

**UNIVERSIDADE FEDERAL DE MINAS GERAIS**  
Escola de Engenharia  
Programa de Pós-Graduação em Saneamento, Meio Ambiente e Recursos Hídricos

Denis Fürstenau Plec

**INFLUENCE OF HYDRODYNAMICS ON PHYTOPLANKTON BEHAVIOUR IN  
LAKES IN URBAN AREAS THROUGH HIGH-FREQUENCY MEASUREMENTS AND  
THREE-DIMENSIONAL NUMERICAL MODELLING**  
**Application to Lake Champs-sur-Marne (France) and Lake Pampulha (Brazil)**

Belo Horizonte  
2020

Denis Fürstenau Plec

**INFLUENCE OF HYDRODYNAMICS ON PHYTOPLANKTON BEHAVIOUR IN  
LAKES IN URBAN AREAS THROUGH HIGH-FREQUENCY MEASUREMENTS AND  
THREE-DIMENSIONAL NUMERICAL MODELLING**  
**Application to Lake Champs-sur-Marne (France) and Lake Pampulha (Brazil)**

Tese apresentada ao Programa de Pós-graduação em Saneamento, Meio Ambiente e Recursos Hídricos da Universidade Federal de Minas Gerais e École Doctorale Sciences, Ingénierie et Environnement Université Paris-Est, como requisito parcial à obtenção do título de Doutor em Saneamento, Meio Ambiente e Recursos Hídricos.

Área de concentração: Recursos Hídricos

Linha de pesquisa: Hidrodinâmica e Modelagem Matemática

Orientador: Nilo de oliveira nascimento e Brigitte Vinçon-Leite.

Coorientador: Talita SILVA

Belo Horizonte  
2020

P724i	<p>Plec, Denis Fürstenau.  Influence of hydrodynamics on phytoplankton behaviour in lakes in urban areas through high-frequency measurements and three-dimensional numerical modeling [recurso eletrônico] : Application to Lake Champs-sur-Marne (France) and Lake Pampulha (Brazil) / Denis Fürstenau Plec. - 2020. 1 recurso online (248 f. : il., color.) : pdf.</p> <p>Orientadores: Nilo de Oliveira Nascimento, Brigitte Vinçon-Leite.  Coorientadores: Talita Silva, Bruno Lemaire.</p> <p>Tese (doutorado) - Universidade Federal de Minas Gerais, Escola de Engenharia.</p> <p>Anexos: f. 207-206.</p> <p>Bibliografia: f. 194-206.  Exigências do sistema: Adobe Acrobat Reader.</p> <p>1. Engenharia sanitária - Teses. 2. Recursos hídricos - Desenvolvimento - Teses. 3. Cianobactéria - Teses. 4. Hidrodinâmica - Teses. 5. Pampulha, Lagoa da (MG) - Teses. I. Nascimento, Nilo de Oliveira. II. Vinçon-Leite, Brigitte. III. Silva, Talita Fernanda das Graças. IV. Lemaire, Bruno J. V. Universidade Federal de Minas Gerais. Escola de Engenharia. VI. Título.</p> <p style="text-align: right;">CDU:</p>
628(043)	



UNIVERSIDADE FEDERAL DE MINAS GERAIS  
Escola de Engenharia  
*Programa de Pós-Graduação em Saneamento, Meio Ambiente e Recursos Hídricos*  
Avenida Antônio Carlos, 6627 - 4º andar - 31270-901 - Belo Horizonte – BRASIL  
Telefax: 55 (31) 3409-1882 - [posgrad@desa.ufmg.br](mailto:posgrad@desa.ufmg.br)  
<http://www.smarh.eng.ufmg.br>

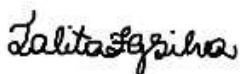
## FOLHA DE APROVAÇÃO

Influence of Hydrodynamics on Phytoplankton Behaviour in Lakes in Urban Areas Through High-Frequency Measurements and Three-Dimensional Numerical Modelling – Application to Lake Champs-Sur-Marne (France) and Lake Pampulha (Brazil)

**DENIS FURSTENAU PLEC**

Tese defendida e aprovada pela banca examinadora constituída pelos Senhores:

NILO DE OLIVEIRA NASCIMENTO 

TALITA FERNANDA DAS GRAÇAS SILVA 

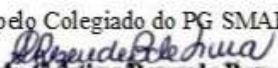
BRIGITTE JEANNE GABRIELLE VINÇON-LEITE 

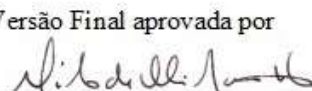
CRISTOVÃO VICENTE SCAPULATIEMPO FERNANDES 

OLIVIER FOCHE-GROBLA 

ORLANE ANNEVILLE 

SÉRGIO KOIDE 

Aprovada pelo Colegiado do PG SMARH  
  
**Profª Sonaly Cristina Rezende Borges de Lima**  
**Coordenadora**

Versão Final aprovada por  
  
**Prof. Nilo de Oliveira Nascimento**  
Orientador

Belo Horizonte, 18 de dezembro de 2020.

## Acknowledgement

I would like to take this opportunity to express my appreciation to professor Nilo and professor Brigitte. Thank you for calling and choosing me to participate in this research. Thank you for your help on the scientific plan. To professor Nilo, thank you for displaying the importance of having a kind nature. Thank you, professor Brigitte, for guiding me and showing me what to do and how not to do.

I am particularly grateful for the assistance given by my coordinators, professor Talita. The import support in decision making was crucial for my progress. I would like to thanks Bruno Lemaire, I should have walked closer during the period in France.

I would like to offer my special thanks to CAPES and French National Research Agency (ANR) for providing crucial financial support.

I also address my thanks to all the members of my jury.

I would like to express my thanks to all the staff of LEESU and EHR. Thank you, Phillipe and Mohammed for the support in field measurements. Thanks for all PhD students from Brazil and France.

I would also like to thank all my friends and family members that provided me with great support during the research process. Without you the work would not have been possible to conclude.

My special thanks to Bianca, Nicholas, Thiago, Janete and my brother Swen. Thank you all for assisting me with your knowledge of the English language.

Thank you all for helping me to be here.

I would also take this opportunity to thank God. He has taking care of me during every breath I have taken. I foresaw the Lord always before me, for he is at my right hand that I may not be shaken, therefore my heart rejoices, and my tongue is glad. You will make me full of gladness with your presence (Acts 2:25-26a; 28b)

## Resumo

O objetivo principal dessa tese é o de caracterizar a hidrodinâmica de lagos urbanos rasos para melhor entender a sua influência na variabilidade espacial e temporal da biomassa de fitoplâncton utilizando monitoramento em alta frequência e modelagem numérica tridimensional. Para alcançar esse objetivo, foram investigados dois estudos de casos experimentais: Lago de Champs-sur-Marne, um pequeno e raso lago urbano na França, e a Lagoa da Pampulha, um reservatório urbano raso de médio porte, no Brasil.

A pesquisa mostrou que um modelo hidrodinâmico tridimensional calibrado e um modelo ecológico, associados a monitoramento em alta frequência, são essenciais para entender a hidrodinâmica de lagos rasos e para compreender a variabilidade temporal e espacial do comportamento de fitoplâncton e cianobactérias. Na pesquisa, foram destacadas estratégias para avaliar a variabilidade espacial e temporal da biomassa de cianobactérias e a relevância em compreender a hidrodinâmica lacustre com o propósito do manejo das águas. Também foram destacadas a importância de descrever corretamente eventos de misturas e estratificações térmica e de monitorar forçantes meteorológicas externas, para poder representar corretamente as variabilidades temporais e espaciais em modelos ecológicos.

Na pesquisa, dois diferentes lagos foram estudados. O primeiro foi o lago de Champs-sur-Marne, um lago urbano pequeno e raso que foi formado devido a extração de areia. O lago não possui contribuição de cursos de água que renovam o seu armazenamento. Ele é alimentado pelo lençol freático, oriundo do escoamento subterrâneo do rio Marne que está localizado em sua proximidade. O segundo estudo de caso foi a Lagoa da Pampulha, um reservatório urbano raso de médio porte. A Lagoa da Pampulha é um reservatório artificial que é alimentado por 8 tributários, possui tempo de residência de 89 dias (considerando a vazão média de longo termo). Ambos os lagos estudados possuem problemas com explosões de cianobactérias. O lago de Champs-sur-Marne é frequentado por crianças de sua área urbana vizinha, entretanto, atividades recreativas no lago são repentinamente proibidas durante o verão devido a riscos à saúde humana causados por explosões de cianobactérias tóxicas. A Lagoa da Pampulha foi originalmente concebida com a finalidade de usos múltiplos, incluindo fonte de captação para abastecimento de água. Entretanto, devido a intenso processo de urbanização em sua bacia hidrográfica a partir da década de 70, a qualidade da água e seu estado trófico foram severamente comprometidas, resultando em um reservatório com condição hipertrófica, o que, associado com a ocorrência de frequentes explosões de cianobactérias, levou a interrupção da captação para finalidade de abastecimento a partir da década de 80.

No lago francês, um modelo hidrológico e ecológico tridimensional foi calibrado usando monitoramento de alta frequência da clorofila-a, da temperatura e velocidade da água. A clorofila-a foi medida na profundidade de 1,5 m. A temperatura foi medida na superfície (0,5 m), profundidade média (1,5 m) e no fundo do lago (2,5 m). A velocidade foi medida da superfície até 2,7 m de profundidade em uma variação intervalar de 0,45 m. Após a calibração do modelo, o comportamento do fitoplâncton foi verificado para cenários com diferentes concentrações de nutriente usando modelo ecológico e usando um traçador para avaliar a influência do vento.

O Período 1 (com 7 dias de duração, do dia 23 a 30 de junho de 2015, correspondendo a 159 valores horários em cada profundidade) foi utilizado para avaliar a hidrodinâmica e o comportamento do fitoplâncton, considerado como um traçador conservativo, por meio de uma simulação de transporte. O Período 2 (com 14 dias de duração, do dia 13 a 27 de julho de 2015, correspondendo a 342 valores horários para cada profundidade) e o Período 3 (com duração de 19 dias, do dia 14 de julho a 01 de agosto de 2016, correspondendo a 456 valores horários para cada profundidade) foram selecionados para simular o modelo hidrodinâmico acoplado com o modelo ecológico. O Período 4 (com duração de 19 dias, do dia 19 de setembro a 12 de outubro, correspondendo a 567 valores horários para cada profundidade) foi utilizado para monitorar e calcular a velocidade da água. A temperatura da água para as 3 profundidades monitoradas foi validada para os 4 períodos simulados.

A pesquisa desenvolvida no lago de Champs-sur-Marne mostrou que:

- ✓ O monitoramento em alta frequência possibilita a análise de variações temporais abruptas da biomassa de fitoplâncton no lago e a influência de forçantes meteorológicas externas no comportamento hidrodinâmico;
- ✓ O modelo tridimensional Delft-3D possibilitou a análise da influência da hidrodinâmica na concentração de fitoplâncton e na sua distribuição espacial heterogênea;
- ✓ A variação da condição de mistura e de estratificação térmica e a complexa funcionalidade hidrodinâmica lacustre pode ser representada por meio de modelagem tridimensional;
- ✓ A modelagem tridimensional pode auxiliar na melhoria da rede de monitoramento, destacando regiões com diferentes comportamentos;
- ✓ A modelagem matemática é uma excelente ferramenta para simular diferentes cenários em situações que existem lacunas de dados de campo;
- ✓ O monitoramento e as simulações mostraram que o comportamento hidrodinâmico do lago Champs-sur-Marne é muito instável e dinâmico. O lago responde rapidamente e intensamente em relação a forçantes meteorológicas. Entretanto, a modelagem hidrodinâmica tridimensional foi capaz de representar esse complexo comportamento;
- ✓ O monitoramento e as simulações numéricas mostraram que o lago não possui estratificação de velocidade em termos da potência da frequência. Foi mostrado que, o comportamento da velocidade, é muito similar e apresenta correlação com a intensidade do vento, onde um valor de 3,0 m/s pode impactar inteiramente a coluna vertical, portanto, uma estação meteorológica *in loco* é importante;

No lago brasileiro, o modelo hidrodinâmico tridimensional Delft3D-flow foi calibrado e validado usando medições de temperatura da água em alta frequência. O período de calibração teve duração de 18 dias, do dia 16 de maio a 03 de junho de 2016, correspondendo a 440 valores horários para cada uma das profundidades

monitoradas, a saber: superfície (0,5 m), 2,5 m, 5,5 m, e fundo (9,5 m). O período de validação, teve duração de 16 dias, do dia 29 de maio a 14 de junho de 2016, correspondendo a 388 valores horários para cada uma das já mencionadas profundidades. Um segundo período de validação teve duração de 88 dias, do dia 15 de maio a 10 de agosto de 2015, correspondendo a 2107 valores horários para a superfície (0,5 m de profundidade), única profundidade disponível no referido período.

A pesquisa desenvolvida na lagoa da Pampulha mostrou que:

- ✓ Os principais parâmetros que apresentam maior sensibilidade para calibrar o comportamento térmico da lagoa é o fator que multiplica a intensidade do vento (*Wind fator*) e o coeficiente de Dalton;
- ✓ Monitoramento em alta frequência, com espaçamento horário, pode detectar repentinas mudanças na temperatura da água, que apresentaram diferentes amplitudes de variações ao longo da coluna vertical de profundidade e, utilizando modelagem tridimensional, foi possível avaliar e investigar as causas das repentinas mudanças na temperatura da água;
- ✓ O modelo tridimensional, associado com monitoramento em alta frequência, mostrou que detectar a vazão afluyente com temperatura inferior a do lago e, conhecendo a trajetória temporal do escoamento ao longo das camadas mais profundas do lago, pode contribuir para implementar e auxiliar técnicas de restauração e ajudar no manejo de águas de lagos urbanos que possuem condições de hipóxia no fundo do lago;
- ✓ O modelo tridimensional foi apto a reproduzir acuradamente as alternâncias das condições de mistura e estratificação térmica para todos os períodos simulados, permitindo uma análise aprofundada da hidrodinâmica de um lago urbano tropical e raso

Como lagos urbanos rasos não tem sido um grande foco de estudo, essa pesquisa pode acrescentar importantes contribuições para o conhecimento sobre a influência da hidrodinâmica no comportamento de fitoplâncton em lagos urbanos e rasos. Na pesquisa, foi mostrado que lagos rasos são muito instáveis e reagem fortemente e rapidamente às condições meteorológicas. A biomassa de fitoplanctons apresenta alta heterogeneidade no tempo e espaço, o que resulta em grande complexidade para monitoramento do seu comportamento. Usando um modelo tridimensional, foi mostrado que a hidrodinâmica desempenha um importante papel para melhor compreender explosões de algas e sua concentração na superfície do espelho de água (*scum formation*). Essa pesquisa mostrou que um modelo hidrodinâmico e ecológico tridimensional calibrado e validado, utilizando monitoramento em alta frequência, é essencial para compreender a qualidade da água em lagos urbanos rasos. Além do mais, utilizando os resultados da modelagem, podem ser feitas sugestões para aprimoramento de uma rede de monitoramento, buscando melhor elucidar o comportamento de cianobactérias. Portanto, essas contribuições científicas também são promissoras para ajudar a avaliar e monitorar a distribuição, resuspensão e sedimentação de nutrientes e poluentes em lagos, além de compreender o fenômeno de explosões de fitoplanctons de maneira mais ampla.

Palavras chaves: Lagos urbanos rasos; fitoplâncton, cianobactérias, hidrodinâmica lacustre, monitoramento em alta frequência, modelagem tridimensional.



## Abstract

The main objective of this thesis is to characterize the hydrodynamics of shallow urban lakes to better understand its influence on spatial and temporal variability of phytoplankton biomass through high-frequency measurements and three-dimensional numerical modelling. To achieve this objective, two experimental study sites were investigated: Lake Champs-sur-Marne, a small and shallow urban lake in France, and Lake Pampulha, a medium-sized and shallow urban reservoir, in Brazil.

The research shows that a calibrated three-dimensional hydrodynamic model and an ecological model using high-frequency monitoring are essential for understanding shallow lakes hydrodynamic and the temporal and spatial behaviour of phytoplankton and cyanobacteria. It was highlighted strategies to assess spatial and temporal variability of cyanobacteria biomass and how relevant is to understand lake dynamics for management purpose and the importance to well describe the mixing and stratification and to measure the external forces for appropriate temporal and spatial dynamic based in ecosystem modelling approach. In this research it was studied two different lakes. The first study site was Lake Champs-sur-Marne, a small and shallow urban lake that was formed during sand extraction quarry. The lake does not have water inflow that renews the water accumulation. It is filled mainly by groundwater, flowing from the water table of the nearby Marne River. The second study site was Lake Pampulha, a medium-sized and shallow urban reservoir. Lake Pampulha is an artificial reservoir that is filled by 8 tributaries, with a residence time of 89 days (considering the annual mean inflow). Both lakes have problems with cyanobacteria blooms. Lake Champs-sur-Marne is frequented by children from a nearby urban area however, water recreational activities in the lake have been repeatedly banned in the summer because of potential health risks caused by toxic cyanobacteria blooms. Lake Pampulha was built for many purposes, including drinking water supply. However, due to an intense urbanisation process in the lake catchment from the 1970s on, the lake water quality and ecological state was severely compromised resulting in a hypereutrophic reservoir, leading to the interruption of drinking water provision from the 1980s, with frequent cyanobacteria blooms.

In the French lake, a three-dimensional hydrodynamic and ecological model was calibrated using high-frequency measurements of chlorophyll-a, temperature, and water velocity. The chlorophyll-a was measured at 1.5 m depth. The water temperatures were measured at surface (0.5 m), middle (1.5 m) and bottom (2.5 m) depths. The velocities were measured with a depth range of 0.45 m from the surface to 2.7 m at the bottom. After the model calibration the phytoplankton behaviour was verified through scenarios with different nutrient concentration using the ecological model and a scenario using a tracer concentration to evaluate the wind influence.

The Period 1 (lasting 7 days, from 23<sup>rd</sup> June 2015 to 30<sup>th</sup> June 2015, corresponding to 159 hourly values for each depth) was used to evaluate hydrodynamic and the phytoplankton considering transport simulation as a conservative tracer. Periods 2 (lasting 14 days, from 13 July to 27 July 2015, corresponding 342 hourly values for each depth) and Period 3 (lasting 19 days, from 14 July 2016 to 01 August 2016, corresponding to 456 hourly values for each depth) were selected to run the coupled hydrodynamic and ecological model. Period 4 (lasting 19 days, from 19 September 2016 to 12 October 2016, corresponding to 567 hourly values for each depth) was used to assess the measured and calculated velocities. The temperature at three measured depths was validated for all of the four periods.

The research carried out in Lake Champs-sur-Marne showed that:

- ✓ High-frequency monitoring enables an analysis of the high temporal variation of biomass in the lake and the influence of different external forces on hydrodynamic behaviour;
- ✓ The three-dimensional model Delft-3D was useful in the analysis of the influence of lake hydrodynamics on phytoplankton concentrations and spatial heterogeneity;
- ✓ Alternation and duration of mixing and stratification conditions and the complex hydrodynamic functioning of the lake could be represented by the three-dimensional model;
- ✓ The three-dimensional model can help to improve lake monitoring design, highlighting regions with different behaviour;
- ✓ Mathematical modelling is a great tool to simulate different scenarios in cases where there are field data gaps;
- ✓ The measurements and simulations showed that the hydrodynamics of Lake Champs-sur-Marne are very unstable and dynamic. The lake reacts rapidly and intensely to meteorological forcing. However, the three-dimensional hydrodynamic model was able to represent these complex hydrodynamics behaviour;
- ✓ The measurements and simulations showed that the lake does not have velocity stratification in terms of power frequency. It was shown that, the velocity behaviour was very similar and presented a strong correlation with wind intensity, in which wind intensity of 3.0 m/s may impact the entire vertical column, therefore, being important an *in loco* meteorological station.

In the Brazilian lake, the three-dimensional hydrodynamic model Delft3D-Flow was calibrated and validated using high-frequency temperature measurements. The calibration period lasted 18 days, from 16<sup>th</sup> May to 03<sup>rd</sup> June 2016, corresponding to 440 hourly data for each one of the four respectively depths: surface (0.5 m), 2.5 m, 5.5 m and bottom (9.5 m). The validation period lasted 16 days, from 29<sup>th</sup> May to 14<sup>th</sup> June 2016, corresponding to 388 hourly values of water temperature for each of the same four depths. A second validation period lasted 88 days, from 15<sup>th</sup> May to 10<sup>th</sup> August 2015, corresponding to 2107 hourly values, for surface (0.5 m) depth was also simulated.

The research carried out in Lake Pampulha showed that:

- ✓ The main sensitivity parameters to calibrate the thermal behaviour of the lake are the Wind factor and Dalton coefficient;
- ✓ High-frequency measurement with hourly time step could detect sudden changes of water temperature with different amplitudes depending on the depth and using three-dimensional model it was possible to investigate the cause of sudden changes in the water temperature;

- ✓ The three-dimensional model, associated with high-frequency measurement, showed that detecting colder freshwater current and knowing the time trajectory throughout the deeper layer of the lake may contribute to implement and leverage restoration techniques and support water management for urban lakes that have hypoxia condition at the bottom of the lake;
- ✓ A three-dimensional model could accurately reproduce the alternation of stratification and mixing conditions along all simulated period, allowing a deeper analysis of a shallow tropical lake hydrodynamics

As shallow urban lakes have been the subject of much less study, this research could add important contributions to knowledge about the influence of hydrodynamics on phytoplankton behaviour in shallow and urban lakes. It was shown that shallow lakes are very instable and react strongly and rapidly to meteorological forces. Phytoplankton biomass displays high heterogeneities in space and time that result in high complexity to be able to measure its behaviour. Using a three-dimensional model, it was shown that hydrodynamics play an important role to better understand algal blooms and scum formation. This study shows that a calibrated and validated three-dimensional hydrodynamic and ecological model using high-frequency monitoring is essential for understanding water quality in shallow urban lakes. Otherwise, using the results of modeling, suggestions could be made to improve the current monitoring locations to better elucidate cyanobacteria behaviour. Therefore, these scientific contributions are promising to help in assessing and measure the distribution and resuspension of nutrients, sedimentation, and pollutants in lakes, and for understanding phytoplankton blooms more broadly.

Keywords: Shallow urban lakes; phytoplankton; cyanobacteria; lake hydrodynamics; high-frequency measurements; three-dimensional model.

## List of figures

Figure 3.1 – Location of Lake Champs-sur-Marne. Adapted from Google Earth® .....	60
Figure 3.2 – Lake aerial photographs. a) 1923 b) 1933 c) 1946 Source: Géoportail® from Huguenard (2015) .....	61
Figure 3.3 – Aerial photographs (a) before the flood in 1969, (b) during a flood in 1970 and (c) after the morphology adaptation in 1971 (source: Géoportail® adapted by (Huguenard, 2015) .....	61
Figure 3.4 – Channel grounding on the island. Source: Adapted from GoogleEarth®. Left: August 2005; Right: April 2014 .....	61
Figure 3.5 – Main features of the island. Source: Adapted from Google Earth® .....	62
Figure 3.6 – Small island created in the south part of the lake in red circle. Source: Adapted from GoogleEarth .....	62
Figure 3.7 – Small beach. Photo: author, March 2017 .....	63
Figure 3.8 – Large beach and equipment installed. Photo: author, March 2017 .....	63
Figure 3.9 – Localization of Lake Pampulha and its tributaries: (1) Olhos d’água; (2) AABB*; (3) Bráunas; (4) Água Funda; (5) Sarandi; (6) Ressaca; (7) Tijuco and (8) Mergulhão. *river not named, popularly known as AABB (Associação Atlética Banco do Brasil – Athletics Association from Brazil Bank). Red lines are the respective catchment of the tributaries. Monitoring station in triangle: (1) Fluviometric (SAR18F – Sarandi and RES17F – Ressaca; (2) Meteorological (A521 - UFMG and 83587 - Belo Horizonte); (3) Lake monitoring in red cycle (P1).....	64
Figure 3.10 – Trajectory of bathymetry measurement in the lake and depth.....	66
Figure 3.11 – Total biomass of phytoplankton and biomass of cyanobacteria expressed as chlorophyll-a (Chl-a). Source: Peiffer, (2016).....	66
Figure 3.12 – Main phytoplankton groups observed in the lake over the last decade (2006-2016) during summer. Source: Peiffer, (2016) .....	67
Figure 3.13 – Location of the monitoring points on the lake of Champs-sur-Marne.....	68
Figure 3.14 – Treatment flowchart for Chl-a. ....	69
Figure 3.15 – Daily boxplot for chlorophyll-a fluorescence measured at points A and B during January 2016.....	70
Figure 3.16 – Daily boxplot for chlorophyll-a fluorescence measured at points A and B during March 2016.....	71
Figure 3.17 – Scheme shows ADCP measurement method. Source: Nortek, (2008) .....	74
Figure 3.18 – Nutrient concentration measured in Lake Champs-sur-Marne. ....	75
Figure 3.19 – Bathymetry map (SUDECAP, 2014). P <sub>1</sub> is the monitoring point of the lake .....	77
Figure 3.20 – Example of □-grid (on the left) and Z-grid (on the right) available in the Delft3D model (Deltares, 2013).....	92
Figure 3.21 – Three-dimensional view for an element computation of grid of Delft3D (Deltares, 2013) .....	92
Figure 3.22 – Sets of thin dams in the computation grid. (Deltares, 2013).....	92
Figure 3.23 – Mathematical mesh used in Delft3D simulation for Lake Champs-sur-Marne. Yellow lines are thin dams .....	93
Figure 3.24 – Vertical resolution for □□ and Z-grid in point P <sub>1</sub> . Blue X represents the measurement depths. ....	94
Figure 3.25 – Water Inflows locations (blue lines), thin dam locations (yellow line), monitoring point (P <sub>1</sub> - cyan cross) and spillway location (red line).....	96
Figure 3.26 – Location of the tracer input and the points evaluated. ....	101
Figure 3.27 – Tracer input and fluorescence measured at point B .....	101
Figure 3.28 – Wind direction and speed (m/s) for Orly Station during the period from 23 <sup>rd</sup> June 2015 to 30 <sup>th</sup> June 2015.....	102
Figure 3.29 – Wind velocity (m/s) for Orly Station during the period from 23 <sup>rd</sup> June 2015 to 30 <sup>th</sup> June 2015.....	102
Figure 4.1 – Chl-a measurements using MPX and BBE for all points.....	105
Figure 4.2 – Chl-a measurements using MPX in point A and laboratory analysis of water samples from a point near the beach.....	105

Figure 4.3 – Radiation, atmosphere temperature, wind intensity and direction, cloud cover and humidity during period 1 (23 <sup>rd</sup> June 2015 to 30 <sup>th</sup> June 2015).....	107
Figure 4.4 – Comparison of the temperature between measured and simulated data for period 1 (23 <sup>rd</sup> June 2015 to 30 <sup>th</sup> June 2015) at point A.....	108
Figure 4.5 – Stratification behaviour at points A, B and C from 23 <sup>rd</sup> June 2015 to 30 <sup>th</sup> June 2015.....	109
Figure 4.6 – Comparison of the stratification condition between measured (a) and simulated (b) data from 23 <sup>rd</sup> June 2015 to 30 <sup>th</sup> June 2015 in Point A. Red arrows represent partial mixing events.	110
Figure 4.7 – Comparison between the simulated temperature for point A, Beach and Channel for period 1 (23 <sup>rd</sup> June 2015 to 30 <sup>th</sup> June 2015). .....	111
Figure 4.8 – Surface simulated temperature for period 1 on 24 June 2015 at 14 hours. ....	111
Figure 4.9 – Comparison of the temperature at points A, B and C at 3 depths for period 1 (26 <sup>th</sup> June 2015 to 30 <sup>th</sup> June 2015). .....	112
Figure 4.10 – Radiation, atmosphere temperature, wind intensity and direction, cloud cover and humidity during period 2 (13 July 2015 to 27 July 2015).....	113
Figure 4.11 – Comparison of the temperature between measured and simulated data from period 2 (13 to 27 July 2015) at point A.....	114
Figure 4.12 – Temperature isocontours during simulation period 2 (13 July 2015 to 27 July 2015) ..	115
Figure 4.13 – Water temperature at point A during period 2 (13 July 2015 to 27 July 2015) .....	115
Figure 4.14 – Radiation, atmosphere temperature, wind intensity and direction, cloud cover and humidity, during period 3 (14 July 2016 to 01 August 2016).....	116
Figure 4.15 – Comparison of the temperature between measured and simulated data for period 3 (14 July 2016 to 01 August 2016) at point A .....	117
Figure 4.16 – Stratification behaviour for measured (left) and simulated (right) for period 3 (14 July 2016 to 01 August 2016) .....	117
Figure 4.17 – Radiation, air temperature, wind intensity and direction, cloud cover and humidity during period 4 (19 September 2016 to 12 October 2016).....	118
Figure 4.18 – Comparison of the temperature between measured and simulated data from period 4 (19 September 2016 to 12 October 2016).....	119
Figure 4.19 – Simulated water temperature from period 4 (19 September 2016 to 12 October 2016) at point A.....	119
Figure 4.20 – Total velocity profile near point B in Lake Champs-sur-Marne. (a) Measured data (m/s) (b) Simulated values (m/s) for period 4.....	121
Figure 4.21 – Difference between simulated and measured total velocity profile near point B in Lake Champs-sur-Marne.....	121
Figure 4.22 – Power Spectra of simulated and measured total velocity profile near point B in Lake Champs-sur-Marne for surface (0.5m), middle (1.5) and bottom (2.5 m) depths .....	122
Figure 4.23 – Power spectra of simulated and measured total velocity profiler near point B in Lake Champs-sur-Marne for surface (0.5 m), middle (1.5 m) and bottom (2.5 m) depths.....	122
Figure 4.24 – Measured daily average water velocity for the average vertical profile, surface (0.5 m), middle (1.5 m) and bottom (2.5 m) depths.....	123
Figure 4.25 – Simulated daily average water velocities for the average vertical profile, surface (0.5 m), middle (1.5 m) and bottom (2.5 m) depths.....	123
Figure 4.26 – Temperature and total Chlorophyll-a during monitoring period with ADCP, corresponding to period 4 .....	124
Figure 4.27 – Tracer concentration over time for the simulation with original wind direction .....	125
Figure 4.28 – Map of the tracer concentrations on 24 <sup>th</sup> , and 29 <sup>th</sup> June at 10h a. m. for (a) standard direction, (b) West wind (c) Northwind in the surface layer (0.5 m).....	126
Figure 4.29 – Water temperature and chlorophyll-a monitoring at point A during 2015. The simulated period is between the black vertical lines.....	127
Figure 4.30 – Water temperature and chlorophyll-a monitoring at point B during 2015. The simulated period is between the black vertical lines.....	127
Figure 4.31 – Water temperature monitoring at point C during 2015. The simulated period is between the black vertical lines.....	127
Figure 4.32 – Water temperature and chlorophyll-a for the calibration period (13 to 27 July 2015) at point A. The black lines represent the dates of the vertical profiles with BBE fluorometer.....	128

Figure 4.33 – Water temperature and chlorophyll-a for the calibration period (13 to 27 July 2015) at point B. The black lines represent the dates of the vertical profiles with BBE fluorometer. ....	128
Figure 4.34 – Water temperature for the calibration period (13 to 27 July 2015) at point C.....	128
Figure 4.35 – Chlorophyll-a at point A and B for the calibration period (13 to 27 July 2015).....	129
Figure 4.36 – Daily Box-Plot of chlorophyll-a behaviour at point A and B for the calibration period (13 to 27 July 2015).....	129
Figure 4.37 – Fraction contribution of each algal group measured at point A and B for the calibration period (13 to 27 July 2015) .....	131
Figure 4.38 – Active radiation measured in vertical profile on 30 <sup>th</sup> June 2015 .....	132
Figure 4.39 – Active radiation attenuation equation for a vertical profile on 30 <sup>th</sup> June 2015 .....	132
Figure 4.40 – Simulated and measured Chl-a concentrations at 1.5 m depth at point A using default sedimentation values. ....	133
Figure 4.41 – Fraction contribution of each algal group measured at point A for the calibration period (13 to 27 July 2015) using default sedimentation velocities .....	133
Figure 4.42 – Simulated and measured Chl-a concentrations at 1.5 m depth at point A using using 0.50 m/day for cyanobacteria sedimentation velocities .....	134
Figure 4.43 – Fraction contribution of each algal group measured at point A for the calibration period (13 to 27 July 2015) using 0.50 m/day for cyanobacteria sedimentation velocities. ....	134
Figure 4.44 – Simulated and measured Chl-a concentrations at 1.5 m depth at point A using 0.50 m/day for cyanobacteria sedimentation velocities and 0.75 m/day for Green algae .....	135
Figure 4.45 – Fraction contribution of each algal group measured at point A for the calibration period (13 to 27 July 2015) using 0.50 m/day for cyanobacteria sedimentation velocities and 0.75 m/s for green algae .....	136
Figure 4.46 – Simulated and measured Chl-a concentrations at 1.5 m depth at point A using 0.50 m/day for cyanobacteria sedimentation velocities and 1.0 m/day for green algae.....	137
Figure 4.47 – Fraction contribution of each algal group measured at point A for the calibration period (13 to 27 July 2015) using 0.50 m/day for cyanobacteria sedimentation velocities and 1.0 m/day for green algae.....	137
Figure 4.48 – Chlorophyll-a concentration during simulation from 13 to 27 July 2015 at point A.....	139
Figure 4.49 – Dissolved Oxygen concentration during simulation from 13 to 27 July 2015 at point A .....	140
Figure 4.50 – Simulated and measured vertical Dissolved Oxygen concentration on 22/07/2015 at point A.....	140
Figure 4.51 – Nitrate ( $\text{NO}_3^-$ gN/m <sup>3</sup> ) concentration during simulation from 13 to 27 July 2015 at point A .....	141
Figure 4.52 – Ortho-Phosphate ( $\text{PO}_4^{3-}$ gP/m <sup>3</sup> ) concentration during simulation from 13 to 27 July 2015 at point A.....	141
Figure 4.53 – Ammonium ( $\text{NH}_4^+$ gN/m <sup>3</sup> ) concentration during simulation from 13 to 27 July 2015 at point A.....	142
Figure 4.54 – Chlorophyll-a simulated on 16 July at 16 h.....	143
Figure 4.55 – Chlorophyll-a simulated on 19 July at 21 h.....	143
Figure 4.56 – Chlorophyll-a simulated on 20 July at 04 h.....	144
Figure 4.57 – Chlorophyll-a simulated on 20 July at 07 h.....	144
Figure 4.58 – Chlorophyll-a simulated on 21 July at 07 h.....	145
Figure 4.59 – Chlorophyll-a simulated on 23 July at 09h.....	145
Figure 4.60 – Total Chlorophyll-a and temperature monitoring in point A during 2016. The simulated period corresponds to black vertical lines .....	146
Figure 4.61 – Temperature and Chlorophyll-a for the validation period (14 July to 01 August 2016). Black lines show when the vertical profile was performed.....	146
Figure 4.62 – Vertical algae distribution measured on 18 July 2016 at Point A.....	147
Figure 4.63 – Vertical algae distribution measured on 18 July 2016 at Point B.....	147
Figure 4.64 – Vertical algae distribution measured on 18 July 2016 at Point C.....	148
Figure 4.65 – Vertical contribution of each algal group measured during the verification period (18 July 2016 to 01 August 2016).....	148

Figure 4.66 – Dissolved oxygen concentration at point A, B and C. The green line represents the mean valued used as initial concentration in element depths for the verification period (18 July 21016 to 01 August 2016).....	149
Figure 4.67 – Simulated and measured chlorophyll concentrations at 1.5m depth at point A. The shaded dark grey area represents the range of the hourly concentrations measured, and the shaded light grey area represents the limits of simulated biomass. ....	150
Figure 4.68 – Average contribution of each algal group measured and simulated in the validation period (18 July 2016 to 01 August 2016).....	151
Figure 5.1 – Water temperature and chlorophyll-a, measured in Lake Pampulha at point P <sub>1</sub> .....	155
Figure 5.2 – Water temperature (Surface (0.5 m), 2.5 m, 5.5 m and 9.5 m depths) and Chlorophyll-a at surface (0.5 m) measured in Lake Pampulha at station P <sub>1</sub> .....	155
Figure 5.3 – Chlorophyll-a measured in Lake Pampulha and sensor cleaning events (vertical black lines) prior to Phoslock treatment .....	156
Figure 5.4 – Chlorophyll-a measured in Lake Pampulha and sensor cleaning events (vertical black lines) during Phoslock treatment.....	157
Figure 5.5 – Linear regression between air temperature and inflow water temperature. Red line represents the 1:1 relationship between variables. ....	157
Figure 5.6 – Fitted sine function for daily maximum and minimum water temperatures .....	158
Figure 5.7 – Fitted sine function for daily maximum and minimum air temperatures.....	158
Figure 5.8 – Hourly inflow water temperature generated using linear regression and the MSSWF method and observed inflow water temperature during April and May 2013.....	159
Figure 5.9 – Water temperature (°C) measured at point P <sub>1</sub> for 0.5, 2.5, 5.5 and 9.5 m depth during the first simulated period (16 <sup>th</sup> May to 03 <sup>rd</sup> June 2016) .....	160
Figure 5.10 – Radiation, air temperature, wind intensity and direction, cloud cover and humidity measured at a meteorology station during the calibration period (16 <sup>th</sup> May to 03 <sup>rd</sup> June 2016) ..	161
Figure 5.11 – Measured and simulated temperatures with different wind intensity factors for the calibration period (16 <sup>th</sup> May to 03 <sup>rd</sup> June 2016) .....	162
Figure 5.12 – Mean average error (MAE), Relative Error (RE) and R <sup>2</sup> for wind factor calibration....	163
Figure 5.13 – Measured and simulated temperature with 100% measured wind intensity and different Dalton coefficients for the calibration period (16 <sup>th</sup> May to 03 <sup>rd</sup> June 2016) .....	164
Figure 5.14 – Measured and simulated temperature with 0.025 and 0.0025 m <sup>2</sup> /s for background horizontal eddy viscosity and diffusivity .....	165
Figure 5.15 – Measured and simulated temperatures at point P <sub>1</sub> at surface (0.5), 2.5, 5.5 and 9.5 m depths for the calibration period simulated with Sigma and Z grid. ....	167
Figure 5.16 – Water temperature simulated at point P <sub>1</sub> at surface (0.5), 2.5, 5.5 and 9.5 m depths for the calibration period (16 <sup>th</sup> May to 03 <sup>rd</sup> June 2016) with a wind intensity factor of 100%, a Dalton coefficient of 0.0007 and 0.025 m <sup>2</sup> /s for background horizontal eddy viscosity and diffusivity. ....	168
Figure 5.17 – Comparison of measured and simulated water temperature at point P <sub>1</sub> at surface (0.5), 2.5, 5.5 and 9.5 m depths for the calibration period. Red line represents a perfect adjustment. ...	168
Figure 5.18 - Water temperature (°C) measured at point P <sub>1</sub> for 0.5, 2.5, 5.5 and 9.5 m depth during validation period simulated (29 <sup>th</sup> June to 14 <sup>th</sup> June 2016).....	169
Figure 5.19 - Radiation, air temperature, wind velocity and direction, cloud cover and humidity measured at the meteorology station during the validation period simulated (29 <sup>th</sup> May to 14 <sup>th</sup> June 2016) .....	170
Figure 5.20 - Measured and simulated water temperature for the validation period (29 <sup>th</sup> May to 14 <sup>th</sup> June 2016) at surface (0.5 m), 2.5 m, 5.5 m and 9.5 m depths .....	171
Figure 5.21 - Difference of surface (0.5) and bottom (9.5) for measurement and simulated temperatures for the validation period from 29 <sup>th</sup> May to 14 <sup>th</sup> June 2016 at P <sub>1</sub> station. Blue dashed line represents a mixing condition with difference between surface and bottom of 0.25 °C .....	172
Figure 5.22 - Water temperature (°C) simulated at point P <sub>1</sub> for 0.5, 2.5, 5.5 and 9.5 m depth during validation period (29 <sup>th</sup> May to 14 <sup>th</sup> June 2016). ....	172
Figure 5.23 – Measured and simulated temperature at point P <sub>1</sub> at surface (0.5 m), 2.5 m, 5.5 m and 9.5 m depths for the validation period (29 <sup>th</sup> May to 14 <sup>th</sup> June 2016). The red line represents the 1:1 relationship.....	173

Figure 5.24 – Measured and simulated difference temperatures between surface and bottom at point P1 for the validation period simulated (29 <sup>th</sup> May to 14 <sup>th</sup> June 2016). The red line represents the 1:1 relationship. ....	174
Figure 5.25 – Tributaries inflow from 29 <sup>th</sup> May to 14 <sup>th</sup> June 2016. ....	175
Figure 5.26 – Lake water temperature at the surface (0.5 m), on the bottom (9.5 m) and inflow water temperature.....	175
Figure 5.27 – Measured and simulated water temperature at point P <sub>1</sub> at the surface (0.5 m), 2.5 m, 5.5 m, 9.5 m depths for the validation period simulated (29 <sup>th</sup> May to 14 <sup>th</sup> June 2016).....	176
Figure 5.28 – Longitudinal profile of the lake grid in red.....	177
Figure 5.29 – Water temperature during inflow water peak (03 <sup>rd</sup> June 2016 15h) along the longitudinal profile.....	178
Figure 5.30 – Water velocity during inflow water peak (03 <sup>rd</sup> June 2016 15h) along the longitudinal profile.....	179
Figure 5.31 – Water density during inflow water peak (03 <sup>rd</sup> June 2016 15h) along the longitudinal profile.....	180
Figure 5.32 – Velocity behaviour during inflow water peak (03 <sup>rd</sup> June 2016 15h) at the surface.....	181
Figure 5.33 – Velocity behaviour during inflow water peak (03 <sup>rd</sup> June 2016 15h) at bottom layer....	182
Figure 5.34 – Schmidt stability variation during the validation period (29 <sup>th</sup> May to 14 <sup>th</sup> June 2016) at point P1. ....	183
Figure 5.35 – Difference of surface (0.5) and bottom (9.5) for measured and simulated water temperature for the validation period from 29 <sup>th</sup> May to 14 <sup>th</sup> June 2016 at P1 station. Blue dashed line represents a mixing condition with difference between surface and bottom of 0.25 °C. ....	184
Figure 5.36 – Lake number variation during the validation period (29 <sup>th</sup> May to 14 <sup>th</sup> June 2016) at point P1.....	184
Figure 5.37 – Inflow water in Ressaca/Sarandi during the third period simulated.....	185
Figure 5.38 – Water surface temperature measurements during the third simulated period.....	185
Figure 5.39 – Radiation, air temperature, wind velocity and direction, cloud cover and humidity measured at the meteorology station during the third simulated period. ....	186
Figure 5.40 – Measured and simulated temperature at P <sub>1</sub> at surface (0.5 m) depth from 15 <sup>th</sup> May 2015 to 10 <sup>th</sup> August 2015. ....	187
Figure 5.41 – Hourly measured and simulated water temperature at P1 at 0.5 depth from 15 <sup>th</sup> May 2015 to 10 <sup>th</sup> August 2015. ....	188
Figure 42 – Location of Lake Pampulha and its tributaries: (1) Olhos d’água; (2) AABB*; (3) Bráunas; (4) Água Funda; (5) Sarandi; (6) Ressaca; (7) Tijuco and (8) Mergulhão. *river not named, popularly known as AABB ( <i>Associação Atlética Banco do Brasil – Athletics Association from Brazil Bank</i> ). Red lines indicate the respective catchment of the tributaries. Monitoring station in triangle: (1) Fluviometric (SAR18F – Sarandi and RES17F – Ressaca; (2) Meteorological station (A521 -UFMG and 83587 - Belo Horizonte); (3) Lake monitoring (P1, red dot). ....	223
Figure 43 – Lake Pampulha bathymetry, inflow location, thin dam location (yellow line), monitoring point (P1 – cyan cross) and spillway and inflow locations (blue lines). ....	224
Figure 44 – Vertical resolution for□□ and Z-grid in point P1. Blue X represents the measurement depths. ....	226
Figure 45 – Water temperature (°C) measured at point P1 for surface (0.5 m), 2.5 m, 5.5 m and bottom (9.5 m) depth during the calibration period (May 16 <sup>th</sup> to June 3 <sup>rd</sup> 2016) and validation period (May 29 <sup>th</sup> to June 14 <sup>th</sup> 2016). ....	227
Figure 46 – Tributaries inflow water during the calibration period (May 16 <sup>th</sup> to June 3 <sup>rd</sup> 2016) and validation period (May 29 <sup>th</sup> to June 14 <sup>th</sup> 2016). ....	228
Figure 47 – Measured temperature at P1 at surface (0.5 m) depth from May 15 <sup>th</sup> 2015 to August 10 <sup>th</sup> 2015.....	228
Figure 48 –Tributaries inflow water from May 15 <sup>th</sup> 2015 to August 10 <sup>th</sup> 2015. ....	228
Figure 8 – Radiation, air temperature, wind intensity and direction, cloud cover and humidity measured at a meteorology station during the calibration period (May 16 <sup>th</sup> to June 3 <sup>rd</sup> 2016) and validation period (May 29 <sup>th</sup> to June 14 <sup>th</sup> 2016). ....	229
Figure 9 – Radiation, air temperature, wind velocity and direction, cloud cover and humidity measured at the meteorology station during May 15 <sup>th</sup> 2015 to August 10 <sup>th</sup> 2015. ....	230



Figure 51 – Wind velocity and direction, Air temperature and humidity, Cloud Cover and Radiation measured in the meteorology station for Calibration (May 16 <sup>th</sup> to June 3 <sup>rd</sup> 2016), Validation 2016 (May 29 <sup>th</sup> to June 14 <sup>th</sup> 2016) and Validation 2015 (May 15 <sup>th</sup> to August 10 <sup>th</sup> 2015). Box plots represent minimum, first quartile, median, third quartile, and maximum values for each meteorological variable. ....	231
Figure 52 – Wind direction (degree) and velocity (m/s): Calibration period (May 16 <sup>th</sup> to June 3 <sup>rd</sup> 2016), Validation period in 2016 (May 29 <sup>th</sup> to June 14 <sup>th</sup> 2016) and Validation period in 2015 (May 15 <sup>th</sup> to August 10 <sup>th</sup> 2015). ....	231
Figure 12 – Measured and simulated temperatures for the calibration period from May 16 <sup>th</sup> to June 3 <sup>rd</sup> 2016 at P1 station. ....	234
Figure 13 – Difference of surface (0.5 m) and bottom (9.5 m) for measurement and simulated temperatures for the calibration period from May 16 <sup>th</sup> to June 3 <sup>rd</sup> 2016 at P1 station. Blue dashed line represents a mixing condition with difference between surface and bottom of 0.25 °C and grey lines represent differences of 1.0 and 2.0 °C. ....	234
Figure 14 – Water temperature (°C) simulated at point P1 for surface (0.5 m), 2.5 m, 5.5 m and bottom (9.5 m) depth during the calibration period (May 16 <sup>th</sup> to June 3 <sup>rd</sup> 2016). ....	235
Figure 15 – Measured and simulated temperature for the validation period (May 29 <sup>th</sup> to June 14 <sup>th</sup> 2016) at surface (0.5 m), 2.5 m, 5.5 m and 9.5 m depths. ....	236
Figure 16 – Difference of surface (0.5 m) and bottom (9.5 m) for measurement and simulated temperatures for the validation period from May 29 <sup>th</sup> to June 14 <sup>th</sup> 2016 at P1 station. Blue dashed line represents a mixing threshold with difference between surface and bottom of 0.25 °C. ....	237
Figure 17 – Simulated temperature for the validation period (May 29 <sup>th</sup> to June 14 <sup>th</sup> 2016) at surface (0.5 m), 2.5 m, 5.5 m and 9.5 m depths. ....	237
Figure 18 – Measured and simulated temperature at P <sub>1</sub> station at surface (0.5 m) depth from May 15 <sup>th</sup> to August 10 <sup>th</sup> 2015. ....	238
Figure 19 – Computed inflow water temperature used as an input during the validation period (May 29 <sup>th</sup> to June 14 <sup>th</sup> 2016). Red dash line represents the sensitivity analysis with an inflow water temperature with a constant temperature during June 03 <sup>rd</sup> (scenario D1) and the black dash line during June 02 <sup>nd</sup> to 03 <sup>rd</sup> (scenario D2). ....	239
Figure 21 – Longitudinal transect of the lake model in red and observation points in black cross. ....	239
Figure 22 – Water level variation during the validation period (May 29 <sup>th</sup> to June 14 <sup>th</sup> 2016). ....	239
Figure 23 – Simulated lake water temperature during high inflow on June 03 <sup>rd</sup> 2016 at 13:00 h along the reservoir longitudinal transect. ....	241
Figure 24 – Measured and simulated temperatures at point P1 at the surface (0.5 m), 2.5 m, 5.5 m, 9.5 m depths for the validation period simulated (May 29 <sup>th</sup> to June 14 <sup>th</sup> 2016) and for different inflow water temperatures scenarios. ....	242
Figure 25 – Simulated temperature for the validation period (May 29 <sup>th</sup> to June 14 <sup>th</sup> 2016) at surface (0.5 m), 2.5 m, 5.5 m and 9.5 m depths at the downstream region of the lake (DOWN point in Figure 21). ....	243
Figure 26 – Simulated velocity module at UP point (see Figure 21) for the validation period (May 29 <sup>th</sup> to June 14 <sup>th</sup> 2016) at surface (0.5 m) and bottom (2.0 m). ....	243
Figure 27 – Simulated velocity module at DOWN point (see Figure 21) for the validation period (May 29 <sup>th</sup> to June 14 <sup>th</sup> 2016) at surface (0.5 m) and bottom (13.85 m) ....	243
Figure 28 – Schmidt stability variation during the validation period (May 29 <sup>th</sup> to June 14 <sup>th</sup> 2016) at point P1. ....	244
Figure 29 – Lake number variation during the validation period (May 29 <sup>th</sup> to June 14 <sup>th</sup> 2016) at point P1. ....	244

## List of tables

Table 2.1 – Main results of the comparison of Chl-a measured by FluoroProbe and extraction methods .....	38
Table 2.2 - Indicators evaluated for the 2012 National Lakes Assessment from the United States. (NLA, 2012) .....	53
Table 3.1 – Lake Pampulha climate characteristics for values measured between 1961 and 2001 at Belo Horizonte’s meteorological station from INMET. Source: (CPRM, 2001) .....	65
Table 3.2 – Technical specification of Lake Champs-sur-Marne devices for Chlorophyll-a .....	68
Table 3.3 – Characteristics of measuring devices on the Lake of Champs-sur-Marne. Source: Khac et al., 2018.....	74
Table 3.4 – Characteristics of measuring devices on the Lake Pampulha .....	78
Table 3.5 – Lake Pampulha tributaries catchment area. From Felisberto et al., (2015).....	78
Table 3.6 – Adopted parameters for Delft3D-Flow model in Lake Champs-sur-Marne (From Scriban 2015) .....	95
Table 3.7 – Total outflow of Lake Pampulha. (from Felisberto et al., 2015).....	96
Table 3.8 – Phytoplankton physiology.....	98
Table 3.9 – Phytoplankton stoichiometry .....	99
Table 3.10 – Phytoplankton typology and sedimentation velocity .....	99
Table 3.11 – Simulated period in Lake of Champs-sur-Marne .....	100
Table 3.12 – Values of the tracer input .....	101
Table 4.1 – Results of the temperature simulations .....	120
Table 4.2 – Water velocity determination coefficient for measured and simulated values with wind.....	124
Table 4.3 – Initial condition values used for the calibration period (13 to 27 July 2015).....	131
Table 4.4 – Mathematical performance indicators for coupled hydrodynamic calibration.....	138
Table 4.5 – Initial condition values of the simulation in 2016.....	149
Table 4.6 – Range of nutrients used in 2016 simulations .....	149
Table 4.7 – Simulation performance for the 2016 scenario .....	150
Table 5.1 – Mathematical indicators for the hourly water temperature estimation methods. ....	159
Table 5.2 – Mathematical indicators for temperature with different values of attenuation of the wind intensity .....	163
Table 5.3 – Mathematical indicators for temperature with different values of Dalton coefficient .....	165
Table 5.4 – Mathematical indicators for lake temperature varying background eddy viscosity and diffusivity values .....	166
Table 5.5 – Mathematical indicators for lake temperature using Z-grid option.....	166
Table 5.6 – Set of parameter values for hydrodynamic simulation in Lake Pampulha.....	168
Table 5.7 – Mathematical indicators for the validation period (29 <sup>th</sup> May to 14 <sup>th</sup> June 2016). ....	173

## List of abbreviations, initials, and symbols

ADCP	Acoustic Doppler Current Profiler
ANA	National Water Agency
ANN	Artificial Neural Networks
ANR	National Research Agency
BOD	Biochemical Oxygen Demand
BWD	Bathing Water Directive
CAEDYM	Computational Aquatic Ecosystem Dynamics Model
CDOM	Colored Dissolved Organic Matter
CFL	Courant-Friedrichs-Lewy
CHL-a	Chlorophyll-a (Chl-a)
CORIF	<i>Île-de-France</i> Ornithological Center
DOC	Dissolved organic carbon
DON	Dissolved Organic Nitrogen (DON)
DOP	Dissolved Organic Phosphorus (DOP)
DYRESM	Dynamic Reservoir Simulation Model
EEA	European Environment Agency
EIA	Environmental Impact Study
ETAF	Fluvial Water treatment Plant
EU	European Union
EU DWD	European Union Drinking Water Directive
EWACS	Early Warning System
FINEP	Financier of Studies and Projects
FP	Fluorescence Probes
GLM	General Lake Model
GPS	Global Position System
HABs	Harmful Algal Blooms
HPLC	High-Performance Liquid Chromatography
IBAMA	Brazilian Institute of the Environment and Renewable Natural Resources
INMET	National Institute of Meteorology of Brazil
LED	Light-Emitting Diode
MAE	Mean Average Error
MDS	MultiDimensional Scaling
MNHN	National Museum of Natural History
MPx	Multi-Parametric Probe
MSSWF	Modified Sine and Sinusoidal Wave Functions Model
NARS	National Aquatic Resource Surveys

NLA	National Lakes Assessment
NOAA	National Oceanic and Atmospheric Administration
OD	Dissolved Oxygen
PBH	Municipality of Belo Horizonte
PCA	Principal Component Analysis
PROPAM	Environmental Development Program
RE	Relative Error
RMSE	Root Mean Square Error
SWMM	StormWater Management Model
TR	Reference Term
WFD	Water Framework Directive
WHO	World Health Organization

## Table of Contents

<b>1. INTRODUCTION</b> .....	<b>22</b>
<b>1.1. GENERAL SCIENTIFIC CONTEXT</b> .....	<b>22</b>
<b>1.2. THESIS OBJECTIVES</b> .....	<b>24</b>
<b>2. LITERATURE REVIEW</b> .....	<b>26</b>
<b>2.1. MAIN HYDRODYNAMIC PROCESSES IN LAKE ECOSYSTEMS</b> .....	<b>26</b>
<b>2.2. PHYTOPLANKTON AND CYANOBACTERIA IN LAKE ECOSYSTEMS AND THEIR RELATION WITH HYDRODYNAMICS</b> .....	<b>27</b>
<b>2.3. PHYTOPLANKTON MONITORING COMPOSITION</b> .....	<b>32</b>
2.3.1. <i>BBE Fluorescence probes</i> .....	<i>34</i>
2.3.2. <i>Use of Phycocyanin</i> .....	<i>38</i>
2.3.3. <i>Phytoplankton monitoring with satellite remote sensing</i> .....	<i>39</i>
2.3.4. <i>Interferences on phytoplankton measurements</i> .....	<i>40</i>
<b>2.4. PHYTOPLANKTON MODELLING APPROACHES</b> .....	<b>41</b>
2.4.1. <i>Wind-driven criteria</i> .....	<i>43</i>
2.4.2. <i>Deterministic approach</i> .....	<i>43</i>
2.4.3. <i>Artificial neural networks and statistical techniques</i> .....	<i>46</i>
2.4.4. <i>Warning system for surface water blooms using statistical models</i> .....	<i>48</i>
<b>2.5. REGULATORY CONTEXT OF LAKE WATER QUALITY</b> .....	<b>49</b>
2.5.1. <i>The guidelines of the World Health Organization</i> .....	<i>49</i>
2.5.2. <i>European Water Framework Directive</i> .....	<i>50</i>
2.5.3. <i>Clean Water Act of the United States</i> .....	<i>52</i>
2.5.4. <i>Brazil Regulation</i> .....	<i>53</i>
<b>2.6. URBAN LAKE CHARACTERISTICS AND CHALLENGES</b> .....	<b>55</b>
<b>2.7. LAKE CHAMPS-SUR-MARNE STUDY SITE</b> .....	<b>56</b>
<b>2.8. LAKE PAMPULHA STUDY SITE</b> .....	<b>58</b>
<b>3. MATERIALS AND METHODS</b> .....	<b>60</b>
<b>3.1. STUDY SITES</b> .....	<b>60</b>
3.1.1. <i>Lake Champs-sur-Marne</i> .....	<i>60</i>
3.1.2. <i>Lake Pampulha</i> .....	<i>64</i>
<b>3.2. MEASUREMENTS</b> .....	<b>66</b>
3.2.1. <i>Lake Champs-sur-Marne</i> .....	<i>66</i>
3.2.1.1. <i>Bathymetry</i> .....	<i>66</i>
3.2.1.2. <i>Phytoplankton Sampling</i> .....	<i>66</i>
3.2.1.3. <i>High-frequency measurements</i> .....	<i>67</i>
3.2.1.4. <i>Campaigns</i> .....	<i>72</i>
3.2.1.5. <i>Measurement of the water velocity</i> .....	<i>73</i>
3.2.1.6. <i>Nutrients Monitoring</i> .....	<i>75</i>
3.2.1.7. <i>Meteorological Monitoring</i> .....	<i>76</i>
3.2.2. <i>Lake Pampulha</i> .....	<i>76</i>
3.2.2.1. <i>Bathymetry</i> .....	<i>76</i>
3.2.2.2. <i>High-frequency</i> .....	<i>77</i>
3.2.2.3. <i>Water Inflow Monitoring</i> .....	<i>78</i>
3.2.2.4. <i>Meteorological Monitoring</i> .....	<i>81</i>
<b>3.3. MODEL FORMULATION</b> .....	<b>81</b>
3.3.1. <i>Hydrodynamic model formulation</i> .....	<i>81</i>
3.3.2. <i>Water quality model formulation</i> .....	<i>87</i>
<b>3.4. MODEL CONFIGURATION</b> .....	<b>91</b>
3.4.1. <i>Lake Domain</i> .....	<i>93</i>
3.4.2. <i>Hydrodynamic Model configuration</i> .....	<i>94</i>
3.4.3. <i>Water Quality Model configuration</i> .....	<i>97</i>

3.5.	<b>LAKE CHAMPS-SUR-MARNE SIMULATIONS</b> .....	99
3.5.1.	<i>Hydrodynamic simulations</i> .....	99
3.5.2.	<i>Phytoplankton transport simulation</i> .....	100
3.5.3.	<i>Coupled hydrodynamic and ecological simulation</i> .....	102
3.6.	<b>LAKE PAMPULHA SIMULATION</b> .....	103
3.6.1.	<i>Calibration period</i> .....	103
3.6.2.	<i>Validation period</i> .....	103
3.6.3.	<i>Longer validation period</i> .....	103
3.7.	<b>PERFORMANCE INDICATORS</b> .....	103
4.	<b>LAKE CHAMPS-SUR-MARNE RESULTS</b> .....	104
4.1.	<b>COMPARISON BETWEEN DIFFERENT CHL-A FLUORESCENCE MEASURING DEVICES</b> .....	104
4.2.	<b>HYDRODYNAMIC SIMULATIONS</b> .....	106
4.2.1.	<i>Results of the temperature simulations</i> .....	106
4.2.2.	<i>Results of the velocity simulations</i> .....	120
4.2.3.	<i>Phytoplankton biomass transport simulation</i> .....	125
4.3.	<b>COUPLED HYDRODYNAMIC AND ECOLOGICAL SIMULATION</b> .....	126
4.3.1.	<i>Calibration Period</i> .....	126
4.3.2.	<i>Verification Period</i> .....	145
4.4.	<b>LAKE CHAMPS-SUR-MARNE CONCLUSIONS AND DISCUSSIONS</b> .....	151
5.	<b>LAKE PAMPULHA RESULTS</b> .....	154
5.1.	<b>ANALYSIS AND VALIDATION OF MEASURED DATA</b> .....	154
5.2.	<b>INFLOW WATER TEMPERATURE</b> .....	157
5.3.	<b>HYDRODYNAMIC SIMULATIONS</b> .....	160
5.3.1.	<i>Calibration period</i> .....	160
5.3.2.	<i>Validation period</i> .....	169
5.3.3.	<i>Longer validation period</i> .....	184
5.4.	<b>LAKE PAMPULHA CONCLUSION AND DISCUSSION</b> .....	188
6.	<b>GENERAL CONCLUSIONS</b> .....	192
7.	<b>REFERENCES</b> .....	194
8.	<b>ANNEX</b> .....	207
8.1.	<b>SPECIFIC GROWTH RATE OF DIATOMS, GREEN AND MICROCYSTIS</b> .....	207
8.2.	<b>ALERT LEVELS FOR TOXIC CYANOBACTERIA IN RECREATIONAL WATERS</b> .....	208
8.3.	<b>CHLOROPHYLL-A TREATMENT</b> .....	209
8.4.	<b>ADCP SETTINGS FOR LAKE OF CHAMPS-SUR-MARNE, FRANCE</b> .....	210
8.5.	<b>FLUOROPROBE PARAMETERS</b> .....	213
8.6.	<b>FLUOROPROBE USAGE PROTOCOL</b> .....	214
8.7.	<b>FLUOROPROBE SPECIFICATIONS</b> .....	216
8.8.	<b>RESULTS OF THE HYDRODYNAMIC MODEL</b> .....	217
8.9.	<b>PAPER ACCEPTED IN RBRHR</b> .....	218

## 1. INTRODUCTION

The general scientific context of this thesis will be presented in this initial chapter alongside its objectives.

### 1.1. General scientific context

Lakes and reservoirs in metropolitan areas provide many ecosystem services. They are frequently part of the urban stormwater drainage network and also offer many recreational activities. They contribute to the landscape composition and the quality of life for neighbourhoods and users. Urban lakes are increasingly recognized as essential biotypes for maintaining ecological continuity and for supporting biodiversity in urban and peri-urban areas.

In France, the majority of urban lakes are of artificial origin, either stormwater retention basins or as a result of quarrying activities, especially sand extraction (Catherine, 2009). Around Paris (also known as the *Île-de-France* region), 99% of the lakes measure less than 0.5 km<sup>2</sup> in area, many of them are used for leisure and recreation activities such as swimming and sailing, as is Lake Champs-sur-Marne, which is the first case study in the present research.

In Brazil, many large cities were developed around lakes or were equipped with a reservoir, such as Paranoá reservoir in Brasília, the capital of Brazil; Guarapiranga and Billings reservoirs in the city of São Paulo, built in the beginning of the 20<sup>th</sup> century for drinking water and hydropower purposes; Rodrigo de Freitas, Jacarepaguá and Tijuca lakes in Rio de Janeiro; Conceição lake in Florianópolis; Mundaú lake in Maceió; among others. All these lakes and reservoirs are urban, as is Lake Pampulha in Belo Horizonte, which is the second case study in the present research.

Environmental changes at a local scale, within their watersheds, and at a global scale are affecting the water quality and ecological functioning of urban lakes (Birch and McCaskie, 1999; Friese et al., 2010; Li-Kun et al., 2017), resulting in an increase in phytoplankton biomass and the occurrence of potentially toxic cyanobacteria and health risks (Davidson et al., 2016; Ho and Michalak, 2015; Jöhnk et al., 2008). Cyanobacteria concentrations and algal toxin levels also provide ecological information for lakes and an estimate of how the main stressors are impacting lake quality (NLA, 2012; European Parliament and Council, 2000a; WHO, 1998).

Among all organisms that compose the phytoplankton in lake environments, cyanobacteria are the most problematic regarding public health because of their toxic potential (Beniston, 2004; Huisman et al., 2005; Jöhnk et al., 2008; Silva, 2014). Cyanobacteria blooms represent a high risk to human health and economic costs for several water uses, especially for drinking water (Codd et al., 1999; Hitzfeld B C et al., 2000; Shimoda and Arhonditsis, 2016). According to WHO (2003), values higher than 50 µg/L of cyanobacteria are considered critical to human health. Neuro and hepatotoxins released by some cyanobacteria species can cause paralysis and liver damage. Livestock deaths and human illnesses associated with cyanobacterial toxins have already been reported in many countries (Chorus and Bartram, 1999). Greater attention should be given to urban lakes due to human exposure to toxins on the lake surface.

Several of the most important toxins of cyanobacteria are concentrated in surface blooms, resulting in scum formation (Ibelings et al., 2003). The production of cyanobacterial toxins mainly happens after a bloom formation and accumulation on the surface. Codd et al. (1999), pointed out higher toxin production on water surface. Cyanobacteria concentration varies in surface blooms events. According to Ibelings et al. (2003), when the concentration at the surface water exceeds 10 gC/m<sup>3</sup> (about 200 µg/L), a surface bloom is assumed to be present. It is paramount that processes governing the spatial and temporal distribution of phytoplankton, particularly of cyanobacteria, are studied and understood.

Phytoplankton and cyanobacterial dynamics are not only influenced by their biological properties, but also by environmental factors such as water quality, hydrodynamics, nutrient availability, in addition to meteorological conditions, such as solar radiation, wind and air temperature.

The major factors that determine phytoplankton growth, physical-chemical and biological processes are nutrients, solar radiation, water temperature and grazing (Phlips et al., 2002; Reynolds, 1998; Van Donk, 1984). Water temperature impacts phytoplankton dynamic succession and community composition (Elliott, 2012; Grimaud et al., 2017; Jöhnk et al., 2008; Phlips et al., 2002; Reynolds, 1998; Van Donk, 1984; Vinçon-Leite and Casenave, 2019). Thermal stratification and a longer residence time of the water within the lake can boost the phytoplankton production. Due to low turbulence, lake ecosystems can provide the required conditions for phytoplankton species and water deterioration. Changes in the distribution of phytoplankton suggest a response to the dynamics of the surface mixed layer and to lateral advection (Huang et al., 2016; Li Wei et al., 2013; Liu et al., 2014; Wang et al., 2017; Wu et al., 2013, 2010). Lateral advection, affected by wind-driven current, is one of the main factors that cause biomass accumulation in specific areas due to scum formation (surface blooms). Water mixing events have a major impact on the vertical turbulence and temperature structure, affecting phytoplankton and cyanobacteria developments (Jöhnk et al., 2008). Thus, an understanding of water circulation and its interference on water quality bears great importance (Li-Kun et al., 2017; Qin et al., 2015; Wu et al., 2015; Zbiciński and Ziemińska-Stolarska, 2017).

As most urban lakes are small and shallow, they react strongly and rapidly to external hydrological and meteorological forces. As a consequence of this weak stability, the hydrodynamic processes in shallow lakes are complex. Understanding the hydrodynamic processes and their influence on the ecological state of urban lakes is of great importance. Wu (2013), highlighted the need to investigate the influence of short-term hydrodynamics on cyanobacteria in shallow lakes, as the complex cyanobacteria motion in natural water bodies are poorly understood.

The ecological state of a lake is determined by physical-chemical and biological indicators (Qi et al., 2018; Xu et al., 2001). Interactions on lakes occur all over the system at all-time scales: from chemical reactions within seconds, through phytoplankton growth in day-night cycles, to population density changes over seasons and the interannual variability in the appearance and the disappearance of phytoplankton species (Khac et al., 2018). Not only such dynamics develop within their own rhythm, but they are also disturbed and interrupted by other factors. Therefore, high-resolution and high-frequency measurements are necessary to better understand them. However, high-resolution and high-frequency monitoring are very rare, especially in small and shallow urban lakes, the focus of this research. Currently, fluorometric probes are available for phytoplankton *in situ* monitoring, providing an estimation of phytoplankton biomass through high-frequency measurement of chlorophyll-a (Chl-a) fluorescence. It is possible to detect specific classes of phytoplankton through the spectral signature of their pigment fluorescence. Chl-a fluorescence is measured through excitation at one or more specific wavelengths. However, measured values depend on the water characteristics (interference of coloured dissolved organic matter), the algal species (different pigment contents, the age of the population, stage of growth, cell size) and the measuring device design. Such sensors are quite valuable for field monitoring, but they also present many limitations and uncertainties (Catherine et al., 2012; McQuaid et al., 2011; Silva et al., 2016). A recent review (Zamyadi et al., 2016) demonstrates that the presence of Chl-a among other phytoplankton in a mixed population could lead to an error of 2% to 600% of *in situ* fluorescence measurements.

The main characteristics that hinder an accurate and meaningful monitoring of the phytoplankton biomass, as well as the identification of toxin-producing species, are the great heterogeneity of space-time biomass concentration and measurement interferences. However, Chl-a has been widely used as a phytoplankton biomass proxy, because it is simpler and faster than other methods.

Considering the complexity of lake ecosystems (especially small and shallow urban lakes), reliable mathematical models supported by high quality measurements are valuable tools to organize and



quantify ecological knowledge. Modelling studies aiming to understand phytoplankton groups are of utmost importance, as evidenced by the increase in studies over recent years (León et al., 2005; Li-Kun et al., 2017; Qin et al., 2015; Shimoda and Arhonditsis, 2016).

Coupling phytoplankton modelling with monitoring is a way to understand ecological behaviour and the causal factors of phytoplankton growth and behaviour. Mathematical models can also help to better develop monitoring programs due to their contribution in understanding the processes and environmental factors involved, predicting the time and space distribution of phytoplankton (Zhang et al., 2017). Mathematical models may help lake managers by providing information for better management of lake ecological problems (Birch and McCaskie, 1999). Due to the complex ecological and hydrodynamic behaviour of lakes, with high heterogeneity in space and time, three-dimensional models play an important role in better understanding all of the processes involved (Gong et al., 2016; Soullignac et al., 2017, 2018; Zbiciński and Ziemińska-Stolarska, 2017). Three-dimensional models help to understand and predict lake ecosystem behaviour in response to external pressures, like climate forcing, nutrient loading, and pollutant input (Chanudet et al., 2012; Evelyn Aparicio Medrano et al., 2013).

Monitoring and modelling the evolution of phytoplankton and cyanobacteria biomasses still involves many uncertainties (Li-Kun et al., 2017; Robson, 2014; Shimoda and Arhonditsis, 2016). Impreciseness of the measured data values coupled with uncertainty regarding how representative they are of water conditions pose a challenge when modelling phytoplankton behaviour.

Hydrodynamic modelling provides a better understanding and evaluation of the spatial and temporal heterogeneity of the distribution of phytoplankton biomass. An accurate representation of temperature stratification is of particular significance in regulating the vertical transport of nutrients, phytoplankton, and oxygen (Boegman et al., 2003; Gonçalves et al., 2016; Grimaud et al., 2017; Simpson et al., 2015). Hydrodynamic behaviour changes the distribution of phytoplankton biomass in response to the dynamics of the vertical layers and lateral advection. Therefore, lake hydrodynamics modelling plays a large role in tracking and better understanding phytoplankton blooms and scum formation (Prakash et al., 2007).

Several mathematical models are available and make use of different modelling approaches. The majority use deterministic equations to describe the physical-chemical and biological processes involved, whereas other models use a statistical approach as an alternative to improve the weak predictive power of deterministic models. Nonetheless, the better modelling approach to evaluate phytoplankton behaviour in lakes depends on specific objectives and data availability. Modelling all processes involved in phytoplankton behaviour requires a large amount of data and parameter configuration, which are not always available. Hence, in this research, different modelling approaches were addressed with the purpose of evaluating the potential and applicability of each. Using hydrodynamic simulation and coupled hydrodynamic and ecological simulation in different scenarios will be analysed to improve the knowledge and the influence of the hydrodynamic of shallow lakes in ecological behaviour.

## **1.2. Thesis objectives**

The main objective of this thesis is to characterize the hydrodynamics of shallow urban lakes to better understand its influence on spatial and temporal variability of cyanobacteria biomass through high-frequency measurements and three-dimensional numerical modelling. To achieve this objective, two experimental study sites were investigated: Lake Champs-sur-Marne, a small and shallow urban lake in France, and Lake Pampulha, a medium-sized and shallow urban reservoir in Brazil.

The two main reasons which led to the selection of these specific lakes were: (1) they are study sites of major research projects in France and in Brazil, respectively; and (2) they are quite diverse regarding urban and climate contexts, as well as the availability of monitoring data. The contrast between these

two case studies offers a rich opportunity for model testing and assessing main lake hydrodynamic and ecological behaviour.

Based on these two study sites, Lake Champs-sur-Marne in France and Lake Pampulha in Brazil, the following sub-objectives were addressed:

- ✓ Show the importance of high resolution and high-frequency measurements to better understand shallow lakes hydrodynamics and phytoplankton and cyanobacteria biomass distribution in time and space;
- ✓ Use and analyze the capability of a three-dimensional model to describe the influence of hydrodynamic and weather conditions on shallow lakes to better understand their relation to cyanobacteria dynamics;
- ✓ Identify a modelling tool able to support water management decision-making at a urban scale.

The main hypothesis of the thesis is that high-frequency measurement and three-dimensional modelling, allow to better access the influence of hydrodynamic in cyanobacteria biomass dynamic in shallow lakes and that a calibrated three-dimensional model helps to improve the existing and future monitoring programs.

In the French lake, a three-dimensional hydrodynamic and ecological model that uses mathematical optimization for phytoplankton growth was calibrated and verified using high-frequency measures.

High-frequency monitoring of temperature was used to analyze external forces and their influence on alternation and duration of mixing and stratification conditions (one of the main processes that can boost the phytoplankton production in favour of cyanobacteria). High-frequency measurements of chlorophyll-a and vertical profiles performed during campaigns were used to evaluate and assess model performance in representing phytoplankton behaviour and groups distribution.

Water velocity was measured using ADCP (Acoustic Doppler Current Profiler) technology. The measured period was also simulated and a model performance assessment was carried out using spectral analysis. Additionally, the measured and simulated values were correlated to wind intensity to evaluate the lake response to this external factor. Due to the high influence of wind, different wind scenarios were performed to evaluate the influence on the hydrodynamics of phytoplankton behaviour.

Due to the high importance of nutrient concentration in phytoplankton growth and the large amount of information necessary (normally not completely available) to correctly simulate all physical-chemical and biological processes, a calibrated three-dimensional optimization model was used to evaluate phytoplankton growth behaviour using a range of nutrient concentrations.

In the Brazilian lake, a three-dimensional hydrodynamic model was calibrated and validated using high-frequency measurements. Due to the absence of inflow water temperature information, methods to estimate hourly values were evaluated. Based on mathematical indicators, the best one was used to set the inflow water temperature. High-frequency measurement of temperatures were combined with the modelling result to evaluate the influence of meteorological external forcing and lake morphology on the thermal behaviour of the lake at different depths.

This doctoral research was embedded at LEESU-ENPC (France) within OSS-Cyano research project supported by ANR (French National Research Agency) for Lake Champs-sur-Marne from April 2016 to July 2017, and from August 2017 to the end of 2019 at EHR-UFGM (Brazil) with MoMa-SE research project for Lake Pampulha, supported by CAPES and ANA (Brazilian National Water Agency).

## 2. LITERATURE REVIEW

Taking into account the current research on the behavior of phytoplankton and cyanobacteria in shallow urban lakes, a literature review was performed on the following subjects: (i) Main hydrodynamic processes in lake ecosystems; (ii) Phytoplankton and cyanobacteria in lake ecosystems, in order to describe the processes that are important in their spatial and temporal distribution; (iii) Phytoplankton and cyanobacteria monitoring, in order to present the main techniques and methods used and their advantages and limitations; (iv) The main phytoplankton and cyanobacteria modelling approaches and results were surveyed in the literature, since there are many different approaches and mathematical models; (v) The regulatory context of lake water quality, as the regulatory requirements of urban lake management differ with each region, a survey of the main water quality indicators was performed and their relevance to the concentration of phytoplankton and cyanobacteria; (vi) Urban lakes, in order to know the specificities and problems involved in their ecosystems; (vii) and (viii) A review of the previous research performed in each of the studied lakes, respectively.

### 2.1. Main hydrodynamic processes in lake ecosystems

The main physical governing principles of lake water motion are the conservation laws of mass, momentum and energy, all these statements have the form of balance laws. A balance equation in continuum physics is a computation for the change in content, over a certain domain, of an extensive physical quantity (Epstein, 2009).

Concerning lakes hydrodynamic, it can be described by the Navier-Stokes equations. Its equations are partial differential equations for the velocity, pressure, temperature, and mass concentrations of different tracers (sediment, nutrients, salinity and others). Considering the diffusion processes of actives or passives tracer substances the transport equation of mass shall also be considerate. To arrive at partial differential equations for the variables its relations for molecular and turbulent fluxes and for the turbulent energy production must be established.

In the mathematical formulation, boundary condition must be established. These conditions are not trivial once because, due to external factors, water surfaces deform and evaporation occurs. At the bottom and along lake shore, boundary conditions must also be formulated, thus, the non-uniformity in topography must receive attention. At the lake bottom one usually assumes no-slip or sliding over the basal surface. In the first case the bottom is material, in the second it is not, but drainage vanishes (Hutter, 1984a).

When setting the equations, it is normal to assume some simplifications, such as the shallow water approximation in which lies the hydrostatic equations and Boussinesq assumption. The Boussinesq assumption supposes that density differences are small, except when they appear in terms multiplied by the gravity acceleration. One implication of this assumption is the classical incompressibility assumption. The shallow water approximation implies further simplification, the most significant is in the turbulent fluxes in which the momentum equations reduce to only two horizontal component equations. This simplification has some limitations, not properly representing zones of upwelling and downwelling. Thus, vertical velocities must be small in comparison to horizontal velocities (Hutter, 1984a).

Waves in lakes are primarily generated by external meteorological forces. Gravity waves arise through the action of gravity on water. They often have longer duration period and larger wavelengths compared to the water depth. The rotation of the Earth introduces the Coriolis force, acting at right angles to the velocity vector which leads to the existence of inertial or rotation waves (Hutter, 1984b). Gravity waves are impacted by the earth rotation, in general, the bigger the lake's size, most significant is the impact. Short surface waves are the response of the water lake to wind force acting, contributing to the upper layer turbulence. Their periods are seconds, and their wavelengths small as compared to the water depth.

Hydrodynamic of lakes deals with the identification of the impacts of external factors (wind, inflow water, solar radiation, precipitation) in water and particular matter movement. External factors that impact turbulence on the lake water are wind intensity, precipitation, and water inflow (Li Wei et al., 2013; Wang et al., 2017; Wu et al., 2013). Meteorological forcing provided a more complete picture of the lake's dynamic responses (Mortimer, 1984).

Sharip et al. (2018) concluded that the major factors that impact hydrodynamic of lakes and its circulation pattern may have distinct variation between wind driving, inflows from tributaries or convective motion due to water temperature gradient under low wind condition. The thermal stratification condition of lakes typically has an upper layer in which the mean density is low and the water temperature is high, and the deepest depth with higher mean density and lower temperature. The transition zone is generally narrow and vertical temperature gradients are strong. The upper layer is called epilimnion, the lower layer hypolimnion and the transition zone metalimnion. The location of the largest mean temperature gradient is referred as the thermocline.

The hydrodynamic patterns, due to mixing events or temperature gradient in agreement with forcing of the atmospheric, may also be affected by continuous abstraction of water. Wherein, water pump and higher evaporation rates can significantly impact and drop of water level in a lake. Even the water turbidity may affect the water circulation, because reduction of solar radiation in vertical depth profile, increase surface temperature that induces vertical density gradient. Sharip et al. (2018) concluded that in Bera Lake located in Malaysia, during the night, at the deeper area of the lake, warmer temperature moved to shallower area at the surface, while cooler water in the shallow areas move to the deeper areas at the lake bottom. The flow characteristic due to thermal forcing is strongly influenced by the inertia of the water, presenting a lag of a few hours between the surface heating and the movement of the water (Monismith et al., 1990). Current velocities induced by differential temperature gradient were reported between 1.6 and 2.0 cm/s (Monismith et al., 1990) and 1.5 to 2.8 cm/s (Lovstedt and Bengtsson, 2008).

In an environmental ecosystem the unsteadiness of the forcing acting in a water body will not act in isolation and the spatial and time variation associated with topographic effects, makes the lake hydrodynamic an intriguing and complex concern. This pattern of flow may be of significance to the ecology of a lake, presenting a formidable task to a numerical representation (Imberger and Petterson, 1989). Cyanobacteria concentrations and algal toxin levels provide ecological information for lakes and an estimate of how the main stressors are impacting lake quality (NLA, 2012; European Parliament and Council, 2000a; WHO, 1998).

## **2.2. Phytoplankton and cyanobacteria in lake ecosystems and they relation with hydrodynamics**

In freshwater, phytoplankton refers to small (0.2 - 200  $\mu\text{m}$ ) unicellular organisms. These micro-organisms have very low mobility and follow the motion of water currents and the wind. They may interfere in water turbidity when high in density (WHO, 2003b). They are not individually visible to the naked eye, normally only noticeable when colonies are formed, which can be various colours, including green (Chlorophyta and Euglenophyta, rich in chlorophyll a and b), blue (Cyanophyta, rich in phycocyanin), brown (Bacillariophyta, Chrysophyta and Dinophyta, rich in xanthophylls), or red (Cryptophyta, rich in phycoerythrin). Thus, the pigments analysis may be used to phytoplankton identification.

Cyanobacteria are a subset of phytoplankton, but feature specific traits: some of the characteristics of bacteria and some of eukaryotic algae. They contain photosynthetic pigments and additional pigments, such as phycocyanin—a blue-green pigment—and phycoerythrin, a red pigment (Andrew Brierley, 2017). Toxins produced by some cyanobacteria may cause harm to human health due to freshwater uses (water supply, bathing, fishing, among others) (Jöhnk et al., 2008). Thus, in lake environments, among

all of the organisms which compose phytoplankton, cyanobacteria are the most problematic in terms of public health.

Toxins can be classified according to their mode of action, such as hepatotoxins (e.g. *microcystines*, *nodularines*, and *cylindrospermopsine*), neurotoxins (e.g. *anatoxine-a* and *saxitoxines*), skin irritants (*lipopolysaccharides*), and others (Huisman et al., 2005). These harmful algal blooms (HABs) are a critical source of concern because they affect not only the health of a population and water ecosystem, but the life and economy of a region.

Like other algae, cyanobacteria are photoautotrophic organisms, producing their food via the use of chlorophylls (and other pigments), to fix carbon as a starch through the process of photosynthesis.

Cyanobacteria are one of the very few groups of organisms in which some of the genus can fix (or, “convert”) inert atmospheric nitrogen into an organic form, such as nitrate or ammonia. Cyanobacteria reproduce asexually and photosynthesis also plays a vital and important role in their reproduction and growth.

Shimoda and Arhonditsis (2016), highlighted that the literature on phytoplankton and cyanobacteria has dramatically increased over recent years (2010-2012). The annual number of publications suddenly soared in 1991 and has continued to grow (Merel et al., 2013).

This growth in interest should continue because of the increase in the frequency of bloom events. For instance, June to September 2003, one of the hottest summers in Europe (5 °C higher than the local average), should be interpreted as a warning sign and a potentially important cause which can increase the incidence of harmful algal blooms (Beniston, 2004; Jöhnk et al., 2008).

According to Ibelings et al. (2003), several of the most important toxic biomasses of cyanobacteria are concentrated in scum (surface blooms). Therefore, determining which factors influence blooms and scum formation will be closely considered here.

Many species of freshwater algae may proliferate quite intensively in eutrophic (i.e., nutrient-rich) waters. However, they do not form dense surface blooms (scum) as some cyanobacteria species do, such as:

- (a) *Microcystis*;
- (b) *Aphanizomenon*; and,
- (c) *Planktothrix*.

Cyanobacteria concentration varies in scum events. According to Ibelings et al. (2003), when the concentration at the surface layer exceeds 10 gC/m<sup>3</sup> (about 200 µg/L), a surface bloom (scum) is assumed to be present.

Increased competitiveness between *Microcystis* and other scum-forming cyanobacteria occurs due to the buoyancy capacity, due to changing environmental conditions, based on the following three mechanisms (Konopka, 1982; Reynolds et al., 1987; Bormans et al., 1999):

- (a) Collapse of gas vesicles under rising turgor pressure;
- (b) Kinetic regulation of gas vesicle synthesis (or cell growth relative to gas-vesicle production rates), which induces changes in buoyancy;
- (c) Accumulation of photo-synthetically fixed carbon in the form of glycogen.

The dynamics of cyanobacteria in lakes are henceforth addressed, alongside the biological, physical, and chemical processes that are involved in their behaviour. These lake processes may present horizontal and vertical heterogeneity due to external factors, such as wind, heat exchanges, and river inflow (Jöhnk et al., 2008), which also contribute to thermal stratification, in which the water temperature also affects these processes (Bormans et al., 1999).

The interaction between algae dynamics and nutrient concentration are very complex, due to the fact that they correlate to variations in water temperature, solar radiation intensity, nutrient value and hydrodynamic processes (Gong et al., 2016).

During surface bloom formations, a population of buoyant cyanobacteria accumulates in a distinct scum on the lake surface in the absence of wind mixing. These upward-floating buoyant cyanobacteria can form dense blooms on the water surface (Zohary and Robarts, 1990; Visser et al., 1996).

Surface blooms (scums) only occur in conditions of low water turbulence and high algal biomass (Li Wei et al., 2013). External factors that impact turbulence on the vertical column of lake water are wind intensity, precipitation, and water inflow. Wang et al., (2017) concluded that surface blooms are able to persist with a wind intensity of less than 3.1 m/s. Wu (2013) concluded that wind events greater than 6.0 m/s resulted in vertical mixing of algal biomass and an eventual disappearance of surface blooms, and Liu et al. (2014) concluded that wind intensity of 4.0 m/s leads to sediment resuspension. Missaghi et al., (2016) concluded that water turbulence controls growth and vertical distribution.

Thus, mixing events had a major impact on vertical turbulence and temperature structure, affecting phytoplankton and cyanobacteria development. Jöhnk et al., (2008) analyzed the influence of artificial mixing processes on Lake Nieuwe Meer (Netherlands). With artificial mixing, thermal stratification generally disappeared within a few days, in addition to the *Microcystis* population becoming efficiently suppressed. The authors, however, suggested that *Microcystis* populations were even stronger during the following period without artificial mixing. Such behaviour, reported by Jöhnk et al. (2008), shows the complexity of lake management and decision making which leads to an effective improvement of water quality.

During periods with no artificial mixing processes on Lake Nieuwe Meer (Netherlands), *Microcystis* reached concentrations near the water surface of 30 to 50 times higher than near the thermocline, an indication that many *Microcystis* cells floated upwards when the mixing process was not active. During events of artificial mixing, phytoplankton concentration was homogeneous in the vertical direction. Due to this observation, lake managers decided to induce permanent mixing. The authors also concluded that the *Microcystis* increase also occurred due to high water temperatures, exceeding the optimum temperature for diatoms and green algae, combined with rapid sedimentation caused by reduced turbulent mixing. Diatoms and green algae showed a weaker response to the intermittent mixing regime. This result points to the relevance and influence of lake thermal behaviour on algae blooms, which can easily be monitored and indicate lake mixing events. Zhao et al. (2013), used the lake water temperature to calibrate and validate the hydrodynamic model.

Khac et al. (2018), through high-frequency monitoring, notices that cyanobacteria are one of the dominant groups of phytoplankton blooms throughout lake stratification periods. The conditions for water column stratification are identified by Huber et al. (2012) as an increase in incident radiation and air temperature with a decrease in wind speed. Shimoda and Arhonditsis (2016) highlight that, in freshwater, water temperature is an important regulatory factor for phytoplankton and cyanobacteria growth rate. Rinke et al., (2009) concluded that light and water temperature are the main factors. However, during low external forcing, biological processes also represent significant effects (Gonçalves et al., 2016).

Jöhnk et al. (2008) calibrated the growth rate response related to temperature for diatoms, green algae, and *Microcystis*. They show that *Microcystis* has a lower maximum specific growth rate than diatoms

and green algae at temperatures below 23°C. Nonetheless, in higher water temperature, the specific growth rate of *Microcystis* shows a strong increase. This result conveys the crucial relation of interspecies competition with water temperature. Figure A1 (Annex) shows the effect of temperature on the maximum specific growth rates of *Microcystis*, diatoms and green algae. However, Grimaud et al., (2017) highlight that the growth rate curve depends on the way that the biomass is measured, and that if Chl-a concentration is used, the growth rate curve will be biased, especially due to the capacity of phytoplankton to adapt their pigment when temperature changes.

Phytoplankton phenology indicates that thermal stratification of the water column is also determinant in some cyanobacteria dominance. In shallow lakes, intense stratification extending over more than three weeks favoured the dominance of cyanobacteria (Huber et al., 2012). The genus *Anabaena* seems to be favoured by strong stratification and a stable water column. According to the data analysis, the author concluded that nutrients are an important variable for cyanobacterial dominance. However, lake stratification is the reason for the duration and intensity of bloom and scum formation. This shows the importance of lake hydrodynamics related to weather variability concerning cyanobacteria behaviour.

Melo et al. (2017), evaluated the impacts of a period of water scarcity on a metropolitan drinking water reservoir named Serra Azul, located in the Southeast region of Brazil. The reduction of water volume in the reservoir changed its vertical thermal behaviour, resulting in the loss of the warm monomictic characteristic during the drought period. Thus, the fluxes of dissolved oxygen and nutrients could impact the productivity of drinking water in the reservoir, due to the potential degradation factor for water quality, creating a risk to the urban water supply. Lee and Biggs, (2015) analysed four hypereutrophic urban water supply reservoirs and showed that thermal stratification reduces nutrient transport from hypolimnion into the photic epilimnion region and limits hypolimnion aeration, concluding that thermal and hydrodynamics impact algal production. Mixing episodes of the water column in lakes or reservoirs may also affect the availability of nutrients in the surface layer (Silva, 2014).

In the literature, some conclusions about cyanobacteria growth behaviour are contradictory, especially regarding vertical distribution. This may occur due to the difficulty in determining the predominant species, their characteristics and the high complexity of species competition. A few conclusions are drawn concerning nutrients and cyanobacteria biomass in the following paragraphs.

Paerl and Otten (2016) concluded that the proliferation of nitrogen-fixing cyanobacteria species occurs due to an unbalanced stoichiometric ratio in favour of phosphorus. Another *Microcystis* characteristic is the ability to sequester both dissolved inorganic forms of nitrogen (DIN; as  $\text{NO}_3^-$  and  $\text{NH}_3^+$ ) and organic forms, including urea, amino acids, and other high molecular weight organic compounds.

Experiments (Berman and Chava, 1999) without inorganic nutrient intake generally shows a dominance of *Microcystis* in the end, which tends to confirm that this species is particularly competitive for N and P resources when deficient (Paerl and Otten 2016). Vilas et al. (2018) highlight that blooms of nitrogen-fixing cyanobacteria occurred under nitrogen limitation during the growing season and thermal stratification condition. According Kolzau et al. (2014) concentration ratio below 18.5 for TN:TP indicates nitrogen limitation.

Since 1992, in water bodies in Australia, Bormans et al., (1999) have carried out field studies of cyanobacterial growth and distribution with significant vertical separation between light and nutrients. The conclusion was that cyanobacterial migration does not occur in order to access nutrients at a greater depth. Much of the work on cyanobacteria and its flotation focused on *Microcystis*, *Anabaena*, *Aphanizomenon*, and *Oscillatoria*. According to Bormans et al. (1999), in natural systems, algal buoyancy appears to be substantially dependent on solar radiation rather than nutrients, being consistent with the carbohydrate ballast mechanism.

Otherwise, Bormans et al., (1999), suggest that although it may be possible for *Microcystis* to migrate below the thermocline to reach nutrients, field analyses led to the conclusion that the vertical distribution

of *Microcystis* also responds to the dynamics of the surface mixed layer. Huber et al. (2012) concluded that thermal stratification might favour cyanobacteria due to optimal buoyancy conditions or indirectly by facilitating nutrient release from sediment, although turbulence may remain low to allow for dominance of a buoyant species.

Long-term time series of surface-layer-integrated algal abundance and nutrient profiles from both Maude Weir and Chaffey Reservoirs (Webster et al., 1997) provide further evidence against vertical migration of cyanobacteria to reach nutrients.

Even under low concentrations of nitrate, ammonia and phosphate (<5 mg/L) along stably stratified conditions, *Microcystis* colonies in Lake Okaro, New Zealand, formed surface scums that disappeared with either convective mixing at night or wind mixing during the day (Walsby and McAllister, 1987). The conclusion reached by the authors points to the important role of hydrodynamic behaviour concerning scum formation.

Changes in the spatial distribution of Chl-a suggest a response either to the dynamics of the mixed surface layer or to lateral advection. However, lateral advection, affected by wind-driven current, is one of the key factors that cause biomass accumulation in specific areas due to bloom formation on the surface of the lakes. In Lake Geneva, the timing of phytoplankton growth could be explained by the spatial variability of hydrodynamic and thermal stratification dynamics (Soullignac et al., 2018). Wang et al. (2017) concluded that turbulence greatly influenced the horizontal transport of cyanobacteria. Huber et al. (2012) concluded that meteorological variability might determine whether cyanobacteria surface blooms will happen. Ibelings et al. (1991) indicate that surface bloom formation is a preexisting cyanobacteria population which accumulates at the surface, rather than surface blooms resulting from growth at the surface.

Using high-frequency measurements of water turbidity and temperature, Liu et al. (2014) found that, in a shallow lake, hydrodynamics are an important factor which influenced the inherent optical coefficient (water attenuation coefficient and light absorption), strongly affecting ecological processes.

In the North Basin of Lake Biwa, Japan, Ishikawa et al. (2002), measured the horizontal spatial variation of nutrients across a gyre caused by the water current. The distribution of buoyant cyanobacteria in the lake showed a higher biomass concentration at the surface layer than at the centre of the gyre. Nutrient concentrations were lower in the centre, while higher inshore. Thus, this biomass accumulation in the center of the lake seems not to be caused by offshore growth. Using ADCP (Acoustic Doppler Current Profiler) technology, the authors measured the horizontal advection. Over two days, the period needed to cover the North Basin area, current measurements were done using a 300-kHz ADCP (RD Instrument). The average horizontal current velocities were between 0.08 and 0.16 m/s in epilimnion depth near the edge of the gyre, enabling the advective transport of biomass. The observation data of Ishikawa et al., (2002) imply that offshore accumulation of buoyant cyanobacteria (gyre-*Microcystis*) resulted in a combination of advection influence and bloom-forming conditions from inshore regions. Wu et al. (2010) used an ADCP to verify the influence of water current and wind draft in the *Microcystis* horizontal accumulation. Current data were recorded every 10 minutes with a vertical resolution of 20 cm. Current directions were observed to not always correlate with wind direction. The authors concluded that the effect of wind conditions on the horizontal distribution of *Microcystis* blooms is mainly influenced by water surface drift and that direct measurements would need to be performed for confirmation.

Qin et al. (2015) also used ADCP to measure water currents, with the data showing that a strong storm moved organic matter from bottom to surface during a full mixing of the water column with a vertical velocity of 1 cm/s. The authors indicated that a surface cyanobacterial bloom formation happened due to physical aggregation through collision during the turbulent period. Wu (2013), noted that persistent hydrodynamic disturbance may cause aggregation, in which small colonies of *Microcystis* become large colonies.



Using bed-mounted ADCP measurements, Simpson et al., (2015) noted that stable stratification inhibits the direct downward transfer of surface stresses induced by wind. During thermal mixing conditions, total lake kinetic energy increases compared to stable stratification periods.

Mezemat (2014) used spectral analysis to evaluate the impact of rain events on the hydrodynamics of Créteil, a small and shallow lake in France. The analysis allows the author to assess the impact of stormwater discharge. The spectral behaviour value was shown to vary little according to the depth of the shallow lake.

Due to low flow rate in lakes, Li-Kun et al. (2017) used water temperature measurements to validate a hydrodynamic model.

Soullignac et al. (2017) used temperature profiles measurements and current velocity (using ADCP), captured at the centre of a small and shallow lake, to calibrate and validate a three-dimensional hydrodynamic model. The authors highlight that hydrodynamic calibration is an important step to perform ecological simulations and to discern phytoplankton distribution in space and time.

The distribution of phytoplankton and cyanobacteria in lakes is strongly affected by wind-driven currents and also by spatial heterogeneity on environmental conditions (Cyr, 2017; Wang et al., 2017; Huang et al., 2014; Wu, 2015; Wu, 2013).

Wang et al. (2017) accentuate that the effect of light, wind and current in cyanobacteria distribution is still inadequate. The authors indicate that cyanobacteria behaviour is a dynamic balance between water turbulence and wind drift, in which shallow lakes have a high degree of spatial and temporal biomass variability.

Spatial and temporal heterogeneities are responsible for several issues and, in order to study the behaviour of phytoplankton in lakes, a better understanding of the mechanisms that result in heterogeneities is required (Yang et al., 2013). Complex questions about the factors which influence bloom initiation, growth rate, group composition, and spatial and temporal distribution are still in vogue (Huber et al., 2012; Merel et al., 2013; Shimoda and Arhonditsis, 2016). Wang et al. (2017), highlighted the fact that the spatial and temporal motion of cyanobacteria in shallow lakes (especially *Microcystis*, very common in urban lakes) needs to be better investigated in order to understand the migratory behaviour due to horizontal advection and vertical buoyancy process.

Thus, hydrodynamic conditions appear to be an important factor for biomass concentration and scum formation and require further study.

### **2.3. Phytoplankton monitoring composition**

Monitoring phytoplankton assemblage by species and total biomass is mandatory to improve knowledge of their behaviour in space and time to improve lake and reservoir management (Birch and McCaskie, 1999; Merel et al., 2013). Depending on which species or groups are present, biomass behaviour can differ, such as whether scums may occur.

In order to preserve the quality of the water and thereby safety for human health, monitoring cyanobacteria species and toxins needs to be precise and accurate, so as to provide a successful risk management strategy for recreational activities, drinking water production and other water uses. Assessing biomass concentration and species or group composition is not an easy task. Interference in measurements may result in a misinterpretation of differing group compositions. Some of these interferences will be discussed in the following sections.

There are a broad variety of methods available to monitor phytoplankton biomasses, from species identification with cell counting using microscopy to satellite images of water surface at a larger spatial scale. Considering that phytoplankton biomass and community composition are very variable in space and time, monitoring requires methods capable of capturing this variability.

Several methods to determine algal biomass are used, none of which are completely reliable, as discussed in the forthcoming paragraphs.

Pigments are characterized and quantified either by chromatographic methods such as HPLC (High-Performance Liquid Chromatography) (Mackey et al., 1996; Wright et al., 1991) or based on their specific excitation/emission spectrum (i.e., spectrofluorometric approach) (Beutler et al., 2002). Both methods are now widely applied in studies of phytoplankton community composition, although they do not allow the same level of taxonomic identification as microscopic methods. The microscopic method is used to determine phytoplankton density and group composition through microscopic enumeration of samples taken. It is well known that, due to sensitive to prolonged storage of some phytoplankton types, samples should be examined and counted as soon as possible. Therefore, the use of microscopes to classify phytoplankton requires identification by skilled and experienced operators which can introduce uncertainty. Therefore, the study of phytoplankton community composition requires labour-intensive microscopic methods and experienced staff.

A spatial and temporal approach by sampling and cell counting is an expensive and time-consuming approach because it requires many samples to be analyzed in order to follow trends, as well as a highly trained operator. Another limitation of sampling is that very thin horizontal phytoplankton layering occurs on occasion. Samples taken without proper guidance will likely miss these zones.

To study the composition of phytoplankton communities, microscopic analysis is very useful, but it does not allow for a high-frequency (spatial and temporal) analysis. The time required to sampling a water body and obtain the final results generally excludes the use of these methods for supervision or monitoring tasks (Beutler et al., 2002).

To overcome this issue, fluorescence-based approaches that use specific excitation of pigment antennae found among the main phytoplankton phylogenetic groups have been proposed and have spread rapidly.

*In situ* fluorometers or portable spectrofluorometers were developed with the purposes of reducing the delay between sampling and laboratory analyses and also to provide a better spatial evaluation of algae communities. One such device, the FluoroProbe (FP, BBE Moldaenke), uses spectral fluorescence measurements to quantify phytoplankton biomass (expressed in  $\mu\text{g/L}$  of Chl-a) and to discriminate different phytoplankton groups *in situ*.

Spectrometry determination of chlorophyll-a has been widely used as a phytoplankton-biomass proxy because it is simpler and faster than microscopy analysis.

As an example, a study of the spatial and temporal evolution of the cyanobacterium *Planktothrix rubescens* in Lake Bourget, France, Leboulanger et al. (2002), used a spectrofluorimetric probe (FluoroProbe, BBE Moldaenke) and microscopic cell counts. The study presented a strong linear correlation between both types of data and high spatiotemporal variability. However, a linear correlation does not necessarily mean that the measured values are the same or close.

Lake Erie was used by Ho and Michalak (2015) as a case study to explore the state of knowledge of processes that control HABs (Harmful Algal Blooms). Ambiguous conclusions about HAB occurrences were found to be caused by differences in the methods used to track them. Therefore, the authors suggest that to better understand the link between the causes and consequences of HABs, it is crucial to improve existing and future monitoring programs.

However, one of the main difficulties is the delay between sampling and analysis, which limits the number of samples and, consequently, the frequency of spatial and temporal monitoring (Dworaket al., 2005). Portable spectrofluorometers (FP) provide better spatial and temporal monitoring of Phytoplankton biomass (MacIntyre et al., 2010). Therefore, FP probes will be the focus of the next section.

### 2.3.1. BBE Fluorescence probes

*In vivo* chlorophyll analysis measures chlorophyll fluorescence within a living cell. The advantage of this type of analysis is that it is quick and simple and does not require special sample preparation or extraction.

Many studies were conducted in order to assess the reliability of the fluorescence probes for measuring phytoplankton biomass in different lakes worldwide (Beutler et al., 2002, 2004; Catherine et al., 2012; Escoffier et al., 2015; McQuaid et al., 2011; Silva et al., 2016; Yentsch and Phinney, 1985; Zamyadi et al., 2016).

Depth profiles can be measured with a submersible probe. Profiles measured in the morning and noon are an example of the application of this probe in the study of algal migration showing vertical migration, especially for dinoflagellates (Beutler et al. 1998).

Using fluorescence probes (FP), major taxonomic groups of phytoplanktonic organisms may be identified. Consequently, these devices have been rapidly adopted by members of the scientific community (Catherine et al., 2012) and water resource technical community. Their uses were described in detail by Beutler et al. (2002).

Algal populations fluorometric differentiation is done based on energy transfer and fluorescence emission. Therefore, algal colour is a useful taxonomic criterion in which algal taxonomic groups differ significantly in their fluorescence excitation spectrum response (Beutler et al., 2002).

To categorize “spectral groups”, fingerprints of excitation spectra of chlorophyll (Chl) fluorescence can be used of microalgae *in vivo* and *in situ*; through, for example, vertical profiles achieved within a few seconds. Investigated spectral groups of algae needs specific photosynthetic antenna pigments composition and, consequently, a specific excitation spectrum of the Chl fluorescence, such as HPLC.

FP allows the rapid quantification of phytoplankton biomass and facilitate the characterization of phytoplankton spatial heterogeneity within the water column through the selective excitation of accessory pigments. BBE Fluoroprobe covers (i) ‘green’ algae (Chlorophyta and Euglenophyta) rich in chlorophyll a and b, (ii) ‘brown’ xanthophylls containing algae (Bacillariophyta, Chrysophyta and Dinophyta), (iii) ‘blue’ phycocyanin-rich algae (Cyanophyta) and (iv) ‘red’ phycoerythrin-rich algae (Cryptophyta).

The evaluation of Chl-a concentration of algal groups is based on a fit of the measured spectra by each fingerprint. To obtain the norm spectra in laboratory and *in vivo* experiments, a bench-top fluorometer was set up by Beutler et al (2002). This methodology is important for knowing which phytoplankton groups are present; however, some important aspects that can cause errors need to be known.

For Chl-a concentrations between 80 ng/L and 80 µg/L, the fluorometric method is reasonably precise (standard deviation below 25%). For Chl-a concentrations above 400 µg/L, fluorescence re-absorption results in samples errors due to a light intensity gradient (Beutler et al., 2002).

Another important issue associated with interference in measurements between different groups is reported by Beutler et al (2002), who performed experiments to assess such interferences. The results

showed that, for Chl-a below 400 ng/l and above 20 µg/L, significant errors were observed in the measurements for the least-concentrated algal groups. Whenever the ratio between the highest and lowest Chl-a measurements reaches a value of approximately 20:1, the Chl-a concentration of the least-concentrated algal group was not correctly determined, normally being overestimated.

A limitation of the use of spectrofluorimetric probes is related to the linearity of their response. In Lake Pampulha (Silva et al., 2016), the FP probe response, above 100 µg Chl-a/ L, was no longer linear, leading to underestimated chlorophyll concentrations above this limit when compared to laboratory spectrophotometric analyses. This could also be observed in the calibrated fingerprints that reduce the difference for total phytoplankton between spectrophotometric and FP measurements.

For the use of FP, the following criteria are considered:

- (a) Constant fluorescence excitation spectra (independent of the physiological status of the cells);
- (b) Linear independence of the norm spectra.

*In situ* experiments were conducted by Beutler et al (2002). The author compared the measurements with those of HPLC determinations for a wide Chl-a range. Results were compared to total Chl content measured fluorometrically and through HPLC analyses. The fluorescence measurements were in good agreement with the HPLC analyses.

In the next section, some studies conducted in different regions around the world with the use of Fluoroprobe will be considered. For validation, the usual methodology is to compare the FP values with those obtained through extraction methods (HPLC or biovolume). Strong correlations are normally obtained. Besides the correlation, it is also important to evaluate and compare the values obtained through each method. Comparing the measured FP values with those of the extraction method, most of the results presented lower values for FP, although some presented higher.

Based on a large dataset for the Marne reservoir from 2006 and 2007, Rolland et al. (2010), point out that the Fluoroprobe appears to be a reliable tool to monitor phytoplankton. A high correlation was obtained between the total Chl concentrations given by the BBE Fluoroprobe and the total Chl concentrations provided by the spectrophotometric analysis ( $\rho = 0.93$ ,  $n = 243$ ,  $p < 0.0001$ ), but the BBE FluoroProbe tends to obtain lower Chl-a concentrations than measured with spectrophotometry. According to the author, these differences in measured values, in a range from 0.1 to 40.4 µg/L, can occur because extracted chlorophyll methods usually provide a higher concentration estimate than fluorescence.

To validate the use of Fluoroprobe, samples obtained by a Van Dorn sampling bottle were compared with measurements from the FP, from the surface down to 0,5 m above the bottom, resulting between 10 and 15 data points for every meter of the water column that were performed every 0.5 s. To compare the measurement with those from the Van Dorn sampling bottle, which is 80 cm long, the values were integrate and averaged also along 80 cm along the measurement depths. The results obtained using a single depth (i.e. 3, 6 or 8 m) were also compared, and no significant difference between the two methods was found (Rolland et al., 2010). The Chl-a of the sample was extracted and measured spectrophotometrically, whereas phytoplankton counts and identification were performed with a microscope.

The total equivalent Chl-a concentrations measured by the Fluoroprobe and the total biovolume (obtained after microscopic counting) were with a high significant correlation ( $\rho = 0.6$ ,  $p < 0.0001$ ,  $n = 243$ ).

Gregor and Marsalek (2004), also revealed an excellent correlation between the total (equivalent) Chl-a measured by the BBE Fluoroprobe and the Chl-a determined by spectrophotometry after pigment

extraction ( $r = 0.97$ ,  $p < 0.05$ ,  $n = 18$ ). Gregor et al. (2005), found a similar relationship ( $r = 0.95$ ,  $p < 0.01$ ,  $n = 96$ ). Nonetheless, the spectrofluorometric values (for equivalent Chl-a) were 26% lower than spectrophotometric ones for chlorophyll-a concentrations. Pinckney et al. (1994) obtained the same results, but with 24% lower values comparing spectrofluorometry with spectrophotometry and 3% lower when compared to high-performance liquid chromatography. This difference probably was due to the fact that when the BBE Fluoroprobe is calibrated by high-performance liquid chromatography (HPLC) analysis, it usually reports lower Chl-a concentrations than spectrophotometric methods, especially if ethanol is used for the extraction process (Rolland et al., 2010).

The compositions of phytoplankton communities in a group of 50 shallow lakes near Paris region in France were measured between 27 July and 10 August 2006, using a BBE FluoroProbe (Catherine et al., 2012). Chlorophyll-a concentrations ranged from 0.8 to 264.7  $\mu\text{g/L}$ . Depth profiles were recorded with an average vertical downward velocity of the probe.

A strong correlation ( $r = 0.969$ ,  $p\text{-value} < 0.001$ ) was found between Chl-a concentration estimates given by FP and by laboratory spectrophotometric analysis. Measurements obtained by the spectrophotometric analyses were 1.8 times higher than those given by the FP.

Total Chl-a estimates obtained by spectrophotometric analysis and FP measurements were well correlated with total biovolume data spectrophotometric ( $r = 0.873$ ,  $p\text{-value} < 0.001$ ) and FluoroProbe data ( $r = 0.890$ ,  $p\text{-value} < 0.001$ ).

FP data were corrected by the mean Chl-a/BV ratio obtained for each group. The  $R^2$  statistics increased from 0.73 to 0.77, showing that using the average Chl-a/BV ratio of the four 'spectral' groups improves the estimation of total biomass by FP to some extent.

Catherine et al. (2012), demonstrated that FP data yield better estimates of total phytoplankton biovolume than spectrophotometric chlorophyll-a measurements do.

Five reservoirs located in the south of the Czech Republic were monitored with a FluoroProbe from April to September 2003 (Gregor et al., 2005). These reservoirs (one recreational and the other four for drinking water supply) have varying levels of eutrophication and composition of their phytoplankton communities. The whole depth profile was measured bi-weekly or monthly throughout.

At the depths where the FP detected a peak or changes in phytoplankton quantity/composition, discrete samples were collected for laboratory analysis (Chl-a for the standard spectrophotometry method and microscopic taxonomic identification and cell counting).

The correlation of Chl-a concentrations determined by FP and the standard spectrophotometry method was high ( $r = 0.95$ ,  $n = 96$ ), although with lower values for the FP ( $\text{FP/Samples} = 0.74$ ), even when a single algal group was dominant. The amount of fluorescence emitted was influenced by different physiological states and the density of photosynthetic pigments in cells during growth.

Another influence on fluorescence signal reception was caused by dense cyanobacterial blooms, especially in the case of colonial species. Such interference probably arises because of reabsorbance and scattering of the excitation light, as well as of the Chl-a emission when a bloom is dense (Gregor et al., 2005). In dense phytoplankton biomass, the light and fluorescence emitted by phytoplankton cells are shaded, scattered and re-absorbed, resulting in an underestimation of biomass and a non-linear response by the probe.

Physical variables such as lower water temperature, windy weather, and wave action may also influence the density of the colonies, disintegrating them over the vertical profile. Other potential sources of

variability include different sampling strategies (continuous measurement vs. discrete sampling), sample treatment, and mode of transportation to the laboratory.

Reservoirs with high phytoplankton biomass may yield greater concordance of the two methods, whereas discrepancies may be greater in lower biomass reservoirs because oligotrophic waters should have higher species diversity with lower cell counts (Gregor et al., 2005). Furthermore, achieving strong concordance between cell counts and FP data may be difficult with complex phytoplankton communities, due to the high variability in cell biovolume.

Gregor et al. (2005) concluded that the use of FP appears to be a good tool for water quality management. It can be used in the detection of natural horizontal and vertical variability in phytoplankton communities or for the early detection of cyanobacterial blooms. According to the authors, the use of microscopy analysis should provide information about dominant species and verify the approximate measured ratio of algal groups.

In North Inlet, Richardson et al. (2010) correlated and estimated the biomass of cyanobacteria, cryptophytes, diatoms with dinoflagellates and greens. The comparison was done with the use of a multiple-fixed-wavelength spectral fluorometer Algae Online Analyzer (AOA, BBE-Moldaenke, Kiel, Germany) with the use of a FP, which allowed for an online evaluation of the measurements. They were compared to those from a high-performance liquid chromatography (HPLC) and chemical taxonomy (ChemTax) based taxonomic assessments.

According to the data, total Chl-a concentrations measured by HPLC and multiple-fixed-wavelength spectral fluorometer showed similar variations, although absolute concentrations were significantly higher than those measured by HPLC. Total phytoplankton biomass values were overestimated at a range of 1.2 to 3.4 times ( $R^2$  between 0.89 and 0.92), with the best agreement at 12:00 and the worst overnight. However, by doing this comparison between real-time measurements and samples collected approximately every 3 hours and sometimes weekly, the relative taxonomic composition was well categorized, correctly showing the dominance of chromophyte and green algae and a minor contribution from cryptophytes and cyanobacteria. The authors concluded that the use of the multiple-fixed-wavelength spectral fluorometer seems to be a useful tool for monitoring phytoplankton group composition, that can be used in an early warning system alert for harmful algal blooms.

For tropical lakes, scarce fluorometric data are available. The performance of a spectrofluorometer was assessed in a tropical reservoir with default and calibrated fingerprints (Silva et al., 2016). Measurements with the FP were compared to biovolumes and laboratory spectrophotometric analyses of phytoplankton sampled in Lake Pampulha (Brazil). All samples were highly dominated by cyanobacteria species.

The excitation spectrum of cyanobacteria species found in Lake Pampulha was determined in laboratory and compared with the default fingerprints for cyanobacteria provided by the probe manufacturer (FP-BBE FluoroProbe, Moldaenke, Germany).

The total phytoplankton biovolume was significantly correlated to Chl-a concentration measured by FP ( $r = 0.64$ ,  $p = 0.001$ ,  $n = 23$ ). Cyanobacteria biovolume also presented a significant correlation to the cyanobacteria chlorophyll estimated by the probe ( $r = 0.60$ ,  $p = 0.002$ ,  $n = 23$ ). Even using the default fingerprints (no site-specific correlation), these results show that FP was able to achieve a quite good assessment of total phytoplankton biomass in Lake Pampulha.

Spectrophotometric results and FP measurements for total phytoplankton were weakly correlated ( $r = 0.43$ ,  $p = 0.01$ ,  $n = 35$ ). While analyzing the results for concentrations lower than  $100 \mu\text{g/L}$ , the correlation was higher ( $r = 0.84$ ,  $p < 0.001$ ,  $n = 25$ ), probably due to non-linearity for values over  $100 \mu\text{g/L}$  ( $r = 0.17$ ,  $p = 0.63$ ,  $n = 10$ ).

Compared to spectrophotometry, the total biomass measured with the FP was largely underestimated between 50% and 75%. Underestimation was stronger for higher Chlorophyll concentrations and varied depending on the dominant species (Silva et al., 2016).

### 2.3.2. Use of Phycocyanin

Phycocyanin fluorescence is considered as a specific proxy of cyanobacteria biomass detection (Khac et al., 2018). Zamyadi et al., (2012) validated the use of *in vivo* phycocyanin fluorescence in laboratory ( $r$  between 0.99 and 0.90,  $p < 0.01$ ) and environmental conditions ( $r$  between 0.91 and 0.89,  $p < 0.01$ ) with high and significant correlations between conventional laboratory methods analysis and online *in vivo* PC fluorescence probe. Hence, the authors proposed an online alert system to monitor potentially toxic cyanobacteria in the raw water of drinking water treatment plants in Quebec. The phycocyanin fluorescence values, however, were always lower than by extraction. In laboratory condition, the values were 48 to 52% lower, while 84 to 96% lower in environmental conditions.

A chlorophyll-a peak indicates growth of phytoplankton, not always corresponding to a peak of cyanobacteria. Therefore, the main advantage of using phycocyanin fluorescence monitoring is that its peak can be associated with cyanobacteria blooms (Khac et al., 2018).

A Phycocyanin probe approach, to quantify cyanobacteria, is a method that can be performed rapidly online, is stable and selective, and needs infrequent calibration. Online phycocyanin probes have become a powerful tool for detecting and quantifying cyanobacteria, despite the fact that interferences can affect the fluorescence due to external factors, such as cell physiology, light condition, and water quality (Kong et al., 2017).

For phytoplankton community composition, microscope analysis is very useful, but does not allow for high-frequency (spatial and temporal) analysis. FluoroProbe (FP) is regularly considered a useful tool to help in the detection of natural horizontal and vertical variability in phytoplankton communities and in the early detection of cyanobacterial blooms.

The total Chl-a measured by FP, when compared to laboratory spectrophotometry analysis, generally presents a high correlation. However, FP values are frequently lower with different degrees of underestimation (Catherine et al., 2012; Gregor and Marsalek, 2004; Silva et al., 2016), but are sometimes higher (Beutler et al., 2002; Richardson et al., 2010). FP as an *in vivo* fluorescence method can be used with periodic correlation to quantitative extraction methods that include fluorometric, spectrophotometric or HPLC method (Table 2.1).

**Table 2.1** – Main results of the comparison of Chl-a measured by FluoroProbe and extraction methods

Source	Comparison	Mathematical Indicators	Conclusion
Pinckney et al. (1994)	Fluoroprobe and Spectrophotometric analysis	Not presented	FP with 16% lower value
	Fluoroprobe and High-performance liquid chromatography	Not presented	FP with 3% lower value
Beutler et al (2002)	Fluoroprobe and High-performance liquid chromatography	Not presented	FP typically overestimated Chl-a, when ratio between the greatest and the smallest Chl-a is
Gregor and Marsalek (2004)	Fluoroprobe and Spectrophotometric analysis	$r = 0.97, p < 0.05, n = 18$	FP with 17% lower values

Source	Comparison	Mathematical Indicators	Conclusion
Gregor et al. (2005)	Fluoroprobe and Spectrophotometric analysis	$r = 0.95, p < 0.01, n = 96$	FP with 26% lower values
Rolland et al. (2010)	Fluoroprobe and Spectrophotometric analysis	$\rho = 0.93, n = 243, p < 0.0001$	FP with lower values in most of times
	Fluoroprobe and Biovolume after microscopic counting	$\rho = 0.6, p < 0.0001, n = 243$	Biovolume presented in $\mu\text{m}^3/\text{L}$ and FP in $\mu\text{g}/\text{L}$ . Values with a weak correlation
Zamyadi et al., (2012)	Phycocyanin fluorescence and Spectrophotometric	$r$ between 0.99 and 0.91, $p < 0.01$	Phycocyanin <i>in vivo</i> 48 to 96% lower
Catherine et al. (2012)	Fluoroprobe and Spectrophotometric analysis	$r = 0.969, p < 0.001$	FP with 55% lower values
	Fluoroprobe and Biovolume after microscopic counting	$r = 0.890, p < 0.001$	Biovolume presented in $\mu\text{m}^3/\text{L}$ and FP in $\mu\text{g}/\text{L}$ . Applying $\text{FP}_{\text{tot}}/\text{BV}_{\text{tot}}$ equation FP presented higher values
Richardson et al., 2010	Fluoroprobe and High-performance liquid chromatography	$r > 0.90, p = 0.000$	FP values 20% to 240% higher
Silva et al., 2016	Fluoroprobe and Spectrophotometric analysis	$r = 0.84, p < 0.001, n = 25$ , for values $< 100 \mu\text{g}/\text{L}$	FP with 50% to 75% lower values
	Fluoroprobe and Biovolume	$r = 0.17, p = 0.63, n = 10$ , for values $> 100 \mu\text{g}/\text{L}$	FP with lower values (50 to 400%)
		$r = 0.64, p = 0.001, n = 23$	FP higher values (50 to 300%)

### 2.3.3. Phytoplankton monitoring with satellite remote sensing

Monitoring phytoplankton using satellite remote sensing can be used to evaluate the influence of lake hydrodynamics on scum accumulation. Remote sensing has the advantage of a large spatial scale which is important in identifying scum accumulation in specific regions on lakes or reservoirs.

The need for more effective phytoplankton monitoring has recently led to a growth in the development of satellite remote (Blondeau-Patissier et al., 2014). Satellite images that use colour technology to detect the presence of scums and algorithm to estimate phytoplankton biomass may be used for mapping, monitoring, and detection of phytoplankton scum. This methodology is favoured by its spatial scale with relatively frequent sampling and the capacity for rapid response, due to near real-time data retrieval (Head and Pepin, 2010). Using satellite imagery, Qin et al. (2015) were able to detect a strong increase in scum, in which the scum surface increased from 92 km<sup>2</sup> to almost 400 km<sup>2</sup> in less than 24 hours.

This approach can also be used in the reduction of spatial uncertainties associated with limited water sample analyses (Dörnhöfer et al., 2018). Its main weaknesses are its dependence on good weather with no cloud coverage, a limited capacity to establish and distinguish taxonomic information, and that images only provide information on the water surface.

Another difficulty in interpreting the phytoplankton concentration through images is the high number of available algorithms that interpret the colours and assess the phytoplankton concentration. According



to Clark et al. (2017), different algorithms have distinct performances which vary with phytoplankton concentration, taxonomy, and satellite used.

Glasgow et al. (2004) concluded that increased use and continuing advancements of real-time remote monitoring are becoming an important tool for evaluating water quality. Although satellite images provide great flexibility at spatial and temporal scales of monitoring, they also have limitations and need to be used with caution.

Traditional multi-site measurements, as well as different techniques such as optical remote sensing from space, show phytoplankton heterogeneities along the horizontal axis and time scale. Their distribution still remains without explanation, because of the complexity in monitoring and correlating processes and mechanisms that cause these heterogeneities (Grimaud et al., 2017; Moreno-Ostos et al., 2007). Spatial and temporal variations of phytoplankton biomass happen on very short scales. Direct estimation of chlorophyll-a to deduce phytoplankton biomass may contain errors. Thus, phytoplankton succession and variability in natural systems remains a challenge in aquatic ecosystem research.

#### **2.3.4. Interferences on phytoplankton measurements**

Attention should be paid to the interpretation of measurements as far as phytoplankton biomass is concerned, since inconsistencies might be present.

Some physiological processes affect the functioning of the photosynthetic system in phytoplankton and could potentially explain some of the remaining unexplained variance (Catherine et al., 2012).

The following biological and environmental issues affect results:

##### **(a) Health of the organism**

Healthy phytoplankton will produce a lower fluorescence response per unit chlorophyll rather than senescent (“dying”) phytoplankton cells.

##### **(b) Physiological stress**

Physiological stress is observed among large variations in the fluorescence number for a single species when exposed to nitrogen or phosphorus deficiency. For instance, the fluorescence number for a small centric diatom, *Cyclotella nana*, may range from 0.095 for nitrogen-enriched cells to 0.40 for chlorotic cells which were severely deficient in nitrogen (Kiefer, 1973).

The pigment of different species of cultures changes, resulting in a 50% increase, when nutrients reach a limitation level. Different development stages of phytoplankton also contribute to variation in the pigment cells (Beutler et al., 2002).

Changes in phenology in response to nutrient starvation or high light may lead to a Chl-a misestimation of up to 2-3 times (Beutler et al., 2002).

##### **(c) Light adaptation of the cell**

The amount of chlorophyll per cell can vary due to light availability. Phytoplankton cells adapted to bright light conditions will produce a lower fluorescence response per unit chlorophyll than dark-adapted phytoplankton.

Variations in fluorescence in a water column are common. Photoinhibition of cellular fluorescence accounts for only a part of the total variation in fluorescence value. Phytoplankton fluorescence is at its

maximum at night and minimum at midday. Cellular chlorophyll-a at 10 m fluoresced twice the intensity of that at a depth of 1.0 m depth because of photoinhibition of cellular fluorescence due to the light-dependence at the surface (Kiefer, 1973).

Under conditions of low phytoplankton biomass and high irradiance, significant signal attenuation was found at the surface layer (Catherine et al., 2012).

**(d) Morphology of the cell**

Composition and shape of the cell and surrounding cellular material can interfere with the fluorescent signal.

**(d) Water turbidity**

Turbidity can cause scattering or shading effects depending upon the chemical composition of the suspended matter.

**(e) Dissolved organic matter**

Colored dissolved organic matter (CDOM or yellow substances) may lead to some degree of error in total Chl-a estimates (MacIntyre et al., 2010; Twiss, 2011), which depends on the ratio between CDOM and total phytoplankton biomass.

**(f) Extraction method**

A significant part of unexplained variance might originate from the extraction method and/or the algorithm used to estimate Chl-a from absorption data. Chl-a is generally extracted mechanically (e.g., homogenization, grinding, sonication) using organic solvents (e.g., acetone, ethanol, methanol, DMSO) (Catherine et al., 2012).

**(g) Counting of dead cells**

Some data points were identified as outliers due to their low Chla/BV ratios, which could reflect a higher dominance of low Chl-a containing phytoplankton or bias due to the counting of dead cells in preserved samples (Catherine et al., 2012). Through MDS (MultiDimensional Scaling) analysis, the authors stated that environmental stress could lead Cryptophytes and Cyanobacteria SFS to appear similar to Chlorophytes SFS, leading to misidentification.

## **2.4. Phytoplankton modelling approaches**

Considering the complexity of lake ecosystems with high spatial and temporal variability, the high cost in monitoring, errors, interference in phytoplankton measurements and different methods available, mathematical models supported by consistent monitoring data are valuable tools to organize and quantify ecological knowledge of lakes. Lake and reservoir managers need modelling tools to predict bloom events to better handle the damage caused (Harris and Graham, 2017). According to Robson (2014), ecological modelling may generally be able to provide relevant management action prediction in cases of strong physical drivers.

Impreciseness of measured data values and uncertainty of how representative they are of water conditions pose an important challenge in modelling phytoplankton behaviour. Mathematical models can help to develop efficient monitoring programs due to their contribution to understanding the processes involved in phytoplankton behaviour. Several mathematical models are available, though their use demands considerations.

A common methodology to choose and implement a model can, in general terms, be organized according to the followed steps:

- (a) Definition of objectives and problems to be solved;
- (b) Survey of data and information available about the study area;
- (c) Definition of the model extent, grid size, number of layers (in case of a vertical simulation);
- (d) Collecting and processing data of the domain (e.g.: bathymetric data);
- (e) Processing field measurements for calibration and verification data;
- (f) Defining simulation scenarios;
- (g) Preparing boundary and initial conditions;
- (h) Calibration of the model parameters;
  - (h1) Performing a sensitivity analysis;
  - (h2) Defining the calibration runs to be executed;
  - (h3) Evaluating the quality of results and iterating on the calibration process if necessary;
  - (h4) Determining and executing verification runs and accessing the final accuracy of simulations.
- (i) Validation of the model;
- (j) Uncertainty analysis;
- (k) Conclusions.

Calibration and validation are important steps when using mathematical models. However, these concepts are ill-defined and interpreted differently by many modellers (Los et al., 2008). Meanwhile, Refsgaard and Henriksen (2004) propose the following terminologies, adopted in this research, for calibration and validation:

- (a) Model Calibration: Adjustment of parameter values of a model to obtain a model response of the reality within the range of accuracy established in performance criteria.
- (b) Model Validation: Substantiation that possesses a satisfactory range of accuracy model within its domain of applicability, consistent with the intended application of the model.

Therefore, concluding that a model is good and validated means testing the usefulness of the model according to specific objectives (Alexandrov et al., 2011; Los et al., 2008; Mankin et al., 1975). According to Robson (2014), if a model involves many different processes, it becomes too complex to be properly verified.

Davidson et al. (2016) identified a range of modelling methodologies, showing their strengths and weaknesses when applied to evaluations of phytoplankton behaviour. The methodologies evaluated were: (i) Risk assessment style models, (ii) Lagrangian models, (iii) Ecosystem-based models, (iv) Individual-based models, (v) Statistical models, and (vi) Coupled observational-modelling systems. However, most of the examples were referenced with coastal or offshore applications. The application for these regions offers great value to coastal zone management and aquaculture industry.

The high number of lakes and reservoirs in urban and peri-urban areas is also of concern regarding the risk of cyanobacteria presence. Mooij et al., (2010) presented a survey of existing models and their approaches to lake ecosystem modelling application. The primary focuses included the followed approaches: (i) statistical models, (ii) dynamic models, (iii) optimizations algorithms, (iv) neural networks, and (v) Kalman filters and fuzzy logic.

The authors classified the models using multiple criteria concerning model components and model characteristics (see Table 1 Mooij et al., 2010). It was concluded that the most important aspect for choosing a model is to analyze the principle that led to the development of each approach and the premises chosen during the development of the model. Thus, to set the better ecological model, determining the optimal complexity of the phytoplankton model is a crucial issue (Shimoda and Arhonditsis 2016).

Over the past four decades, many models have been developed to lake ecosystem and, since the availability of tested models is significant, it seems more effective to apply or adopt an existing model instead of creating a new one (Mooij et al., 2010).

Using multiple modelling approaches helps to create an integrated view of the functioning of lake ecosystems. However, this is rarely done in the context of aquatic system modelling (Robson, 2014). Therefore, a best single approach that can always be used does not exist; the best approach depends upon the objective of the modelling and the data available. Thus, in literature it is very common to find couple models that used different coupled approaches (Cao et al., 2016; Dimberg and Olofsson, 2016; Soullignac et al., 2018; Wang et al., 2017; Wynne et al., 2011; Zbiciński and Ziemińska-Stolarska, 2017).

Thus, to evaluate phytoplankton behaviour in lakes, the best model and modelling approaches depend on the specific objectives and data availability. The next sections will address some of the approaches available in the literature concerning ecological models.

#### 2.4.1. Wind-driven criteria

Raine et al. (2010) used a model based on the criterion that wind-driven water exchanges result in exchanges of phytoplankton, which, associated with bay volume during thermal stratification, resulted in toxic events. This wind index presented a high degree of success in Bantry Bay in southwestern Ireland. This approach is advantageous to determine scum formation events temporarily.

In Taihn Lake, a large and shallow lake, Wu et al. (2010), calculated that the horizontal distribution of *Microcystis* concentration was strongly affected by wind conditions and surface drift during short events (from 21 to 25 August). It was concluded that wind speed and direction can cause considerable heterogeneity in the horizontal distribution of plankton populations with a clear higher concentration in downwind areas. *In situ* growth could be helpful for horizontal redistribution of cyanobacteria, however, with a small contribution in short-term bloom events (Wu et al., 2013). This small *in situ* growth contribution could also be reforced, according to measurements performed by the authores, due to weak correlation between Chl-a and dissolved nutrient.

#### 2.4.2. Deterministic approach

Traditionally, a deterministic model is expressed mathematically in partial differential equations. Concerning algae behaviour, it is based on the theories of the dependence of algae growth on physical and biochemical environmental variables.

Models that use deterministic ecosystem were very promising in the early 1980s, when computers capacity became more available (Rigler and Peters, 1995). However, they were very criticized in the 1990s for requiring a large amount of data, for being overly complex, and for not resulting to scientific contribution or demonstrating predictive power.

From a management point of view, there is also a demand for real-time forecasting, for example, of cyanobacteria blooms in lakes with leisure use. The accuracy of traditional deterministic models in predicting this type of event is usually not very high (Mooij et al., 2010). The authors concluded that it would be fruitful to combine current deterministic and statistical model approaches for improvements.

As an alternative to real-time forecasting systems of phytoplankton blooms, the authors suggest the use of statistical model approaches, such as Kalman filters and fuzzy logic. These approaches will be discussed in section 2.4.3 and 2.4.4.

### 2.4.2.1. Hydrodynamic modelling

Lake hydrodynamics are the main factor for the accumulation and transport of blooms over a short time (Li Wei et al., 2013). When creating and analyzing a hydrodynamic model, focusing on thermal and stratification dynamics to predict lake ecological behaviour is a good approach for areas where insufficient data are available (Frassl et al., 2018).

In 2009, the National Oceanic and Atmospheric Administration (NOAA) developed a forecasting system to forecast bloom transport and trajectories using high temporal resolution imagery. A particle tracker with a hydrodynamic model was used to approximate the bloom trajectory. Bloom events happened during a period of low wind intensity and warm water temperature, favourable conditions for bloom maintenance and buoyancy processes (Wynne et al., 2013). Bulletin alerts were sent to local managers, health departments, researchers and other stakeholders. The authors recommended the improvement of the system by using a three-dimensional hydrodynamic model for a more comprehensive examination of vertical distributions. Thus, modelling the vertical mixing would improve analyses assessing the recurrence of high surface biomass.

Concerning shallow lakes or reservoirs, due to the complex ecological behaviour, characterized by having a high heterogeneity in space and time, modelling of lake hydrodynamics plays a large role in better understanding algal blooms and scum formation (Prakash et al., 2007; Wang et al., 2017), for which three-dimensional hydrodynamic models are important tools to understand the processes that control phytoplankton behaviour (Soulignac et al., 2017, 2018; Wynne et al., 2013; Zbiciński and Ziemińska-Stolarska, 2017).

Soulignac et al. (2017) validated a three-dimensional hydrodynamic model (Delft3D-FLOW) on Lake Créteil, a small and shallow urban lake in France with an area of 0.4 km<sup>2</sup> and average depth of 4.5 m. Monitoring of the lake, based on high-resolution and high-frequency sensors, consisted of continuous temperature measurements at five depths at the centre of the lake and three depths at two other stations, as well as current speed profiles from the centre of the lake. The model was verified for 18 different one-month periods. An hourly time step was used and considered consistent with the timescale of biological processes.

In the model, the wind drag coefficient and light extinction coefficient were calibrated. The MAE (mean average error) was used as a performance indicator applied for simulated and observed data.

The calibrated wind drag coefficient and extinction coefficient were calibrated to reproduce the proper temperature differences between the surface (0.5 m depth) and bottom (4.5 m) measured values in all simulated periods. A limitation of the hydrodynamic model used is that it does not vary Secchi depth values during each simulation period. Secchi is a disk used to measure water transparency or turbidity. The transparency of the water is considerate as the depth at which the disk is no longer.

Even with this model limitation, the author concluded that the use of a mean extinction coefficient (associated with Secchi depth) is better for monthly periods. This is due to high temporal variability in water characteristic in which mean values represent thermal behaviour of the lake well.

The author concluded that the model was capable of reproducing water temperature and the alternation between stratification and mixing conditions. The monthly values for the mean absolute error (MAE) in water temperature presented were between 0.25 and 2.34 °C. The length of thermal stratification periods ranged from a few hours up to 40 days.

The author highlighted that a large amount of measurements for a thermal comparison is very rare, especially for small and shallow urban lakes, where, for the first time, to assess the performances of the three-dimensional hydrodynamic model, high temporal resolution data were used.

Soullignac et al. (2018) used a calibrated and validated hydrodynamic model with remote sensing to explain and predict some surface phytoplankton heterogeneities in Lake Geneva.

The results demonstrated that the model was able to reproduce the evolution of the lake thermal vertical structure on a smaller time-scale, detailing the thermal structure of the lake over time, providing explanations for horizontal heterogeneities in Chl-a abundances.

After analyzing the hydrodynamic behaviour in the lake, the authors concluded that surface Chl-a heterogeneities were related to upwelling events. The important role of wind in determining surface phytoplankton abundance was highlighted, where it can cause upwelling current that result in surface Chl-a heterogeneities.

The author suggested that an ecological model coupled to the hydrodynamic model would help to better evaluate and understand phytoplankton dynamics and heterogeneities in lakes. A three-dimensional hydrodynamic model coupled to ecological models could be used to give information about the Chl-a in the vertical direction which may vary between different portions of the lake.

#### **2.4.2.2. Hydrodynamic model coupled with an ecological model**

Most of the models of phytoplankton abundance that simulate and predict their behaviour are based on a deterministic approach. However, modelling an environmental ecosystem is challenging due to the high complexity of interactions and processes involved, including physical, chemical, and biological processes (Lou et al., 2017).

In order to investigate competition for light between cyanobacteria, diatoms, and green algae in eutrophic lakes, Jöhnk et al. (2008) developed a one-dimensional hydrodynamic model coupled to a one-dimensional phytoplankton model in Lake Nieuwe Meer (Netherlands). The use of modelling enabled studies of different climate scenarios. Therefore, Jöhnk et al. (2008) selected three years (1956, 1991 and 2003) characterized by contrasting summer temperatures, wind speeds, and cloud cover.

The parameters evaluated for the hydrodynamic calibration were wind speed, drag coefficient, and background attenuation coefficient. For all other parameters, standard values of typical lakes in the region were used. The wind measured was scaled by a factor of 0.92 (wind speed reduction by 8%). The drag coefficient was adjusted to fit the stratification behaviour of the lake. The background attenuation coefficient for the underwater light field (according to Lambert–Beer's law) was calibrated, yielding a value of  $0.7 \text{ m}^{-1}$ . This was close to measured values of  $0.6 \text{ m}^{-1}$  in Lake Nieuwe Meer.

For the phytoplankton model, cyanobacterium *Microcystis*, diatoms, and green algae were considered. The maximum growth rate parameters for each were determined by using laboratory measurements available in the literature. For *Microcystis*, values presented by Reynolds (1997) were used. For diatoms, a general temperature-dependent curve was fitted to laboratory measurements of the freshwater diatom *Asterionella*, presented by Butterwick et al., (2005). For green algae, the authors reported that the literature did not provide suitable data for Lake Nieuwe Meer, so the parameter was calibrated against the seasonal phytoplankton data.

Temperature stratification and population dynamics of the phytoplankton species predicted by the calibrated model were considered in good agreement with the observed values.

Through model results, high temperatures appeared to increase cyanobacteria growth rates (Jöhnk et al., 2008). Moreover, high temperatures also increased the stability of the water column, thereby reducing vertical turbulent mixing, which shifts the competitive balance in favour of buoyant cyanobacteria.

D-Water Quality is another widely-used model. It is a deterministic ecosystem model developed by Deltares that uses mathematical optimization for phytoplankton growth. It has been applied in several studies regarding algal succession (Los and Brinkman, 1988). A set of coefficients, which was established for 30 lakes worldwide and supposed to be representative of many temperate freshwater systems, was applied and validated on a complicated network system of ditches, canals, shallow and deep lakes (Los, 2009).

Smits (2009) calibrated D-Water Quality for a tropical freshwater system and obtained a more generic set of process coefficients for the water quality processes in tropical regions. However, the highly nonlinear relationship between phytoplankton abundance and various water parameters is still unknown because monitoring data are incomplete.

On the D-Water Quality, the Delft3D-ECO model needs to be run coupled with a hydrodynamic model (Delft3D-Flow) which calculates velocity, temperature and water density. This model was used in this research and will be described in Chapter 3.

Furthermore, according to Mooij et al. (2010), approaches that use a coupled hydrodynamic-ecological model can improve our understanding of the physical, chemical and biological processes influencing water quality dynamics. Some aspects, though, remain unclear such as: (i) whether all important ecosystem feedback mechanisms are well represented and; (ii) how the processes influence the lake ecosystem. These limitations can have a profound impact on their ability to predict complex system dynamic responses to environmental changes in different scenarios for phytoplankton predictions.

### **2.4.2.3. Biogeochemical models**

Shimoda and Arhonditsis (2016) reviewed studies performed from 1980 to 2012. They assessed the capacity of 124 aquatic biogeochemical models to reproduce the dynamics of two or more phytoplankton groups in natural environmental conditions. Most of the studied locations were in the Northern hemisphere, especially in European freshwater and marine ecosystems.

The authors concluded that modellers do not consistently use conventional methodological steps during their application. With no sensitivity analysis, optimization techniques were rarely used during model calibration and a third of the studies did not report any validation. A critical analysis of the results obtained points to the current lack of science on this subject using biogeochemical models.

### **2.4.3. Artificial neural networks and statistical techniques**

Prediction is a broad statement. Due to a high misunderstanding in the literature, some definitions are important. When a prediction is made for instances within a range of observed time points, it is called interpolation. When a prediction is made outside of a range of observed time points, it is called extrapolation. Forecasting is inherently tied to the time domain, when predictions of future observation need to be performed (Wilhelm, 2015).

NOAH (2006) assesses the feasibility of using artificial neural networks (ANN) as a real-time tool for accurately forecasting cyanobacteria counts. ANN has the potential to identify critical climate, hydrologic, and water quality variables which may influence phytoplankton levels. It was applied to a single reservoir within a watershed and for a water treatment plant that obtains its water supply directly from two different rivers.

Artificial neural networks technology differs from traditional deterministic modelling approaches which attempt to explicitly represent the governing laws with physical-based equations for forecasting system states of interest. Instead, ANNs represent a learning paradigm approach, in which predictor variables are obtained by processing representative historical events through their architecture, and state-transition equations which predict system responses as a function of the input.

In the study (NOAH, 2006), several hundred artificial neural networks models of different types were developed and tested for the phytoplankton bloom forecasting problem for one to two weeks prediction horizon. Their predictive performances were compared against measured values.

The result pointed out that the use of artificial neural networks accurately predicted only large changes in phytoplankton populations. This performance is mainly due to non-linear phytoplankton behaviour, the noise in the data, and the relatively small number of historical events available. This result shows the main problems in phytoplankton study: (i) the many processes involved that result in non-linear behaviour, (ii) difficulty in measurements due to many interferences and (iii) lack of available data.

Modelling results also indicate that limiting nutrients are important for accurate forecasting phytoplankton counts in reservoirs. However, impreciseness of measured data values and uncertainty of how representative they are of lake conditions poses an important issue in modelling phytoplankton behaviour. Therefore, for the authors, predicting phytoplankton succession and variability in natural systems remains a challenge.

Hence, historical data sets with sufficient quality and quantity are required to better represent the highly complex behaviour of the algal surface water. The collection of additional data may generate a larger number of events for model development and artificial neural networks testing, allowing more analysis and improving forecasting capability (NOAH, 2006).

As a conclusion, the authors suggest that the systematic elimination of input variables combined with additional sensitivity analyses may improve system understanding and optimal sets of model input variables. Also, as a consequence, monitoring programs could be improved and artificial neural networks forecasting accuracy could increase.

According to Lou et al. (2017), artificial neural networks alone are unable to handle linear and nonlinear processes equally well, like phytoplankton growth that present nonlinear behaviour for higher concentration (above 50 mg/L according Gregor and Marsalek (2004)). This methodology needs a high amount of data and an extended training time. Therefore, the authors suggested multivariate statistical techniques that can lead to better monitoring, modelling, and forecasting results.

Lou et al. (2017) proposed a multivariate statistical technique prediction and forecast models for monthly phytoplankton abundance time series in Macau Main Storage Reservoir (MSR). Twice a month, the authors monitored 23 parameters at a depth of 0.5 m at 3 different points (inlet, outlet, and the middle of the reservoir) over 11 years to develop a more accurate model for explaining the algal bloom mechanisms. The monitored parameters were: Turbidity, Temperature, Ph, Conductivity,  $\text{Cl}^-$ ,  $\text{So}_4^{2-}$ ,  $\text{SiO}_2$ , Alkalinity,  $\text{HCO}_3^-$ , DO,  $\text{NO}_3^-$ ,  $\text{NH}_4^+$ , TN,  $\text{UV}_{254}$ , Fe,  $\text{PO}_4^{3-}$ , TP, Suspended Solid, TOC, HRT, Water Level, Precipitation, and Phytoplankton abundance.

Numerical results presented that the predictions were, a  $R^2$  of 0.764, RMSE of 0.291 and MAE of 0.236 and the forecasting results were a  $R^2$  of 0.875, RMSE of 0.219 and MAE of 0.120. For the validation period, the mathematical indicators were quite the same. Therefore, the authors concluded that the multivariate statistical technique was suitable and can be adopted for further studies. However, a large amount of data was necessary (23 parameters at 0.5 m depth in 3 different points). In order to identify the water parameters that were significantly correlated with phytoplankton abundance, with the purpose of a decreased number of parameters to monitor, a correlation analysis and PCA (Principal component



analysis) were done. The results suggest that most of the variation can be explained by nutrients, physical parameters, and soluble salts. However, PCA did not reduce the number of variables in the study, but served as a mean to identify those parameters that had the greatest contribution to variation in the water quality of reservoirs.

Based on the results, the authors recommended that for future water quality monitoring programs, more effort should be placed on increasing the sampling frequency at different times, instead of increasing sampling points. They suggest that a couple of monitored points are enough to extract information for further analysis. This conclusion results in great relevance to the current research because high-frequency monitoring was used.

#### **2.4.4. Warning system for surface water blooms using statistical models**

In urban areas, eutrophication and cyanobacterial blooms will not be solved in a short time (Li Wei et al., 2013). Therefore, it is important to predict the probability and intensity of cyanobacterial blooms in water bodies used for drinking water or recreation activities. An alternative for lake management is the use of probability of occurrence for blooms. Simple models can be used to estimate the probability of algal blooms (Li Wei et al., 2013).

The use of statistical model approaches is an alternative to improve the weak predictive power of deterministic models. For operational short-term applications, statistical models are more accessible and more rapid (Khac et al., 2018). In this case, specific processes, that cannot be easily be described using deterministic equations, are modelled using knowledge rules. Examples of the use of a Kalman filter with an application for phytoplankton predictions can be found in Allen et al. (2016) and Mao et al., (2009).

Because of high spatial variability and an hourly timescale for the formation of surface water surface blooms (scum), early warning of scum events is a challenge (Ibelings et al., 2003). Models have rarely been used to forecast daily blooms even though they are a good daily management tool to provide predictions on water quality for local authorities (Li Wei et al., 2013).

After a water supply crisis in Wuxi, China in May 2007, millions of residents were forced to depend on bottled drinking water. For better management in such a situation, allowing for efficient decisions over short timeframes, an early warning of cyanobacterial bloom occurrence would be very useful (Li Wei et al., 2013).

Li Wei et al. (2013) used a forecasting model that included the weight of algal biomass, wind velocity, and weather conditions to predict the probability of bloom occurrences. According to the authors, the occurrence of a short-term bloom event is nonlinearly related to many environmental factors, but the key ones are algal biomass, wind velocity and rainfall. By using the numerical short-term cyanobacterial simulations (next 3 days), 97 cyanobacterial blooms forecasting reports were created and sent to the authorities from April to September in 2009 and 2010. The forecast results were checked using remote sensing images and boat survey data. The spatial distribution of forecasted blooms matched the observations approximately 80% of the time.

Qin et al. (2015) developed and tested a cyanobacterial bloom reduction strategy programme for Lake Taihu in China, combining surface cyanobacterial bloom monitoring, forecasting, alert warning and risk management. The probability of surface cyanobacteria bloom prediction was calculated by the product of chlorophyll biomass (predicted by Li Wei et al. (2013) mathematical model), wind strength and precipitation. The algal biomass (Chl-a) prediction model was run twice a week, in which measured values were used as the initial conditions for every simulation. Using the cyanobacterial bloom monitoring and forecasting system alert the lake management was improved. Better emergency

responses could be enacted, such as (i) flushing, (ii) algal collection and removal, (iii) emergency water quality measures, (iv) setting up barriers around inlet water drinking water plant and (v) use of specific chemicals products (potassium permanganate oxidation and powdered activated carbon adsorption) for removing volatile sulfide chemicals and dimethyl trisulfide and cyanotoxin. These measures could guarantee no drinking water contamination during the program.

Ibelings et al. (2003) designed and tested an early warning system (EWACS) for a large lake, which predicts the occurrence of cyanobacterial scums (surface concentration higher than 10 gC/m<sup>3</sup>) formation in qualitative terms, based on wind speed, irradiance and time-of-day data. Based on 12 years of NOAA images, this approach, combining a biomass model with a fuzzy expert system, was tested and validated on Lake IJsselmeer in the Netherlands.

In the study, scums were observed in 23 images. The model could give a proper prediction in 19 cases (83%). In 290 images, surface blooms were absent, and the model gave a proper prediction in 270 cases (93%). Therefore, for the prediction of absence and presence of blooms, the model performs very well. The two most dominant genera present during the study period of cyanobacteria were *Microcystis* and *Aphanizomenon*.

Thus, good scum prediction performance clearly requires good weather forecasts. The unpredictability of the forecast increases with the duration. Therefore, for early warning against surface blooms, a period of 72 hours seems to be sufficient (Ibelings et al., 2003)

The authors highlight that the most important meteorological factor that affects scums formation is wind speed. They simulated a realistic measure of uncertainty adding meteorological data with a variation of wind speed of  $\pm 0.4$  m/s. The results appeared to not be very sensitive to this limited uncertainty in wind speed. The authors conclude that fuzzy models appear less susceptible to error propagation when compared to full deterministic models of bloom formation based on differential equations.

Another example of the successful use of fuzzy logic to predict cyanobacteria bloom can be found in Laanemets et al. (2006), applied to *Nodularia* in the Baltic, and Blauw et al. (2010) which predicted foam on beaches.

In fuzzy logic, the stated variables are expressed in a qualitative way. A disadvantage of this approach is that it may not develop deeper knowledge on bloom formation by not addressing all of the physical, chemical and biological processes involved. Nonetheless, knowing the probability of bloom occurrence for the next few days, a greater effort for monitoring can be carried out punctually and efficiently, configuring a better and more efficiently monitoring program if bloom events were confirmed and measurements performed.

## **2.5. Regulatory context of lake water quality**

Management actions are usually based on regulatory codes. Therefore, the next sections present the main directives for lakes around the world. Three types of regulation were addressed: (i) regulations related to environmental conservation, (ii) regulations related to direct contact with water, such as recreational water bodies, and (iii) regulations related to drinking water.

### **2.5.1. The guidelines of the World Health Organization**

The World Health Organization (WHO) established exposure risk guidelines for chlorophyll-a, cyanobacterial cell counts, and microcystin. This literature is widely used to determine the risk of exposure to algal toxins. Due to more accessibility in monitoring, it is important to note that chlorophyll-

a concentrations and cyanobacteria cell counts serve as proxies for the potential presence of algal toxins. Therefore, they are also used as an ecological indicator.

Due to the harmful effects of toxic cyanobacteria, water authorities worldwide have adopted management strategies to improve handling of bloom events. The main components of these strategies are the identification of threshold levels, which define the alert levels framework and specific interventions due to the risk involved. For human health protection, three levels of probability for health effects (WHO, 2003a) are defined, based on the presence of cyanobacteria chlorophyll-a:

- (a) Low level, up to 10 µg/L;
- (b) Moderate level, up to 50 µg/L; and
- (c) High level for the formation of scums.

For recreational activities, specific countries normally use an alert framework with two or three levels, based on a short-term cyanobacterial cell numbers or biovolume assessment at the recreational site. The lowest level, 'Surveillance Mode', normally does not imply in any public action, it simply advises authorities to continue or intensify their monitoring. The next higher level, 'Alert Mode', adopted at different levels, is a consequence of an indicator such as microcystin or cyanobacterial cell counts or biovolume (Figure A2 Annex). Different countries have different alert thresholds (Ibelings et al., 2015).

For recreational water bodies, the risk is potentially more difficult to assess because of the numerous points where people may enter or move around the lake and the heterogeneous and rapidly changing distributions of cyanobacterial populations, particularly for scums which may accumulate and be transported by the wind. Therefore, the use of mathematical modelling is a great tool to overcome this difficulty, although no guideline emphasizes its use.

Regarding cyanobacterial toxins other than microcystin, the WHO Guidelines for Drinking-Water Quality consider that there are insufficient data to derive a value for cyanobacterial toxins. Therefore a guideline value for total microcystin (free plus cell-bound) is 1 µg/L in drinking water (WHO, 1998).

The WHO has also proposed an Alert Level Framework for the management of drinking water sources (Chorus and Bartram, 1999), where the criteria can change according to local monitoring history data.

Alert Level 1 represents that the cyanobacterial population is 2,000 cells/mL or 0,2 mm<sup>3</sup>/L biovolume or 1µg/L for microcystins. Values below these limits are classified as Vigilance Level with regular monitoring. Alert Level 1 conditions require action to decide about the continuation of drinking water based on the water treatment efficacy and total toxin detected.

The threshold criterion for Alert Level 2 is cyanobacterial biomass over 100,000 cells per ml (10 mm<sup>3</sup>/L biovolume or 50 µg/L chlorophyll-a), and with the presence of toxins performed by chemical or bioassay techniques. It describes a toxic bloom with high biomass and probably scums regions. Alert Level 2 represents a significant increase in the risk of human health effects from the supply of water by a system with not a enough efficiency.

### **2.5.2. European Water Framework Directive**

In order to mitigate the degradation of water resources and to ensure the sustainability of marine and freshwaters, the European community stated water quality criteria through the Water Framework Directive (WFD) (European Parliament and Council, 2000). The WFD presents indicator parameters

for predicting microbiological health risks and achieving a high level of protection of inland surface waters, transitional waters, coastal waters, and groundwater.

The main objective of the WFD is to assure that all European Member States implement the necessary measures in order to prevent deterioration of the status of all the water bodies and to restore them to a good water status by 2015. It was revised by the Environment Agency to acquire good status in at least 60% of waters by 2021 and in as many water bodies as possible by 2027. According to WFD, good status conveys that the biological and chemical quality elements for the surface water body show a low difference from natural condition.

In the WFD, biological quality elements refer to phytoplankton, macrophytes, phytobenthos, benthic invertebrate fauna, and fish fauna. Regarding phytoplankton, the focus of this study, a good status allows only slight changes in the composition and abundance of planktonic taxa. Such changes do not indicate any accelerated growth of algae, resulting in undesirable disturbance to the balance of present organisms in the water body or to the physic-chemical quality of the water.

About lake monitoring, the frequency should be established respecting the parameter variability resulting from both natural and anthropogenic conditions. The chosen frequency needs to achieve an acceptable level of confidence and precision with at least a 6-month frequency for the phytoplankton and every 3-months for physical-chemical parameters (thermal condition, oxygenation, salinity, nutrients and acidification status). Due to the high dynamic of phytoplankton behaviour this frequency certainly does not capture all phytoplankton growth peaks and associated risks.

In the European Union a specific regulation directed by the Bathing Water Directive (BWD), is applied to bathing waters, a practice which is common for some urban lakes. The first directive in the European Union (EU) was started in the 1970s, with the purpose to safeguard public health and clean bathing waters. More recently, the revised Bathing Water Directive (2006/7/EC) replaces the former one (76/160/EC) (European Parliament, 2006).

This BWD establishes:

- (a) The monitoring and classification of bathing water quality;
- (b) The management of bathing water quality; and
- (c) The provision of information to the public on bathing water quality.

This directive shall be applied to any element of surface water where the competent authority expects people to bath, as well as where a permanent bathing prohibition is not imposed or no permanent advice against bathing has been issued.

The 2006 BWD simplified and updated the rules based on scientific knowledge and environmental management experience, providing clear information to citizens about the quality of bathing waters. According to the directive, every European Member State is required to monitor and assess bathing water quality for at least two parameters (Intestinal enterococci and *Escherichia coli*). A sample needs to be taken shortly before the start of each bathing season, and no fewer than four samples need to be collected and analyzed per bathing season (Annex IV, European Parliament, 2006).

The regulation implements the “bathing water profile”. The public must be informed of the bathing water quality through these bathing water profiles. The profile shall present: (i) a description of the bathing water ( physic, geographic and hydrologic characteristics); (ii) an identification of pollution causes (with the expected frequency and duration) that may impact bathing waters and harm bather health; and (iii) an assessment of the potential of cyanobacteria proliferation, macro-algae and phytoplankton at the monitoring point. Every water management action must be explained.

In addition, if necessary, other parameters could also be considered, such as the presence of cyanobacteria or microalgae. When cyanobacteria blooms occur in bathing water, monitoring need to be performed to catch the health risks. If proliferation does start and risks have been identified, the public need immediately to be alerted and measures taken to prevent exposure.

If short-term pollution is detected, adequate management measures must be taken to prevent, reduce or eliminate the causes of pollution. Actions as surveillance, early warning systems and monitoring are indicated.

Brief information on the bathing water status for each monitored lake is available online through the European Environment Agency website. Additionally, the European Environment Agency (EEA) and the European Commission publish the annual European bathing water quality report that indicates the quality of water for bathing.

While the BWD describes risk assessment and regulations only in general terms, not specifying values for quality parameters other than Intestinal enterococci and *Escherichia coli*, most EU member states have created more specific regulations, most of which are based on analysis of cyanobacterial biomass and criteria of the drinking water. The European Union Drinking Water Directive (EU DWD) provides a general degree of protection, without mentioning cyanobacteria specifically (Ibelings et al., 2015).

### **2.5.3. Clean Water Act of the United States**

In order to restore and preserve the physical, biological and chemical integrity of the waters of United States, the Clean Water Act (CWA) of 1972, establishes regulating quality standards for surface water (USA EPA, 2015).

The National Aquatic Resource Surveys (NARS) has statistical surveys of coastal waters, lakes and reservoirs, rivers and streams, and wetlands with indicators as enterococci, algal toxin (microcystins), chlorophyll-a, phytoplankton and dissolved oxygen. It provides information about lakes and estimates how the main stressors are impacting the lake quality. It also provides a history of the improvement of lake water quality measures. NARS is organized by four individual surveys:

- (a) National Coastal Condition Assessment
- (b) National Lakes Assessment
- (c) National Rivers and Streams Assessment
- (d) National Wetland Condition Assessment

The objective of National Lakes Assessment is to identify the state of the lakes, ponds, and reservoirs across the United States every five years (NLA, 2012). The first data collection was conducted in 2007. The methodology is based on selecting lakes randomly to represent the population of lakes.

To evaluate biological state, trophic state, recreational suitability, and reasons that are affecting the biological quality of lakes, a set of physical, biological, and chemical indicators are used and measured (Table 2.2).

**Table 2.2** - Indicators evaluated for the 2012 National Lakes Assessment from the United States. (NLA, 2012)

Biological	Chemical	Physical	Recreational
Benthic	Acidification	Drawdown	Algal toxin (microcystin)
Chlorophyll-a	Atrazine	Human disturbance	Cyanobacteria
Zooplankton	Dissolved oxygen	Lakeshore habitat	
	Nitrogen	Physical habitat complexity	
	Phosphorus		
	Sediment mercury	Shallow water habitat	

Recreational activities (human use) indicators, presented in the fourth column of Table 2.2 are used to assess whether a lake can support recreational uses such as swimming, fishing, and boating.

To address recreational and human health-related considerations, the NLA examines concentrations of the algal toxin microcystin, along with cyanobacteria cell counts and chlorophyll-a concentrations as indicators of the potential for the presence of algal toxins.

NLA analysts assessed three indicators regarding recreational conditions: 1) Microcystin, a toxin produced by cyanobacteria; 2) Cyanobacteria; and 3) Chlorophyll-a.

While quality criteria values for microcystin are established, other cyanotoxins, or any other algal toxins are not presented. The criteria are based on the WHO guidelines (USEPA, 2009).

#### 2.5.4. Brazil Regulation

One of the study sites of the present research is in Brazil. Therefore, the next sections will address Brazilian regulations, presenting the main CONAMA resolutions and environmental licenses.

In Brazil, one of the objectives of law n° 9.433/97 established that water of appropriate quality, according to its use, shall be assured to current and future generations. This law also establishes the classification of water bodies according to current and potential water uses as one of the instruments of the National Water Resources Management Policy.

CONAMA Resolution No. 357 from 17 March 2005 provides the classification of water bodies (freshwater, brackish or saline) and environmental guidelines. It defines types of water bodies, as well as their classification that will be important for the destination of its multiple uses, such as human consumption, animal watering, leisure, and use in industries.

Fresh water bodies are classified according to the quality required for their prevailing uses in five quality classes:

- (a) Special Class. Water intended for human consumption after treatment with disinfection;
- (b) Class One. Water intended for human consumption after simplified treatment and recreation of primary contact (swimming, water skiing, and diving);
- (c) Class two. Water intended for human consumption after simplified treatment and recreation with primary contact (swimming, water skiing, and diving), irrigation, aquaculture, and fishing activities
- (d) Class three. Water intended for human consumption after conventional or advanced treatment, irrigation with no direct contact, fishing activities, recreation with secondary contact (contact with water is sporadic or accidental, and the possibility of ingesting water is small, as in fishing and navigation) and animal water supply;

(e) Class four. Water intended for navigation and landscaping.

Other parameters are also present in the resolution (a total of 36 inorganic and 56 organic parameters). In Special Class waters, the natural conditions of the body of water shall be maintained.

Resolution 274/00 of CONAMA specifically addresses the use of water bodies for swimming and water sports, such as fishing and navigation. The resolution establishes that the water quality of these bodies should be classified as proper or improper, according to limit values of faecal coliforms (thermotolerant) and *Escherichia coli*, sampled at the same point. Preferably, sampling should be done on days and at locations of greatest use by the public.

Water will be considered improper when, for the point sampled, one of the following occurrences is verified:

- (a) Value obtained at the last sampling is greater than 2500 faecal coliforms (thermotolerant), 2000 *E. coli*, or 400 enterococci per 100 millilitres;
- (b) Presence of solid or liquid waste, including sewage, oil, grease, or other substances capable of presenting health risks or turning recreation unpleasant;
- (c) pH <6.0 or pH > 9.0 (fresh water), apart from natural conditions;
- (d) Algae bloom or other organisms, until it is established that they do not offer risk to human health;
- (e) Other factors that contraindicate, temporarily or permanently, primary contact with water.

In Brazil, another instrument to ensure the availability of water at an appropriate quality are environmental licenses. Although these licenses are not applied exclusively to urban lakes, the focus of this research, a brief description will be provided due to the similarity of monitoring and ecological modelling demands in lakes and reservoirs.

To obtain an environmental license for new projects, such as reservoirs and hydroelectric dams, environmental studies (EIA/RIMA) are required. The EIA (environmental impact study) is a technical document that analyzes the possible impacts generated by a project and suggests alternative technologies and locations. The RIMA (environmental impact report) has the function of clarifying the information contained in the EIA for the population.

Brazil has great hydropower potential. For each new hydropower project, the Brazilian Institute of the Environment and Renewable Natural Resources (IBAMA) emits a Reference Term (TR). This TR aims to determine the comprehensiveness, procedures and general criteria for the elaboration of the EIA and the respective RIMA.

For high impact projects, one of the requirements is to present a specific prognosis of hydrodynamics and water quality resulting from the implementation of the proposed reservoir through mathematical models. The study should present, among other requirements:

- (a) Technical justifications for the mathematical model chosen;
- (b) Model the different systems that will be formed (reservoir, downstream stretch and downstream of the return of flows, in the case of power generation)
- (c) Hydrodynamic model calibration;
- (d) Inform the technical literature used;
- (e) Uncertainties of the model input data;

(f) The output data of the water quality model containing: water residence time, water temperature, dissolved oxygen (OD), Biochemical Oxygen Demand (BOD), phosphorus, nitrogen compounds (nitrogen, nitrite, and nitrate) and chlorophyll-a;

(g) Evaluate through simulated results the possibility of thermal, chemical and biological stratifications.

Due to the high potential of water in Brazil for water supply and electricity generation, the scope of the current research can also be applied in other areas beyond urban regions.

## 2.6. Urban lake characteristics and challenges

Urban lakes are frequently part of the urban stormwater drainage network and offer a diversity of recreational activities, contributing to the landscape composition and urban quality of life. They are increasingly recognized as essential biotopes for maintaining ecological continuities and for supporting biodiversity in urban and peri-urban areas.

Global changes and anthropic activities in densely occupied catchments of urban lakes result in heavy pressures that strongly affect lake water quality. High nutrient loads boost the production of phytoplankton biomass. Associated with heat waves, high nutrient loads also increase the occurrence of cyanobacteria blooms, which may affect the uses of the lake. As an example, in situations in which the body is used as a source of drinking water, a potential degradation factor for water quality may result in a risk for the urban water supply (Li Wei et al., 2013; Melo et al., 2017).

There is increasing interest worldwide about the protection and management of urban lakes. This can be seen stated in the Millennium Development Goals from United Nations (United Nations, 2015) and in the European Union Water Framework Directive (European Parliament and Council, 2000). On a global scale, the majority of lakes are small lakes with an area smaller than 1 km<sup>2</sup> (Downing et al., 2006). For example, in the Île-de-France region around Paris, 99% of lakes have an area smaller than 0.5 km<sup>2</sup>, which is the minimum size for lakes monitored within the European Water Framework Directive (Soulignac et al., 2017). However, it is recognized that in some regions where there are many small water bodies, this directive needs to be adapted (REFCOND, 2003).

Urban lakes have been less studied than non-urban ones, and more knowledge about their ecological functioning is required for improving their management (Birch and McCaskie, 1999a; Gong et al., 2016; Soulignac et al., 2017).

For good lake management, modelling how phytoplankton populations dynamically change is very useful. However, the high complexity of the nonlinearity of water variables and their interactions make modelling phytoplankton growth rather challenging (Zhang and Lou, 2017; Gong et al., 2016)

Even in small and shallow urban lakes, the spatial distribution of phytoplankton biomass generally displays large heterogeneities (Ibelings et al., 2003; Pobel et al., 2011; Porat et al., 2001; Welker et al., 2003). Therefore, three-dimensional modelling is required for simulating the spatial heterogeneity of phytoplankton distribution and, more specifically, of cyanobacteria biomasses, which have the potential to produce toxins (Leon et al., 2011; Gong et al., 2016).

Hydrodynamic behaviour in shallow urban lakes is complex due to weak stability (Pobel et al., 2011; Soulignac et al., 2017). This limited stability causes alternating periods of thermal stratification and mixing condition events (polymictic lakes). Hence, ecological processes and lake water quality are strongly affected by hydrodynamics. Therefore, three-dimensional models support the understanding and prediction of lake ecosystem behaviour in response to many external pressures, such as climate forcing, nutrient loading, and pollutant input (Chanudet et al., 2012; Evelyn Aparicio Medrano et al., 2013; Soulignac et al., 2018).



External forcing is generally very heterogeneous in space and time, such as stormwater inflow and meteorological conditions. In shallow lakes, meteorological forcing may impact the greater part of the water column, affecting physical-chemical and biological processes. Processes involved in phytoplankton distribution in space and time occur all over the system at all time scales, from chemical reactions within seconds, through phytoplankton growth in day-night cycles, to population density changes over seasons and the interannual variability in the appearance and the disappearance of phytoplankton species (Khac et al., 2018). As a result, high-resolution and high-frequency measurements are necessary to capture all changes to and the relationship between factors, such as mixing of the water column, light, and nutrient availability.

These factors influence the physiological rhythm of phytoplankton. To fully grasp the spatial and temporal variations of phytoplankton communities, it is important to develop efficient monitoring programs. This helps with the analysis of the evolution of various impacts of external forcing, and achieves an efficient management of water resources and the protection of aquatic ecosystems.

Measuring devices provide essential observations on the functioning of urban lake ecosystems. Providing data and tools for the hydrodynamic, physical-chemical and biological processes occurring in lakes is vital to perform extensive research on ecological processes.

Monitoring and modelling play an important role to better comprehend and predict urban lake ecosystem behaviour and help with lake management challenges. Warnings of ecological state and knowledge of lake dynamics help create and modify a lake management plan (Grimm et al., 2000). Thus, efficient monitoring and modelling systems are increasingly required for the management of lake ecosystems and freshwater bodies in general. Mathematical models are important tools to understand the spatial heterogeneity and temporal distribution of water quality in lakes and the sensitivity to external driving forces in different scenarios (Yi et al., 2016).

## **2.7. Lake Champs-sur-Marne study site**

One of the study sites in this research is Lake Champs-sur-Marne in France. In this section, a brief presentation and discussion of previous studies conducted at this lake is presented. The lake is a small and shallow urban lake located near Paris, France. A complete description of this lake can be found in section 3.1.

Scriban (2015), using the Delf3D-FLOW model, performed a sensitivity and calibration study for the thermal behaviour of Lake Champs-sur-Marne. The calibration methodology applied will be explained in this section because it was taken as a basis for the current research.

Meteorological data were obtained from the Orly airport meteorological station. Orly airport is about 22 km southwest of the lake. Wind intensity and direction measurements are carried out 10 m above the ground. As Lake Champs-sur-Marne is small, the wind that reaches the surface of the lake is greatly influenced by the trees around the lake. Therefore, the evaluation of a reduction factor of wind intensity was applied.

The parameters evaluated in the hydrodynamic model calibration were: Secchi depth (water transparency), a reduction factor of wind intensity and water albedo. Albedo is defined as the ratio of irradiance reflected to the irradiance received by a surface.

With an initial water temperature from field measurements, meteorological data were used as input values in the model. An evaluation of water transparency values with a range between 0.5 and 3 m, in 0.5 m intervals, was carried out for the period from 23<sup>rd</sup> June to 06<sup>th</sup> July 2015 (13 days). The best results, based on the mean absolute error (MAE) and the coefficient of determination ( $R^2$ ) of agreement

between calculated and observed data for 3 depths (surface, middle, and bottom depths), were with a water transparency of 1.0 m.

With the Secchi value fixed at 1.0 m (representing 1.0 m of water transparency), a range of wind factors between 0.50 and 1.0 were tested with variation intervals of 0.1 m. The best results were obtained with a wind factor of 0.6 (meaning 40% wind intensity attenuation).

A range of albedo values from 0.06 to 0.1 were also tested. This parameter is used to calculate the input solar radiance used in the simulation. The best result was obtained with an albedo of 0.08 (meaning that only 8% of the irradiance does not penetrate the water body).

However, analyzing the results obtained, even the best results presented temperatures at the bottom which were too high, as well as an evolution of the temperature in the middle of the water column with excessive values during the day, inconsistent with measured values. Therefore, with albedo fixed at 0.08 and wind factor at 0.6, the Secchi values were tested again, but with a variation of 0.1 m instead of 0.5 m.

The best results were with a Secchi value of 0.7 m. The agreement with measured values was very good, presenting a MAE of 0.51, 0.50 and 0.34 and  $R^2$  of 0.924, 0.916 and 0.916 respectively, for the surface, middle and bottom depths.

This calibration methodology allowed for considerable improvement in the results. Comparing the mean with the three depths evaluated, the model performance indicators during calibration achieved initial values of MAE of 0.95 °C and  $R^2$  of 0.365 and ended with an MAE of 0.45 °C and  $R^2$  of 0.905.

Huguenard (2015) observed that, for Lake Champs-sur-Marne, water temperature is the most influential parameter on Cyanobacteria occurrences (*Microcystis*, *Aphanizomenon* and *Anabaena*). Cyanobacteria development is lower in extreme temperatures. However, another hypothesis for this behaviour is the competition between species, with the presence of dinoflagellates being the possible cause for Cyanobacteria low development at higher temperatures (Peiffer, 2016).

Through the database, the following outcomes were observed: three genera of cyanobacteria develop at air temperatures above 13 °C; *Aphanizomenon* shows higher biomass for temperatures above 22°C; the genus *Microcystis* does not develop at temperatures above 20 °C, and *Anabaena* shows higher biomass for temperatures between 17 and 19 °C.

In order to analyze the relationship between air temperature and cyanobacteria biomass, the degree-day method was applied to the 2015 dataset (Peiffer, 2016). This method (McMaster and Wilhelm, 1997) consists of calculating heat accumulation for the growth of the organisms. The reference temperature adopted was 13° C, according to previous observations. The average air temperature of the previous 10 days was used. A very significant correlation was obtained ( $r = 0.81$ )

This correlation shows that an accumulation of warm days is a variable which influences the growth and biomass of phytoplankton.

Khac et al. (2018) used high-frequency measurements (every 5 minutes) of physical-chemical variables (water temperature, conductivity, pH, dissolved oxygen), chlorophyll-a fluorescence (proxy of total phytoplankton biomass), and phycocyanin fluorescence (proxy of cyanobacteria biomass) to observe that periods of cyanobacteria blooms correspond with phytoplankton development during lake stratification. The authors used the average ratio of phycocyanin to chlorophyll-a ( $\mu\text{g Chl-aL}^{-1}/\mu\text{g PCL}^{-1}$ ) to reinforce this conclusion.

Khac et al. (2018) also highlighted that the use of high-frequency monitoring was able to detect hourly, daily and seasonal variations of different environmental and ecological variables that would not be possible to observe through weekly or monthly sampling, the more traditional measurement approaches.

## 2.8. Lake Pampulha study site

The other study site in this research was Lake Pampulha in Brazil. In this section, a brief presentation and discussion of previous studies conducted on this lake is presented. Silva (2014) applied an integrated modelling approach to the lake and its watershed. For modelling the quantity and quality of urban runoff in the lake watershed, the model chosen was the StormWater Management Model - SWMM 5.0. The SWMM model was calibrated using an automatic calibration routine based on a genetic algorithm. The Nash-Sutcliffe coefficients obtained via SWMM calibration and validation were 0.70 and 0.72, respectively. The unidimensional model DYCD, short for DYRESM-CAEDYM (dynamic reservoir simulation model-computational aquatic ecosystem dynamics model) was applied to simulate the phytoplankton dynamics in Lake Pampulha.

With initial physical, chemical, biological conditions and meteorological forcing the DYCD model was calibrated and validated for the simulation of phytoplankton dynamics before being coupled with SWMM model. The DYCD model has more than 70 parameters for the simulation of each phytoplankton group. The values of each parameter also depend on the specific characteristics of the ecosystem. To identify the parameters that could significantly influence phytoplankton dynamics, a sensitivity analysis was conducted. The value of each parameter was changed and the impact on the model performance was recorded. After the sensitivity analysis, 18 parameters proved to affect the model's performance by more than 10% in the prediction of phytoplankton biomass. These parameters were then used in the model calibration. Most of these parameters were about algal physiology and algal stoichiometry.

Concerning the calibration performed, the frequency of available temperature data was monthly, thus the model was just able to represent in general terms the dominant processes that occur in the water. Concerning the biomass of cyanobacteria, the results of DYCD were also compared with a low amount of data (8 values from April 2008 to March 2010 and 14 values from October 2011 to October 2012). The model could reproduce the general trends of growth and decrease in phytoplankton biomass. The ecological model was unable to represent the high variability of observed total suspended solids (TSS) and nutrient concentrations. The model was not able to reproduce total phosphorus (TP) and  $\text{NO}_3^-$  concentrations. For most of the observed concentrations, a lower variation was presented in the simulated concentrations results, in which TP concentrations were overestimated and  $\text{NO}_3^-$  were underestimated (Silva et al., 2019).

Belico (2017) investigated the dynamic of the Lake Pampulha in relation to rain episodes using monthly samples performed during 2013 and 2015, and high-frequency temperature measurements at water surface during 2011 to 2015. The model obtained a Root Mean Square Error (RMSE) with a range of 0.59 to 1.01 °C for thermal profiles and 1,08 °C for surface high-frequency measures. The simulated water temperature presented an overestimation during winter seasons. The phytoplankton biomass model presented high sensitivity for physiology parameters. The RMSE was in the range of 72.31 to 86.17  $\mu\text{gChl-a/L}$ . The nutrient concentrations were not calibrated and validated. Using the measurement values and the General Lake Model (GLM-AED) model results, the author concluded that rainfall events during summer were not able to change the stratification condition to a mixing condition. During winter and dry seasons, a mixing condition was more observed, accompanied or not by rainfall events. Concerning the impact of rainfall in the ecological of the lake the author concluded that the conductivity and chlorophyll concentration decrease during rainfall events and present lower daily amplitude. The author also highlighted that the phytoplankton biomass migrates to deeper depth during rainfall events (2 to 4 meters deeper).

In the present research, analyses will be performed through high-frequency measurements for Lake Pampulha. Measurements were performed at surface (0.5 m), 2.5 m, 5.5 m and bottom (9.5 m). The measurement in high-frequency performed in these four depths will be compared to three-dimensional hydrodynamic model results, allowing a deeper analysis of the lake hydrodynamics.

### 3. MATERIALS AND METHODS

In the present research, two experimental study sites were investigated: Lake Champs-sur-Marne, a small and shallow urban lake in France, and Lake Pampulha, a medium-sized and shallow urban reservoir in Brazil.

Lake Champs-sur-Marne (Figure 3.1), created as a result of sand extraction, is a small and shallow lake, with a water surface of 0.12 km<sup>2</sup>, an average depth of 2.3 m, and a maximum depth of 4.0 m. It is mainly fed by groundwater flowing from the water table of the nearby Marne River.

Lake Pampulha was built in the 1930s for many purposes, including drinking water supply. The lake has a water surface area of approximately 2.0 km<sup>2</sup> and a volume of about 10 million m<sup>3</sup>, according last bathymetry measured in November 2014. Its maximum depth is 16 m and the average depth is 5 m. The Lake Pampulha catchment, composed of 8 main tributaries, has a surface area of about 98 km<sup>2</sup> and approximately five hundred thousand inhabitants. It is a very urbanised area with more than 70% of the surface anthropised (Matos et al., 2017).

This research focuses on the time evolution of phytoplankton biomass and the lake hydrodynamic behaviour over short periods using a three-dimensional model and high-frequency measurements. The third chapter presents the two sites studied in the section 3.1, the measurement devices for each lake in the section 3.2, the model formulations are presented in the section 3.3, the model configuration and parameters in the section 3.4, the inputs for the performed simulations are present in the section 3.5 for Lake Champs-sur-Marne and in the section 3.6 for Lake Pampulha, and the mathematical indicators used to evaluate the model performance in the section 3.7.

#### 3.1. Study Sites

##### 3.1.1. Lake Champs-sur-Marne

The study site, Lake Champs-sur-Marne, is located about 20 km east of Paris (Figure 3.1) in a green space. The park has a surface area of 0.4 km<sup>2</sup> and is frequented by children from a nearby urban area. Recreational activities include kayaking, sailing, swimming, wall-climbing, and soccer, among others.



**Figure 3.1** – Location of Lake Champs-sur-Marne. Adapted from Google Earth®

Aerial photos (Figure 3.2) show the lake region during the sand extraction quarry which formed the lake. The lake is filled mainly by groundwater, flowing from the water table of the nearby Marne River,

currently located around 80 m north of the lake. The lake has been developed as a leisure base by the Department of Seine-Saint-Denis since the 1970s (Huguenard, 2015).

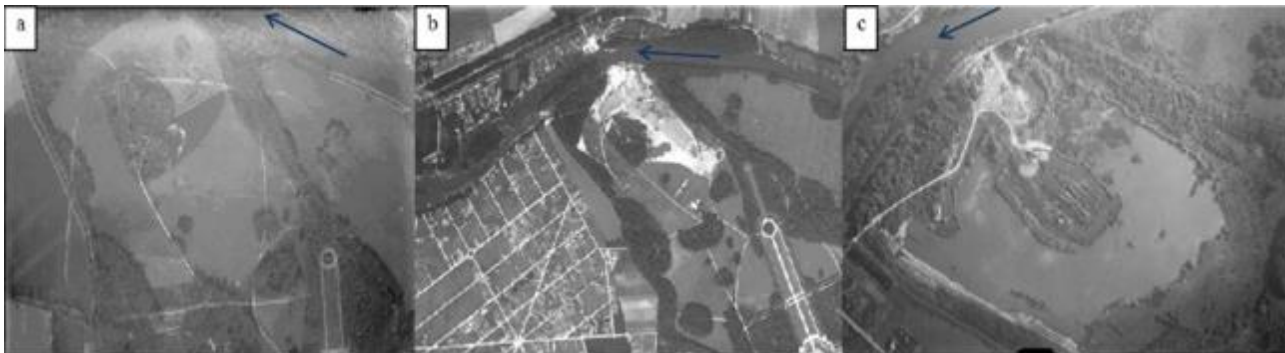


**Figure 3.2** – Lake aerial photographs. a) 1923 b) 1933 c) 1946 Source: Géoportail® from Huguenard (2015)

After an extensive flood in 1970, the morphology of the lake was modified by the rehabilitation of the banks on its northeastern boarder (Figure 3.3). This part of the lake, which is the closest to the river, was regularly impacted by flooding of the Marne river.



**Figure 3.3** – Aerial photographs (a) before the flood in 1969, (b) during a flood in 1970 and (c) after the morphology adaptation in 1971 (source: Géoportail® adapted by (Huguenard, 2015)

Another important characteristic is the island in the centre of the lake. Some parts were reprofiled in order to soften their banks. A channel (dead arm) located on the eastern side, which had accumulated an enormous amount of organic matter, has been filled in with material from the reprofiling of the banks (Figure 3.4), between approximately 2009 and 2014. The reason for this intervention was not clear for the current lake manager, although it was probably performed due to poor water quality in this channel.



**Figure 3.4** – Channel grounding on the island. Source: Adapted from GoogleEarth®. Left: August 2005; Right: April 2014

Two principal channels divide the main island (Figure 3.5), both have 1.3 m deep and less than 150 m long.



**Figure 3.5** – Main features of the island. Source: Adapted from Google Earth®

A small island was also created in the south part of the lake to provide a nesting area for birds (Figure 3.6).



**Figure 3.6** – Small island created in the south part of the lake in red circle. Source: Adapted from GoogleEarth

Since the late 1990s, birds have been regularly present on the lake. The dominant species are *Phalacrocorax carbo* (great cormorant), which are found mostly in the winter, *Branta canadensis* (Canada geese) throughout the year, and *Ardea cinerea* (grey heron). Other species present include the common gallinule (*Poule d'Eau*), great crested grebe (*Grêbe Huppée*), and mallards (*Canard Colvert*). These birds are mainly located on and near the central island. Measures to regulate bird populations have been implemented by means of cutting trees and scaring systems, but with limited success.

Ornithological monitoring was also carried out by CORIF (Centre *ornithologique d'Île-de-France*) until 2008, before being taken over by agents of CD 93 (Seine Saint-Denis County), to monitor the evolution of the most important populations present at the lake and associated health risks.

Since 2004, sanitary problems have appeared due to fecal indicator bacteria and to the presence of cyanotoxins, caused by the proliferation of cyanobacteria. Since then, swimming in the lake has been repeatedly banned in the summer because of potential health risks caused by toxic cyanobacteria blooms.

The northern part of the lake has two beaches for swimming. The small beach was first delimited by floating buoys in the late 1980s and restored in the early 1990s. Deposits of sediments were dragged up and replaced by laying an impermeable tissue and a layer of gravel and sand. Currently, the water at the

small beach does not communicate with the lake (Figure 3.7). According to park employees, approximately 10% of its total volume of water is manually renewed daily through hoses from the park.



**Figure 3.7** – Small beach. Photo: author, March 2017

The large beach was created more recently, first by floating buoys, then by a floating bridge made of wood and stainless steel (Figure 3.8). A net has been placed under the floating pontoon to limit the expansion of filamentous algae. A rotary harrow aerated the water. Barley straw and aerators were set up between 2010 and 2012 to try to solve the problem of cyanobacteria and to mix the water column. The barley straw was put in bales under the floating bridge, and the aerators were fixed between the pontoon and the net.



**Figure 3.8** – Large beach and equipment installed. Photo: author, March 2017

In April 2006, 4100 kg of Aquaclean P (a nitrophilic-bacteria-based product) were gradually poured in the water over three days to increase its transparency. Other products such as herbicides and algacides were used to manage the macrophytes present in the water body, which presented a constraint for the passage of boats. A sediment analysis, which was carried out following dredging in 2008, highlighted the high load of nutrients and copper near the beaches and the central island. The exported sediments were deposited on the island (Huguenard, 2015).

Since 2012, there have been continuous occurrences of algae blooms and no new solution for improving the lake water quality has been proposed. MNHN suppose low oxygen and high cyanotoxin concentrations to be the main causes of fish death, which occurred in 1990, 2000, 2010 and September 2015 (Huguenard, 2015).



### 3.1.2. Lake Pampulha

Lake Pampulha is an artificial reservoir located in Belo Horizonte, a city of 2.5 million inhabitants (IBGE, 2014) located in the Southeast region of Brazil. Lake Pampulha and its modern urban ensemble were designed by architect Oscar Niemeyer and built in the 1940s.

The lake was created in 1938 and was first conceived to fulfil multiple objectives: water supply, flood control, urban landscape, leisure and amenity provision. Due to an intense urbanisation process in the Pampulha stream catchment from the 1970s on, the lake water quality was severely compromised, leading to the interruption of drinking water provision from the 1980s with frequent cyanobacteria blooms and lake siltation (Silva, 2014). The climate characteristics of the lake were described by Silva (2014) and summarized in Table 3.1. A hydrographic map of the Pampulha catchment with the location of Lake Pampulha and its 8 tributaries can be found in Figure 3.9.

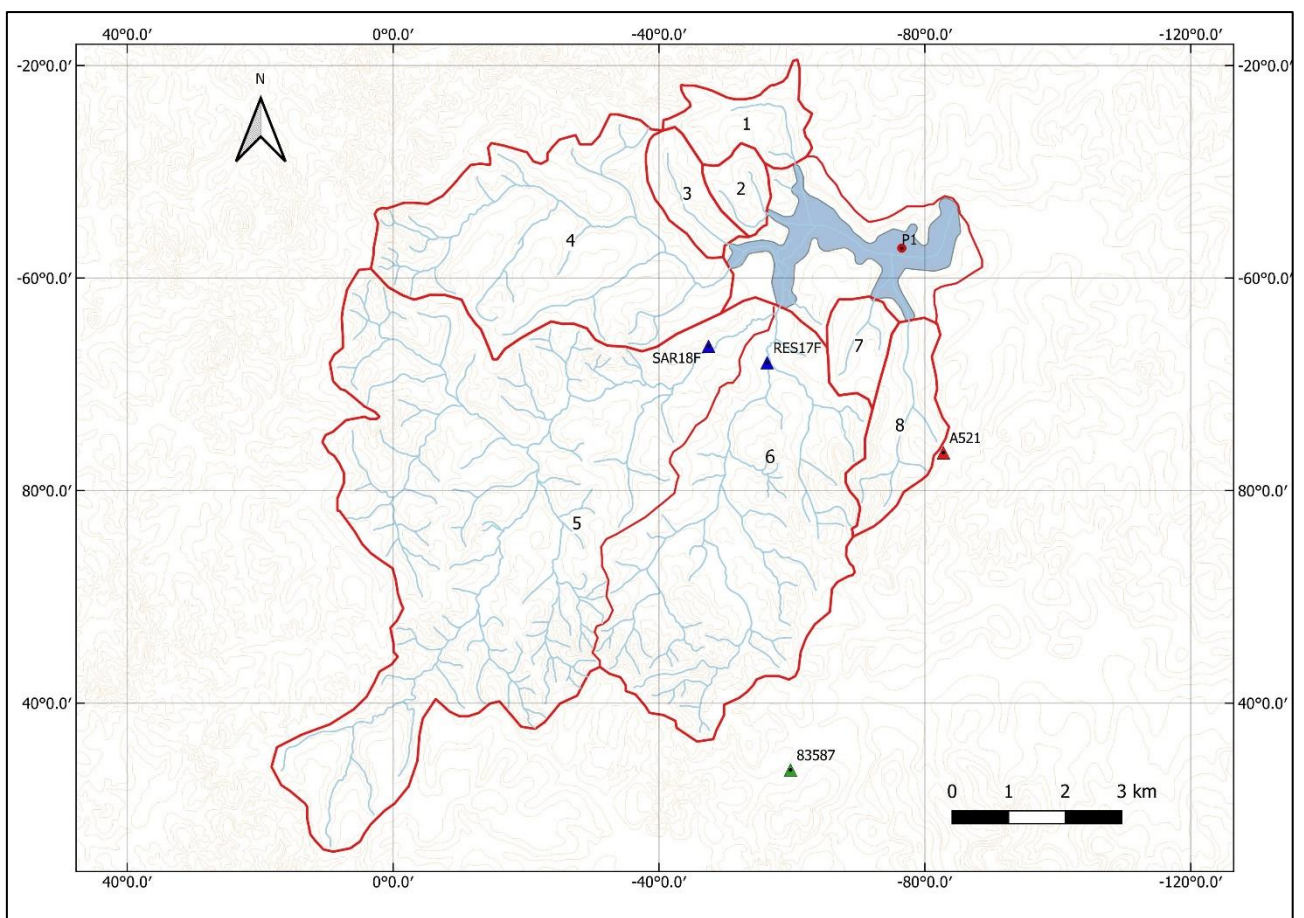


**Figure 3.9** – Localization of Lake Pampulha and its tributaries: (1) Olhos d'água; (2) AABB\*; (3) Bráunas; (4) Água Funda; (5) Sarandi; (6) Ressaca; (7) Tijuco and (8) Mergulhão. \*river not named, popularly known as AABB (Associação Atlética Banco do Brasil – Athletics Association from Brazil Bank). Red lines are the respective catchment of the tributaries. Monitoring station in triangle: (1) Fluviometric (SAR18F – Sarandi and RES17F – Ressaca; (2) Meteorological (A521 -UFMG and 83587 - Belo Horizonte); (3) Lake monitoring in red cycle (P1)

**Table 3.1** – Lake Pampulha climate characteristics for values measured between 1961 and 2001 at Belo Horizonte’s meteorological station from INMET. Source: (CPRM, 2001)

Climate	Tropical altitude
Air temperature	Maximum monthly of 28.8 °C (February)
	Minimum monthly of 13.1 °C (July)
Dry season	April to September (monthly minimum 14 mm)
Rainfall season	October to March (monthly maximum 320 mm)

Due to high sedimentation, dredging works have been carried out in Lake Pampulha in 1979, 1996, 2000-2006 and 2013-2014 (Silva, 2014).

In 2003, within the framework of the Pampulha Lake Watershed Recovery and Environmental Development Program (PROPAM), a fluvial water treatment plant (ETAF) was established after the confluence of the Ressaca and Sarandi rivers, the main tributaries to Lake Pampulha. The treatment capacity of this plant is 750 L/s. This flow corresponds to the dry season average flow of the Ressaca and Sarandi streams (Silva, 2014).

Lake Pampulha and its catchment have been monitored since 2011 under a collaborative project between the municipality of Belo Horizonte and UFMG. The lake is part of a long-term collaborative research project involving LEESU-ENPC and UFMG, which also started in 2011.

In 2016, the lake Pampulha has become a UNESCO World Heritage site, which boosted public sector to seek for water quality improvement actions. Thus, through the consortium *Pampulha Viva* (comprised of the companies CNT Ambiental, Millennium Tecnologia Ambiental e Hidrosciência) the municipality of Belo Horizonte (PBH) committed to invest about R\$ 30 million for recovering the water quality of Lake Pampulha over 12 months, starting in March 2016 (Diário Oficial do Município, 2016). Phoslock® and Enzilimp® were applied in the lake in order to remove phosphorus from the water column and to reduce coliforms and the Biochemical Oxygen Demand – BOD (Barçante et al., 2020). The treatment was renewed for another year at the cost of about R\$ 16 million. Efforts to improve sanitation infrastructure in the Pampulha catchment were also carried out aiming at collecting 95% of sewage at an investment of R\$ 875 million from 2004 to 2016 (PMS, 2017).

Even after major efforts to improve sanitation infrastructure in the Pampulha catchment, episodes of blooms in Lake Pampulha are still frequent (Photo 1).



**Photo 1** – Presence of algae in Lake Pampulha. (Photo: author, 22 July 2018)

## 3.2. Measurements

### 3.2.1. Lake Champs-sur-Marne

#### 3.2.1.1. Bathymetry

Lake Champs-sur-Marne bathymetry was measured in August 2016 (Figure 3.10) using an echo sounder, a Global Position System (GPS) and a small boat at low navigation speed. During measurement, a spacing of 20 m between the trajectories from west to east was approximately maintained.

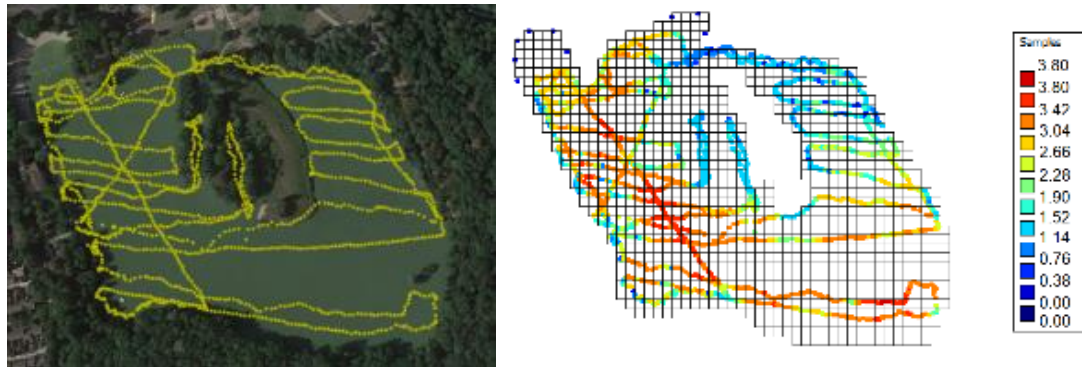


**Figure 3.10** – Trajectory of bathymetry measurement in the lake and depth

#### 3.2.1.2. Phytoplankton Sampling

Since 2006, in order to comply with bathing regulations in France (Parlement européen, 2006) to identify cyanobacteria species, phytoplankton biomass has been monitored near the large beach, where children usually swim. Samplings are taken by the county of Seine-Saint-Denis (93) and the *Muséum National d'Histoire Naturelle* (MNHN) at a frequency that varies from monthly, between November and January, to weekly, between April and October.

Based on laboratory biomass extraction and spectrophotometric analysis of samples taken on the floating bridge from the large beach (Figure 3.8), the evolution of the phytoplankton biomass between 2006 and 2015 (Figure 3.11) was studied by Peiffer (2016). It shows high total Chlorophyll-a concentrations during most summers and peaks of Chlorophyll-a concentrations associated with cyanobacteria. These values indicate a strong dominance of Cyanobacteria (Huguenard, 2015; Peiffer, 2016).

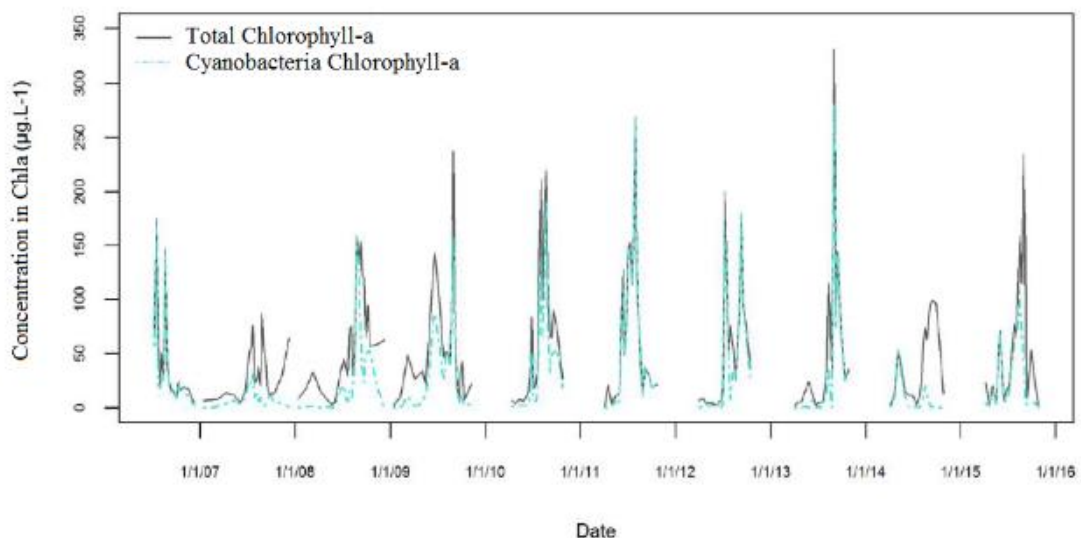


**Figure 3.11** – Total biomass of phytoplankton and biomass of cyanobacteria expressed as chlorophyll-a (Chl-a). Source: Peiffer, (2016)

According to Peiffer (2016), the main phytoplankton groups observed in the lake during the last decade (2006-2015) are Green algae, Diatoms, Cyanobacteria, and Dinoflagellates. During summer the dominant groups (Figure 3.12) are (i) Cyanobacteria (mainly *Anabaena*, *Aphanizomenon* and *Microcystis*), and (ii) Dinoflagellates (mainly *Ceratium* and *Peridinium*) (Peiffer, 2016).

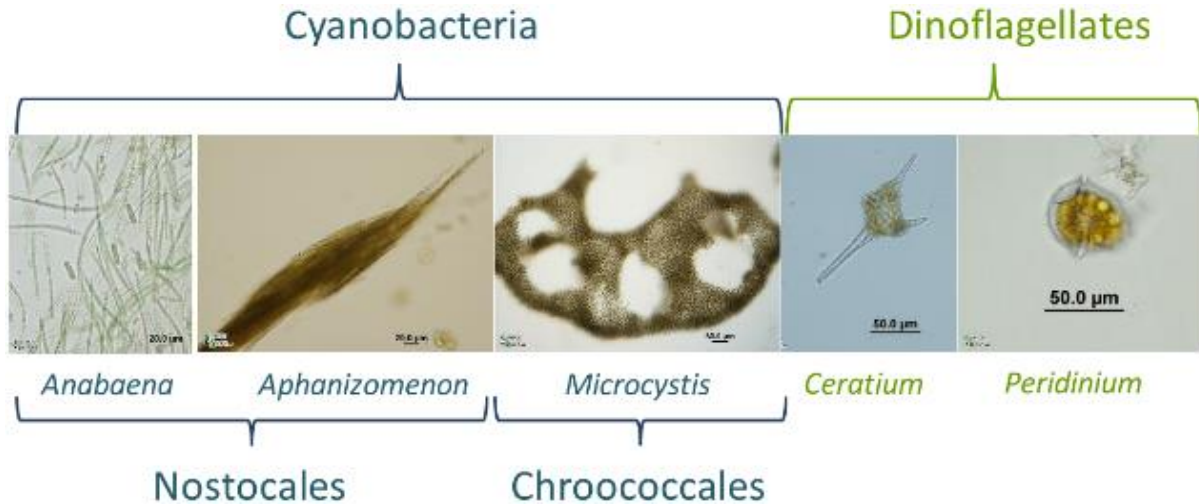


**Figure 3.12** – Main phytoplankton groups observed in the lake over the last decade (2006-2016) during summer. Source: Peiffer, (2016)

The dynamics of phytoplankton succession was described by Huguenard (2015) and generally happens as follows:

*Anabaena* appears first during the year, followed by *Aphanizomenon* and then by *Microcystis*. The genus *Aphanizomenon* reaches maximum annual biomass between mid-July and the end of August. *Aphanizomenon* developed very little in 2014 and did not exceed the concentration of 4 µgChl-a/L.

The genus *Anabaena* reached a maximum concentration of 148 µgChl-a/L in 2012. It developed very little in 2011 with a concentration less than 6 µgChl-a/L. The maximum annual biomass of *Anabaena* is reached between May and August, either before or simultaneously with the genus *Aphanizomenon*. There is a peak of annual development and sometimes smaller development peaks as in 2008 and 2015.

Cyanobacteria of the genus *Microcystis* had a maximum concentration of 173 µgChl-a/L in September 2012. Their development is indeed greater between August and September.

Nitrogen-fixing cyanobacteria, such as *Anabaena* and *Aphanizomenon*, develop at the beginning of summer. In sequence, non-nitrogen fixing cyanobacteria appear, such as *Microcystis*. It is then assumed that the senescence of diazotrophic cyanobacteria biomass provides the necessary nutrients for the development of *Microcystis*. This happens because the decomposition of detritus results in nutrient bioavailability through mineralization. Nutrients can become available in the water column through the remineralisation process of organic matter and autolysis. Autolysis represents the fraction of dead cells which are directly available (dissolved) to grow new algae through cellular degeneration (Los, 2009).

### 3.2.1.3. High-frequency measurements

Since May 2015, as part of OSS-Cyano project framework funded by the French Research Agency (ANR), high-frequency monitoring has been implemented. Sensors fixed under buoys have been continuously measuring temperature, dissolved oxygen, conductivity and chlorophyll-a (Chl-a) fluorescence at a 5-minute time step (Figure 14) at three points: A, B, and C. According to the bathymetry, each monitoring point has a respective depth of: A, 3 m; B, 2.8 m; and C, 3.2 m.

High-frequency measurements of temperature, conductivity (NKE), and dissolved oxygen (Anderaa) are performed at 3 depths (0.5, 1.5 and 2.5 m).

A Turner Design optical sensor measures the Chl-a Fluorescence in the middle of the water column (1.5 m). The sensor is an accurate single-channel detector. It is designed for integration into multi-parameter systems from which it receives power and delivers a voltage output proportional to the concentration of the fluorophore, particle, or compound of interest (Turner Design, 2017). The sensor has technical specifications presented in Table 3.2.

**Table 3.2** – Technical specification of Lake Champs-sur-Marne devices for Chlorophyll-a

Variable	Point	Measuring range	Wave-length	Detection Limit
Chlorophyll-a	A & C	0 to 50 $\mu\text{gChl-a/L}$	460 nm (excitation) and 696 nm (emission)	0.03 $\mu\text{g/L}$
	B	0 to 500 $\mu\text{gChl-a/L}$		

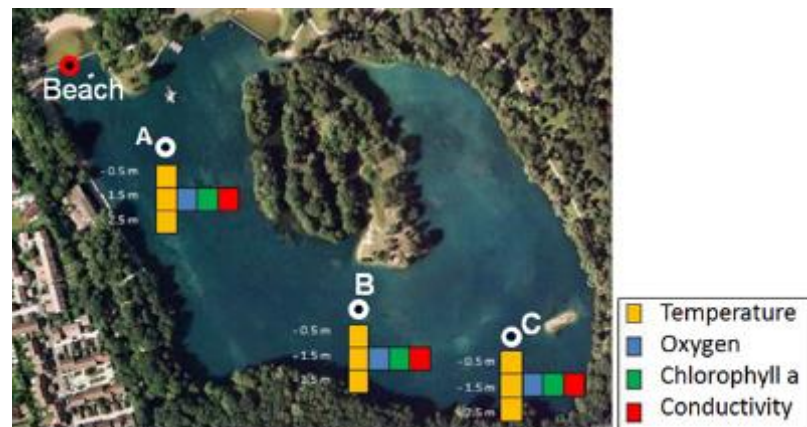


**Figure 3.13** – Location of the monitoring points on the lake of Champs-sur-Marne

The measurements of chlorophyll-a at 5-minute intervals present great temporal variability. Additionally, some measured values are not representative of the actual phytoplankton concentrations due to biofouling in the sensor of the multi-parametric probe (MPx™, NKE, France). Therefore, treatment was carried out to validate the data.

For the data treatment, the criterion used was that the current concentration (at time step  $t$ ), for values greater than 10  $\mu\text{gChl-a/L}$ , cannot have increased by more than 2 times the average concentration of the last 30 minutes. If the value was exceeded this, it was not considered in the time series. Figure 3.14 shows the flowchart used in the treatment process. Empirical observation of the time series (ANNEX 8.3) was used as a basis to define the criterion cutoff as greater than 2 times.

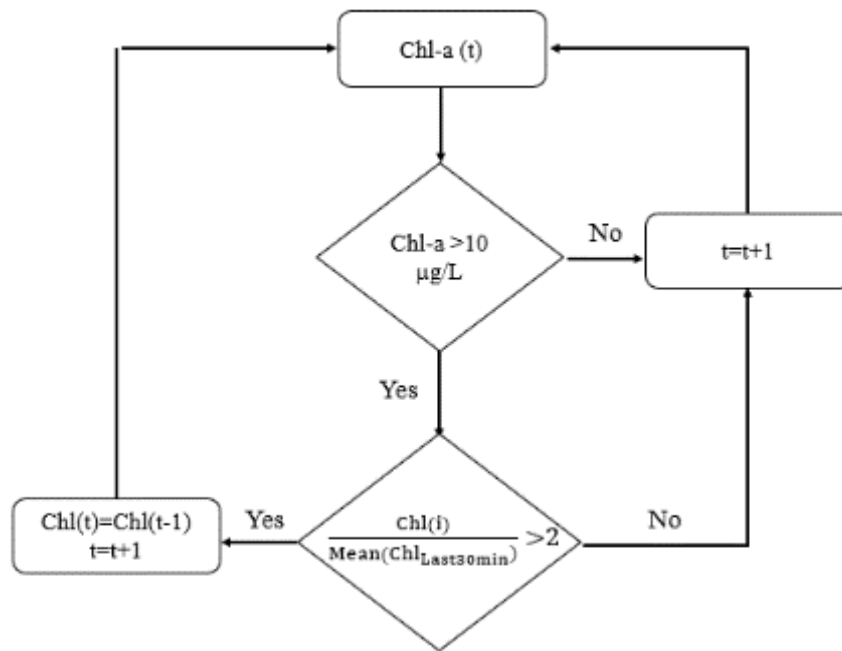


**Figure 3.14** – Treatment flowchart for Chl-a.

For the daily duration, boxplots at Points A and B are present in Figure 3.15 and Figure 3.16. The outliers were discarded. Figures 16 and 17 also show that in some period, heterogeneity was observed on the lake, even between points A and B, which were close to each other. For example, on 19 January 2016 and 8 March 2016, point B presented two times the values of point A.

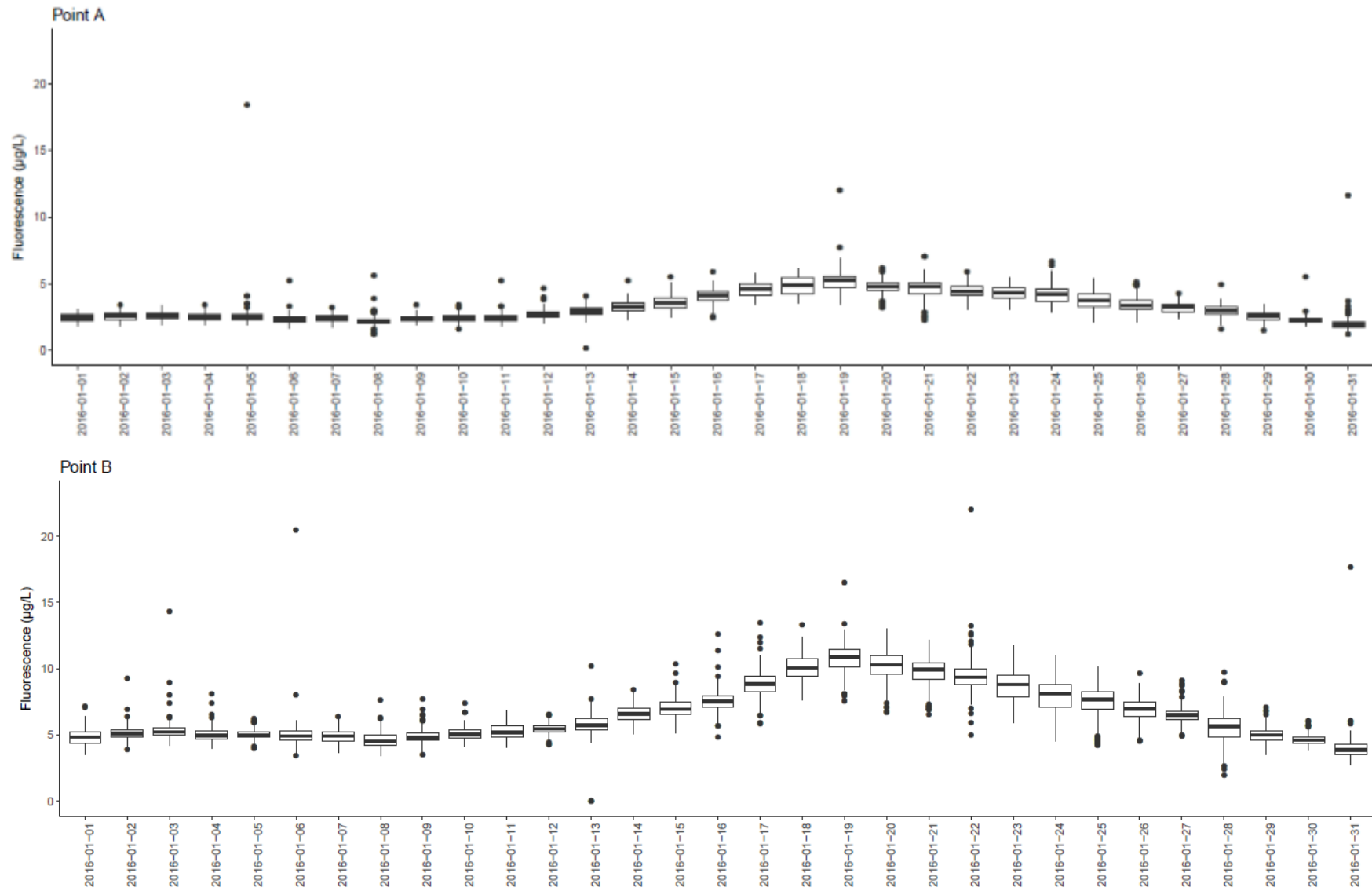


**Figure 3.15** – Daily boxplot for chlorophyll-a fluorescence measured at points A and B during January 2016

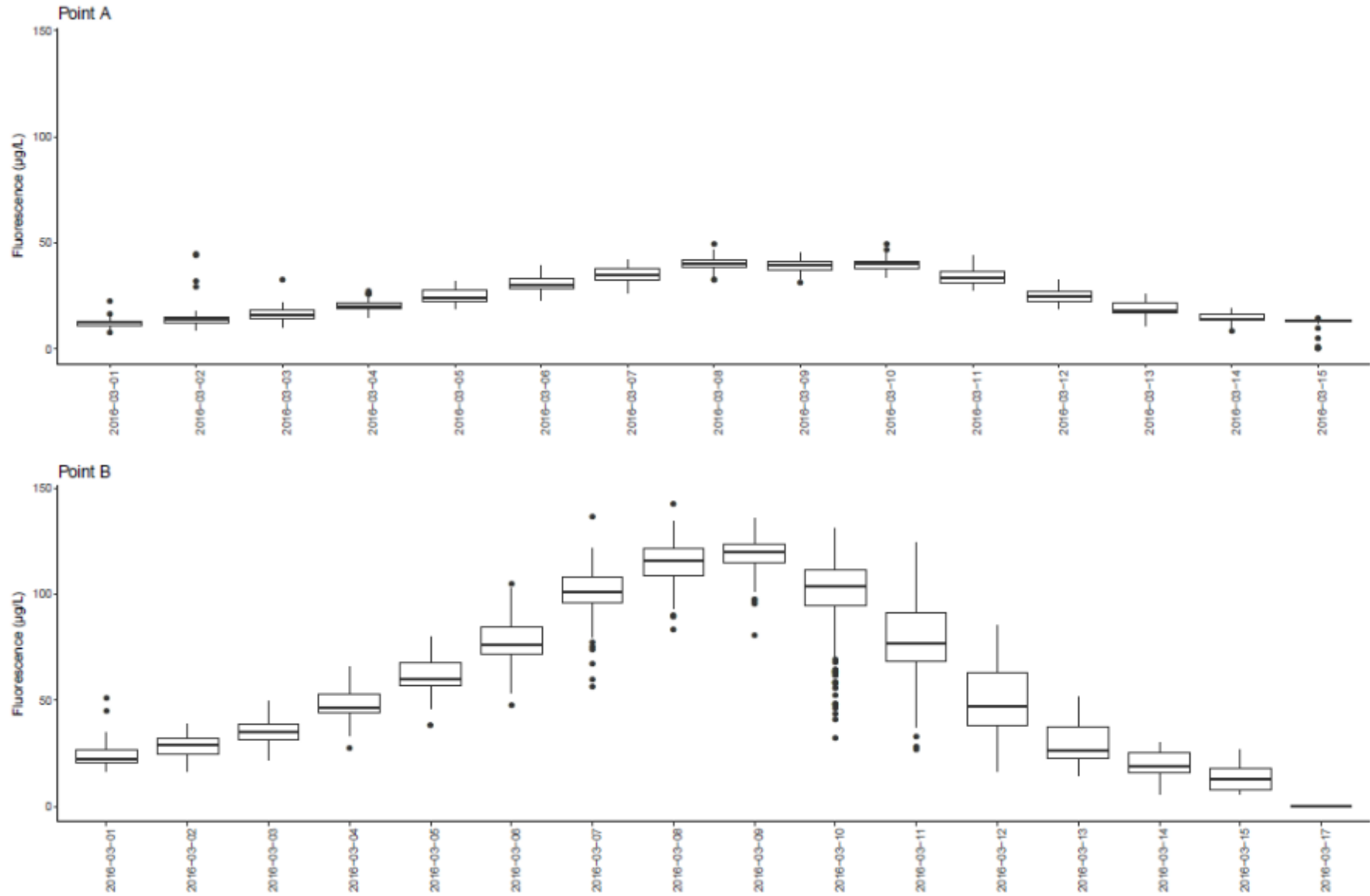


Figure 3.16 – Daily boxplot for chlorophyll-a fluorescence measured at points A and B during March 2016



To obtain accurate and repeatable measurements, it is important to keep the sensor clean. However, the measured concentration may vary depending on factors such as speciation, light history, algal stresses and pigment ratios. According to the manual from Turner Design (2017), a non-linear response should not occur with measuring range setting between 0 and 50  $\mu\text{gChl-a/L}$ .

Concerning temperature measurements, the treatment consisted of the suppression of measurements registered during the cleaning of the equipment. This situation was easily detected by the instantaneous variation of pressure measured by the sensor.

#### 3.2.1.4. Campaigns

In parallel, fortnightly campaigns have been carried out at the same points. A set of independent measuring devices were deployed for discrete profile measurements in the lake, in order to complement the continuous measurements or to calibrate the continuous measuring sensors:

- ✓ Two fluorometric probes (FluoroProbe, BBE Moldaenke™): FluoroProbe for measuring 4 phytoplankton families and Algae Torch for measuring phycocyanin and total chlorophyll;
- ✓ A multiparameter probe for measuring temperature, conductivity, pH and dissolved oxygen (Seabird SBE 19™);
- ✓ An active radiation probe for photosynthesis (Li-Cor Li-193);

The active radiation measurements with Li-Cor were done according to the following procedure:

- ✓ Stop the boat;
- ✓ Place the Li-Cor probe near the surface for 1 minute;
- ✓ Place the Li-Cor probe immediately below the surface of the water for 1 minute;
- ✓ Go down 50 cm and let the Li-Cor probe measure for 30 seconds;
- ✓ Continue in depth increments of 50 cm at a duration of 30 seconds for each new depth until reaching the bottom;
- ✓ Recover the sensor;
- ✓ If a change in cloud cover occurred, discard the measurements and start again.

For algae group differentiation, 6 LEDs (light-emitting diode) are used by the BBE fluorometers of fluorescence excitation. The LEDs emit light at 6 selected wavelengths (370 nm, 470 nm, 525 nm, 570 nm, 590 nm and 610 nm):

- (a) Chlorophyceae (green algae) show a broad maximum of fluorescence at 470nm;
- (b) Cyanophyceae (blue-green algae) have their maximum peak at 610nm;
- (c) Cryptophyceae, a significant maximum can be found at 570nm;
- (d) Dinophyceae have their maximum peak at 525nm.

The LED (370 nm) is used to measure yellow substances (dissolved organic matter) in water. At 370 nm, the differences between algae (low signal) and yellow substances (high signal) are detected.

In the BBE fluorometer, the fluorescence signal for each LED is averaged over a given measuring time and given at the end. The sum of all detected concentrations of algae classes is the total chlorophyll (BBE Moldaenke, 2012).

An important step is treatment validation of the measurements. The first step is to subtract the offset signal (that does not come from the algae). There are two types of offsets that the software analyses automatically:

1. The signal from the BBE fluorometer itself, from the electronics and the optical system;
2. The signal from fluorescent substances in the water that are not algae.

The first signal solely depends on the BBE fluorometer and has a small relatively range variation, and it do no need to be calibrated. However, the second must be calibrated because depends on the sample.

After subtracting the signal that does not come from the algae, the measured values are associated to each algae class. A statistical calculation of the BBE software finds the best combination of concentrations of algae classes for the measured signals. The value is compensated by adding the turbidity multiplied by two factors: a FluoroProbe dependent factor and a FluoroProbe independent factor. The dependent factor is calculated from the FluoroProbe fingerprints.

The correction is done for each LED wavelengths (Equation 1).

$$\begin{aligned} \text{Offset cor.} &= \text{Offset} + \text{Turbidity} * \text{FactorFluoroProbe(LED)} * \text{FactorReflexion(LED)} + \\ \text{Raw value cor.} &= \text{Raw val.} * (1 + \text{Turbidity} * \text{Factor mitigation (LED)}) \end{aligned} \quad \text{Equation 1}$$

Turbidity is used to compensate for two effects:

1. The higher offset due to additional reflection of the particles;
2. The change in the signal (raw value) due to the attenuation of the light.

To correct and convert *in vivo* chlorophyll data into actual chlorophyll data, BBE uses multiple regressions (Equation 2).

$$y = mx + mz + b \quad \text{Equation 2}$$

Where:

y = corrected chlorophyll value; mx = coefficient (slope) for *in vivo* Chl-a; mz = coefficient (slope) for turbidity; b = y intercept.

During measurement, the sample spectrum is storage into the device of the instrument and later need to be sent to an external computer. The concentration of every algae division is given in  $\mu\text{g}$  chlorophyll-a/L.

All fluorescence measurements are converted into equivalent Chl-a concentrations for 4 phytoplankton groups: (i) Green algae; (ii) Cyanobacteria; (iii) Diatoms and (iv) Dinoflagellates.

Regularly cleaning of the FluoroProbe windows is strongly recommended. Cleaning intervals have been every 2 weeks in summers and monthly in winter, when the concentration of algae and particles were lower. ANNEX 8.5 presents the FluoroProbe parameters adopted, ANNEX 8.6 presents the usage protocol and ANNEX 8.7 shows the FluoroProbe specifications. A multiparameter probe for measuring vertical profiles of temperature, conductivity, pH and oxygen (Seabird SBE19) was used.

### 3.2.1.5. Measurement of the water velocity

Water current velocities were measured from 19 September 2016 to 12 October 2016 with an Acoustic Doppler current profiler (2 MHz Aquadopp Nortek ADCP), developed by Nortek AS. It measures high-quality, accurate, and unbiased three-component (East, North, Up) current velocity using acoustic Doppler technology (Nortek, 2008).

Velocities were measured near point B (Figure 3.13). The measurements were carried out with a burst interval of 3 minutes, with an averaged interval of 30 s. This means that in 3 minutes, 30 s were measured and the output is the average value calculated in the 3 directions.

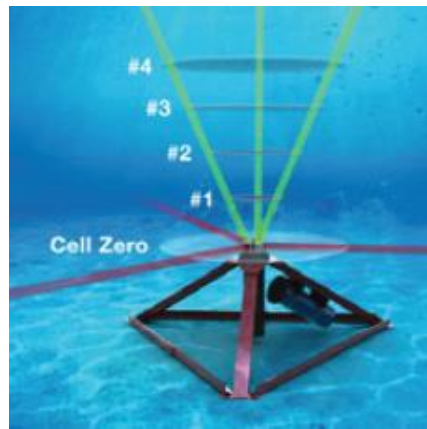


**Figure 3.17** – Scheme shows ADCP measurement method. Source: Nortek, (2008)

The ADCP was oriented towards the surface. Therefore, it was necessary to assess acoustic interference from the surface echo. That configuration was queried out in the lake during device installation. The final configuration was with a depth range of 0.45 m from the surface to 2.7 m at the bottom, with a vertical resolution of 5 cm. The distance of each numbered cell (Figure 3.17) was set to 0.45 m. A standard current profiler cannot measure currents near the equipment (blanking distance). The blanking distance was set to 20 cm. The setup file of the ADCP is presented in Annex **Erro! Fonte de referência não encontrada.** The characteristics of all measuring devices used in Lake of Champs-sur-Marne are summarised in Table 3.3.

**Table 3.3** – Characteristics of measuring devices on the Lake of Champs-sur-Marne. Source: Khac et al., 2018

Variable	Sensor	Monitoring Point	Monitoring Depth	Measuring Range	Sensor Resolution	Measuring Precision
Temperature	NKE - SP2T10	A, B, C	0.5 m & 2.5 m	-5 °C to +35 °C	0.05 °C	0.020 °C at 20 °C
	NKE - MPx	A, C	1.5 m	-5 °C to +35 °C	0.05 °C	0.050 °C
	NKE - SAMBAT	B	1.5 m	-5 °C to +35 °C	0.01 °C	0.050 °C
Conductivity	NKE - MPx	A, C	1.5 m	0 to 2 mS/cm	0.0004 mS/cm	<0.010 mS/cm
	NKE - SAMBAT	B	1.5 m	0 to 2 mS/cm	0.001 mS/cm	0.020 mS/cm
Dissolved Oxygen	Anderaa (NKE - MPx)	A, C	1.5 m	0–120% (0–16 mg/L)	0.01%	5%
	Ponsel (NKE—SAMBAT)	B	1.5 m	0–200% (0–20 mg/L)	0.01%	1%
Chlorophyll-a	TurnerDesign—Cyclops7 (NKE—MPx)	A, C	1.5 m	0–50 µg/L	<0.008 µg/L	0.03 µg/L
	TurnerDesign—Cyclops7	B	1.5 m	0–500 µg/L	<0.008 µg/L	0.03 µg/L

Variable	Sensor	Monitoring Point	Monitoring Depth	Measuring Range	Sensor Resolution	Measuring Precision
	(NKE—SAMBAT)					
Current	Doppler Nortek Aquadopp HR-Profiler	B	0.6–2.8 m	0-10 cm/s	0.01 cm/s	1% (0.5 cm/s)

### 3.2.1.6. Nutrients Monitoring

In 2015, the consulting company I.D.EAUX (I.D. Eaux, 2015) performed, at the large beach (Beach point in Figure 3.13) nutrient concentration samples. The obtained nutrient concentrations of nitrate, ammonium and orthophosphate are presented in Figure 3.18. The concentrations values were acquired from I.D.EAUX technical report. Unfortunately, no details of the methodology applied in the laboratory analyses were describe.

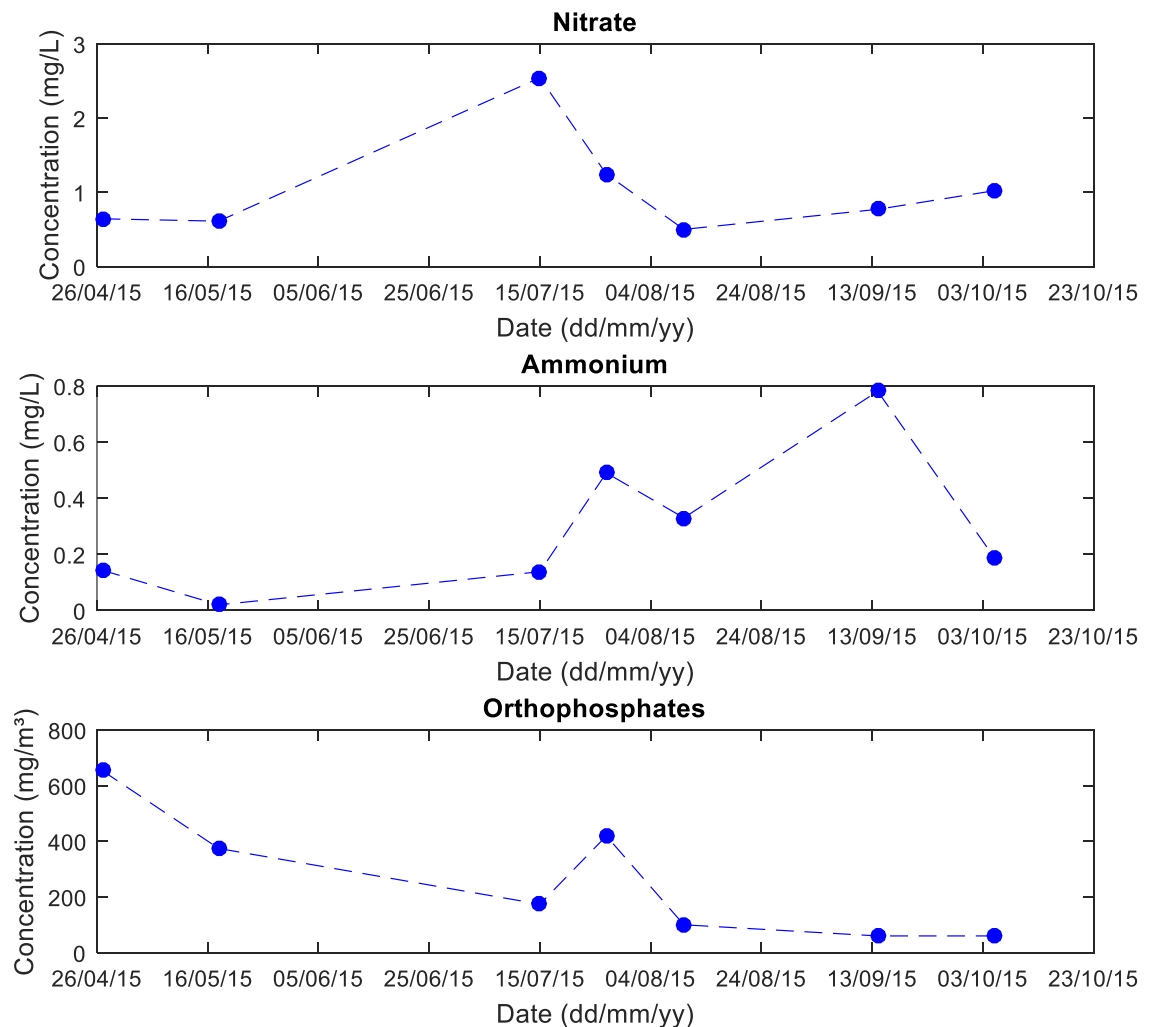


**Figure 3.18** – Nutrient concentration measured in Lake Champs-sur-Marne.

### 3.2.1.7. Meteorological Monitoring

The meteorological conditions (cloud cover, wind speed and direction, relative humidity and air temperature), were collected from the meteorological station (Météo-France) at Orly airport. The station is located approximately 22 km from the southwest side of the lake. The data were downloaded during 2016 from the Meteociel website (<http://www.meteociel.fr/>).

The net solar energy incident (Equation 3) on the surface of the lake, used as input in the Delft3D model, was calculated from cloudiness, albedo, solar radiation data and latitude, according to Equation 3 (Deltares, 2013).

$$Q_S = (1 - \delta)(1 - \alpha) * (1 - \alpha) * Q_0(1 - 0.65F^2) \quad \text{Equation 3}$$

Where:

$Q_S$  = Net solar energy incident on the surface of the water (W/m<sup>2</sup>)

$Q_0$  = Energy solar radiation data from the meteorological station (W/m<sup>2</sup>)

$\delta$  = Fraction of the energy absorbed by the atmosphere, equal to 0.2 (-)

$\alpha$  = Albedo of water (-)

$F$  = Cloudiness (-)

According to the results obtained by Scriban (2015), the albedo value of the water for Lake Champs-sur-Marne is 0.08.

## 3.2.2. Lake Pampulha

### 3.2.2.1. Bathymetry

The last Lake Pampulha bathymetry was performed by SUDECAP in November 2014 after dredging in the upstream region.

The bathymetry (Figure 3.19) of Lake Pampulha can be divided into four regions: (i) The upstream channel of the Ressaca and Sarandi rivers, (ii) an upstream region with a very shallow depth (about 1.5 m depth), (iii) a transition region, where the depth goes from 1.5 m to almost 13 m, and (iv) a deeper region further downstream.

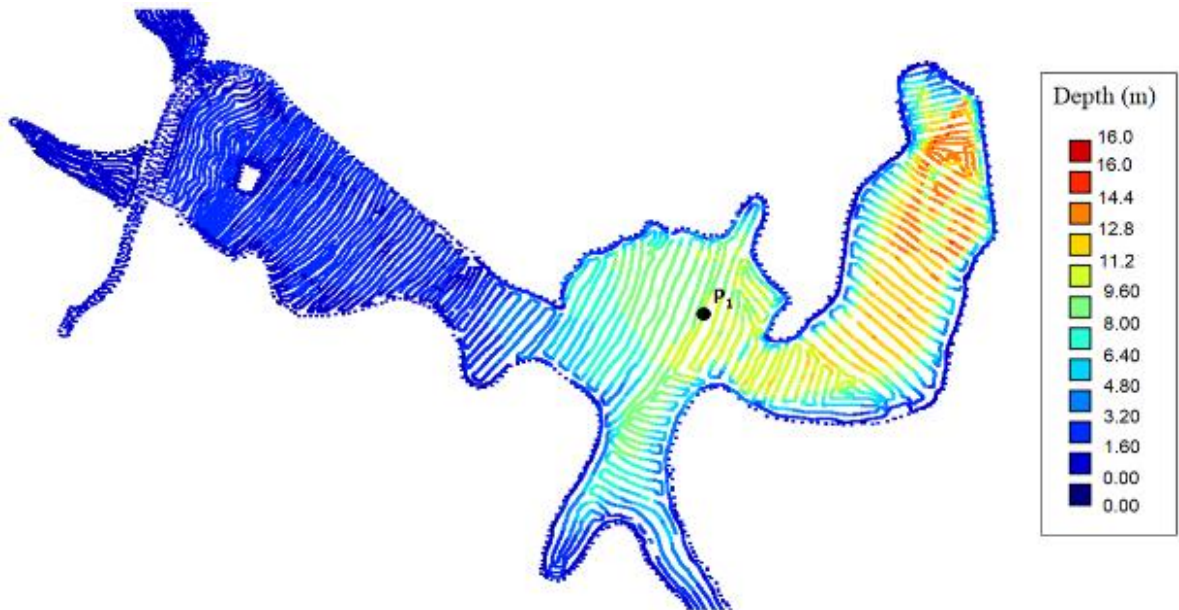


**Figure 3.19** – Bathymetry map (SUDECAP, 2014). P<sub>1</sub> is the monitoring point of the lake

### 3.2.2.2. High-frequency

Since 2011, the monitoring of Lake Pampulha has been conducted in partnership between the Phycology laboratory at the UFMG Institute of Biological Sciences (ICB) and the municipality of Belo Horizonte, with the support of different research funding frameworks. Lake Pampulha high frequency data used in this work were previously collected by collaborators of the research group and monitoring methods are fully described in Silva (2014) and Belico (2017). This monitoring shows that cyanobacteria are dominant in Lake Pampulha throughout the year, with rare exceptions (Silva, 2014).

With a consolidated database, it was possible to calibrate and validate a one-dimensional numerical model of Lake Pampulha (Silva, 2014). This present research focuses on three-dimensional modelling and high-frequency monitoring in the framework of the project MoMa-SE funded by CAPES, a Brazilian research funding agency, and the National Water Agency (ANA).

Since February 2015, a high-frequency monitoring scheme has been implemented in Lake Pampulha. A previous project (Maplu-2) funded monitoring devices, supported by FINEP (Brazilian research funding agency). At station P<sub>1</sub> located at 19° 51' 5" south and 43° 58' 35" west (Figure 3.19), underwater sensors have been continuously measuring temperature, chlorophyll-a (Chl-a) fluorescence, conductivity and dissolved oxygen. The total depth at the monitoring station P<sub>1</sub> is 10 m. Therefore, the 9.5 monitoring depth was considered as the bottom.

High-frequency monitoring has been performed at the surface (0.5 m depth) for temperature and Chl-a fluorescence at a time step of 30 minutes during February 2015 to August 2018. The temperature has also been performed at three other depths (2.5 m, 5.5 m and 9.5 m) during 18 months (February 2016 to August 2017) at a 1-hour time step (Table 3.4). In parallel, fortnightly campaigns have been carried out at the same point for obtaining complete profiles of temperature, conductivity, dissolved oxygen and pH with a multi-parametric probe YSI 556 (YSI, EUA), and water transparency was measured using a Secchi Disk in fortnightly campaigns at a monthly frequency.

**Table 3.4** – Characteristics of measuring devices on the Lake Pampulha

Variable	Sensor	Monitoring Point	Monitoring Depth	Measuring Range	Sensor Resolution	Measuring Precision	Time step
Temperature	NKE	P1	0.5 m; 2.5;5.5 & 9.5 m	-5 °C to +35 °C	0.05 °C	0.020 °C at 20 °C	30 min & 1 h
Chl-a	NKE	P1	0.5 m	0- 500 µg/L	<0.008 µg/L	0.03 µg/L	1 hour

The data treatment carried out for the study in Lake Pampulha consisted of discarding the measured values when the sensors were removed from the water for cleaning and maintenance.

### 3.2.2.3. Water Inflow Monitoring

Lake Pampulha has 8 tributaries (Figure 3.9). Concerning the lake water inflow, since 2011 monitoring stations integrate a Hydrological Monitoring System operated by PBH (Siqueira et al., 2019). In the 8 tributaries of Lake Pampulha, monitoring stations are just present on the main tributaries, Sarandi stream (station SAR18F, 2,8 km upstream the lake), located at 19° 52' 01" south and 44° 0' 33" west and Ressaca stream (station RES17F, 2,0 km upstream the lake), located at 19° 52' 11" south and 43° 59' 57" west. These streams represent 70% of the reservoir inflow (CPRM, 2001). These stations do not measure water discharge, thus they are limnometric stations. The watersheds of the Sarandi and Ressaca rivers and the localisation of limnometric stations are shown in Figure 3.9.

Nogueira (2015) determined the rating curve for both station in each respective confluence. These rating curves were used to obtain the inflow time series of the limnometric stations. The other tributaries do not have monitoring. Thus, the time series for each was calculated based on the inflow time series of the reference station multiplied by the ratio of each tributary's catchment area (Table 3.5) and the catchment area of the reference station (Equation 4). The Sarandi station (SAR18F) was used as the reference station because it was the only station that presented monitoring values during 2015 and 2016, the period used in the current research.

$$Q(t)_{trib} = Q(t)_{ref} * \frac{A_{trib}}{A_{ref}} \quad \text{Equation 4}$$

Where:

$Q(t)_{trib}$  = Tributary inflow water (m<sup>3</sup>/s) in time t

$Q(t)_{ref}$  = Reference station inflow water (m<sup>3</sup>/s) in time t

$A_{trib}$  = Tributary catchment area (km<sup>2</sup>)

$A_{ref}$  = Reference station catchment area (km<sup>2</sup>)

**Table 3.5** – Lake Pampulha tributaries catchment area. From Felisberto et al., (2015)

Tributaries	Catchment area (km <sup>2</sup> )
Ressaca	21
Sarandi	41
Água Funda	17
AABB	0.7
Olhos D'Água	3.0
Mergulhão	3.4
Tijuco	1.8
Braúnas	2.0

Concerning water temperature inflow, a monitoring station close to the fluvial water treatment plant (ETAF), downstream the confluence of the Ressaca and Sarandi rivers, monitored inflow temperature for only a short period of two months (April and May 2013).

For small and shallow streams, it is possible to estimate water temperature using air temperature (Stefan and Preud'homme, 1993). Lake Pampulha tributaries all have small catchment and are shallow rivers, an aspect reinforced during periods of drought (the period of focus due to a higher occurrence of blooms). According to the limimetric station, the Sarandi river presented a maximum depth of 2.8 m during the flood period in 2015 and 0.90 m during the drought period.

Two methods to estimate hourly water temperature in rivers were evaluated. The first one was a linear regression with air temperature and the second method evaluated was the Modified Sine and Sinusoidal Wave Functions Model (MSSWF).

A linear regression model is the simplest regression model (Equation 5), which was used in many previous studies (Chen and Fang, 2015; Hébert et al., 2015; Stefan and Preud'homme, 1993).

$$T_w(t) = a * T_a(t) + b \quad \text{Equation 5}$$

Where:

$T_w(t)$  = water temperature (°C) in time t

$T_a(t)$  = air temperature (°C) in time t

a and b = scalar and translation coefficients

Recently, to improve the accuracy of hourly water temperature estimation the MSSWF method was proposed by Chen Gang and Fang Xing (2016). The sine function (Equation 6) is used to calculate daily air and water temperature.

$$T(t) = \bar{T} + T_{am} * \sin(\omega t - \theta) \quad \text{Equation 6}$$

Where:

$T(t)$  = air temperature (°C) in time t

$\bar{T}$  = annual mean temperature of air or water (°C)

$T_{am}$  = amplitude of sine function (°C)

t = day of year (DOY) scalar and translation coefficients

$\omega$  = angular frequency of temperature variations (radians day<sup>-1</sup>)

$\theta$  = phase shift (radians)

Sine functions have previously been used to estimate daily maximum and minimum water temperatures in rivers for which the MSSWF method was used to estimate hourly water temperatures (Equation 7 to Equation 12).

For  $0 \leq H < RISE + Lag_{Max}$  and  $t_{Wmax} < H \leq 24$

$$T_w(H) = T_{Wave} + AMP * \cos\left(\frac{\pi * H'}{10 + RISE}\right) \quad \text{Equation 7}$$

For  $RISE + Lag_{Max} \leq H < T_{Wmax}$

$$T_w(H) = T_{Wave} - AMP * \cos\left(\frac{\pi * (H - RISE - Lag_{Max})}{T_{Wmax} - RISE - Lag_{Max}}\right) \quad \text{Equation 8}$$

In which :

$$T_{Wave} = \frac{T_{Wmin} + T_{Wmax}}{2} \quad \text{Equation 9}$$



$$AMP = \frac{T_{Wmax} - T_{Wmin}}{2} \quad \text{Equation 10}$$

If  $H < RISE + Lag_{Max}$   
 $H' = H + 8$  Equation 11

If  $H > t_{Wmax}$   
 $H' = H - 16$  Equation 12

Where:

$T_w(H)$  = water temperature (°C) at time H (h)

$RISE$  = time of sunrise in hours (h)

$Lag_{Max}$  = mean lag time of maximum water air temperature in hours (h)

$t_{Wmax}$  = time (h) of maximum water temperature

$T_{Wmin}$  and  $T_{Wmax}$  = minimum and maximum daily temperature (°C), obtained by Equation 6

To improve the sine function model accuracy of the sine function model, the difference between observed temperature and estimated temperature from the fitted sine function is calculated (observed temperature – estimated temperature) and the deviation for maximum and minimum water temperature is linearly correlated with the deviation for corresponding air temperature (Equation 13 and Equation 14). Therefore, water temperature variation is connected to air deviation.

$$DiffT_{Wmax} = A * DiffT_{Amax} + B \quad \text{Equation 13}$$

$$DiffT_{Wmin} = C * DiffT_{Amin} + D \quad \text{Equation 14}$$

Where:

A, B, C and D = regression coefficients

$DiffT_{Wmax, Wmin, Amax, Amin}$  = deviation for daily maximum and minimum water and air temperature

To compare and decide between linear regression and the MSSWF method, the mean absolute error (MAE), the root mean square error (RMSE) and the Nash-Sutcliffe efficiency (NSE) were used.

$$NSE = 1 - \frac{\sum(T_{stm} - T_{obs})^2}{\sum(\bar{T}_{obs} - T_{obs})^2} \quad \text{Equation 15}$$

Where:

$\bar{T}_{obs}$  = mean values of the observed water temperature

In summary, the MSSWF method follows six steps, using daily maximum and minimum air temperatures, to estimate the hourly water temperature of a stream:

- a) Uses fitted sine functions (Equation 6) to estimate daily maximum and minimum water temperatures, and daily maximum and minimum air temperatures;
- b) Calculates differences between observed and estimated daily maximum and minimum for air and water temperatures;
- c) Calculates the linear regression between the differences of the daily maximum and minimum water temperatures for the maximum and minimum air temperatures (Equation 13 and Equation 14);

- d) Corrects the estimated daily maximum and minimum water temperatures from fitted SFs by adding  $DiffT_{W_{max}}$  and  $DiffT_{W_{min}}$ , calculated by linear regression from the air temperature;
- e) Calculates hourly water temperatures using Equation 7 and Equation 8.

#### 3.2.2.4. Meteorological Monitoring

Meteorological data (air temperature, air moisture, wind intensity and direction, and cumulative hourly solar radiation and precipitation) measured during 2015 and 2016 were provided by the National Institute of Meteorology of Brazil (INMET). The nearest automatic weather station (a521) is located inside the UFMG campus, about 3 km from Lake Pampulha.

The nebulosity data are recorded at the meteorology station Belo Horizonte (83587), located 9.5 km from Lake Pampulha. This station provides nebulosity data three times a day (0h, 12h, and 18h) and these values were linearly interpolated to hourly values for simulation.

### 3.3. Model Formulation

In this research, Delft3D suite software (Deltares, 2013) was used. It is composed of several modules, grouped around an interface allowing interaction with one another. Two modules were employed, Delft3D-Flow for hydrodynamics, D-Water Quality for phytoplankton dynamics. According the water quality model formulation (presented in Item 3.3.2) a numerical mathematical optimization is used, this approach is the main reason to the choice of the model. Using a mathematical optimization, it is possible to model the complex phytoplankton species competition and adaptation in different environmental conditions with less mathematical expressions.

#### 3.3.1. Hydrodynamic model formulation

##### 3.3.1.1. Navier-Stokes equations

The hydrodynamic module Delft3D-FLOW solves in three dimensions the Navier-Stokes equations for an incompressible fluid, under shallow water and Boussinesq assumptions. The essence of the Boussinesq assumption is that it ignores density difference except where they appear in terms multiplied by  $g$  (gravity acceleration). In the vertical momentum equation, the vertical accelerations are neglected, which leads to hydrostatic pressure condition. In three-dimensional models, the vertical velocities are taken into account by the continuity equation. Therefore, the model has better application in shallow water that have stably stratification, in case of unstable stratification and strong vertical circulation, measures need to be taken to evaluate the model applicability.

The system of partial differential equations (Equation 16 to Equation 20) in combination with initial and boundary conditions is solved on a finite difference grid (Deltares, 2013).

Delft3D-FLOW simulates three-dimensional unsteady flow and transport phenomena resulting from meteorological forcing. The condition of velocities, water elevations, density, salinity, vertical eddy viscosity and vertical eddy diffusivity are calculated by Delft3D-FLOW. This model is fully described in the Delft3D-FLOW User Manual (Deltares, 2014a).

The main hydrodynamic equations are continuity (Equation 16), conservation of momentum according to the horizontal (Equation 17 and Equation 18), and the equation of energy conversation (Equation 19). The momentum conservation equation in the vertical direction is reduced to the hydrostatic pressure equation.

$$\frac{\partial u}{\partial x} + \frac{\partial v}{\partial y} + \frac{\partial w}{\partial z} = 0 \quad \text{Equation 16}$$

$$\begin{aligned} \frac{\partial u}{\partial t} + u \frac{\partial u}{\partial x} + v \frac{\partial u}{\partial y} + w \frac{\partial u}{\partial z} \\ = -\frac{1}{\rho} \frac{\partial p}{\partial x} + \frac{\partial}{\partial x} \left( v_H \frac{\partial u}{\partial x} \right) + \frac{\partial}{\partial y} \left( v_H \frac{\partial u}{\partial y} \right) + \frac{\partial}{\partial z} \left( v_V \frac{\partial u}{\partial z} \right) + f_v \end{aligned} \quad \text{Equation 17}$$

$$\frac{\partial v}{\partial t} + u \frac{\partial v}{\partial x} + v \frac{\partial v}{\partial y} + w \frac{\partial v}{\partial z} = -\frac{1}{\rho} \frac{\partial p}{\partial y} + \frac{\partial}{\partial x} \left( v_H \frac{\partial v}{\partial x} \right) + \frac{\partial}{\partial y} \left( v_H \frac{\partial v}{\partial y} \right) + \frac{\partial}{\partial z} \left( v_V \frac{\partial v}{\partial z} \right) - f_u \quad \text{Equation 18}$$

$$\frac{\partial T}{\partial t} + u \frac{\partial T}{\partial x} + v \frac{\partial T}{\partial y} + w \frac{\partial T}{\partial z} = \frac{\partial}{\partial x} \left( D_H \frac{\partial T}{\partial x} \right) + \frac{\partial}{\partial y} \left( D_H \frac{\partial T}{\partial y} \right) + \frac{\partial}{\partial z} \left( D_V \frac{\partial T}{\partial z} \right) + \frac{S}{\rho C_{pw}} \quad \text{Equation 19}$$

Where:

$x, y, z$  = coordinates (m)

$u, v, w$  = three components of the vector velocity (m/s)

$f$  = frequency of Coriolis (1/s)

$p$  = pressure (Pa)

$T$  = water temperature (°C)

$\rho$  = water density (kg/m<sup>3</sup>)

$v_H, v_V$  = horizontal and vertical coefficient of turbulent viscosity (m<sup>2</sup>/s)

$D_H, D_V$  = horizontal and vertical coefficient of turbulent heat diffusion (m<sup>2</sup>/s)

$S$  = heat per volume (W/m<sup>3</sup>)

$C_{pw}$  = specific heat of water (J/°C.kg)

### 3.3.1.2. Heat balance

Due to the importance of thermal behavior of lakes for the current research, the main equations and considerations of the model were described. The equations exposed in the sequence have the objective of presenting the equations and parameters involved in the calibration of the thermal model of the lake. For a full description, the Delft3D-FLOW User Manual (Deltares, 2014a) shall be consulted.

The heat exchange at the free surface is considered as resulting from the separate effects of solar (short wave) and atmospheric (longwave) radiation, and heat loss, represented in terms of back radiation, evaporation, and convection. The total heat flux ( $Q_{tot}$ ) through the free surface is calculated according to Equation 20.

$$Q_{tot} = Q_{sn} + Q_{an} - Q_{br} - Q_{ev} - Q_{co} \quad \text{Equation 20}$$

Where:

$Q_{tot}$  = total heat flux (J/m<sup>2</sup>.s)

$Q_{sn}$  = net incident solar radiation (J/m<sup>2</sup>.s) (short wave)

$Q_{an}$  = net incident atmospheric radiation (J/m<sup>2</sup>.s) (long wave)

$Q_{br}$  = back radiation (J/m<sup>2</sup>.s) (long wave)

$Q_{ev}$  = evaporative heat flux (J/m<sup>2</sup>.s) (latent heat)

$Q_{co}$  = convective heat flux (J/m<sup>2</sup>.s) (sensible heat)

The heat exchange at the lake bottom is assumed to be zero. Representing a simplification in the model, that may lead to an over-estimate the water temperature in shallow lakes. Also, the effect of precipitation on water temperature is not considered.

Not all radiation is absorbed at the water's surface. A portion is transmitted to deeper water. Short wave radiations can penetrate over 3 to 30 m, depending on the water transparency, while longer wave radiations are absorbed at the surface. Therefore, it is important to know the equation and assumption of the model concerning heat exchange.

The absorption of heat in the water column is calculated by an exponential decay function (Lambert-Beer law) of the distance H from the water surface (Equation 21).

$$Q = \int_0^H e^{-\gamma h} dh \quad \text{Equation 21}$$

Where:

$Q$  = heat absorbed at the water column (J/m<sup>2</sup>.s)

$\gamma$  = extinction coefficient (m<sup>-1</sup>)

$h$  = distance to the water surface in meters (m)

$H$  = total water depth (m)

The extinction coefficient (Equation 22) is related to water transparency (Secchi depth). The Delft-3D flow model assumes that the Secchi value is constant during the simulation.

$$\gamma = \frac{1.7}{\text{Secchi}} \quad \text{Equation 22}$$

Cloud cover reduce the radiation that reaches the water surface. Cloudiness is expressed by a cloud cover fraction  $F_c$  (fraction of the sky covered by clouds). A part of the radiation that reaches the water surface is also reflected.

Back radiation is part of the total long-wave radiation flux, the so-called effective back radiation ( $Q_{eb}$  - Equation 23).

$$Q_{eb} = Q_{br} - Q_{an} \quad \text{Equation 23}$$

Atmospheric radiation depends on the vapour pressure ( $e_a$ ), which depends on relative humidity, air temperature ( $T_a$ ), and cloud cover ( $F_c$ ). Back radiation depends on surface temperature ( $T_s$ ). The effective back radiation ( $Q_{eb}$  - Equation 23) is computed through vapour pressure ( $e_a$  [mbar]), emissivity factor ( $\epsilon$ ), the proportionality constant of the increase of intensity radiation due to temperature increases named Stefan-Boltzmann's constant ( $\sigma$  [J/(m<sup>2</sup>.s.K<sup>4</sup>)]), and cloud cover fraction ( $F_c$ ), according to Equation 24.

$$Q_{eb} = \epsilon \sigma T_s^4 (0.39 - 0.05\sqrt{e_a})(1 - 0.6F_c^2) \quad \text{Equation 24}$$

The evaporative heat flux ( $Q_{ev}$  [J/m<sup>2</sup>.s] - Equation 25) is a flux process that takes place between water and air.

$$Q_{ev} = L_v E \quad \text{Equation 25}$$

Where:

$L_v$  = latent heat of vapourization (J/kg)

$E$  = evaporation rate ( $\text{kg/m}^2\text{s}$ ), defined as the mass of water evaporated per unit area per unit time

The evaporation rate is computed from the difference in relative humidity, rather than from the difference in vapour pressure. The evaporative heat flux (Equation 26) is composed by a forced convection (due to wind effect) and a contribution by free convection (due to density differences between air and water that results in buoyant forces).

$$Q_{ev} = Q_{ev,forced} + Q_{ev,free} \quad \text{Equation 26}$$

The free convection of latent and sensible heat is also calculated by the model. The latent heat flux due to forced convection is giving by Equation 27.

$$Q_{ev,forced} = L_v \rho_a f(U_{10}) \{q_s(T_s) - q_a(T_a)\} \quad \text{Equation 27}$$

Where:

$\rho_a$  is the air density ( $\text{kg/m}^3$ ),  $q_s$  and  $q_a$  are the specific humidity of respectively saturated air and remote air,  $T_s$  is the water surface temperature ( $^\circ\text{C}$ ) and  $T_a$  is the air temperature ( $^\circ\text{C}$ ) and  $f(U_{10})$  is the wind function (Equation 28)

$$f(U_{10}) = c_e U_{10} \quad \text{Equation 28}$$

Where:

$c_e$  is the Dalton number (-)

$U_{10}$  is the velocity ( $\text{m/s}$ ) measured at 10 m height.

The Dalton number is a model parameter commonly used in the literature to calibrate models of water temperature simulation (Polli et al., 2019; Soullignac et al., 2017; Vinnå et al., 2017).

Free convection of latent heat (Equation 29) is the other part of heat loss due to evaporation. This term is driven by buoyant forces due to density differences. Evaporation due to free convection is important in circumstances where inverse temperature/density gradients are present and wind speeds are almost negligible.

$$Q_{ev,free} = \left[ 0.14 \left\{ \frac{g \vartheta_{air}^2}{0.7^2 \bar{\rho}_a} \right\} (\rho_{a10} - \rho_{a0}) \right]^{1/3} L_v \bar{\rho}_a \{q_s(T_s) - q_a(T_a)\} \quad \text{Equation 29}$$

Where  $g$  is the acceleration of gravity ( $\text{m/s}^2$ ),  $\vartheta_{air}$  is the air viscosity ( $\text{m}^2/\text{s}$ ),  $\rho_{a0}$  is the saturated air density ( $\text{kg/m}^3$ ),  $\rho_{a10}$  is the remote air density (10 m above water level) ( $\text{kg/m}^3$ ) and  $\bar{\rho}_a$  is the average air density ( $\text{kg/m}^3$ ),  $T_s$  is the water surface temperature ( $^\circ\text{C}$ ) and  $T_a$  is the air temperature ( $^\circ\text{C}$ ).

Convective heat flux is split into two parts, in the same manner as evaporative heat flux. Convective heat flux is divided into a contribution by forced convection and a contribution by free convection. The sensible heat flux is due to forced convection (Equation 30).

$$Q_{co,forced} = \rho_a c_p g(U_{10})(T_s - T_a) \quad \text{Equation 30}$$

Where  $c_p$  is the specific heat of air ( $\text{J}/(\text{kgC})$ ).

The wind-speed function  $g(U_{10})$  is defined by the Stanton number  $C_h$  times the wind velocity at 10 m high (Equation 31). The Stanton number is a model parameter commonly used in the literature to

calibrate models of water temperature simulation (Polli et al., 2019; Soullignac et al., 2017; Vinnå et al., 2017).

$$g(U_{10}) = C_H U_{10} \quad \text{Equation 31}$$

The free convection of sensible heat is calculated according to Equation 32.

$$Q_{co,free} = \left[ 0.14 \left\{ \frac{g \vartheta_{air}^2}{0.7^2 \bar{\rho}_a} \right\} (\rho_{a10} - \rho_{a0}) \right]^{1/3} * \bar{\rho}_a c_p (T_s - T_a) \quad \text{Equation 32}$$

Where  $g$  is the acceleration of gravity ( $m/s^2$ ),  $\vartheta_{air}$  is the air viscosity ( $m^2/s$ ),  $\rho_{a0}$  is the saturated air density ( $kg/m^3$ ),  $\rho_{a10}$  is the remote air density (10 m above water level) ( $kg/m^3$ ) and  $\bar{\rho}_a$  is the average air density ( $kg/m^3$ ),  $c_p$  is the specific heat of air ( $J/(kgC)$ ),  $T_s$  is the water surface temperature ( $^{\circ}C$ ) and  $T_a$  is the air temperature ( $^{\circ}C$ ).

### 3.3.1.3. Turbulent Eddy Viscosity and Diffusion

In shallow water condition, turbulent viscosity ( $\nu$  [ $m^2/s$ ] - Equation 33) and turbulent diffusion ( $D$  [ $m^2/s$ ] - Equation 34) are calculated differently in the horizontal and vertical directions. In turbulent flows, the diffusion mechanism is not only performed by molecular motions, but also intensified by eddy motions. Thus, when modeling turbulence, the intensify diffusion coefficient is performed by adding turbulent viscosity to molecular diffusion. Vertical terms are very small compared to horizontal terms. The most part of the horizontal eddy viscosity is related with the horizontal turbulent motions and forcing contribution. The concept of the turbulent stress component is defined as the product between a flow, grid-dependent eddy viscosity coefficient and the corresponding components of the mean rate-of-deformation tensor. The eddy viscosity coefficients are grid-dependent, meaning that they differ in fine or coarse computation grids affect its value. Every time that a mesh has a different size of elements, this parameter needs to be analysed.

In the horizontal direction, the coefficients of turbulent eddy viscosity ( $\nu_H$  [ $m^2/s$ ]) and diffusion ( $D_H$  [ $m^2/s$ ]) are calculated according to Equation 33 and Equation 34, respectively (Deltares, 2014a).

$$\nu_H = \nu_V + \nu_H^{back} \quad \text{Equation 33}$$

$$D_H = D_V + D_H^{back} \quad \text{Equation 34}$$

Where:

$\nu_V$  = vertical eddy viscosity ( $m^2/s$ )

$D_V$  = vertical diffusion coefficient ( $m^2/s$ )

$\nu_H^{back}$  = background horizontal coefficient of turbulent viscosity ( $m^2/s$ )

$D_H^{back}$  = background horizontal coefficient of turbulent diffusion ( $m^2/s$ ).

The background horizontal eddy viscosity and diffusion represent unresolved and complicated hydrodynamic phenomena not calculated by the turbulent model.

In the vertical direction, the coefficients of turbulent eddy viscosity ( $\nu_V$  [ $m^2/s$ ]) and diffusion ( $D_V$  [ $m^2/s$ ]) are calculated according to Equation 35 and Equation 36.

$$v_V = v_{mol} + \max(v_{3D}, v_V^{back}) \quad \text{Equation 35}$$

$$D_V = \frac{v_{mol}}{\sigma_{mol}} + \max(D_{3D}, D_V^{back}) \quad \text{Equation 36}$$

Where:

$v_{mol}$  = kinematic viscosity of water (m<sup>2</sup>/s)

$\sigma_{mol}$  = molecular Prandtl number for heat diffusion

$v_{3D}$  = turbulent viscosity (m<sup>2</sup>/s), computed by a three-dimensional-turbulence closure model k-ε

$v_V^{back}$  = background vertical coefficient of turbulent viscosity (m<sup>2</sup>/s)

$D_{3D}$  = turbulent diffusivity (m<sup>2</sup>/s), computed by a three-dimensional-turbulence closure model k-ε

$D_V^{back}$  = background vertical coefficient of turbulent diffusivity (m<sup>2</sup>/s)

The background vertical eddy viscosity and diffusion represent unresolved and complicated hydrodynamic phenomena not calculated by the turbulent model.

#### 3.3.1.4. Shear Stress

The shear stress at the bottom layer of the lake is defined according to Equation 37.

$$\vec{\tau}_b = \frac{g\rho|\vec{u}_b|\vec{u}_b}{C_d^2} \quad \text{Equation 37}$$

Where:

$\vec{u}_b$  = velocity of the horizontal velocity in the first layer just above the bottom (m/s)

$C_d$  = Chezy coefficient (m<sup>0.5</sup>/s)

$g$  = acceleration due to gravity (m/s<sup>2</sup>)

$\rho$  = water density (kg/m<sup>3</sup>)

The shear stress at the water surface due to wind intensity is defined according to Equation 38.

$$|\vec{\tau}_s| = \rho_a C_d U_{10}^2 \quad \text{Equation 38}$$

Where:

$\tau_s$  = magnitude of the surface stress (Pa)

$C_d$  = wind drag coefficient (-)

$U_{10}$  = velocity (m/s)

$\rho_a$  = air density (kg/m<sup>3</sup>)

#### 3.3.1.5. Numerical method

The set of partial differential equations in combination with an appropriate set of initial and boundary conditions is to be solved in the model through the numerical method of finite differences.

An explicit time integration method was used in the model. Therefore, the stability requirement of the explicit method in numerical analysis typically leads to the Courant-Friedrichs-Lewy (CFL) condition (Equation 39). The equation of momentum is solved by a multidirectional upwind explicit numerical scheme and the equation of heat by the second Van Leer numerical scheme, known as the “5-Ocean” model.

$$CFL = 2\Delta t \sqrt{gH} \sqrt{\frac{1}{\Delta x^2} + \frac{1}{\Delta y^2}} < 1 \quad \text{Equation 39}$$

Where:

$\Delta t$  = time step (s)

$g$  = gravity acceleration (m/s<sup>2</sup>)

$H$  = water depth (m)

$\Delta x$  = mesh size in x direction (m)

$\Delta y$  = mesh size in y direction (m)

### 3.3.2. Water quality model formulation

D-Water Quality is the water quality module of the Delft3D modelling suite. It solves the fundamental advection-diffusion equation (Equation 40) on a predefined computational grid and for a wide range of model substances. D-Water Quality allows great flexibility in the substances to be modelled, as well as in the processes to be considered.

In the model configuration, it is necessary to choose and activate which physical, biochemical and biological processes and substances will be simulated. Information on flow fields (water temperature, bed shear stress, vertical dispersion and water velocity) is derived from Delft3D-FLOW.

To simulate the development of algal biomass and all processes involved, two modules (routines), ECO and BLOOM, were used.

ECO simulates the concentrations of nutrients (N, P, Si), organic matter, dissolved oxygen, and active substances (Smits, 2009).

$$\frac{\partial C}{\partial t} = -\frac{\partial Cu}{\partial x} - \frac{\partial Cv}{\partial y} - \frac{\partial Cw}{\partial z} + \frac{\partial}{\partial x} \left( D_x \frac{\partial C}{\partial x} \right) + \frac{\partial}{\partial y} \left( D_y \frac{\partial C}{\partial y} \right) + \frac{\partial}{\partial z} \left( D_z \frac{\partial C}{\partial z} \right) + S(x, y, z) \quad \text{Equation 40}$$

Where:

$C$  = concentration (kg/m<sup>3</sup>)

$u, v$  and  $w$  = components of velocity (m/s) in  $x, y$  and  $z$  direction

$D_{x,y,z}$  = component of the dispersion tensor (m<sup>2</sup>/s) in  $x, y, z$  direction

$S(x, y, z)$  = change of concentration due to a source (contribution or withdraw) (kg/(m<sup>3</sup>.s))

BLOOM models phytoplankton species competition and adaptation in different environmental conditions, such as limiting nutrients and light (Los, 2009). Each phytoplankton group or species have different requirements for resources (e.g. nutrients, light), different ecological properties and present different condition states (Los, 2009).

For every species of phytoplankton considered, BLOOM distinguishes them between three phenotypes: under nitrogen-limiting conditions, under phosphorus-limiting conditions and under light-limiting conditions. Therefore, it is possible to evaluate which restriction was a limiting factor to the distribution of each species (Smits, 2009).

Each phenotype has distinct physiology (growth rates, mortality rates and respiration rates), stoichiometry (nutrient-carbon ratios, and Chl-a carbon ratios) and sedimentation rates. The model uses the concept of phenotypes to model the physiological stress and species adaptations of each phytoplankton group and/or species in different environmental limiting condition.



The objective of the BLOOM model was described by (Los, 2009) as follows:

“Selecting the best-adapted combination of phytoplankton types at a certain moment and at a certain location consistent with the available resources, the existing biomass levels at the beginning of a time interval and the potential rates of change of each type.”

Competition between phytoplankton species is one of the main processes considered in BLOOM. Through numerical mathematical optimisation, BLOOM finds the distribution of biomass of each alga modelled at a time step, thus representing the variations in the fluorescence caused by a different environmental condition.

### 3.3.2.1. Biomass distribution

It is challenging and complicated to model phytoplankton behaviour in terms of mathematical expressions based on differential equations governed by parameters. One of the main difference of the BLOOM model, compared to other phytoplankton models, is that to overcome the difficulty in defining all differential equations and parameters, the BLOOM model uses the approach of numerical optimisation based on a linear programming method. To achieve this, a mathematical set of equations (objective and constraint functions) was formulated and the main ones will be presented here. For more detail, the model is fully described in the Open Process Library manual (Deltares, 2014b).

BLOOM calculates the maximum of the biomass distributed in all algae types (objective function, according to Equation 41). It uses a linear programming method to optimise the distribution of available resources (energy and nutrients), always respecting the growth constraints imposed (maximum growth and maximum mortality). Competition between species is determined by the ratio of the resource requirement to the net growth rate, meaning how much a species requires to grow and how fast the species can grow (Los, 2009).

Considering the constraint of nutrients, light energy, growth rate and mortality rate, the mass distribution of each algae type is the one for which the total net biomass of the phytoplankton community is maximal. Equation 41 shows in mathematical terms the objective of the linear programming solution of BLOOM. The constraints for the phytoplankton growth will be described in sections 3.3.2.2 to 3.3.2.5.

$$\text{Maximize } \sum_k Pn_k B_k \quad \text{Equation 41}$$

Where:

$B_k$ = Concentration biomass of algae type k (g/m<sup>3</sup>)

$Pn_k$ = net production rate constant of algae type k (1/day)

### 3.3.2.2. Nutrients

The presentation of nutrient equations in the model is taken from Los (2009). The requirements for nitrogen, phosphorus and silica (only used by diatoms groups) are specified by coefficients for each alga type, as a parameter of each nutrient (N, P and Si) per unit biomass concentration.

The total available concentration of each nutrient (Equation 42) is equals to the sum of: (i) The amount in the total living biomass of algae; (ii) the amount in dead algae (detritus); and (iii) the amount dissolved in the water. Nutrient recycling depends on the remineralisation and sedimentation rate of dead phytoplankton cells (temperature dependent) and a fraction that is directly available (dissolved) to grow new algae through autolysis (cellular degeneration).

$$Cnut = Cnut + \sum_{i=1}^{i=n} (anut_{k,i} * Calg_i) + Cnut_{detritus} \quad \text{Equation 42}$$

Where:

$Cnut$  = concentration of dissolved inorganic nutrient k (gN/m<sup>3</sup>, gP/m<sup>3</sup> or gSi/m<sup>3</sup>)

$anut_{k,i}$  = stoichiometric constant of nutrient k of specie i (gN/C, gP/C or gSi/C)

$Cnut$  = concentration of organic nutrient k (gN/m<sup>3</sup>, gP/m<sup>3</sup> or gSi/m<sup>3</sup>) in detritus

### 3.3.2.3. Energy

Algae need to absorb light for photosynthesis and growth. The relationship between growth and light intensity is crucial for each algae type.

The amount of light energy which a phytoplankton is exposed to varies depending on: (i) the cloud cover that varies the irradiance during the day, (ii) the vertical position of the phytoplankton cells that varies over time, as well as (iii) the species, which react differently to irradiance variations in intensity per unit of time. All these variations change the growth rate over time.

The attenuation of light intensity is an exponential function of depth times the total extinction coefficient, according to the law of Lambert-Beer (Equation 43)

$$I_{i+1} = I_i * \exp^{-et*H} \quad \text{Equation 43}$$

Where:

$I_i$  = light intensity at layer I (W/m<sup>2</sup> or J/s.m<sup>2</sup>)

$et$  = total extinction coefficient unit (1/m)

$H$  = depth (m)

The total extinction coefficient ( $et$  - Equation 44) of visible light is calculated as the sum of seven partial extinction coefficients.

$$et = eat + emt + ept + edt + est + eot + eb \quad \text{Equation 44}$$

Where:

$eat$  = partial extinction coefficient of algae biomass (1/m)

$eb$  = background extinction coefficient (1/m)

$edt$  = partial extinction coefficient of dissolved organic matter (1/m)

$ept$  = partial extinction coefficient of particulate detritus (1/m)

$emt$  = partial extinction coefficient of macrophytes (1/m)

$est$  = partial extinction coefficient of suspended inorganic matter (1/m)

$eot$  = partial extinction coefficient of other substances as a function of salinity (1/m)

$et$  = total extinction coefficient (1/m)

According to Equation 44, algae biomass, suspended and dissolved organic matter (detritus), suspended inorganic matter, the water itself and all remaining dissolved substances contribute as partial extinction coefficient. All these components are calculated based on concentrations and specific extinction coefficients (Equation 45 to Equation 49).

$$eat = \sum_1^n ea_i * Calg_i \quad \text{Equation 45}$$

$$ept = \sum_1^n ea_j * Cpoc_j \quad \text{Equation 46}$$

$$edt = ed * Cdoc \quad \text{Equation 47}$$

$$est = \sum_1^n es_k * Cim_k \quad \text{Equation 48}$$

$$eot = eo * \left(1 - \frac{SAL}{SAL_{max}}\right) \quad \text{Equation 49}$$

Where:

Calg<sub>i</sub> = biomass concentration of algae species group i (gC/m<sup>3</sup>)

Cpoc<sub>j</sub> = concentration of particulate detritus component j (gC/m<sup>3</sup>)

Cim<sub>k</sub> = concentration of suspended inorganic matter fraction k (gC/m<sup>3</sup>)

ea = specific extinction coefficient of an algae species type (m<sup>2</sup>/gC)

ed = specific extinction coefficient of dissolved organic carbon (m<sup>2</sup>/gC)

eo = spec. ext. coefficient of other substances based on relative salinity (1/m)

ep = specific extinction coefficient of a particulate detritus component (m<sup>2</sup>/gC)

es = spec. ext. coefficient of a suspended inorganic matter fraction (m<sup>2</sup>/gDM)

SAL = actual salinity (g/kg)

SAL<sub>max</sub> = maximal salinity (g/kg)

i = index for algae species [-]

j = index for detritus components [-]

k = index for suspended inorganic matter fractions [-]

n = number for algae species

m = number of detritus components

Water characteristics and all other remaining substances that also contribute to light extinction are computed in the form of a background extinction coefficient. The background extinction coefficient (eb) and the partial extinction coefficient of macrophytes (emt) are constant and defined as inputs (Deltares, 2014b).

It should be noted here that the extinction coefficient is calculated differently between the hydrodynamic (Equation 22) model and the ecological model (Equation 44). In practical terms, this means that in the hydrodynamic simulation, the coefficient is constant throughout the simulation period, while in the ecological simulation, it varies along time.

### 3.3.2.4. Growth limits

The maximum gross growth rate,  $Pg_k^{max}$ , in the BLOOM model can be specified as an equation which varies as a power function (Equation 50) or as a linear function (Equation 51) to water temperature (Los, 2009).

$$Pg_k^{max} = (P_{1k}P_{2k})^T \quad \text{Equation 50}$$

$$Pg_k^{max} = P_{1k} * (T - P_{2k}) \quad \text{Equation 51}$$

Where:

$P_{1k}$  and  $P_{2k}$  are type-specific model coefficients (-)

T is the temperature (°C)

The final growth rate is obtained by multiplying the maximum gross growth rate (Equation 50 or Equation 51 with the production efficiency factor ( $E_k$  [-]), which is contingent on light response and the number of hours of daylight for each algae group. Lastly, biomass variation is calculated by Equation 52.

$$\frac{dB_k}{dt} = (Pg^{max}_k * E_k - M_k - R_k) * B_k \quad \text{Equation 52}$$

Where:

$M_k$  = specific mortality rate constant of type k (-)

$R_k$  = specific respiration rate constant of type k (-)

### 3.3.2.5. Mortality limits

In a unfavourable environmental conditions, to avoid a complete removal of a algae specie in a single time-step, the decrease of each algae species has also a constrain. The minimum biomass (Equation 53) value of a species is obtained assuming there is no production, but only mortality.

$$B_k^{min} = B_k^0 \exp[-M_k * \Delta t] \quad \text{Equation 53}$$

Where:

$B_k^{min}$  (g.m-3) = minimum dry biomass of type k at the end of time interval  $\Delta t$

$B_k^0$  (g.m-3) = dry initial biomass of type k

$M_k$  (day-1) = specific mortality rate constant of type k

## 3.4. Model Configuration

The Delft3D models require a computation domain, specification of boundary conditions, initial conditions and the selection of model parameter values that need to be provided for each module. Therefore, the next sections will present model configurations.

In a computation domain, it is necessary to define the grid (mesh), bathymetry and number of vertical layers. For the vertical direction, two types of vertical grid are supported in Delft3D (Figure 3.20):

(a) With the  $\sigma$ -grid option the vertical layer thickness varies with the depth while the number of active layers is constant; and

(b) With the Z-grid option, the layer thickness is fixed and the number of active layers varies with the depth. The layer thickness at the top is determined by the actual water level and at the bottom by the local topography.

The type and thickness of the vertical layer determine depths at which the model calculates and prints the results. Figure 3.21 shows the exact point of model print for an element.

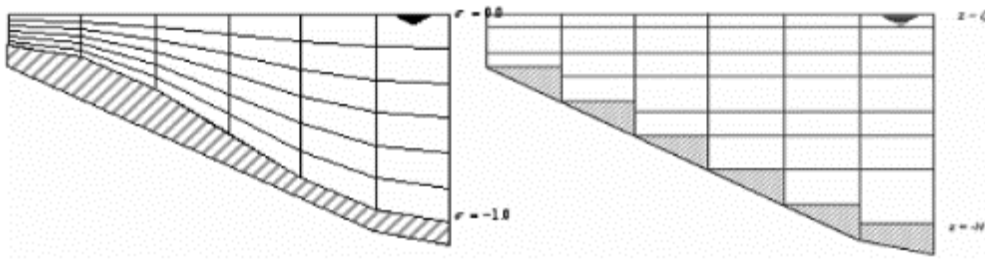
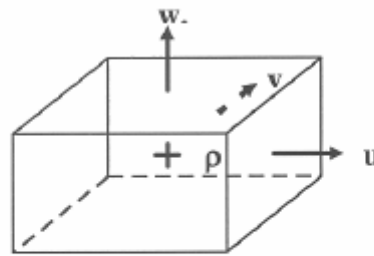


**Figure 3.20** – Example of  $\sigma$ -grid (on the left) and Z-grid (on the right) available in the Delft3D model (Deltares, 2013)



Legend:

- + water level ( $\zeta$ ) / density ( $\rho$ ) point
- velocity point ( $u, v$  or  $w$ )

**Figure 3.21** – Three-dimensional view for an element computation of grid of Delft3D (Deltares, 2013)

Some computation domains require a high refinement of the mesh to represent physical features that are not in other regions. Using many elements in the grid, due to refinement, results in a higher computational time. Different refinement along the computation domain results in different size of adjacent elements that may cause numerical instabilities. To overcome these problems, it is possible to use thin dams.

Thin dams (Figure 3.22) are one dimensional objects (infinitely thin) that can be set on the edges of grid elements. They prevent flow between two adjacent grid elements (cell), but they do not separate the bathymetry on both sides. These elements can be used to describe some specific structure in the model domain, thus avoiding refinement.

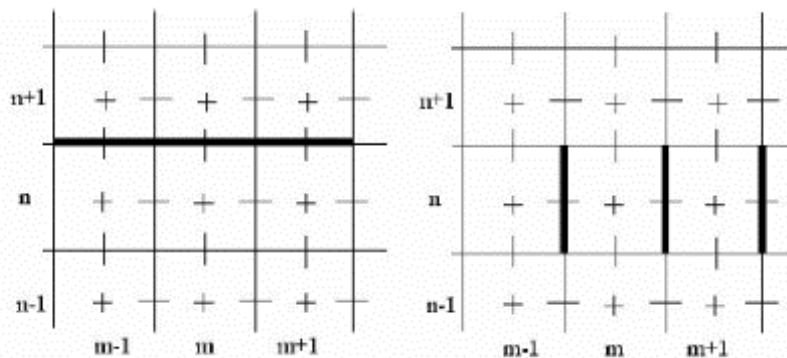


**Figure 3.22** – Sets of thin dams in the computation grid. (Deltares, 2013)

### 3.4.1. Lake Domain

#### 3.4.1.1. Lake Champs-sur-Marne domain

For Lake Champs-sur-Marne, the mesh used (Figure 3.23) was the one used by Scriban (2015) with 1165 horizontal elements and 12 vertical, with mesh elements of  $10\text{ m} \times 10\text{ m} \times 0.33\text{ m}$  (latitude, longitude and depth). In this mesh, the number of vertical layers was defined in a way that also incorporates the depths at which the sensors are located. The Z-grid method was used because the water depth is very homogeneous. Thin dams were used to represent the channels in the central island and artificial barriers near the beaches.



**Figure 3.23** – Mathematical mesh used in Delft3D simulation for Lake Champs-sur-Marne. Yellow lines are thin dams

#### 3.4.1.2. Lake Pampulha domain

For Lake Pampulha, the mesh used has 10 layers along the vertical ( $\sigma$ -grid method) and 4019 grid elements in the horizontal, 40190 elements in total (Figure 3.25). For the horizontal grid, near the boundaries (Figure 3.25) the grid was refined. Grid refinement in the horizontal direction means that in some region of the domain, smaller mesh sizes were used. The advantage is a higher accuracy and less instability in the boundary areas. Lake Pampulha was configured with a grid with mesh elements varying from  $10 \times 10$  to  $50 \times 20$  (latitude, longitude). Thin dams were used to represent the inflow channel coming from the Ressaca and Sarandi rivers (Figure 3.25).

The bathymetry characteristics of Lake Pampulha, greatly vary from upstream to downstream, with an upstream region of very shallow depth (about 1.5 m depth), a transition region, where the depth goes from 1.5 m to almost 13 m and a deeper region further downstream. Thus, during calibration of the hydrodynamic model the  $\sigma$ -grid and Z-grid options were used to compare the model performance and the influence of the grid type.

The Z-grid option does not change the thickness of each vertical layer, which may help to represent the thermocline depth and water stratification. The  $\sigma$ -grid option for the vertical grid layer thickness has the advantage to preserve the number of active layers along the whole grid. Thus, in the shallower part of the lake the vertical resolution was higher (0.15 cm). At monitoring point P1, the Z-grid and  $\sigma$ -grid were very close, with 1-m thickness vertical layers (Figure 3.24). The  $\sigma$ -grid option allows analysing the hydrodynamic of the lake at the bottom of the lake in a same layer in continuity; otherwise, using the Z-grid option the bottom of the lake would be represented in different layers.

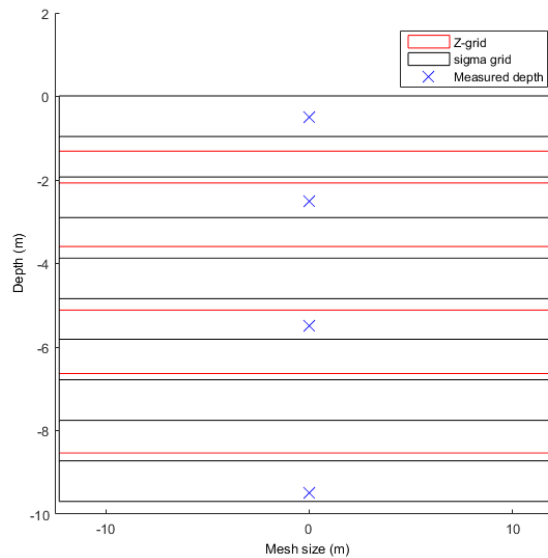


**Figure 3.24** – Vertical resolution for  $\sigma$  and Z-grid in point P1. Blue X represents the measurement depths.

## 3.4.2. Hydrodynamic Model configuration

### 3.4.2.1. Lake Champs-sur-Marne

To configure a boundary condition, its location, type and some related input data are necessary. The following types of boundary conditions are available in the flow model: (a) Water level, (b) Velocity, (c) Neumann (water level gradient)—this option means that the model determines the solution of water level and velocity at the boundaries by imposing the water level gradient instead of a fixed water level or velocity; (d) Discharge or flux (total or per grid cell).

As Lake Champs-sur-Marne is mainly fed by groundwater flowing from the water table of the nearby Marne River, no inflow was considered. Therefore, not open boundary was set. For the initial condition for each period simulated, the water temperatures were initialised with values observed at the point stations at the beginning of each period. For velocity, the water was supposed to be at rest, a usual assumption in three-dimensional hydrodynamic simulation (Soulignac et al., 2017).

Secchi depth, the reduction factor for wind intensity, water salinity, the albedo of the lake water surface, the minimum horizontal background eddy viscosity and diffusivity of heat were set according to Scriban (2015). The wind reduction factor is justified due to various trees, approximately a dozen meters high, around the lake, which reduce the intensity of the wind on the lake surface in comparison to the values measured at the Orly airport station. Three other parameters (Dalton coefficient, Stanton coefficient and wind drag coefficient) involved in the surface boundary conditions were modified from default values by Scriban (2015) during the calibration step. The Dalton coefficient is involved in the wind function (Equation 28) used in the computation of the evaporative heat flux. The Stanton coefficient appears in the wind function, used for the computation of the sensible heat flux (Equation 30 and Equation 31). The wind drag coefficient is involved in the computation of the surface wind shear-stress (Equation 38). These values (Table 3.6) were derived from a previous research conducted on a similar urban lake nearby (less than 15 km away) (Soulignac et al., 2017). As already mentioned in section 3.3.1.3 the horizontal eddy viscosity and diffusion depend on the mesh size of the horizontal grid and on the intensity of the flow. For Lake Créteil a value of  $0.01 \text{ m}^2/\text{s}$  for a mesh size of  $20 \times 20 \text{ m}$  was used (Soulignac et al., 2017). The authors presented a comparison between mesh characteristics and parameter values for four lake applications of the three-dimensional hydrodynamic model Delft3D-

FLOW. Therefore, a value of  $0.0025 \text{ m}^2/\text{s}$  was adopted for Lake Champs-sur-Marne (mesh size of  $10 \times 10 \text{ m}$ ).

**Table 3.6** – Adopted parameters for Delft3D-Flow model in Lake Champs-sur-Marne (From Scriban 2015)

Parameter	Value
Secchi (m)	0.7
Wind Factor	0.6
Albedo	0.08
Horizontal Viscosity ( $\text{m}^2/\text{s}$ )	0.0025
Horizontal Diffusivity ( $\text{m}^2/\text{s}$ )	0.0025
Dalton	0.0015
Stanton	0.00145
Wind Drag	0.0013

In the model configuration, it is necessary to activate specific processes such as the temperature and wind processes. The following constants received the values in all simulations: acceleration of gravity of  $9.81 \text{ m/s}^2$ , water density of  $1000 \text{ kg/m}^3$  and air density of  $1 \text{ kg/m}^3$ .

For bottom shear stress, the Chezy formulation was chosen with uniform values of  $65 \text{ m}^{0.5}/\text{s}$  (default value), with free slip condition in wall roughness. The  $k-\varepsilon$  model for three-dimensional turbulence was chosen. It is a second-order turbulence closure model, in which turbulent kinetic energy  $k$  and the turbulent kinetic dissipation  $\varepsilon$  are prescribed by a transport equation. This model is used for stratified flow and thermocline evolution (Deltares, 2014a).

The computational time step was set to 30 s. This value respects the Courant-Friedrichs-Levy stability criterion (see section 3.3.1.5). The outputs of the model were set for an hourly time step on each mesh element.

### 3.4.2.2. Lake Pampulha

For Lake Pampulha, the 8 tributaries were defined in the domain boundary condition as time series discharge. The water inflows of the Bráunas, Água Funda, Sarandi and Ressaca rivers were set as a single boundary, named Ressaca and Sarandi (Figure 3.25). The hourly water temperature was evaluated by applying two methods using air temperature (see section 3.2.2.3).

For the downstream boundary, all outflows were concentrated in the spillway located at the dam. The type of boundary was set as the water level, according to the spillway rating curve (Table 3.7) defined by Felisberto et al. (2015).



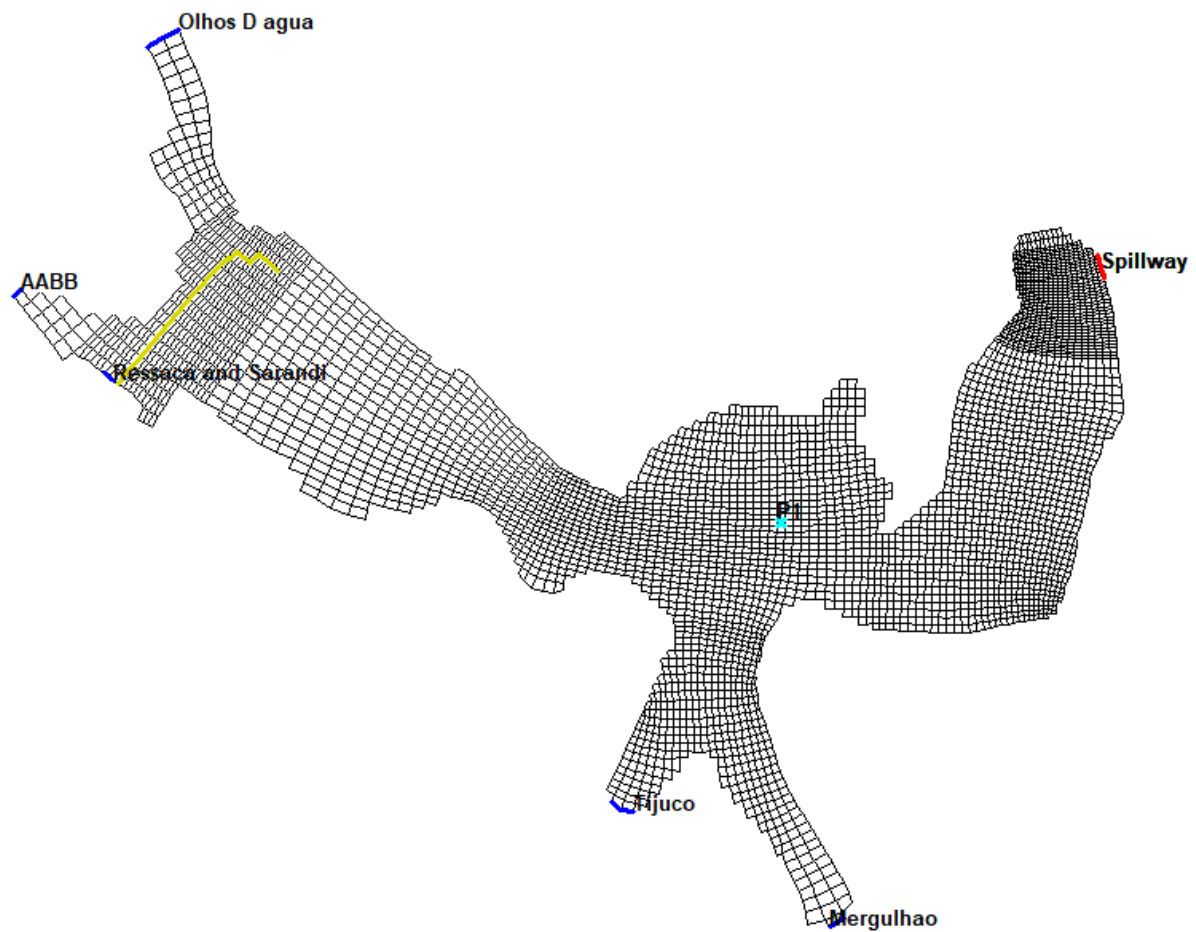


**Figure 3.25** – Water Inflows locations (blue lines), thin dam locations (yellow line), monitoring point (P1 - cyan cross) and spillway location (red line)

**Table 3.7** – Total outflow of Lake Pampulha. (from Felisberto et al., 2015)

Water Level (m)	Total outflow (m <sup>3</sup> /s)
0.0*	0
0.5	121
1.0	201
1.5	282
2.0	368
2.5	459
3.0	555
3.5	655

\* Zero water level corresponds to an altimetric quote of 801.0 m.

In the model configuration the following constants were given in all simulations: acceleration of gravity at 9.81 m/s<sup>2</sup>, water density at 1000 kg/m<sup>3</sup>, air density at 1 kg/m<sup>3</sup> and water salinity at 0.15 ppt, according mean field conductivity measurements applying the Practical Salinity Scale of 1978 (PSS–78) formulated and adopted by UNESCO (1981).

For bottom roughness, the Chezy formulation was chosen with uniform values of 65 (m<sup>1/2</sup>.s<sup>-1</sup>) with free slip condition in wall roughness. The background horizontal viscosity and diffusivity were considered as calibration parameters due to the variation of the size of the elements in the mesh. Vertical eddy viscosity and diffusivity were adopted as negligible. The k–ε model for three-dimensional turbulence was chosen.

Secchi depth (0.3 m) was defined according to measured values. As the Secchi depth values presented almost no variation, it was not chosen as a calibration parameter. Wind factor, Dalton coefficient, Stanton coefficient, horizontal viscosity and diffusivity were estimated during the model calibration.

Wind factor values were tested in a range of 40% higher and 40% lower than measured values, varying by 20% for each scenario. This range of values was defined according to a review of the literature and also based on the methodology of Scriban (2015).

Dalton and Stanton coefficient values were calibrated focusing on the heat exchange between water and air (Equation 27 and Equation 30). Default values were adopted for the wind drag coefficient (0.00063).

A calibration round was also performed considering the water tributary flow. The selected simulation period corresponds to the dry period in the Southeast region of Brazil, starting in April and ending at the end of September. The discharge curves were obtained by Nogueira (2015) using hydraulic simulation to the total hydrological cycle (period of floods and drought) and some measured values. Due to these uncertainties inherent to few flow measurements, a second rating curve was evaluated based only on the dry period simulations and measured values.

The last parameters analysed in the calibration were the background horizontal eddy viscosity ( $v_H$  - [m<sup>2</sup>/s] - Equation 33) and diffusivity ( $D_H$  [m<sup>2</sup>/s] - Equation 34). This step was performed due to variations in the size of the mesh elements. For the model of Lake Pampulha, the mesh elements vary from 50x20 to 10x10 m (Figure 3.25). Two values of background horizontal eddy viscosity and diffusivity were evaluated, 0.025 and 0.0025 m<sup>2</sup>/s respectively.

### 3.4.3. Water Quality Model configuration

The water quality model, D-Water Quality, makes use of the hydrodynamic variable values (velocities, water elevation, density, vertical eddy viscosity and vertical eddy diffusivity) calculated by Delft3D-FLOW. For the water quality model, the Delft3D-ECO module was chosen for Lake Champs-sur-Marne.

In the water quality model, it is necessary to define processes and substances that will be modelled (section 3.3.2). The active processes and substances were selected according to a similar study performed by Soullignac, 2016. The processes included were: (a) Reaeration of oxygen; (b) Algae growth and mortality; (c) Mineralization of organic matter; (d) Nitrification; (e) Phosphate adsorption and precipitation.

The ecological model applied to Lake Champs-sur-Marne has 32 substances that can be grouped into five groups:

- (a) First group: Dissolved oxygen (DO);
- (b) Second group: Particulate mineral matter (IM1);
- (c) Third group: Dissolved mineral matter: ammonium (NH<sub>4</sub>), nitrate (NO<sub>3</sub>), reactive phosphorus (PO<sub>4</sub>), phosphorus attached to IM1 (AAP), reactive silica (SiO<sub>2</sub>) and silica contained in opal (Opal);
- (d) Fourth group: Organic matter. Particulate organic carbon is divided into four fractions whose decomposition rates are different: POC1, POC2, POC3 and POC4. Particulate organic nitrogen is divided into four fractions: PON1, PON2, PON3 and PON4. Particulate organic phosphorus is divided into four fractions: POP1, POP2, POP3 and POP4. Dissolved organic carbon (DOC), dissolved organic nitrogen (DON) and dissolved organic phosphorus (DOP);
- (e) Fifth group: Algae groups.

For the phytoplankton simulation, the BLOOM module was chosen. The selection of the variables representing the main phytoplankton groups was performed according to previous research conducted on Lake Champs-sur-Marne (Huguenard, 2015; Peiffer, 2016). The main phytoplankton groups observed in the lake during the last decade (2006-2015) are Green algae, Diatoms, Cyanobacteria and Dinoflagellates. During summer the dominant groups are (i) Cyanobacteria, mainly *Anabaena*, *Aphanizomenon* and *Microcystis*, and (ii) Dinoflagellates, mainly *Ceratium* and *Peridinium* (Peiffer, 2016). Therefore, 4 state variables to describe the phytoplankton assemblage were defined: the concentrations of Cyanobacteria, Diatoms, Dinoflagellates and Green algae.

After choosing the variables, it is necessary to set the initial biomass. The measurements provided by the FluoroProbe BBE and the Multi-parametric probe (MPx) were used to define the initial concentration of each phytoplankton group. With the measured FluoroProbe BBE vertical profiles, it was determined the representativeness of each of the 4 phytoplankton groups. The respectively concentration for each group was defined by multiplying the percentage of each group by the chlorophyll-a measured through the Multi-parametric probe, meaning that the MPx chlorophyll-a is distributed among the 4 groups. The high-frequency measurements, performed by the Multi-parametric probe MPx, were used to compare the time evolution of total phytoplankton with the total concentration of phytoplankton simulated. The distribution of the phytoplankton groups measured by the BBE was used to compare the phytoplankton composition computed by the model and to evaluate the model calibration.

In order to evaluate the algae accumulation at the beach, a correlation analysis between the values measured by the fluorescence sensors at point A (the monitored point closest to the large beach) and the Chl-a concentrations obtained by laboratory analysis of the water samples collected at the large beach was performed.

Nutrients are described by the following variables: Ammonium, Nitrate and Ortho-Phosphate concentrations. Input values used were based on I.D. Eaux report (2015). Dissolved oxygen concentration is also a state variable of the biological model and input values are required. For these reasons, measurements of Multi-parametric Probe (Seabird SBE 19™) were used. Organic matter was not measured, and a zero value was adopted.

An important process in the model is the calculation of the light conditions in the water. The light extinction coefficient (Equation 44) was defined based on irradiation data measured along the vertical profile through PAR (Photosynthetically active radiation) by Li-Cor Li 193. This process will be better described in section 4.3. The BLOOM module requires a large set of species coefficients, related to phytoplankton physiology (Table 3.8), algal stoichiometry (Table 3.9) and specific extinction coefficients and sedimentation velocities (Table 3.10). All the values presented are the model default ones.

**Table 3.8 – Phytoplankton physiology**

Phytoplankton	Phenotype	Max. Production*	Temp. Coeff. Production**	Equation
Diatoms	Energy	0.35	1.06	Equation 50
	P & Si	0.35	1.054	
Flagellates	Energy	0.35	1.05	Equation 51
Green	Energy	0.068	0	
	Nitrogen	0.068	3	
	Phosphorus	0.068	3	
Bluegreen (Cyanobacteria)	Energy	0.056	3	
	Nitrogen	0.048	5	
	Phosphorus	0.048	5	

\*P<sub>1</sub> and \*\*P<sub>2</sub> in Equation 50 and Equation 51

**Table 3.9 – Phytoplankton stoichiometry**

Phytoplankton	Phenotype	N/C	P/C	Chla/C
Diatoms	Energy	0.21	0.018	0.04
	P & Si	0.188	0.0113	0.025
Flagellates	Energy	0.275	0.018	0.029
Green	Energy	0.275	0.0238	0.033
	Nitrogen	0.175	0.015	0.025
	Phosphorus	0.2	0.0125	0.025
Bluegreen (Cyanobacteria)	Energy	0.225	0.0188	0.033
	Nitrogen	0.125	0.0188	0.02
	Phosphorus	0.15	0.015	0.02

**Table 3.10 – Phytoplankton typology and sedimentation velocity**

Phytoplankton	Phenotype	Extinction*	Sedimentation (m/s)
Diatoms	Energy	0.27	1.0
	P & Si	0.1875	1.5
Flagellates	Energy	0.225	0.5
Green	Energy	0.225	0.5
	Nitrogen	0.1875	1
	Phosphorus	0.1875	1
Bluegreen (Cyanobacteria)	Energy	0.4	0.0
	Nitrogen	0.2875	0.0
	Phosphorus	0.2875	0.0

\*ea in Equation 45

Many coefficients of the D-Water Quality model have either fixed values or preferred values that have been determined by extensive calibrations for many different water systems (Deltares, 2014b; Los, 2009). Consequently, the values are considered as generic and model calibration can usually be restricted to just a few coefficients, such as the decomposition rate constants, the nitrification rate constant and the sedimentation and resuspension velocities (Deltares, 2013). In the calibration step of the model, only the sedimentation velocities were changed. According to Brennen et al. (2018), many different sedimentation values are used in literature, the standard values vary from 0.1 to 1.0 m/day. The values also change between groups and species and according to concentration and colony sizes (Larocque et al., 1996). For Diatoms and Dinoflagellates, the default settling velocities values were used. For cyanobacteria and Green algae, the velocity was calibrated. For biogeochemical processes, default parameters were used.

### 3.5. Lake Champs-sur-Marne simulations

#### 3.5.1. Hydrodynamic simulations

The criteria used to select the simulation periods are as follows: (a) A mixed condition at the beginning of the period, and (b) A thermal stratification during most of the period. This focus on thermal behaviour was chosen because the thermal stratification of the water is one of the main processes that can boost phytoplankton production in favour of cyanobacteria. The reason to start with a mixed condition, concerning phytoplankton growth, is that vertical distribution of the nutrients and Chl-a concentration is rarely known. So, a mixed condition allows considering a uniform distribution in the water column.

According to [these](#) criteria, the resulting periods of simulation are presented in Table 3.11:

**Table 3.11** – Simulated period in Lake of Champs-sur-Marne

Period	Date	Number of hourly values	Used for
01	23 <sup>rd</sup> June to 30 <sup>th</sup> June 2015	159	Phytoplankton transport (tracer)
02	13 <sup>rd</sup> July to 27 <sup>th</sup> July 2015	342	Coupled hydrodynamic and ecological
03	14 <sup>th</sup> July to 01 <sup>st</sup> August 2016	456	
04	19 <sup>th</sup> September to 12 <sup>nd</sup> October 2016	567	ADCP measurement

These periods were used to validate the adopted parameters (Table 3.6) for hydrodynamic simulation and to evaluate the behaviour of the lake and the influence of hydrodynamic and weather conditions.

Period 1 was also used to evaluate the phytoplankton transport (specific methodology in section 3.5.2). Periods 2 and 3 were selected to run the coupled hydrodynamic and ecological simulation (specific methodology in section 3.5.3). During period 4, water velocities were measured using an Acoustic Doppler current profiler (ADCP). Therefore, this period was simulated to assess the velocities calculated by the model.

For a better evaluation between measured and simulated velocities, the time step resolutions for both data need to be the same. Due to low water velocity values, a time step smaller than an hourly resolution presented inappropriate behaviour due to a high amount of noise and erratic behaviour (without a pattern). Furthermore, an hourly resolution in the model also avoids generating a very large amount of data in the simulation with smaller time steps. Therefore, for a coherent comparison, average hourly values of simulated and total current velocity measured were used.

The model performance assessment was carried out using spectral analysis. One of the main features of flows in a lake is that they contain a wide range of dynamically active scales. To access the information of scale values, it is important to carry out a spectral study of the fields and simulated values (Mezmate, 2014; Soullignac et al., 2017). This was carried out using the fast Fourier transform (FFT), which is a tool used for analysing and measuring signals from field data acquisition devices (Cerna and Audrey, 2013), in which was used to find the frequency components of the water velocity in time. Through spectrum analysis, it is possible to acquire time-domain signals and measure the frequency content. Comparing the measured and simulated spectra it is possible to evaluate the model performance. Comparison was performed in the surface, middle and bottom depth values. Additionally, the measured and simulated daily values were also correlated to wind intensity to evaluate the model performance in representing the lake response to this external factor on the same depths and for the average vertical profile.

### 3.5.2. Phytoplankton transport simulation

This simulation (for the period 1 from 23<sup>rd</sup> June to 30<sup>th</sup> June 2015) was performed to investigate the impact of hydrodynamics on phytoplankton transport. Phytoplankton biomass was considered as a conservative tracer, with neither growth nor decay. In this way, this simulation was performed only with the hydrodynamic model (Delft3D-Flow) and the effect of the hydrodynamics on the spatial distribution of the tracer was studied.

According to the lake manager observations, it was assumed that the blooms generally start at the southern end of the island. Therefore, the initiation of a cyanobacteria bloom was simulated as an input spot at the water surface (0.5 m depth) near point B (Figure 3.26). The model results were considered at points A, C, D and at the beach (Figure 3.26).

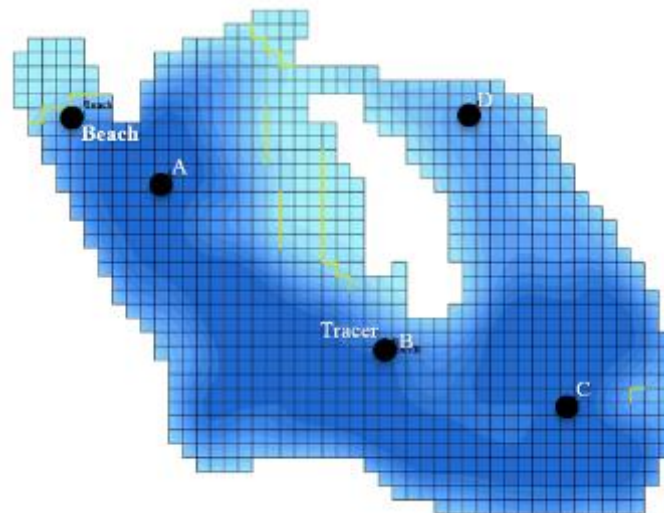


**Figure 3.26** – Location of the tracer input and the points evaluated.

A constant inflow of  $0.1 \text{ m}^3/\text{s}$ , with the concentration varying in time according to Table 3.12, was set for the tracer input. These values are close to the Chlorophyll concentrations measured at point B during this period (Figure 3.27). The measured concentration of Chl-a in the lake at the beginning of the period was  $5 \mu\text{g/L}$ . Therefore the initial tracer concentration was also set with this value.

**Table 3.12** – Values of the tracer input

Time	Flow ( $\text{m}^3/\text{s}$ )	Tracer Concentration ( $\mu\text{g/L}$ )
23/06/2015 10:00	0.1	5.0
25/06/2015 10:00	0.1	20.0
27/06/2015 10:00	0.1	20.0
28/06/2015 10:00	0.1	5.0
30/06/2015 00:00	0.1	5.0

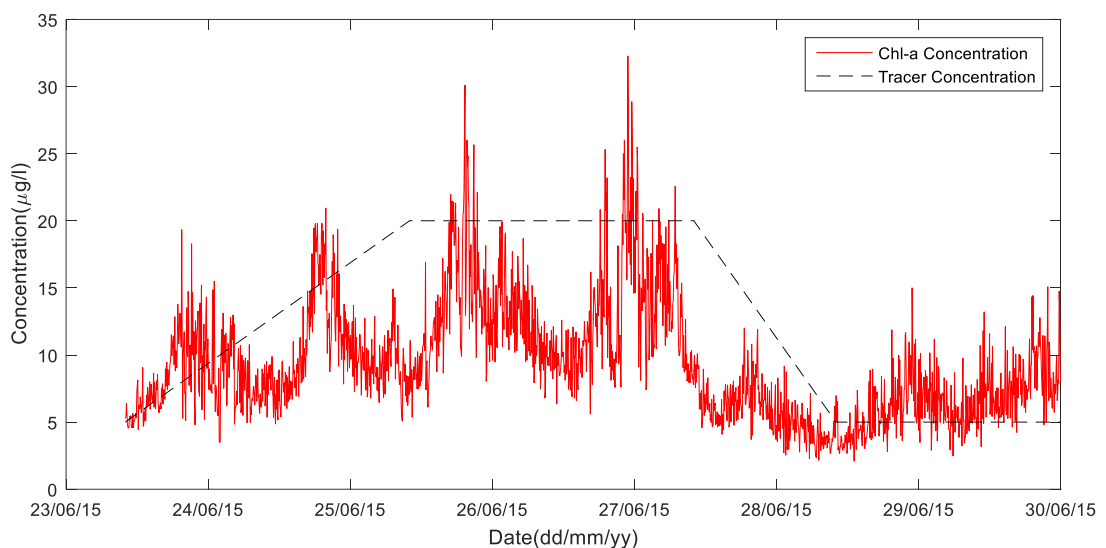


**Figure 3.27** – Tracer input and fluorescence measured at point B

Three simulations were performed to evaluate the influence of wind direction on the hydrodynamics and tracer concentration. The first simulation, called the reference simulation, was done with an unchanged wind direction (Figure 3.28). The wind speed from the Orly Station was reduced by 40%, according to the calibrated hydrodynamics results (Figure 3.29). The second and third scenarios were performed by

changing the direction of the wind to western (wind coming from the west) and northern (wind coming from the north) directions. Namely, in the second simulation with a western wind, it means that the wind comes only from the west; and in the third scenario with a northern wind, it comes only from the north. In all scenarios, the same wind speed was used as in the reference simulation.

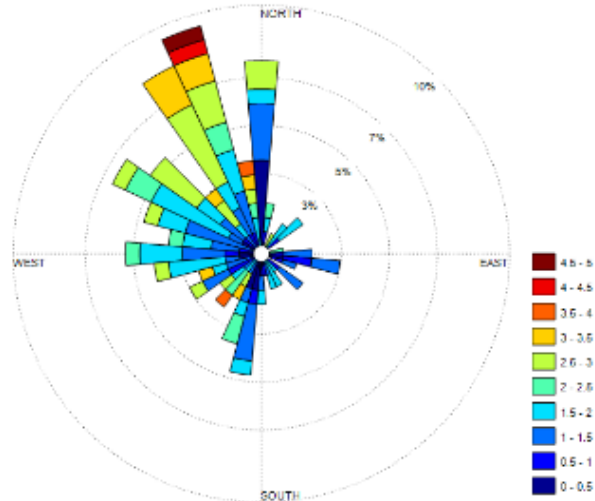


**Figure 3.28** – Wind direction and speed (m/s) for Orly Station during the period from 23<sup>rd</sup> June 2015 to 30<sup>th</sup> June 2015

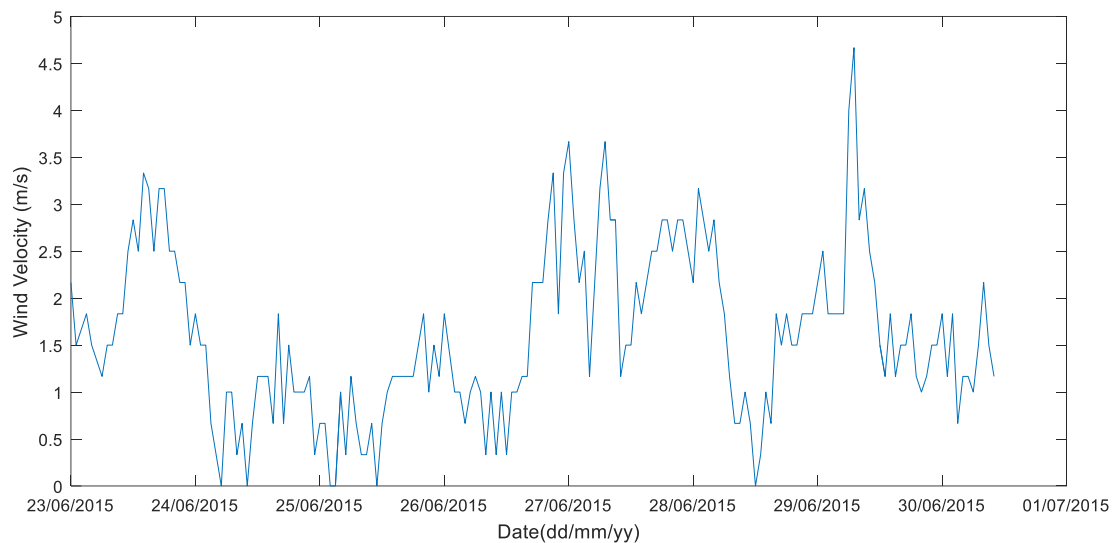


**Figure 3.29** – Wind velocity (m/s) for Orly Station during the period from 23<sup>rd</sup> June 2015 to 30<sup>th</sup> June 2015

### 3.5.3. Coupled hydrodynamic and ecological simulation

In parallel with the criteria used to select a period to simulate the hydrodynamics of the lake, criteria were defined for selecting periods of ecological simulation. The criteria used were: (i) Occurrence of Chl-a concentration higher than 10  $\mu\text{g/L}$ , considering the threshold stated at 10 $\mu\text{g}$  Chl-a/L for a first warning level in bathing waters; (ii) Presence and dominance of cyanobacteria in sampling monitoring on the large beach during the period and (iii) Availability of vertical fluorometric profile, in order to know the algal group assemblage. To evaluate the performance of the coupled hydrodynamic and ecological model, two periods were simulated for two different years, with the previously established criteria being respected. The first period, from 13<sup>th</sup> to 27<sup>th</sup> July 2015 (two-week duration), was used as

calibration. The second period, from 14<sup>th</sup> July to 01<sup>st</sup> August 2016 (18 days), was used as a verification period. A sensitivity assessment was performed based on the minimum, mean and maximum values of the nutrients database to verify the biomass behaviour.

### 3.6. Lake Pampulha Simulation

Two different periods in 2016 were chosen for hydrodynamic simulations. The first was used as a calibration period and the second as validation. The criteria used were the same as those of the Champs-sur-Marne hydrodynamic simulation: (a) a mixed condition at the beginning of the period; and (b) a thermal stratification during most of the period. A third period was selected in 2015 to evaluate the hydrodynamic behaviour of the lake for a longer period.

#### 3.6.1. Calibration period

The first period, used for the calibration of the Delft3D-Flow parameters, lasts 18 days (n= 440), from 16<sup>th</sup> May 2016 to 03<sup>rd</sup> June 2016. This period includes mixing and thermal stratification conditions. A mixing condition was classified when the difference of temperature of surface and bottom was less than 0.1 °C.

#### 3.6.2. Validation period

The second period, lasting 16 days (n= 388), from 29<sup>th</sup> May to 14<sup>th</sup> June 2016, was used for the validation of Delft3D-Flow. This period includes the mixing and thermal stratification conditions.

#### 3.6.3. Longer validation period

After hydrodynamic calibration and validation, a third period was selected and simulated. The purpose of the simulation was to evaluate the hydrodynamic behaviour of the lake for a longer period. The period selected for simulation was from 15<sup>th</sup> May to 10<sup>th</sup> August 2015, a duration of almost three months.

### 3.7. Performance indicators

Three mathematical indicators were used to compare simulated and measured water temperature and Chl-a fluorescence (in the case of Lake Champs-sur-Marne). These indicators were computed using the hourly outputs of the model and the hourly averaged measured values. The mean absolute error (MAE) indicates the difference between the simulated and measured values. The coefficient of determination ( $R^2$ ) represents the proportion of the variance of measured values that is predictable by the simulation, an  $R^2$  of 1.0 means the measured values can be predicted without error. The relative error (RE) is the ratio of the sum of the absolute errors to the sum of mean measured data.

$$MAE = \frac{1}{n} \sum_{i=1}^{i=n} |y_i - \hat{y}_i| \quad \text{Equation 54}$$

$$R^2 = \frac{\sum_{i=1}^{i=n} (y_i - \hat{y}_i)^2}{\sum_{i=1}^{i=n} (y_i - \bar{y}_i)^2} \quad \text{Equation 55}$$

$$RE = \frac{\sum_{i=1}^{i=n} |y_i - \hat{y}_i|}{\sum_{i=1}^{i=n} \hat{y}_i} * 100 \quad \text{Equation 56}$$

Where:

$y_i$  = data simulated in time interval i

$\hat{y}_i$  = data measured in time interval i

$\bar{y}_i$  = average of data measured

n = number of measured values



## 4. LAKE CHAMPS-SUR-MARNE RESULTS

This chapter will present the results for the study site of Champs-sur-Marne, located in France. Each section in this chapter has a specific objective. As seen in section 2.3 of the Literature Review, Chl-a concentration, used as a proxy for phytoplankton biomass, may contain significant differences when measured through different devices. Thus, section 4.1 will present the results of a comparison between different measurements of Chl-a fluorescence performed in the lake.

Hydrodynamics play an important role in cyanobacteria behaviour in lakes. Thermal stratification might favour cyanobacteria growth due to optimal buoyancy conditions, while mixing events may facilitate nutrient release from the sediment, allowing an increase in phytoplankton. Thus, section 4.2 will present the results of a hydrodynamic simulation, covering lake thermal and velocity behaviour.

Phytoplankton and cyanobacteria modelling can be performed with different approaches, each with certain advantages and limitations, as seen in section 2.4 of the Literature Review. Section 4.2.3 will present the results of phytoplankton biomass transport through hydrodynamic model simulations, focusing on the influence of wind in spatial and temporal distribution. Section 4.3 will present the results of the coupled hydrodynamic and ecological simulation, covering the model performance in the representation of total phytoplankton behaviour and species competition. A first period was selected to calibrate the model based in Chl-a measurements. Based on the parameters defined in the calibration period, a second period was selected to verify the behaviour of biomass. In order to investigate the model sensitivity to nutrient concentrations, a range of nutrient concentrations was simulated. Finally, Section 4.4 will present conclusions and discussions of results of this study site.

### 4.1. Comparison between different Chl-a fluorescence measuring devices

In Lake Champs-sur-Marne, as seen in section 3.2, Chl-a Fluorescence was measured at three different points (Figure 3.13) using (i) a high-frequency multi-parametric probe (MPX) at 1.5 m depth (middle of the water column) and (ii) a BBE FluoroProbe, to obtain vertical profiles in fortnightly campaigns. Near the large beach, at weekly and monthly frequencies, samples were collected to identify phytoplankton and cyanobacteria species after laboratory analysis.

In order to assess the consistency of Chl-a measurements, the correlation between Chl-a fluorescence measured by the MPX sensor and Chl-a measured by the spectrofluorometer (BBE) was obtained.

To obtain the correlation, the time and depth of measurements need to be consistent. Therefore, the considered MPX values were obtained through the average of all values observed during the instant of vertical profiles measurement. For the BBE vertical profiles, the considered values were calculated through the average of the values 16 cm above and below of the MPX depth (1.5 m). This range of value was defined to maintain the same vertical refinement of the mathematical model mesh (33 cm).

The values considered at all points for both devices are strongly correlated ( $R^2=0.94$ ,  $n=25$ ,  $p<0.0001$  Figure 4.1). However, the values measured by the fixed fluorescence sensor (MPX) presented values almost three times lower than the BBE sensor at the same point (Equation 57). This difference is difficult to justify, since the equipment have periodic maintenance and use the principle of light excitation to measure Chl-a Fluorescence, however, MPX uses just one wavelength while BBE employs six.

$$Chl_{BBE} = 2.88 * Chl_{MPX}$$

Equation  
57

This result did not change significantly when each point was analysed separately and when the full vertical profile was considered ( $R^2=0.90$ ,  $n=25$ ,  $p<0.0001$  and  $Chl_{BBE} = 2.90 * Chl_{MPX}$ ).

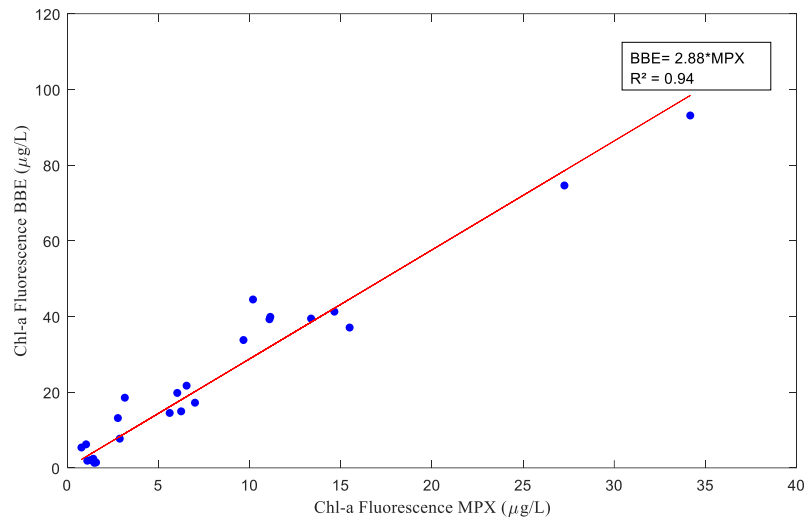


**Figure 4.1** – Chl-a measurements using MPX and BBE for all points

To link the high-frequency monitoring results, a correlation analysis was performed between the values measured by the fluorescence sensors at point A (FluoA) and the Chl-a concentrations obtained by laboratory analysis of the water samples collected at the large beach (ChlBeach). The beach is located approximately 100 m from point A.

The fluorescence sensor data are about 4.4 times smaller than lab analysis values (Equation 58), but they show a reasonable correlation ( $R^2 = 0.63$ ,  $n = 30$ ,  $p < 0.00001$  - Figure 4.2)

$$Chl_{Beach} = 4.37 * Fluo_A$$

**Equation 58**

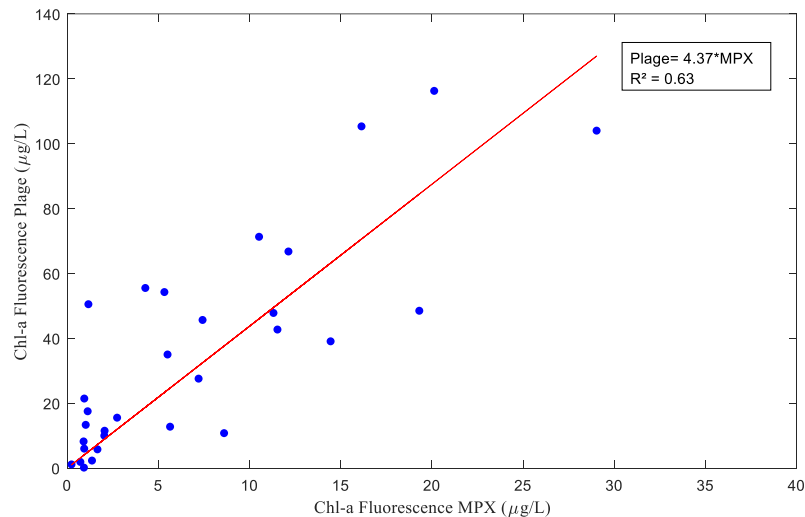


**Figure 4.2** – Chl-a measurements using MPX in point A and laboratory analysis of water samples from a point near the beach

Equation 58 may indicate a phytoplankton accumulation at the large beach higher than Equation 57 that presented different values due to the use of different devices. This situation corresponds with reports from staff, who affirms that the large beach tends to present an accumulation of phytoplankton. Unfortunately, the influence inherent to the different measurement methods and the distance between the point A and the large beach could not be evaluated. Therefore, it was recommended to add a

monitoring point at the large beach using MPX and BBE devices to evaluate the hypothesis of biomass accumulation in the large beach. Due to this data limitation, this accumulation hypothesis will be evaluated through mathematical modelling in the next sections.

## **4.2. Hydrodynamic Simulations**

### **4.2.1. Results of the temperature simulations**

As presented in the Literature Review, water temperature and nutrient concentration are the main variables that determine phytoplankton and cyanobacteria growth, and thermal stratification is one of the main processes that can boost phytoplankton production in favour of cyanobacteria. Unfortunately, nutrient data are scarce for Lake Champs-sur-Marne (section 3.2.1.6). High-frequency thermal monitoring is a rare case in the literature, even more due to the characteristics of shallow, small and urban lakes. Therefore, the next sections (4.2 and 4.2.3) will present Lake Champs-sur-Marne's thermal behaviour and the performance of Delft3D-Flow in representing it.

With the calibration parameters (sections 3.4.1 and 3.4.2.1), the temperature behaviour of Lake Champs-sur-Marne was simulated for 4 different periods, in summer and autumn, as follows:

1. 23<sup>rd</sup> June 2015 to 30<sup>th</sup> June 2015
2. 13<sup>rd</sup> July to 27<sup>th</sup> July 2015
3. 14<sup>th</sup> July 2016 to 01<sup>st</sup> August 2016
4. 19<sup>th</sup> September 2016 to 12<sup>nd</sup> October 2016

For the period 1 (23<sup>rd</sup> June 2015 to 30<sup>th</sup> June 2015) an initial mixed water condition of 20.8 °C and meteorological inputs (Figure 4.3) were set in the Delft3D-Flow model. The results for the temperature at 3 depths (0.5, 1.5 and 2.5 m) are presented in Figure 4.4 for point A. For the other points (B and C), the results were similar and are presented in ANNEX 8.8.

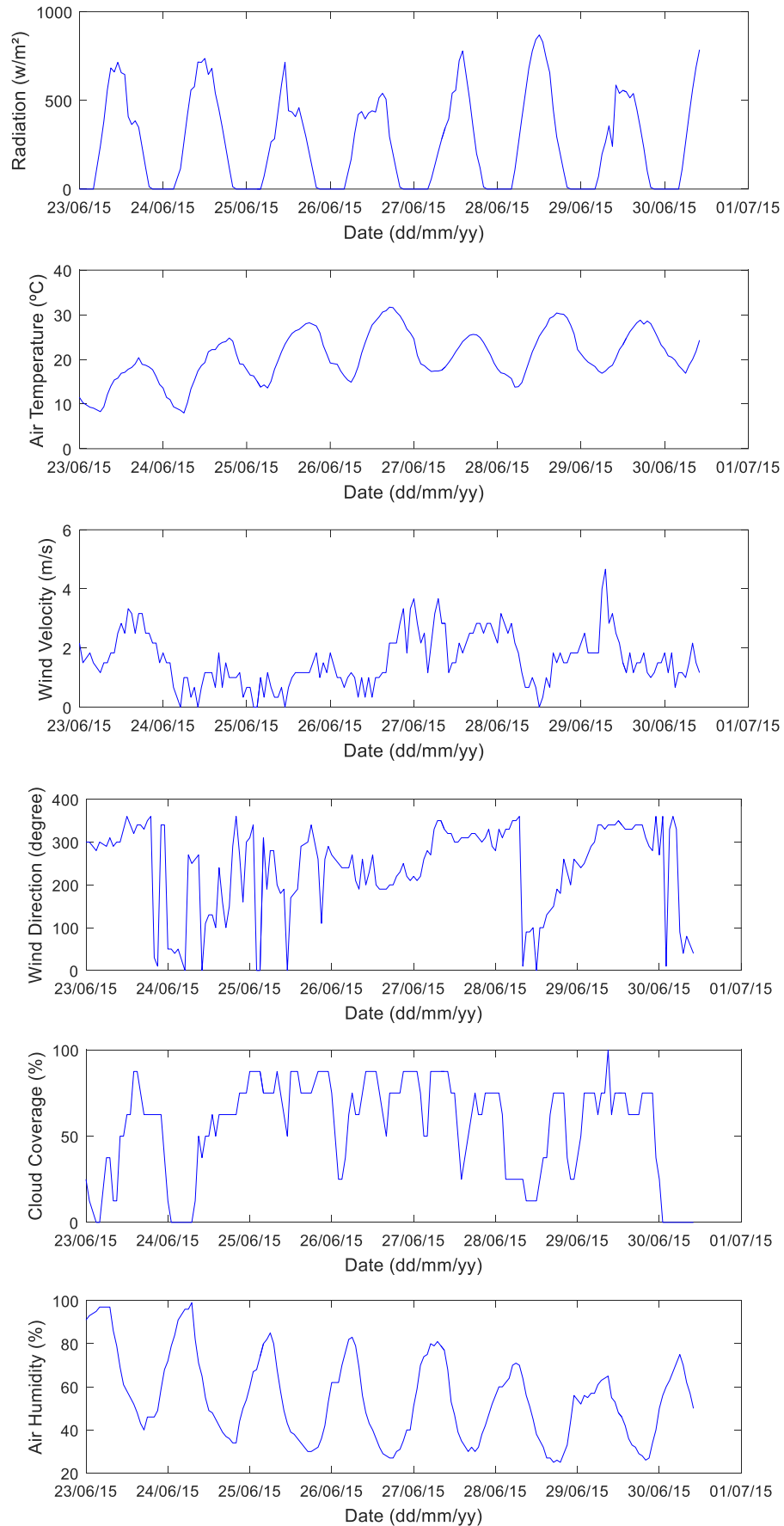


**Figure 4.3** – Radiation, atmosphere temperature, wind intensity and direction, cloud cover and humidity during period 1 (23<sup>rd</sup> June 2015 to 30<sup>th</sup> June 2015)

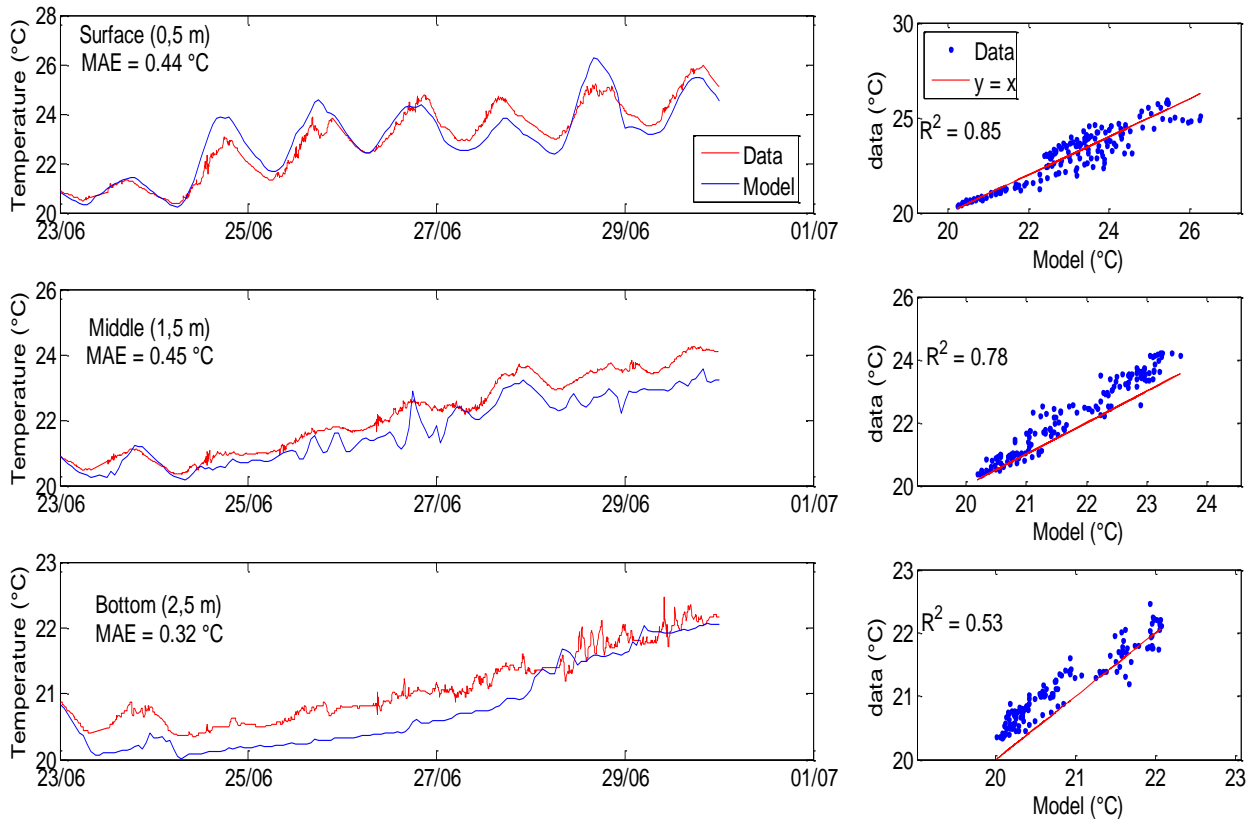


**Figure 4.4** – Comparison of the temperature between measured and simulated data for period 1 (23<sup>rd</sup> June 2015 to 30<sup>th</sup> June 2015) at point A

The agreement between the modelled and observed temperatures can be considered quite good. The simulated surface temperature correctly represented peaks and daily cycles with an  $R^2$  of 0.85. At the middle and bottom depths, the model also represented the thermal behavior well. Graphically, at the bottom depth, it seems that the model could not simulate the temperature adequately, being colder for most of the period. The  $R^2$  for the bottom depth was not very high (0.53). However, the MAE was the smallest (0.32°C) in comparison to other depths (0.44 °C at the surface and 0.45°C at the middle depth) and the temperature variation was also lower. Therefore, this result shows that the model can be considered as validated.

Analysing the temperature for each monitored point separately and comparing the measured data for the three depths with those simulated (Figure 4.5) allow us to note that the stratification period is well represented. The partial mixing event on 27<sup>th</sup> and 28<sup>th</sup> June at the surface and middle depths, was correctly predicted by the model.

The alternation of mixing and stratification was well reproduced (arrows in Figure 4.6). The general heating behaviour of the lake during the simulated period was observed and simulated. Water temperature began at 20.8 °C (23<sup>rd</sup> June) and, after a week, the surface was 5° C warmer and the bottom more than 1.0 °C warmer as well. This warmer condition could also be observed in air temperature (Figure 4.3), which presented a daily cycle with an increase in the minimum temperatures.

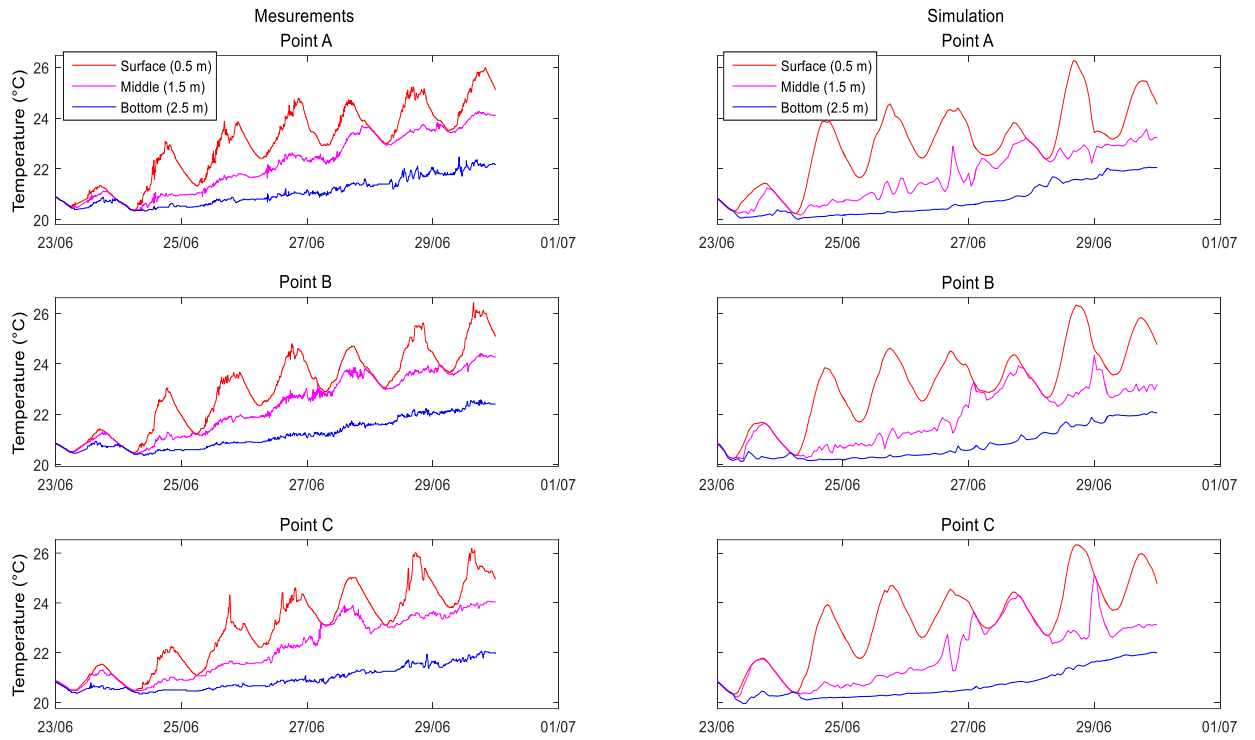


**Figure 4.5** – Stratification behaviour at points A, B and C from 23<sup>rd</sup> June 2015 to 30<sup>th</sup> June 2015

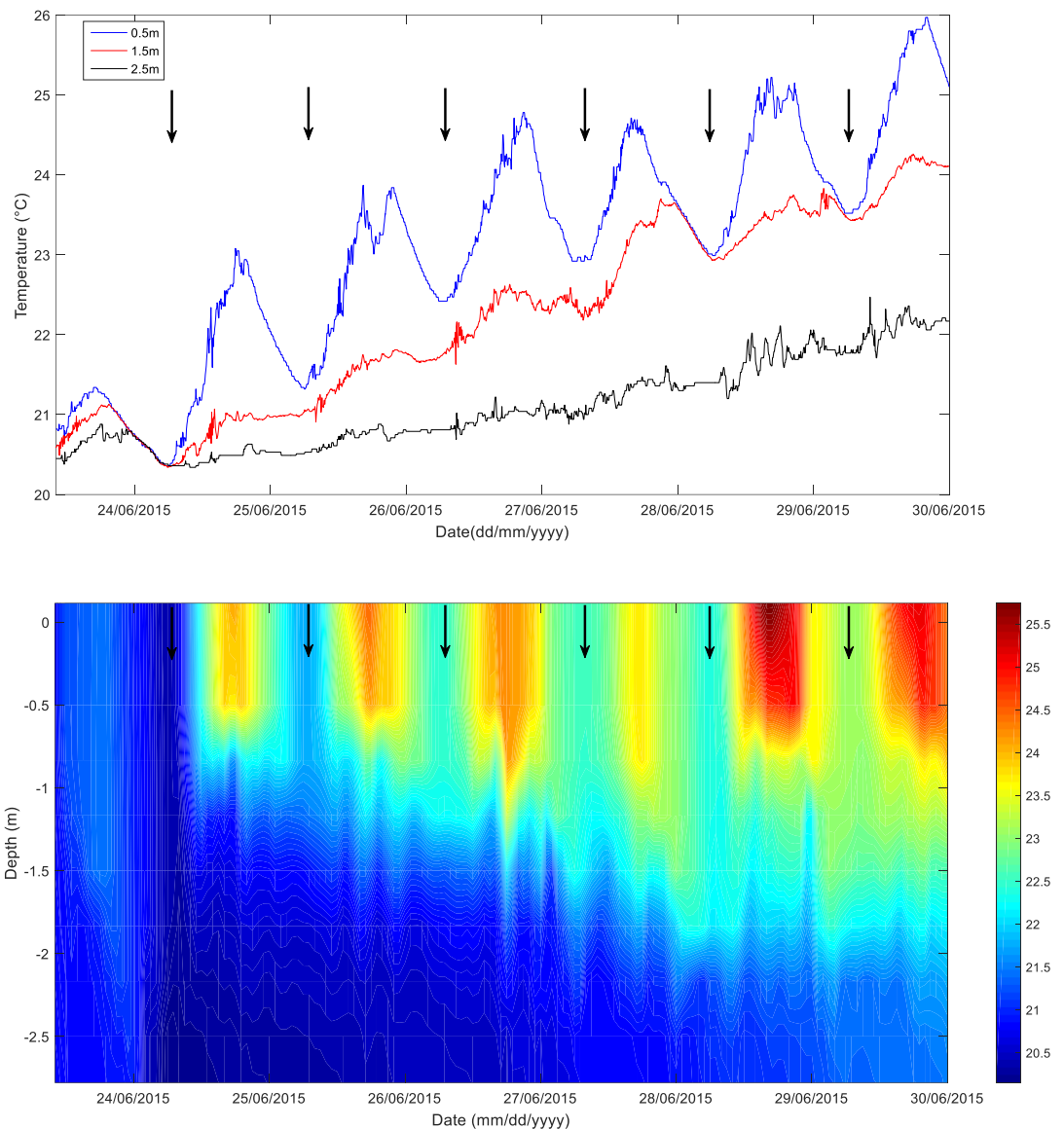


**Figure 4.6** – Comparison of the stratification condition between measured (a) and simulated (b) data from 23<sup>rd</sup> June 2015 to 30<sup>th</sup> June 2015 in Point A. Red arrows represent partial mixing events.

The comparison of the temperature between point A (maximal depth of 3 m), B (maximal depth of 2.8 m) and C (maximal depth of 3.2 m) are presented in Figure 4.9 for the three monitored depths (0.5, 1.5 and 2.5 m). The thermal behaviour is quite homogenous for the three points. On the surface, the temperatures are practically the same for all three points. Small differences were well represented at the middle depth and partially at the bottom. This homogeneity is because the points have almost the same depths and are in similar regions of the lake. Therefore, the model result was used to evaluate the thermal behaviour in different regions.

The simulated temperature behaviour at the surface (0.5 m depth) for point A (3 m depth), Beach (1.9 m depth) and in the channel on the central island (1.3 m depth) are presented in Figure 4.7 and in Figure 4.8 in the lake surface in 24<sup>th</sup> June 2015 at 14 hours representing a different water temperature as example. For these points, the thermal behaviour is no longer homogenous. All points have the same daily cycles. However, the thermal amplitude is not the same.

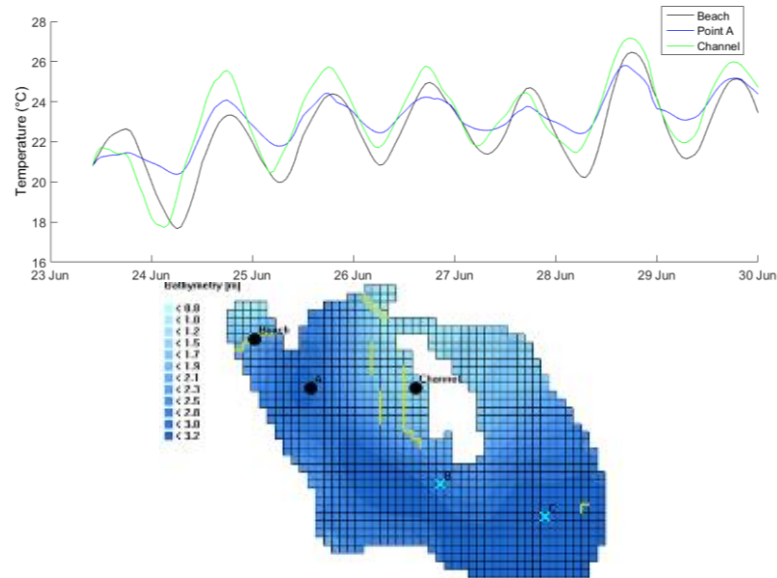


**Figure 4.7** – Comparison between the simulated temperature for point A, Beach and Channel for period 1 (23<sup>rd</sup> June 2015 to 30<sup>th</sup> June 2015).

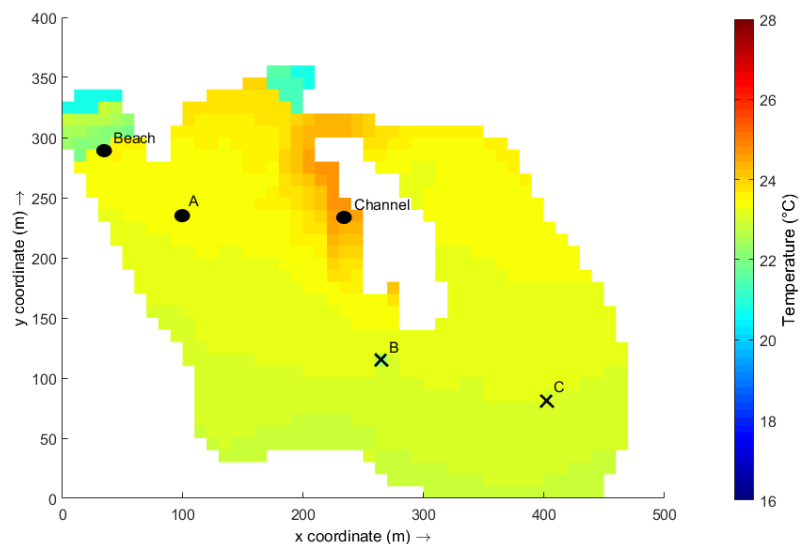


**Figure 4.8** – Surface simulated temperature for period 1 on 24 June 2015 at 14 hours.

The thermal and hydrodynamic heterogeneity of the lake can also boost the occurrence of heterogeneity concentration in the lake. It is important to highlight that the east channel has less communication with the rest of the lake (Figure 3.4), which may affect the water temperature and phytoplankton behaviour. Section 3.1.1 presented a description of the central island. Therefore, a monitoring point on the channel located at the central island is recommended to better evaluate this behaviour.



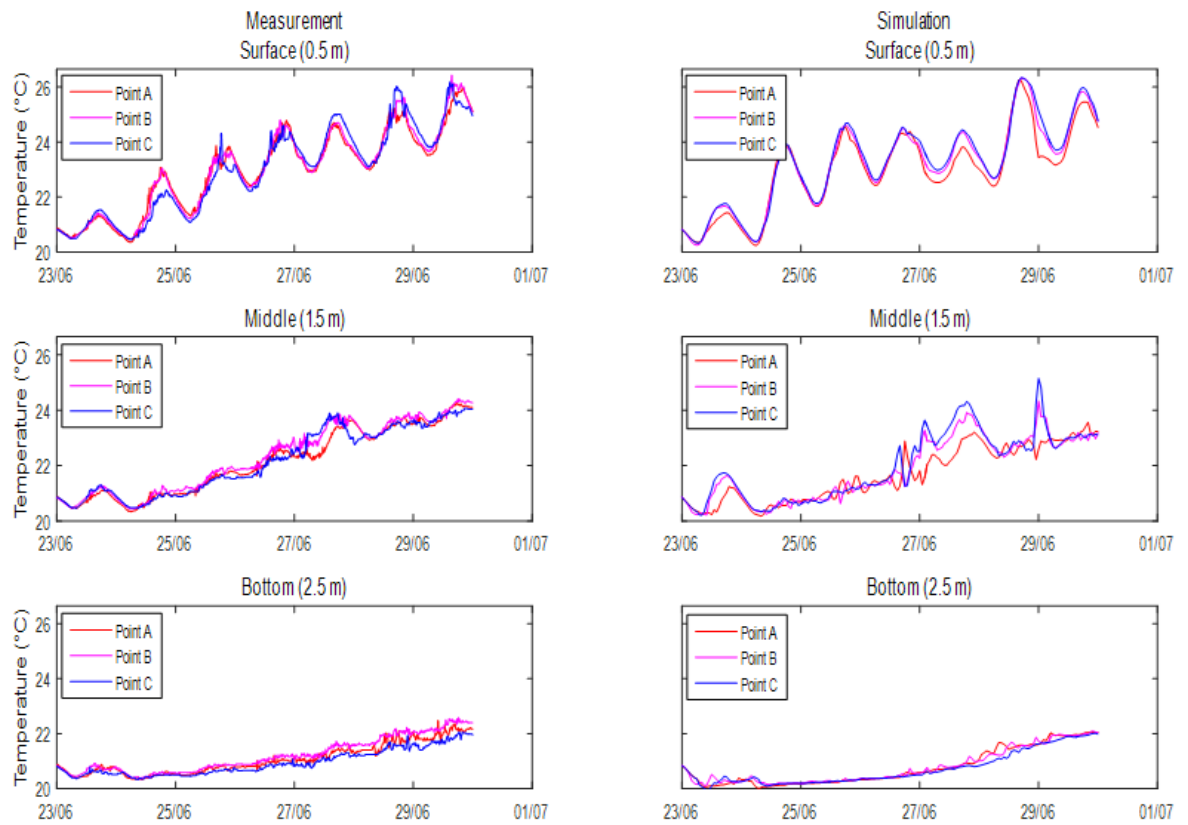


**Figure 4.9** – Comparison of the temperature at points A, B and C at 3 depths for period 1 (26<sup>th</sup> June 2015 to 30<sup>th</sup> June 2015).

With the same parameters used in the simulation for period 1, period 2 (13<sup>rd</sup> July 2015 to 27<sup>th</sup> July 2015) was simulated. For initial conditions, a uniform mixed temperature of 23.4 °C was set for all grid elements according to measurements. Meteorological conditions for the period are presented in Figure 4.10. Temperature results for simulation 2 are presented in Figure 4.11. The hydrodynamic model was able to represent the temperature behaviour accurately. For all depths, MAEs were less than 0.5 °C and with an  $R^2$  higher than 0.7.

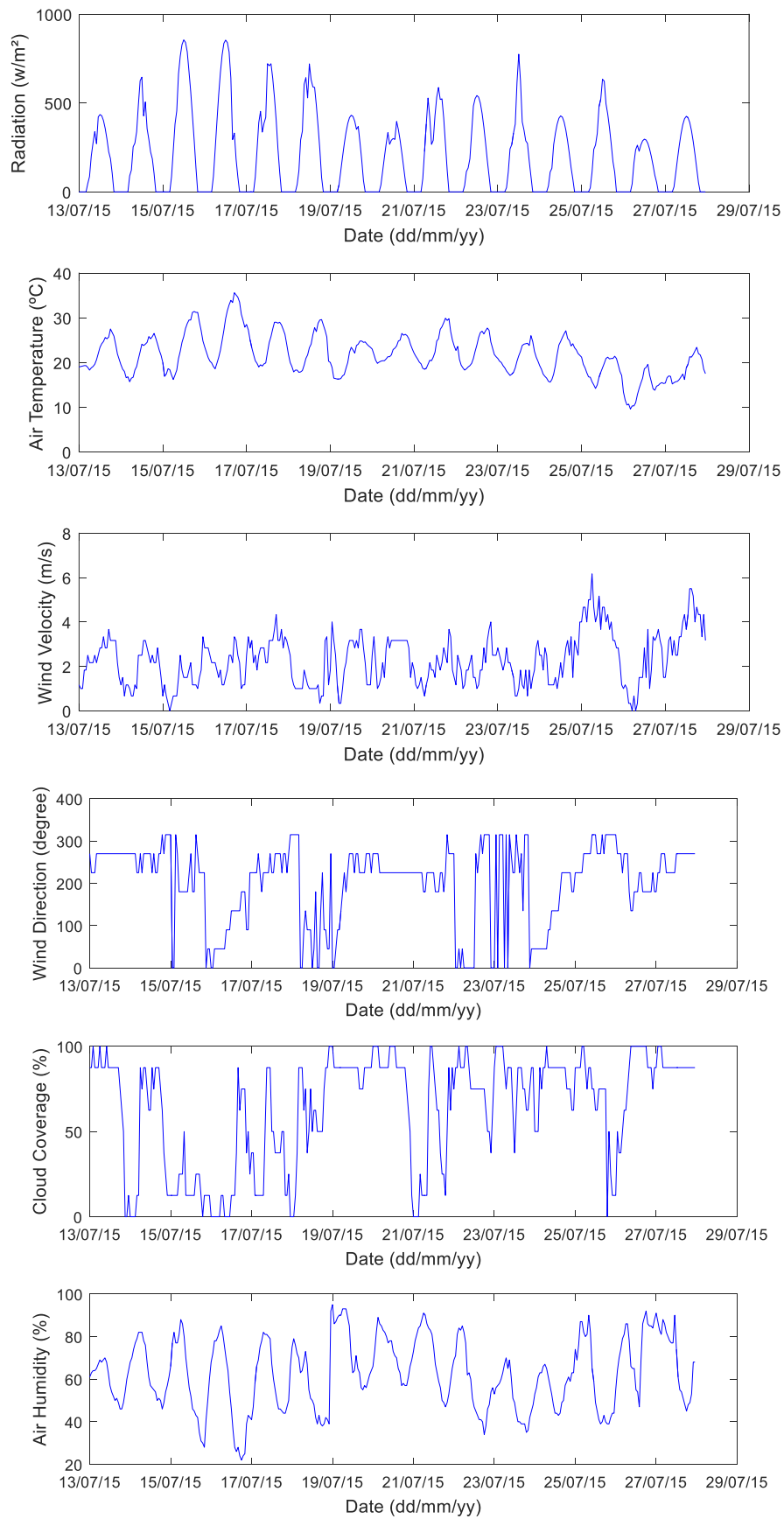


**Figure 4.10** – Radiation, atmosphere temperature, wind intensity and direction, cloud cover and humidity during period 2 (13 July 2015 to 27 July 2015)

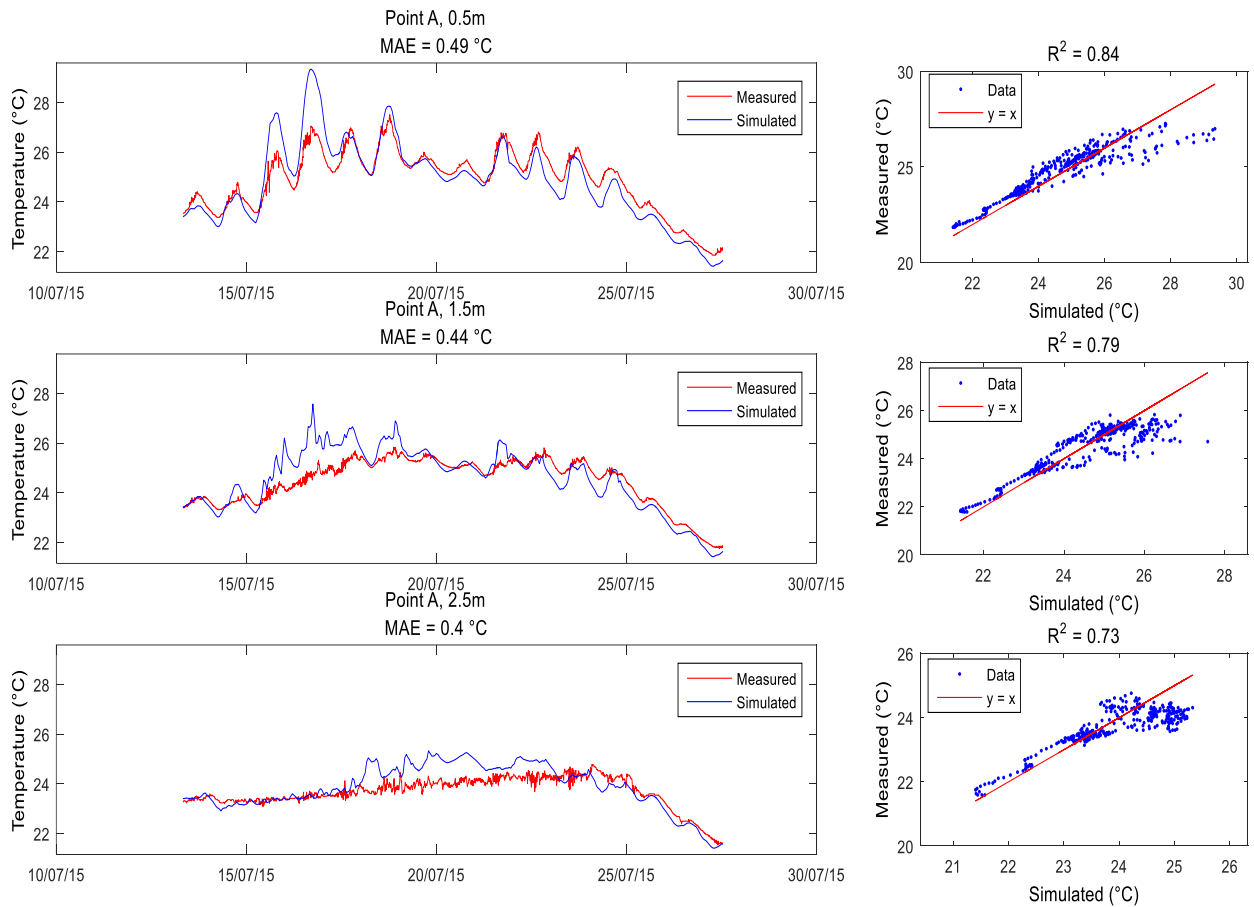


**Figure 4.11** – Comparison of the temperature between measured and simulated data from period 2 (13 to 27 July 2015) at point A

According to Figure 4.11 the results for 16 and 17 July show that the model reaches values above those measured at 0.5 and 1.5 m depths and a correct temperature for the bottom depth of 2.5 m. For the simulated period, this difference between measured and simulated values was only observed on these two days. Thus, it may have occurred due to a discrepancy of meteorological inputs because of the distance between the Orly station and the lake (22 km). Due to the high importance of meteorological conditions, *in loco* measurement is recommended.

Analysing the duration of stratification (Figure 4.12 and 4.13), it is possible to observe that the simulated behaviour in the model had a complete mixing event on 20 July, but in the measured temperature data, the mixing condition was partial. It is clearly noticeable that on 20 July the measured surface water did not present a significant heating intensity as on other days, continuing with a daily maximum below 26°C. This low surface temperature behaviour happened due to lower solar intensity (Figure 4.10). On 19 and 20 July, the maximum daily radiation was 26% and 32% lower respectively than the mean daily maximum of the period. Figure 4.13 shows that the model could represent this lower water surface heating very well. Therefore, the discrepancy for this mixing event on day 20 was the temperature at the bottom. Figure 4.11 shows that the model reached even higher values at the bottom depth than those measured. This difference started on 17 July, which was the hottest day of the period, with a maximum temperature of 35°C. This high temperature, associated with a high wind intensity, which reached a maximum value of 4 m/s, caused the bottom to warm up. Section 4.2.2 will show, through water velocity measurements, that wind velocity of 3.0 m/s can impact the entire vertical profile, even with only one high hourly wind value. Therefore, this high wind intensity on 17 July did not likely occur at the lake. The following day (after 17 July), stratification was again observed, although the bottom (2.5 m) remained slightly warmer in the model until the complete mixing event on 20 July.

A mixing event repeated after 24 July; however, this condition remains for a longer period in measured data and simulated results. The water presented cooling behaviour at the surface and at 1.5 m depth, and heating behaviour at the bottom depth. This behaviour was present in observed and simulated data. On 25 July, a period of wind intensity greater than 3.0 m/s began, with a peak of 6.0 m/s. This high wind intensity was associated with low radiation and decreased atmosphere temperature. These weather conditions resulted in a complete and intense mixing condition. The model could represent this condition very well.

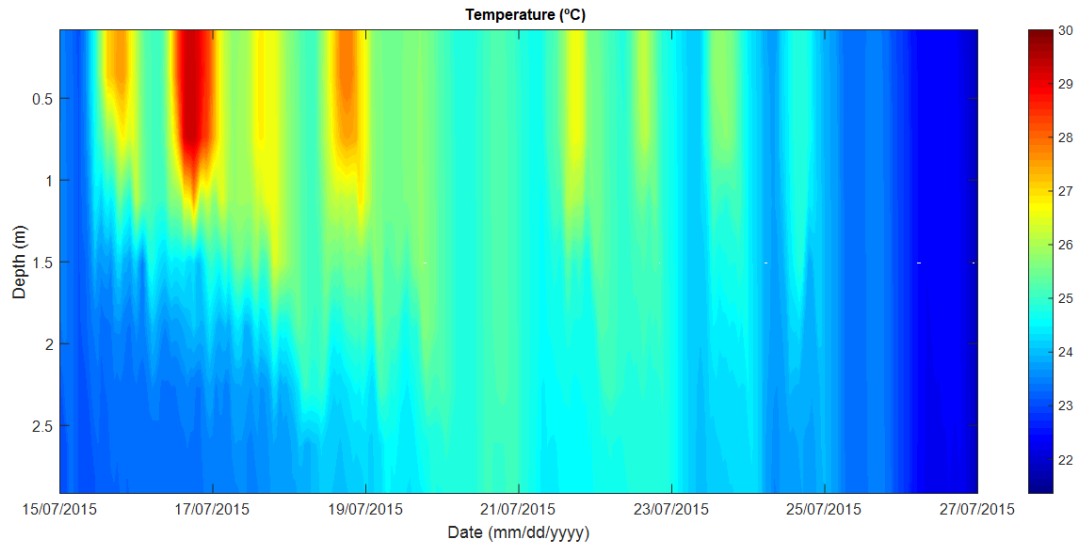


**Figure 4.12** – Temperature isocontours during simulation period 2 (13 July 2015 to 27 July 2015)

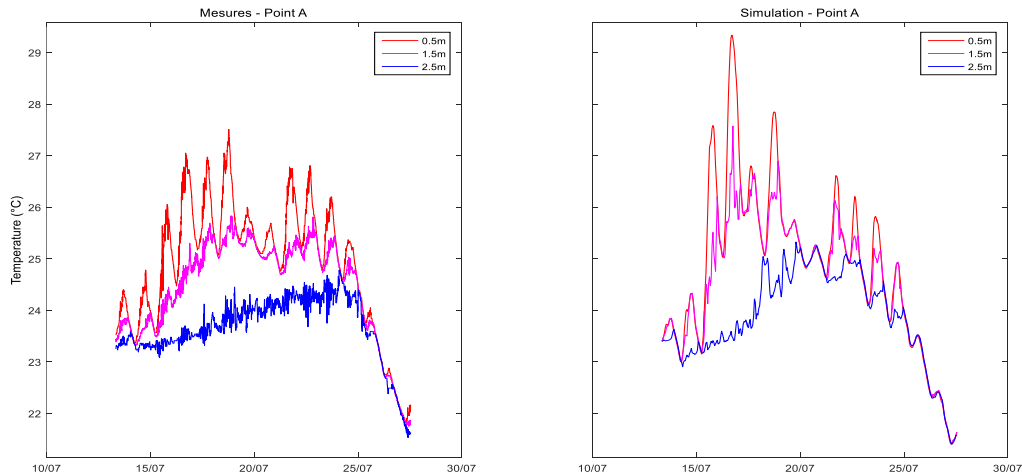


**Figure 4.13** – Water temperature at point A during period 2 (13 July 2015 to 27 July 2015)

Period 2 showed how complex the thermal dynamics of a small shallow lake are, with frequent mixing and thermal stratification events. Period 2 also showed that the model was able to well represent this dynamic, even with the uncertainty of the meteorological data that were measured 22 km from the lake. For period 3 (14 July 2016 to 01 August 2016), the initial thermal condition was set with a uniform temperature of 22.7 °C for all grid elements. Figure 4.14 presents the meteorological inputs. Figure 4.15 shows the simulated temperature. The results were fairly good with all  $R^2$  higher than 0.7. The MAE indicator on the surface and at 1.5 m presented values of 0.77 and 0.63°C, slightly higher than previous simulations. This occurred as the simulated temperature peaks were higher than the peaks measured for the first week of the period. However, after the first week, the thermal amplitude was correctly simulated. The bottom depth presented a better result ( $R^2$  of 0.89 and MAE of 0.48 °C).

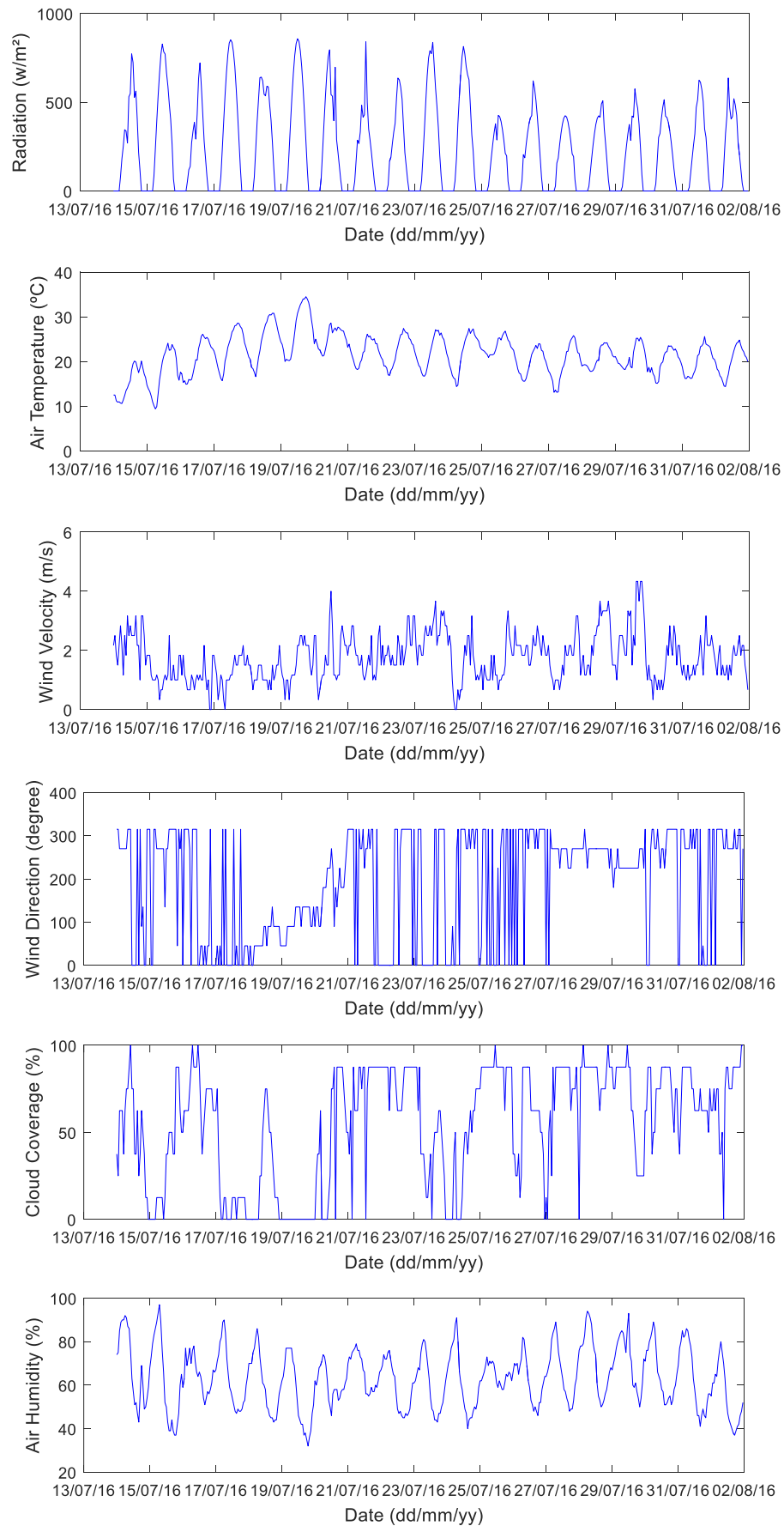


**Figure 4.14** – Radiation, atmosphere temperature, wind intensity and direction, cloud cover and humidity, during period 3 (14 July 2016 to 01 August 2016)

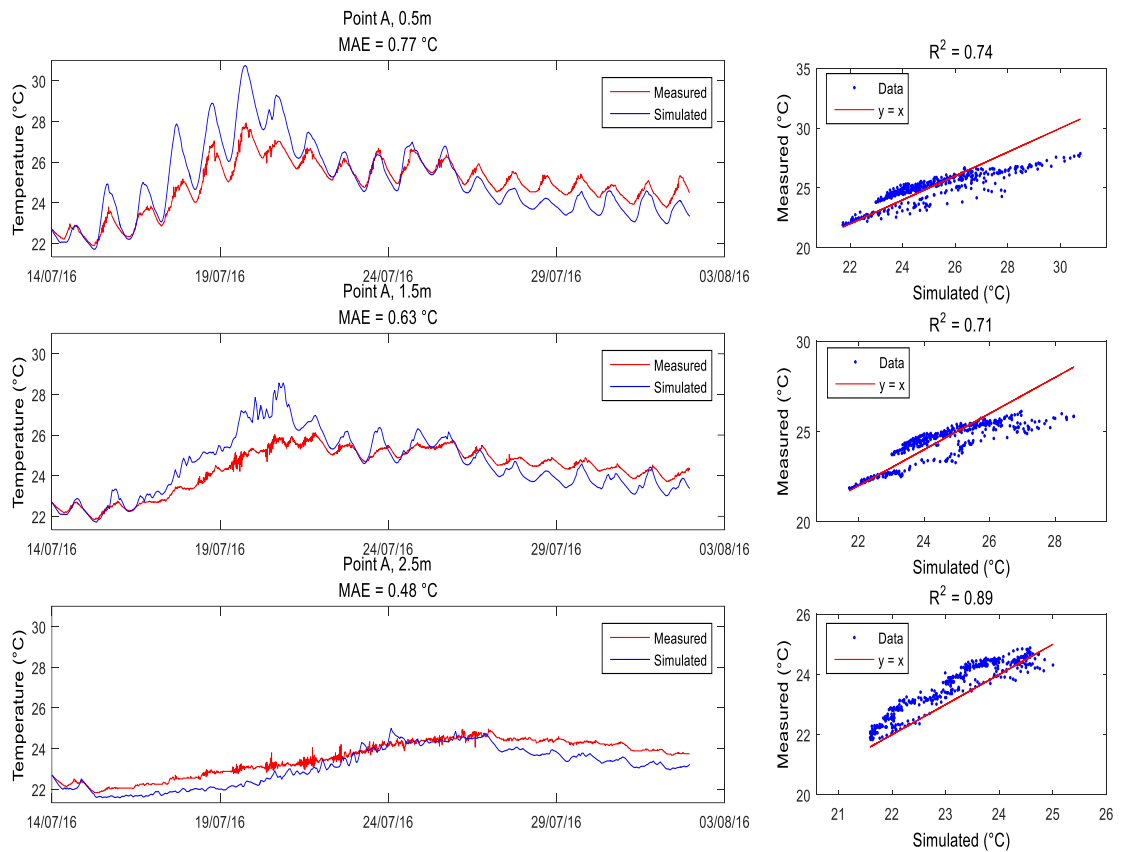


**Figure 4.15** – Comparison of the temperature between measured and simulated data for period 3 (14 July 2016 to 01 August 2016) at point A

In the first week of the period, the high-temperature values at the shallowest depths were associated with an increase in atmospheric temperature and low wind intensity (less than 2 m/s).

Analysing the thermal stratification, its duration and the timing of the mixing events, it is observed that the model predicted the thermal behaviour of the period correctly, even with a higher amplitude at the beginning of the period at the water surface (Figure 4.16).

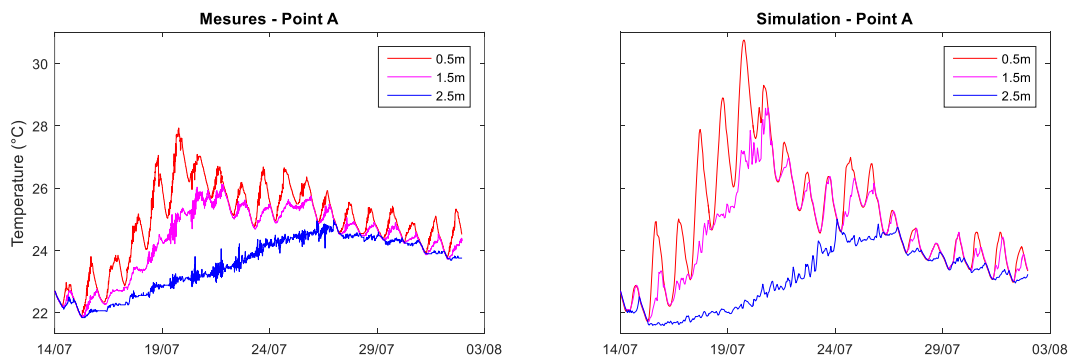


**Figure 4.16** – Stratification behaviour for measured (left) and simulated (right) for period 3 (14 July 2016 to 01 August 2016)

For period 4 (19 September 2016 to 12 October 2016) the initial thermal condition was set with a uniform temperature of 20.5 °C for all grid elements. The meteorological values are presented Figure 4.17.

Temperature results for period 4 are presented in Figure 4.18 with thermal behaviour in Figure 4.19. Observed data and simulated results showed a cooling process. The result presented a MAE lower than  $0.6^{\circ}\text{C}$  and a  $R^2$  higher than 0.98. Simulating this period, it was possible to note that the model performed well in representing a cooling process.

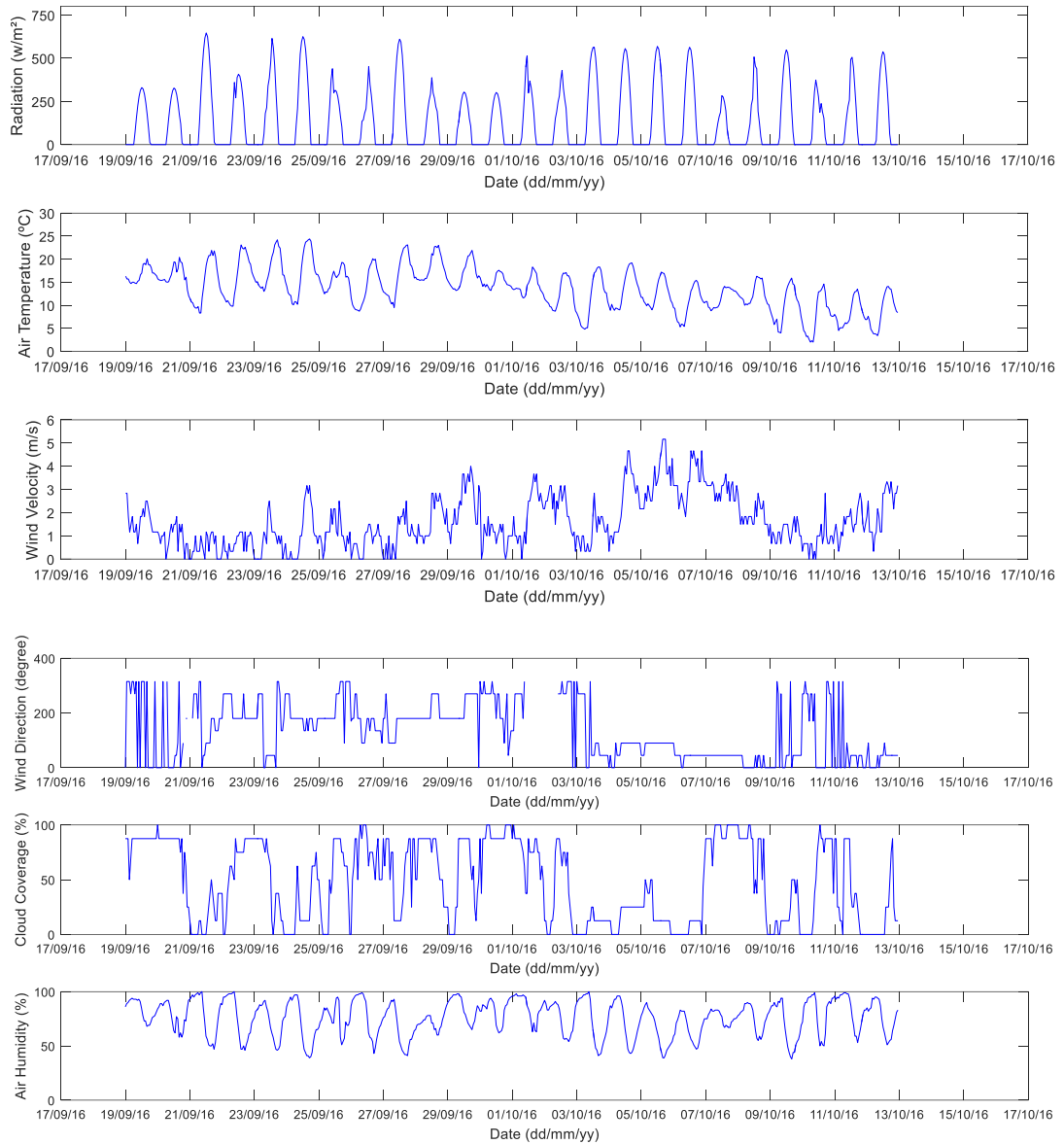


**Figure 4.17** – Radiation, air temperature, wind intensity and direction, cloud cover and humidity during period 4 (19 September 2016 to 12 October 2016)

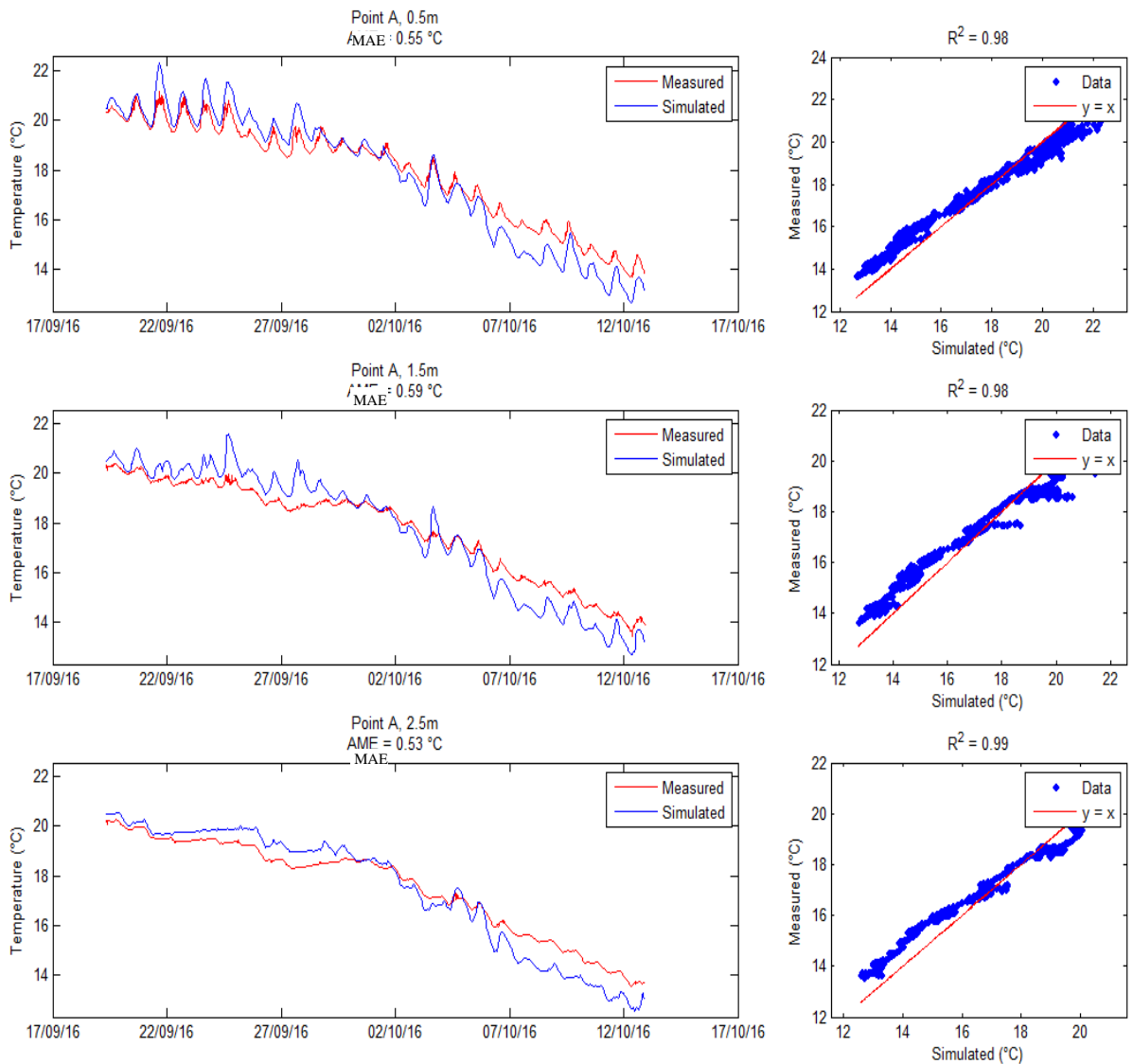


**Figure 4.18** – Comparison of the temperature between measured and simulated data from period 4 (19 September 2016 to 12 October 2016)

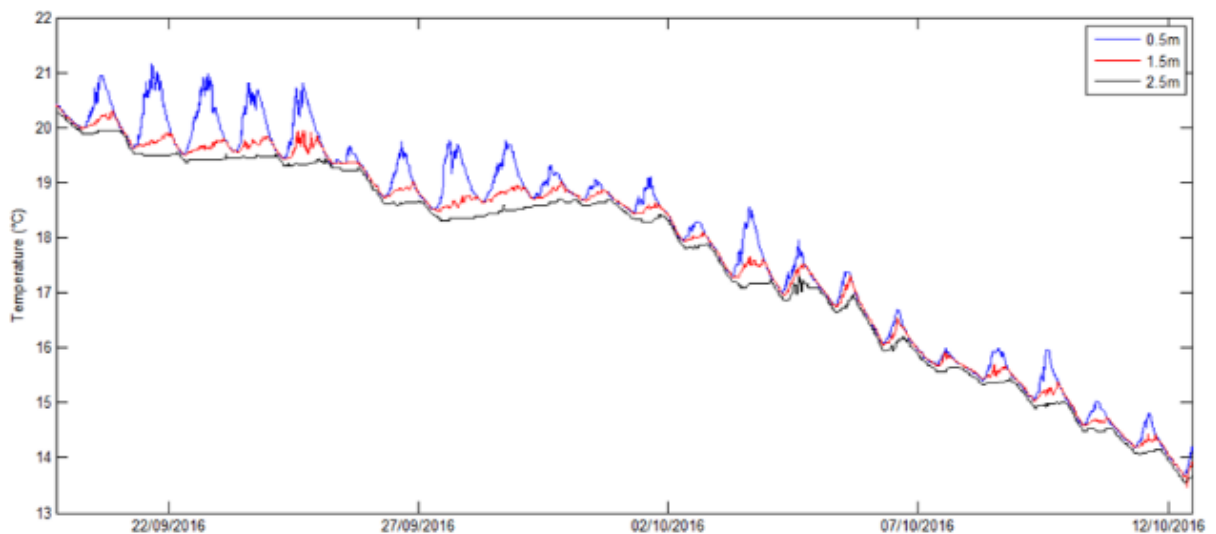


**Figure 4.19** – Simulated water temperature from period 4 (19 September 2016 to 12 October 2016) at point A



Period 4 presented higher values of wind intensity, especially after 05 October, in which observed wind intensities were higher than 3 m/s. Higher values of wind intensity associated with cold air temperature resulted in an almost uniform temperature in the vertical water column (Figure 4.19).

With the results of the four simulated periods, it is conclusive that the model reproduces the water temperature accurately (Table 4.1). The Mean Absolute Errors (MAE) for the temperature simulations were between 0.4 to 0.77 °C and  $R^2$  values between 0.53 to 0.99 for different weather condition (summer and autumn). The alternations between stratifications and mixing conditions and their durations were well reproduced by the model. The analyses of simulations and monitored results indicate that the data of the Orly meteorological station, located 22 km from the lake, reproduce the meteorological condition of the lake well for the most part. However, some discrepancies may have affected the performance of the model and on-site meteorological monitoring would be necessary to confirm this hypothesis.

**Table 4.1** – Results of the temperature simulations

Period	Surface (0.5 m)		Middle (1.5 m)		Bottom (2.5 m)	
	MAE	$R^2$	MAE	$R^2$	MAE	$R^2$
(1) 23 <sup>rd</sup> to 30 <sup>th</sup> June 2015	0.44	0.85	0.45	0.78	0.32	0.53
(2) 13 <sup>rd</sup> to 27 <sup>th</sup> July 2015	0.49	0.84	0.44	0.79	0.40	0.73
(3) 14 <sup>th</sup> July to 01 <sup>st</sup> Aug. 2016	0.77	0.74	0.63	0.71	0.48	0.89
(4) 19 <sup>th</sup> to 12 <sup>th</sup> Sept. 2016	0.55	0.98	0.59	0.98	0.53	0.99

#### 4.2.2. Results of the velocity simulations

Water current velocities were measured from 19<sup>th</sup> September 2016 to 12<sup>nd</sup> October 2016 (defined as period 4) with an Acoustic Doppler current profiler (ADCP). The velocity profiles were sampled every 3 minutes and spread from 0.6 to 2.8 m depth near point B, with a resolution of 5 cm in the vertical direction (section 3.2.1.5).

Hourly simulated values and the hourly average of measured data are presented in Figure 4.22. The measured and simulated values are in the same range. Figure 4.21 presents the differences between the simulated and measured values.

The model satisfactorily represented the time at which the water current reaches the higher values and its vertical distribution. The first week of October was the period which presented the highest water velocity measured by the ADCP (maximum velocity of 0.038 m/s). This could also be simulated by the model (maximum velocity of 0.040 m/s). This period also presented the highest wind intensity (Figure 4.3), with many episodes above 4.0 m/s.

On 29 October, the ADCP measured a water velocity increase that was not propagated along the entire water column. The velocity increase occurred up to 1.5 m depth. This event and the vertical profile could also be represented in the model. However, on 29 October a velocity increase was calculated by the model but was not measured by the ADCP. In this episode, the wind intensity used in the model was close to 3 m/s, whereas the real value at the lake was most likely smaller.

Analysing the vertical velocity profile with the intensity of the wind (Figure 4.3), it is observed that wind intensity near 3 m/s has the potential to impact the entire vertical profile. Between 24 and 25 September, only one value of wind intensity was higher than 3.0 m/s. This was enough to impact the entire vertical profile.

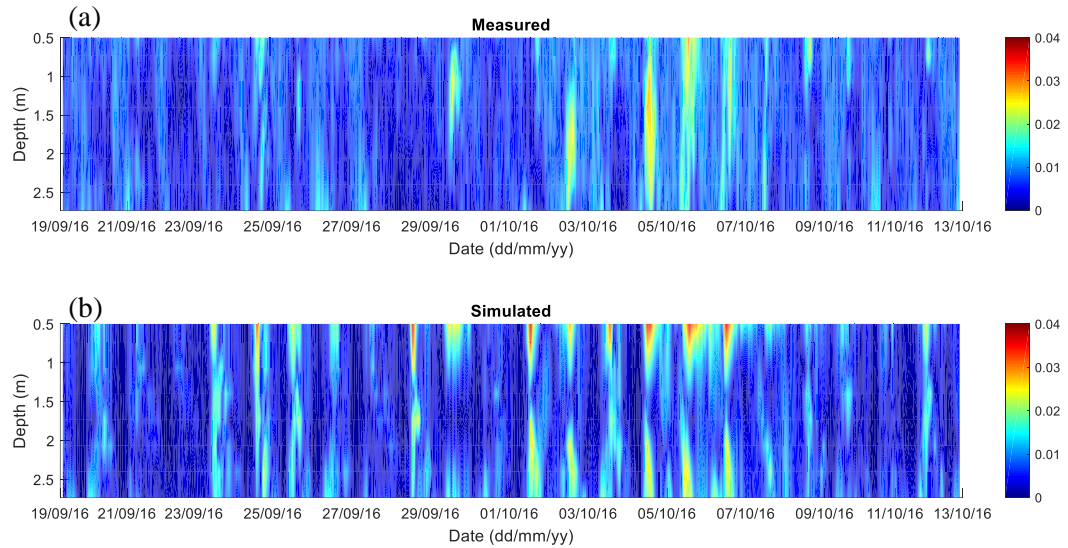


**Figure 4.20** – Total velocity profile near point B in Lake Champs-sur-Marne. (a) Measured data (m/s)  
(b) Simulated values (m/s) for period 4

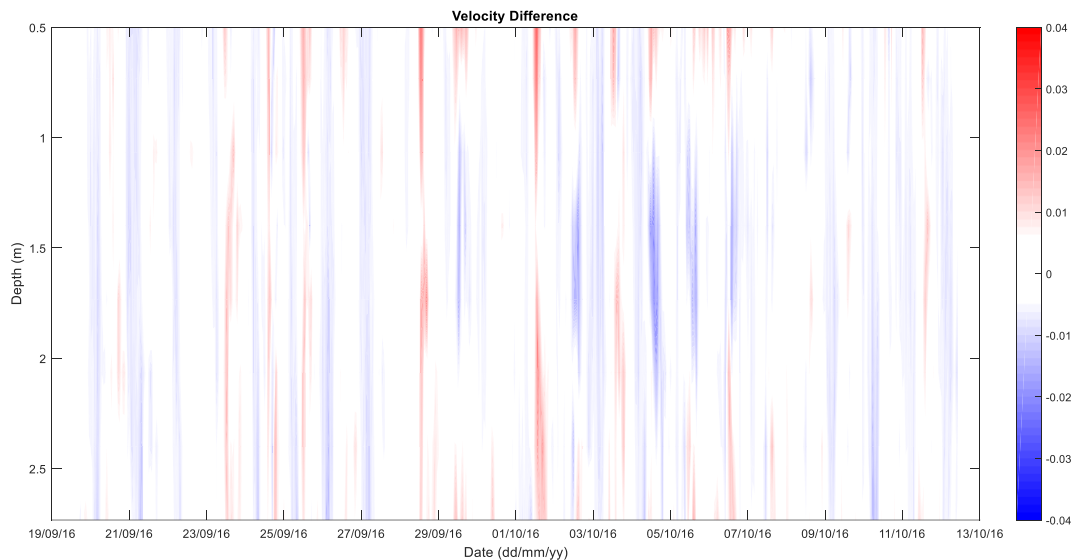


**Figure 4.21** – Difference between simulated and measured total velocity profile near point B in Lake Champs-sur-Marne

Additionally, spectral analyses were obtained for the measured and simulated velocities. The fast Fourier transformation (FFT) was used to find the frequency components of the water velocity in time. FFTs produce the average frequency content of a signal over the entire time that the signal was acquired. Figure 4.22 shows the bi-log comparison between simulated and measured values for the surface (0.5 m), middle (1.5 m) and bottom (2.5 m) depths. Due to the same behaviour in a log-log plot (Figure 4.22), it is noted that the model could simulate the same frequency as the measured values. The 24-hour frequency presented the higher power spectrum. For daily cycles (24 hours on the x axis), the model

overestimates the power spectrum in comparison to the measurement signals for the surface depth. However, for the middle (1.5 m) and bottom (2.5 m) depths, the power was well captured.

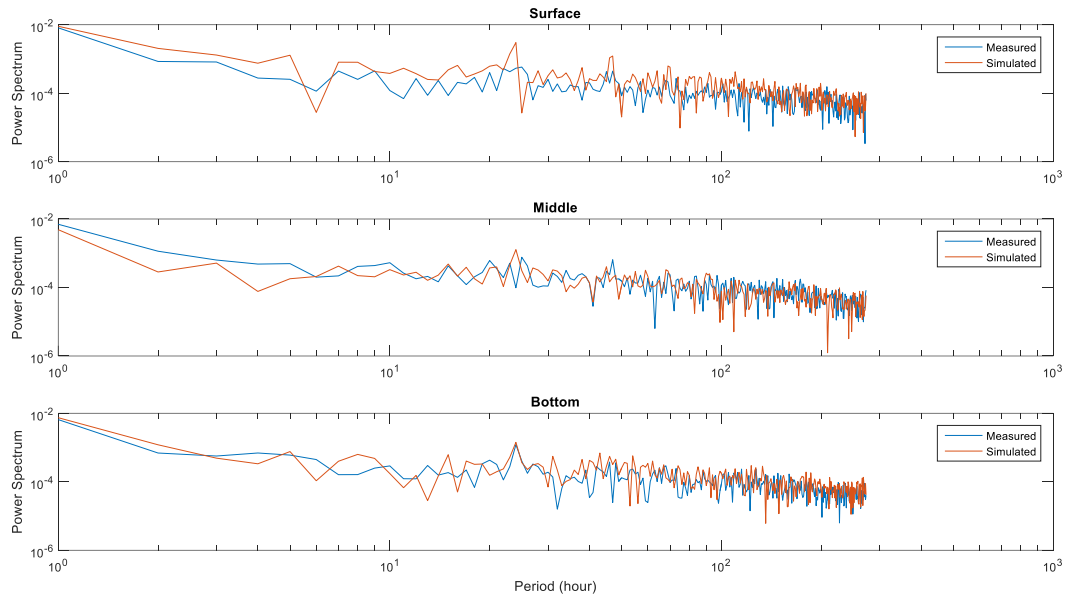


**Figure 4.22** – Power Spectra of simulated and measured total velocity profile near point B in Lake Champs-sur-Marne for surface (0.5m), middle (1.5) and bottom (2.5 m) depths

According to Pannard et al. (2011), the lake is stratified if the power spectrum at different depths presents a different behaviour. For the studied lake, the three depths have the same scales and temporal distribution, thus the different depths have the same spectra (Figure 4.23). Therefore, it was noted that the lake does not have velocity stratification in terms of power frequency. This was observed in measured and simulated values. As a result, the model could also represent this behaviour.

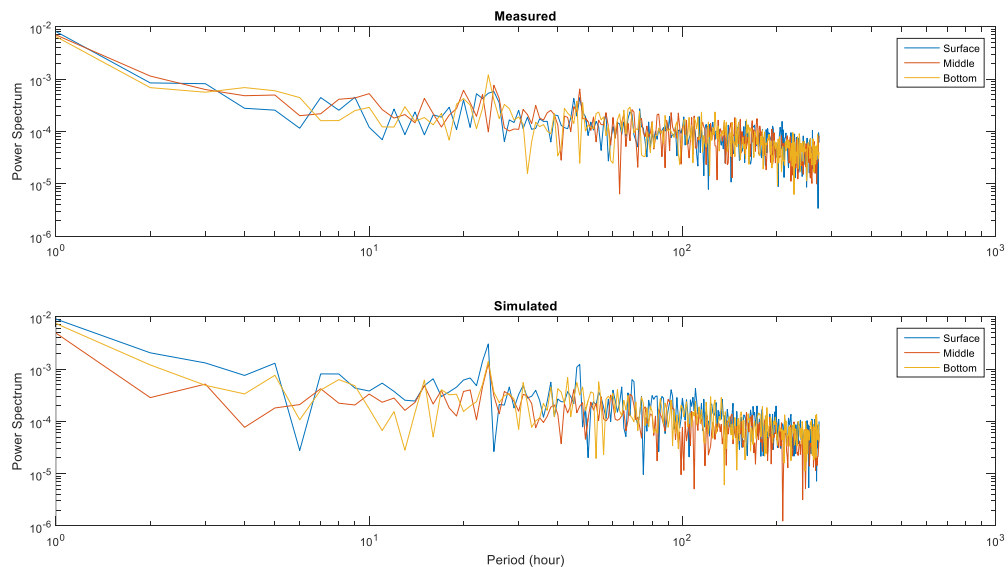


**Figure 4.23** – Power spectra of simulated and measured total velocity profiler near point B in Lake Champs-sur-Marne for surface (0.5 m), middle (1.5 m) and bottom (2.5 m) depths

To reinforce this analysis of the vertical distribution of water velocity, the average daily measured values of the water velocities were analysed at the surface, middle, bottom and for the average vertical profile. Figure 4.24 shows that for all three depths, as well as for the average vertical profile the behaviour was very similar. The velocity behaviour presents a strong determination coefficient with wind intensity for surface ( $R^2 = 0.72$ ) and middle ( $R^2 = 0.76$ ) depths and a moderate determination coefficient ( $R^2 = 0.30$ ) for the bottom (Table 4.2). At the bottom depth (2.5 m), the behaviour was not well captured during the first week, in which wind velocities presented lower values. However, during October, wind intensity and determination coefficient increased ( $R^2 = 0.58$ ). Concerning the simulated values, Figure 4.25 shows the average daily values. The surface velocities presented values slightly above the expected values for winds velocities above 4 m/s. The middle depth did not present a strong determination coefficient with wind intensity, as expected ( $R^2 = 0.39$ , Table 4.2). However, Wu et al. (2013) concluded that the horizontal flow intensity was strongly correlated with wind speed with a value of  $R^2 = 0.43$ .

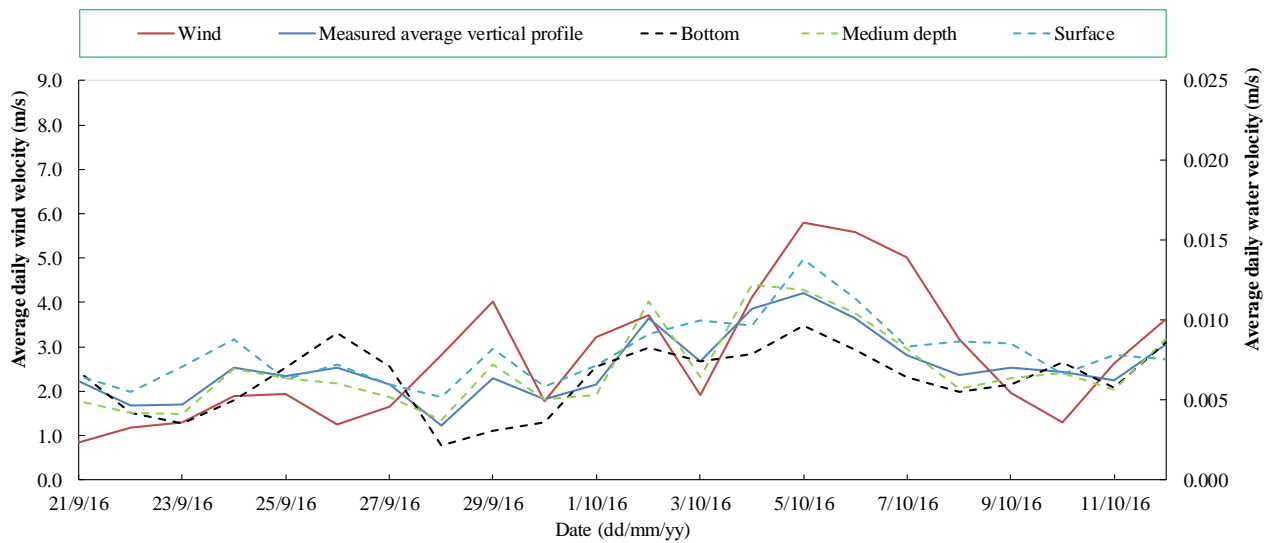


**Figure 4.24** – Measured daily average water velocity for the average vertical profile, surface (0.5 m), middle (1.5 m) and bottom (2.5 m) depths

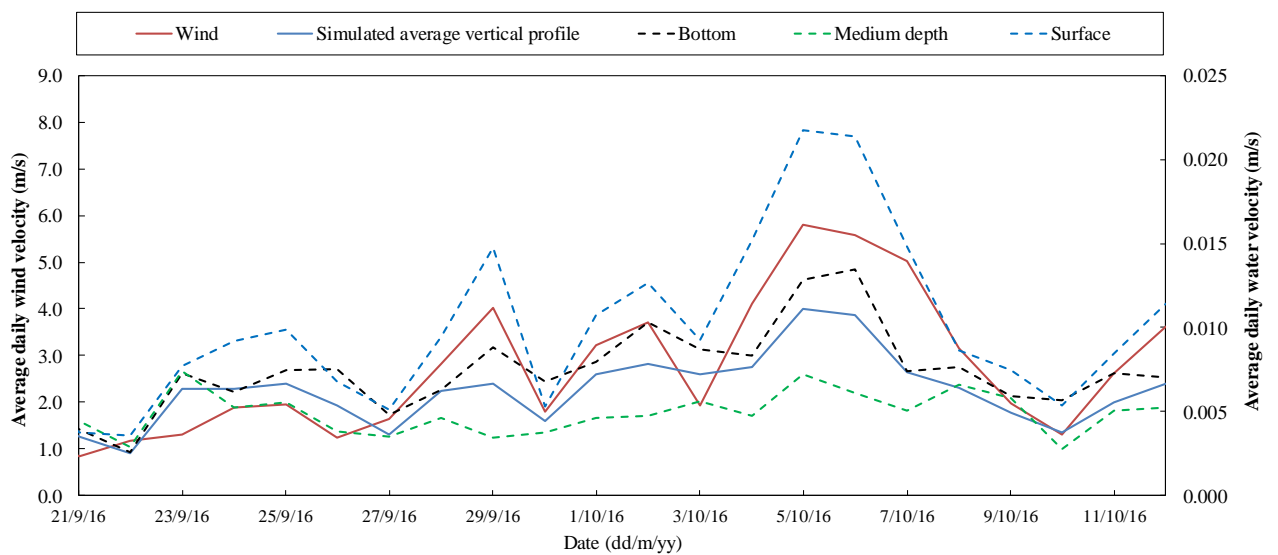


**Figure 4.25** – Simulated daily average water velocities for the average vertical profile, surface (0.5 m), middle (1.5 m) and bottom (2.5 m) depths

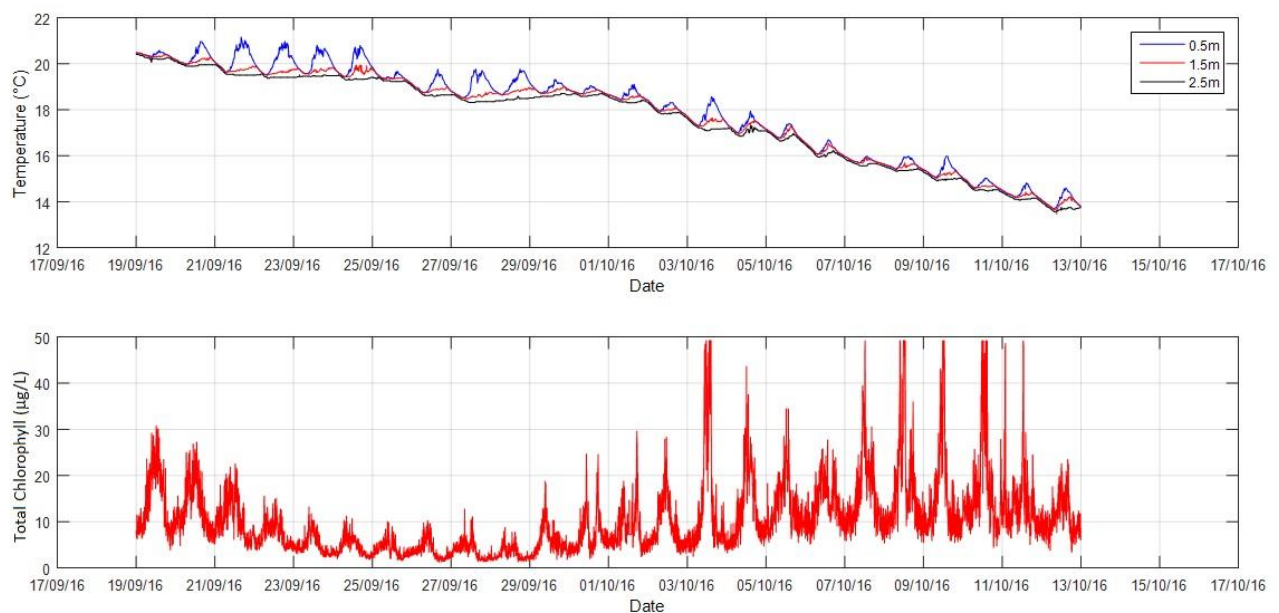
**Table 4.2** – Water velocity determination coefficient for measured and simulated values with wind

Depth	R <sup>2</sup>	
	Measured (°C)	Simulated
Vertical profile	0.70	0.85
Surface (0.5 m)	0.72	0.95
Middle (1.5 m)	0.76	0.39
Bottom (2.5 m)	0.30	0.76

The measurements and simulations show that the hydrodynamics of Lake Champs-sur-Marne are very unstable and dynamic. The lake reacts rapidly and intensely to meteorological forcing. However, the three-dimensional hydrodynamic model was able to represent these complex hydrodynamics.

With the results, it is possible to conclude that a hydrodynamic model is a tool which helps to better understand spatial water temperature distribution, water current, and the spatial patterns of mixing events. These conditions influence the behaviour of phytoplankton blooms in small shallow lakes, due to the process of sedimentation, the resuspension and transport of nutrients and water stratification.

On 03 October, a period of higher wind intensity and water velocity began. According to thermal behaviour and chlorophyll-a measurements (Figure 4.26), this period coincided with the beginning of a stronger water temperature reduction associated with a significant increase in the phytoplankton biomass. Therefore, this biomass increase may have been caused by a potential nutrient resuspension caused by higher velocity at the bottom and/or by the change in interspecies competitiveness due to the temperature drop (Annex 8.1). Wu et al. (2013) suggested a sediment resuspension in Lake Taihu (maximum depth less than 3.0 m) during an event with a mean current horizontal velocity of 8.5 cm/s and a maximum of 12.2 cm/s, much higher than the measured values at Lake Champs-sur-Marne, which presented maximum values smaller than 1.5 cm/s (Figure 4.24). Concerning the hypothesis of a change in interspecies competitiveness due to the temperature drop, the vertical profiles with BBE, measuring the concentration for each algae group, unfortunately do not coincide with these events, preventing the confirmation of this hypothesis.

**Figure 4.26** – Temperature and total Chlorophyll-a during monitoring period with ADCP, corresponding to period 4

### 4.2.3. Phytoplankton biomass transport simulation

This section presents the simulation results for the period of 23<sup>rd</sup> June to 30<sup>th</sup> June 2015 (period 1), which investigates the phytoplankton transport and the influence of the hydrodynamics on its spatial distribution. The simulation was performed using only the Delft3D-Flow model and the parameters (Table 3.6) of hydrodynamic simulation. Therefore, phytoplankton biomass was considered as a conservative tracer, with neither growth nor decay (section 3.5.2).

The time evolution of the tracer concentration at the surface layer with the original wind direction is plotted at 4 points: A, C, D and at the large beach (Figure 3.26). The results are compared to the threshold for a first warning level of 10  $\mu\text{g}$  Chl-a/L for bathing waters.

At the beach, the tracer passed the threshold for a bathing warning one day after the beginning of the simulated bloom. At point D, this threshold was passed two days later. This result indicates that the hydrodynamics of a shallow lake may result in heterogeneous behaviour on the lake. Concerning tracer accumulation, Figure 4.27 shows that at point A and at the large beach, higher values were present by the end of the simulation period.

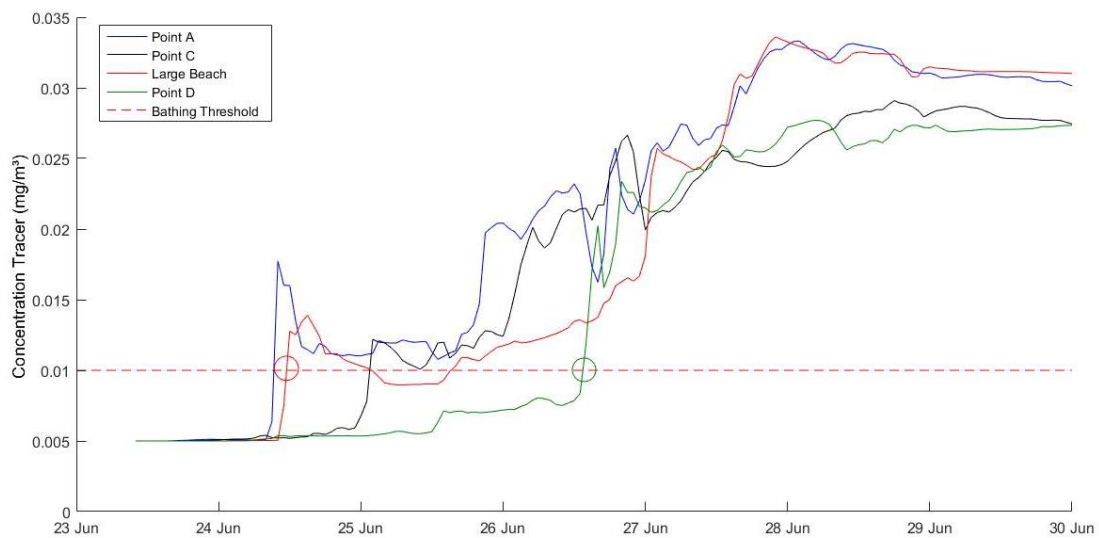


**Figure 4.27** – Tracer concentration over time for the simulation with original wind direction

In the simulations with other wind directions, changing the direction of the wind to western (wind coming from the west) and northern (wind coming from the north), tracer concentrations were also higher at point A and at the large beach (western area of the lake Figure 4.28). This is probably due to the impact of the island, which protects the eastern area in cases of wind coming from the west or north.

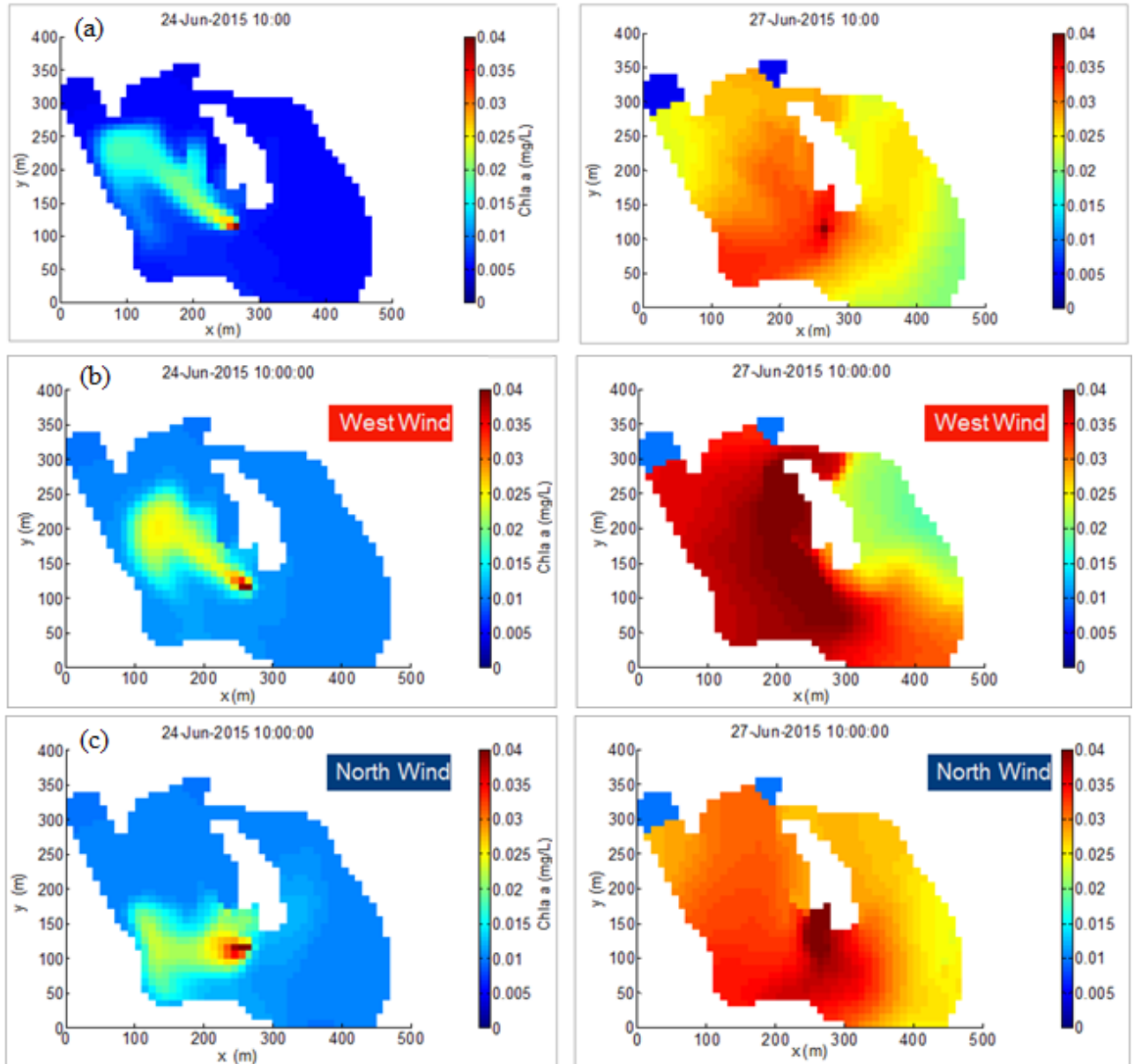


**Figure 4.28** – Map of the tracer concentrations on 24<sup>th</sup>, and 29<sup>th</sup> June at 10h a. m. for (a) standard direction, (b) West wind (c) Northwind in the surface layer (0.5 m)

These results illustrate how the modelling outcomes could be used to identify a better potential location for the beach and the importance of hydrodynamics and wind effects on the lake.

### 4.3. Coupled hydrodynamic and ecological simulation

#### 4.3.1. Calibration Period

The simulation of the biomass in Lake Champs-sur-Marne was performed by coupling hydrodynamic (Delft-3D Flow) and ecological modules (ECO). It focused on the time and spatial evolution of the cyanobacteria, over two short summer periods with the purpose to evaluate the influence of hydrodynamics. The first selected period was in 2015. The monitored water temperature at points A, B and C at 3 depths for 2015 are presented in Figure 4.29A, Figure 4.30A and Figure 4.31, while the chlorophyll-a fluorescence at 1.5 m depth for the points A and B in Figure 4.29B and Figure 4.30B, respectively. Unfortunately, during 2015 at point C, Chl-a was not measured.

According to previously established criteria (section 3.5.3), the selected period to simulate and calibrate the coupled hydrodynamic and ecological models, was from 13 to 27 July 2015 (a duration of two weeks). For an overview of the selected period in relation to 2015, this period is highlighted by vertical black lines in Figure 4.29 to Figure 4.31, respectively for point A, B and C.

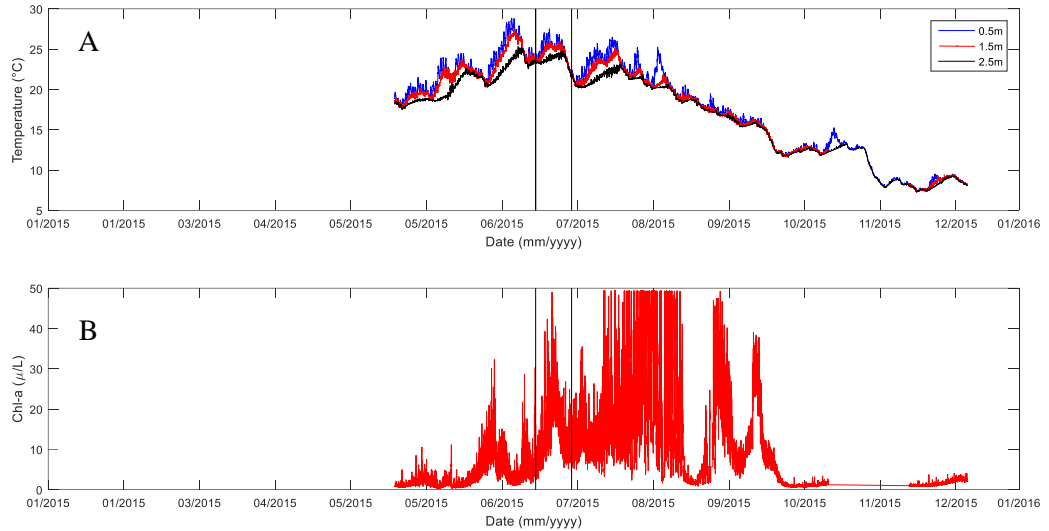


**Figure 4.29** – Water temperature and chlorophyll-a monitoring at point A during 2015. The simulated period is between the black vertical lines

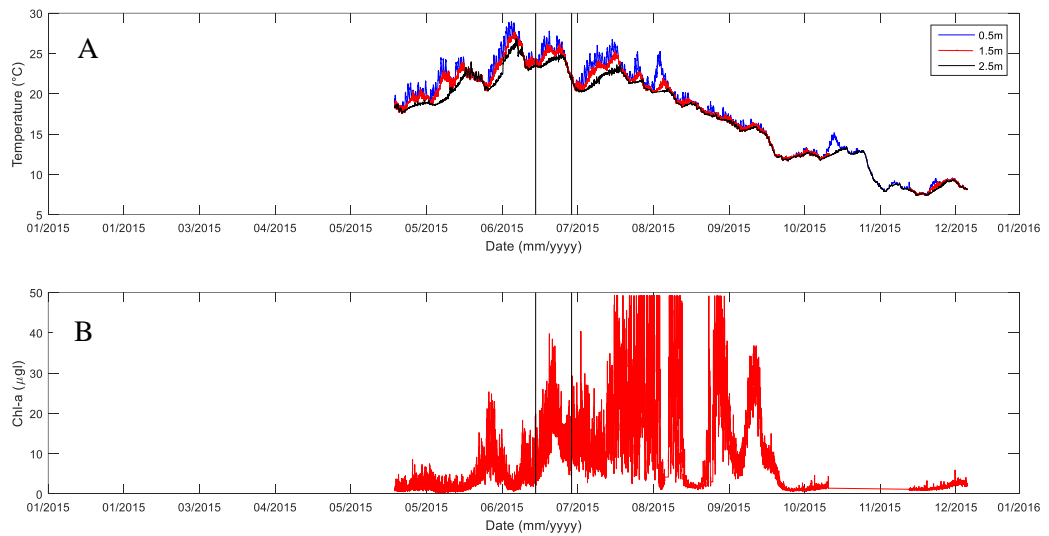


**Figure 4.30** – Water temperature and chlorophyll-a monitoring at point B during 2015. The simulated period is between the black vertical lines

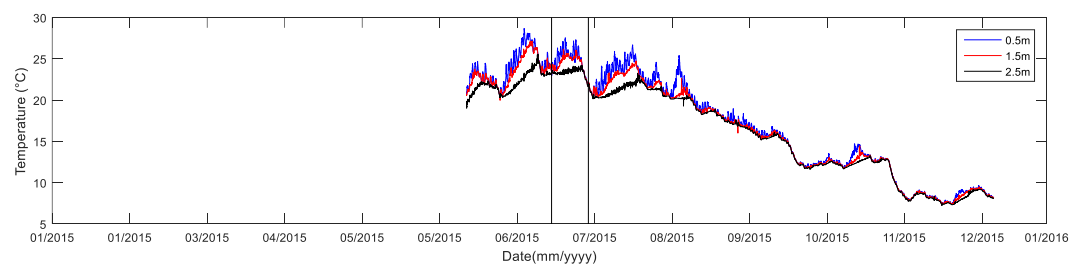


**Figure 4.31** – Water temperature monitoring at point C during 2015. The simulated period is between the black vertical lines



The water temperature and Chl-a variation for the simulated period are presented in Figure 4.32 to Figure 4.34, for points A, B and C respectively. The vertical black lines show when the vertical profile, measured with BBE fluorometer, were performed for 4 algal groups.

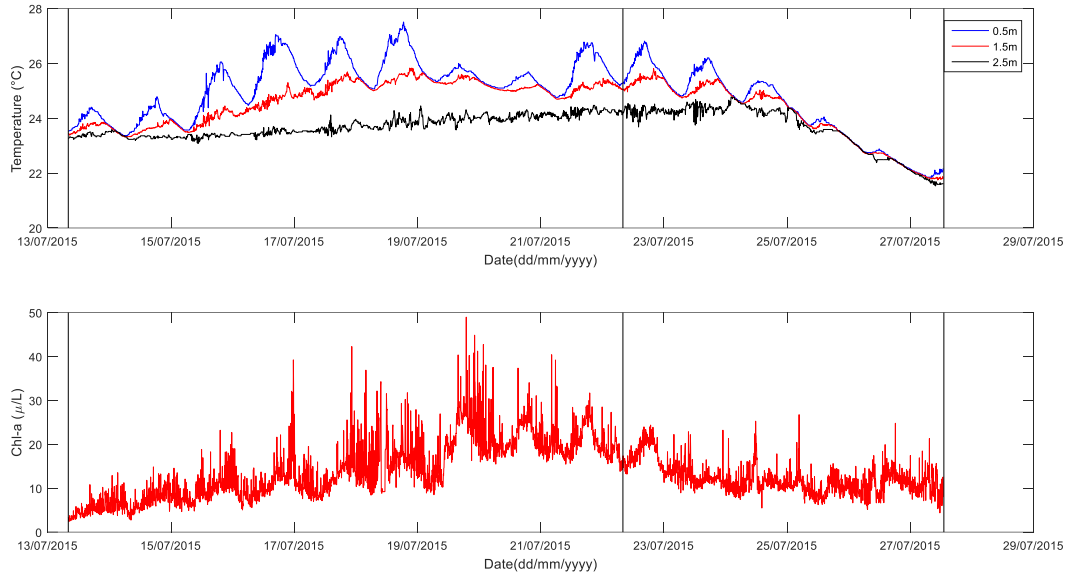


**Figure 4.32** – Water temperature and chlorophyll-a for the calibration period (13 to 27 July 2015) at point A. The black lines represent the dates of the vertical profiles with BBE fluorometer.

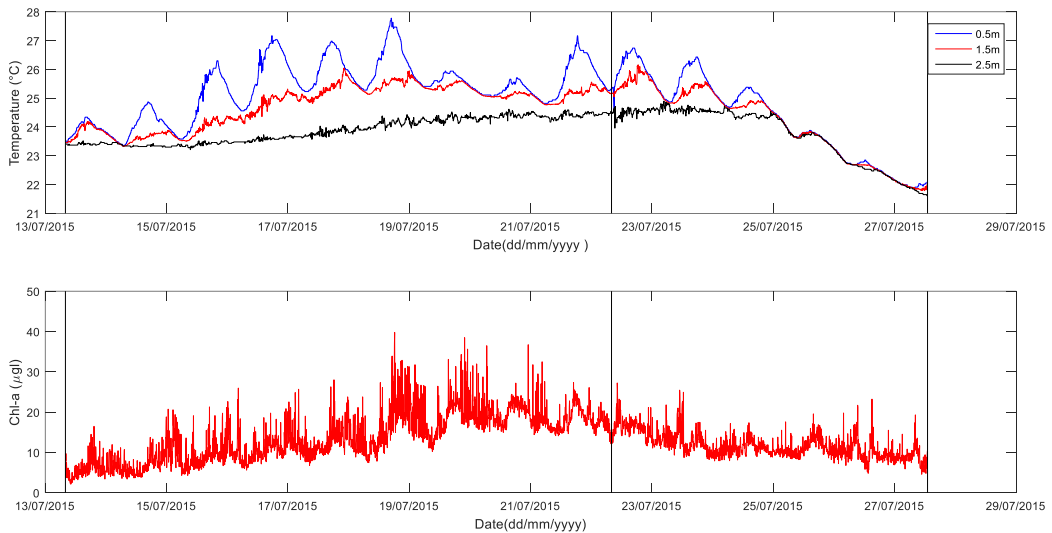


**Figure 4.33** – Water temperature and chlorophyll-a for the calibration period (13 to 27 July 2015) at point B. The black lines represent the dates of the vertical profiles with BBE fluorometer.

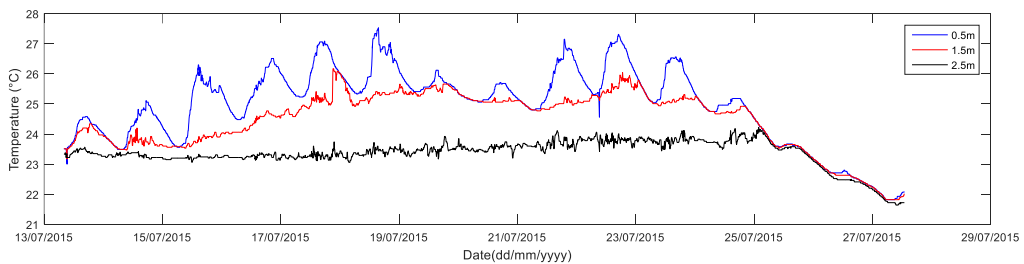


**Figure 4.34** – Water temperature for the calibration period (13 to 27 July 2015) at point C

Similar behaviour was noted for Chl-a measured at points A and B (Figure 4.35), also observable in the daily box-plot presented in Figure 4.36. This homogeneity is probably because the points are located near each other and at points that have the same characteristics on the lake.

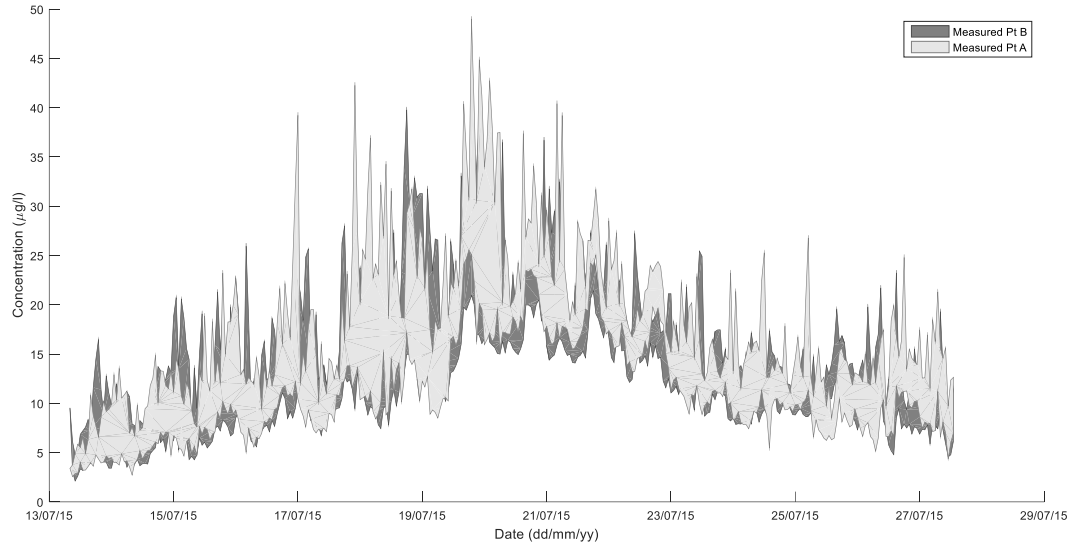


**Figure 4.35** – Chlorophyll-a at point A and B for the calibration period (13 to 27 July 2015)

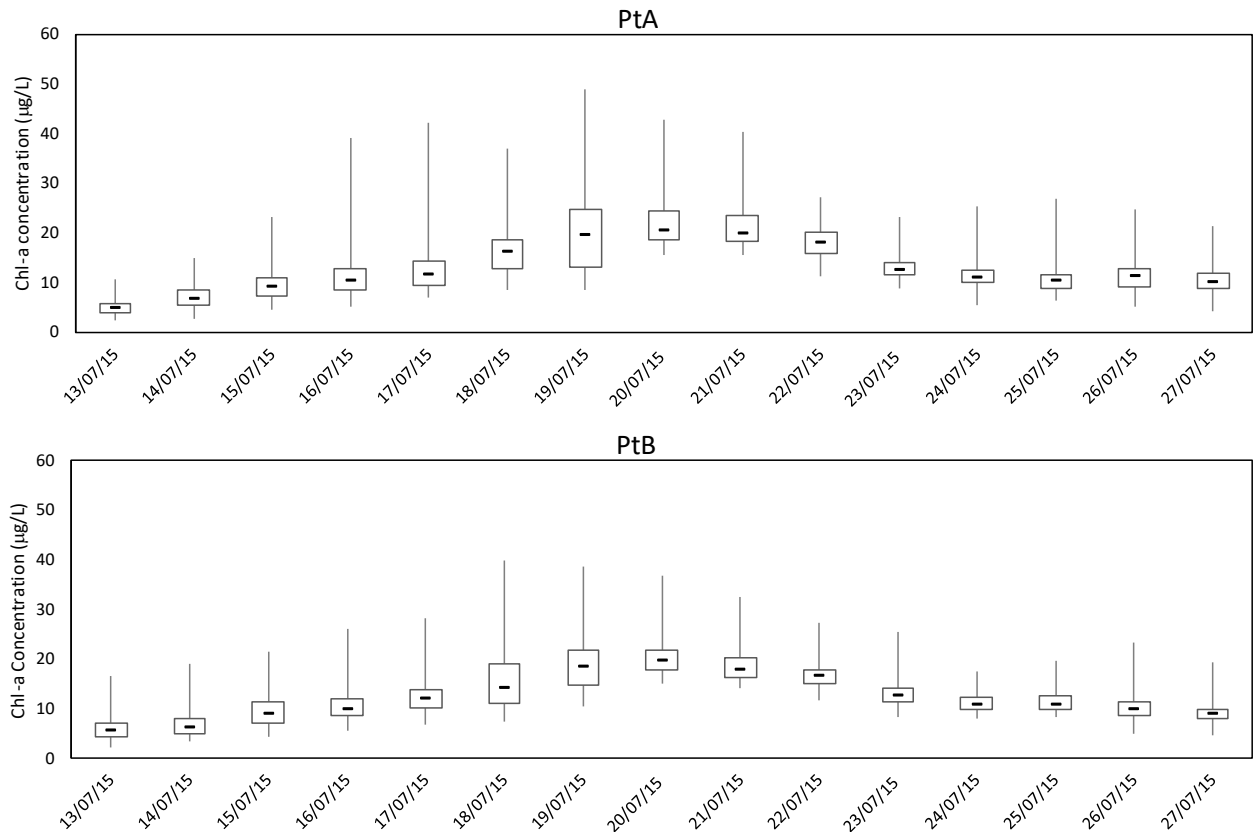


**Figure 4.36** – Daily Box-Plot of chlorophyll-a behaviour at point A and B for the calibration period (13 to 27 July 2015)

Despite high-frequency monitoring not taking place in heterogeneous zones, it is believed that the lake features a complex spatial dynamic in relation to the phytoplankton biomass. Despite a different monitoring methodology, this characteristic can be observed in samples taken near the large beach.

Installing one of the high-frequency sensor points (or acquiring an additional Chl-a sensor) at this bathing zone is recommended to capture more precisely the dynamic of the phytoplankton biomass and validate with greater assertion the heterogeneous spatial characteristic. Therefore, it was recommended to add a monitoring point at the large beach using MPX and BBE devices to evaluate the hypothesis of biomass accumulation in the large beach.

Under mixing conditions on 13 July, the beginning of the period, Chl-a fluorescence was approximately 5 µg/L, with a maximum value, close to 45 µg/L at point A and 40 µg/L at point B, measured on 20 July.

In the same manner as thermal behaviour, Chl-a fluorescence also displays a daily cycle pattern, as discussed in section 3.5. Some rapid increases in the total fluorescence were observed during water stratification. For example, on 18 July, the concentration grew from 8 to 34 µg/L in less than 6 hours. This behaviour shows the importance of high-frequency measurements, since daily sampling would not register such behaviour.

A strong thermal stratification lasted for 10 days during the period evaluated here. The surface and bottom temperature reached a difference of almost 4°C on 18 July. The surface water temperature varies greatly on a daily frequency, with a maximum amplitude of nearly 3°C. The bottom temperature remains more stable. For the ecological simulation, the hydrodynamic results (period 2 – section 4.2.1) were used as input.

To set the species contribution to the total phytoplankton biomass in the model, the Chl-a fluorescence measured by the fixed fluorescence sensor was first verified to be consistent with the Chl-a measured by the spectrofluorometer (BBE). The values measured by both devices were strongly correlated ( $R^2=0.95$ ,  $n=25$ ,  $p<0.0001$ , section 4.1).

According to the spectrofluorometer vertical profiles performed during the calibration period, also used to evaluate and perform model calibration, the fraction of Chl-a for each of the 4 phytoplankton groups at points A and B are presented in Figure 4.37. The phytoplankton assemblage changed over time with very similar values between points. The initial concentration of each phytoplankton is set in the model in units of gC/m<sup>3</sup> and the mean values between the points were used. The stoichiometry for each group was used to convert Chl-a into carbon (Table 3.9 - section 3.4.3). However, for a better understanding, the presentation of the unity of µgChl-a/L was standardized. According to period selection criteria, Cyanobacteria constituted an important percentage, between 25 and 60% of the biomass in the three profiles of the period.

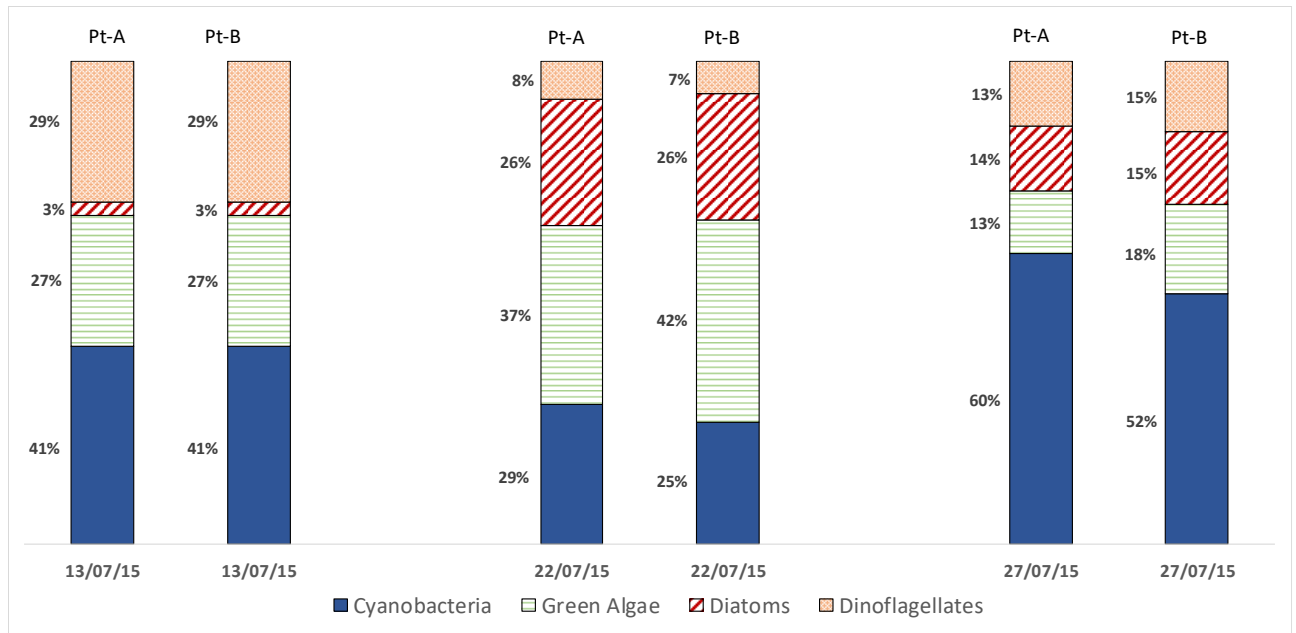


**Figure 4.37** – Fraction contribution of each algal group measured at point A and B for the calibration period (13 to 27 July 2015)

In the simulation, nutrients were described by the following dissolved inorganic variables: Ammonium, Nitrate and Ortho-Phosphate concentrations. Dissolved organic, particulate and inorganic matter forms were set to zero in initial conditions because they were not monitored. Otherwise, according to Dupuis and Hann (2009), dissolved inorganic forms are more readily available for assimilation over a short-term period, such as a duration of a month. Nutrient concentrations were derived from field measurements done on 15 July 2015 (ID EAUX, 2015). Dissolved oxygen concentration is also a stated variable of the biological model. The field values, used as initial conditions, are presented in Table 4.3. The initial dissolved oxygen concentration was obtained from the multi-parameter profile. As the lake is mixed at the beginning of the simulation, uniform initial concentrations were also adopted for the whole domain. This homogeneous condition could also be observed in other lakes in which nutrients concentrations showed no clear spatial differences (Barbosa et al., 2018; Beghelli et al., 2016; Vilas et al., 2018). To establish nutrient and chemical stratification, more than 200 days of thermal stratification are necessary (Barbosa et al., 2018).

**Table 4.3** – Initial condition values used for the calibration period (13 to 27 July 2015)

Variable	Values
Dissolved Oxygen ( $\text{g/m}^3$ )	10.0
Ammonium ( $\text{gN/m}^3$ )	0.107
Nitrate ( $\text{gN/m}^3$ )	0.574
Ortho-Phosphate ( $\text{gP/m}^3$ )	0.057
Cyanobacteria ( $\mu\text{gChl-a/L}$ )	2.04
Diatoms ( $\mu\text{gChl-a/L}$ )	0.15
Dinoflagellates ( $\mu\text{gChl-a/L}$ )	1.45
Green algae ( $\mu\text{gChl-a/L}$ )	1.36

The light extinction coefficient (Equation 44) was defined based on irradiation data measured along the vertical profile through PAR (Photosynthetically active radiation) using the Li-Cor equipment. According to the procedure described (section 3.2.1.4), measurements were performed for 30 seconds at depth intervals of 50 centimetres apart. The natural logarithm values of active radiation are presented in Figure 4.38 and were measured for the closest day (30<sup>th</sup> June 2015) to the start of the simulation.

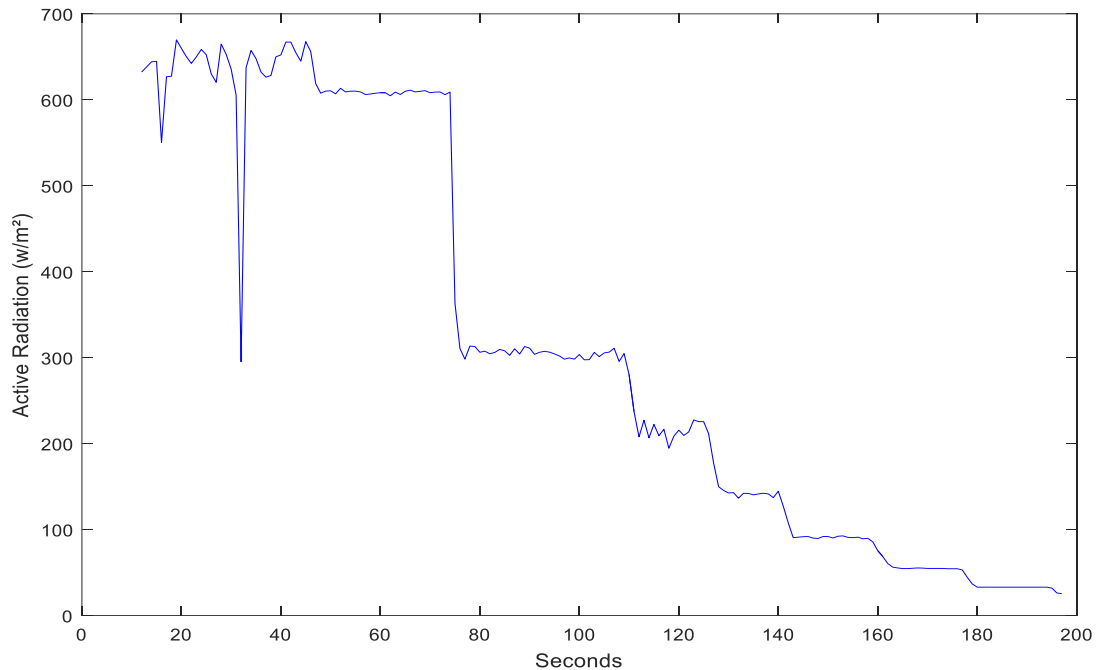


**Figure 4.38** – Active radiation measured in vertical profile on 30<sup>th</sup> June 2015

The median value of the active radiation for each depth and the respective depth are presented by the points in Figure 4.39. The attenuation of the radiation coefficient was determined according to the Lambert-Beer law (Equation 44), corresponding to the angular coefficient of the linear curve. The value obtained was 0.93 (Figure 4.39). This value was used as a process parameter in the model.

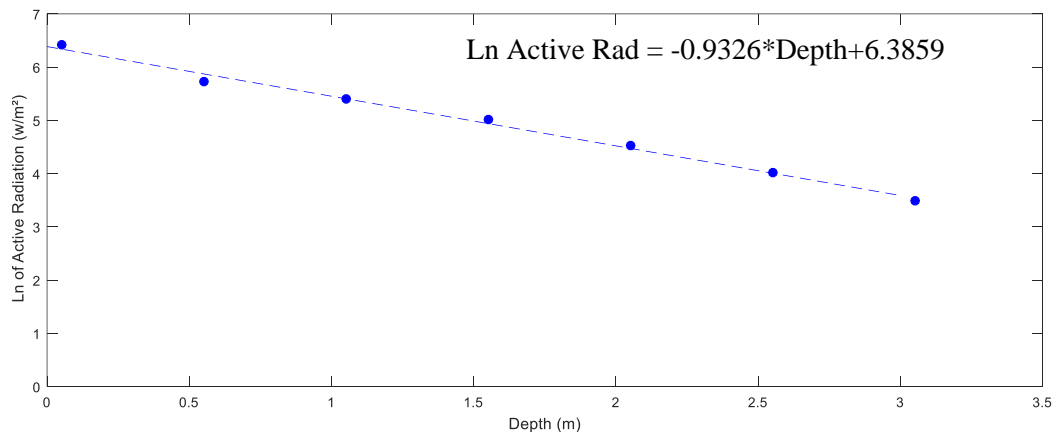


**Figure 4.39** – Active radiation attenuation equation for a vertical profile on 30<sup>th</sup> June 2015

The performance indicators were calculated using the hourly mean of the measured Chl-a data and the model results at 1.5 m depth. The vertical average contributions of each algal groups were used to calibrate algae groups competition. According to Deltares (2013), the calibration can usually be restricted to just a few coefficients, such as the decomposition rate constants, the nitrification rate constant and the algae sedimentation and resuspension velocities. Due to scarce nutrient database, the chosen calibration coefficients were the sedimentation and resuspension velocities of each algae group for the energy phenotype.

Using the default values (Table 3.10) and initial concentration (Table 4.3), the concentration of Chl-a at point A is presented in Figure 4.40 (point B presented very similar behaviour). The grey shaded area represents the range of the hourly concentrations measured every 5 minutes. It is observed that the simulated Chl-a presented much higher values. The performance indicators were:  $R^2$  of 0.41, MAE of 15.5  $\mu\text{g/L}$  and RE of 115%. Concerning algae group competition, Figure 4.41 shows that cyanobacteria

had a higher contribution than measured in the two vertical profiles (22 and 27 July). The MAE considering all phytoplankton groups was of 20% on 22 July and 7% on 27 July.

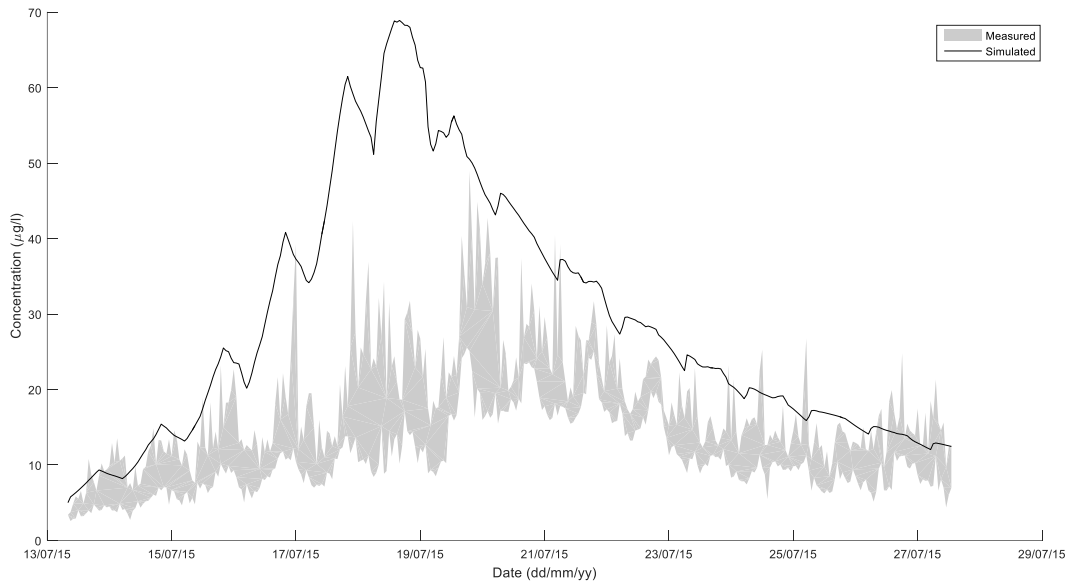


**Figure 4.40** – Simulated and measured Chl-a concentrations at 1.5 m depth at point A using default sedimentation values.

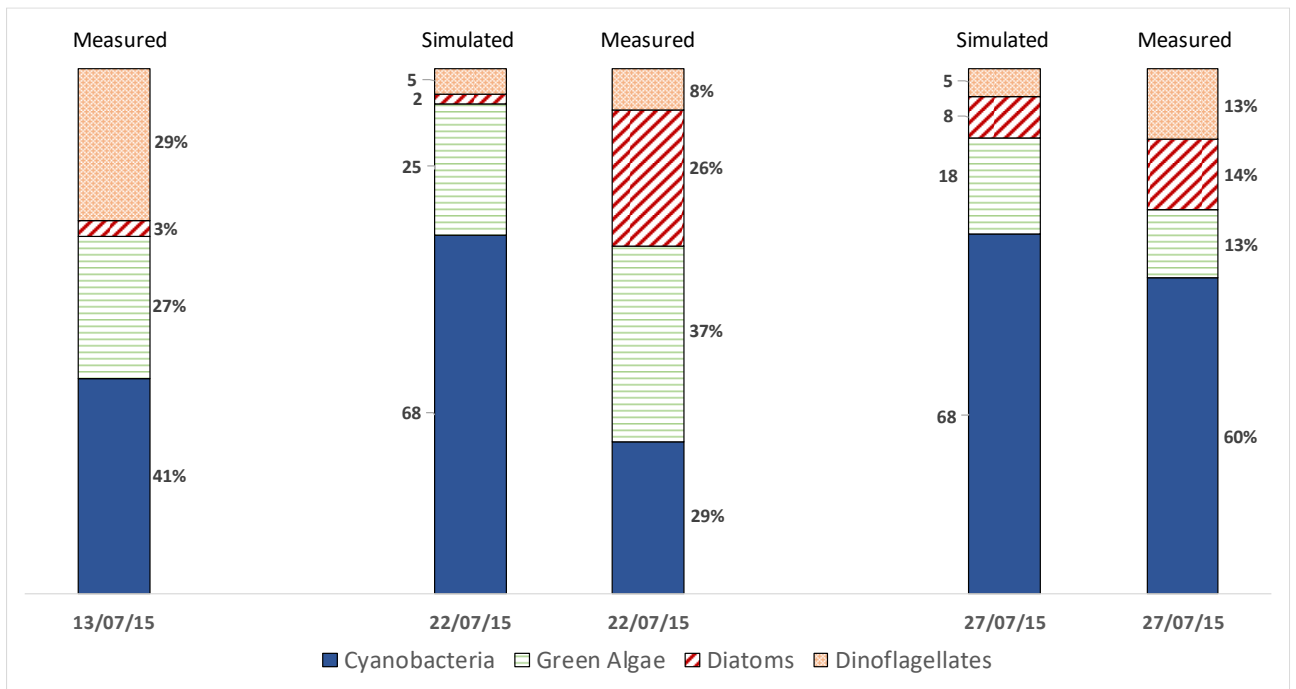


**Figure 4.41** – Fraction contribution of each algal group measured at point A for the calibration period (13 to 27 July 2015) using default sedimentation velocities

Setting the sedimentation velocity of cyanobacteria to 0.5 m/day for the energy phenotype, the simulated Chl-a presented a reduction (Figure 4.42). The performance indicators MAE and RE showed an improvement (MAE of 8.8 µg/L and RE of 65%) but the R<sup>2</sup> decreased (R<sup>2</sup> of 0.32). Concerning algae group competition (Figure 4.43), the MAE of all phytoplankton group contributions was of 11% on 22 July and 6% on 27 July, presenting an improvement. The cyanobacteria group presented a decreased contribution in the two vertical profiles (22 and 27 July), as intended. However, the green algae

contribution now presented values that were too high, especially on 27 July, in which the simulated values was 25%, while the measured was 13%. Thus, the sedimentation velocity of green algae was increased.

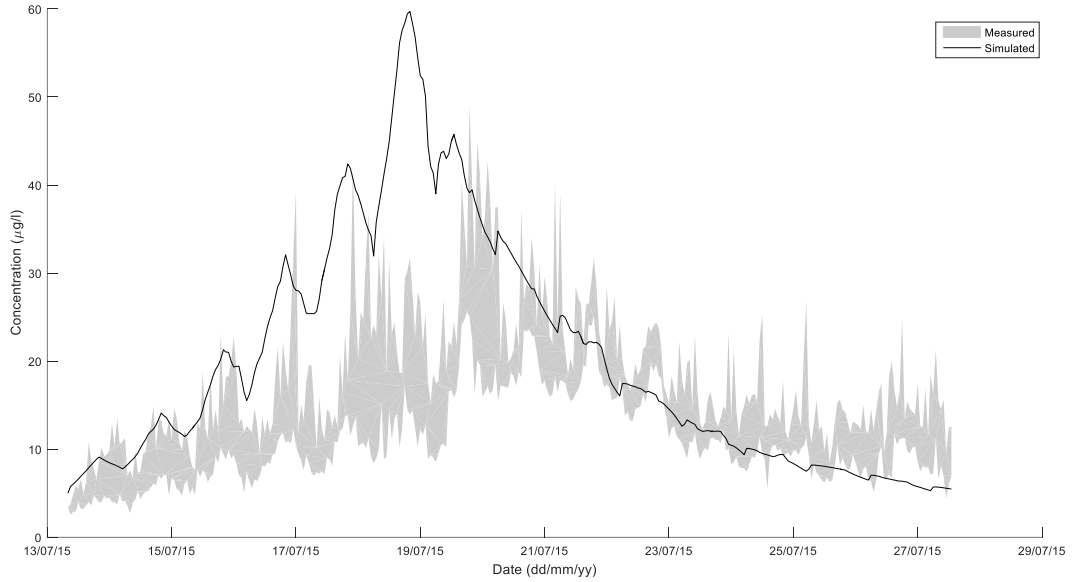


**Figure 4.42** – Simulated and measured Chl-a concentrations at 1.5 m depth at point A using using 0.50 m/day for cyanobacteria sedimentation velocities

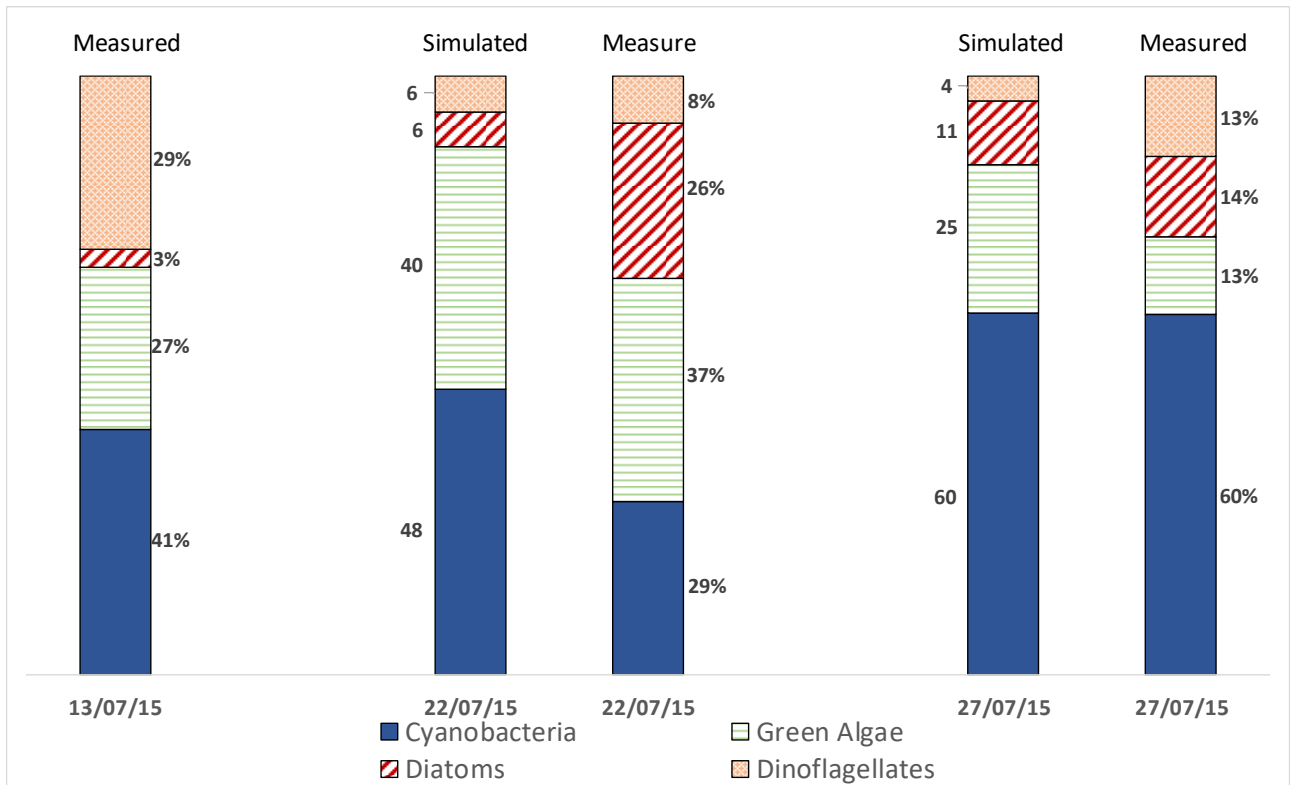


**Figure 4.43** – Fraction contribution of each algal group measured at point A for the calibration period (13 to 27 July 2015) using 0.50 m/day for cyanobacteria sedimentation velocities.

To evaluate the behaviour of the biomass and competitiveness between species, two values of sedimentation velocity were tested for the green algae group. First, a value of 0.75 m/day was tested. Figure 4.44 shows that Chl-a presented a decrease at peak values, especially between 17 and 19 July. All performance indicators showed an improvement ( $R^2$  of 0.51, MAE of 7.6  $\mu\text{g/L}$  and RE of 56%). Concerning algae group competition (Figure 4.45), the MAE of all phytoplankton group contributions was of 13% on 22 July and 8% on 27 July. The green algae group presented a decrease in contribution from 40% to 31% on 22 July and from 25 to 17% on 27 July. This reduced contribution of green algae resulted in an increased contribution by the cyanobacteria group, which presented an increase from 48% to 55% on 22 July, and from 60% to 72 % on 27 July. For other groups, the values did not present a significant change.

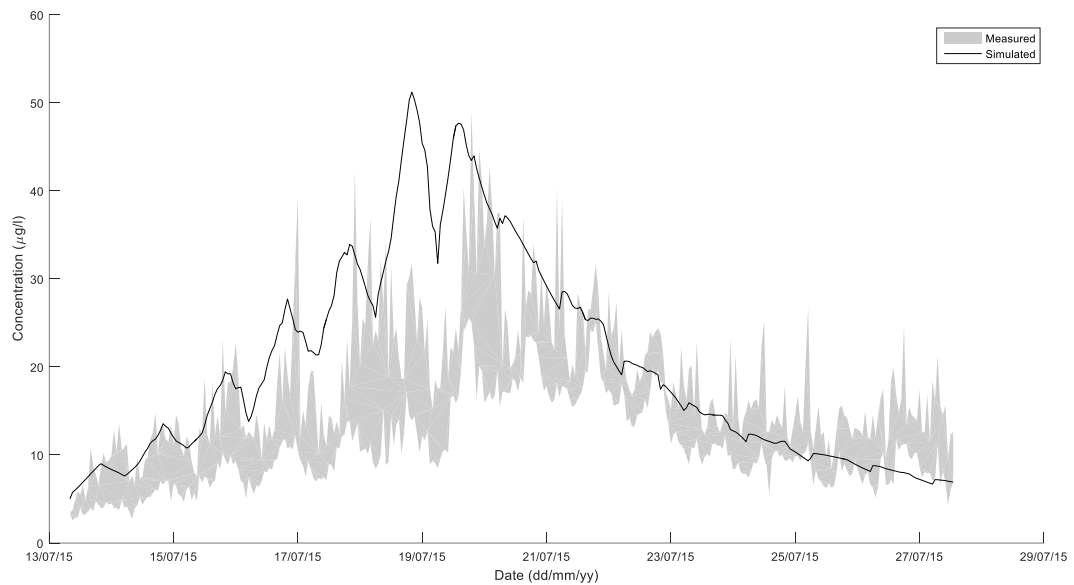


**Figure 4.44** – Simulated and measured Chl-a concentrations at 1.5 m depth at point A using 0.50 m/day for cyanobacteria sedimentation velocities and 0.75 m/day for Green algae



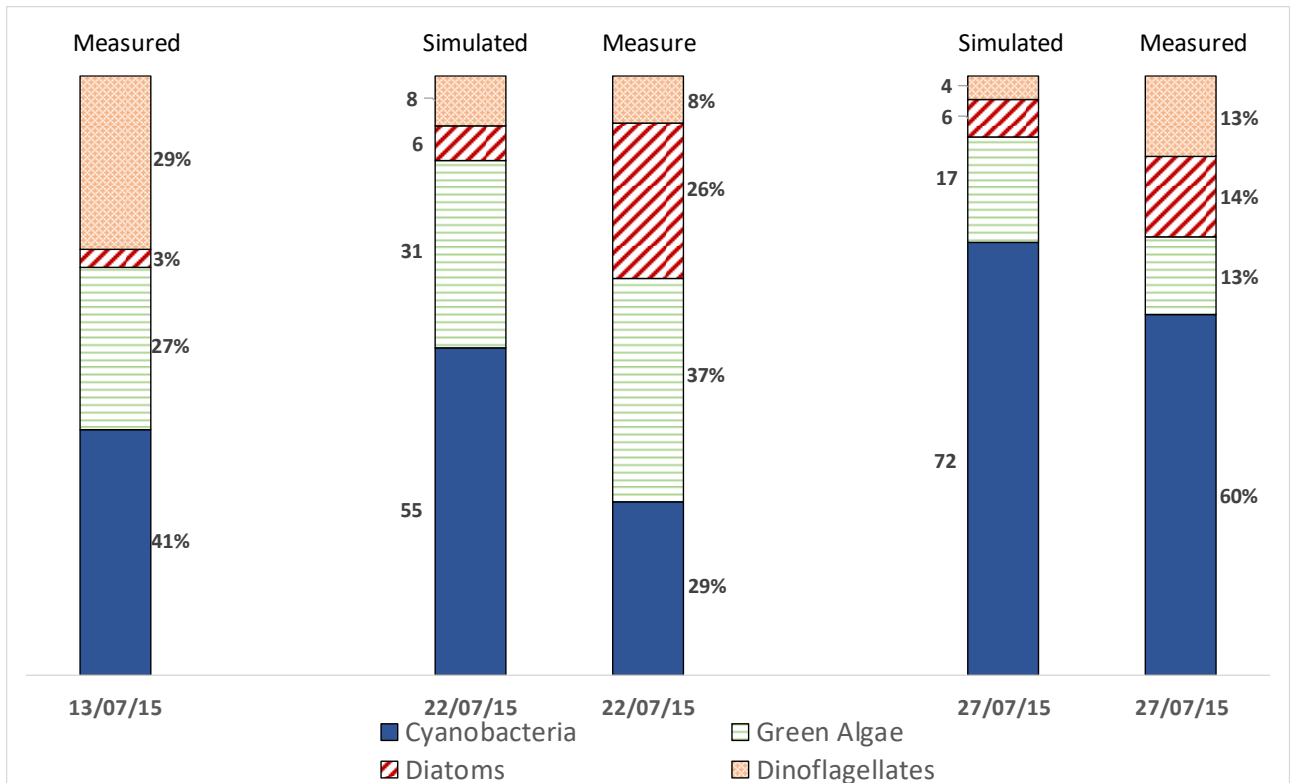


**Figure 4.45** – Fraction contribution of each algal group measured at point A for the calibration period (13 to 27 July 2015) using 0.50 m/day for cyanobacteria sedimentation velocities and 0.75 m/s for green algae

The second sedimentation velocity tested was 1.0 m/day. Figure 4.46 shows that Chl-a had a better adjustment to the measured values. The performance indicators also showed an improvement ( $R^2$  of 0.72, MAE of 7.5  $\mu\text{g/L}$  and RE of 55%). Concerning the resulted algal group competition (Figure 4.47) and comparing with green algae default sedimentation velocity (Figure 4.43), green algae presented a strongly decrease contribution from 40% to 19% on 22 July and from 25% to 17% on 27 July. However, the cyanobacteria contribution increased significantly, with its contribution increasing to 65% on 22 July and to 72% on 27 July. For 22 July, the simulated cyanobacteria contribution was much higher than the measured values, on 27 July it was closer. For 22 July, the MAE of all phytoplankton group contributions was 19% on 22 July and 08% on 27 July. Thus, based on the Chl-a mathematical indicators, in which  $R^2$  presented a better value and the fact that the MAE of species contribution does not change significantly, the sedimentation velocity of 1.0 m/day was chosen for the green algae group. Table 4.4 shows the performance indicator in each simulation.

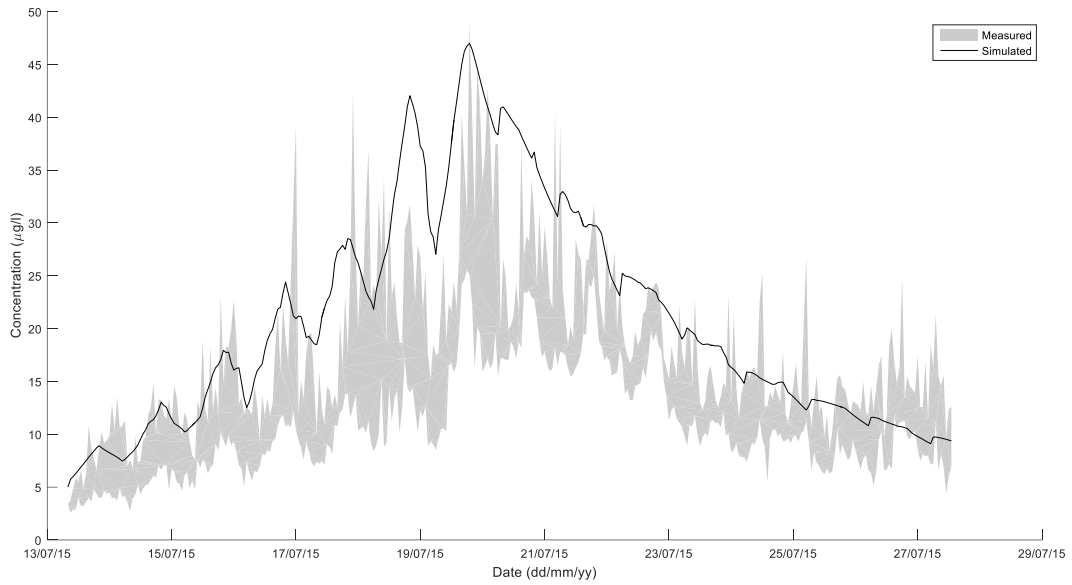


**Figure 4.46** – Simulated and measured Chl-a concentrations at 1.5 m depth at point A using 0.50 m/day for cyanobacteria sedimentation velocities and 1.0 m/day for green algae

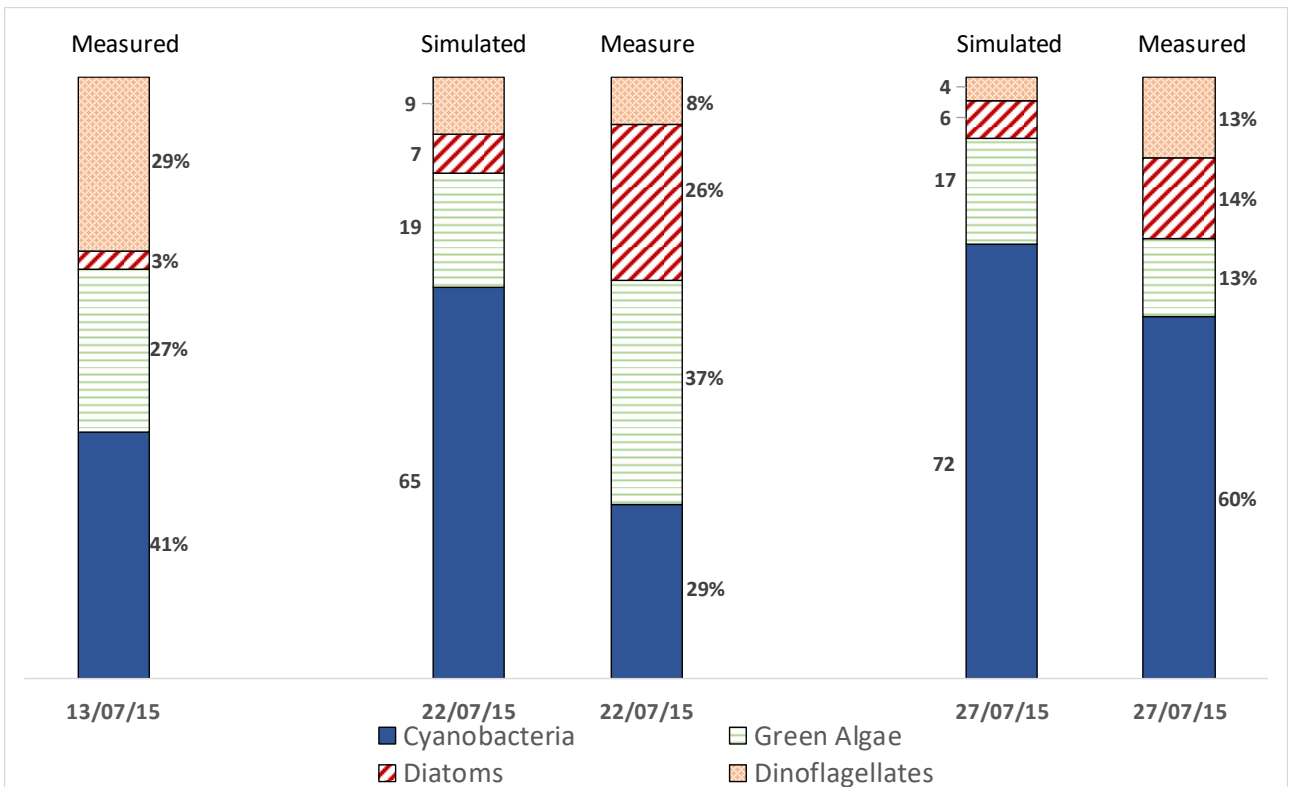


**Figure 4.47** – Fraction contribution of each algal group measured at point A for the calibration period (13 to 27 July 2015) using 0.50 m/day for cyanobacteria sedimentation velocities and 1.0 m/day for green algae

**Table 4.4** – Mathematical performance indicators for coupled hydrodynamic calibration

Phytoplankton group	Phenotype	Sedimentation (m/s)	R <sup>2</sup>	MAE (µg/L)	RE (%)			
Diatoms	Energy	1.0	0.41	15.5	115			
	P & Si	1.5						
Flagellates	Energy	0.5						
Green	Energy	0.5						
	Nitrogen	1.0						
	Phosphorus	1.0						
Bluegreen (Cyanobacteria)	Energy	0.0						
	Nitrogen	0.0						
	Phosphorus	0.0						
Diatoms	Energy	1.0				0.32	8.8	0.65
	P & Si	1.5						
Flagellates	Energy	0.5						
Green	Energy	0.5						
	Nitrogen	1.0						
	Phosphorus	1.0						
Bluegreen (Cyanobacteria)	Energy	0.5						
	Nitrogen	0.0						
	Phosphorus	0.0						
Diatoms	Energy	1.0	0.51	7.6	0.56			
	P & Si	1.5						
Flagellates	Energy	0.5						
Green	Energy	0.75						
	Nitrogen	1.0						
	Phosphorus	1.0						
Bluegreen (Cyanobacteria)	Energy	0.5						
	Nitrogen	0.0						
	Phosphorus	0.0						
Diatoms	Energy	1.0				0.72	7.5	0.55
	P & Si	1.5						
Flagellates	Energy	0.5						
Green	Energy	1.0						
	Nitrogen	1.0						
	Phosphorus	1.0						
Bluegreen (Cyanobacteria)	Energy	0.5						
	Nitrogen	0.0						
	Phosphorus	0.0						

Based on the Chl-a fluorescence values, measured at 1.5 m depth at point A and point B, the model was able to represent the biomass behaviour. During the first six days (13 to 19 July), the values simulated by the model remained at the top of the growth region. On 19 July, fast growth was measured and simulated. The maximum hourly concentration measured growth varied from 18.5 µg/L (05 h) to 49.0 µg/L (19 h). The hourly simulated value of 27.04 µg/L (06 h) grew to 47.0 µg/L (19 h). However, on 19 July, after this fast growth, the measured values decreased to 21.6 µg/L (14 h) and the model decrease to 38.4 µg/L and then to 30.6 µg/L on 21 July (05 h) with a measured value with 24.6 µg/L on the same moment. From 20 to 27 July, the biomass presented a downward tendency, which the model also represented. In addition to total biomass, the distribution among species was also compared in order to

verify that the algal succession. Even with some limitation, algal succession was well captured by the model, and the algae group distribution presented a good indicator to calibrate the total biomass.

The isocontour map of the Chl-a simulated in the water column at point A is presented in Figure 4.48. It is noted that the highest concentration was between 18 and 21 July, with a slightly higher concentration at concentration.

Concerning dissolved oxygen concentration, Figure 4.49 shows the isocontour map, in which the higher values correspond to moments of higher Chl-a concentration, due to algae oxygen production. From 13 to 20 July, a period of increased dissolved oxygen occurred, the same period as the higher increase of biomass. Between 18 and 19 July, a slight oxygen stratification was observed. This period also coincided with a slight biomass stratification. However, according to the vertical profile performed on 22 July 2015, the simulated oxygen stratification was much lower than the measured one (Figure 4.50), especially at bottom depth, in which the measured values were less than 2.0 mg/L and the simulated persisted near 15 mg/L. To improve the oxygen vertical distribution, the decomposition and mineralization processes that provide oxygen consumption need to be improved. After 21 July, with the beginning of a biomass decrease, a decrease in dissolved oxygen is also observed, decreasing to the saturated value.

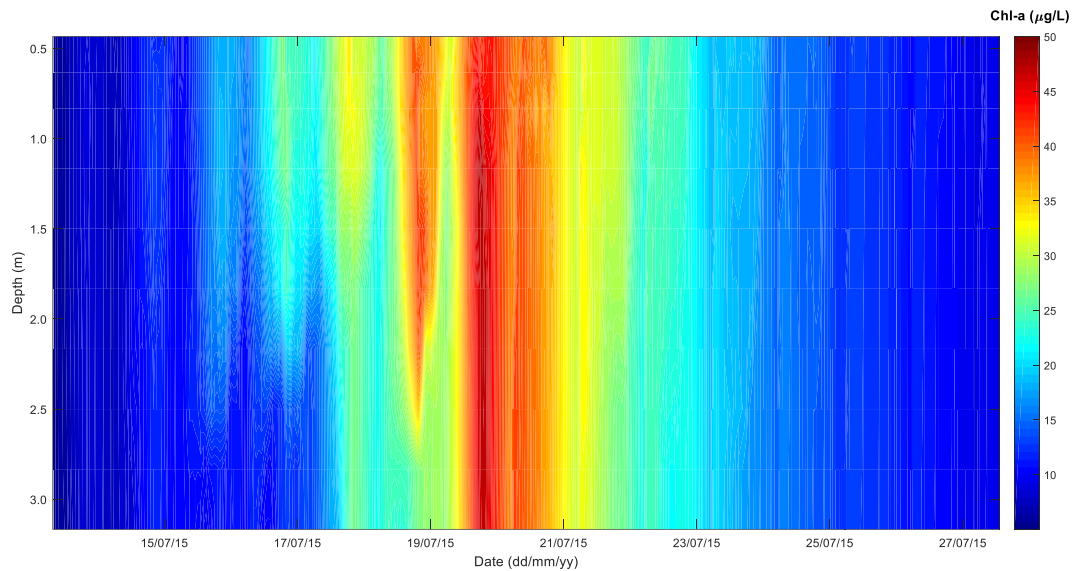


**Figure 4.48** – Chlorophyll-a concentration during simulation from 13 to 27 July 2015 at point A

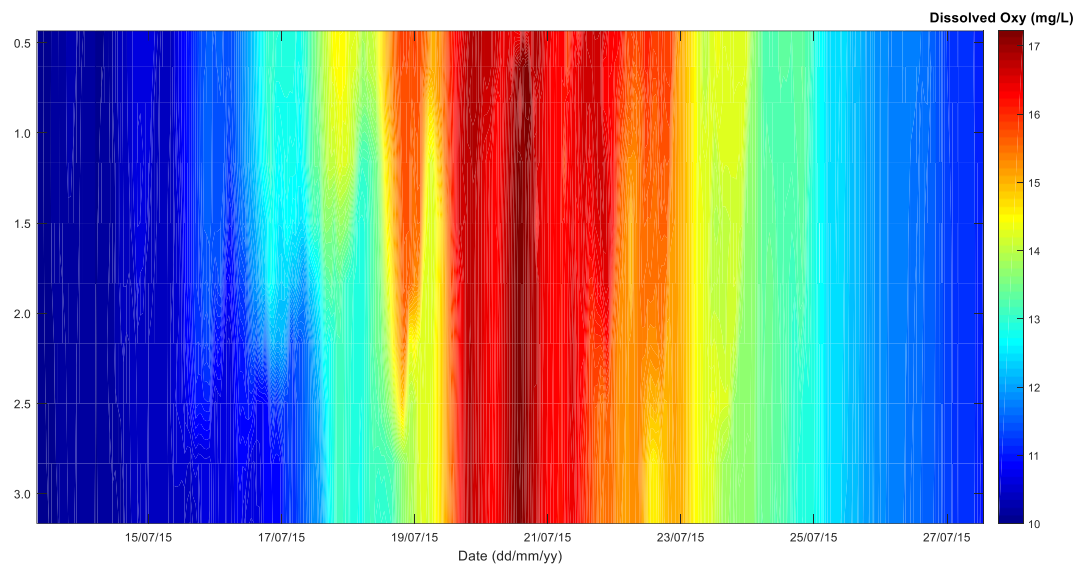


**Figure 4.49** – Dissolved Oxygen concentration during simulation from 13 to 27 July 2015 at point A

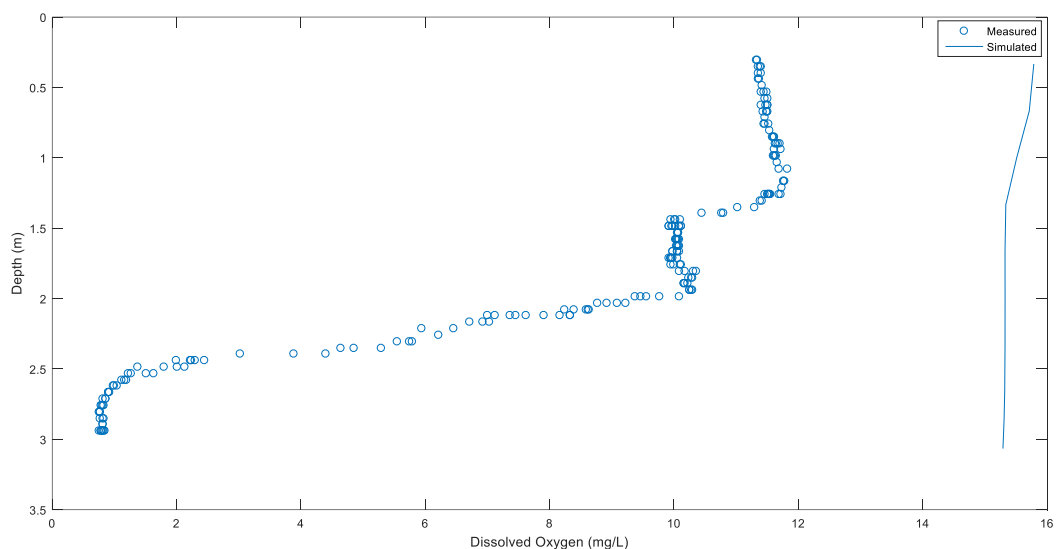


**Figure 4.50** – Simulated and measured vertical Dissolved Oxygen concentration on 22/07/2015 at point A

The evolution of the Nitrate, Ortho-Phosphate and Ammonium concentration in the water column are presented in Figure 4.51 to Figure 4.53 respectively. Unfortunately, due to poor nutrient information, these results could not be validated. Therefore, not all processes have been equally tested and calibrated. However, the absence of nitrate after 20 July demands attention and some consideration must be given.

Some cyanobacteria species (i.e. *Aphanizomenon* and *Anabaena*) are N-fixer, meaning they can take up nitrogen from the atmosphere as an additional source. This source is included as a separate nutrient in the model and is assumed to be infinite. This process was tested, but the results could not be calibrated. Therefore it was deactivated in the simulations.

Based on the active constraint of the optimisation model, represented by the phenotype (see section 3.3.2), the decrease of the biomass in the model started due to the dissolved nitrate. The nitrate concentration and the total biomass concentration dropped dramatically on 20 July. Very low nitrate

concentrations were also measured in other lakes (Zbiciński and Ziemińska-Stolarska, 2017; Beghelli et al., 2016). Right after the decrease of nitrate concentration, phosphate concentration also presented a strong decrease.

Algae mortality produces detritus and inorganic nutrients via autolysis. Mineralisation of detritus in the water column and in the bottom sediment produces inorganic nutrients. Therefore, after 20 July, the available nutrient necessary to the simulated biomass persistence was due to autolysis and mineralisation. As the dissolved nitrate and phosphate concentration is limiting, the model optimisation procedure distributes the full resource. Thus, the nitrate, and in the sequence the phosphate, are completely assimilated and consumed, avoiding a dissolved concentration value overbalance in the water column. In the model, in the case of a resource limitation, the biomasses of the phytoplankton are set to a level at which the resource is completely exhausted.

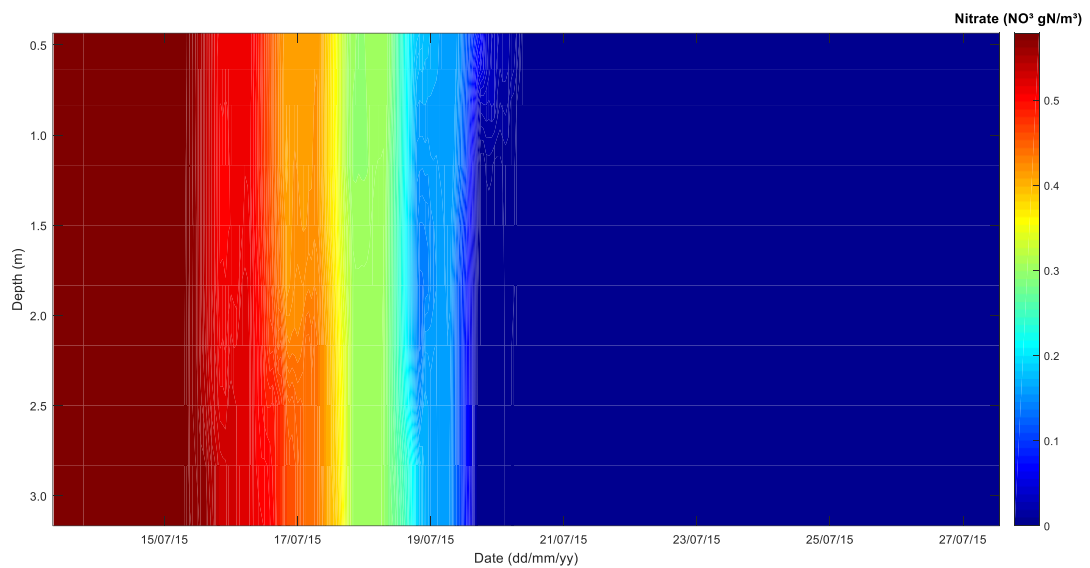


**Figure 4.51** – Nitrate ( $\text{NO}_3^-$  gN/m<sup>3</sup>) concentration during simulation from 13 to 27 July 2015 at point A

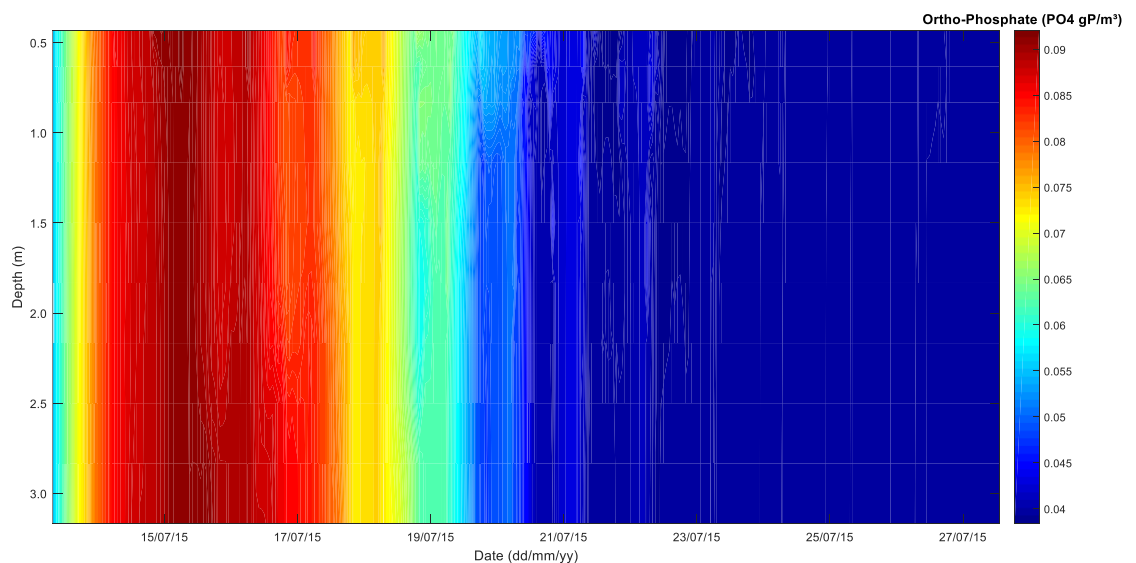


**Figure 4.52** – Ortho-Phosphate ( $\text{PO}_4$  gP/m<sup>3</sup>) concentration during simulation from 13 to 27 July 2015 at point A

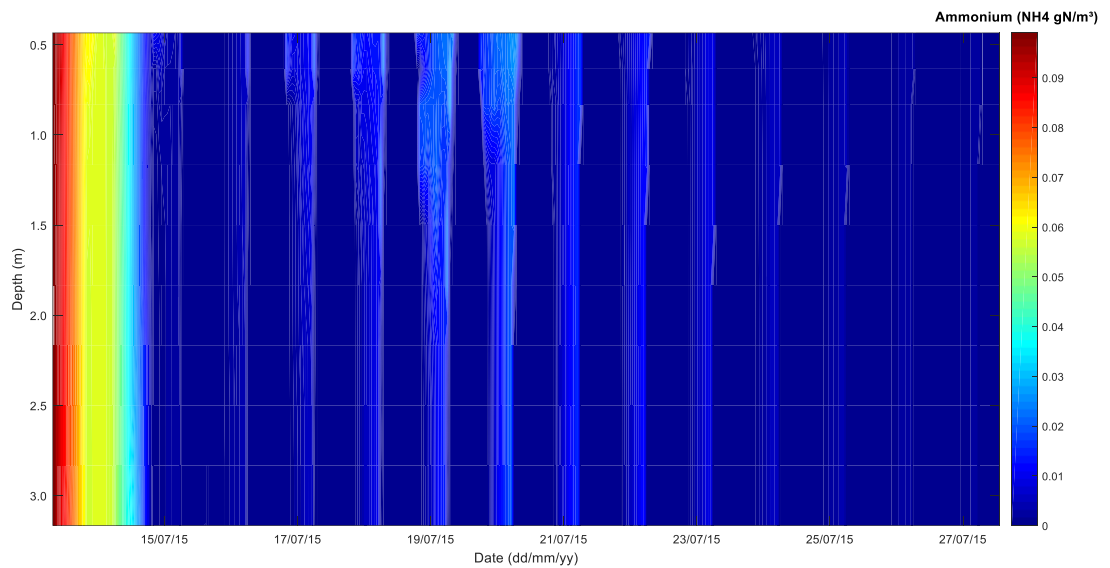


**Figure 4.53** – Ammonium ( $\text{NH}_4$   $\text{gN/m}^3$ ) concentration during simulation from 13 to 27 July 2015 at point A

These simulation results show that the model is able to adequately reproduce observed Chl-a concentration under a wide range of conditions. However, a limitation in the stratification behaviour of the cyanobacteria remains. The results also show that the nutrient cycle needs to be better investigated. However, the model pointed to the potential impacts of nitrate reductions in the biomass behaviour of algae behaviour.

The results of the simulation were evaluated regarding the production of a biomass accumulation on the large beach, due to an increase in biomass and the hydrodynamic behaviour of the lake (as exposed in section 4.2.3). However, this was not observed. According to Figure 4.55 to Figure 4.59, a lower biomass concentration on the east side of the lake was simulated, as obtained in section 4.2.3 using hydrodynamic simulation.

On 16 July, the model result did not present a significant surface heterogeneity (Figure 4.54). The simulated heterogeneity started on 19 July and persisted more evidently until 21 July. In the same period higher measured and simulated Chl-a values were observed.

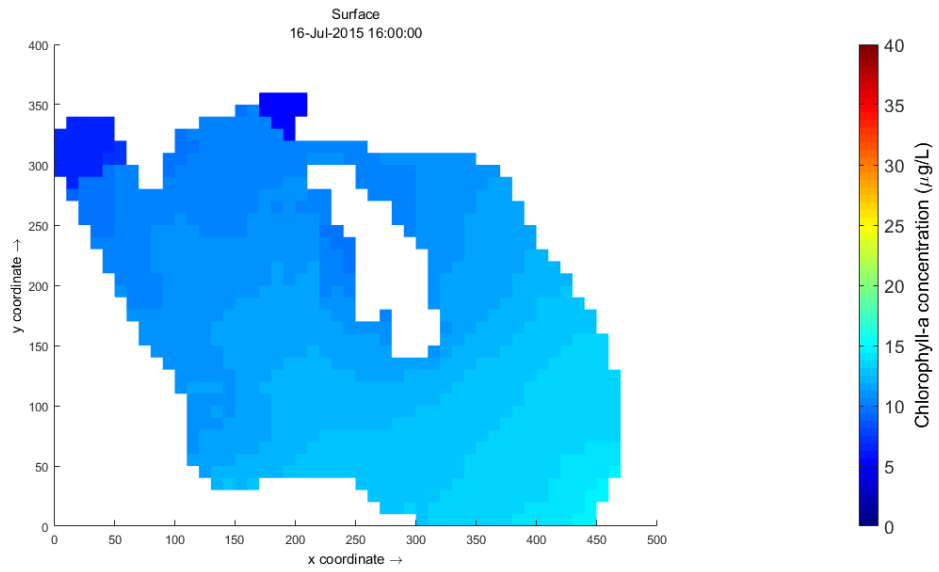


**Figure 4.54** – Chlorophyll-a simulated on 16 July at 16 h

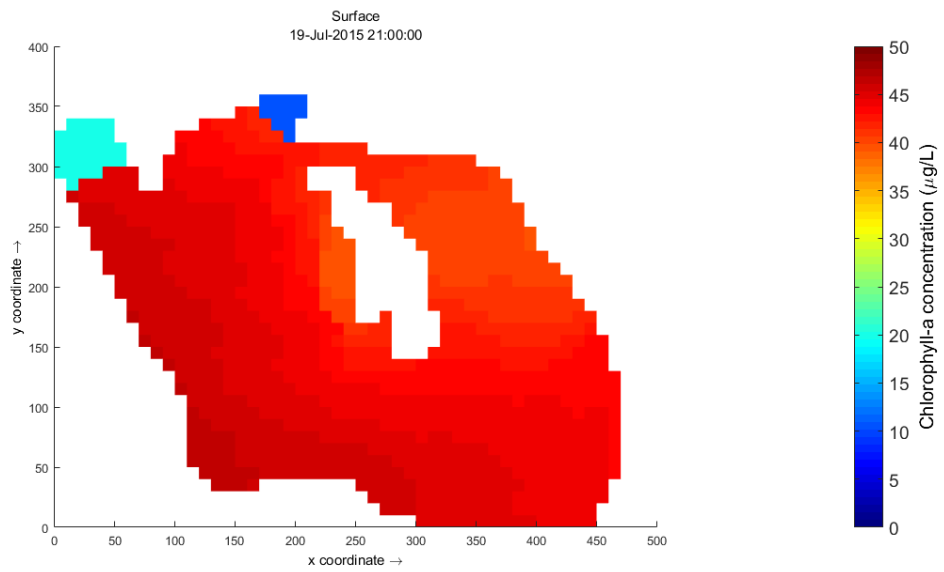


**Figure 4.55** – Chlorophyll-a simulated on 19 July at 21 h



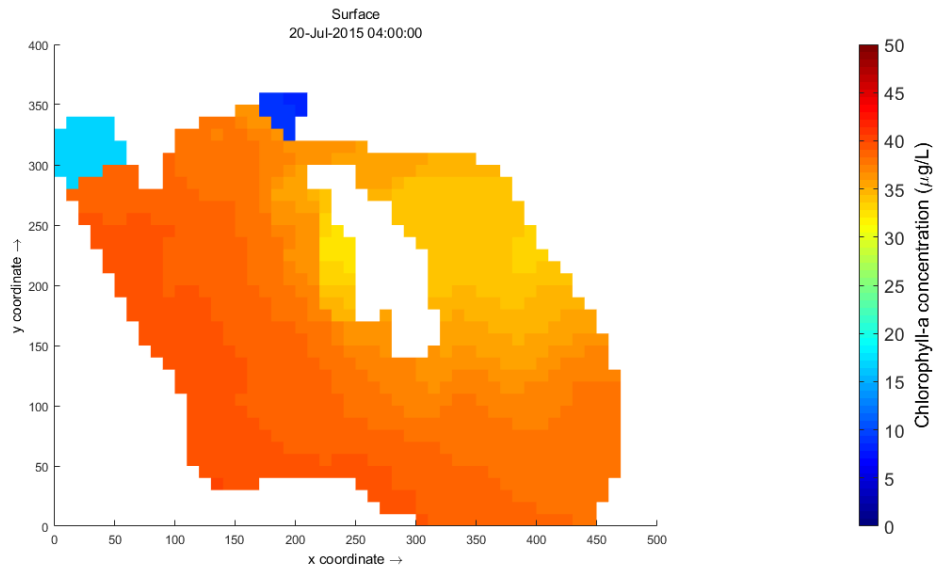


**Figure 4.56** – Chlorophyll-a simulated on 20 July at 04 h

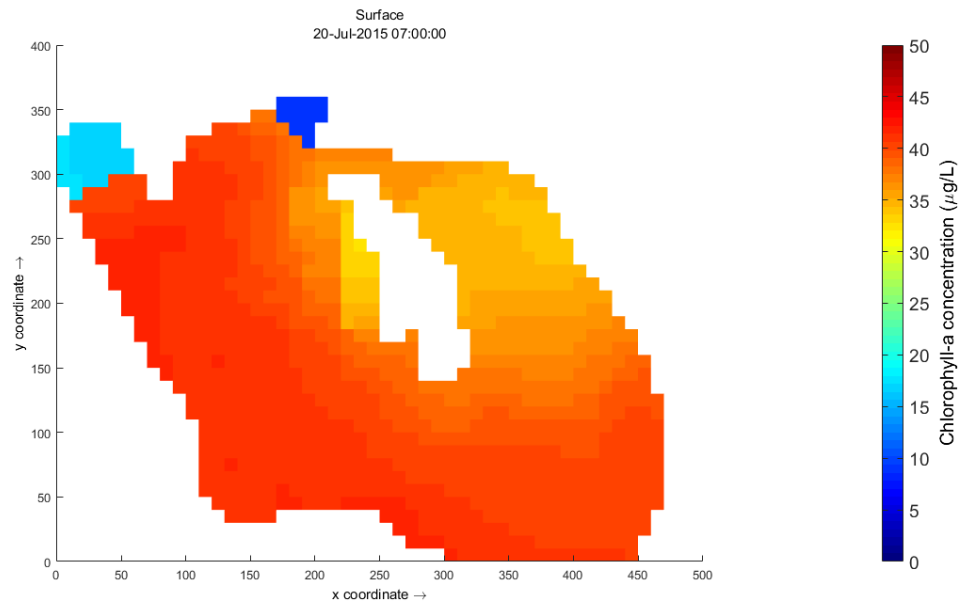


**Figure 4.57** – Chlorophyll-a simulated on 20 July at 07 h

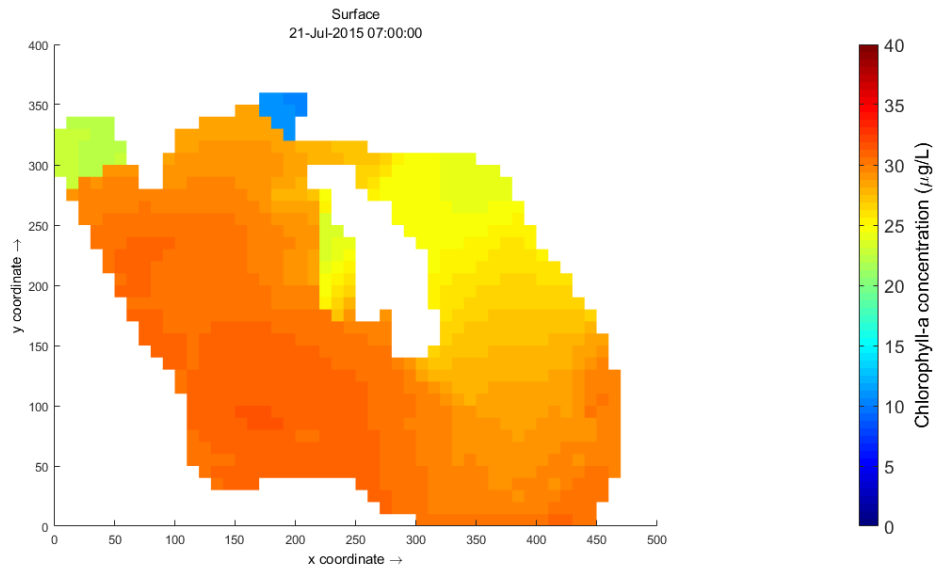


**Figure 4.58** – Chlorophyll-a simulated on 21 July at 07 h

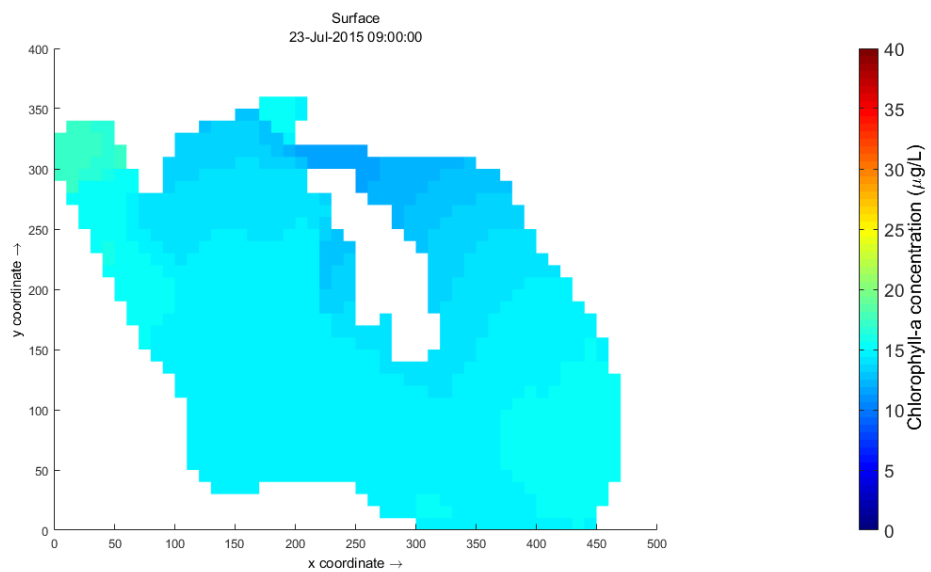


**Figure 4.59** – Chlorophyll-a simulated on 23 July at 09h

The hydrodynamic simulations and the simulation coupling with ecological model pointed that the east side of the lake presented a lower biomass concentration during the period with stronger increase. Thus, it is recommended to install a monitoring point on this side of the lake (point D – Figure 3.26) to validate this hypothesis.

### 4.3.2. Verification Period

The verification period was selected according to the same criteria as the calibration period, as well as the same time of year, but in 2016. The selected period extends from 14 July to 01 August 2016 (18 days). Figure 4.60 presents the temperature at 3 depths and the total Chl-a at 1.5 m depth during 2016. Figure 4.61 presents only the selected period and the dates of field campaigns. It represents the vertical profiles of Chl-a fluorescence from 4 algal groups measured through BBE, which are represented by vertical black lines.

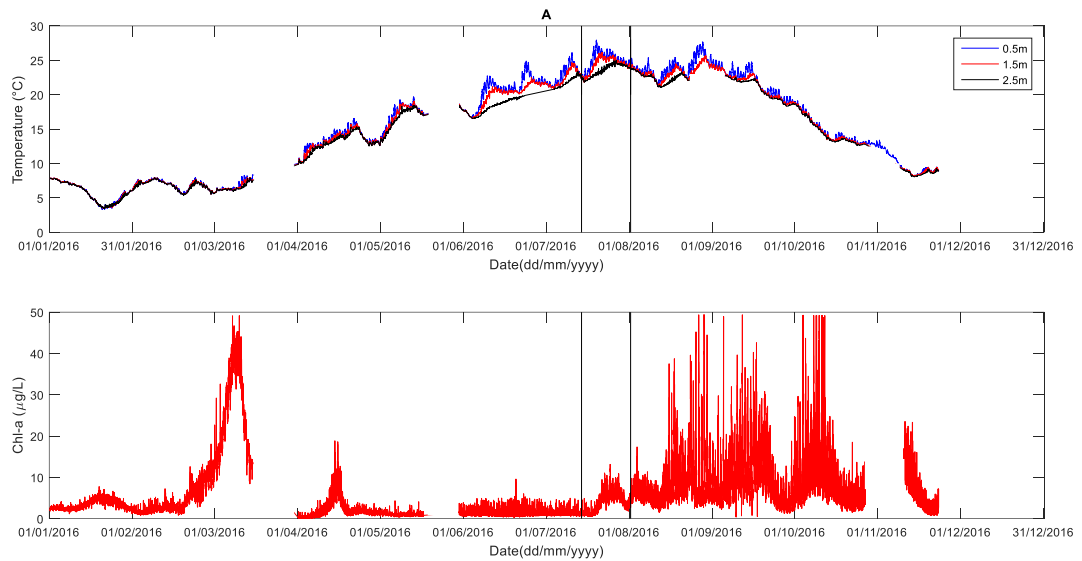


**Figure 4.60** – Total Chlorophyll-a and temperature monitoring in point A during 2016. The simulated period corresponds to black vertical lines

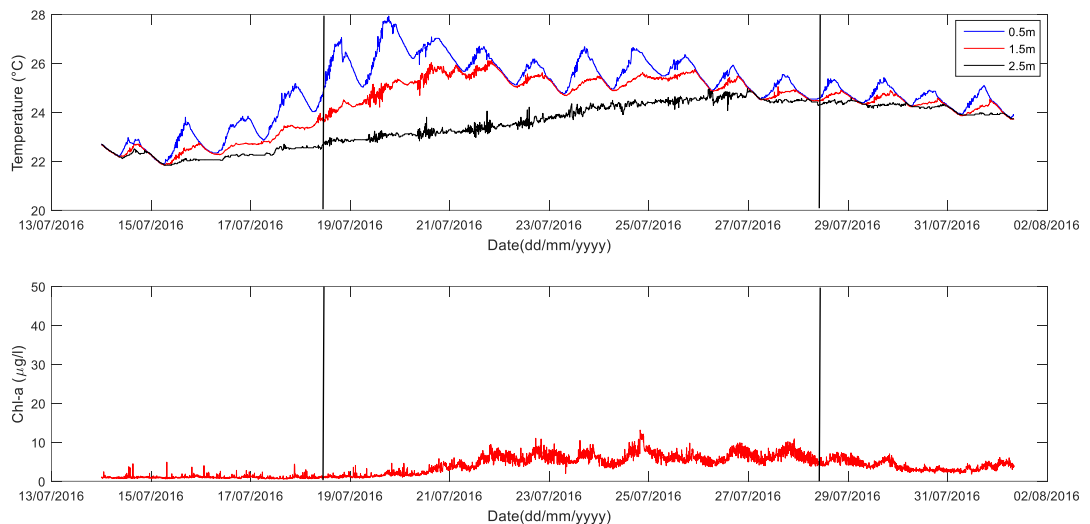


**Figure 4.61** – Temperature and Chlorophyll-a for the validation period (14 July to 01 August 2016). Black lines show when the vertical profile was performed

At the beginning of the period, in thermal mixing conditions, total Chl-a was approximately 1  $\mu\text{g/L}$ . Thermal stratification rapidly appeared on 15 July 2016. However, total Chl-a started to increase just one week later and reached its maximum, approximately 12  $\mu\text{g/L}$ , on 25 July 2016, 10 days after the beginning of stratification. The maximum Chl-a concentration (12  $\mu\text{g/L}$ ) in this period is almost four times lower than in the calibration period of 2015 (45  $\mu\text{g/L}$ ).

The water quality model has a limitation for the calculation of the minimum biomass for each phytoplankton group. Therefore, the start of the ecological simulation was shifted to 18 July, when the biomass was 2.4  $\mu\text{gChl-a/L}$ , above the model minimum limit. Thus, it was evaluated whether setting a uniform condition as initial condition was still possible. The vertical algae group concentration, performed with BBE on 18 July 2016, are presented in Figure 4.62 to Figure 4.64, for points A, B and C respectively. According to these figures, the observed vertical concentrations do not present a vertical

stratification. It is also noted that the algae group contributions were uniformly distributed between the points (Figure 4.65). Thus, a uniform condition of 2.4  $\mu\text{gChl-a/L}$  was set in the model, in which the applied relative species distribution is presented in Table 4.5.

Cyanobacteria represented about 85 % of the total Chl-a during the first week (14 July to 18 July). However, during the last part of the period, green Algae increased and represented 80 % of the Chl-a on 28 July 2016. The stoichiometry ratio for each group was used to convert Chl-a into carbon (section 3.4.3 in Table 3.9).

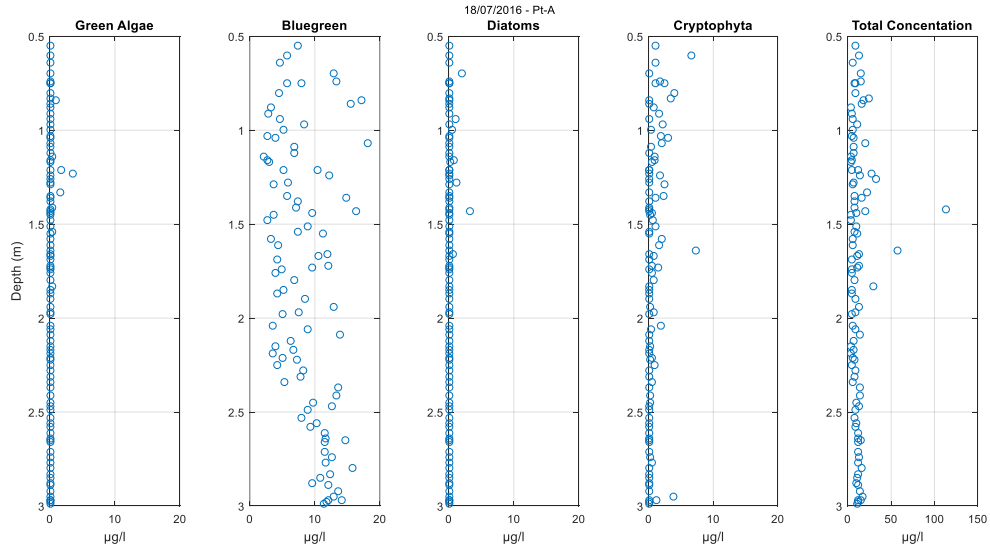


**Figure 4.62** – Vertical algae distribution measured on 18 July 2016 at Point A

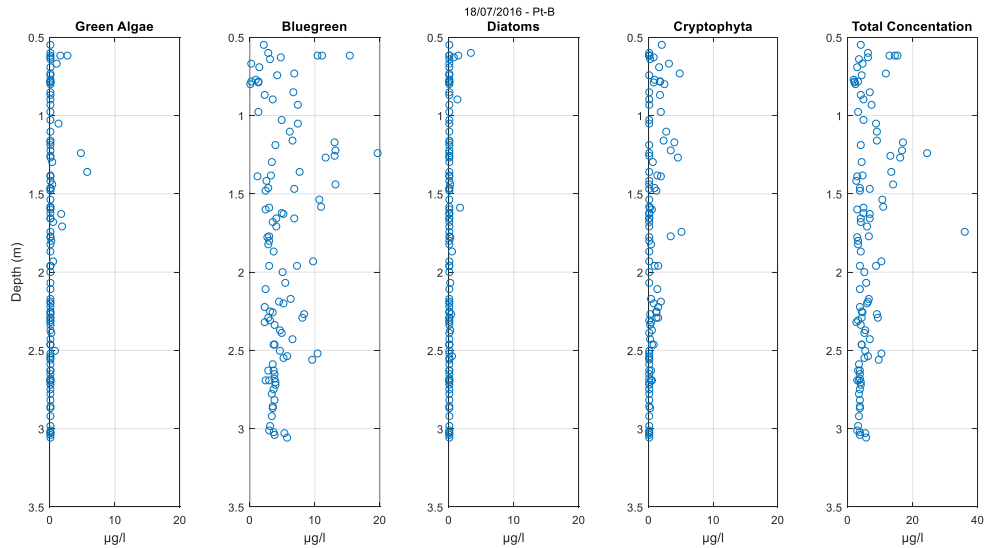


**Figure 4.63** – Vertical algae distribution measured on 18 July 2016 at Point B

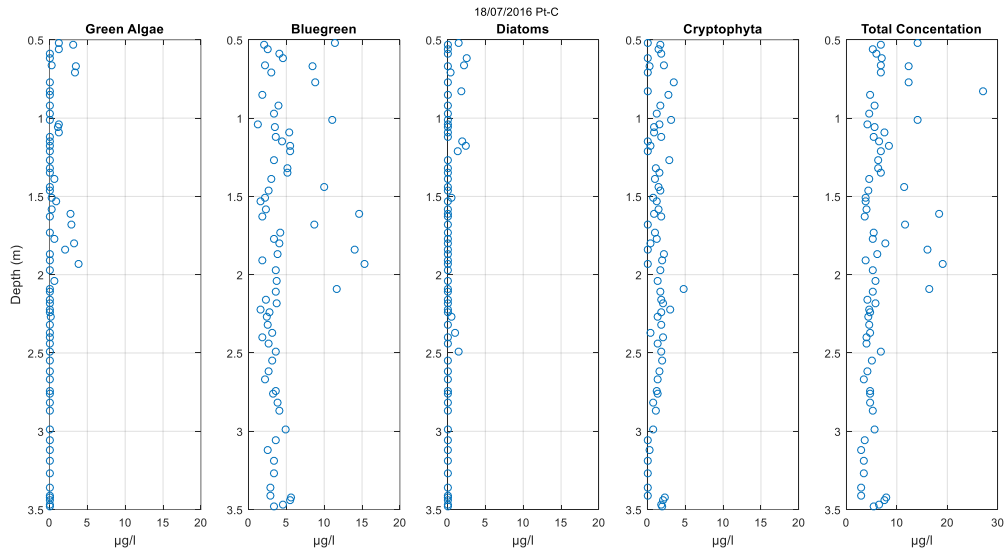


**Figure 4.64** – Vertical algae distribution measured on 18 July 2016 at Point C

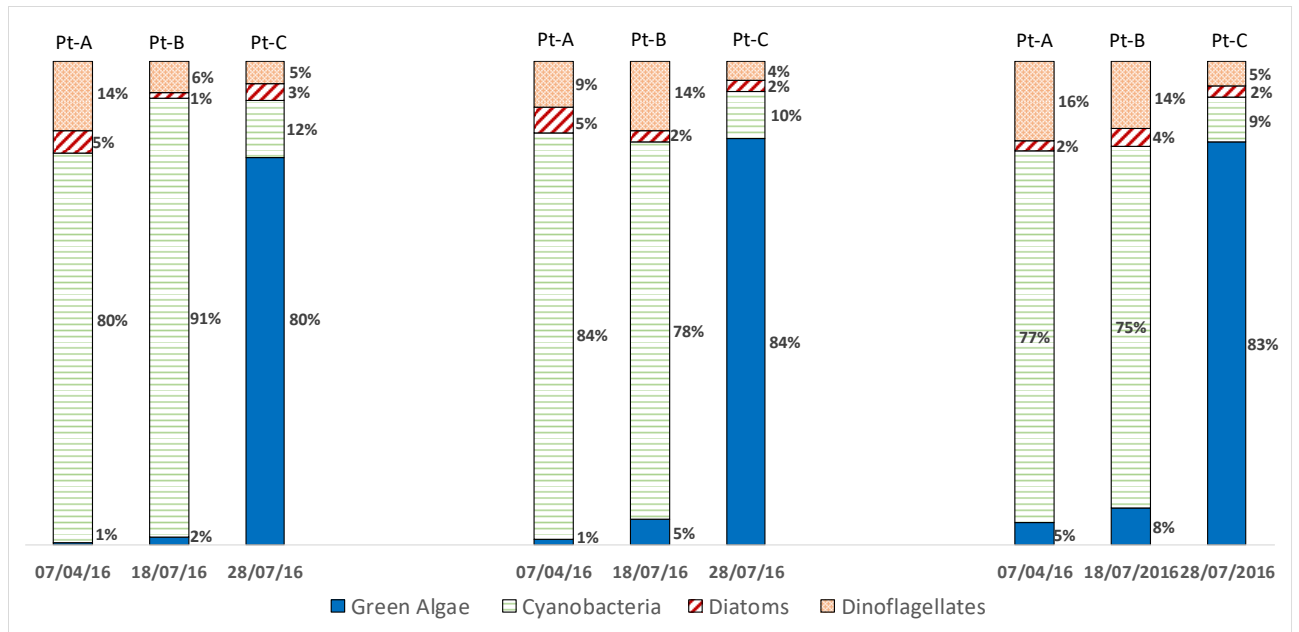


**Figure 4.65** – Vertical contribution of each algal group measured during the verification period (18 July 2016 to 01 August 2016)

Concerning dissolved oxygen, the initial condition was obtained from the multi-parameter probe profiles. The vertical profile at point A, B and C, performed on 18 July 2016, are presented in Figure 4.66. As the three points presented a similar vertical profile, the vertical mean values between each point were set as initial condition, meaning that all points in the domain presented the mean values presented in Figure 4.66.

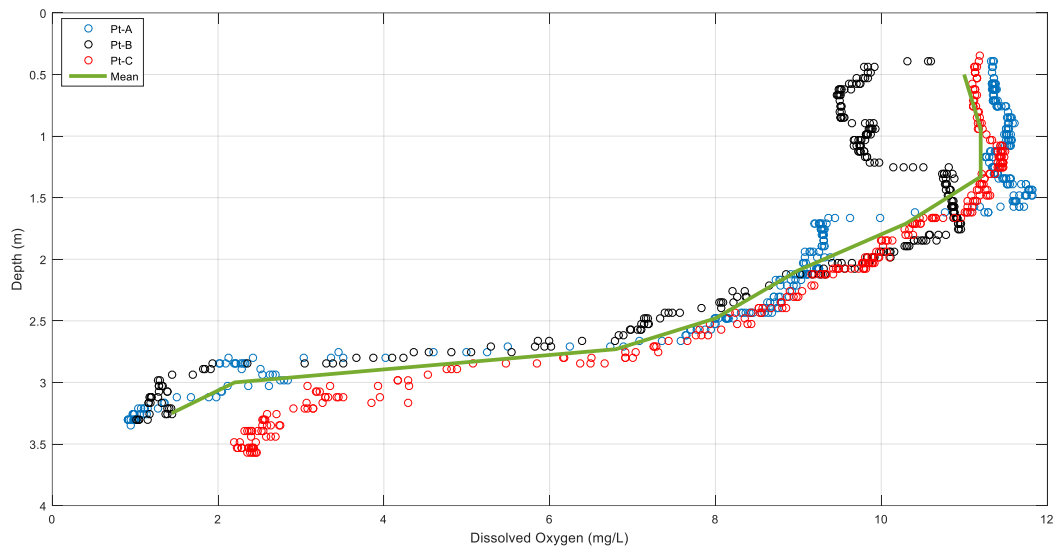


**Figure 4.66** – Dissolved oxygen concentration at point A, B and C. The green line represents the mean valued used as initial concentration in element depths for the verification period (18 July 21016 to 01 August 2016)

**Table 4.5** – Initial condition values of the simulation in 2016

Variable	Values
Dissolved Oxygen (mg/L)	11.2 to 1.5
Cyanobacteria ( $\mu\text{gChl-a/L}$ )	1.96
Diatoms ( $\mu\text{gChl-a/L}$ )	0.07
Dinoflagellates ( $\mu\text{gChl-a/L}$ )	0.27
Green algae ( $\mu\text{gChl-a/L}$ )	0.1

For 2016, a nutrient data analysis was not performed. Therefore, a sensitivity assessment was performed based on the minimum, mean and maximum values of the nutrient database (Table 4.6). The selected period makes it possible to evaluate the advantage of a hydrodynamic model coupled to an ecological model even when some data are missing.

**Table 4.6** – Range of nutrients used in 2016 simulations

Elements	Min	Mean	Max
Ammonium ( $\text{gN/m}^3$ )	0.107	0.202	0.607
Nitrate ( $\text{gN/m}^3$ )	0.138	0.202	0.574
Ortho-Phosphate ( $\text{gP/m}^3$ )	0.057	0.129	0.213

The results of the simulated Chl-a concentrations compared to the measured values at 1.5 m depth are presented in Figure 4.67. The dark grey shaded area represents the range of hourly concentrations measured, and the light grey shaded area represents the range of biomass simulated, varying according to the concentration of nutrients.

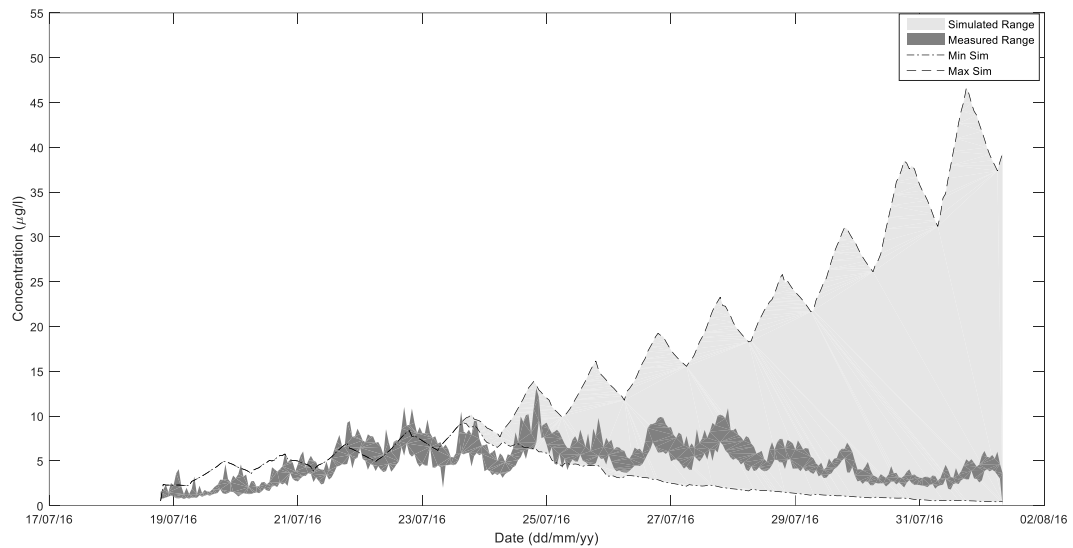


**Figure 4.67** – Simulated and measured chlorophyll concentrations at 1.5m depth at point A. The shaded dark grey area represents the range of the hourly concentrations measured, and the shaded light grey area represents the limits of simulated biomass.

Regardless of the low availability of nutrient data, the model was able to well-represent the slow biomass increase during the first 6 days of the simulated period.

From 25 to 29 July, the simulated values were dependent on the nutrients concentrations. Table 4.7 presents performance indicators for the simulations, according to the nutrient concentrations used.

**Table 4.7** – Simulation performance for the 2016 scenario

Nutrients	RE	R <sup>2</sup>	MAE (µg/L)
Min*	65 %	0.41	2.50
Mean*	121 %	0.77	4.67
Max*	200 %	0.39	7.67

\*Values on Table 4.6

On 18 and 28 July 2016, the main phytoplankton groups were assessed in the water column through the spectrofluorometer vertical profiles (BBE). Figure 4.68 presents the simulated and measured depth-averaged relative biomass with minimum nutrients concentrations. The model did not correctly predict the proportion between each simulated group and the total biomass, representing a limitation of the simulation. However, the biomass concentration was low, so this discrepancy is quantitatively less significant (Figure 4.61).

For a predictive application, such as an early alert system, knowing that the biomass will not increase significantly over the next days, even during a condition of heating and stratification, could be an important information for the lake manager.

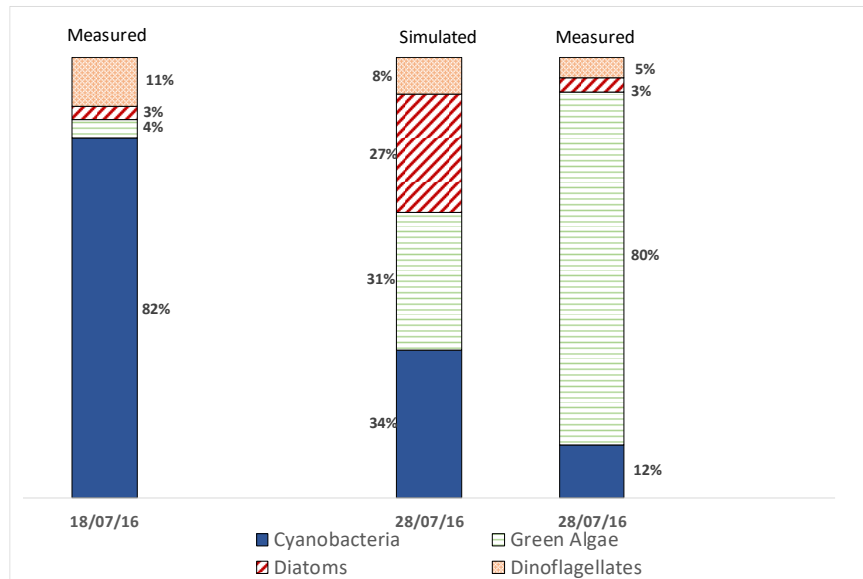


**Figure 4.68** – Average contribution of each algal group measured and simulated in the validation period (18 July 2016 to 01 August 2016)

#### 4.4. Lake Champs-sur-Marne conclusions and discussions

Hydrodynamics play an important role in cyanobacteria behaviour in lakes. Thermal stratification might favour cyanobacteria growth due to optimal buoyancy conditions, while mixing events may facilitate nutrient release from the sediment, allowing an increase in phytoplankton. Thus, the Delft3D-Flow model performance was first assessed on Lake Champs-sur-Marne for water temperature simulation using high-frequency data. For all four different simulated periods,  $R^2$  ranged from 0.53 to 0.99, similar to results obtained in others studies (Missaghi and Hondzo, 2010; Zhao et al., 2013). For instance, in Lake Yilong (Zhao et al., 2013), the  $R^2$  calculated with data from 15 field campaigns ranged between 0.65 and 0.74.

The MAE values of water temperature obtained for Lake Champs-sur-Marne were compared with values obtained in a similar small and shallow lake, Lake Créteil. A detailed analysis of Delft3D-Flow performance was conducted by Soullignac et al. (2017). In summer, the MAE computed with high-frequency data ranged between 0.34 and 0.62 °C. MAE values for Lake of Champs-sur-Marne ranged within the same magnitude, between 0.32 and 0.77 °C for four period using high-frequency data. The Period 1 (lasting 7 days, from 23<sup>rd</sup> June 2015 to 30<sup>th</sup> June 2015, corresponding to 159 hourly values), periods 2 (lasting 14 days, from 13<sup>th</sup> July to 27<sup>th</sup> July 2015, corresponding 342 hourly values), period 3 (lasting 19 days, from 14<sup>th</sup> July 2016 to 01<sup>st</sup> August 2016, corresponding to 456 hourly values) and period 4 (lasting 19 days, from 19<sup>th</sup> September 2016 to 12<sup>th</sup> October 2016, corresponding to 567 hourly values) were used to validated the model.

In our research, an important source of uncertainty in the hydrodynamic simulations comes from the geographical distance (22 km) of the meteorological data recording station. Though the main features of meteorological forcing can be considered similar in both locations, some are expected to differ, especially the hourly values for the wind (speed and direction), the relative humidity and cloud cover. Our research could explain and discuss uncertainties that result in specific discrepancies between measured and simulated data in the lake, showing that a shallow lake has a high sensibility to external forcing, thus, *in loco* meteorological measurement is more recommended (section 4.2.1).

Current flow, measured every three minutes through ADCP with a resolution of 5 cm in the vertical direction, enabled an analysis of the influence of water mixing on the vertical column, phytoplankton behavior and the influence of wind on a small and shallow lake.



One of the main features of flows in a lake is that they contain a wide range of dynamically active scales. To access the information of scale values, it is important to carry out a spectral analysis of observed and simulated data (Mezemate, 2014). Through spectrum analysis, it is possible to acquire time-domain signals and measure the frequency content. Comparing the measured and simulated spectral it is possible to evaluate the model performance.

According to the results, the three-dimensional hydrodynamic model could satisfactorily represent the time at which the water current reaches the higher values and its vertical distribution. Using a fast Fourier transformation (FFT), it is noted that the model could simulate the same frequency behaviour for the measured velocity values. According to Pannard et al. (2011), the lake has a stratification behaviour if the power spectrum at different depths presents a different behaviour. The measurements and the simulation show that the lake does not have velocity stratification. It was shown that, for all three depths and for the average vertical profile the velocity behaviour was very similar and presented a strong correlation with wind intensity, in which wind intensity of 3.0 m/s may impact the entire vertical column.

Li-Kun et al. (2017) used water temperature measurements to validate a hydrodynamic model. In our results, it was possible to note that a calibrated and validated model to the thermal behaviour of the lake could also well represent the current flow.

Regarding phytoplankton modelling, the performance of the different models was harder to compare with the available literature. The heterogeneity of the field survey frequency, measuring devices and the aggregate level of phytoplankton species make it particularly difficult to achieve quantitative comparisons. Nevertheless, according to a broad analysis of the performance of phytoplankton models conducted by Shimoda, Arhonditsis (2016) in the literature, simulations of total phytoplankton have  $R^2$  values ranging from 0.01 to 0.92, with a median of 0.28, and relative errors (RE) ranging from 12% to 141% with a median value of 39%. The performance indicators of our simulations are within the best part of the range, an  $R^2$  of 0.72 and a RE of 55% for the calibration (2015) period and an  $R^2$  of 0.41 and RE of 65% for the verification period (2016) in the low nutrient scenario.

The vertical average contributions of each algal group were also used to calibrate the algae group competitions. The sedimentation velocities for each algae group were changed to calibrate the model. The final velocities were in the same range as the literature and close to values presented in Yu et al., (2018), which used 0.3 to 1.2 m/day for *Chlorella* (green-algae) and in the range of algae sediment standard values which varies from 0.1 to 1.0 m/day (Brennen et al., 2018).

Among the many sources of uncertainty that can affect the ecological model accuracy, the main concerns identified were: (i) the uncertainty of the chlorophyll-a field data; and (ii) the lack of reliable nutrient measurements.

Chl-a is used as a proxy to assess phytoplankton biomass. It can be measured with different types of sensors. Although based on the principle of specific excitation at one or several specific wavelengths, they produce different values depending on the water characteristics (interference of colored dissolved organic matter), the algal species (different pigment contents), and the design of the measuring device. However, the sensors play an important role in field monitoring despite their limitation and uncertainties (Silva, et al., 2016; Catherine, et al., 2012; McQuaid, et al., 2011).

Better availability of nutrient data is required to improve the modelling of phytoplankton succession which is shaped by the interplay between light, temperature, and nutrient limitation. Knowledge of the nutrient concentrations would allow us to better calibrate and validate the parameters involved in the equations for the mineralization and release processes, including dissolved oxygen concentration. In the simulations from July 2015 and 2016, according to the model, the decline of the phytoplankton growth was caused by low concentration of nitrates. No field data were available to confirm it. However, very low nitrate concentration impacting phytoplankton growth was also verified in other lakes (Zbiciński and Ziemińska-Stolarska, 2017; Beghelli et al., 2016). According to Kolzau et al. (2014) concentration

ratio below 18.5 for TN:TP indicate nitrogen limitation. A UV spectral photometer sensor for nitrogen and carbon measurements was acquired by the LEESU laboratory and will be installed in the lake in the near future. With this sensor, a real-time response will be possible. With high-frequency nutrient measurements, calibration and validation of the parameters involved in mineralization processes can be improved.

Ecological simulations were based on few nutrient concentrations. Notwithstanding, it could be seen that the model presented good results in modeling phytoplankton increase, decrease behaviour and the timing of the beginning of biomass growth was correctly represented. The model is also a reliable tool for simulating different scenarios, in cases where there are information gaps. A great advantage of the used model is the linear optimization method to determine biomass distribution. Despite some limitations and the difficulty in collecting all required field data, this model seems to be a helpful tool for lake management and to determine specific monitoring points. With the objective of evaluating the spatial and temporal behaviour of algae biomass in the lake, the installation of a high-frequency sensor near to the large beach and on the east side of the lake is recommended. To evaluate the vertical migration, it is also recommended to install a sensor at same point at different depth, as near the surface.

Based on model results, it was noticed that the temporal and spatial biomass distribution is influenced by advection forces. The water velocities and direction calculated by Delft-3D influence the transport of cyanobacterial biomass. It was possible to take advantage of using different modeling approaches (with and without coupling ecological module) to evaluate the transport features and spatial and temporal biomass behaviour. Wu (2013, 2015) also pointed that hydrodynamic and blooming behaviour leads to high spatial and temporal heterogeneity in a shallow lake. Ishikawa (2002) concluded that buoyant colonies accumulate through large-scale horizontal hydrodynamic processes. Wang (2017), using ABM (Agent-based models), observed that cyanobacteria biomass changes their position according to horizontal convection but strongly depended on buoyancy vertical migration process. According to the author, buoyancy regulation and vertical turbulence due to wind are the two main factors that influence the cyanobacteria migration in his case study.

The coupled models, also made it possible to evaluate the influence of hydrodynamics on spatial and temporal distribution of phytoplankton biomass. This approach can also be used to improve specific monitoring campaigns. Knowing where scum is likely to occur and accumulate may help in the challenge of obtaining field data and study this phenomenon.

Due to the great variability of hydrodynamic behaviour in shallow urban lakes and external driving forces, high-frequency monitoring coupled with a three-dimensional model may help to achieve a system to catch cyanobacterial bloom events and scum formations. Hence, high-frequency monitoring and three-dimensional modelling corroborate for a clearer understanding of phytoplankton and cyanobacteria concentrations.

Using high-frequency field data to demonstrate that a change in hydrodynamic behaviour has the potential to influence cyanobacterial blooms presents a considerable challenge. However, using 3D modeling, calibrated for specific points, indicates that the lake hydrodynamic is a process that affect spatial and temporal biomass distribution in a shallow lake. Otherwise, using the result of modeling, suggestions could be done to improve the current monitoring locations to better elucidate the cyanobacteria behaviour. To complement field observations, remote sensing images can also improve the monitoring program, especially to evaluate the lake heterogeneity.

## **5. LAKE PAMPULHA RESULTS**

This fifth chapter will present the results for the study site of Lake Pampulha, located in Brazil. Section 5.1 will present data treatment and analysis carried out for Lake Pampulha. Section 5.2 will present the results of two methods applied to estimate the water temperature of tributary inflows based on the available air temperature data. Section 5.3 will present the hydrodynamic results for the calibration period (18 days), the validation period (11 days) and a third period as a longer validation period (88 days). Model performance of simulated periods was evaluated using hourly values. Based on the hourly measurements and simulation results, these periods enable an analysis of different external forces and the hydrodynamic behaviour of the lake. Section 5.4 will present conclusions and discussions.

### **5.1. Analysis and validation of measured data**

The first data treatment carried out for Lake Pampulha consisted of discarding values measured during cleaning and maintenance events, in which the sensors were removed from the water.

The high-frequency measurements performed at station P<sub>1</sub> (19° 51' 5" south and 43° 58' 35" west) captured water temperature and Chl-a fluorescence at the surface (0.5 m depth) at 30-minute time steps from February 2015 to August 2018. The temperature was also measured at 3 other depths (2.5 m, 5.5 m and 9.5 m) over 18 months (from February 2016 to August 2017) at 1-hour time steps. Figure 5.1 presents the time series for the monitored depths and Figure 5.2 presents an overview of the time series for the period with temperature measurement at 0.5, 2.5, 5.5 and 9.5 m depth.

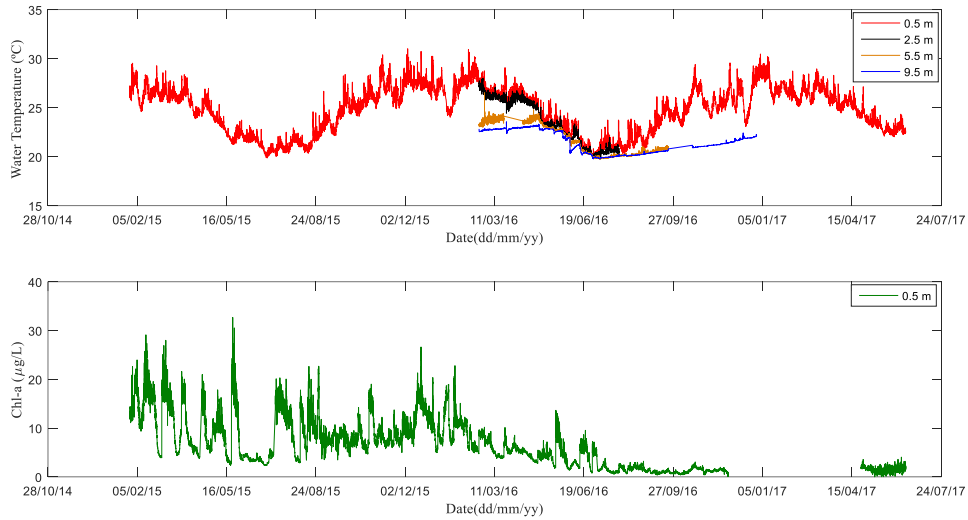


**Figure 5.1** – Water temperature and chlorophyll-a, measured in Lake Pampulha at point  $P_1$

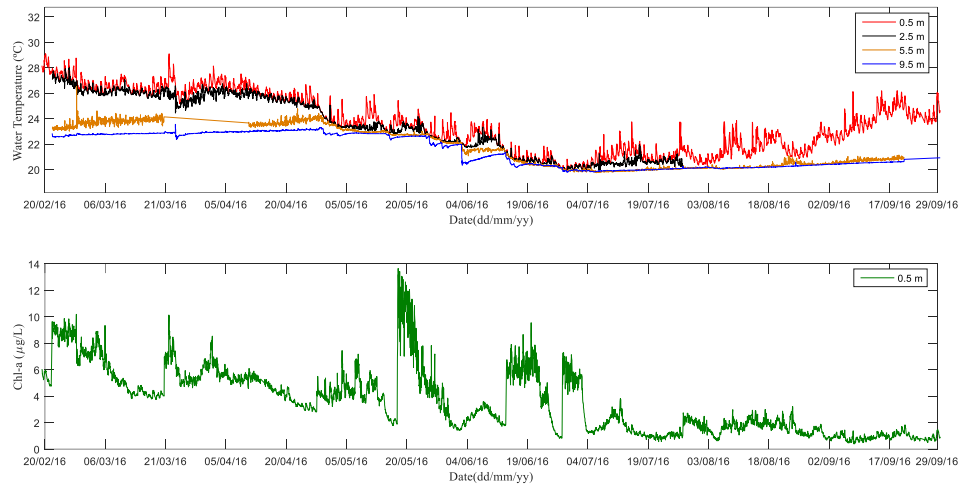


**Figure 5.2** – Water temperature (Surface (0.5 m), 2.5 m, 5.5 m and 9.5 m depths) and Chlorophyll-a at surface (0.5 m) measured in Lake Pampulha at station  $P_1$

Concerning surface water temperature, it is possible to identify two main cycles in the lake: an annual cycle and a daily cycle. On the annual cycle, higher temperatures (25 to 30 °C) are observed during the summer season (December to February) and lower temperatures (19 to 23 °C) during the winter (June to August). For the daily cycle, the surface water temperature varies greatly with a maximum amplitude of nearly 3°C.

In relation to Chl-a fluorescence in the lake, two main periods are identified: prior to Phoslock treatment (before March 2016) in which Chl-a values consistently exceed 5 µg/L with peaks around 30 µg/L, and during Phoslock treatment (after March 2016) with Chl-a values mostly below 5 µg/L.

Chl-a fluorescence appears to follow a monthly cycle, with higher values at the beginning of the month and lower values at the end of the month. However, this characteristic suffered interference from the sensor cleaning, especially during the period of higher concentrations. Chl-a fluorescence prior to Phoslock treatment and during Phoslock treatment are respectively presented in Figure 5.3 and Figure 5.4. The sensor cleaning events are represented by black vertical lines.

After a period of higher values, the sensor seems to measure a systematic decrease in the values recorded. Immediately after the sensor cleaning, it registers higher values again (Figure 5.3). This probably happened due to phytoplankton incrustation on the sensor. During the period with Phoslock treatment, this behaviour was less preponderant (Figure 5.4). Due to this strong bias, the Chl-a measurements could not be used. This shows the great difficulty in high-frequency phytoplankton monitoring. More frequent maintenance may help, although this would increase costs.

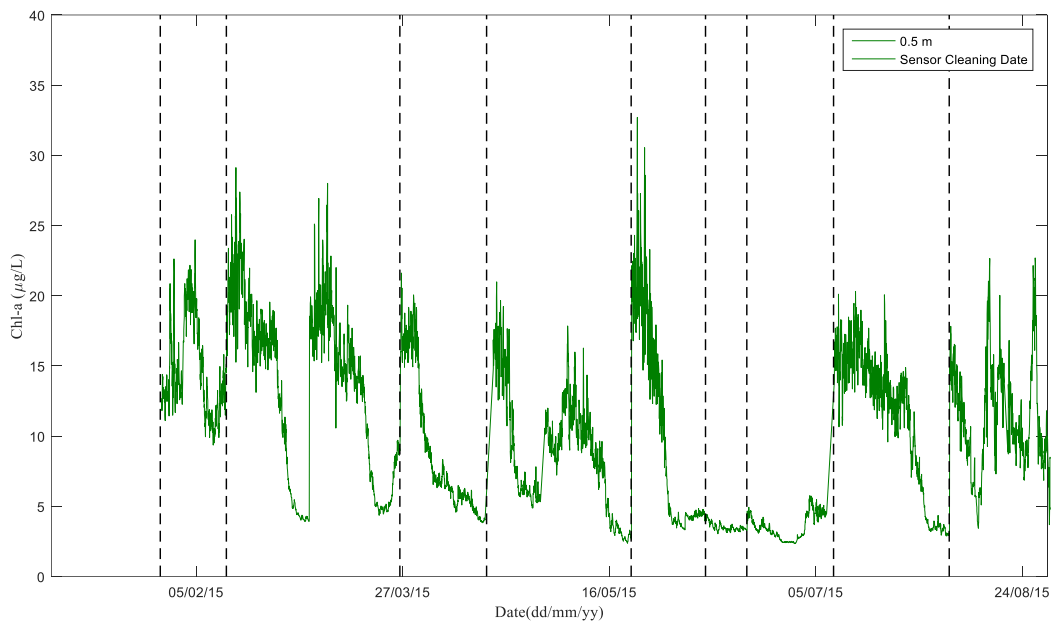


**Figure 5.3** – Chlorophyll-a measured in Lake Pampulha and sensor cleaning events (vertical black lines) prior to Phoslock treatment

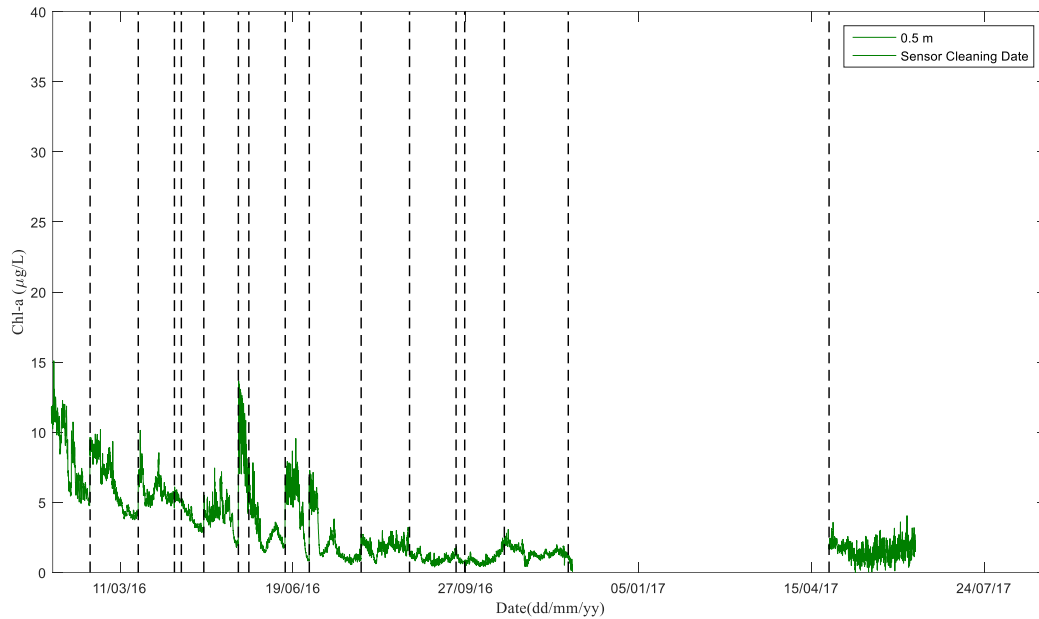


**Figure 5.4** – Chlorophyll-a measured in Lake Pampulha and sensor cleaning events (vertical black lines) during Phoslock treatment

## 5.2. Inflow water temperature

Inflow water temperature was measured during April and May 2013 in Ressaca and Sarandi tributaries. Using these data two methods were applied to estimate the inflow water temperature for the simulated period using air temperature.

The result of the linear regression (Equation 59) between hourly air temperature and hourly inflow water temperature is presented in Figure 5.5. Generally, water inflow temperature is colder in comparison to air temperature.

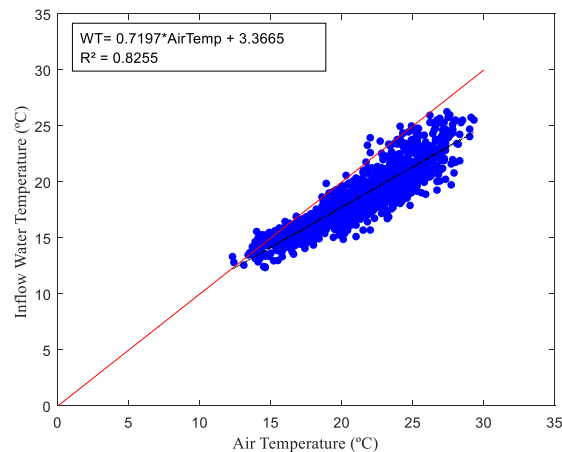


**Figure 5.5** – Linear regression between air temperature and inflow water temperature. Red line represents the 1:1 relationship between variables.

$$WT = 0.7197 * AitTemp + 3.3665$$

**Equation  
59**

Where:

WT = Water Temperature (°C)

AitTemp = Air Temperature (°C)

Applying the MSSWF method to the two months of water temperature monitoring (April and May 2013), the fitted sine functions for daily water and air temperature are presented in Figure 5.6 and Figure 5.7 respectively. The respective equations are presented in Equation 60 to Equation 63.

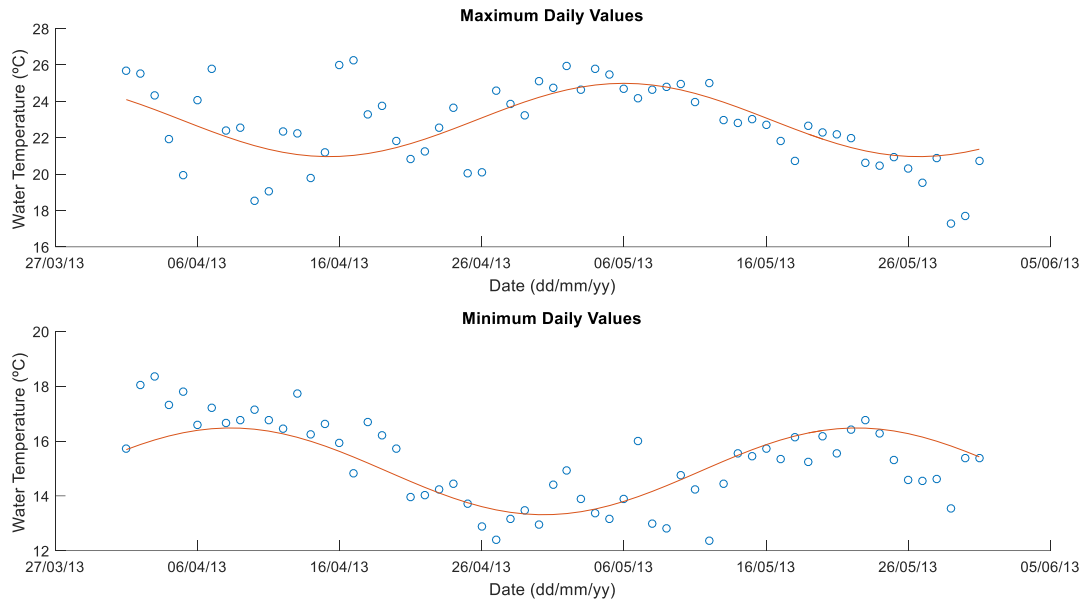


**Figure 5.6** – Fitted sine function for daily maximum and minimum water temperatures

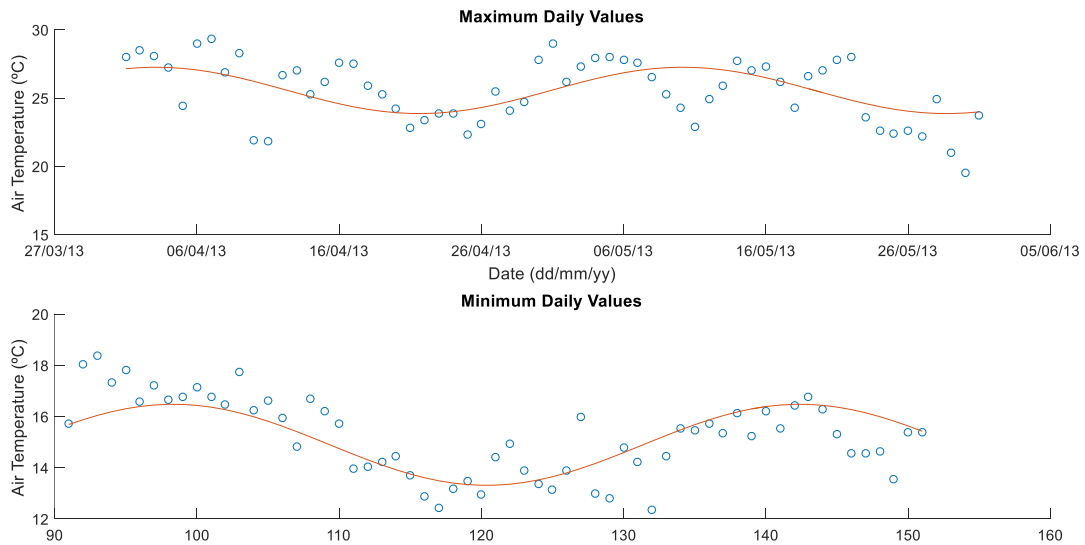


**Figure 5.7** – Fitted sine function for daily maximum and minimum air temperatures

$$T_{Wmax} = 22.65 + 4.50 * \sin(0.209 * t) \quad \text{Equation 60}$$

$$T_{Wmin} = 15.23 + 3.00 * \sin(0.209 * t) \quad \text{Equation 61}$$

$$T_{Amax} = 25.55 + 4.90 * \sin(0.209 * t) \quad \text{Equation 62}$$

$$T_{Amin} = 16.47 + 4.25 * \sin(0.209 * t) \quad \text{Equation 63}$$

The linear correlation between the differences between the daily maximum and minimum water temperatures and the maximum and minimum air temperatures are presented in Equation 64 ( $R^2 = 0.76$ ) and Equation 65 ( $R^2 = 0.77$ ).

$$DiffT_{Wmax} = 0.77 * DiffT_{Amax} - 0.0015 \quad \text{Equation 64}$$

$$DiffT_{Wmin} = 0.83 * DiffT_{Amin} + 0.0009 \quad \text{Equation 65}$$

The measured and estimated time series using the MSSWF and linear regression are presented in Figure 5.8.

The generated water temperature hourly time series, using linear regression and the MSSWF method, were compared to the measured hourly time series. The mathematical indicators for each method are presented in Table 5.1. Compared to MSSWF, linear regression presented better values for all indicators. Thus, for the simulations, linear regression was used to estimate the hourly inflow water temperature.

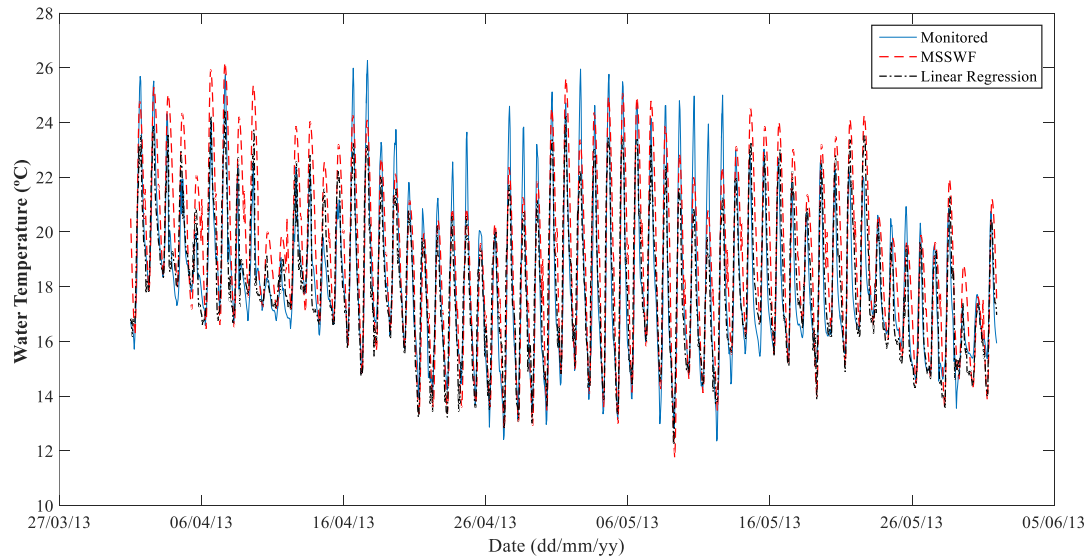


**Figure 5.8** – Hourly inflow water temperature generated using linear regression and the MSSWF method and observed inflow water temperature during April and May 2013

**Table 5.1** – Mathematical indicators for the hourly water temperature estimation methods.

Method	Indicators	Values
Linear Regression	MAE (°C)	1.05
	$R^2$	0.82
	NSE	0.82
MSSWF	MAE (°C)	2.26
	$R^2$	0.75
	NSE	0.56

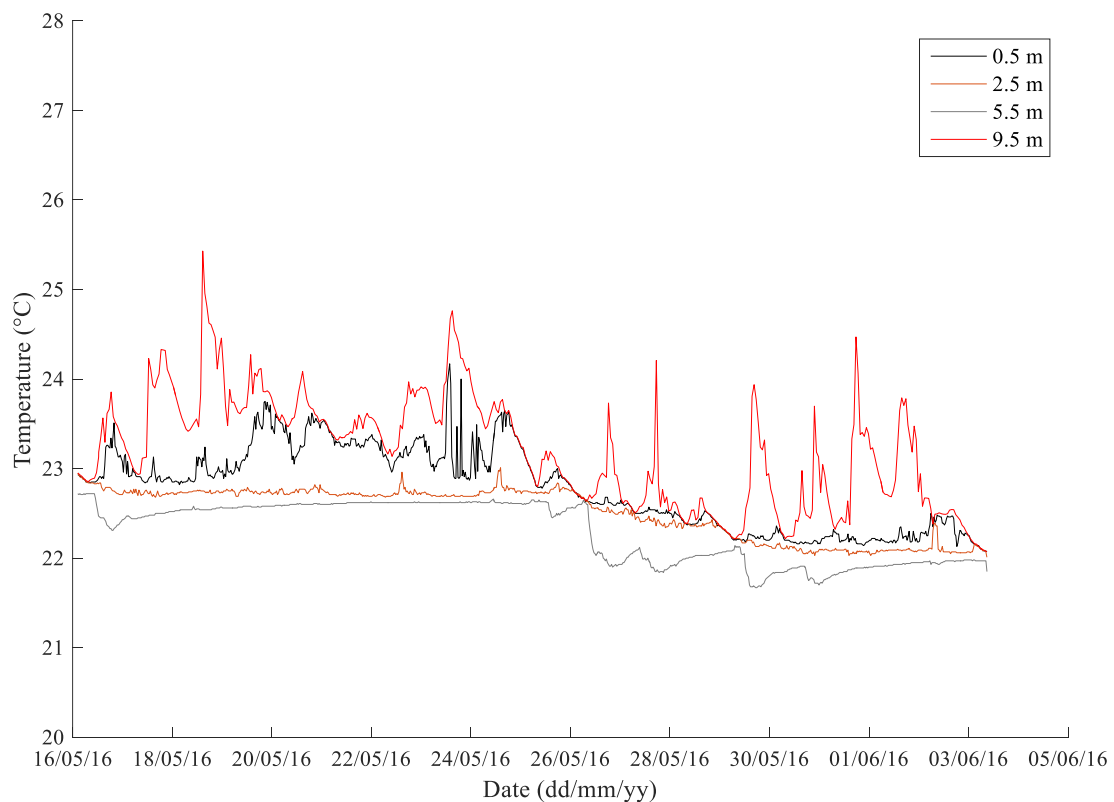


### 5.3. Hydrodynamic Simulations

#### 5.3.1. Calibration period

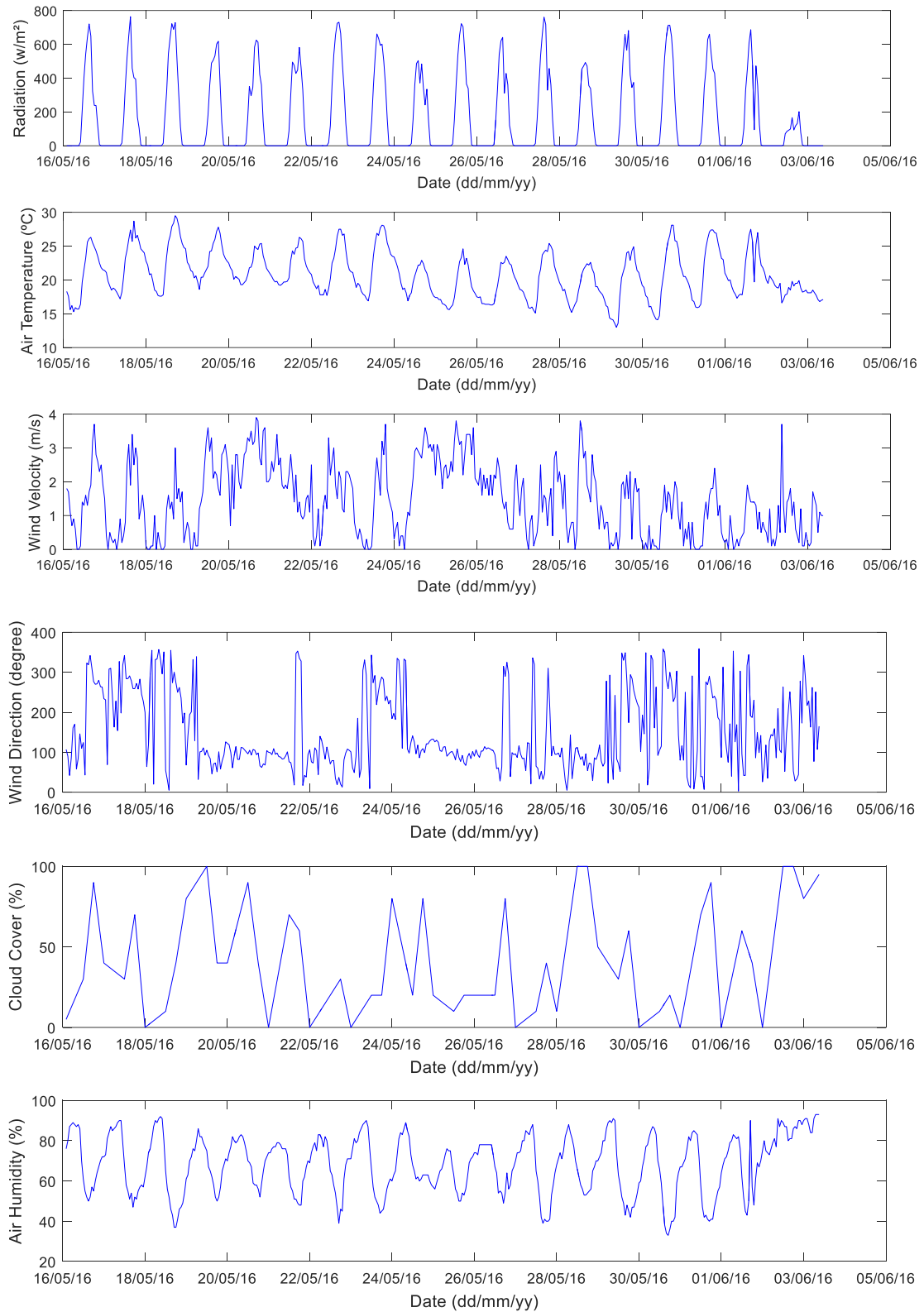
For the calibration period, from 16<sup>th</sup> May to 03<sup>rd</sup> June 2016, a period of 18 days (n=440), the Delft3D-Flow model was run. This period was selected because it was the first monitored period with mixing and thermal stratification conditions. The water temperature was measured during this period at four depths at station P<sub>1</sub>, which has a maximum depth of 10 m, is plotted in Figure 5.9.

The period started with a mixed thermal condition of about 22.9 °C. This temperature value was set as the initial temperature condition for the lake simulation for all grid elements. Over the following days, the lake presented stratification with warming in the first 2.5 meters of the water column. Another mixing event was detected on 26<sup>th</sup> May of 22.6 °C. After 26<sup>th</sup> May, the deeper sensor (9.5 m) showed a cooling of almost 1° C while the surface sensor revealed daily warming events. This second stratification period lasted three days, ending with a mixing event on 29<sup>th</sup> May of 22.1 °C. During the whole period, the maximum temperature difference between the surface and bottom was 2.9 °C (18<sup>th</sup> May at 15:00).



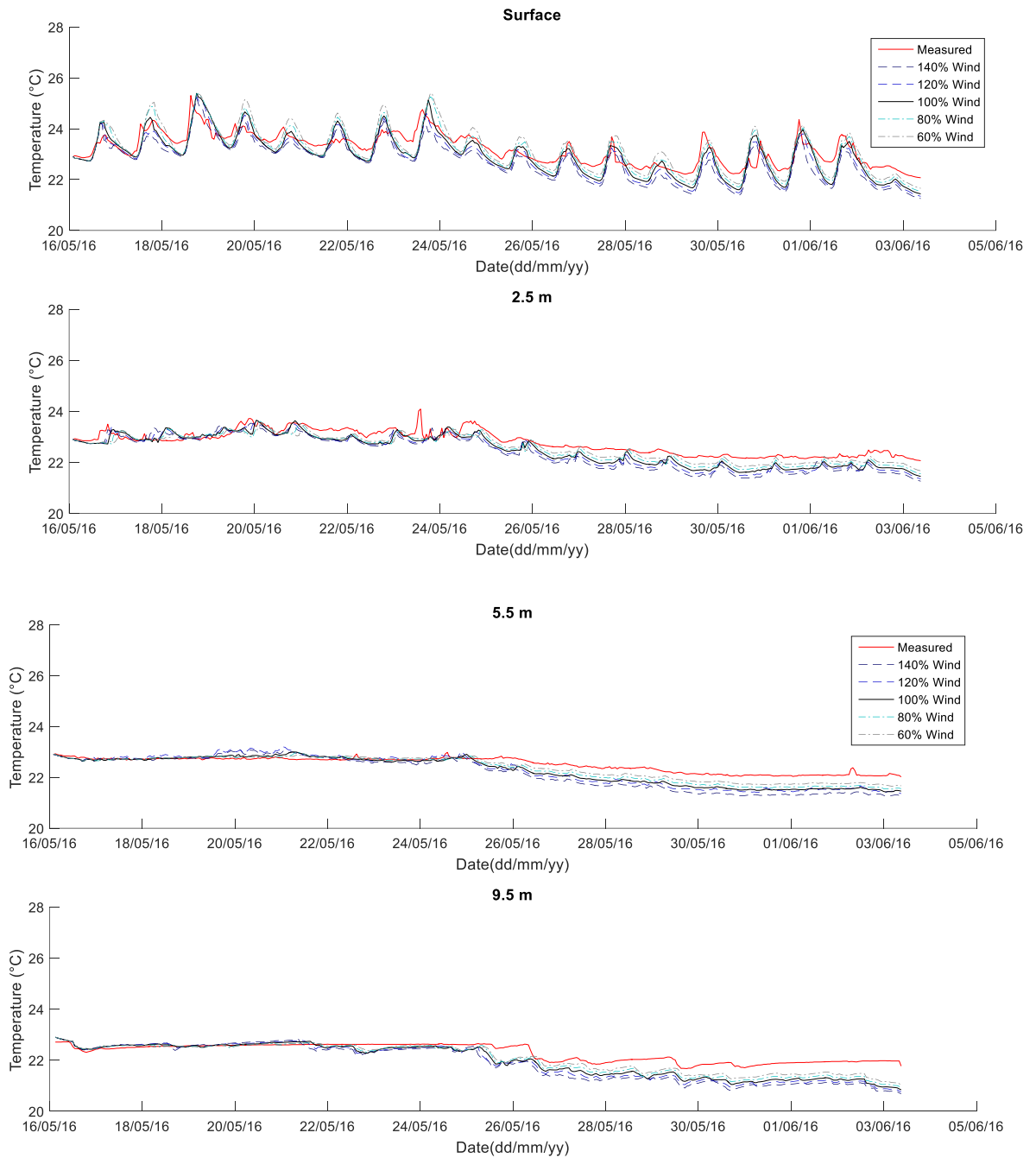
**Figure 5.9** – Water temperature (°C) measured at point P1 for 0.5, 2.5, 5.5 and 9.5 m depth during the first simulated period (16<sup>th</sup> May to 03<sup>rd</sup> June 2016)

Wind factor values were tested for a range from 40% higher to 40% lower than measured values, varying by 20% for each scenario. The measurements of radiation, air temperature, wind intensity and direction, cloud cover and humidity from a meteorology station over the calibration period are presented in Figure 5.10.



**Figure 5.10** – Radiation, air temperature, wind intensity and direction, cloud cover and humidity measured at a meteorology station during the calibration period (16<sup>th</sup> May to 03<sup>rd</sup> June 2016)

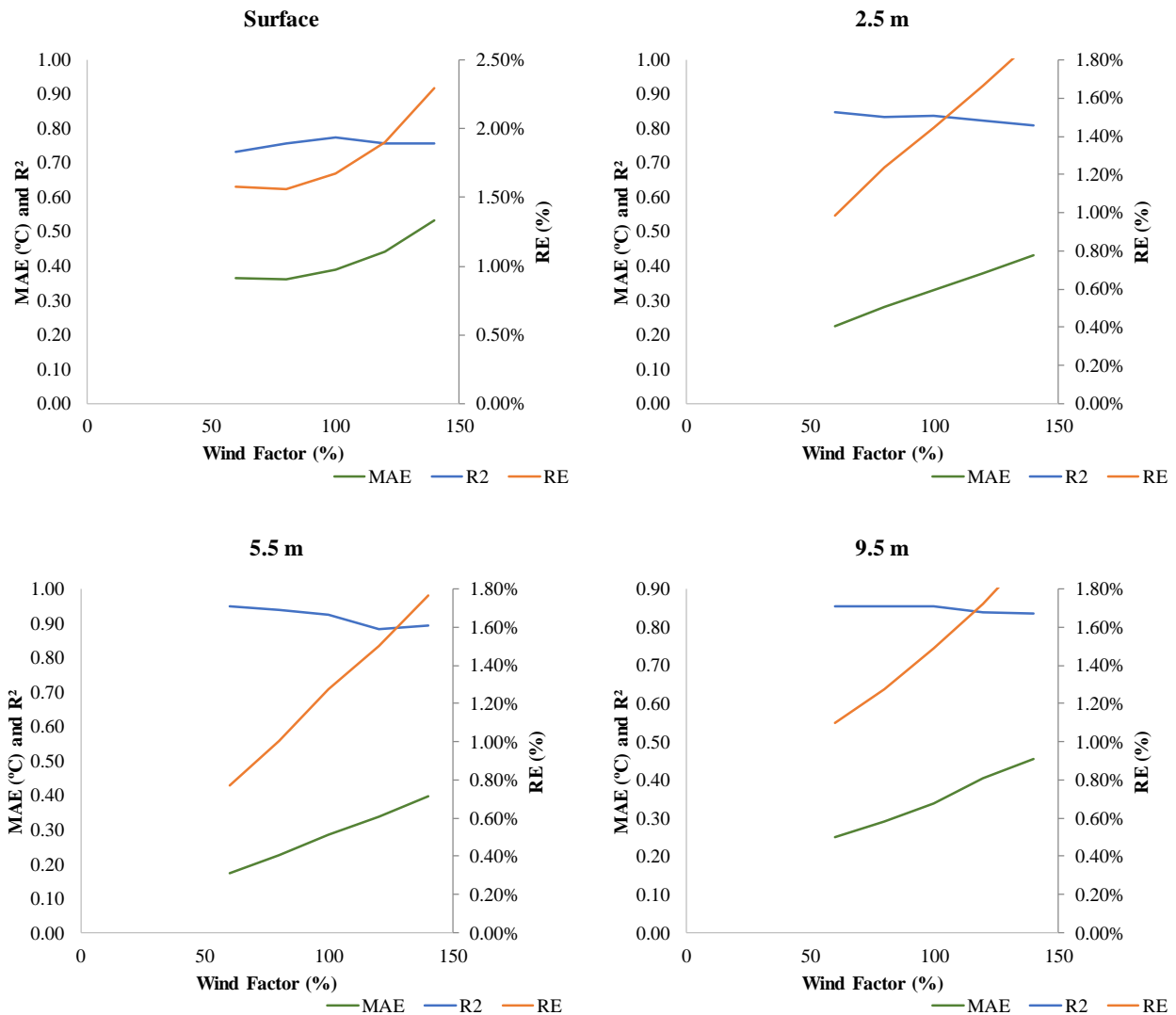
Measured and simulated temperatures at the surface (0.5 m), 2.5, 5.5 and 9.5 m depths, with different wind factors are presented in Figure 5.11. For all depths, the lower the wind factor, the better the adjustment between measured and simulated values (Table 5.2 and Figure 5.12). At the surface, the simulated values presented a higher amplitude variation compared to measured values. For the 2.5, 5.5 and 9.5 m depths, a systematic error present in all simulations was discovered after 25<sup>th</sup> May, in which the simulations calculated colder temperatures values than measured. Therefore, it was decided to evaluate other parameters to correct this error using the measured wind intensity values.



**Figure 5.11** – Measured and simulated temperatures with different wind intensity factors for the calibration period (16<sup>th</sup> May to 03<sup>rd</sup> June 2016)

**Table 5.2** – Mathematical indicators for temperature with different values of attenuation of the wind intensity

Depth (m)	Indicators	140%	120%	100%	80%	60%
0.5	MAE (°C)	0.53	0.44	0.39	0.36	0.37
	RE (%)	2.29	1.9	1.67	1.56	1.57
	R <sup>2</sup>	0.76	0.76	0.77	0.76	0.73
2.5	MAE (°C)	0.43	0.38	0.33	0.28	0.22
	RE (%)	1.90	1.66	1.45	1.24	0.99
	R <sup>2</sup>	0.81	0.82	0.84	0.83	0.85
5.5	MAE (°C)	0.40	0.34	0.29	0.23	0.17
	RE (%)	1.77	1.50	1.27	1.00	0.77
	R <sup>2</sup>	0.89	0.88	0.93	0.94	0.95
9.5	MAE (°C)	0.46	0.40	0.35	0.29	0.24
	RE (%)	2.05	1.81	1.55	1.30	1.07
	R <sup>2</sup>	0.89	0.89	0.89	0.89	0.89

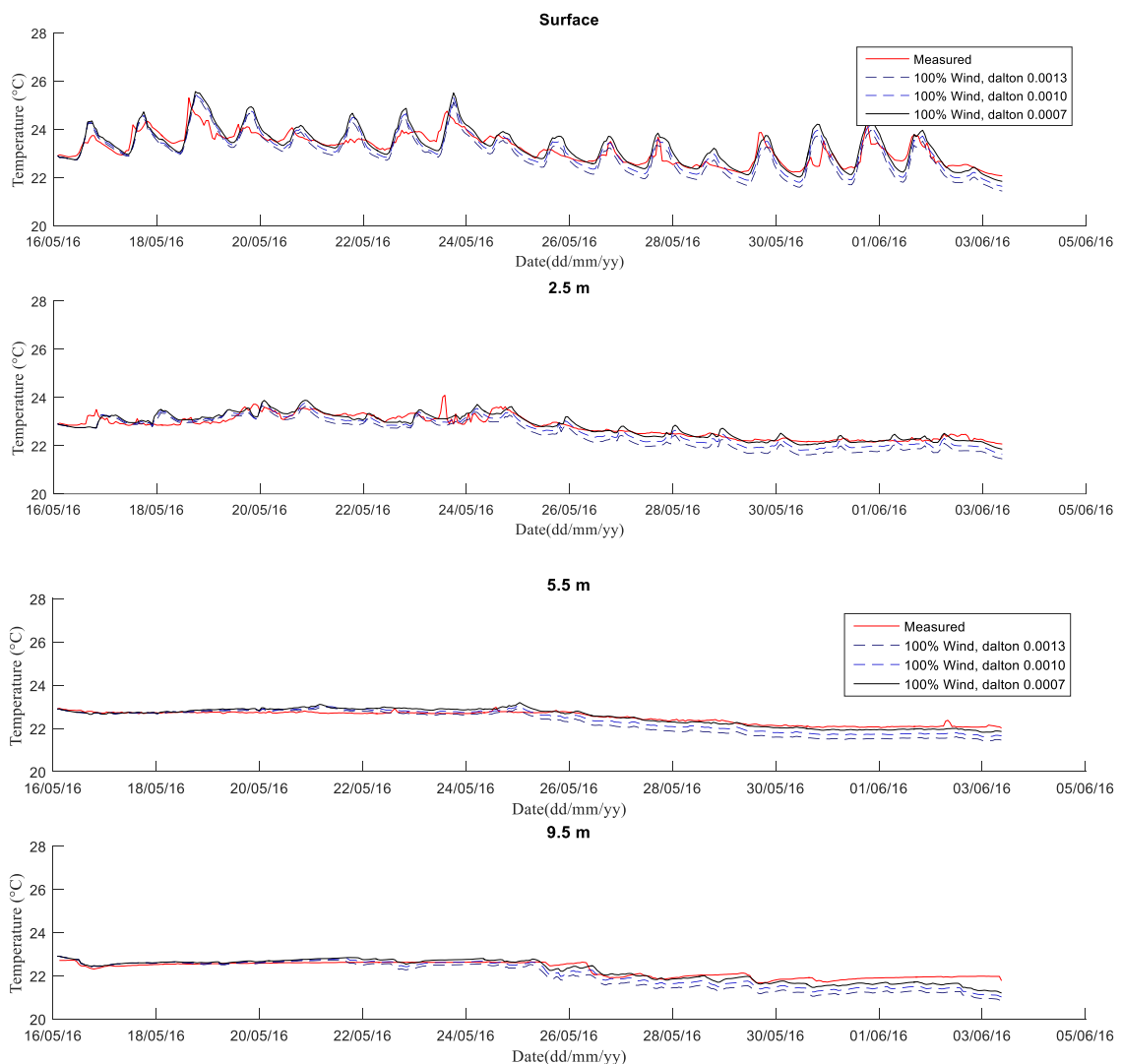
**Figure 5.12** – Mean average error (MAE), Relative Error (RE) and R<sup>2</sup> for wind factor calibration

Dalton and Stanton coefficient values were calibrated focusing on the heat exchange between water and air. Initial values were set with default values (Dalton and Stanton equal to 0.0013). The simulated amplitudes were higher than measured (Figure 5.11). This means that the heating exchange between water and air was lower than simulated by the model. Setting wind intensity equal to measured values (wind intensity factor

equal to 100%), the Dalton and Stanton coefficients were changed separately. A decrease of the Stanton coefficient to 0.0007 (almost 50% lower) did not result in significant changes (maximum temperature decreased less than 0.1 °C). Thus, the default value of 0.0013 was chosen. Meanwhile, the results of changing the Dalton coefficient were more significant. When decreasing Dalton coefficient, water surface temperature presented a lower thermal amplitude at the surface and at the other depths, for which the adjustments were also better. Figure 5.13 shows the comparison of simulated and measured values using Dalton coefficient values of 0.0013, 0.0010 and 0.0007.

Table 5.3 shows the mathematical indicators. For the MAE, the improvement using the value of 0.0007 was 0.09, 0.18, 0.16 and 0.18 °C respectively at the surface (0.5), 2.5, 5.5 and 9.5 m depths. For the RE, the improvement was 0.38%, 0.79%, 0.69% and 0.80%. For  $R^2$ , the indicator does not present a significant change (decreasing by 0.04 at the surface and increasing by 0.01 at 5.5 and 9.5 m depth). Even with the indicator values not presenting very different values from the simulation, the systematic error (to colder simulated temperature for deeper depth) was improved (Figure 5.13).

Water surface cooling was less intense for lower Dalton coefficients (less heat exchange with the atmosphere during nights), as shown in Figure 5.13. The surface water temperature remaining warmer (in comparison to the simulation with the default Dalton coefficient) also resulted in warmer temperatures at greater depths. As the better adjustment was with the value of 0.0007 for the Dalton coefficient (Table 5.3), this value was chosen.

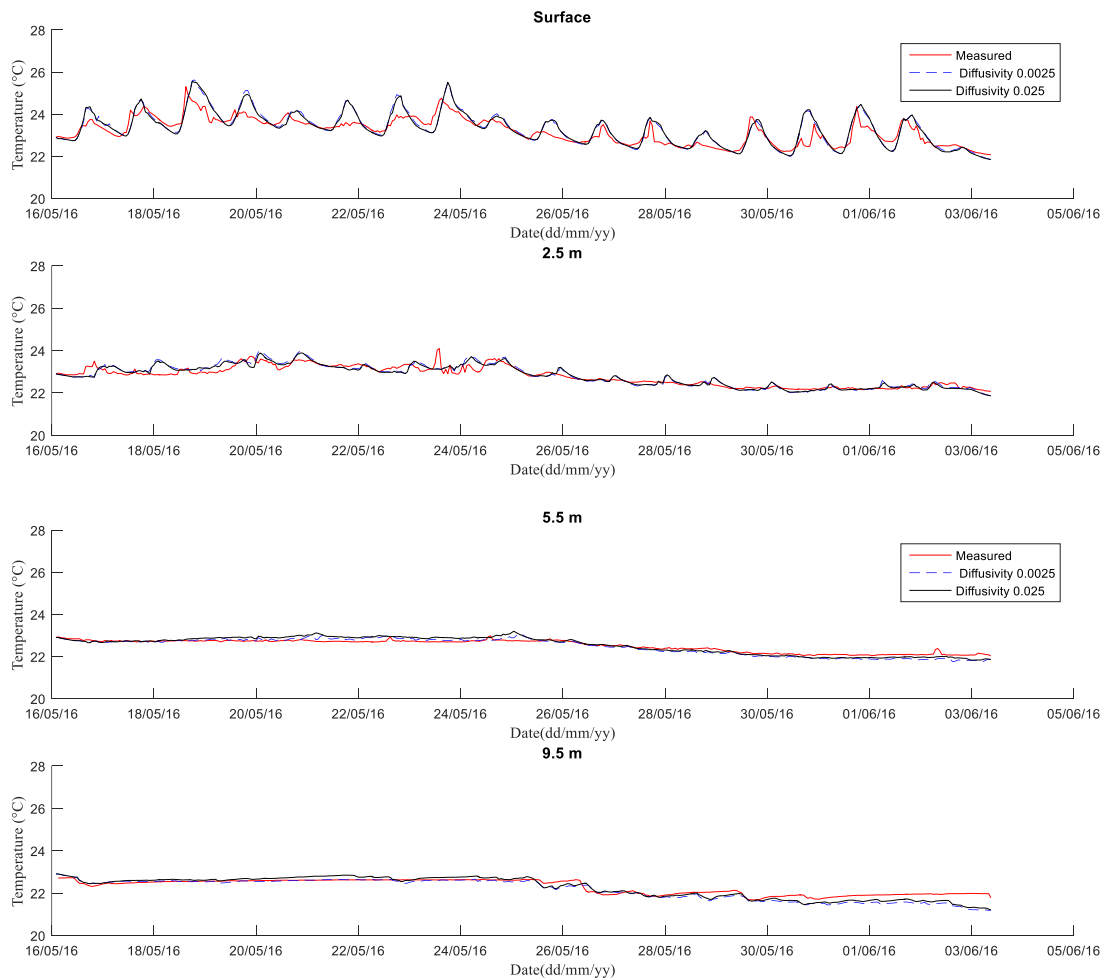


**Figure 5.13** – Measured and simulated temperature with 100% measured wind intensity and different Dalton coefficients for the calibration period (16<sup>th</sup> May to 03<sup>rd</sup> June 2016)

**Table 5.3** – Mathematical indicators for temperature with different values of Dalton coefficient

Depth (m)	Indicators	Dalton		
		0.0013	0.0010	0.0007
0.5	MAE (°C)	0.39	0.32	0.30
	RE (%)	1.68	1.37	1.30
	R <sup>2</sup>	0.77	0.76	0.73
2.5	MAE (°C)	0.33	0.22	0.15
	RE (%)	1.42	0.94	0.63
	R <sup>2</sup>	0.84	0.84	0.84
5.5	MAE (°C)	0.29	0.20	0.13
	RE (%)	1.24	0.85	0.55
	R <sup>2</sup>	0.93	0.94	0.93
9.5	MAE (°C)	0.35	0.23	0.16
	RE (%)	1.50	1.01	0.70
	R <sup>2</sup>	0.89	0.90	0.90

Other parameters analysed in the calibration were background horizontal eddy viscosity ( $v_H$  - [m<sup>2</sup>/s] - Equation 33) and diffusivity ( $D_H$  [m<sup>2</sup>/s] - Equation 34). Figure 5.14 presents measured and simulated temperatures for the surface (0.5), 2.5, 5.5 and 9.5 m depths and Table 5.4 presents the mathematical indicators evaluated for background horizontal eddy viscosity and diffusivity values (0.025 and 0.0025 m<sup>2</sup>/s).

**Figure 5.14** – Measured and simulated temperature with 0.025 and 0.0025 m<sup>2</sup>/s for background horizontal eddy viscosity and diffusivity

**Table 5.4** – Mathematical indicators for lake temperature varying background eddy viscosity and diffusivity values

Depth (m)	Indicators	Background Eddy viscosity and diffusivity	
		0.025 (m <sup>2</sup> /s)	0.0025 (m <sup>2</sup> /s)
0.5	MAE (°C)	0.30	0.30
	RE (%)	1.30	1.30
	R <sup>2</sup>	0.73	0.75
2.5	MAE (°C)	0.15	0.16
	RE (%)	0.63	0.69
	R <sup>2</sup>	0.84	0.83
5.5	MAE (°C)	0.13	0.12
	RE (%)	0.55	0.50
	R <sup>2</sup>	0.93	0.95
9.5	MAE (°C)	0.16	0.16
	RE (%)	0.70	0.70
	R <sup>2</sup>	0.90	0.88

According to Table 5.4, the changes were not very significant (0.01 °C for the MAE, 0.05 % for the RE and 0.02 for R<sup>2</sup>), thus the value of 0.025 m<sup>2</sup>/s was chosen.

A calibration round was also performed considering the water tributary flow. A rating curve was evaluated based only on the dry period simulations and measured values. However, no different values were obtained.

The Z-grid option was also used to compare the model performance and the influence of the grid type. Using the Z-grid option, a non-homogenous vertical distribution was necessary to provide more active layers in the lake upstream region, avoiding numerical instabilities due to inflows during the simulations. The type and thickness of the vertical layer determine the depths at which the model prints the results. The depth for each layer is computed in the middle of each vertical element, therefore, the results for each type of mesh were interpolated to the corresponded measuring depth.

The mathematical indicators using the Z-grid (Table 5.5) were also good however, a slightly worse, especially in surface (0.5 m) and 2.5 m for RE and MAE. At bottom depth (9.5 m), using Z-grid the simulated values presented slightly warmer values after 26<sup>th</sup> May.

**Table 5.5** – Mathematical indicators for lake temperature using Z-grid option

Depth (m)	Indicators	Grid option	
		$\sigma$ -grid	Z-grid
0.5	MAE (°C)	0.30	0.40
	RE (%)	1.30	1.68
	R <sup>2</sup>	0.73	0.72
2.5	MAE (°C)	0.15	0.18
	RE (%)	0.64	0.77
	R <sup>2</sup>	0.84	0.86
5.5	MAE (°C)	0.13	0.08
	RE (%)	0.56	0.34
	R <sup>2</sup>	0.93	0.95
9.5	MAE (°C)	0.16	0.16
	RE (%)	0.70	0.72
	R <sup>2</sup>	0.90	0.90

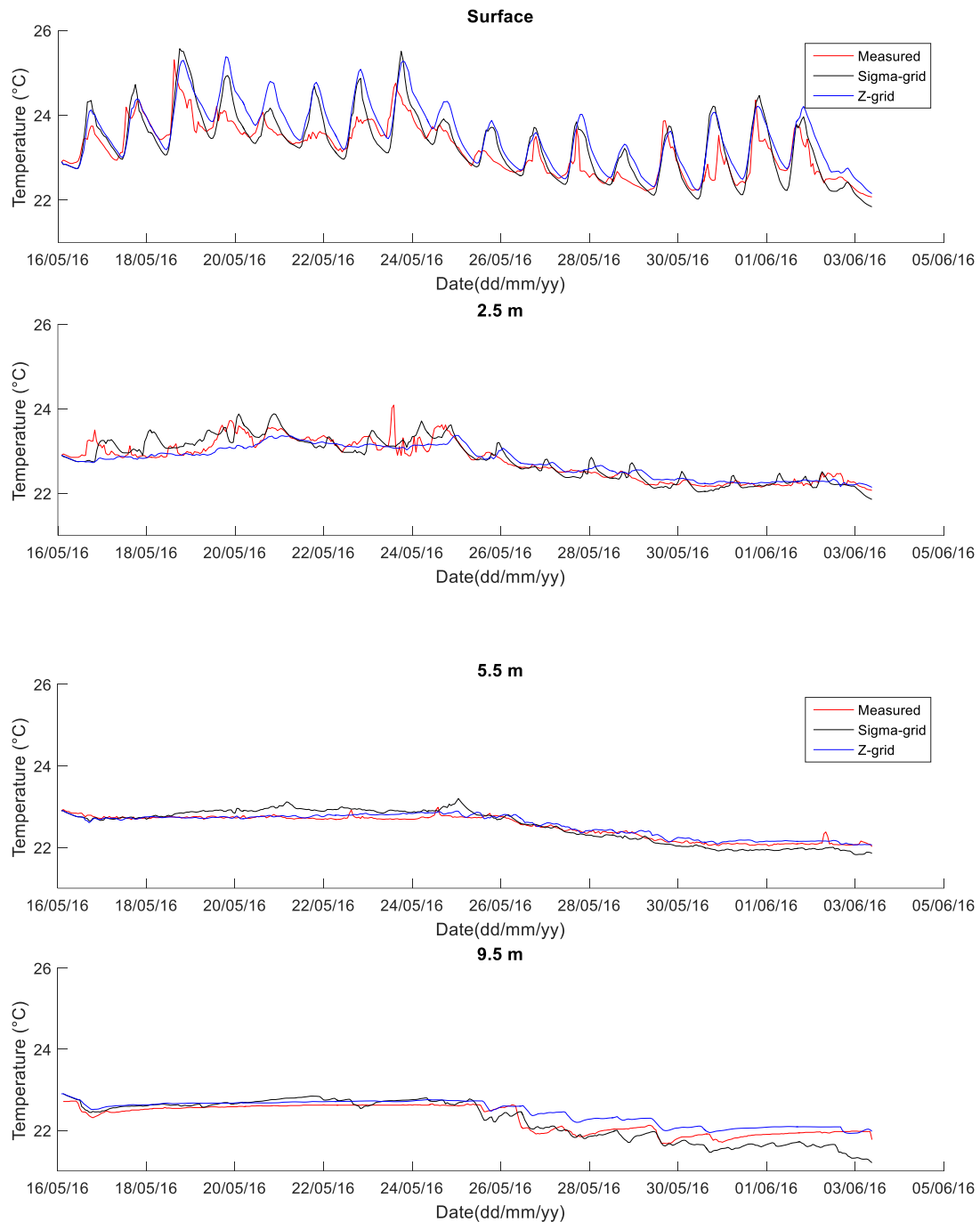


**Figure 5.15** – Measured and simulated temperatures at point P1 at surface (0.5), 2.5, 5.5 and 9.5 m depths for the calibration period simulated with Sigma and Z grid.

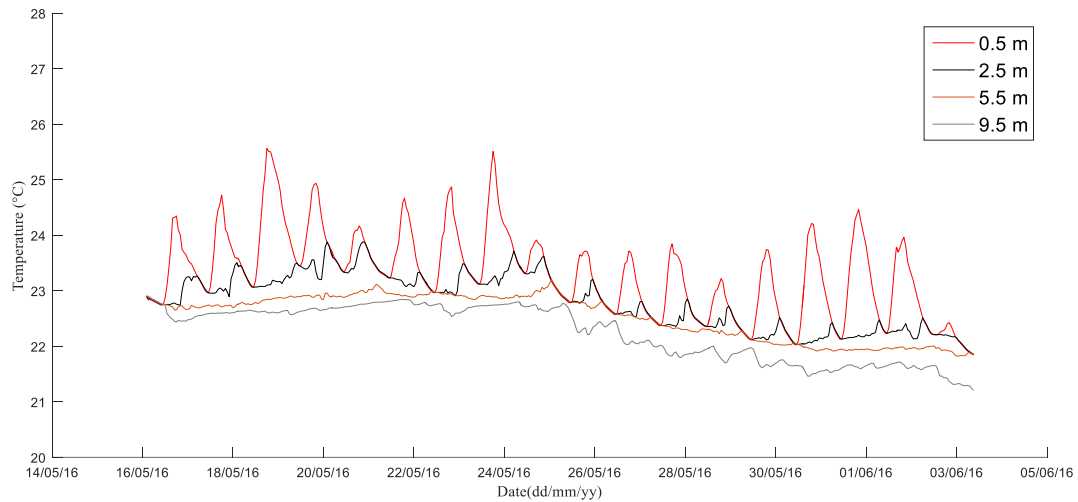
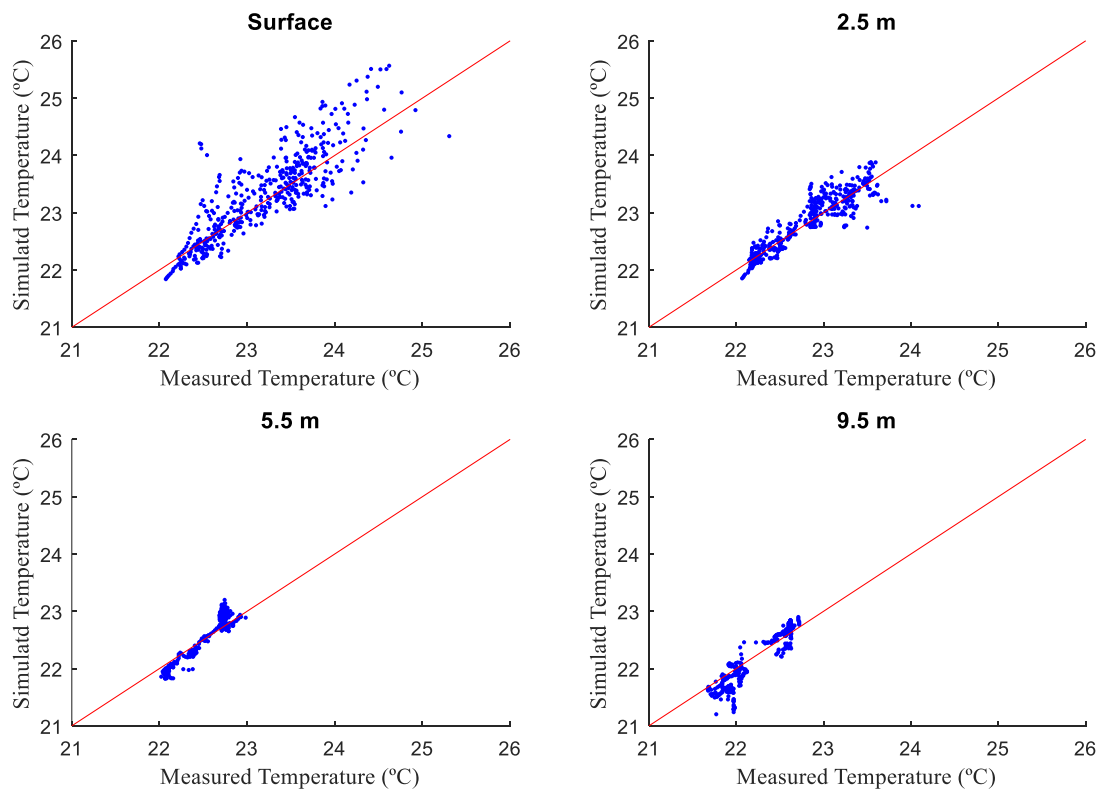
The final set of parameter values are shown in Table 5.6. The time series of simulated water temperature at the four depths for the best parameter set are presented in Figure 5.16. Figure 5.17 shows a comparison of measured and simulated values. The red line represents a perfect adjustment between measured and simulated temperatures.

The model could accurately represent the main events and measured characteristics: (i) the daily time scale for surface warming; (ii) the cooling at the bottom on 26<sup>th</sup> May; (iii) the mixing conditions on 2<sup>th</sup> and 26<sup>th</sup> May and partially the mixing event on 29<sup>th</sup> May, in which the differences between the surface and bottom temperature were 0.07 and 0.15 °C respectively for the measured and simulated values.



**Table 5.6** – Set of parameter values for hydrodynamic simulation in Lake Pampulha

Parameter	Value
Secchi (m)	0.3 (measured)
Wind Factor	1.0 (calibrated)
Background Horizontal Eddy Viscosity (m <sup>2</sup> /s)	0.025 (calibrated)
Background Horizontal Eddy Diffusivity (m <sup>2</sup> /s)	0.025 (calibrated)
Dalton	0.0007 (calibrated)
Stanton	0.0013 (default)
Wind Drag	0.00063 (default)

**Figure 5.16** – Water temperature simulated at point P<sub>1</sub> at surface (0.5), 2.5, 5.5 and 9.5 m depths for the calibration period (16<sup>th</sup> May to 03<sup>rd</sup> June 2016) with a wind intensity factor of 100%, a Dalton coefficient of 0.0007 and 0.025 m<sup>2</sup>/s for background horizontal eddy viscosity and diffusivity**Figure 5.17** – Comparison of measured and simulated water temperature at point P<sub>1</sub> at surface (0.5), 2.5, 5.5 and 9.5 m depths for the calibration period. Red line represents a perfect adjustment.

### 5.3.2. Validation period

The water temperature time series at four depths at station P<sub>1</sub>, which has a maximum depth of 10 m, is plotted for the validation period, from 29<sup>th</sup> May to 14<sup>th</sup> June 2016, a period of 16 days (n = 388), in Figure 5.18.

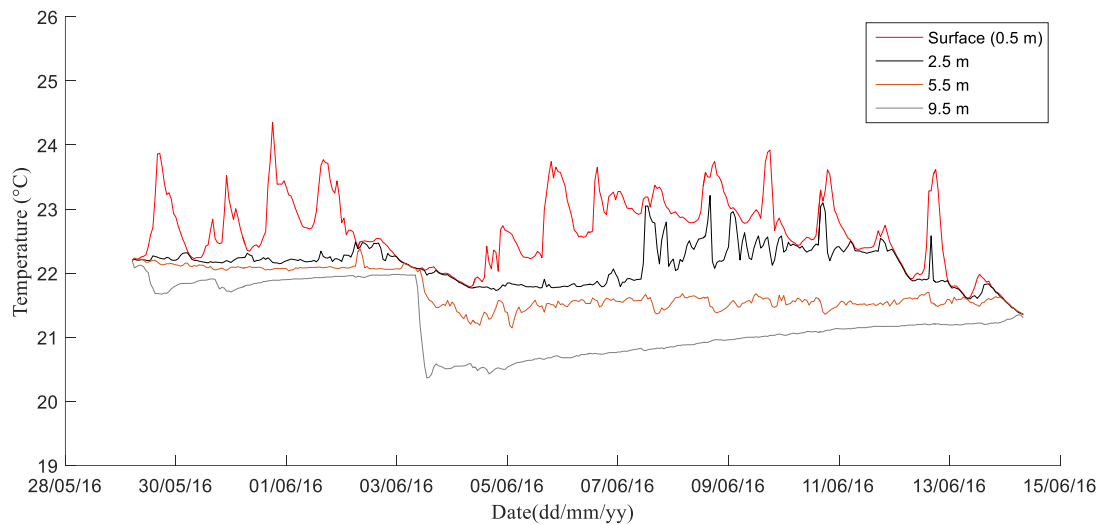


**Figure 5.18** - Water temperature (°C) measured at point P<sub>1</sub> for 0.5, 2.5, 5.5 and 9.5 m depth during validation period simulated (29<sup>th</sup> June to 14<sup>th</sup> June 2016)

The period started with a mixed thermal condition of about 22.2 °C. Over the first five days it was observed almost a daily stratification and mixing condition alternation.

On 03<sup>rd</sup> June, the water temperature column was mixed around 22.0 °C. Then, four hours later, at 09:00 the lake started a stratification with strong cooling at 5.5 and 9.5 m depth. At 9.5 m depth, the water temperature presented a decrease of almost 2°C over 4 hours. At 5.5 m depth, the decrease was 0.8 °C over 12 hours.

After this cooling on 03<sup>rd</sup> June, the water at 5.5 m depth remained with a relatively constant temperature of 21.5 °C for the whole period. In contrast, heating was observed at 9.5m depth at a constant rate of 0.08°C per day. At 2.5 m depth, the temperature remained constant until 07<sup>th</sup> June when it began to increase. At the surface (0.5 m), water warming started on 04<sup>th</sup> June, presenting a daily heating and cooling cycle for almost the whole period. The meteorological inputs during the period simulated are presented in Figure 5.19.

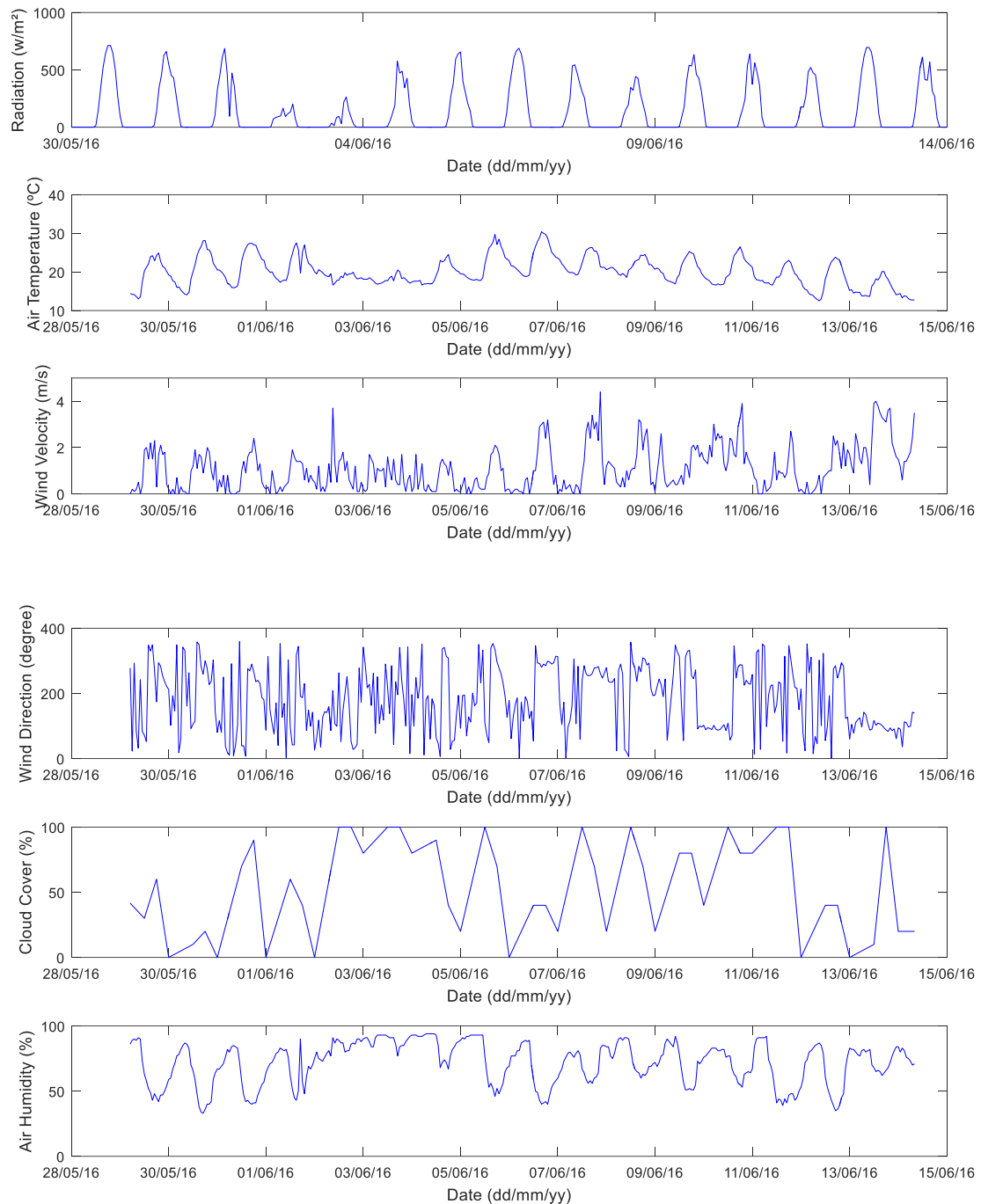


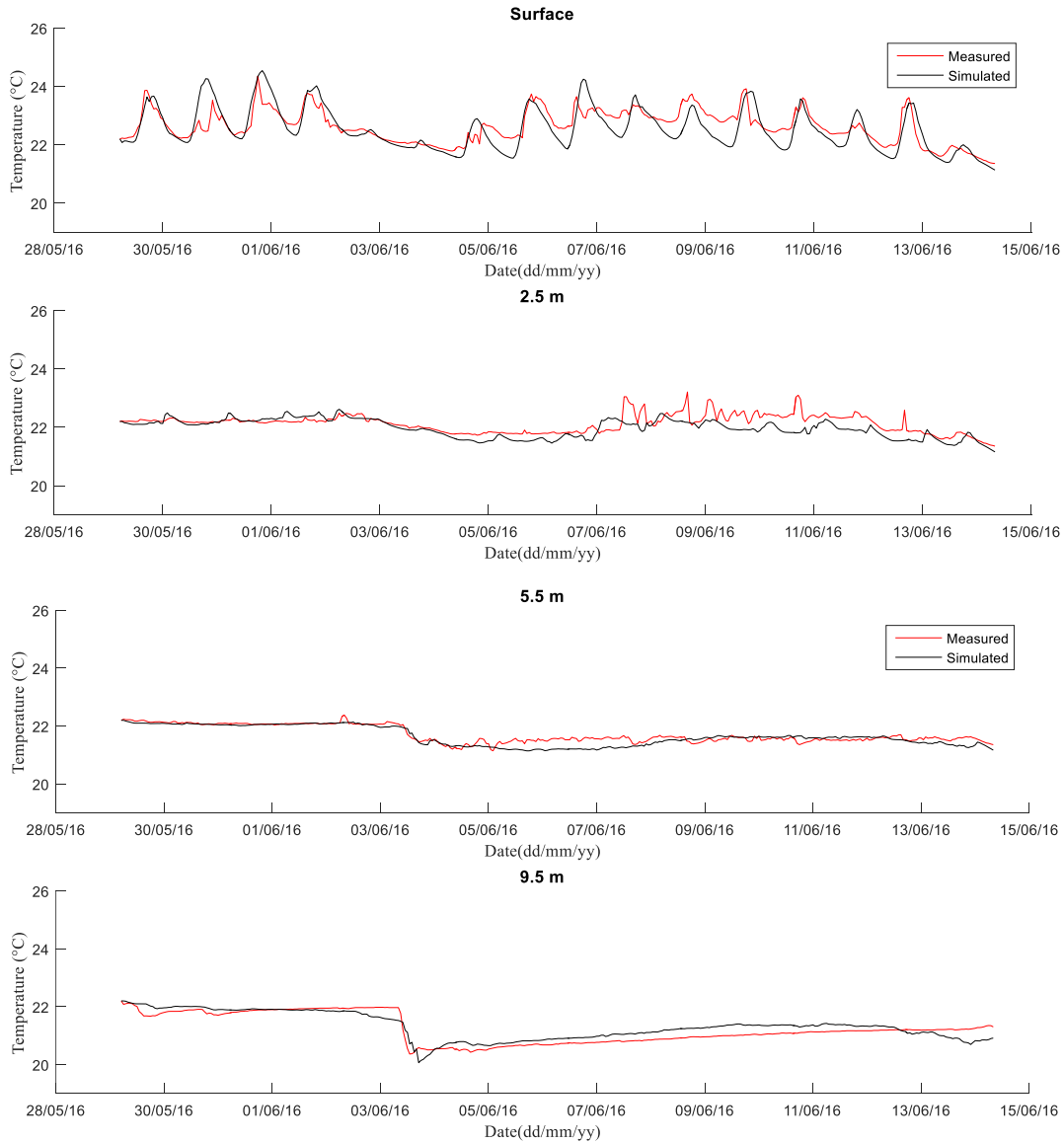
**Figure 5.19** - Radiation, air temperature, wind velocity and direction, cloud cover and humidity measured at the meteorology station during the validation period simulated (29<sup>th</sup> May to 14<sup>th</sup> June 2016)

For the validation period, the Delft3D-Flow model was run using the same parameters and criteria established through the calibration period (Table 5.6).

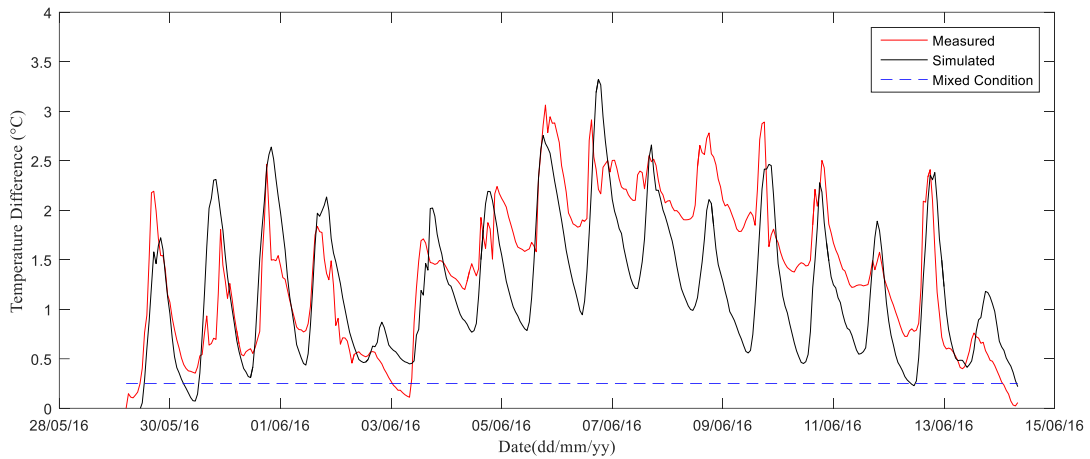
For all depths, the MAE and RE between the measured and simulated values were quite good (Table 5.7 and Figure 5.20), with maximum values of 0.45 °C and 1.51 %, respectively. The  $R^2$  ranged from 0.41 to 0.81, also considered as a good result. According the mathematical indicators, the model performance can be considered validated.

The validation period in 2016 started on 29<sup>th</sup> May with a uniform water temperature of 22.2°C. Over the first five days it was observed almost a daily stratification and mixing condition alternation. According Figure 5.24, on 30<sup>th</sup> May the difference between surface and bottom temperature was 0.35 °C for measured values and 0.07

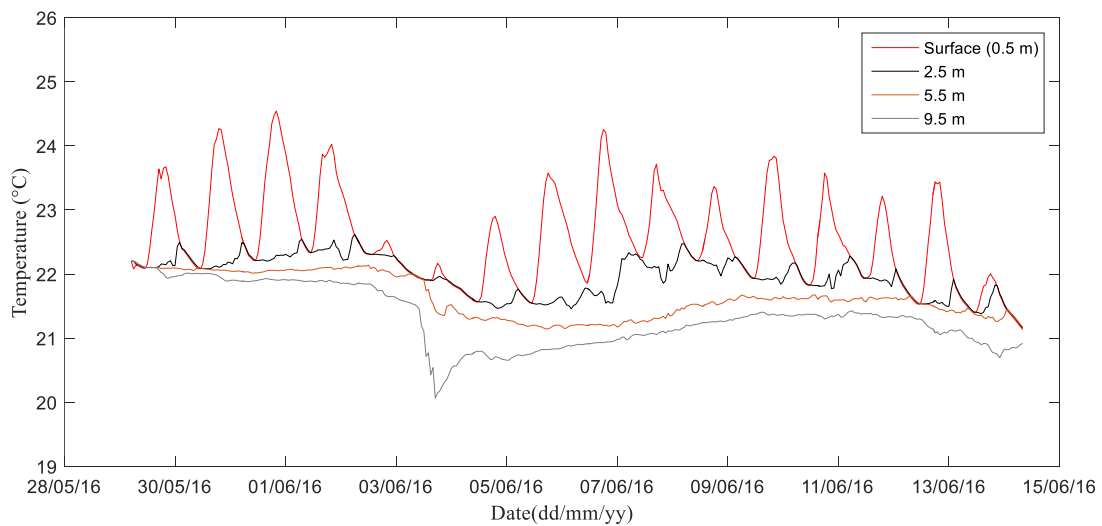
°C for simulated values. On 31<sup>st</sup> May, this difference was 0.53 and 0.31 °C, on 01<sup>st</sup> June it was 0.77 and 0.44 °C and 02<sup>nd</sup> June 0.11 and 0.46 °C, respectively for measured and simulated values. According to Figure 5.20, the model could represent the cooling event at 5.5 and 9.5 m depth on 03<sup>rd</sup> June. Until 05<sup>th</sup> June, comparing with the measured values, the simulated water surface presented a good adjustment, however, after this date the simulated values presented higher amplitude with lower low values. This discrepancy resulted in higher differences between surface and bottom simulated water temperature (Figure 5.21). Figure 5.22 shows the temperature dynamic by simulation. According to Figure 5.22, the model could detect the water cooling on 03<sup>rd</sup> June and the subsequent water warming at 5.5 and 9.5 depths. Figure 5.23 shows the scatter plots between measured and simulated temperature for the four measured depths, and Figure 5.26 shows the scatter plots of the water temperature difference between surface and bottom layers, both of them show that the model performed well.



**Figure 5.20** - Measured and simulated water temperature for the validation period (29<sup>th</sup> May to 14<sup>th</sup> June 2016) at surface (0.5 m), 2.5 m, 5.5 m and 9.5 m depths



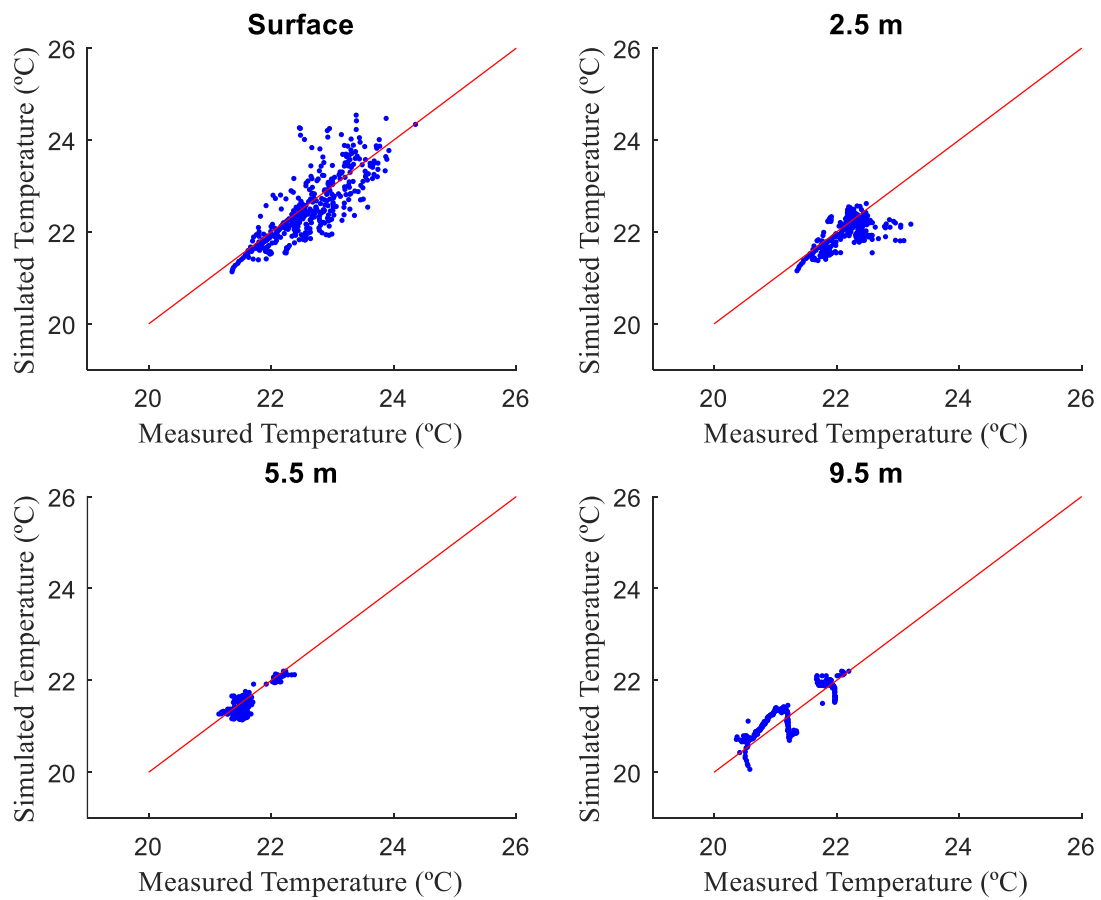
**Figure 5.21** - Difference of surface (0.5) and bottom (9.5) for measurement and simulated temperatures for the validation period from 29<sup>th</sup> May to 14<sup>th</sup> June 2016 at P1 station. Blue dashed line represents a mixing condition with difference between surface and bottom of 0.25 °C



**Figure 5.22** - Water temperature (°C) simulated at point P<sub>1</sub> for 0.5, 2.5, 5.5 and 9.5 m depth during validation period (29<sup>th</sup> May to 14<sup>th</sup> June 2016).

**Table 5.7** – Mathematical indicators for the validation period (29<sup>th</sup> May to 14<sup>th</sup> June 2016).

Depth (m)	Indicators	Validation Period
Surface (0.5)	MAE (°C)	0.34
	RE (%)	1.51
	R <sup>2</sup>	0.63
2.5	MAE (°C)	0.23
	RE (%)	1.04
	R <sup>2</sup>	0.41
5.5	MAE (°C)	0.12
	RE (%)	0.56
	R <sup>2</sup>	0.80
Bottom (9.5)	MAE (°C)	0.20
	RE (%)	0.95
	R <sup>2</sup>	0.81

**Figure 5.23** – Measured and simulated temperature at point P<sub>1</sub> at surface (0.5 m), 2.5 m, 5.5 m and 9.5 m depths for the validation period (29<sup>th</sup> May to 14<sup>th</sup> June 2016). The red line represents the 1:1 relationship.

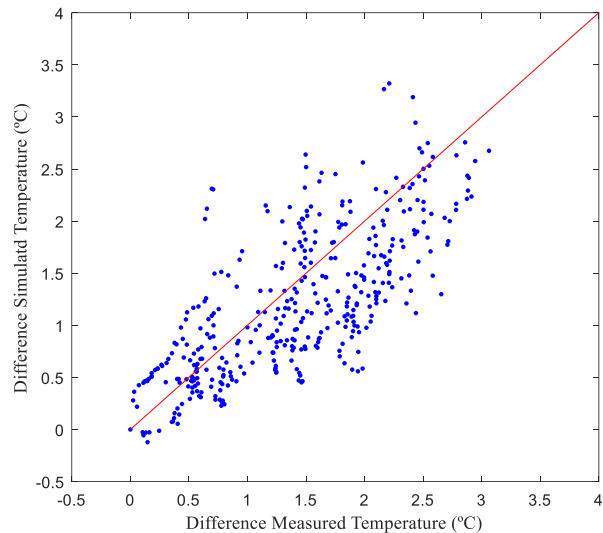


**Figure 5.24** – Measured and simulated difference temperatures between surface and bottom at point P1 for the validation period simulated (29<sup>th</sup> May to 14<sup>th</sup> June 2016). The red line represents the 1:1 relationship.

On 03<sup>rd</sup> June 2016, the water temperature presented a strongly decreased. Due to the high specific heat content of water, a strong variation was not expected, even less with an exclusively variation in the deepest layer. The model was used as a tool to better understand what could be the reason for such specific cooling presented only below 5.5 m and more intense at 9.5 m depth.

On 03<sup>rd</sup> June, increased inflow (Figure 5.25) was noted. In the simulation, even with higher inflow, the simulated water level variations at station P1 were less than 12 cm during the passage of the higher inflow.

According to the computed water inflow temperature (Figure 5.26), the tributary water, just before the water cooling, presented a lower temperature (16.1 °C) and, therefore, a higher density, compared to the lake temperature (uniform at 22 °C). This colder inflow entered the reservoir during the previous 24 hours of a high discharge event of the tributaries. The model suggests that the propagation of the inflow water on 03<sup>rd</sup> June occurred through the bottom of the lake. This behaviour is quite consistent; however, the inflow water temperature was not measured to prove this hypothesis. Therefore, to evaluate the influence of the inflow water temperature, the period was also simulated considering the water inflow at a constant temperature of 22°C, which corresponds to the mixing water temperature in the lake on June 03<sup>rd</sup>. In this simulation, the sharp temperature decrease did not occur at 5.5 m neither at the bottom (9.5 m) depths. Figure 5.27 shows the comparison for the measured and simulated values for different inflow water temperatures (varying and constant).

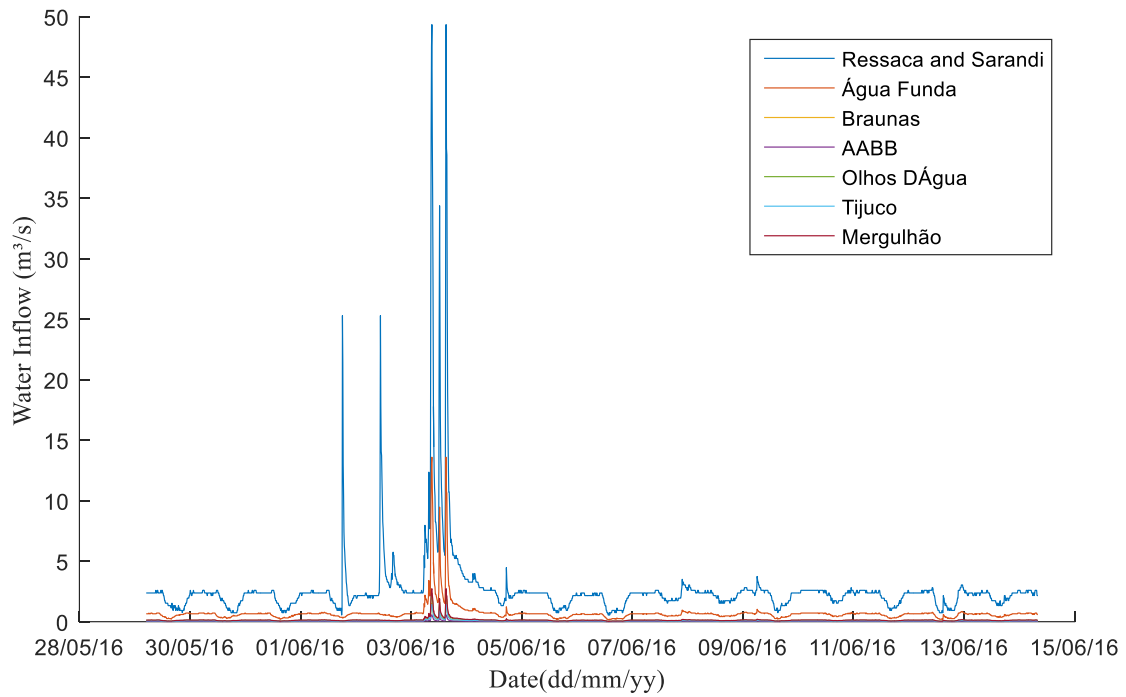


**Figure 5.25** – Tributaries inflow from 29<sup>th</sup> May to 14<sup>th</sup> June 2016.

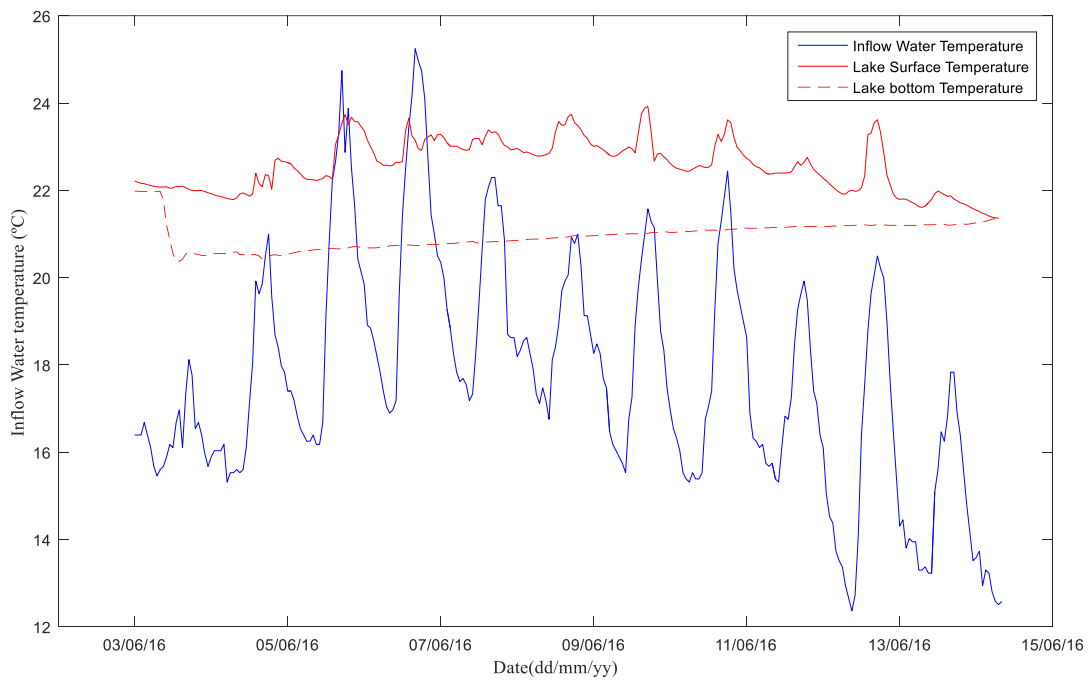


**Figure 5.26** – Lake water temperature at the surface (0.5 m), on the bottom (9.5 m) and inflow water temperature



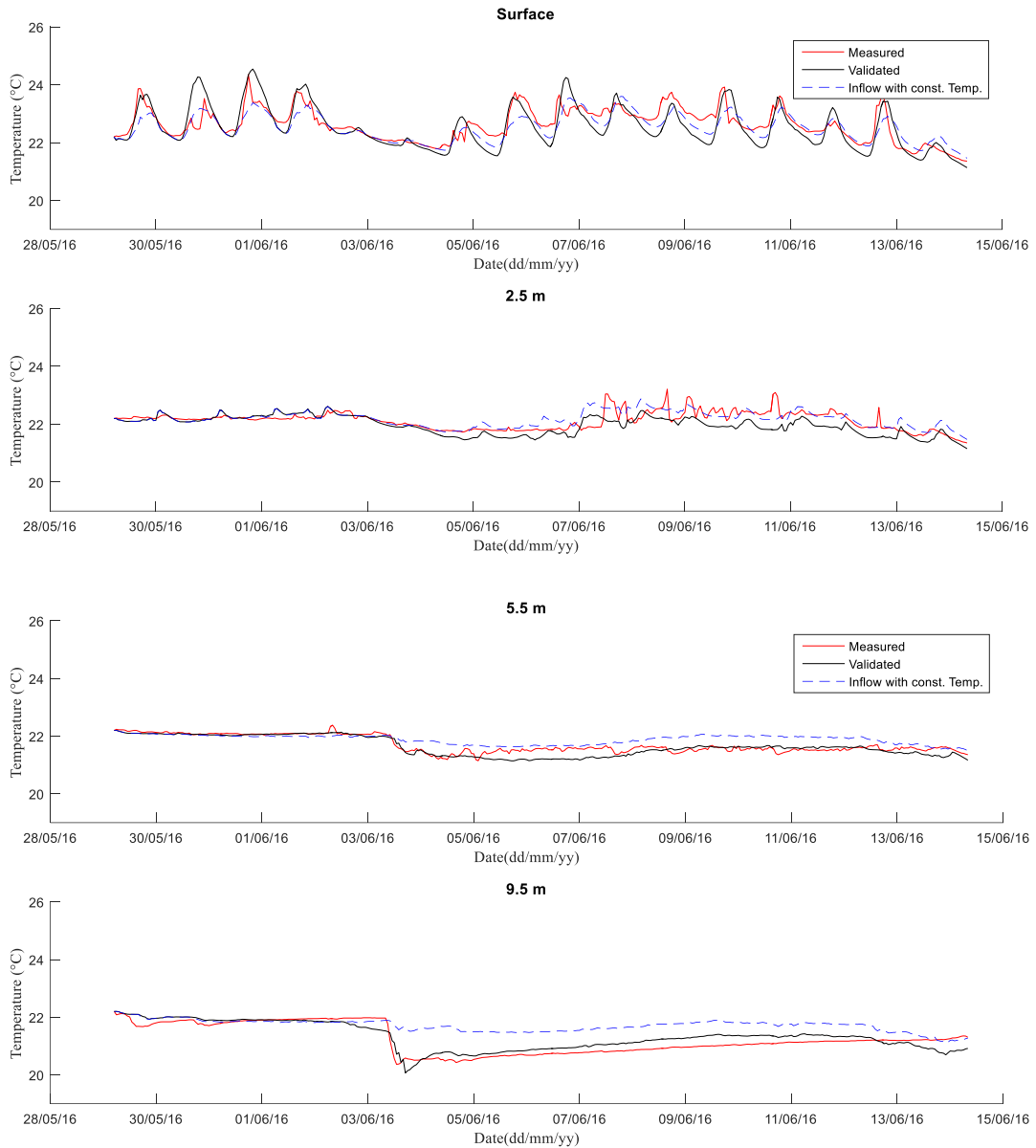


**Figure 5.27** – Measured and simulated water temperature at point P<sub>1</sub> at the surface (0.5 m), 2.5 m, 5.5 m, 9.5 m depths for the validation period simulated (29<sup>th</sup> May to 14<sup>th</sup> June 2016)

A longitudinal profile was defined in the grid (Figure 5.28) to evaluate the current propagation in an event with colder inflow water temperature. The event with colder inflow water occurred on 03<sup>rd</sup> June 2016 at 15:00, when the inflow water was 16.1 °C and the lake was mixed at 22 °C. The water temperature, velocity and density are shown in Figure 5.29 to Figure 5.33.

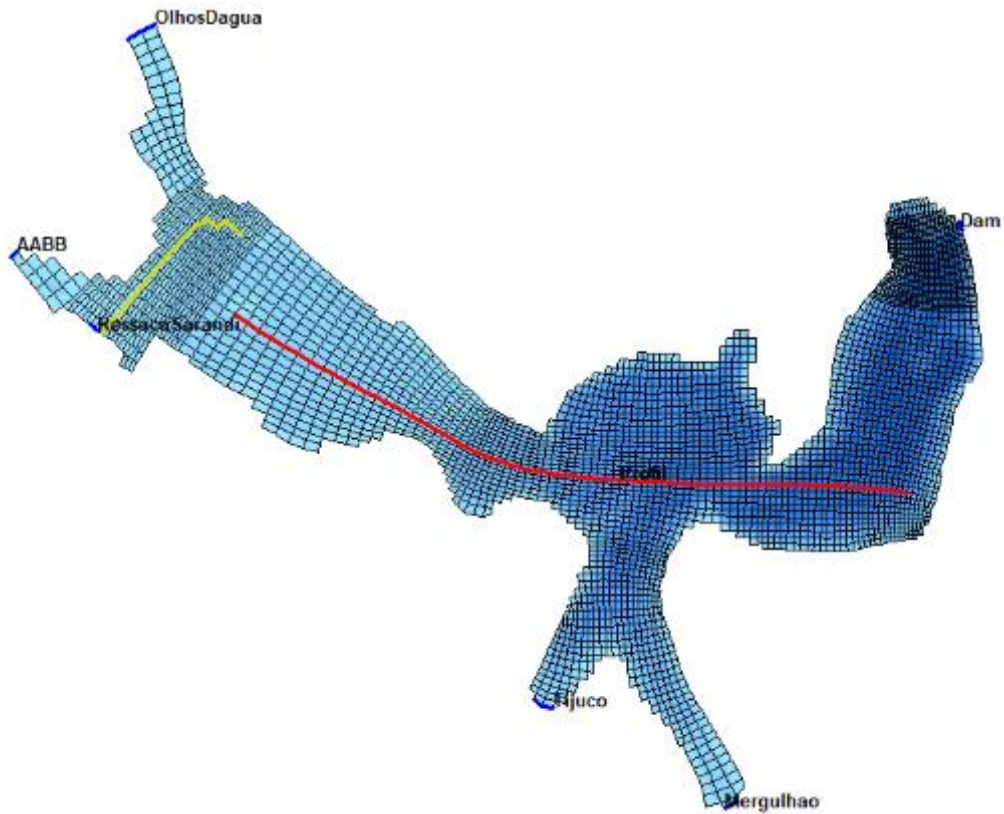


**Figure 5.28** – Longitudinal profile of the lake grid in red

The inflow water sank to deeper layers of the lake in a section of morphology change, 1500 m far from the inflow channel (Figure 5.29 and Figure 5.30). The total velocity exceeded 10 cm/s. Even after almost 2000 m from the inflow section, the current in the bottom layer was still noticeable at depths greater than 10 m in the deeper part of the lake.

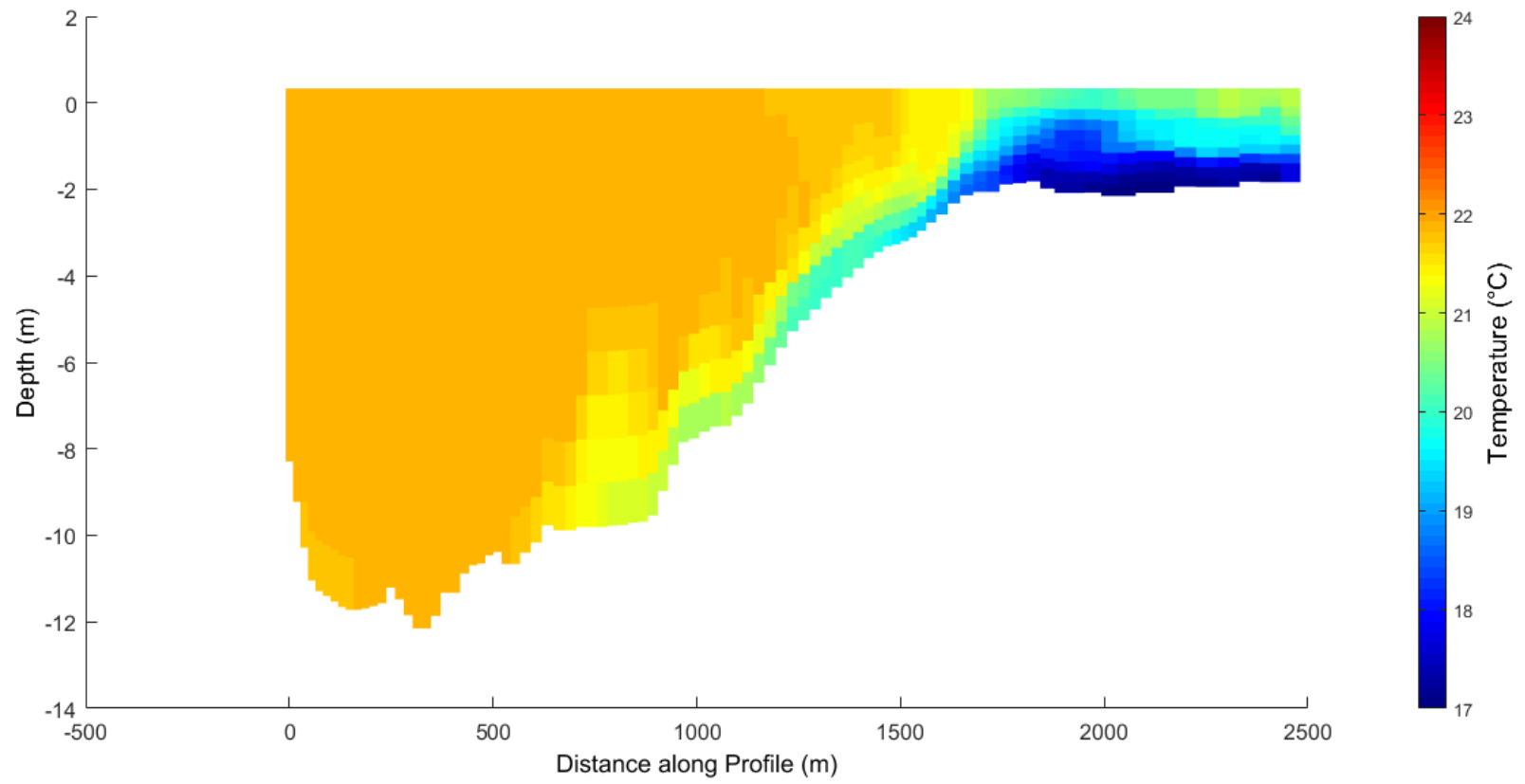


**Figure 5.29** – Water temperature during inflow water peak (03<sup>rd</sup> June 2016 15h) along the longitudinal profile

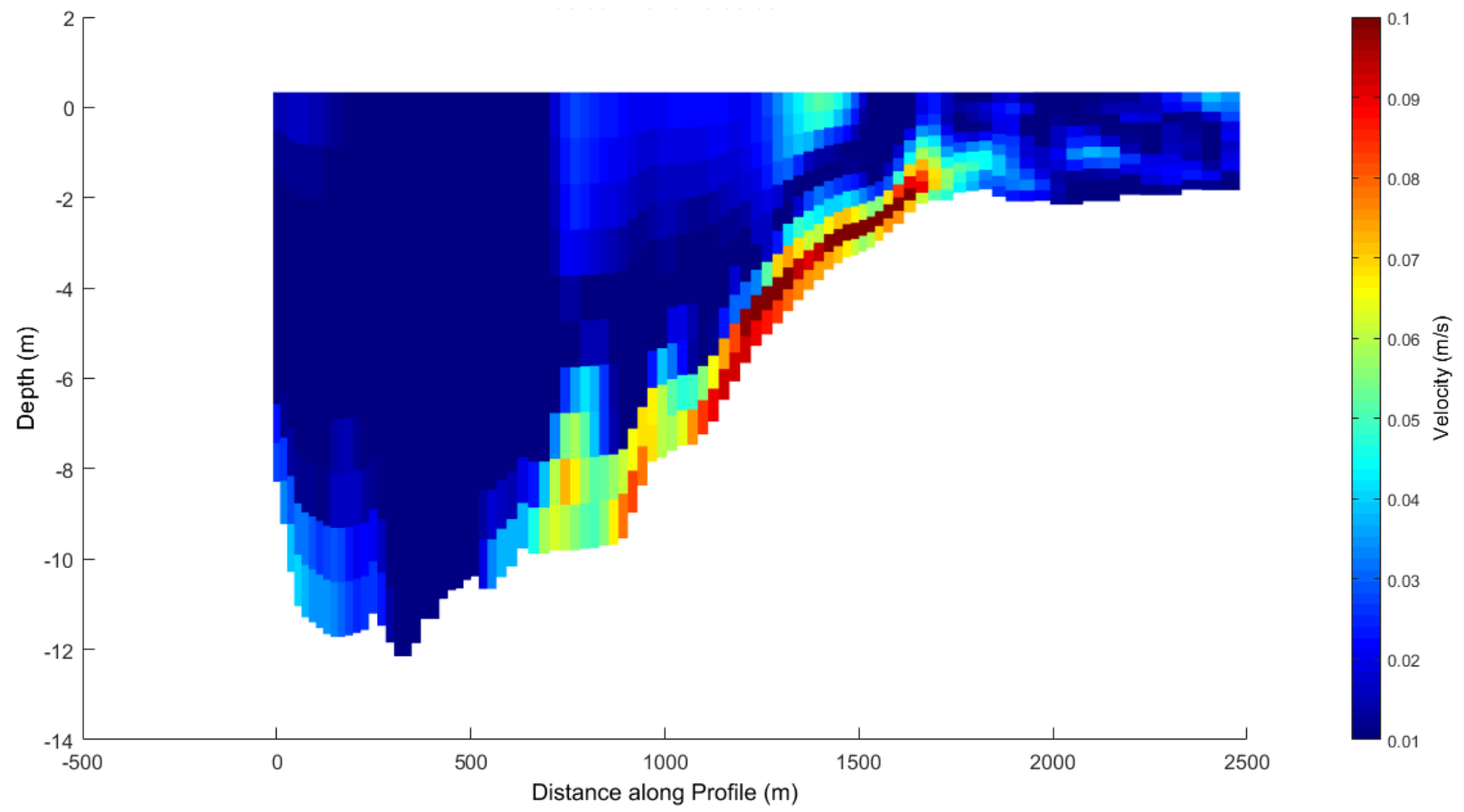


**Figure 5.30** – Water velocity during inflow water peak (03<sup>rd</sup> June 2016 15h) along the longitudinal profile

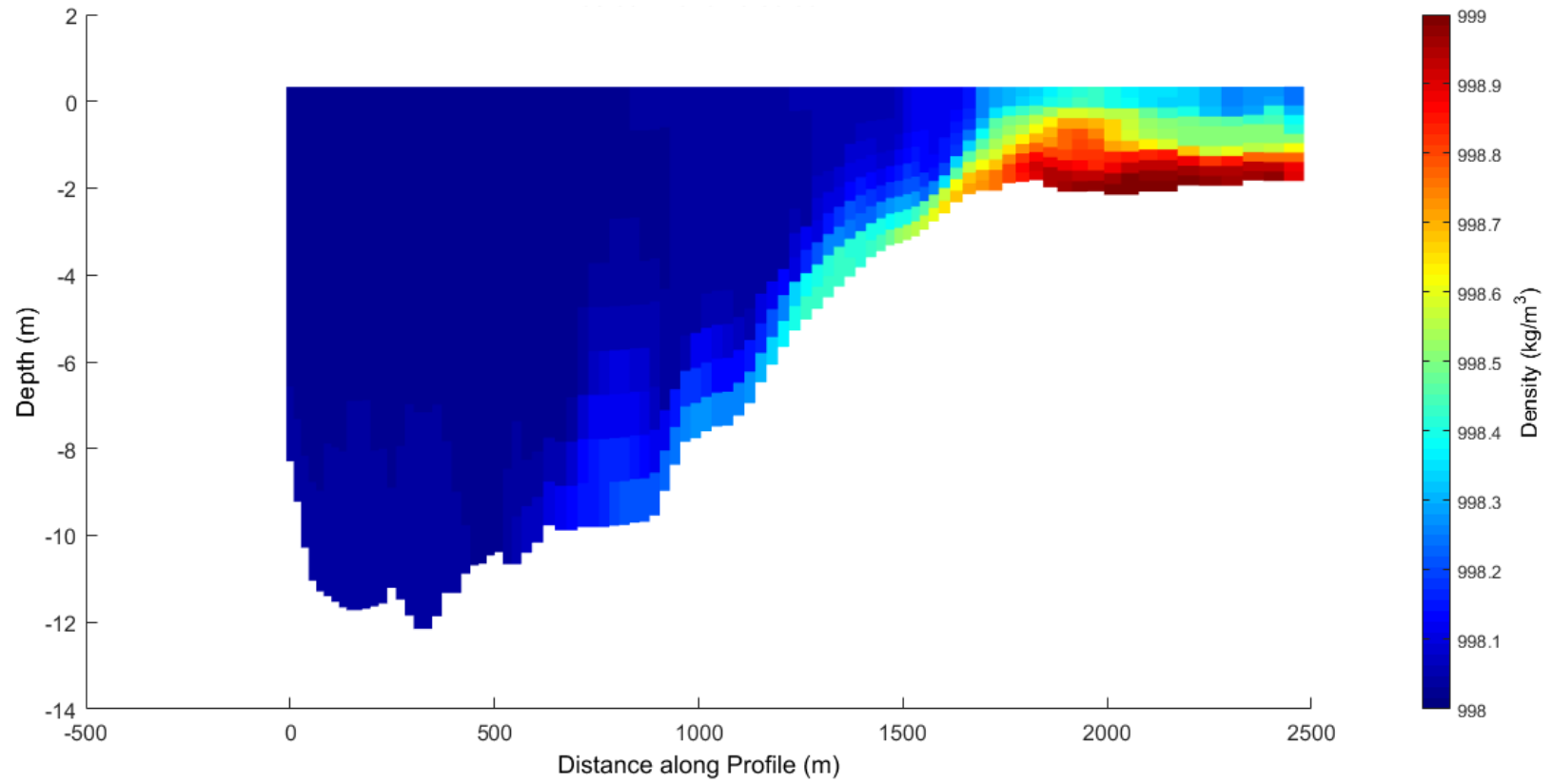


**Figure 5.31** – Water density during inflow water peak (03<sup>rd</sup> June 2016 15h) along the longitudinal profile

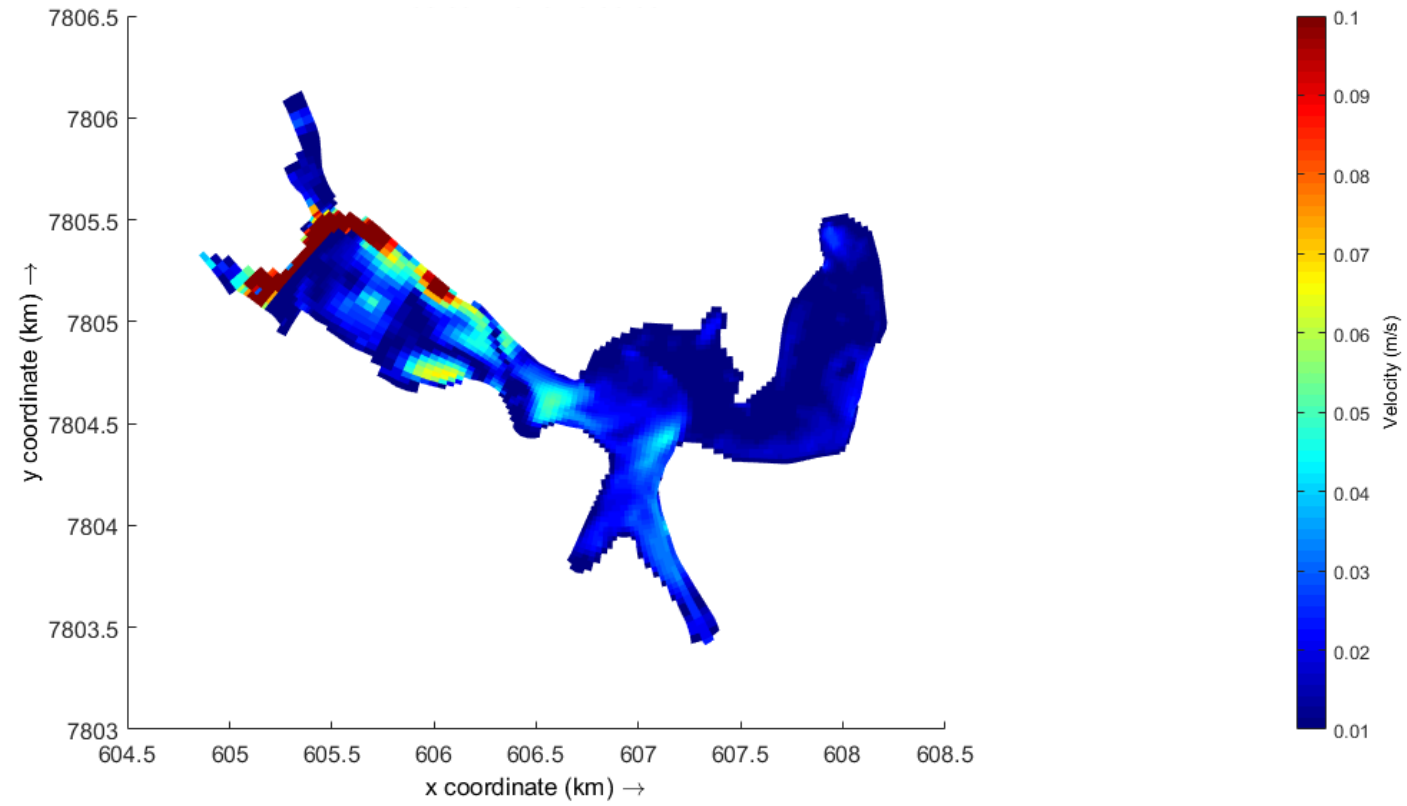


**Figure 5.32** – Velocity behaviour during inflow water peak (03<sup>rd</sup> June 2016 15h) at the surface

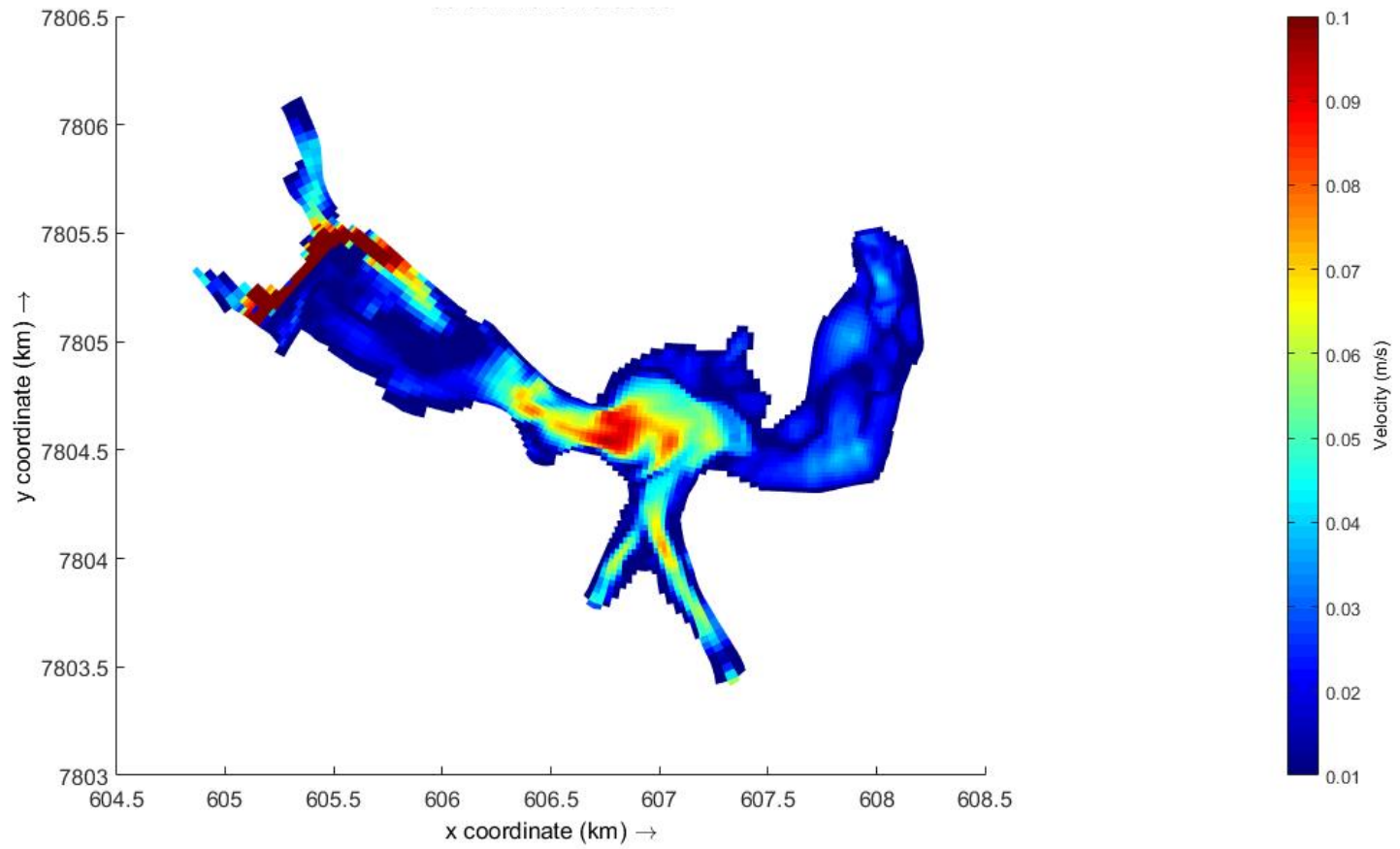


**Figure 5.33** – Velocity behaviour during inflow water peak (03<sup>rd</sup> June 2016 15h) at bottom layer

To analyse the impact of the stream inflow in the lake thermal stratification, Schmidt stability index and Lake number were computed using Lake Analyzer (Read et al. (2011)). Schmidt Stability represents the resistance to mechanical mixing (Idso, 1973), meaning the energy required to completely mix a stratified lake and the Lake Number, defined by Imberger and Patterson (1990), is the ratio of the strength of stratification (Schmidt Stability) to the effect of the wind stress.

For the period, Schmidt stability shows a pattern in day-night oscillations (Figure 5.34), induced by the heating and cooling alternation period, corresponding to the same pattern of the water temperature difference between surface and bottom (Figure 5.35). However, just before the cooling of the bottom depth on 03<sup>rd</sup> June it was observed a mixing condition that strongly reduced the value of Schmidt Stability index. This mixing condition reduced the daily variation on 03<sup>rd</sup> June, changing the pattern, showing a smaller amplitude. Before the mixing event, the daily variation was around 14 J/m<sup>2</sup>, on 03<sup>rd</sup> June it reduced to 4 J/m<sup>2</sup>. Figure 5.34 also shows that the model could represent this Schmidt stability dynamic. However, after 05<sup>th</sup> June, a weaker agreement between measurements and simulated results (Figure 5.20), led to higher differences between surface and bottom depth (Figure 5.35), directly impacting the Schmidt stability index computed from simulated results.

Lake number below 1 means that the lake stratification is weak with respect to wind stress and the lake will probably mix. According Figure 5.34 and Figure 5.36, the Lake Number peaks were coincident with the Schmidt Stability peaks for measured and simulated values. The water inflow during 03<sup>rd</sup> and 04<sup>th</sup> June resulted in the cooling of the bottom of the lake. On 05<sup>th</sup> June, after the cooling of the bottom depth, it is observed a greater difference of water temperature between surface and bottom, which increased the Lake Number peaks to values higher than 600 J/m<sup>2</sup>. Thus, the stream inflow impacted the lake stratification strength and the three-dimensional model could represent this dynamic.

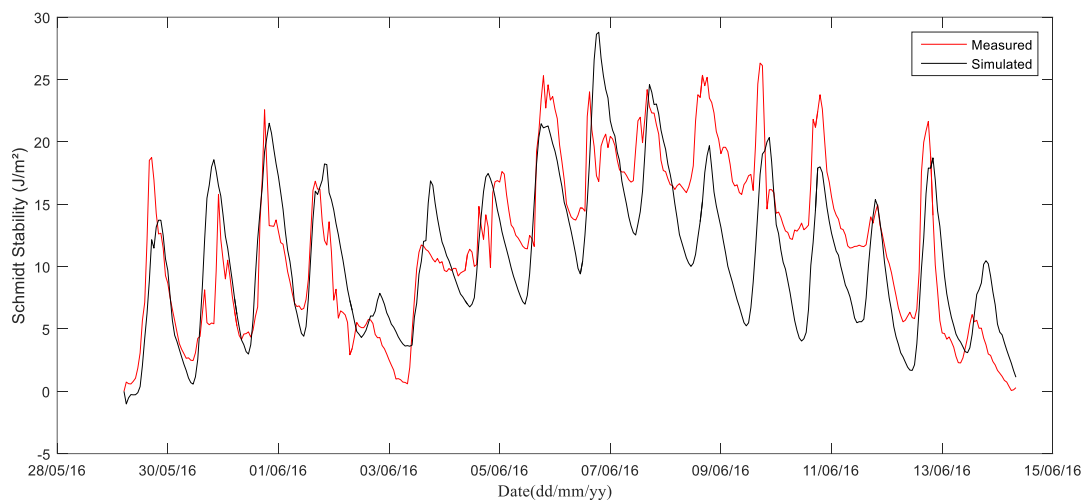


**Figure 5.34** – Schmidt stability variation during the validation period (29<sup>th</sup> May to 14<sup>th</sup> June 2016) at point P1.



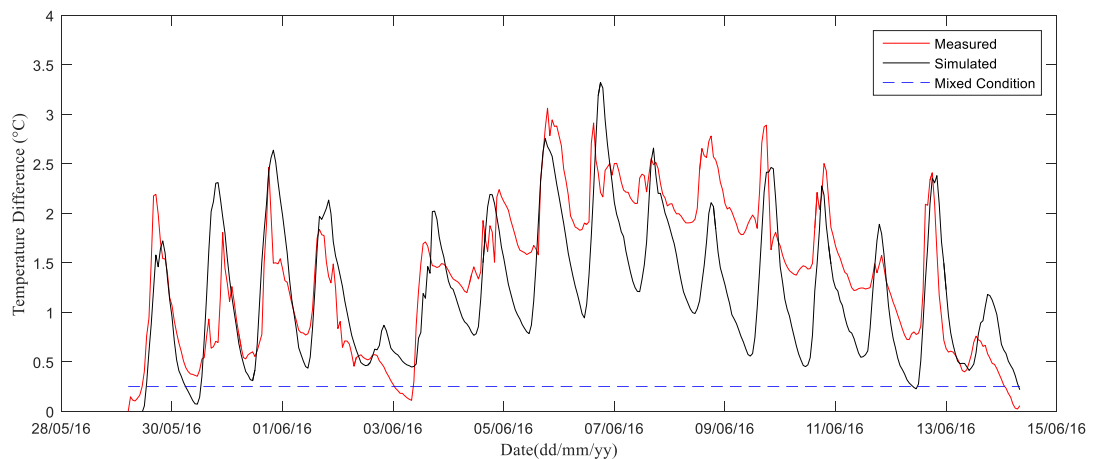


**Figure 5.35** – Difference of surface (0.5) and bottom (9.5) for measured and simulated water temperature for the validation period from 29<sup>th</sup> May to 14<sup>th</sup> June 2016 at P1 station. Blue dashed line represents a mixing condition with difference between surface and bottom of 0.25 °C.

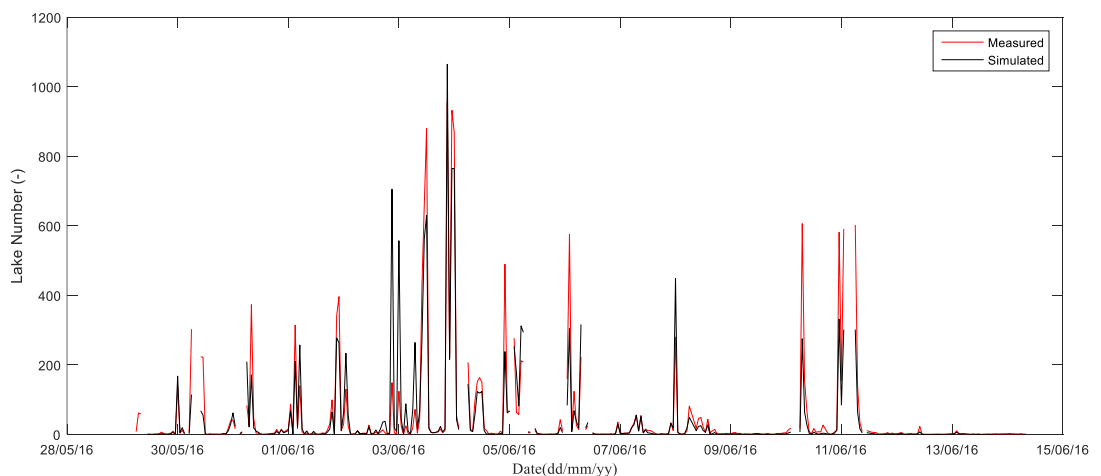


**Figure 5.36** – Lake number variation during the validation period (29<sup>th</sup> May to 14<sup>th</sup> June 2016) at point P1.

### 5.3.3. Longer validation period

With the same parameters used in the calibration and validation periods, a third period was simulated from 15<sup>th</sup> May 2015 to 10 August 2015 ( $n=2107$ ). For this period, only surface temperature was measured (Figure 5.37). This simulation had the purpose of evaluating the performance of the model for a longer period.

The inflow water and meteorological inputs are presented in Figure 5.38 and Figure 5.39. During this period, just on 29<sup>th</sup> May 2015 an inflow water peak was noticed of 29.4 m<sup>3</sup>/s.

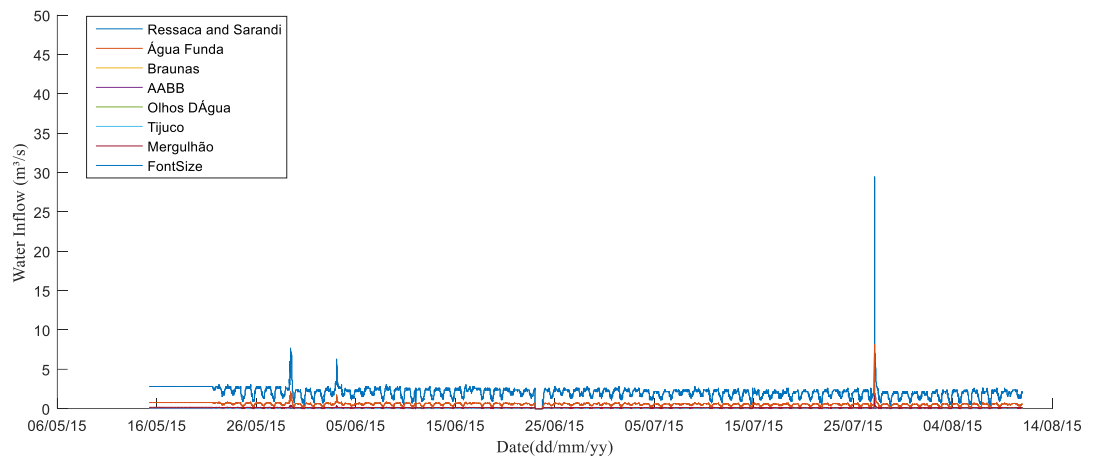


**Figure 5.37** – Inflow water in Ressaca/Sarandi during the third period simulated

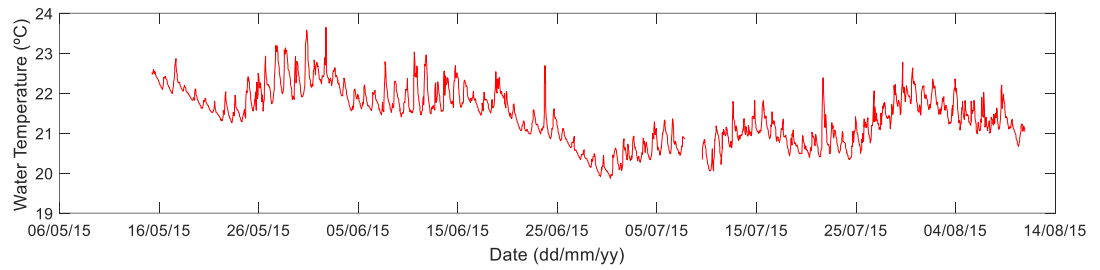


**Figure 5.38** – Water surface temperature measurements during the third simulated period.

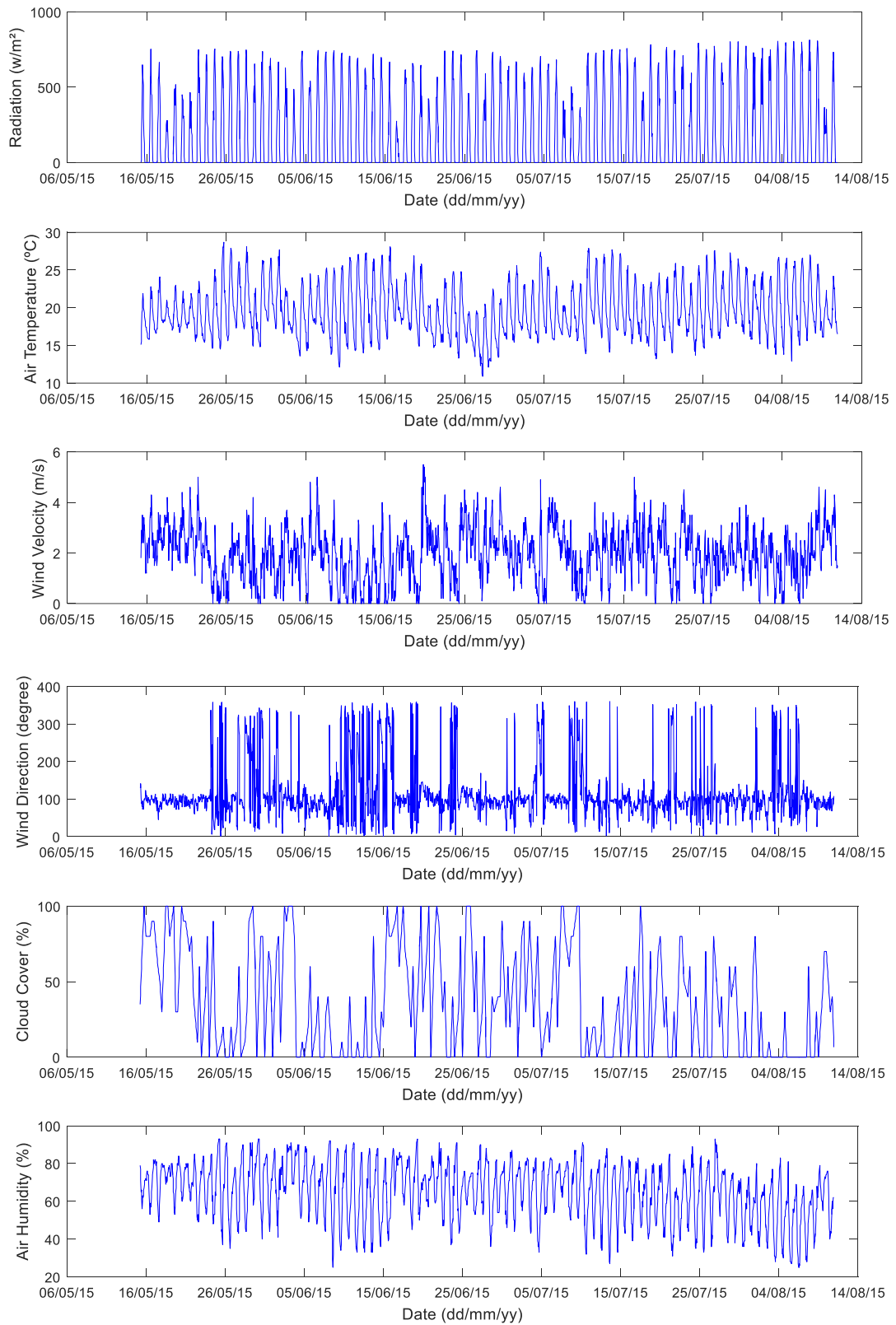


**Figure 5.39** – Radiation, air temperature, wind velocity and direction, cloud cover and humidity measured at the meteorology station during the third simulated period.

The simulation results and data measurements during the period are presented in Figure 5.40. To assess the performance of the hydrodynamic model, the water surface temperature measurements were used.

For a better view of the comparison between measured and simulated results, the figure was split into three graphs. The hourly measured and simulated temperatures (n=2107) is presented in Figure 5.41. Even with a slightly warmer simulated water temperature, the MAE between the measured and simulated values were very good (0.46 °C), the  $R^2$  was quite good (0.54) and the RE also presented very good value (2.12 %).

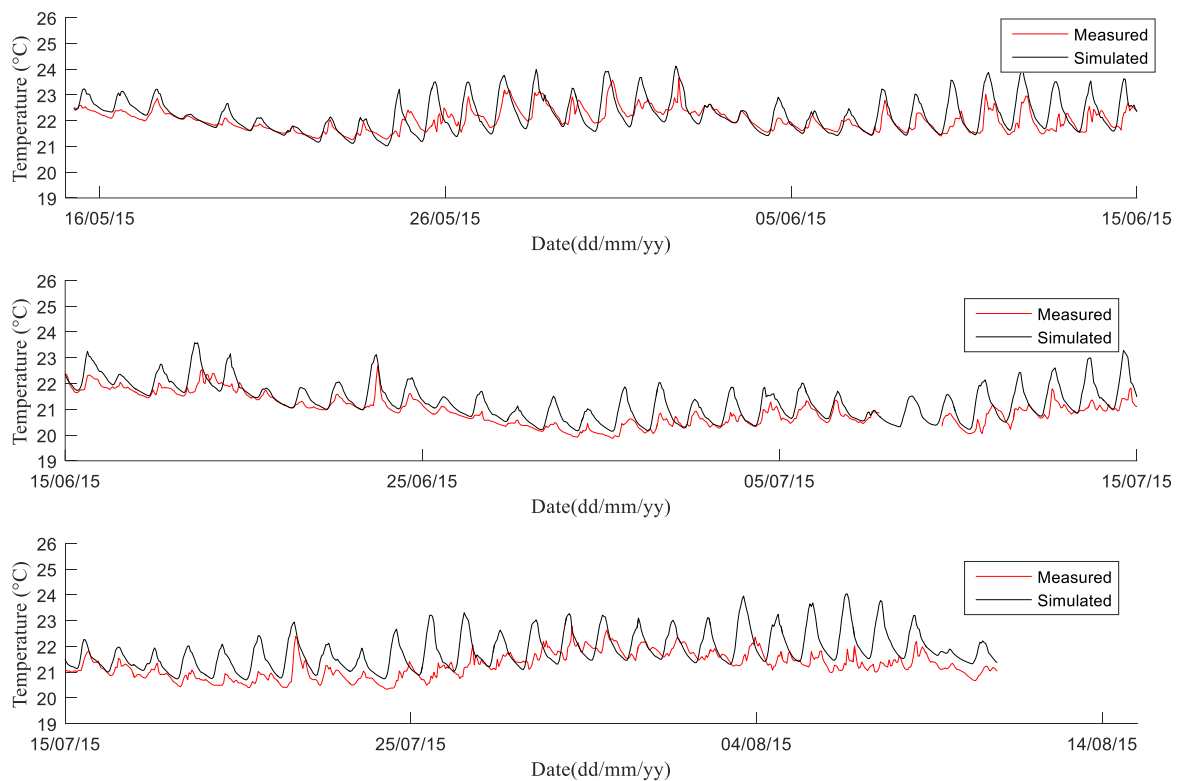


**Figure 5.40** – Measured and simulated temperature at P<sub>1</sub> at surface (0.5 m) depth from 15<sup>th</sup> May 2015 to 10<sup>th</sup> August 2015.

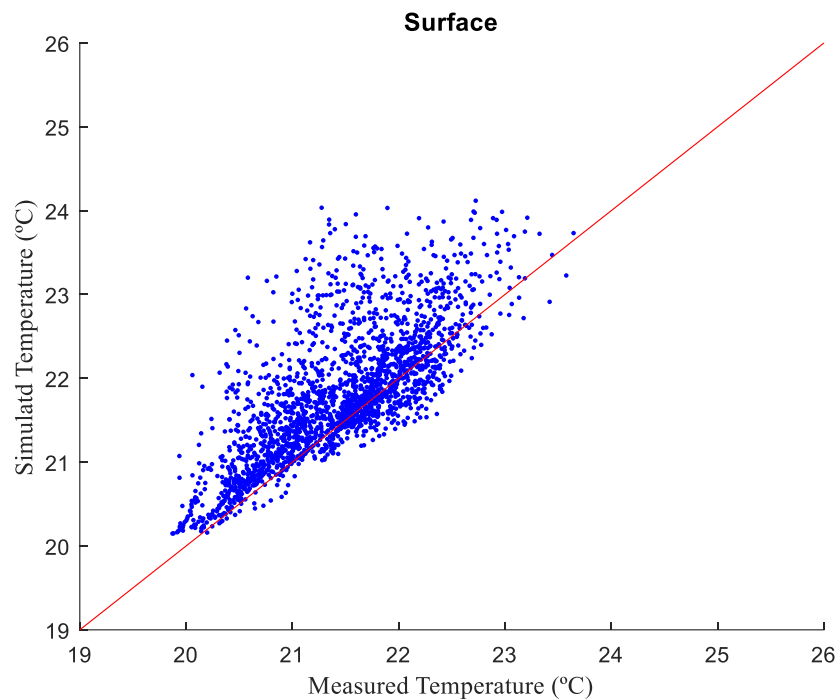


**Figure 5.41** – Hourly measured and simulated water temperature at P1 at 0.5 depth from 15<sup>th</sup> May 2015 to 10<sup>th</sup> August 2015.

#### 5.4. Lake Pampulha conclusion and discussion

A literature review of 15 years (from 2000 to 2015), carried out by Meinson et al. (2016), showed that more than two-thirds of the studies that used high-frequency monitoring in lakes were carried out in northern temperate zone, either in North America or in Europe. The authors also showed that water temperature was the most common measured parameter, because of the sensor reasonable price and low maintenance and the most important, because water temperature is a controlling factor of biological, ecological and chemical processes (MEINSON et al., 2016).

Very few modelling attempts have been performed on small and shallow lakes, and quantitative comparisons of modelling based on high-frequency data are also very scarce (Shimoda, Arhonditsis, 2016). Urban lakes have been less studied than non-urban ones and more knowledge about them is required (Birch and McCaskie, 1999a; Gong et al., 2016; Soullignac et al., 2017).

Due to the complex hydrodynamic behaviour of lakes, with high heterogeneity in space and time, three-dimensional models play an important role in better understanding all processes involved (Gong et al., 2016; Soullignac et al., 2017, 2018; Zbiciński and Ziemińska-Stolarska, 2017). Three-dimensional models help to understand and predict lake ecosystem behaviour in response to external pressures, like climate forcing, nutrient loading, and pollutant input (Chanudet et al., 2012; Evelyn Aparicio Medrano et al., 2013).

In this research, a three-dimensional hydrodynamic model, Delft3D-FLOW, was implemented in Lake Pampulha, a shallow urban tropical lake. It was possible to perform a rare analysis using high-frequency measurement data and a three-dimensional hydrodynamic model using Delft3D-FLOW. For all simulated period, the model performance was evaluated based in hourly values.

For the first simulated period, the model was calibrated by comparing measured and simulated results of the water temperature for 440 hourly values (16<sup>th</sup> May to 03<sup>rd</sup> June 2016). The agreement between the modelled and observed temperatures was quite good. The final results presented, for surface (0.5 m), 2.5 m, 5.5 m and 9.5 m depths respectively: a Mean Absolute Error (MAE) of 0.30 °C, 0.15 °C, 0.13 °C and 0.16 °C; an RE of 1.30%, 0.64%, 0.56% and 0.70%; and an R<sup>2</sup> of 0.73, 0.84, 0.93 and 0.90. The model could accurately reproduce the alternation of stratification and mixing conditions along the period.

For the second simulated period (from 29<sup>th</sup> May to 14<sup>th</sup> June 2016 with 388 hourly values for each depth), the calibration was verified and the agreement between the modelled and observed temperatures was also quite good. The results presented, for the surface (0.5 m), 2.5 m, 5.5 m and 9.5 m depths respectively: a Mean Absolute Error (MAE) of 0.34 °C, 0.23 °C, 0.12 °C and 0.20 °C; an RE of 1.51%, 1.04%, 0.56% and 0.95%, and an R<sup>2</sup> of 0.63, 0.41, 0.80 and 0.81.

For the third period (from 15<sup>th</sup> May to 10<sup>th</sup> August 2015), it was possible to validate the model's performance for a longer period of days using 2107 hourly surface temperature data, representing almost three months. The mathematical indicators between the measured and simulated water surface values were very good with a MAE of 0.45 °C, R<sup>2</sup> was quite good (0.55) and the RE also presented very good value (2.08%).

Mean absolute error (MAE) during all simulation periods for water temperature varied between 0.15 and 0.45 °C and was similar to other three-dimensional model studies. Soullignac et al. (2017) achieved values in a range between 0.25 and 2.34 °C for Lake Crétéil (surface area of 0.4 km<sup>2</sup> and mean depth of 4.5 m,) using hourly temperature values at five depths (0.5, 1.5, 2.5, 3.5 and 4.5 m). In Lake Yilong (surface area of 28.4 km<sup>2</sup> and mean depth of 3.9 m), Zhao et al. (2013) obtained a R<sup>2</sup> between 0.65 and 0.74 calculated from measured data of 15 campaigns throughout one year, same range of our values (0.55 to 0.93). In Lake Minnetonka (maximum depth of 25.0 m and surface area of 8.01 km<sup>2</sup>), Missaghi and Hondzo (2010) obtained a R<sup>2</sup> between 0.91 and 0.98 using 6 months of bi-weekly measured profiles of temperature for calibration and validation period.

Belico (2017) investigated the dynamic of the Lake Pampulha during rain events from 2011 to 2015 with hourly measurements of water temperature at surface and monthly vertical profiles. The unidimensional modelling provided a Root Mean Square Error (RMSE) of 1.08 °C at surface. In our research, the RMSE varied between 0.15 and 0.65 °C.

In shallow lakes, water temperature plays an important role which affects lake ecological behaviour. Thermal stratification and a longer residence time of the water within the lake can boost phytoplankton production. Due to low turbulence, lake ecosystems can provide the required conditions for phytoplankton species and water deterioration. Water mixing events have a major impact on vertical turbulence and temperature structure, affecting phytoplankton and cyanobacteria developments (Jöhnk et al., 2008). Thus, an understanding of water circulation and its interference on water quality bears great importance (Li-Kun et al., 2017; Qin et al., 2015; Wu et al., 2015; Zbiciński and Ziemińska-Stolarska, 2017).

Khac et al. (2018), through high-frequency monitoring, noticed that cyanobacteria are one of the dominant phytoplankton group in blooms episodes during lake stratification periods in Lake Champs-sur-Marne. The conditions for water column stratification are identified by Huber et al. (2012) as an increase in incident radiation and air temperature with a decrease in wind speed. Shimoda and Arhonditsis (2016) highlighted that, in freshwater, water temperature is an important regulatory factor

for phytoplankton and cyanobacteria growth rate. Rinke et al. (2009) concluded that light and water temperature are the main factors.

In this research for Lake Pampulha, it was noted that the thermal amplitude of surface water impacts the thermal behaviour at deeper layers over time. Water surface cooling during the night is less intense for lower Dalton coefficients, which impacts the heat exchange between atmosphere and water. Therefore, the surface water temperature remains warmer for a longer time, resulting in a heating behaviour at greater depths.

Despite using data from only one monitoring station to calibrate the model and despite the limitation in water inflow temperatures measurements, the model was useful to understand and evaluate forcing changes scenarios. The impact of the stream inflow on the reservoir temperature was highlighted by showing that during higher discharge events, when the river temperature is colder than the lake water, it flows through deeper layers of the lake. This contributes to the knowledge of a complex spatio-temporal dynamic of the lake hydrodynamic.

The Lake Pampulha water quality is severely compromised and presents a hypoxia condition at the bottom of the lake (Friese et al., 2010; von Sperling and Campos, 2011). Current velocities in lakes are normally low and water residence is generally high. The water current coming from inflow, through the deeper layers of the lake, may help to renew and aerate the water and impact the ecological status of the lake by affecting the nutrient upwelling fluxes and leverage sediment resuspension and release the nutrients from them, even at 10 m depth and about 2 km from the inlet.

Using the model, it was possible to evaluate different scenarios of inflow water under different weather conditions and how these processes may impact the lake in different regions. Due to the importance of water stratification and hydrodynamics on phytoplankton growth, these results may also help to understanding algal blooms. The good results of the hydrodynamic model allow, for the next steps, to study phytoplankton and ecological dynamics by coupling the water quality module.

The good simulation results also indicate that the meteorological data, collected at a weather station located 3 km from the lake (and from 9.5 km for the cloud cover data) reproduce well the meteorological conditions over the lake for majority of the time. However, the performance of the model may have been affected due to high sensibility of the lake hydrodynamics to external forcing, being affected by some discrepancies, such as nebulosity and wind intensity and direction. Another source of uncertainties was the inflow of water temperature that was estimated using air temperature.

A good model performance was obtained using short simulation period, which is suitable in terms of tri-dimensional computation time demanding and availability of high-frequency time series. However, the simulated periods were not realized for all seasons. The dry season was focalized because it is the period with higher episodes of cyanobacteria blooms. Another limitation of the research was to validate the model using just one measurement station that was in the middle of the lake. However, four different depths were measured. Concerning water stratification and mixing conditions, our results could contribute to the knowledge of the complex behaviour of the lake. Even with our data limitations, it is possible to conclude that our results fetch important information of the thermal behaviour of shallow lake specificities.

These results, using high-frequency monitoring and three-dimensional modelling, are promising to help assessing the distribution of pollutants and nutrients in the lake, sedimentation and resuspension processes, and for understanding algal blooms in shallow lakes.

In this research, the use of a three-dimensional hydrodynamic model was essential to understand the thermal behaviour of a shallow tropical lake. Collaborating to the conclusions of Leon et al. (2011) and Gong et al. (2016) that three-dimensional modelling is required for simulating complex lake behaviours.

The main results of the Lake Pampulha study site was presented in the “Thermal functioning of a tropical reservoir assessed through three-dimensional modelling and high-frequency monitoring” paper. It was accepted in the Brazilian Journal of Water Resources (RBRH) (Annex 8.9).



## 6. GENERAL CONCLUSIONS

In this research, two experimental study sites were investigated: Lake Champs-sur-Marne, a small and shallow urban lake in France, and Lake Pampulha, a medium-sized and shallow urban reservoir in Brazil.

In the French lake, a three-dimensional hydrodynamic and ecological model was calibrated using high-frequency measurements and used to simulate phytoplankton and cyanobacteria biomass in different scenarios. The model was useful to better understand phytoplankton increase and decrease and cyanobacteria biomass in space and time for short-term bloom events. Using high-frequency measurements, it was possible to register some rapid increases in total fluorescence. Not having all necessary data, mathematical models are useful tools to better understand phytoplankton behaviour in space and time by evaluating and simulating different weather scenarios and nutrient concentration conditions. It was possible to take advantage to evaluate the transport features and spatial and temporal biomass behaviour by using different modeling approaches (with and without coupling ecological module).

The coupled models also made it possible to evaluate the influence of hydrodynamics on the spatial and temporal distribution of phytoplankton biomass. This approach can also be used to improve specific measurement campaigns. Knowing where scum is likely to occur and accumulate may help in the challenge of obtaining field data and study this phenomenon.

Current flow, measured at high-frequency through ADCP, enabled an analysis of the influence of water mixing on the vertical column and the influence of wind on a small and shallow lake. The hydrodynamic model could satisfactorily represent the time at which the water current reaches the higher values and its vertical distribution. The measurements and the simulation show that the lake does not have velocity stratification. It was shown that, for all three depths and for the average vertical profile, the velocity behaviour was very similar and presented a strong correlation with wind intensity, in which wind intensity of 3.0 m/s may impact the entire vertical column, therefore, being an important *in loco* meteorological measurement. Due to the great variability of hydrodynamic behaviour in shallow urban lakes and external driving forces, high-frequency monitoring coupled with a three-dimensional model may help to achieve a system to catch cyanobacterial bloom events and scum formations. Helping to improve the network measurement and in better understanding the hydrodynamic of a lake and its different behaviour in specific regions of a lake. Hence, high-frequency monitoring and three-dimensional modelling corroborate for a clearer understanding of phytoplankton and cyanobacteria concentrations.

Using high-frequency field data to demonstrate that a change in hydrodynamic behaviour has the potential to influence cyanobacterial blooms presents a considerable challenge. However, using three-dimensional modeling, calibrated for specific points, indicates that lake hydrodynamics are a key process that affects spatial and temporal biomass distribution in a shallow lake. Otherwise, using the results of modeling, suggestions could be made to improve the current monitoring locations to better elucidate cyanobacteria behaviour. To complement field observations, remote sensing images can also improve monitoring programs, especially to evaluate lake heterogeneity. In a more synthetic form, the Lake champs-sur-Marne results showed:

- ✓ High-frequency monitoring enables an analysis of the high temporal variation of biomass in the lake and the influence of different external forces on hydrodynamic behaviour;

- ✓ The three-dimensional model Delft-3D was useful in the analysis of the influence of lake hydrodynamics on phytoplankton concentrations and spatial heterogeneity;
- ✓ Alternation and duration of mixing and stratification conditions and the complex hydrodynamic functioning of the lake could be represented by the three-dimensional model;
- ✓ The three-dimensional model can help to improve lake monitoring design, highlighting regions with different behaviour;
- ✓ Mathematical modelling is a great tool to simulate different scenarios in cases where there are field data gaps;
- ✓ The measurements and simulations showed that the hydrodynamics of Lake Champs-sur-Marne are very unstable and dynamic. The lake reacts rapidly and intensely to meteorological forcing. However, the three-dimensional hydrodynamic model was able to represent these complex hydrodynamics behaviour;
- ✓ The measurements and simulations showed that the lake does not have velocity stratification in terms of power frequency. It was shown that, the velocity behaviour was very similar and presented a strong correlation with wind intensity, in which wind intensity of 3.0 m/s may impact the entire vertical column, therefore, being an important *in loco* meteorological station.

In the Brazilian lake, a three-dimensional hydrodynamic model was calibrated and validated using high-frequency temperature measurements. In a more synthetic form, the Lake Pampulha results showed:

- ✓ The main sensitivity parameters to calibrate the thermal behaviour of the lake are the Wind factor and Dalton coefficient;
- ✓ High-frequency measurement with hourly time step could detect sudden changes of water temperature with different amplitudes depending on the depth and using three-dimensional model it was possible to investigate the cause of sudden changes in the water temperature;
- ✓ The three-dimensional model, associated with high-frequency measurement, showed that detecting colder freshwater current and knowing the time trajectory throughout the deeper layer of the lake may contribute to implement and leverage restoration techniques and support water management for urban lakes that have hypoxia condition at the bottom of the lake;
- ✓ A three-dimensional model could accurately reproduce the alternation of stratification and mixing conditions along all period simulated, allowing a deeper analysis of a shallow tropical lake hydrodynamics.

As shallow urban lakes have been the subject of much less study, this research could add important contributions to knowledge about the influence of hydrodynamics on phytoplankton behaviour in shallow and urban lakes. It was shown that shallow lakes are very instable and react strongly and rapidly to meteorological forces. Phytoplankton biomass displays high heterogeneities in space and time that result in high complexity to be able to measure its behaviour. Using a three-dimensional model, it was shown that hydrodynamics play an important role to better understand algal blooms and scum formation. This study shows that a calibrated and validated three-dimensional hydrodynamic and ecological model using high-frequency monitoring is essential for understanding water quality in shallow urban lakes.

## 7. REFERENCES

- Alexandrov, G.A., Ames, D., Bellocchi, G., Bruen, M., Crout, N., Erechtkhoukova, M., Hildebrandt, A., Hoffman, F., Jackisch, C., Khaiteer, P., et al. (2011). Technical assessment and evaluation of environmental models and software: Letter to the Editor. *Environ. Model. Softw.* 26, 328–336.
- Allen, B.J., Mansell, E.R., Dowell, D.C., and Deierling, W. (2016). Assimilation of Pseudo-GLM Data Using the Ensemble Kalman Filter. *Mon. Weather Rev.* 144, 3465–3486.
- Andrew Brierley (2017). Plankton. *ScienceDirect* 27, 478–483.
- Barbosa, L.G., Barbosa, F.A.R., Bicudo, C.E. de M., Barbosa, L.G., Barbosa, F.A.R., and Bicudo, C.E. de M. (2018). Is thermal stability a factor that influences environmental heterogeneity and phytoplankton distribution in tropical lakes? *Acta Limnol. Bras.* 30.
- Barçante, B., Nascimento, N.O., Silva, T.F.G., Reis, L.A., and Giani, A. (2020). Cyanobacteria dynamics and phytoplankton species richness as a measure of waterbody recovery: Response to phosphorus removal treatment in a tropical eutrophic reservoir. *Ecol. Indic.* 117, 106702.
- BBE, M. (2012). Submersible Spectrofluorometer with Automatic Algae Class and Chlorophyll Analysis.
- Beghelli, F.G. de S., Frascareli, D., Pompêo, M.L.M., and Moschini-Carlos, V. (2016). Trophic State Evolution over 15 Years in a Tropical Reservoir with Low Nitrogen Concentrations and Cyanobacteria Predominance. *Water. Air. Soil Pollut.* 227, 95.
- Belico, J.C.B. (2017). Impactos de eventos chuvosos na dinâmica físico-química e biológica em reservatórios urbanos estudo de caso: Lagoa da Pampulha.
- Beniston, M. (2004). The 2003 heat wave in Europe: A shape of things to come? An analysis based on Swiss climatological data and model simulations. *Geophys. Res. Lett.* 31.
- Berman, T., and Chava, S. (1999). Algal growth on organic compounds as nitrogen sources. *J. Plankton Res.* 21, 1423–1437.
- Beutler, M., Wiltshire, K.H., Meyer, B., Moldaenke, C., Luring, C., Meyerhofer, M., Hansen, U.P., and Dau, H. (2002). A fluorometric method for the differentiation of algal populations in vivo and in situ. *Photosynth. Res.* 72, 39–53.
- Beutler, M., Wiltshire, K.H., Reineke, C., and Hansen, U.P. (2004). Algorithms and practical fluorescence models of the photosynthetic apparatus of red cyanobacteria and Cryptophyta designed for the fluorescence detection of red cyanobacteria and cryptophytes. *Aquat. Microb. Ecol.* 35, 115–129.
- Birch, S., and McCaskie, J. (1999). Shallow urban lakes: a challenge for lake management. *Hydrobiologia* 395–396, 365–378.
- Blondeau-Patissier, D., Gower, J.F.R., Dekker, A.G., Phinn, S.R., and Brando, V.E. (2014). A review of ocean color remote sensing methods and statistical techniques for the detection, mapping and analysis of phytoplankton blooms in coastal and open oceans. *Prog. Oceanogr.* 123, 123–144.
- Boegman, L., Imberger, J., Ivey, G.N., and Antenucci, J.P. (2003). High-frequency internal waves in large stratified lakes. *Limnol. Oceanogr.* 48, 895–919.

- Bormans, M., Sherman, B.S., and Webster, I.T. (1999). Is buoyancy regulation in cyanobacteria an adaptation to exploit separation of light and nutrients? *Mar. Freshw. Res.* *50*, 897–906.
- Brennen, C.E., Keady, G., and Imberger, J. (2018). A note on algal population dynamics. *IMA J. Appl. Math.* *83*, 783–796.
- Butterwick, C., Heaney, S.I., and Talling, J.F. (2005). Diversity in the influence of temperature on the growth rates of freshwater algae, and its ecological relevance. *Freshw. Biol.* *50*, 291–300.
- Cao, H., Recknagel, F., and Bartkow, M. (2016). Spatially-explicit forecasting of cyanobacteria assemblages in freshwater lakes by multi-objective hybrid evolutionary algorithms. *Ecol. Model.* *342*, 97–112.
- Catherine, A. (2009). Déterminisme des efflorescences et de la toxicité des cyanobactéries en milieu périurbain (Ile-de-France). PhD thesis. Museum National d'Histoire Naturelle.
- Catherine, A., Escoffier, N., Belhocine, A., Nasri, A.B., Hamlaoui, S., Yéprémian, C., Bernard, C., and Troussellier, M. (2012). On the use of the FluoroProbe®, a phytoplankton quantification method based on fluorescence excitation spectra for large-scale surveys of lakes and reservoirs. *Water Res.* *46*, 1771–1784.
- Catherine, A., Mitroi, V., Vinçon-Leite, B., Lucas, F., Bressy, A., Jardillier, L., and Bernard, C. (2015). Rapport de synthèse sur l'évaluation de l'état écologique et sanitaire des plans d'eau d'Ile-de-France (ANR CEP&S PULSE 2011-2015.).
- Cerna, M., and Audrey, H. (2013). The Fundamentals of FFT-Based Signal Analysis and Measurement - Application Note.
- Chanudet, V., Fabre, V., and van der Kaaij, T. (2012). Application of a three-dimensional hydrodynamic model to the Nam Theun 2 Reservoir (Lao PDR). *J. Gt. Lakes Res.* *38*, 260–269.
- Chen, G., and Fang, X. (2015). Accuracy of Hourly Water Temperatures in Rivers Calculated from Air Temperatures. *Water* *7*, 1068–1087.
- Chen, G., and Fang, X. (2016). Estimating Hourly Water Temperatures in Rivers from Air Temperatures. *World Environ. Water Resour. Congr.* 2016.
- Chorus, I., and Bartram, J. (1999). *Toxic Cyanobacteria in Water: a guide to their public health consequences, monitoring and management* (Geneva: World Health Organization).
- Clark, J.M., Schaeffer, B.A., Darling, J.A., Urquhart, E.A., Johnston, J.M., Ignatius, A.R., Myer, M.H., Loftin, K.A., Werdell, P.J., and Stumpf, R.P. (2017). Satellite monitoring of cyanobacterial harmful algal bloom frequency in recreational waters and drinking water sources. *Ecol. Indic.* *80*, 84–95.
- Codd, G.A., Bell, S.G., Kaya, K., Ward, C.J., Beattie, K.A., and Metcalf, J.S. (1999). Cyanobacterial toxins, exposure routes and human health. *Eur. J. Phycol.* *34*, 405–415.
- CPRM (2001). Projeto Pampulha – Estudo Hidrogeológico da Bacia da Lagoa da Pampulha, (PBH).
- Cyr, H. (2017). Winds and the distribution of nearshore phytoplankton in a stratified lake. *Water Res.* *122*, 114–127.

- Davidson, K., Anderson, D.M., Mateus, M., Reguera, B., Silke, J., Sourisseau, M., and Maguire, J. (2016). Forecasting the risk of harmful algal blooms. *Harmful Algae* 53, 1–7.
- Deltares (2013). Delft3D-FLOW - Simulation of multi-dimensional hydrodynamic flows and transport phenomena, including sediments. User Manual Version: 3.15.30059 (Delft Hydraulics, Delft).
- Deltares (2014a). Delft3D-FLOW User Manual. Version: 3.15.36498.
- Deltares (2014b). D-Water Quality, Open Processes Library. User Manual. Version 0.99.33644.
- Diário Oficial do Município (2016). Prefeitura dá início à recuperação da qualidade da água da lagoa da pampulha.
- Dimberg, P.H., and Olofsson, C.J. (2016). A Comparison Between Regression Models and Genetic Programming for Predictions of Chlorophyll-a Concentrations in Northern Lakes. *Environ. Model. Assess.* 21, 221–232.
- Dörnhöfer, K., Klinger, P., Heege, T., and Oppelt, N. (2018). Multi-sensor satellite and in situ monitoring of phytoplankton development in a eutrophic-mesotrophic lake. *Sci. Total Environ.* 612, 1200–1214.
- Downing, J.A., Prairie, Y.T., Cole, J.J., Duarte, C.M., Tranvik, L.J., Striegl, R.G., McDowell, W.H., Kortelainen, P., Caraco, N.F., Melack, J.M., et al. (2006). The global abundance and size distribution of lakes, ponds, and impoundments. *Limnol. Oceanogr.* 51, 2388–2397.
- Dupuis, A.P., and Hann, B.J. (2009). Warm spring and summer water temperatures in small eutrophic lakes of the Canadian prairies: potential implications for phytoplankton and zooplankton. *J. Plankton Res.* 31, 489–502.
- Elliott, J.A. (2012). Is the future blue-green? A review of the current model predictions of how climate change could affect pelagic freshwater cyanobacteria. *Water Res.* 46, 1364–1371.
- Epstein, M. (2009). Balance Laws. In *Encyclopedia of Neuroscience*, M.D. Binder, N. Hirokawa, and U. Windhorst, eds. (Berlin, Heidelberg: Springer), pp. 332–336.
- Escoffier, N., Bernard, C., Hamlaoui, S., Groleau, A., and Catherine, A. (2015). Quantifying phytoplankton communities using spectral fluorescence: the effects of species composition and physiological state. *J. Plankton Res.* 37, 233–247.
- European Parliament (2006). Directive 2006/7/EC of the European Parliament and of the Council of 15 February 2006 concerning the management of bathing water quality and repealing Directive 76/160/EEC.
- European Parliament and Council (2000). Directive 2000/60/EC of the European Parliament and of the Council of 23 October 2000 establishing a framework for Community action in the field of water policy.
- Evelyn Aparicio Medrano, Rob Uittenbogaard, Miguel Dionisio Pires, Bas J. H. van de Wiel, and Herman J.H. Clercx (2013). Coupling hydrodynamics and buoyancy regulation in *Microcystis aeruginosa* for its vertical distribution in lakes. ResearchGate.

Felisberto, H., Rocha, F., and Palmier, L.R. (2015). Mapeamento da área inundada resultante da propagação de onda de cheia oriunda de ruptura hipotética de barragem - estudo de caso: Barragem da Pampulha. SBRH 8.

Frassl, M.A., Boehrer, B., Holtermann, P.L., Hu, W., Klingbeil, K., Peng, Z., Zhu, J., and Rinke, K. (2018). Opportunities and Limits of Using Meteorological Reanalysis Data for Simulating Seasonal to Sub-Daily Water Temperature Dynamics in a Large Shallow Lake. *Water* 10, 594.

Friese, K., Schmidt, G., de Lena, J.C., Arias Nalini, H., and Zachmann, D.W. (2010). Anthropogenic influence on the degradation of an urban lake – The Pampulha reservoir in Belo Horizonte, Minas Gerais, Brazil. *Limnol. - Ecol. Manag. Inland Waters* 40, 114–125.

Glasgow, H.B., Burkholder, J.M., Reed, R.E., Lewitus, A.J., and Kleinman, J.E. (2004). Real-time remote monitoring of water quality: a review of current applications, and advancements in sensor, telemetry, and computing technologies. *J. Exp. Mar. Biol. Ecol.* 300, 409–448.

GmbH, bbe M. (2012). User Manual - FluoroProbe BBE.

Gonçalves, A.L., Pires, J.C.M., and Simões, M. (2016). The effects of light and temperature on microalgal growth and nutrient removal: an experimental and mathematical approach. *RSC Adv.* 6, 22896–22907.

Gong, R., Xu, L., Wang, D., Li, H., and Xu, J. (2016). Water Quality Modeling for a Typical Urban Lake Based on the EFDC Model. *Environ. Model. Assess.* 21, 643–655.

Gregor, J., and Marsalek, B. (2004). Freshwater phytoplankton quantification by chlorophyll alpha: a comparative study of in vitro, in vivo and in situ methods. *Water Res.* 38, 517–522.

Gregor, J., Geriš, R., Maršálek, B., Heteša, J., and Marvan, P. (2005). In situ Quantification of Phytoplankton in Reservoirs Using a Submersible Spectrofluorometer. *Hydrobiologia* 548, 141–151.

Grimaud, G.M., Mairet, F., Sciandra, A., and Bernard, O. (2017). Modeling the temperature effect on the specific growth rate of phytoplankton: a review. *Rev. Environ. Sci. Biotechnol.* 16, 625–645.

Grimm, N.B., Grove, J.G., Pickett, S.T.A., and Redman, C.L. (2000). Integrated Approaches to Long-Term Studies of Urban Ecological Systems Urban ecological systems present multiple challenges to ecologists—pervasive human impact and extreme heterogeneity of cities, and the need to integrate social and ecological approaches, concepts, and theory. *BioScience* 50, 571–584.

Harris, T.D., and Graham, J.L. (2017). Predicting cyanobacterial abundance, microcystin, and geosmin in a eutrophic drinking-water reservoir using a 14-year dataset. *Lake Reserv. Manag.* 33, 32–48.

Head, E.J.H., and Pepin, P. (2010). Monitoring changes in phytoplankton abundance and composition in the Northwest Atlantic: a comparison of results obtained by continuous plankton recorder sampling and colour satellite imagery. *J. Plankton Res.* 32, 1649–1660.

Hébert, C., Caissie, D., Satish, M.G., and El-Jabi, N. (2015). Predicting Hourly Stream Temperatures Using the Equilibrium Temperature Model. *J. Water Resour. Prot.* 07, 322.

Hitzfeld B C, Höger S J, and Dietrich D R (2000). Cyanobacterial toxins: removal during drinking water treatment, and human risk assessment. *Environ. Health Perspect.* 108, 113–122.

- Ho, J.C., and Michalak, A.M. (2015). Challenges in tracking harmful algal blooms: A synthesis of evidence from Lake Erie. *J. Gt. Lakes Res.* *41*, 317–325.
- Horppila, J., Holmroos, H., Niemistö, J., Massa, I., Nygrén, N., Schönach, P., Tapio, P., and Tammeorg, O. (2017). Variations of internal phosphorus loading and water quality in a hypertrophic lake during 40 years of different management efforts. *Ecol. Eng.* *103*, 264–274.
- Huang, J., Gao, J., Hörmann, G., and Fohrer, N. (2014). Modeling the effects of environmental variables on short-term spatial changes in phytoplankton biomass in a large shallow lake, Lake Taihu. *Environ. Earth Sci.* *72*, 3609–3621.
- Huang, J., Xi, B., Xu, Q., Wang, X., Li, W., He, L., and Liu, H. (2016). Experiment study of the effects of hydrodynamic disturbance on the interaction between the cyanobacterial growth and the nutrients. *J. Hydrodyn. Ser B* *28*, 411–422.
- Huber, V., Wagner, C., Gerten, D., and Adrian, R. (2012). To bloom or not to bloom: contrasting responses of cyanobacteria to recent heat waves explained by critical thresholds of abiotic drivers. *Oecologia* *169*, 245–256.
- Huguenard, L. (2015). *L'ingénierie écologique : une réponse face aux enjeux de l'accueil de public sur une base de loisirs en milieu urbain* (Muséum national d'Histoire naturelle).
- Huisman, J., Matthijs, H.C.P., and Visser, P.M. (2005). *Harmful Cyanobacteria* (Dordrecht (The Netherlands): Aquatic Ecology Series).
- Hutter, K. (1984a). Fundamental equations and approximations. In *Hydrodynamic of Lakes*, (Wien: Springer-Verlag), p. 347.
- Hutter, K. (1984b). Linear gravity waves, Kelvin waves and Poincaré waves, theoretical modelling and observations. In *Hydrodynamic of Lakes*, (Wien: Springer-Verlag), p. 347.
- Ibelings, B.W., Mur, L.R., and Walsby, A.E. (1991). Diurnal changes in buoyancy and vertical distribution in populations of *Microcystis* in two shallow lakes. *J. Plankton Res.* *13*, 419–436.
- Ibelings, B.W., Vonk, M., Los, H.F.J., Molen, D.T. van der, and Mooij, W.M. (2003). Fuzzy modeling of cyanobacterial surface waterblooms: validation with NOAA-AVHRR satellite images. *Ecol. Appl.* *13*, 1456–1472.
- Ibelings, B.W., Backer, L.C., Kardinaal, W.E.A., and Chorus, I. (2015). Current approaches to cyanotoxin risk assessment and risk management around the globe. *Harmful Algae* *49*, 63–74.
- I.D. Eaux (2015). *BASE DE LOISIRS DE CHAMPS SUR MARNE - Suivi physico-chimique et biologique*.
- Idso, S.B. (1973). On the concept of lake stability. *Limnol. Oceanogr.* *18*, 681–683.
- Imberger, J., and Patterson, J.C. (1990). Physical Limnology. In *Advances in Applied Mechanics*, J.W. Hutchinson, and T.Y. Wu, eds. (Elsevier), pp. 303–475.
- Imberger, J., and Petterson, J.C. (1989). Physical Limnology. *Adv. Appl. Mech.* 303–475.

- Ishikawa, K., Kumagai, M., Vincent, W.F., Tsujimura, S., and Nakahara, H. (2002). Transport and accumulation of bloom-forming cyanobacteria in a large, mid-latitude lake: the gyre-Microcystis hypothesis. *Limnology* 3, 87–96.
- Jöhnk, K.D., Huisman, J., Sharples, J., Sommeijer, B., Visser, P.M., and Stroom, J.M. (2008). Summer heatwaves promote blooms of harmful cyanobacteria. *Glob. Change Biol.* 14, 495–512.
- Khac, V.T., Hong, Y., Plec, D.F., Lemaire, B.J., Dubois, P., Saad, M., and Vinçon-Leite, B. (2018). An Automatic Monitoring System for High-Frequency Measuring and Real-Time Management of Cyanobacterial Blooms in Urban Water Bodies. *Processes* 6.
- Kiefer, D.A. (1973). Fluorescence properties of natural phytoplankton populations. *Mar. Biol.* 22, 263–269.
- Kolzau, S., Wiedner, C., Rucker, J., Köhler, J., Köhler, A., and Dolman, A.M. (2014). Seasonal Patterns of Nitrogen and Phosphorus Limitation in Four German Lakes and the Predictability of Limitation Status from Ambient Nutrient Concentrations. *PLOS ONE* 9, e96065.
- Kong, Y., Lou, I., zhang, Y., Lou, C., and Mok, kai (2017). Using an Online Phycocyanin Fluorescence Probe for Rapid Monitoring of Cyanobacteria in Macau Freshwater Reservoir. In *Advances in Monitoring and Modelling Algal Blooms in Freshwater Reservoirs*, (Springer), pp. 45–68.
- Konopka, A. (1982). Buoyancy regulation and vertical migration by *Oscillatoria rubescens* in Crooked Lake, Indiana. *Br. Phycol. J.* 17, 427–442.
- Larocque, I., Mazumder, A., Proulx, M., Lean, D.R., and Pick, F.R. (1996). Sedimentation of algae: relationships with biomass and size distribution. *Can. J. Fish. Aquat. Sci.* 53, 1133–1142.
- Leboulanger, C., Dorigo, U., Jacquet, S., Berre, B.L., Paolini, G., and Humbert, J. (2002). Application of a submersible spectrofluorometer for rapid monitoring of freshwater cyanobacterial blooms: a case study. *Aquat. Microb. Ecol.* 30, 83–89.
- Lee, R.M., and Biggs, T.W. (2015). Impacts of land use, climate variability, and management on thermal structure, anoxia, and transparency in hypereutrophic urban water supply reservoirs. *Hydrobiologia* 745, 263–284.
- León, L.F., Imberger, J., Smith, R.E.H., Hecky, R.E., Lam, D.C.L., and Schertzer, W.M. (2005). Modeling as a Tool for Nutrient Management in Lake Erie: a Hydrodynamics Study. *J. Gt. Lakes Res.* 31, 309–318.
- Leon, L.F., Smith, R.E.H., Hipsey, M.R., Bocaniov, S.A., Higgins, S.N., Hecky, R.E., Antenucci, J.P., Imberger, J.A., and Guildford, S.J. (2011). Application of a 3D hydrodynamic–biological model for seasonal and spatial dynamics of water quality and phytoplankton in Lake Erie. *J. Gt. Lakes Res.* 37, 41–53.
- Li Wei, Qin Boqiang, and Zhu Guangwei (2013). Forecasting short-term cyanobacterial blooms in Lake Taihu, China, using a coupled hydrodynamic–algal biomass model. *Ecohydrology* 7, 794–802.
- Li-Kun, Y., Sen, P., Xin-hua, Z., and Xia, L. (2017). Development of a two-dimensional eutrophication model in an urban lake (China) and the application of uncertainty analysis. *Ecol. Model.* 345, 63–74.



- Liu, X., Zhang, Y., Wang, M., and Zhou, Y. (2014). High-frequency optical measurements in shallow Lake Taihu, China: determining the relationships between hydrodynamic processes and inherent optical properties. *Hydrobiologia* 724, 187–201.
- Los, H. (2009). *Eco-hydrodynamic Modelling of Primary Production in Coastal Waters and Lakes Using BLOOM*. IOS Press.
- Los, F.J., and Brinkman, J.J. (1988). Phytoplankton modelling by means of optimization: a 10-year experience with BLOOM II. *Int. Ver. Theor. Angew. Limnol. Verhandlungen* 23.
- Los, F.J., Villars, M.T., and Van der Tol, M.W.M. (2008). A 3-dimensional primary production model (BLOOM/GEM) and its applications to the (southern) North Sea (coupled physical–chemical–ecological model). *J. Mar. Syst.* 74, 259–294.
- Lou, I., Xie, Z., Ung, W., and Mok, K. (2017). Integrating Support Vector Regression with Particle Swarm Optimization for Numerical Modeling for Algal Blooms of Freshwater. In *Advances in Monitoring and Modelling Algal Blooms in Freshwater Reservoirs*, (Springer), pp. 125–142.
- Lovstedt, C.B., and Bengtsson, L. (2008). Density-driven current between reed belts and open water in a shallow lake. *Water Resour. Res.*
- MacIntyre, H.L., Lawrenz, E., and Richardson, T.L. (2010). Taxonomic Discrimination of Phytoplankton by Spectral Fluorescence. In *Chlorophyll a Fluorescence in Aquatic Sciences: Methods and Applications*, D.J. Suggett, O. Prášil, and M.A. Borowitzka, eds. (Dordrecht: Springer Netherlands), pp. 129–169.
- Mackey, M., Mackey, D., Higgins, H., and Wright, S. (1996). CHEMTAX - a program for estimating class abundances from chemical markers: application to HPLC measurements of phytoplankton. *Mar. Ecol. Prog. Ser.* 144, 265–283.
- Mankin, J.B., O'Neill, R.V., Shugart, H.H., and Rust, B.W. (1975). Importance of validation in ecosystem analysis (Oak Ridge National Lab., Tenn. (USA)).
- Mao, J.Q., Lee, J.H.W., and Choi, K.W. (2009). The extended Kalman filter for forecast of algal bloom dynamics. *Water Res.* 43, 4214–4224.
- Matos, A.C. de S., Lemos, R.S., Silva, T.F. das G., Eleutério, J.C., and Nascimento, N. (2017). Evolução do uso e ocupação do solo em mananciais de abastecimento metropolitano na região metropolitana de Belo Horizonte, Estado de Minas Gerais. 8.
- McMaster, G.S., and Wilhelm, W. (1997). Growing degree-days: one equation, two interpretations. *Publ. USDA-ARS UNL Fac.*
- McQuaid, N., Zamyadi, A., Prevost, M., Bird, D.F., and Dorner, S. (2011). Use of in vivo phycocyanin fluorescence to monitor potential microcystin-producing cyanobacterial biovolume in a drinking water source. *J. Environ. Monit.* 13, 455–463.
- Meinson, P., Idrizaj, A., Noges, P., Noges, T., and Laas, A. (2016). Continuous and high-frequency measurements in limnology: history, applications, and future challenges. *Environ. Rev.* 24, 52–63.

- Melo, L., Sila, T.F. das G., and Vinçon-Leite, B. (2017). Modelagem de reservatório metropolitano destinado à produção de água potável: Uma ferramenta para avaliar os impactos da escassez hídrica sobre a hidrodinâmica de ambientes lênticos. ResearchGate.
- Merel, S., Walker, D., Chicana, R., Snyder, S., Baurès, E., and Thomas, O. (2013). State of knowledge and concerns on cyanobacterial blooms and cyanotoxins. *Environ. Int.* 59, 303–327.
- Mezemat, Y. (2014). Analyse et modélisation multifractale des interactions ondes, turbulence et biologie dans le lac de Créteil. ParisEst.
- Missaghi, S., and Hondzo, M. (2010). Evaluation and application of a three-dimensional water quality model in a shallow lake with complex morphometry. *Ecol. Model.* 221, 1512–1525.
- Missaghi, S., Hondzo, M., Sun, C., and Guala, M. (2016). Influence of fluid motion on growth and vertical distribution of cyanobacterium *Microcystis aeruginosa*. *Aquat. Ecol.* 50, 639–652.
- Monismith, S.G., Imberger, J., and Morison, M.L. (1990). Convective motions in the sidearm of a small reservoir. *Limnol. Oceanogr.* 35, 1676–1702.
- Mooij, W.M., Trolle, D., Jeppesen, E., Arhonditsis, G., Belolipetsky, P.V., Chitamwebwa, D.B.R., Degermendzhy, A.G., DeAngelis, D.L., Domis, L.N.D.S., Downing, A.S., et al. (2010). Challenges and opportunities for integrating lake ecosystem modelling approaches. *Aquat. Ecol.* 44, 633–667.
- Moreno-Ostos, E., Silva, S.L.R. da, Vicente, I. de, and Cruz-Pizarro, L. (2007). Interannual and between-site variability in the occurrence of clear water phases in two shallow Mediterranean lakes. *Aquat. Ecol.* 41, 285–297.
- Mortimer, C.H. (1984). Measurements and models in physical limnology. In *Hydrodynamic of Lakes*, (Wien: Springer-Verlag), p. 347.
- NLA, 2012 (2012). 2012 National Lakes Assessment.
- NOAH (2006). Forecasting Algal blooms in Surface Water Systems with Artificial Neural Networks. FINAL REPORT.
- Nogueira, M.M. (2015). Elaboração da curva chave dos córregos Ressaca e Sarandi utilizando métodos computacionais (UFMG).
- Nortek, A. (2008). User Guide - Aquadopp High Resolution.
- Paerl, H.W., and Otten, T.G. (2016). Duelling ‘CyanoHABs’: unravelling the environmental drivers controlling dominance and succession among diazotrophic and non-N<sub>2</sub>-fixing harmful cyanobacteria. *Environ. Microbiol.* 18, 316–324.
- Pannard, A., Beisner, B.E., Bird, D.F., Braun, J., Planas, D., and Bormans, M. (2011). Recurrent internal waves in a small lake: Potential ecological consequences for metalimnetic phytoplankton populations. *Limnol. Oceanogr. Fluids Environ.* 1, 91–109.
- Parlement européen (2006). Directive Européenne 2006/7/CE du Parlement européen et du Conseil concernant la gestion de la qualité des eaux de baignade et abrogeant la directive 76/160/CEE.

Peiffer, R. (2016). Analyse de la dynamique des cyanobactéries dans un plan d'eau urbain. Master Thesis. Ecole des Ponts ParisTech.

Phlips, E.J., Badylak, S., and Grosskopf, T. (2002). Factors Affecting the Abundance of Phytoplankton in a Restricted Subtropical Lagoon, the Indian River Lagoon, Florida, USA. *Estuar. Coast. Shelf Sci.* *55*, 385–402.

Pinckney, J., Papa, R., and Zingmark, R. (1994). Comparison of high-performance liquid chromatographic, spectrophotometric, and fluorometric methods for determining chlorophyll a concentrations in estuarine sediments. *J. Microbiol. Methods* *19*, 59–66.

PMS (2017). POLÍTICA MUNICIPAL DE SANEAMENTO DE BELO HORIZONTE.

Pobel, D., Robin, J., and Humbert, J.-F. (2011). Influence of sampling strategies on the monitoring of cyanobacteria in shallow lakes: Lessons from a case study in France. *Water Res.* *45*, 1005–1014.

Polli, B.A., Bleninger, T., Polli, B.A., and Bleninger, T. (2019). Comparison of 1D and 3D reservoir heat transport models and temperature effects on mass transport. *RBRH* *24*.

Porat, R., Teltsch, B., Perelman, A., and Dubinsky, Z. (2001). Diel buoyancy changes by the cyanobacterium *Aphanizomenon ovalisporum* from a shallow reservoir. *J. Plankton Res.* *23*, 753–763.

Prakash, S., Atkinson, J.F., and Green, M.L. (2007). A semi-lagrangian study of circulation and transport in Lake Ontario. *J. Gt. Lakes Res.* *33*, 774–790.

Qi, L., Huang, J., Huang, Q., Gao, J., Wang, S., and Guo, Y. (2018). Assessing Aquatic Ecological Health for Lake Poyang, China: Part I Index Development. *Water* *10*, 943.

Qin, B., Li, W., Zhu, G., Zhang, Y., Wu, T., and Gao, G. (2015). Cyanobacterial bloom management through integrated monitoring and forecasting in large shallow eutrophic Lake Taihu (China). *J. Hazard. Mater.* *287*, 356–363.

Raine, R., McDermott, G., Silke, J., Lyons, K., Nolan, G., and Cusack, C. (2010). A simple short range model for the prediction of harmful algal events in the bays of southwestern Ireland. *J. Mar. Syst.* *83*, 150–157.

Read, J.S., Hamilton, D.P., Jones, I.D., Muraoka, K., Winslow, L.A., Kroiss, R., Wu, C.H., and Gaiser, E. (2011). Derivation of lake mixing and stratification indices from high-resolution lake buoy data. *Environ. Model. Softw.* *26*, 1325–1336.

REFCOND (2003). Common implementation strategy for the water framework directive (2000/60/EC) - Guidance Document No 10 - Rivers and Lakes – Typology, Reference Conditions and Classification Systems.

Refsgaard, J.C., and Henriksen, H.J. (2004). Modelling guidelines – terminology and guiding principles. *Adv. Water Reserouces* *27* 71–82.

Reynolds, C. (2006). *The Ecology of Phytoplankton* (Cambridge: Cambridge University Press).

Reynolds, C.S. (1998). What factors influence the species composition of phytoplankton in lakes of different trophic status? *Hydrobiologia* *369*, 11–26.

- Reynolds, C.S., Oliver, R.L., and Walsby, A.E. (1987). Cyanobacterial dominance: The role of buoyancy regulation in dynamic lake environments. *N. Z. J. Mar. Freshw. Res.* *21*, 379–390.
- Richardson, T.L., Lawrenz, E., Pinckney, J.L., Guajardo, R.C., Walker, E.A., Paerl, H.W., and MacIntyre, H.L. (2010). Spectral fluorometric characterization of phytoplankton community composition using the Algae Online Analyser®. *Water Res.* *44*, 2461–2472.
- Rigler, F.H., and Peters, R.H. (1995). *Science and Limnology. Int. Rev. Gesamten Hydrobiol. Hydrogr.* *81*, 182–182.
- Rinke, K., Huber, A.M.R., Kempke, S., Eder, M., Wolf, T., Probst, W.N., and Rothhaupt, K.-O. (2009). Lake-wide distributions of temperature, phytoplankton, zooplankton, and fish in the pelagic zone of a large lake. *Limnol. Oceanogr.* *54*, 1306–1322.
- Robson, B.J. (2014). When do aquatic systems models provide useful predictions, what is changing, and what is next? *Environ. Model. Softw.* *61*, 287–296.
- Rolland, A., Rimet, F., and Jacquet, S. (2010). A 2-year survey of phytoplankton in the Marne Reservoir (France): A case study to validate the use of an in situ spectrofluorometer by comparison with algal taxonomy and chlorophyll a measurements. *Knowl. Manag. Aquat. Ecosyst.* *02*.
- Schönach, P., Tapio, P., Holmroos, H., Horppila, J., Niemistö, J., Nygrén, N.A., Tammeorg, O., and Massa, I. (2017). Persistency of artificial aeration at hypertrophic Lake Tuusulanjärvi: A sociohistorical analysis. *Ambio* *46*, 865–877.
- Scriban, A. (2015). Configuration d'un modèle de prévision de l'évolution à court terme des dynamiques hydrodynamiques et biogéochimiques dans le plan d'eau urbain de Champs-sur-Marne. Mémoire de stage de deuxième année. Agro Paris Tech.
- Sharip, Z., Shah, S.A., Jamin, A., and Jusoh, J. (2018). Assessing the Hydrodynamic Pattern in Different Lakes of Malaysia. *Appl. Water Syst. Manag. Model.*
- Shimoda, Y., and Arhonditsis, G.B. (2016). Phytoplankton functional type modelling: Running before we can walk? A critical evaluation of the current state of knowledge. *Ecol. Model.* *320*, 29–43.
- Silva, T.F. das G. (2014). Suivi et modélisation de la dynamique des cyanobactéries dans les lacs urbains au sein de leur bassin versant. Université Paris-Est and Universidade Federal de Minas Gerais.
- Silva, T., Giani, A., Figueredo, C., Viana, P., Khac, V.T., Lemaire, B.J., Tassin, B., Nascimento, N., and Vinçon-Leite, B. (2016). Comparison of cyanobacteria monitoring methods in a tropical reservoir by in vivo and in situ spectrofluorometry. *Ecol. Eng.* *97*, 79–87.
- Silva, T.F.G., Vinçon-Leite, B., Lemaire, B.J., Petrucci, G., Giani, A., Figueredo, C.C., and Nascimento, N. de O. (2019). Impact of Urban Stormwater Runoff on Cyanobacteria Dynamics in A Tropical Urban Lake. *Water* *11*, 946.
- Simpson, J.H., Lucas, N.S., Powell, B., and Maberly, S.C. (2015). Dissipation and mixing during the onset of stratification in a temperate lake, Windermere. *Limnol. Oceanogr.* *60*, 29–41.
- Siqueira, R.C., Moura, P.M., and Silva, T.F. das G. (2019). Methodology for the construction of an urban flood hazard chart. *RBRH* *24*.

- Smits, J.G.C. (2009). Development of Delft3D-ECO. Calibration for a tropical stratified reservoir. Smits, J.G.C. (Delft Hydraulics).
- Soullignac, F. (2016). Tutoriel Delft3D Léman.
- Soullignac, F., Vinçon-Leite, B., Lemaire B. J., Scarati R, Bonhomme, C., Dubois, P., Mezemate, Y., Tchiguirinskaia I, Schertzer, D., and Tassin B (2017). Performance assessment of a 3D hydrodynamic model using high temporal resolution measurements in a shallow urban lake. *Environ. Model. Assess. in press*.
- Soullignac, F., Danis, P.-A., Bouffard, D., Chanudet, V., Dambrine, E., Guénand, Y., Harmel, T., Ibelings, B.W., Trevisan, D., Uittenbogaard, R., et al. (2018). Using 3D modeling and remote sensing capabilities for a better understanding of spatio-temporal heterogeneities of phytoplankton abundance in large lakes. *J. Gt. Lakes Res.*
- von Sperling, E., and Campos, M.O. (2011). Restoration of Lake Pampulha, Brazil by using sanitation and in-lake techniques.
- Stefan, H.G., and Preud'homme, E.B. (1993). Stream Temperature Estimation from Air Temperature I. *JAWRA J. Am. Water Resour. Assoc.* 29, 27–45.
- Tian, X., Pan, H., Köngäs, P., and Horppila, J. (2017). 3D-modelling of the thermal circumstances of a lake under artificial aeration. *Appl. Water Sci.* 7, 4169–4176.
- Turner Design (2017). User's Manual - Cyclops Submersible Sensor.
- Twiss, M.R. (2011). Variations in chromophoric dissolved organic matter and its influence on the use of pigment-specific fluorimeters in the Great Lakes. *J. Gt. Lakes Res.* 37, 124–131.
- UNESCO (1981). Background papers and supporting data on the practical salinity scale 1978. Unesco/ICES/SCOR/IAPSO Joint Panel on Oceanographic Tables and Standards. UNESCO Tech. Pap. Mar. Sci. Doc. Tech. Unesco Sur Sci. Mer.
- United Nations (2015). The Millennium Development Goals Report 2015.
- USA EPA, O. (2015). Clean Water Laws, Regulations, and Executive Orders related to Section 404.
- USEPA (2009). National Lakes Assessment - A Collaborative Survey of the Nation's Lakes.
- Van Donk, E. (1984). Factors influencing phytoplankton growth and succession in Lake Maarsseveen I. *Hydrobiol. Bull.* 18, 69–71.
- Vilas, M.P., Marti, C.L., Oldham, C.E., and Hipsey, M.R. (2018). Macrophyte-induced thermal stratification in a shallow urban lake promotes conditions suitable for nitrogen-fixing cyanobacteria. *Hydrobiologia* 806, 411–426.
- Vinçon-Leite, B., and Casenave, C. (2019). Modelling eutrophication in lake ecosystems: A review. *Sci. Total Environ.* 651, 2985–3001.
- Vinnå, L.R., Wüest, A., and Bouffard, D. (2017). Physical effects of thermal pollution in lakes. *Water Resour. Res.* 53, 3968–3987.

- Visser, P., Ibelings, B., Veer, B.V.D., Koedood, J., and Mur, R. (1996). Artificial mixing prevents nuisance blooms of the cyanobacterium *Microcystis* in Lake Nieuwe Meer, the Netherlands. *Freshw. Biol.* *36*, 435–450.
- Walsby, A.E., and McAllister, G.K. (1987). Buoyancy regulation by *Microcystis* in Lake Okaro. *N. Z. J. Mar. Freshw. Res.* *21*, 521–524.
- Wang, C., Feng, T., Wang, P., Hou, J., and Qian, J. (2017). Understanding the transport feature of bloom-forming *Microcystis* in a large shallow lake: A new combined hydrodynamic and spatially explicit agent-based modelling approach. *Ecol. Model.* *343*, 25–38.
- Webster, I.T., Jones, G.J., Oliver, R.L., Bormans, M., and Sherman, B.S. (1997). Control strategies for cyanobacterial blooms in weir pools (Canberra, CSIRO Land and Water).
- Welker, M., von Dohren, H., Tauscher, H., Steinberg, C.E.W., and Erhard, M. (2003). Toxic *Microcystis* in shallow lake Muggelsee (Germany) - dynamics, distribution, diversity. *Arch. Hydrobiol.* *157*, 227–248.
- WHO (1998). Guidelines for Drinking-Water Quality - Health Criteria and Other Supporting Information.
- WHO (2003a). Guidelines for safe recreational water environments.
- WHO (2003b). Algae and cyanobacteria in fresh water. In *Guidelines for Drinking-Water Quality*, (World Health Organization), pp. 136–158.
- Wilhelm, J. (2015). What is the difference between Prediction and Forecast?
- Wright, D.A., Sherman, W.M., and Dernbach, A.R. (1991). Carbohydrate feedings before, during, or in combination improve cycling endurance performance. *J. Appl. Physiol. Bethesda Md* *1985* *71*, 1082–1088.
- Wu, T., Qin, B., Zhu, G., Luo, L., Ding, Y., and Bian, G. (2013). Dynamics of cyanobacterial bloom formation during short-term hydrodynamic fluctuation in a large shallow, eutrophic, and wind-exposed Lake Taihu, China. *Environ. Sci. Pollut. Res. Int.* *20*, 8546–8556.
- Wu, T., Qin, B., Brookes, J.D., Shi, K., Zhu, G., Zhu, M., Yan, W., and Wang, Z. (2015). The influence of changes in wind patterns on the areal extension of surface cyanobacterial blooms in a large shallow lake in China. *Sci. Total Environ.* *518–519*, 24–30.
- Wu, X., Kong, F., Chen, Y., Qian, X., Zhang, L., Yu, Y., Zhang, M., and Xing, P. (2010). Horizontal distribution and transport processes of bloom-forming *Microcystis* in a large shallow lake (Taihu, China). *Limnologia* *40*, 8–15.
- Wynne, T.T., Stumpf, R.P., Tomlinson, M.C., Schwab, D.J., Watabayashi, G.Y., and Christensen, J.D. (2011). Estimating cyanobacterial bloom transport by coupling remotely sensed imagery and a hydrodynamic model. *Ecol. Appl. Publ. Ecol. Soc. Am.* *21*, 2709–2721.
- Wynne, T.T., Stumpf, R.P., Tomlinson, M.C., Fahnenstiel, G.L., Dyble, J., Schwab, D.J., and Joshi, S.J. (2013). Evolution of a cyanobacterial bloom forecast system in western Lake Erie: Development and initial evaluation. *J. Gt. Lakes Res.* *39*, 90–99.

- Xu, F.L., Tao, S., Dawson, R.W., Li, P.G., and Cao, J. (2001). Lake ecosystem health assessment: indicators and methods. *Water Res.* 35, 3157–3167.
- Yang, L., Lei, K., Meng, W., Fu, G., and Yan, W. (2013). Temporal and spatial changes in nutrients and chlorophyll- $\alpha$  in a shallow lake, Lake Chaohu, China: An 11-year investigation. *J. Environ. Sci.* 25, 1117–1123.
- Yentsch, C., and Phinney, D. (1985). Spectral Fluorescence - an Ataxonomic Tool for Studying the Structure of Phytoplankton Populations. *J. Plankton Res.* 7, 617–632.
- Yi, X., Zou, R., and Guo, H. (2016). Global sensitivity analysis of a three-dimensional nutrients-algae dynamic model for a large shallow lake. *Ecol. Model.* 327, 74–84.
- Yu, Q., Liu, Z., Chen, Y., Zhu, D., and Li, N. (2018). Modelling the impact of hydrodynamic turbulence on the competition between *Microcystis* and *Chlorella* for light. *Ecol. Model.* 370, 50–58.
- Zamyadi, A., McQuaid, N., Prévost, M., and Dorner, S. (2012). Monitoring of potentially toxic cyanobacteria using an online multi-probe in drinking water sources. *J. Environ. Monit. JEM* 14, 579–588.
- Zamyadi, A., Choo, F., Newcombe, G., Stuetz, R., and Henderson, R.K. (2016). A review of monitoring technologies for real-time management of cyanobacteria: Recent advances and future direction. *Trac-Trends Anal. Chem.* 85, 83–96.
- Zbiciński, I., and Ziemińska-Stolarska, A. (2017). Analysis of factors affecting the ecological status of the large water bodies on the basis of monitoring and integrated 3D models. *E3S Web Conf.* 19, 02009.
- Zhang, W., and Lou, I. (2017). Monitoring and Modeling Algal Blooms. In *Advances in Monitoring and Modelling Algal Blooms in Freshwater Reservoirs. General Principles and a Case Study of Macau*, (Springer), pp. 1–14.
- Zhang, W., Lou, I., Ung, W., Kong, Y., and Mok, K. (2017). Application of PCR and Real-Time PCR for Monitoring Cyanobacteria, *Microcystis* spp. and *Cylindrospermopsis raciborskii*, in Macau Freshwater Reservoir. In *Advances in Monitoring and Modelling Algal Blooms in Freshwater Reservoirs*, (Springer), pp. 69–88.
- Zhao, L., Li, Y., Zou, R., He, B., Zhu, X., Liu, Y., Wang, J., and Zhu, Y. (2013). A three-dimensional water quality modeling approach for exploring the eutrophication responses to load reduction scenarios in Lake Yilong (China). *Environ. Pollut.* 177, 13–21.
- Zohary, T., and Robarts, R.D. (1990). Hyperscums and the population dynamics of *Microcystis aeruginosa*. *J. Plankton Res.* 12, 423–432.

## 8. ANNEX

### 8.1. Specific growth rate of Diatoms, Green and Microcystis

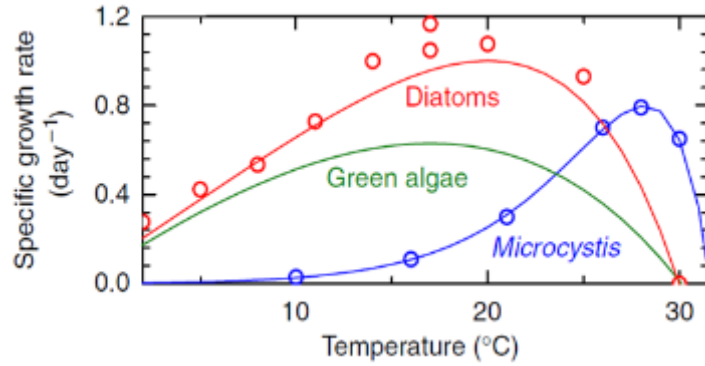


**Figure A1-** Effect of temperature on the maximum specific growth rates of Microcystis (blue line), diatoms (red line), and green algae (green line) representative for Lake Nieuwe Meer. Source: Jöhnk et al., 2008



8.2. Alert levels for toxic cyanobacteria in recreational waters

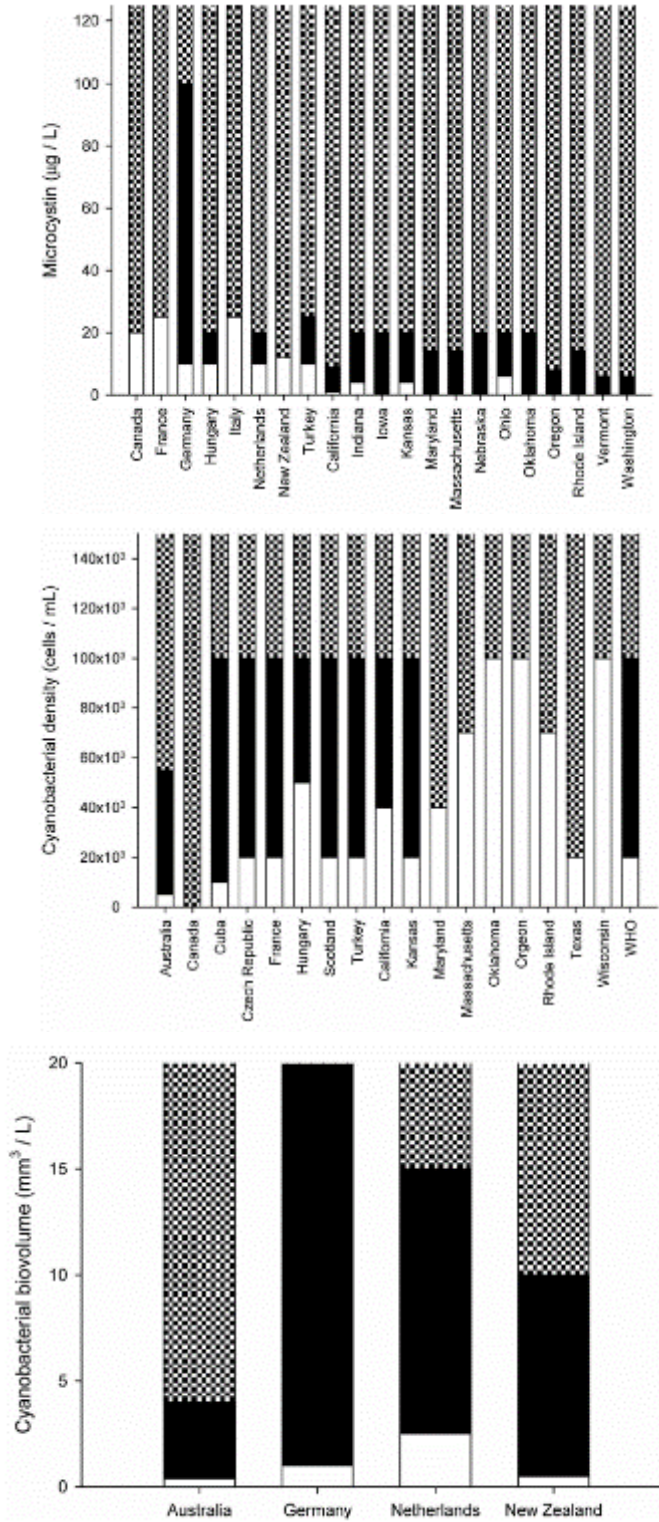


**Figure A2-** Alert levels in recreational waters on basis of microcystins (top panel), cell numbers (middle panel) and biovolume of cyanobacteria (lower panel). White means Surveillance mode, black Alert mode and hatched Action mode. Source: (Ibelings et al., 2015)

### 8.3. Chlorophyll-a treatment

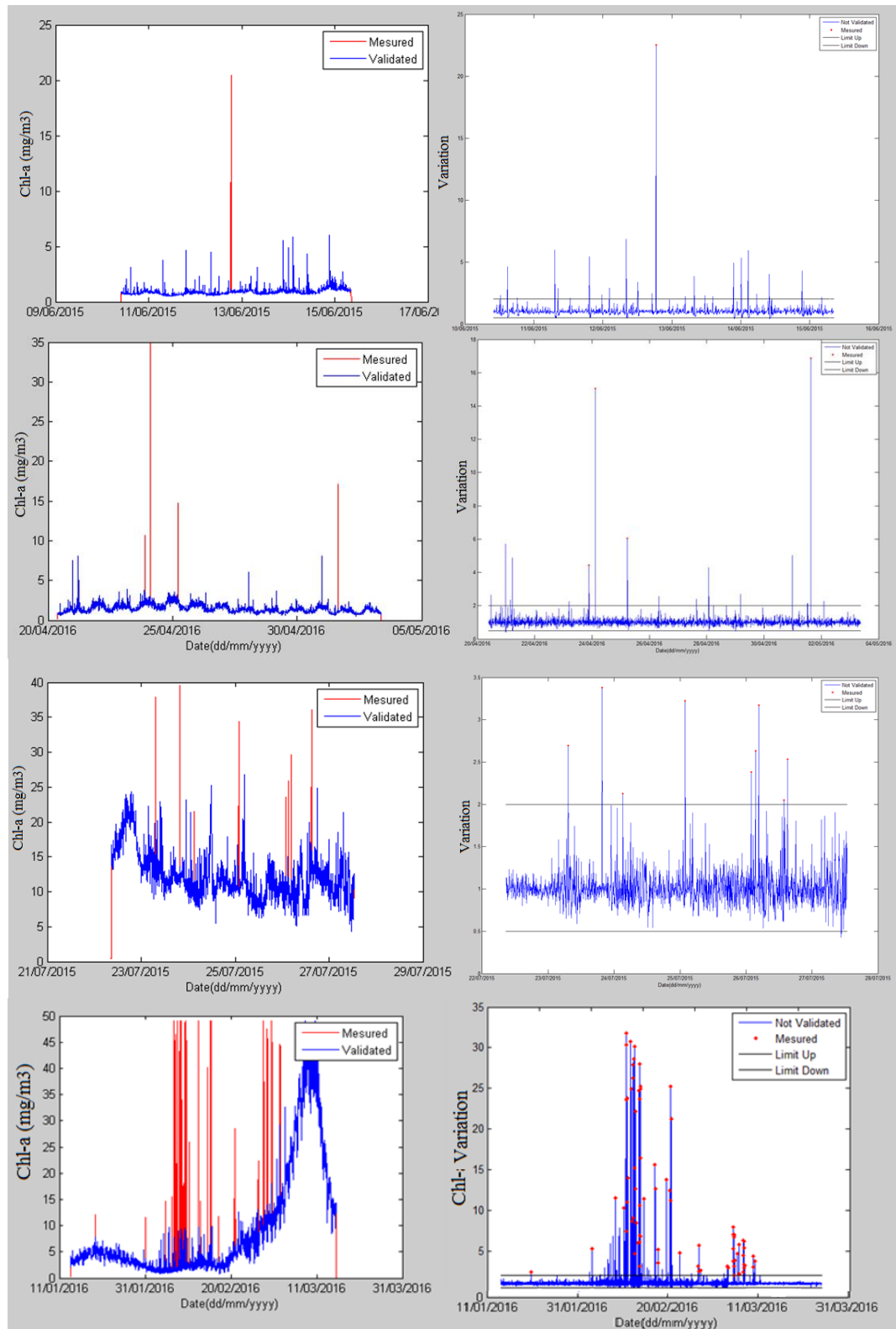


**Figure A3** - Result of data treatment for measurements in Lake of Champs-sur-Marne. Black horizontal lines limit the criterion of valid data. Red lines and point are the inconsiderate data.

#### 8.4. ADCP settings for Lake of Champs-sur-Marne, France

Current time: 19/09/2016 13:14:20

Start at: 19/09/2016 13:17:00

Comment:

point B

-----

Measurement interval (s): 180

Cell size (mm): 50

Orientation: UPLOOKING SHALLOW WATER

Distance to surface (m): 0.40

Pulse distance (m): 2.60

Profile range (m): 2.30

Horas. vel. range (m/s): 0.12

Vert. vel. range (m/s): 0.05

Number of cells: 46

Average interval (s): 30

Blanking distance (m): 0.200

Measurement load (%): 69

Samples per burst: N/A

Sampling rate (Hz): N/A

Compass up. rate (s): 30

Coordinate System: ENU

Speed of sound (m/s): MEASURED

Salinity (ppt): 0

Analog input 1: NONE

Analog input 2: NONE

Analog input power out: DISABLED

File wrapping: OFF

Telltale: OFF

Acoustic modem: OFF

Serial output: OFF

-----  
Assumed duration (days): 30.0

Battery utilization (%): 112.0

Battery level (V): 11.8

Recorder size (MB): 185

Recorder free space (MB): 103.146

Memory required (MB): 8.3

-----  
Instrument ID: AQD 8495

Head ID: ASP 5446

Firmware version: 3.14 HR

-----  
AquaProHR Version 1.09

Copyright (C) Nortek AS

**Deployment Planning** [X]

Standard **Advanced**

**Setup**

Meas/Burst interval (s): 180  Burst sampling

Cell size (mm): 50 Samples: 512

Average interval (s): 30 Rate (Hz): 1

Blanking dist.(m): 0.2 #Beams: 3

Compass upd. rate (s): 30

Measurement load (%): 100 69

Pulse distance (m): 2.6

Extended velocity range

**Deployment planning**

Assumed duration (days): 30

Battery utilization (% of capacity): 112

Number of cells: 46

Profile range (m): 2.3

Horizontal vel. range (m/s): 0.12

Vertical vel. range (m/s): 0.05

Memory required (MB): 8.3

**Data output**

Coordinate system: ENU

File wrapping

**Speed of sound**

Measured  
Salinity (ppt): 0.05

Fixed (m/s): 1525

**Analog inputs**

Input 1: NONE

Input 2: NONE

Output power

Update OK Annuler Appliquer Aide

**Figure A4 - ADCP parameters**

8.5. FluoroProbe parameters

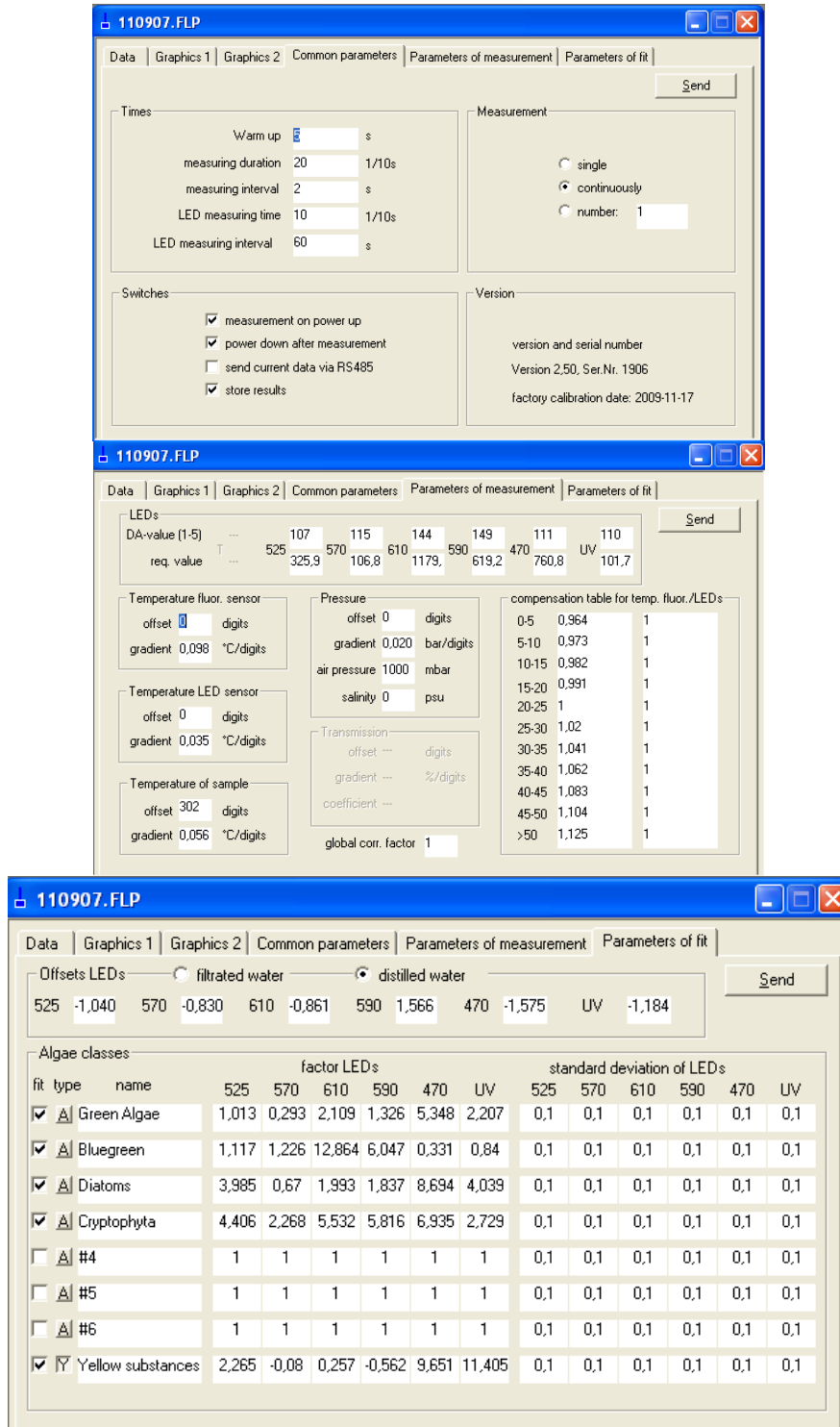


Figure A5 - FluoroProbe parameters

## 8.6. FluoroProbe usage protocol

### 1. Acquisition via l'autostart:

la sonde mesure enregistre les données qui seront lues ultérieurement.

Ce mode permet de ne pas utiliser le PC sur le terrain ainsi que le câble de liaison pendant la mesure.

*Parametrize:*

- Brancher la sonde au câble de 25 m, relier l'autre extrémité du câble au port USB de l'ordinateur via le connecteur en Y.
- Ouvrir le logiciel FluoroProbe.
- Onglet Probe => set up port => COM6 => OK.
- Onglet Probe => test connection. FluoroProbe doit afficher "OK! Probe is ready".
- Onglet Probe => Battery Voltage :  
L'acquisition peut se faire seulement si le voltage est supérieur à 12V .
- Lecture des parameters: Onglet Probe => get data /parameters => parameters only
- Pour changer la fréquence d'acquisition des données, aller dans common parameters. => Measuring interval: changer le temps => send
- Pour effacer les anciennes données: Probe => Delete data  
Mettre 0 si on veut toutes les effacer => Ok.
- Onglet Common parameters. Cocher toutes les cases de switches. => send

*Sur le terrain:*

- Brancher l'autostart à la sonde pour démarrer l'enregistrement.

L'enlever pour arrêter.

Répéter sur les n points de mesure

*Récupération des données de la sonde vers le PC*

- Via connexion entre sonde et PC

- Se connecter à la sonde (faire les 4 1eres étapes du paramétrage)
- Onglet Probe => get data / parameters => data and parameters
- Corriger la pression atmosphérique pour une mesure de la profondeur exacte en utilisant la fonction 'set air pressure' dans le menu
- Sauvegarde Onglet File => save as

- Via USB:

Relier la sonde à la clé USB grâce à l'adaptateur USB. Attendre que la lumière s'allume puis s'éteigne avant de la retirer.

Lire les données sur la clé (classement par date).

## 2. Acquisition directe sur ordinateur

La sonde mesure et envoi en temps réel les données sur le PC

*Paramétrage & terrain:*

- Brancher la sonde au câble de 25 m, relier l'autre extrémité du câble au port USB de l'ordinateur via le raccordur.
- Ouvrir le logiciel FluoroProbe.
- Onglet Probe => set up port => COM6 => OK.
- Onglet Probe => test connection. FluoroProbe doit afficher "OK! Probe is ready". Sinon, vérifier les branchements.
- Onglet Probe => Battery Voltage :  
Voltage > 12V => cliquer sur OK.  
Voltage < 12V => brancher le chargeur entre le câble de 25 m et le raccordur, ainsi qu'au secteur.
- Lecture des parameters: Onglet Probe => get data /parameters => parameters only
- Pour changer la fréquence d'acquisition des données, aller dans common parameters. => Measuring interval: changer le temps => send
- Vérifier dans l'onglet common parameters que seuls les deux derniers switches sont cochés. Sinon les modifier => send
- Onglet Probe => Start measurement. Une fenêtre apparait, ne rien toucher.
- Se placer sur l'onglet data pour voir les relevés
- Onglet Probe => Stop measurement.
- Sauvegarde Onglet File => save as

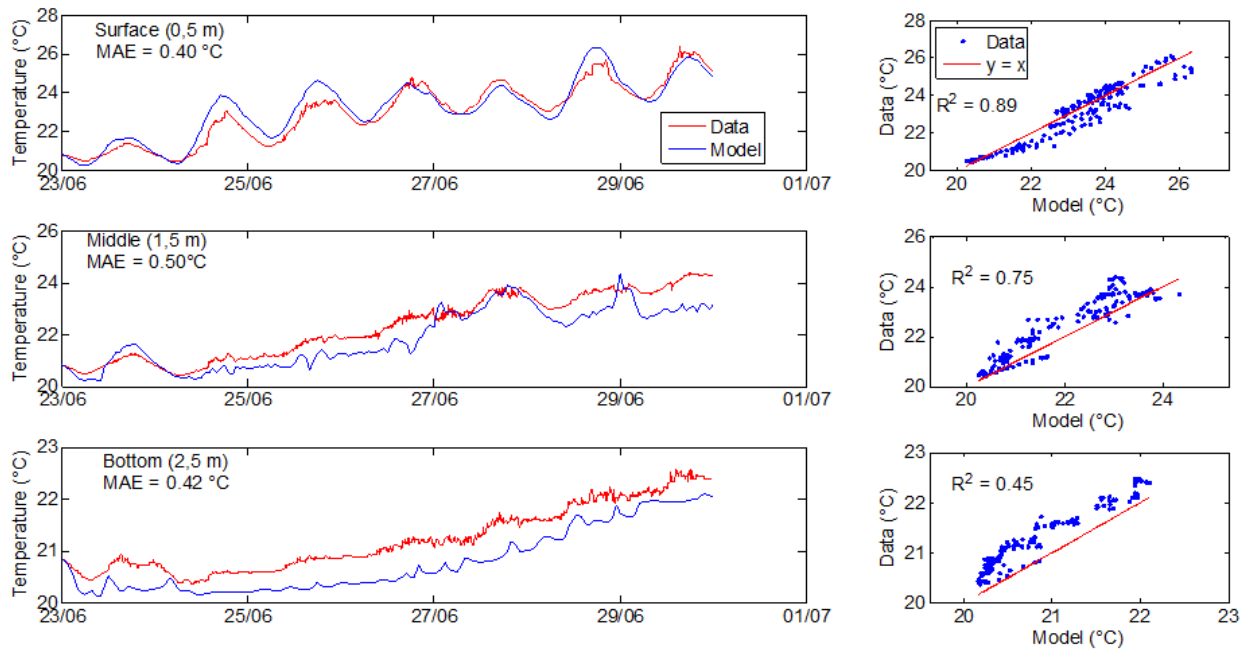


## 8.7. FluoroProbe Specifications

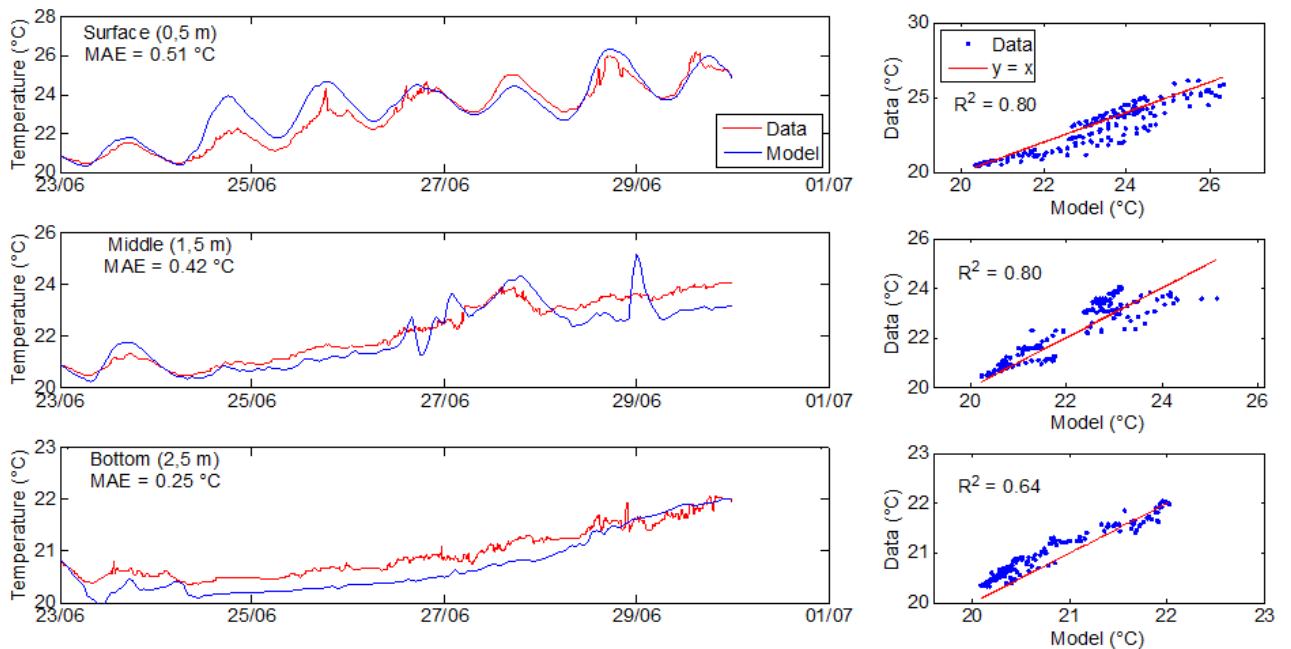
Specifications	
FluoroProbe	
Measurands	total chlorophyll [ $\mu\text{g chl-a/l}$ ]
Chlorophyll	0 - 200 $\mu\text{g chl-a/l}$
Measurement procedure	spectral fluorometry
Resolution	0.05 $\mu\text{g chl-a/l}$
Transmission	0 - 100%
Water temperature	-2 - +40°C
Housing material	reinforced carbon fibre/V4A steel
Weight	4.5 kg
Dimensions (H x D)	450 x 140 mm
Voltage	12 V
Battery capacity	3900 mAh
Operating time	10 h - 30 days
Memory capacity	2 million datasets
Interface	RS485/ RS232 modem (optional)
Maximum diving depth	0 - 100 m 0 - 300 m (extended range 1) 0 - 1000 m (extended range 2)
Options	Workstation 25 (cuvette device) transmission measurement, temperature measurement instrument for benthic algae PDA with software 2, 10, 20, 30, 50, 70, 100 m cables Flow-Through Unit Hydro-Wiper Protective Cage

Figure A6 – FluoroProbe Specifications Source: (BBE, 2012)

## 8.8. Results of the hydrodynamic model



**Figure A7** - Measured and simulated temperature during 23/06/2015 to 30/06/2015 for Point B in Lake of Champs-sur-Marne



**Figure A8** - Measured and simulated temperature during 23/06/2015 to 30/06/2015 for Point C in Lake of Champs-sur-Marne

## **8.9. Paper Accepted in RBRHR**

**THERMAL FUNCTIONING OF A TROPICAL RESERVOIR ASSESSED  
THROUGH THREE-DIMENSIONAL MODELLING AND HIGH-FREQUENCY  
MONITORING**

**Denis Furstenau PLEC<sup>(1)</sup>, Talita Fernanda das Graças SILVA<sup>(2)</sup>, Brigitte VINÇON-LEITE<sup>(3)</sup>, Nilo NASCIMENTO<sup>(4)</sup>**

<sup>(1)</sup> *Department of Hydraulic and Water Resources, Universidade Federal de Minas Gerais, 6627 av. Antônio Carlos, CEP 31270-901 Belo Horizonte, Minas Gerais, Brasil, and LEESU, Ecole des Ponts ParisTech, Univ Paris Est Creteil, Marne-la-Vallée, France, [denis.plec@gmail.com](mailto:denis.plec@gmail.com) – ORCID: 0000-0002-0452-996X*

<sup>(2)</sup> *Department of Hydraulic and Water Resources, Universidade Federal de Minas Gerais, 6627 av. Antônio Carlos, CEP 31270-901 Belo Horizonte, Minas Gerais, Brasil, [talita.silva@ehr.ufmg.br](mailto:talita.silva@ehr.ufmg.br) – ORCID: 0000-0002-4061-9639*

<sup>(3)</sup> *LEESU, Ecole des Ponts ParisTech, Univ Paris Est Creteil, Marne-la-Vallée, France, [b.vincon-leite@enpc.fr](mailto:b.vincon-leite@enpc.fr) – ORCID: 0000-0002-0190-0209*

<sup>(4)</sup> *Department of Hydraulic and Water Resources, Universidade Federal de Minas Gerais, 6627 av. Antônio Carlos, CEP 31270-901 Belo Horizonte, Minas Gerais, Brasil, [niloon@ehr.ufmg.br](mailto:niloon@ehr.ufmg.br) – ORCID: 0000-0002-1212-2000*

**ABSTRACT**

Urban lakes and reservoirs provide important ecosystem services. However, their water quality is being affected by anthropogenic pressures. The thermal regime is a strong driver of the vertical transport of nutrients, phytoplankton and oxygen. Thermal stratification can modify biogeochemical processes. In this paper, a three-dimensional hydrodynamic model was implemented and validated with high-frequency measurement of water temperature. The simulation results were in agreement with the measurements. For all simulation period, the model performance was evaluated based on hourly values, presenting a maximum RMSE of 0.65°C and Relative Error of 2.08%. The results show that high-frequency measurement associated with a three-dimensional model could help to understand and identify the reasons for the changes in the thermal condition of a shallow urban lake. The impact of the stream inflow on the temperature was highlighted, showing that during higher discharge events, when the river temperature is colder than the lake water, it flows into the lake deeper layers. The inflow water sank to the deeper layers where the lake morphology changes. The model showed an impact along the entire lake, showing the importance of monitoring the inflow water temperature. This modelling tool could be further used to study specific patterns of reservoir hydrodynamics.

**Keywords:** Reservoir hydrodynamics; Thermal regime; Lake Pampulha, 3D hydrodynamic model.

**COMPORTAMENTO TÉRMICO EM UM LAGO TROPICAL URBANO  
AVALIADO POR MODELAGEM TRIDIMENSIONAL E MONITORAMENTO  
EM ALTA FREQUÊNCIA**

**RESUMO**

Lagos e reservatórios urbanos fornecem importantes serviços ecossistêmicos. Porém, a qualidade da água está sendo afetada por diversas pressões antrópicas. O regime térmico é de particular importância no transporte vertical de nutrientes, fitoplâncton e oxigênio. A estratificação térmica dos reservatórios pode modificar processos biogeoquímicos. Nesse artigo, um modelo hidrodinâmico tridimensional foi implementado e validado com medição de temperatura da água em alta frequência. Os resultados das simulações ficaram de acordo com os dados medidos. Para todos os períodos simulados, o desempenho

do modelo foi avaliado com base em valores horários, apresentando raiz quadrada do erro quadrático médio de  $0,65^{\circ}\text{C}$  e erro relativo de  $2,08\%$ . Os resultados mostram que as medições de alta frequência associada ao modelo tridimensional ajudaram a compreender e identificar as causas das alterações na condição térmica de um lago urbano raso. O impacto de uma vazão afluyente na temperatura do reservatório foi evidenciado, mostrando que durante eventos de grandes vazões, quando a temperatura do rio é mais fria que a temperatura do lago, ocorre o escoamento desta vazão pelas camadas mais profundas. A vazão afluyente submerge para camadas mais profundas onde a morfologia do lago se altera. O modelo mostrou um impacto por todo o lago, mostrando assim a importância de monitorar a temperatura da água afluyente. Essa ferramenta numérica poderá ser futuramente utilizada para estudos sobre padrões específicos hidrodinâmicos do reservatório.

**Palavras-chaves:** Hidrodinâmica de reservatórios, regime térmico, Lagoa da Pampulha, modelo hidrodinâmico tridimensional.

---

## INTRODUCTION

In urban areas, lakes and reservoirs provide many ecosystem services. Environmental changes at a local scale, within their watersheds, and at a global scale are affecting the water quality and ecological functioning of urban lakes (Birch and McCaskie, 1999; Friese et al., 2010; Li-Kun et al., 2017), resulting in an increase in phytoplankton biomass and the occurrence of potentially toxic cyanobacteria blooms (Davidson et al., 2016; Ho and Michalak, 2015; Jöhnk et al., 2008; Whyte et al., 2014).

In lake ecosystems thermal stratification and a longer residence time of the water can boost the phytoplankton production (Jöhnk et al., 2008). Thermal stratification is of particular significance in regulating the vertical transport of nutrients, phytoplankton, and oxygen (Boegman et al., 2003; Gonçalves et al., 2016; Grimaud et al., 2017; Simpson et al., 2015). Water temperature impacts phytoplankton succession and community composition (Elliott, 2012; Grimaud et al., 2017; Jöhnk et al., 2008; Philips et al., 2002; Reynolds, 1998; Van Donk, 1984; Vinçon-Leite and Casenave, 2019). Wu et al. (2013) highlighted the need to investigate the influence of short-term hydrodynamics on cyanobacteria in shallow lakes, as the complex cyanobacteria motion in natural water bodies is poorly understood. Thus, understanding hydrodynamics and its interference on water quality bears great importance and needs to be investigated (Li-Kun et al., 2017; Qin et al., 2015; Wu et al., 2015; Zbiciński and Ziemińska-Stolarska, 2017).

Most urban lakes are medium-size and shallow (Birch and McCaskie, 1999; Gong et al., 2016). They may react strongly and rapidly to external hydrological and meteorological forcing, presenting many alternation periods of thermal stratification and mixing. Thus, high-frequency measurements are necessary to capture transient changes and to help understanding the relationship between factors that may impact ecological status. However, high-frequency monitoring is rarely used, especially in urban lakes in tropical regions.

Due to the complex interplay between ecological and hydrodynamic processes in lakes, with high heterogeneity in space and time, three-dimensional models help in better understanding the processes involved (Gong et al., 2016; Soullignac et al., 2017, 2018; Zbiciński and Ziemińska-Stolarska, 2017). Usually in hydrodynamic three-dimensional models, hydrodynamic processes are represented in a sub-model that provides water temperature and velocity in time and space to an ecological sub-model. Three-dimensional models are increasingly implemented to better understand the lake ecosystem response to external pressures, like climate forcing, nutrient loading, and pollutant input (Aparicio Medrano et al., 2013; Chanudet et al., 2012; Soullignac et al., 2018; Vinçon-Leite and Casenave, 2019; Yi et al., 2016). However, the use of three-dimensional modelling in urban lakes is much less reported (Soullignac et al., 2017), especially in tropical water bodies which are subjected to distinct conditions of external forcing and may present different responses compared to temperate water bodies. Furthermore, the use of high-frequency measurements in three-dimensional modelling studies in

urban lakes is rarely found. Chanudet et al. (2012) used a three-dimensional model with high-frequency water temperature measurements in the shallow Nam Theun 2 Reservoir (Laos). However, the authors obtained high errors between simulated and measurement values in the reservoir deepest layer, especially during strong thermal stratification events. Soullignac et al. (2017) used three-dimensional model with high-frequency water temperature measurements in the shallow Lake Créteil (France). The authors could well represent the water temperature dynamics over all depths. Jin et al. (2000) used three-dimensional model with high-frequency water temperature measurements in the shallow Lake Okeechobee (USA). The authors obtained a considerable root mean square error of water temperature of 9.18%. Jin et al. (2000) highlighted the wind-induced wave and sediment deposition/resuspension. However, none of them highlighted the impact of the inflow water temperature. Belico (2017) used a unidimensional model in the lake Pampulha (study site of the present article). The one-dimensional model could not rightly simulate the temperature in the deeper layers of the lake. Other modelling studies were previously applied to Lake Pampulha (Silva, 2014; Silva et al., 2016, 2019) however, none of them used three-dimensional modelling with high-frequency measurement in different depths.

This paper presents a rare application of three-dimensional modelling and water temperature high-frequency measurements in a shallow and medium-size tropical urban lake using hourly meteorological and inflow data. The main objective of this study is to associate high frequency measurements and three-dimensional hydrodynamic modelling in order to investigate the influence, during thermal stratification periods, of inflow water discharge and temperature and lake morphology on the lake thermal behaviour.

## MATERIALS AND METHODS

### Study site

Lake Pampulha is a reservoir located in Belo Horizonte, a city with 2.5 million inhabitants (IBGE, 2014) in the southeast of Brazil. Lake Pampulha and its modern urban ensemble, was designed by the architect Oscar Niemeyer and built in the 1940s. The climate characteristics of the lake region are of tropical altitude type (CPRM, 2001) and summarized in Table 8. Dry season occurs from April to September. Annual mean inflow in Lake Pampulha is 1.30 m<sup>3</sup>/s and 2-years return period inflow is 106.7 m<sup>3</sup>/s (Campos, 2004, Table 9).

Located at an altitude of 801m, Lake Pampulha has a surface area of approximately 2.0 km<sup>2</sup> and a volume of about 10 million m<sup>3</sup> at 801 m (spillway crest) with a residence time of 89 days (considering the annual mean inflow). The lake is a shallow reservoir with a maximum depth of 16 m and an average depth of 5 m. The lake has a polymictic thermal regime, in which the thermal stratification of the water column during a few days alternates with mixing episodes. Lake Pampulha catchment,

composed of 8 main tributaries, has a surface area of about 98 km<sup>2</sup> (CPRM, 2001), with more than 70% urbanised (Matos et al., 2017) and approximately 500,000 inhabitants. Lake Pampulha was built for many purposes, including drinking water supply. However, due to an intense urbanisation process in the lake catchment from the 1970s on, the lake water quality was severely compromised resulting in a hypereutrophic reservoir, leading to the interruption of drinking water provision from the 1980s, with frequent cyanobacteria blooms (Silva, 2014) and presenting a hypoxia condition at the bottom of the lake (Friese et al., 2010; von Sperling and Campos, 2011).

In 2016, the lake has become a UNESCO World Heritage site, which boosted public sector to seek for water quality improvement actions. The municipality of Belo Horizonte (PBH) committed to invest about R\$ 30 million to recover the water quality of Lake Pampulha over 12 months, starting from March 2016 (Diário Oficial do Município, 2016). Phoslock® and Enzilimp® were applied in the lake in order to remove phosphorus from the water column and to reduce coliforms and the Biochemical Oxygen Demand – BOD (Barçante et al., 2020). The treatment was renewed for another year at the cost of about R\$ 16 million. Efforts to improve sanitation infrastructure in the Pampulha catchment were also carried out aiming at collecting 95% of sewage at an investment of R\$ 875 million from 2004 to 2016 (PMS, 2017).

### Available data

Concerning the lake water inflow, since 2011 monitoring stations integrate a Hydrological Monitoring System (Figure 42) operated by PBH (Siqueira et al., 2019). Monitoring stations are present only on the two main tributaries, Sarandi stream (station SAR18F, 2.8 km upstream the lake), located at 19° 52' 01" south and 44° 0' 33" west and Ressaca stream (station RES17F, 2.0 km upstream the lake), located at 19° 52' 11" south and 43° 59' 57" west. These streams represent 70% of the reservoir inflow (CPRM, 2001). These stations measure water level. Nogueira (2015) determined the rating curves, i.e. the water level x discharge relationship, for both streams at the monitoring stations. In this study, the rating curves were used to obtain the inflow data from water level measurements during the simulation period. The other tributaries are not monitored. Thus, time series of the inflow discharges were estimated by multiplying the inflow time series of the reference stations by the ratio of each tributary

catchment area divided by the catchment area of the reference stations.

Inflow water temperature was monitored for a short period of two months (April and May 2013) downstream the confluence of Ressaca and Sarandi streams (Silva et al., 2016). In this research we used hourly water inflow temperature. Two methods to estimate hourly water inflow temperature were evaluated. The first one was a linear regression with air temperature, used in previous studies (Chen and Fang, 2015; Hébert et al., 2015; Stefan and Preud'homme, 1993). The second method was the Modified Sine and Sinusoidal Wave Functions Model (MSSWF), proposed by Chen and Fang (2016).

Hourly meteorological data (air temperature, air humidity, wind intensity and direction, and cumulative hourly solar radiation and precipitation) were provided by the National Institute of Meteorology of Brazil (INMET) and used as uniform values in the computation domain. The nearest automatic weather station (a521) is located inside the campus of the *Universidade Federal de Minas Gerais* at 19° 53' 02" south and 43° 58' 10" west, about 3 km from Lake Pampulha (Figure 42). The cloud coverage data are recorded at the meteorological station named Belo Horizonte (83587), located at 19° 56' 04" south and 43° 59' 43" west, 9.5 km from Lake Pampulha (Figure 42). This station provides nebulosity data three times a day (0h, 12h, and 18h) and these values were linearly interpolated to hourly values for simulation.

The most recent Lake Pampulha bathymetry was measured by PBH in November 2014. Based on the bathymetry data (Figure 43), the reservoir can be divided into four regions: (i) the upstream channel of Ressaca and Sarandi streams, (ii) an upstream very shallow region (about 1.5 m depth), (iii) a transition region, where the depth varies from 1.5 m to almost 13 m, and (iv) a deeper region further downstream. The inflow channel of the Ressaca and Sarandi streams was represented as thin dams in the model. In Delft3D-Flow, thin dams are infinitely thin and defined on the edges of elements. They prevent flow exchange between the two contiguous computational cells keeping the total wet surface and the volume of the model (Deltares, 2014). At station P<sub>1</sub> (10 m depth, Figure 42), located at 19° 51' 5" south and 43° 58' 35" west, high-frequency water temperature monitoring (Table 10) was performed at the surface (0.5 m) at a time step of 30 minutes and at 2.5 m, 5.5 m and 9.5 m depth at a 1-hour time step in 2015 and 2016 (monitoring performed within MAPLU-2 research project). Water transparency was measured using a Secchi Disk at a monthly frequency.

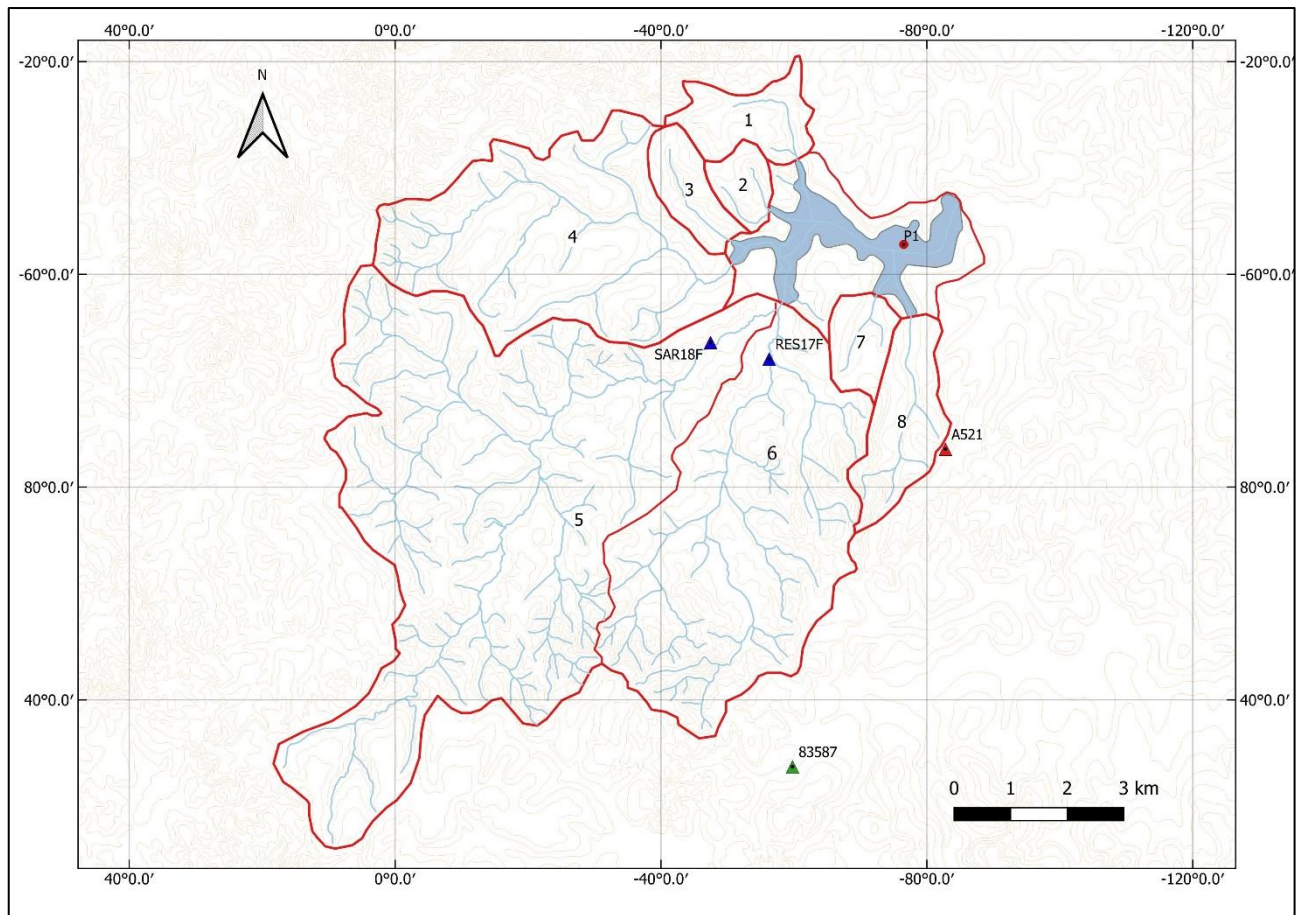


**Figure 42** – Location of Lake Pampulha and its tributaries: (1) Olhos d’água; (2) AABB\*; (3) Bráunas; (4) Água Funda; (5) Sarandi; (6) Ressaca; (7) Tijuco and (8) Mergulhão. \*river not named, popularly known as AABB (*Associação Atlética Banco do Brasil* – Athletics Association from Brazil Bank). Red lines indicate the respective catchment of the tributaries. Monitoring station in triangle: (1) Fluviometric (SAR18F – Sarandi and RES17F – Ressaca; (2) Meteorological station (A521 -UFMG and 83587 - Belo Horizonte); (3) Lake monitoring (P1, red dot).



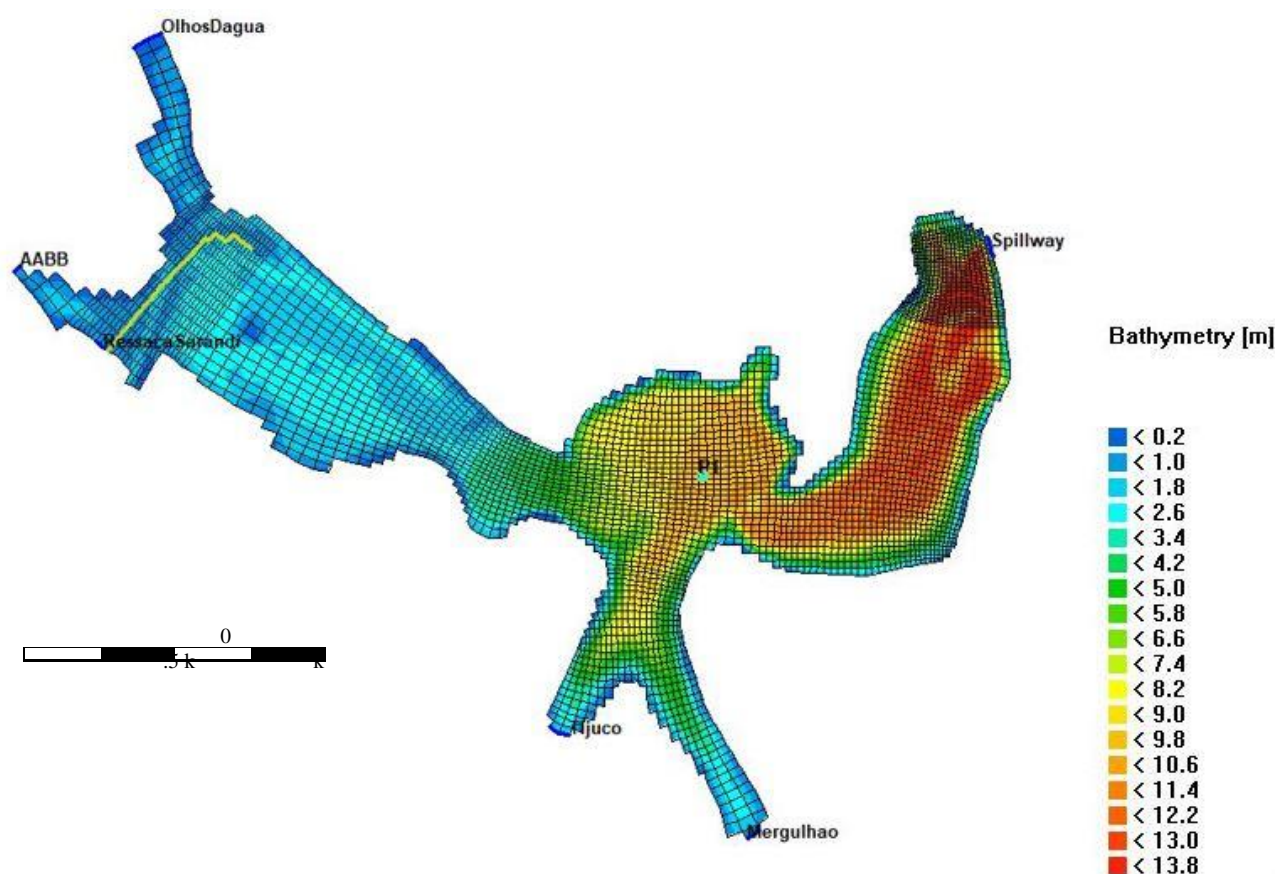


**Figure 43** – Lake Pampulha bathymetry, inflow location, thin dam location (yellow line), monitoring point (P1 – cyan cross) and spillway and inflow locations (blue lines).

**Table 8** – Lake Pampulha climate characteristics measured between 1961 and 2001 at Belo Horizonte’s INMET meteorological station. Source: (CPRM, 2001)

Climate	Tropical altitude
Air temperature	Monthly maximum of 28.8 °C (February) Monthly minimum of 13.1 °C (July)
Dry season	April to September (monthly minimum 14 mm)
Rainfall season	October to March (monthly maximum 320 mm)

**Table 9** – Lake Pampulha discharge frequency. Source: (Campos, 2004)

Return Period	Discharge (m <sup>3</sup> /s)
Annual mean flow	1.30
2 years	106.7
10 years	172.0
50 years	234.0
100 year	261.0

**Table 10** – Characteristics of measuring devices at Lake Pampulha P1 station

Variable	Sensor manufacturer	Monitoring Depth	Monitoring period	Frequency	Measuring Range	Sensor Resolution	Measuring Precision
Water Temperature	NKE	0.5 m	05/2015 to 06/2016	1 hour	-5 °C to +35 °C	0.05 °C	0.020 °C at 20 °C
		2.5, 5.5, 9.5	02/2016 to 06/2016	1 hour			

incident atmospheric radiation ( $Q_{an}$ ) is the effective back radiation, computed by the Equation 3.

$$Q_{eb} = Q_{br} - Q_{an} = 5.58 * 10^{-8} T_s^4 * (0.39 - 0.05 \sqrt{e_a}) * (1 - 0.6 F_c^2) \quad (68)$$

## Hydrodynamic modelling

The three-dimensional hydrodynamic model Delft3D-Flow was used. It solves in three dimensions the Reynolds Averaged Navier-Stokes (RANS) equations for an incompressible fluid, under the shallow water and the Boussinesq assumptions. In the vertical, a hydrostatic pressure equation is considered, and the velocities are computed from the continuity equation. The k- $\epsilon$  model, a second-order turbulence closure model was chosen. The model computes the horizontal and vertical turbulent coefficient by transport equation for the turbulent kinetic energy and kinetic energy dissipation based in Kolmogorov and Prandtl concept. A full description can be found in Deltares (2014) section 9.4.2.

Hourly data of water temperature were used to calibrate the parameters of the heat exchange module included in the three-dimensional model. Thus, the heat exchange main equations (Deltares, 2014), will be presented. In the model, the heat exchange module is named as "Ocean". The heat exchange at the free surface is considered as resulting from the separate effects of solar (short wave) and atmospheric (longwave) radiation, and heat loss, represented in terms of back radiation, evaporation and convection. The total heat flux ( $Q_{tot}$ ) through the free surface is calculated according to Equation 1.

$$Q_{tot} = Q_{sn} + Q_{an} - Q_{br} - Q_{ev} - Q_{co} \quad (66)$$

where  $Q_{sn}$  = net incident solar radiation ( $J/m^2.s$ ) (short wave),  $Q_{an}$  = net incident atmospheric radiation ( $J/m^2.s$ ) (long wave),  $Q_{br}$  = back radiation ( $J/m^2.s$ ) (long wave),  $Q_{ev}$  = evaporative heat flux ( $J/m^2.s$ ) (latent heat),  $Q_{co}$  = convective heat flux ( $J/m^2.s$ ) (sensible heat).

The net incident solar radiation flux ( $Q_{sn}$ ) that will reach water surface is calculated as a function of short wave radiation for a clear sky condition, in which a part is reflected by the water surface (surface Albedo) and the magnitude is reduced by cloud cover (Equation 2).

$$Q_{sn} = (1 - \alpha) Q_{sc} * (1 - 0.4 F_c - 0.38 F_c^2) \quad (67)$$

Where  $\alpha$  is the albedo reflection coefficient (dimensionless),  $Q_{sc}$  is the solar radiation for a clear sky condition ( $J/m^2.s$ ) and  $F_c$  is the sky clouds that cover the sky (%). The albedo coefficient used was 0,06 (default value) and the time series of solar radiation and cloud cover are input data.

Concerning the long wave radiations, the difference between the back radiation ( $Q_{br}$ ) and the net

where  $T_s$  is the water surface temperature ( $^{\circ}C$ ) and  $e_a$  is the vapour pressure (mbar).

Not all the radiation is absorbed at the water surface. A portion is transmitted to deeper water. The absorption of radiation in the water column is calculated by an exponential decay function (Lambert-Beer law). The evaporative heat flux ( $Q_{ev}$ ) is composed by a forced convection term ( $Q_{ev,forced}$ ), caused by wind, and by a free convection term ( $Q_{ev,free}$ ), due to buoyant forces from density differences between air and water (Equation 4).

$$Q_{ev} = Q_{ev,forced} + Q_{ev,free} \quad (69)$$

The forced convection of latent heat is calculated according Equation 5.

$$Q_{ev,forced} = L_v \rho_a f(U_{10}) \{q_s(T_s) - q_a(T_a)\} \quad (70)$$

where  $L_v$  is the latent heat of vaporisation ( $J/kg$ ),  $\rho_a$  is the air density ( $kg/m^3$ ),  $q_s$  (dimensionless) and  $q_a$  (dimensionless) are the specific humidity of respectively saturated air and remote air (10 m above water level),  $T_s$  is the water surface temperature ( $^{\circ}C$ ),  $T_a$  is the air temperature ( $^{\circ}C$ ) and  $f(U_{10})$  is the wind ( $m/s$ ) function (Equation 6).

$$f(U_{10}) = c_e U_{10} \quad (71)$$

where  $c_e$  is the Dalton number (dimensionless) and  $U_{10}$  is the wind velocity ( $m/s$ ) measured at 10 m height.

The free convection of latent heat is calculated according Equation 7.

$$Q_{ev,free} = \left[ 0.14 \left\{ \frac{g \theta_{air}^2}{0.7^2 \rho_a} \right\} (\rho_{a10} - \rho_{a0}) \right]^{1/3} \bar{\rho}_a L_v (q_s(T_s) - q_a(T_a)) \quad (72)$$

The convective heat flux (sensible heat), is also composed by a forced (Equation 8) and free term (Equation 9).

$$Q_{co,forced} = \rho_a c_p c_H U_{10} (T_s - T_a) \quad (73)$$

Where  $\rho_a$  is the air density ( $kg/m^3$ ),  $c_p$  is the specific heat of air ( $0.24 \text{ cal}/(g \text{ } ^{\circ}C)$ ),  $c_H$  is the Stanton number (dimensionless) and  $U_{10}$  is the wind velocity ( $m/s$ ) measured at 10 m height.

$$Q_{co,free} = \left[ 0.14 \left\{ \frac{g \vartheta_{air}^2}{0.7^2 \bar{\rho}_a} \right\} (\rho_{a10} - \rho_{a0}) \right]^{1/3} \bar{\rho}_a c_p (T_s - T_a) \quad (74)$$

where  $g$  is the acceleration of gravity ( $m/s^2$ ),  $\vartheta_{air}$  is the air viscosity ( $m^2/s$ ),  $\rho_{a0}$  is the saturated air density ( $kg/m^3$ ),  $\rho_{a10}$  is the remote air density (10 m above water level) ( $kg/m^3$ ),  $\bar{\rho}_a$  is the average air density ( $kg/m^3$ ),  $c_p$  is the specific heat of air ( $J/(kgC)$ ).

Wind intensity and direction measurements, used as uniform in the computation domain (spatial variations of wind speed were not considered), are carried out 10 m above the ground. Therefore, for the wind at lake surface ( $U_{Lake\ surface}$ ) an evaluation of a correction factor ( $k$ ) of wind intensity was applied (Equation 10). Wind factor values were tested in a range of 40% higher and 40% lower than measured values, varying by 20% for each simulation. According Jöhnk et al. (2008), due to lake geometry and variability of terrain roughness between the lake and the meteorologic station, the wind intensity required to be calibrated. Dalton coefficient, Stanton coefficient, horizontal viscosity and diffusivity were also estimated during the model calibration. Table 11 present the range values tested.

$$U_{Lake\ surface} = U_{10} * k \quad (75)$$

### Model setup

The model requires a computation domain and the specification of boundary and initial conditions. Lake Pampulha was discretized in ten vertical layers and 4019 horizontal grid elements (40190 elements in total). The mesh size varies from 50x20 to 10x10 m (Figure 43). Near the dam and Ressaca and Sarandi inflow the mesh was refined to account for likely higher water current velocities due to inflow and outflow regions.

Bathymetry of Lake Pampulha (Figure 43) greatly varies from upstream to downstream. During calibration of the hydrodynamic model the  $\sigma$ -grid and Z-grid options were used to compare the model performance and the influence of the grid type. The Z-grid option does not change the thickness of each vertical layers, which may help to represent the thermocline depth and water stratification. The  $\sigma$ -grid option has the advantage to preserve the number of active layers along the whole grid. Thus, in the shallower part of the lake the vertical resolution was higher (0.15 cm). At monitoring point P1, the Z-grid and  $\sigma$ -grid were very close, with 1-m thickness vertical layers (Figure 44). The  $\sigma$ -grid option allows to analyse the hydrodynamics at the lake bottom in a same layer in continuity. Otherwise, using the Z-grid option the bottom of the lake would be represented in different layers.

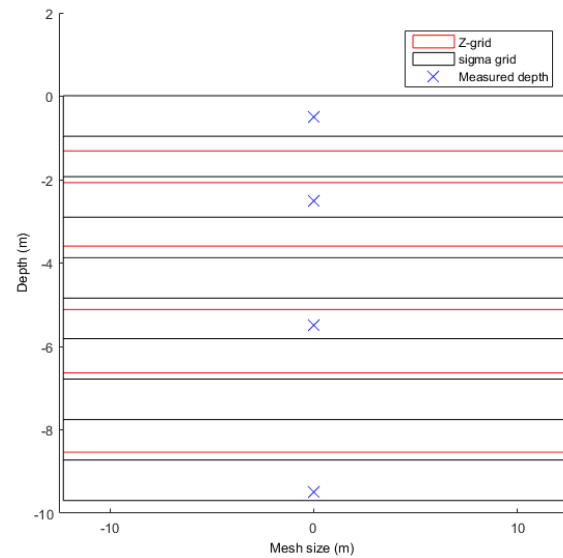


Figure 44 – Vertical resolution for  $\sigma$  and Z-grid in point P1. Blue X represents the measurement depths.

Outflow was concentrated in the free spillway located at the dam (Figure 43). The open downstream boundary was set as the spillway rating curve (Felisberto et al., 2015). Thus, the outflow discharge is defined according to the water level in the spillway. The simulated periods were performed during the dry season, with low inflow (maximum inflow was smaller than 2-year return period flow), representing a water level of about 10 cm higher than the spillway crest. Thus, the initial water level of the lake was considered as the same level of the spillway for all simulated periods.

The initial conditions for the reservoir water temperature at the beginning of each simulation period were obtained from the lake monitoring station. The simulations were initialized with vertically uniform temperature. For velocities, the water was supposed to be at rest as initial condition. For all simulations, the following constants were used: acceleration of gravity at  $9.81\ m^2/s$ , water density at  $1000\ kg/m^3$ , air density at  $1\ kg/m^3$  and water salinity at 0.15 ppt calculated with the mean of field conductivity data from 2015 to 2016 in surface water using the PSS-78 (Practical Salinity Scale of 1978 or Sal78 function) formulated and adopted by UNESCO (1981). For bottom roughness, the Chezy formulation was chosen with uniform values of  $65\ m^{1/2}.s^{-1}$  with free slip condition in wall roughness.

According to Deltares (2014), turbulent viscosity and turbulent diffusion are calculated differently in the horizontal and vertical directions. In turbulent flows, the diffusion mechanism is not only performed by molecular motion, but also intensified by eddy motion. Thus, the diffusion coefficient is computed by adding turbulent viscosity to molecular. Vertical terms are very small compared to horizontal terms.

The Delft3D-Flow model uses background horizontal eddy viscosity and diffusivity coefficients to represent unresolved hydrodynamic processes not calculated by the turbulent model.

Measured Secchi depth presented almost no variation during the simulation periods (between 0.20 and 0.35 m, with a mean of 0.30 m). Secchi depth was set as 0.3 m.

### Calibration parameters

The following parameters were calibrated: wind factor (Equation 10), Dalton coefficient (Equation 6), Stanton coefficient (Equation 8), background horizontal eddy viscosity and eddy diffusivity, using a trial-and-error method. The range of values (Table 11) were defined according literature review (Deltares, 2014; Scriban, 2015; Soullignac et al., 2017; Vinnå et al., 2017).

### Simulation periods

The simulation periods were selected according to the following criteria: (a) vertical uniform temperature of the water column at the beginning of the period; and (b) occurrence of a thermal stratification during the period.

The calibration period lasted 18 days, from May 16<sup>th</sup> to June 3<sup>rd</sup> 2016, corresponding to 440 hourly data of water temperature for each of the four depths (0.5, 2.5, 5.5 and 9.5 m). The water temperature time series measured during this period at four depths at station P1, which has a maximum depth of 10 m, is plotted in Figure 45. The period started with a mixed thermal condition of about 22.9 °C. This temperature value was set as the initial temperature condition for the lake simulation for all grid elements.

The validation period lasted 16 days, from May 29<sup>th</sup> to June 14<sup>th</sup> 2016, corresponding to 388 hourly values of water temperature (Figure 45). The period started with a mixed thermal condition of about 22.2 °C. Tributary inflows

**Table 11** – Range of parameter values tested in calibration

Parameter	Range tested in calibration
Secchi (m)	-
Wind Factor (-)	0.40 to 1.40
Background Horizontal Eddy Viscosity (m <sup>2</sup> /s)	0.0025 to 0.025
Background Horizontal Eddy Diffusivity (m <sup>2</sup> /s)	0.0025 to 0.025
Dalton (-)	0.0013 to 0.0007
Stanton (-)	0.0007 to 0.0013

during the calibration and validation period are presented in Figure 46. A third period, from May 15<sup>th</sup> to August 10<sup>th</sup> 2015 (90 days, 2107 hourly values), was simulated using the calibrated parameters in order to evaluate the model performance on a longer period. For this period, only sub-surface temperature data is available (Figure 47). Tributary inflows during the period are presented in Figure 48. The meteorological variables, respectively in 2016 (calibration and validation) and 2015 (long validation period) are presented in Figure 5.10 and Figure 5.39. Figure 51 presents the box plot with minimum, first quartile, median, third quartile, and maximum values for each meteorological variable. During calibration and validation periods no precipitation were measured at the meteorological station near the lake (station A521, Figure 1). During the period of 2015 no significant precipitation was measured near the lake (maximum of 14.2 mm/h on 27<sup>th</sup> July). The effect of precipitation on the water temperature is not taken into account by the model. According to Figure 52, during the simulated periods, east wind direction is dominant on the reservoir.

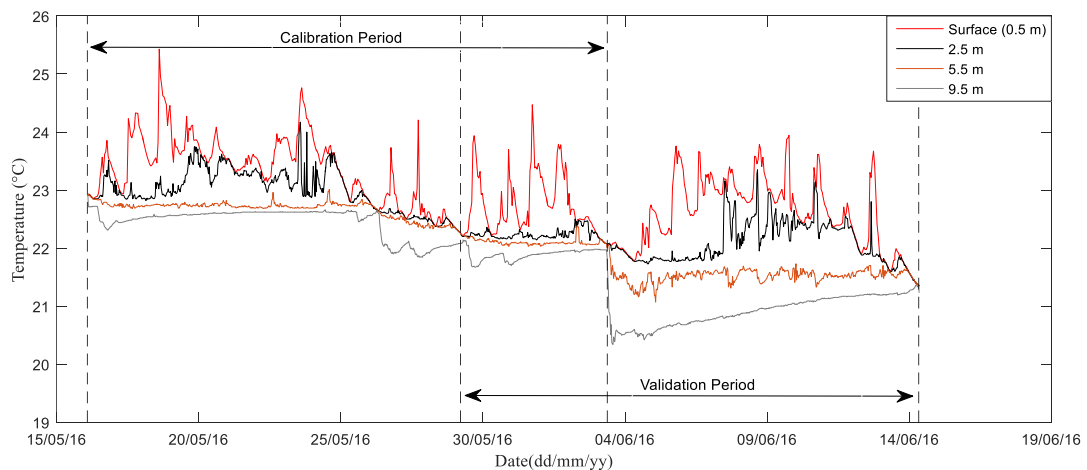


**Figure 45** – Water temperature (°C) measured at point P1 for surface (0.5 m), 2.5 m, 5.5 m and bottom (9.5 m) depth during the calibration period (May 16<sup>th</sup> to June 3<sup>rd</sup> 2016) and validation period (May 29<sup>th</sup> to June 14<sup>th</sup> 2016).

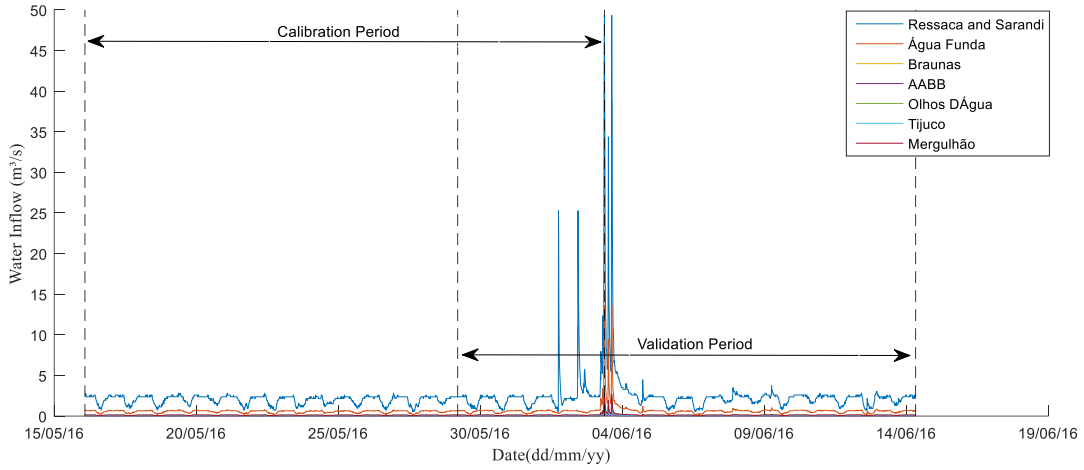


Figure 46 – Tributaries inflow water during the calibration period (May 16<sup>th</sup> to June 3<sup>rd</sup> 2016) and validation period (May 29<sup>th</sup> to June 14<sup>th</sup> 2016).

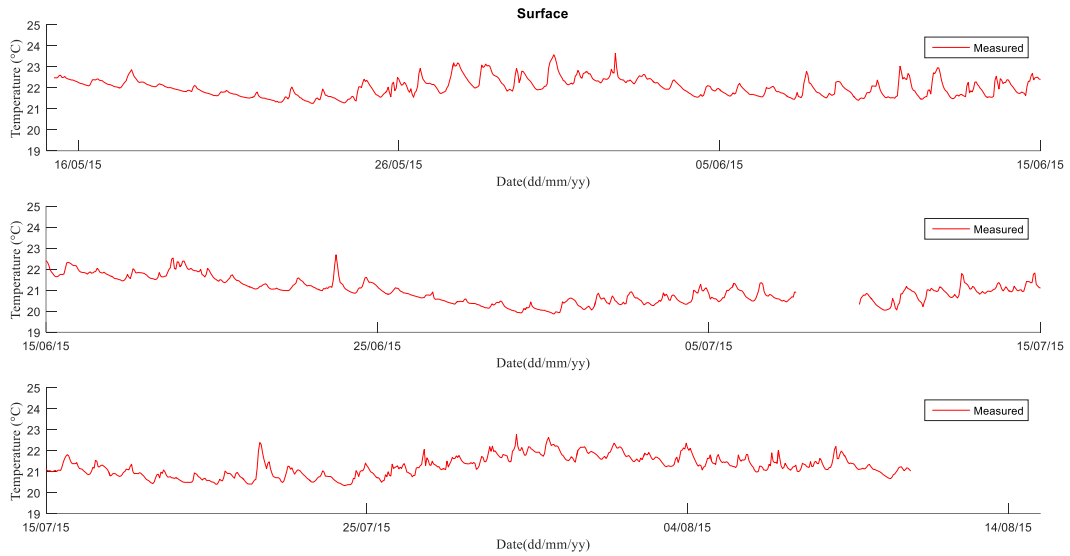


Figure 47 – Measured temperature at P1 at surface (0.5 m) depth from May 15<sup>th</sup> 2015 to August 10<sup>th</sup> 2015.

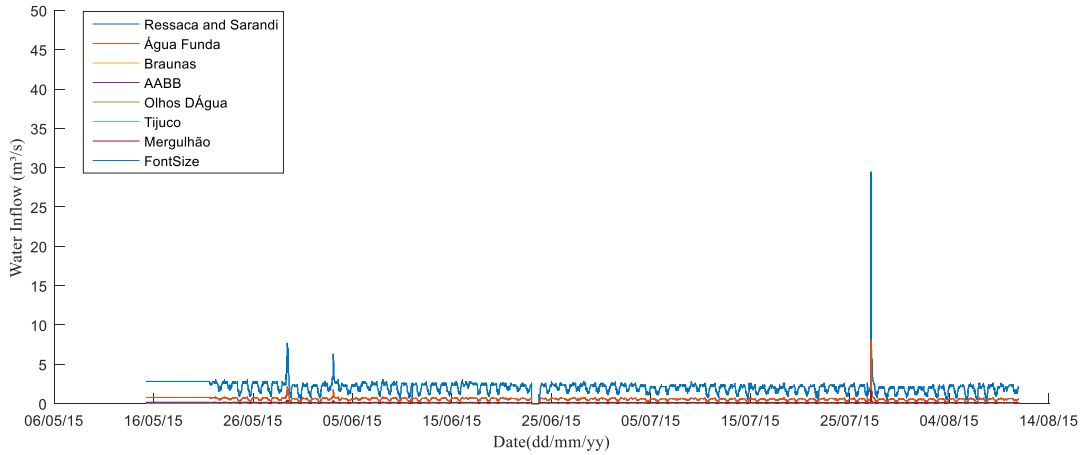
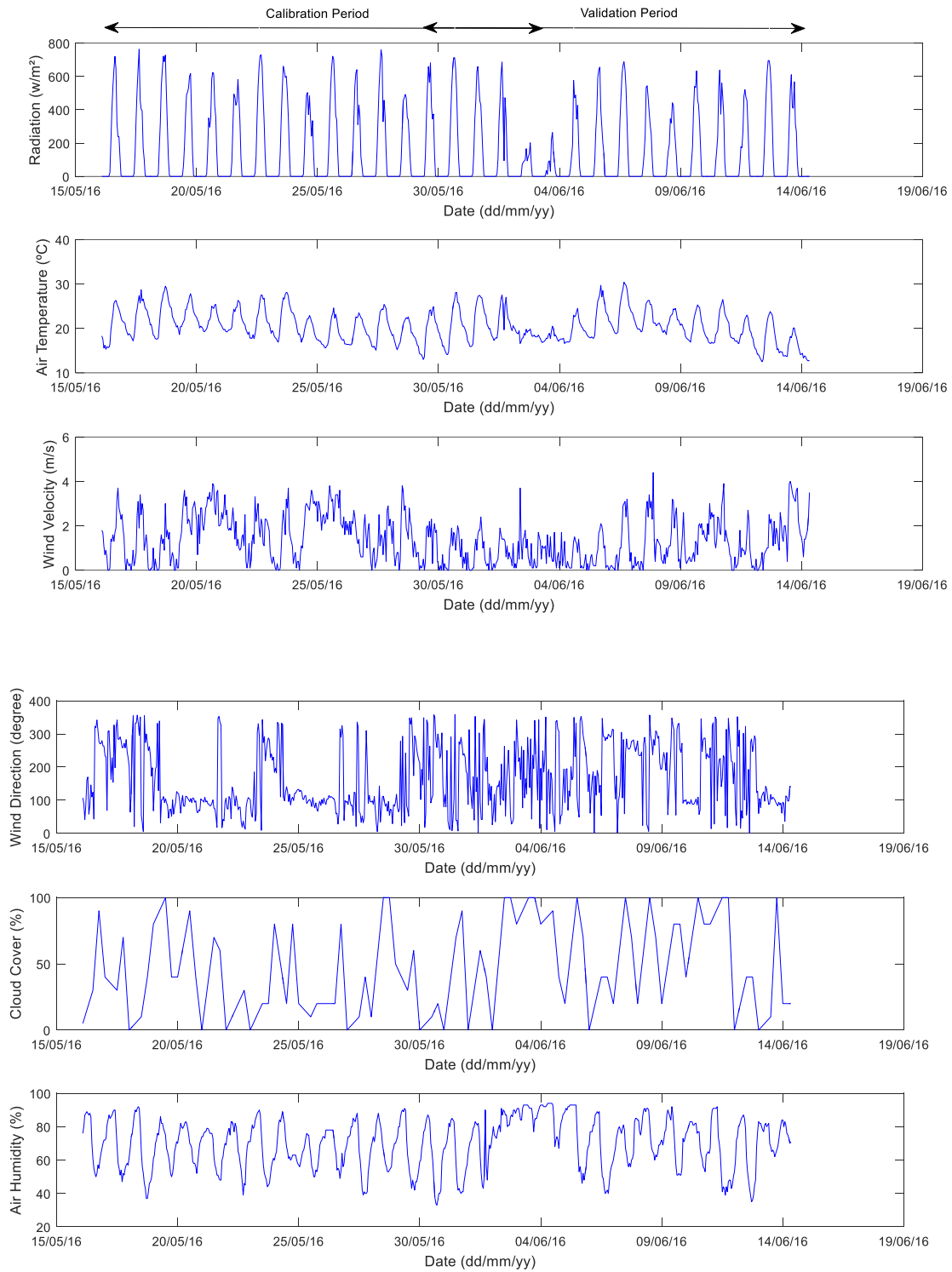
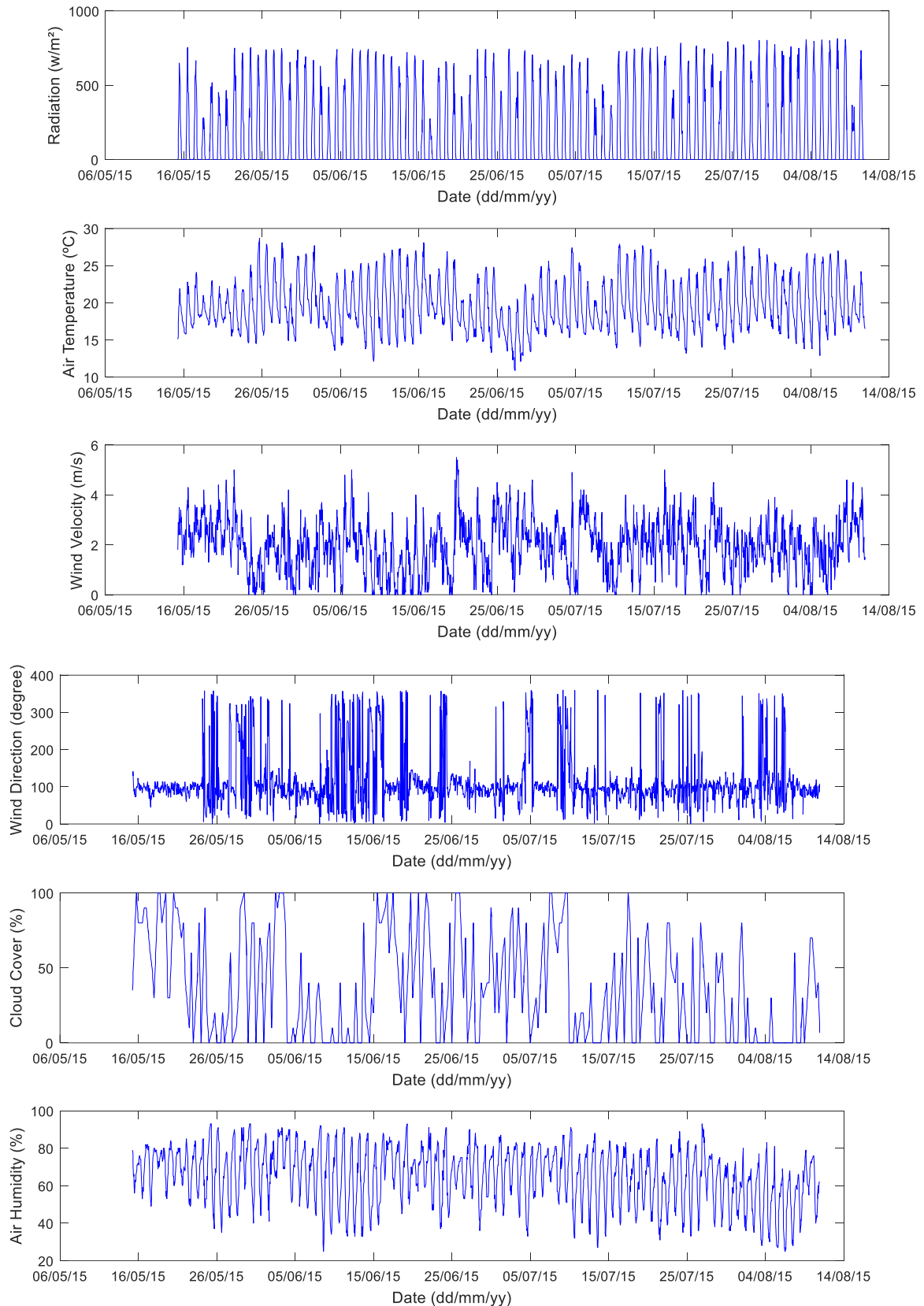


Figure 48 – Tributaries inflow water from May 15<sup>th</sup> 2015 to August 10<sup>th</sup> 2015.



**Figure 8** – Radiation, air temperature, wind intensity and direction, cloud cover and humidity measured at a meteorology station during the calibration period (May 16<sup>th</sup> to June 3<sup>rd</sup> 2016) and validation period (May 29<sup>th</sup> to June 14<sup>th</sup> 2016).



**Figure 9** – Radiation, air temperature, wind velocity and direction, cloud cover and humidity measured at the meteorology station during May 15<sup>th</sup> 2015 to August 10<sup>th</sup> 2015.

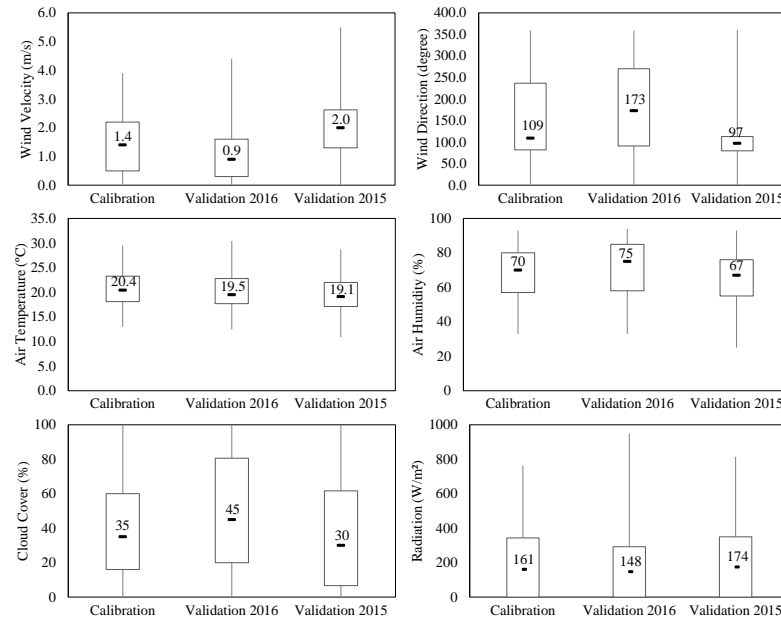


**Figure 51** – Wind velocity and direction, Air temperature and humidity, Cloud Cover and Radiation measured in the meteorology station for Calibration (May 16<sup>th</sup> to June 3<sup>rd</sup> 2016), Validation 2016 (May 29<sup>th</sup> to June 14<sup>th</sup> 2016) and Validation 2015 (May 15<sup>th</sup> to August 10<sup>th</sup> 2015). Box plots represent minimum, first quartile, median, third quartile, and maximum values for each meteorological variable.

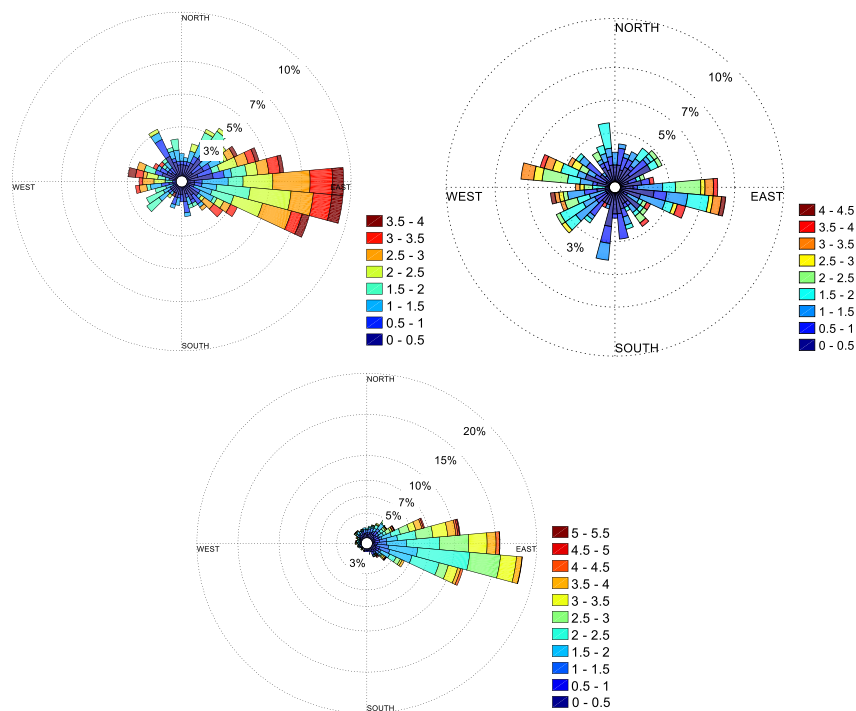


**Figure 52** – Wind direction (degree) and velocity (m/s): Calibration period (May 16<sup>th</sup> to June 3<sup>rd</sup> 2016), Validation period in 2016 (May 29<sup>th</sup> to June 14<sup>th</sup> 2016) and Validation period in 2015 (May 15<sup>th</sup> to August 10<sup>th</sup> 2015).

### Performance indicators

The hydrodynamic model performance during calibration and validation periods was assessed through

comparison between measured and simulated water temperature. Four mathematical indicators were used to compare simulated and measured water temperature: the mean absolute error (MAE), the root mean square error (RMSE), the coefficient of determination ( $R^2$ ) and the



relative error (RE). These indicators were computed using hourly model outputs and hourly-averaged measurements.

Regarding the inflow water temperature estimation, the Nash-Sutcliffe efficiency coefficient, NSE (Equation 11) was used for assessing the goodness of fit. The NSE shows how well a model represents observed data variance compared to the mean value of observed data. NSE varies from  $-\infty$  to 1, the closer to the unity, the better the model performance. A NSE below zero indicates model estimation worse than the mean value of the observed data (Bennett et al., 2013).

$$NSE = 1 - \frac{\frac{1}{n} \sum_{i=1}^n (y_i - y'_i)^2}{\frac{1}{n} \sum_{i=1}^n (y_i - \bar{y})^2} \quad (76)$$

where  $n$  is the number of observations and the number model results,  $y_i$  is the  $i$ th observation,  $\bar{y}$  is the mean value of observations and  $y'_i$  is the  $i$ th model result.

To analyse the impact of the stream inflow in the lake thermal stratification, Schmidt stability index and Lake number were computed using Lake Analyzer (Read et al. (2011).

## RESULTS

### Inflow water temperature

The hourly water inflow temperature was estimated from air temperature using linear regression and MSSWF method. Root mean square error (RMSE), the coefficient of determination ( $R^2$ ) and the Nash-Sutcliffe efficiency (NSE) were used to compare the results of linear regression and of the MSSWF method (Chen and Fang, 2016). Compared to MSSWF, linear regression presented better values for all indicators (Table 5.1). The hourly inflow temperature was computed using a linear regression with air temperature (Equation 12).

$$WT = 0.72 * AirT + 3.37 \quad (77)$$

where  $WT$  is the water temperature ( $^{\circ}C$ ) and  $AirT$  is the air temperature ( $^{\circ}C$ ).

**Table 12** – Mathematical indicators for the hourly water temperature estimation methods

Method	Indicators	Values
Linear Regression	RMSE ( $^{\circ}C$ )	1.02
	$R^2$	0.82
	NSE	0.82
MSSWF	RMSE ( $^{\circ}C$ )	1.50
	$R^2$	0.75
	NSE	0.56

### Model calibration

In the calibration step, wind factor values were tested for a range from 40% higher to 40% lower than 1, varying by 20%. For all depths, the better adjustment between measured and simulated temperature values was obtained for the lower wind factor (0.6), however with no significant differences (Table 13). At the water surface, the simulated values presented a higher variation compared to the measured values for all wind factors. For the 2.5, 5.5 and 9.5 m depths, a systematic error occurs after May 25<sup>th</sup> 2016. The simulated water temperature is colder than the measured values.

Setting wind intensity equal to the measured values (wind intensity factor equal to 1), the Dalton and Stanton coefficients were changed separately. A decrease of the Stanton coefficient to 0.0007 (almost 50% lower) did not result in significant changes (maximum temperature decreased less than 0.1  $^{\circ}C$ ). Thus, the default value of 0.0013 was chosen. Water surface cooling was smaller for lower Dalton coefficients during the night due to lower heat loss. The water surface temperature remaining warmer during the night resulted in warmer temperature at greater depths. Thus, the systematic error (colder simulated temperature for deeper depths) was reduced especially after May 26<sup>th</sup> 2016.

The Z-grid option was also used to compare the influence of the grid type on the model performance. Using the Z-grid option, a non-homogenous vertical distribution was necessary to provide more active layers in the lake upstream region, avoiding numerical instabilities due to inflows. The results for the Z-grid and  $\sigma$ -grid were interpolated to the measuring depth.

The mathematical indicators are very similar (Table 14). The indicators using  $\sigma$ -grid are slightly better in surface (0.5 m) and 2.5 m depth for RE and MAE. Thus, the  $\sigma$ -grid was chosen.

**Table 13** – Mathematical indicators for temperature with different values of wind intensity correction factor (dimensionless)

D epth	Indi cator	1				
		.40	.20	.00	.80	.60
0.5	MAE ( $^{\circ}C$ )	0.53	0.44	0.39	0.36	0.37
	RMSE ( $^{\circ}C$ )	0.60	0.51	0.45	0.43	0.45
	RE (%)	2.29	1.9	1.67	1.56	1.57
	$R^2$	0.76	0.76	0.77	0.76	0.73
2.5	MAE ( $^{\circ}C$ )	0.43	0.38	0.33	0.28	0.22
	RMSE ( $^{\circ}C$ )	0.50	0.44	0.38	0.33	0.27
	RE (%)	1.90	1.66	1.45	1.24	0.99
	$R^2$	0.81	0.82	0.84	0.83	0.85
5.5	MAE ( $^{\circ}C$ )	0.40	0.34	0.29	0.23	0.17
	RMSE ( $^{\circ}C$ )	0.50	0.41	0.36	0.29	0.22
	RE (%)	1.77	1.50	1.27	1.00	0.77
	$R^2$	0.89	0.88	0.93	0.94	0.95
9.5	MAE ( $^{\circ}C$ )	0.46	0.40	0.35	0.29	0.24
	RMSE ( $^{\circ}C$ )	0.57	0.51	0.45	0.38	0.32
	RE (%)	2.05	1.81	1.55	1.30	1.07
	$R^2$	0.89	0.89	0.89	0.89	0.89

**Table 14** – Mathematical indicators for lake temperature using Z-grid and  $\sigma$ -grid option

Depth (m)	Indicator s	Grid type	
		$\sigma$ -grid	Z-grid
0.5	MAE (°C)	0.30	0.40
	RMSE (°C)	0.42	0.51
	RE (%)	1.30	1.68
	R <sup>2</sup>	0.73	0.72
2.5	MAE (°C)	0.15	0.18
	RMSE (°C)	0.20	0.21
	RE (%)	0.64	0.77
	R <sup>2</sup>	0.84	0.86
5.5	MAE (°C)	0.13	0.08
	RMSE (°C)	0.15	0.09
	RE (%)	0.56	0.34
	R <sup>2</sup>	0.93	0.95
9.5	MAE (°C)	0.16	0.16
	RMSE (°C)	0.18	0.19
	RE (%)	0.70	0.72
	R <sup>2</sup>	0.90	0.90

The final parameter values are shown in Table 5.6. Observed and simulated water temperatures at the four depths during the calibration period are presented in Figure 12. Model performance indicators are presented in Table 17. For all depths, RMSE and RE were quite good, with maximum values of 0.42 °C and 1.30%, respectively. The maximum MAE was 0.30 °C, representing a very good performance. The lower R<sup>2</sup> value was 0.73 at water surface layer.

The calibration period started on May 16<sup>th</sup> 2016 with a uniform water temperature of 22.9°C. Over the following ten days, the lake water column stratified with warming in the surface layer to around 25.3°C. Mixing events (temperature difference between surface and bottom less than 0.25 °C) occurred on May 25<sup>th</sup> and 26<sup>th</sup> 2016, with temperature decreasing to 22.6 °C. After May 26<sup>th</sup>, the temperature at 9.5 m depth decreased by almost 1° C and the surface temperature displayed daily warming. A third

stratification period lasted three days, ending with a mixing event on May 29<sup>th</sup> at 22.1 °C. During the whole period, the temperature difference between the surface and 9.5 m depth, at maximum stratification, was 2.9 °C (May 18<sup>th</sup> at 15:00).

Figure 13 shows the difference between surface and bottom layer for measured and simulated water temperature. Figure 14 shows the temperature for the four depths in which measurements were carried out. Table 17 shows the number of days with a difference between surface (0.5 m) and bottom (9.5 m) for measurement and simulated temperatures of 0.25°C to 2.0°C. According to both Figure 13 and Figure 14 and to Table 9, the model could accurately represent the main observed patterns: (i) the daily time scale of surface warming; (ii) the maximum stratification time, (iii) the cooling at the lake bottom on May 26<sup>th</sup>; (iv) the timing of mixing episode on May 25<sup>th</sup>, 26<sup>th</sup> and on 29<sup>th</sup>, in which the difference between the measured and simulated temperature at the lake surface and bottom were respectively of 0.17, 0.04 °C and 0.11 °C for measurement and 0.03, 0.07 and 0.10 for simulation, (v) and the duration of stratification periods.

**Table 36** – Set of parameter values for hydrodynamic simulation in Lake Pampulha

Parameter	Value	Range tested in
Secchi (m)	0.3 (measured)	-
Wind Factor (-)	1.0 (calibrated)	0.40 to 1.40
Background Horizontal Eddy Viscosity (m <sup>2</sup> /s)	0.025 (calibrated)	0.0025 to 0.025
Background Horizontal Eddy Diffusivity (m <sup>2</sup> /s)	0.025 (calibrated)	0.0025 to 0.025
Dalton (-)	0.0007 (calibrated)	0.0013 to 0.0007
Stanton (-)	0.0013 (default)	0.0007 to 0.0013

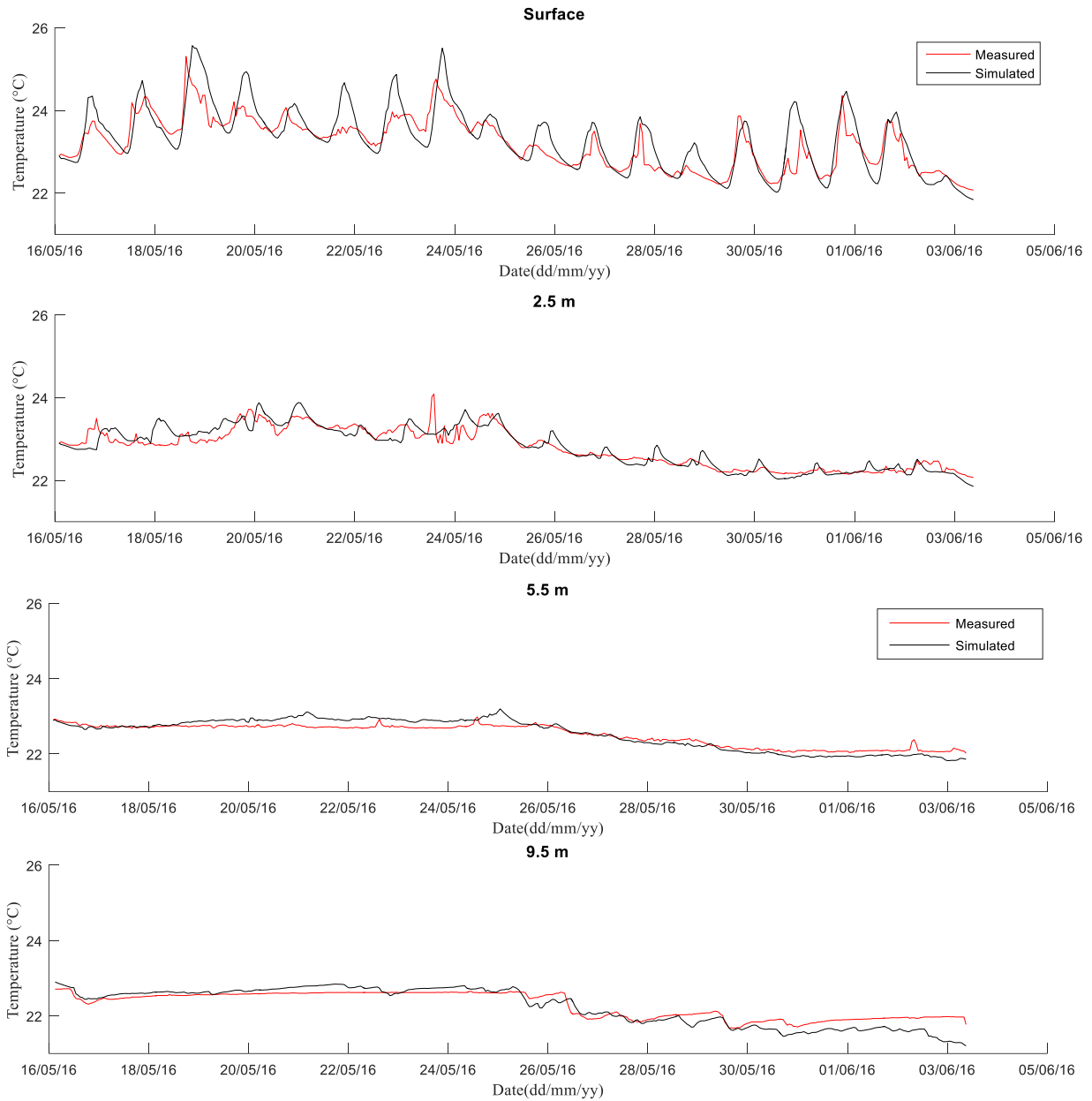


**Figure 12** – Measured and simulated temperatures for the calibration period from May 16<sup>th</sup> to June 3<sup>rd</sup> 2016 at P1 station.

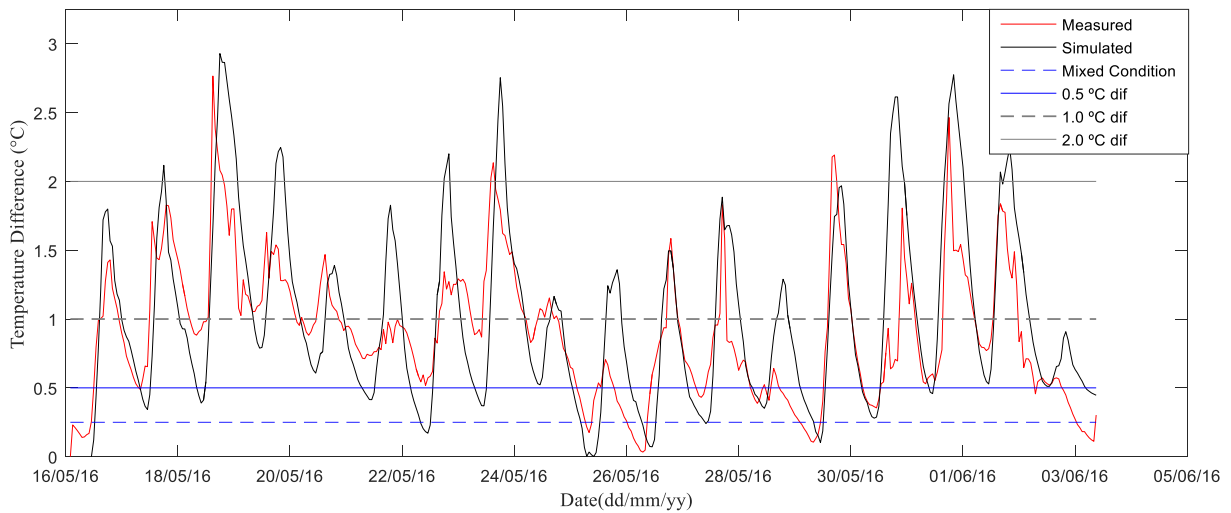


**Figure 13** – Difference of surface (0.5 m) and bottom (9.5 m) for measurement and simulated temperatures for the calibration period from May 16<sup>th</sup> to June 3<sup>rd</sup> 2016 at P1 station. Blue dashed line represents a mixing condition with difference between surface and bottom of 0.25 °C and grey lines represent differences of 1.0 and 2.0 °C.

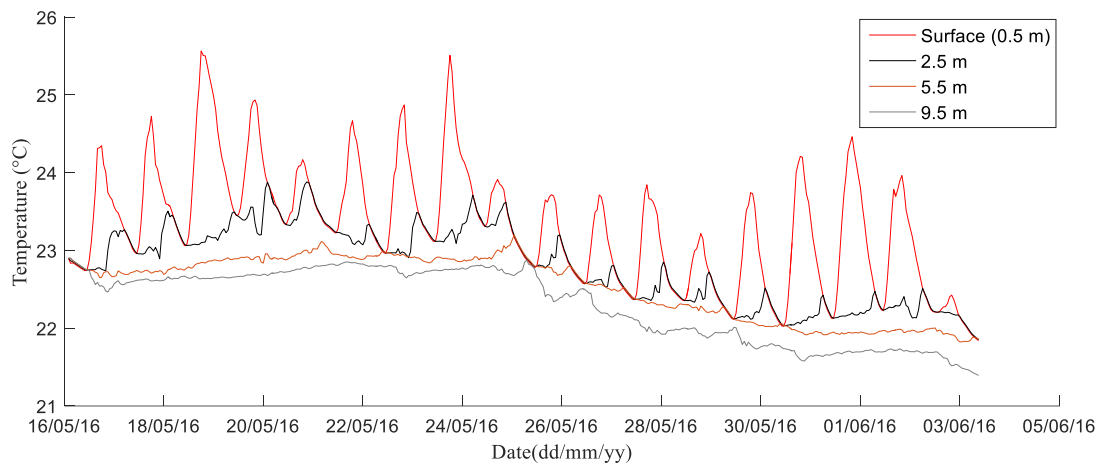


**Figure 14** – Water temperature (°C) simulated at point P1 for surface (0.5 m), 2.5 m, 5.5 m and bottom (9.5 m) depth during the calibration period (May 16<sup>th</sup> to June 3<sup>rd</sup> 2016).

**Table 37** – Number of days with difference between surface (0.5 m) and bottom (9.5 m) for measurement and simulated temperatures for the calibration period from May 16<sup>th</sup> to June 3<sup>rd</sup> 2016 at P1 station

Value	Measure d	Simulated
$\Delta T \leq 0.25^\circ\text{C}$	4	5
$\Delta T \leq 0.50^\circ\text{C}$	9	13
$\Delta T \geq 1.0^\circ\text{C}$	15	17
$\Delta T \geq 2.0^\circ\text{C}$	4	8

### Validation Period in 2016

The model was run with the calibrated parameters values (Table 5.6). For all depths, the RMSE and RE between the measured and simulated values were good (Table 17 and Figure 15), with maximum values of 0.45 °C and 1.51%, respectively. The  $R^2$  ranged from 0.41 to 0.81, also considered as a good result. The MAE presented a very good performance, with a maximum value of 0.34 °C at 0.5 m. According to the mathematical indicators, the model can be considered validated.

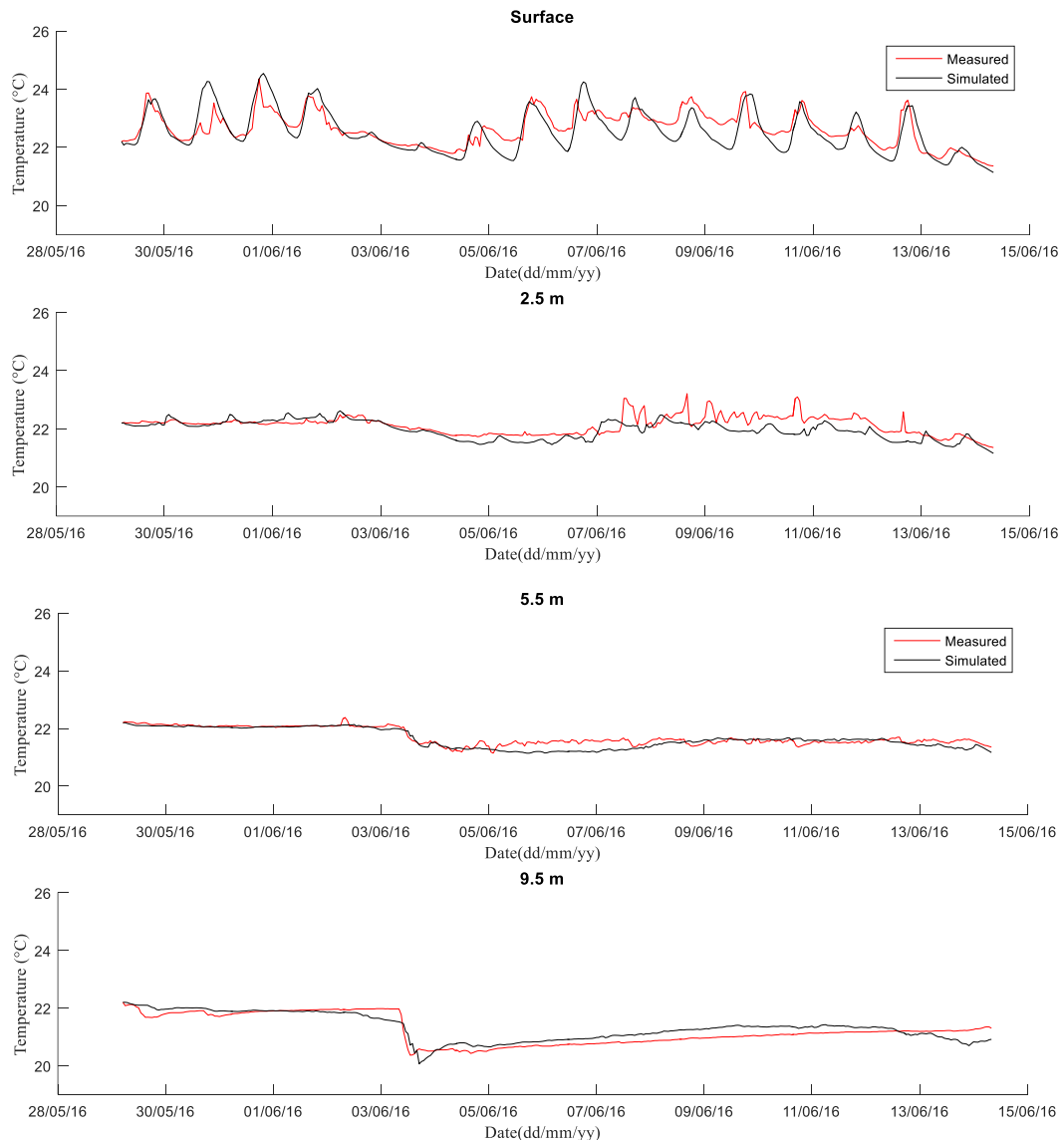
The validation period in 2016 started on May 29<sup>th</sup> with a uniform water temperature of 22.2°C. Over the first five days a daily stratification and mixing alternation was

observed. According to Figure 16, on May 30<sup>th</sup> the difference between surface and bottom temperature was 0.35 °C for measured values and 0.07 for simulated values. On May 31<sup>st</sup>, this difference was 0.53 and 0.31 °C, on 1<sup>st</sup> June it was 0.77 and 0.44 °C and 2<sup>nd</sup> June 0.11 and 0.46 °C, respectively for measured and simulated values. Until 5<sup>th</sup> June, comparing with the measured values, the simulated water surface presented a good adjustment, however, after this date the simulated values presented higher amplitude with lower low values (Figure 15). This discrepancy resulted in higher differences between simulated surface and bottom water temperature (Figure 16).

On 3<sup>rd</sup> June, the water temperature column was uniform around 22.0 °C. Then, four hours later, at 09:00 a strong cooling at 5.5 and 9.5 m depth occurred. At 9.5 m depth, the water temperature decreased by 1.8 °C over 4 hours. At 5.5 m depth, the decrease was 0.8 °C over 12 hours. After this cooling of the bottom layers, the water at 5.5 m depth remained at a relatively constant temperature of 21.5 °C for the whole period. In contrast, warming was observed at 9.5 m depth at a constant rate of 0.08 °C per day. At 2.5 m depth, the temperature remained constant until 7<sup>th</sup> June when it began to increase. This temperature dynamics could also be represented by the simulation (Figure 17).

Table 17 – Model performance indicators for the calibration and validation period

Depth (m)	Performance indicators	Calibration Period	Validation Period 2016
Surface (0.5)	MAE (°C)	0.30	0.34
	RMSE (°C)	0.42	0.45
	RE (%)	1.30	1.51
	R <sup>2</sup>	0.73	0.63
2.5	MAE (°C)	0.15	0.23
	RMSE (°C)	0.20	0.31
	RE (%)	0.64	1.04
	R <sup>2</sup>	0.84	0.41
5.5	MAE (°C)	0.13	0.12
	RMSE (°C)	0.15	0.16
	RE (%)	0.56	0.56
	R <sup>2</sup>	0.93	0.80
Bottom (9.5)	MAE (°C)	0.16	0.20
	RMSE (°C)	0.18	0.24
	RE (%)	0.70	0.95
	R <sup>2</sup>	0.90	0.81

Figure 15 – Measured and simulated temperature for the validation period (May 29<sup>th</sup> to June 14<sup>th</sup> 2016) at surface (0.5 m), 2.5 m, 5.5 m and 9.5 m depths.

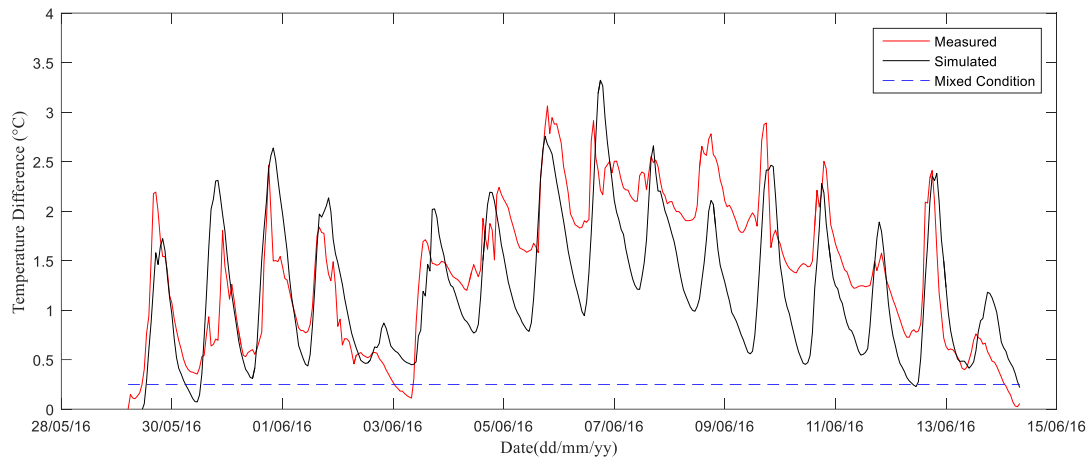


**Figure 16** – Difference of surface (0.5 m) and bottom (9.5 m) for measurement and simulated temperatures for the validation period from May 29<sup>th</sup> to June 14<sup>th</sup> 2016 at P1 station. Blue dashed line represents a mixing threshold with difference between surface and bottom of 0.25 °C.

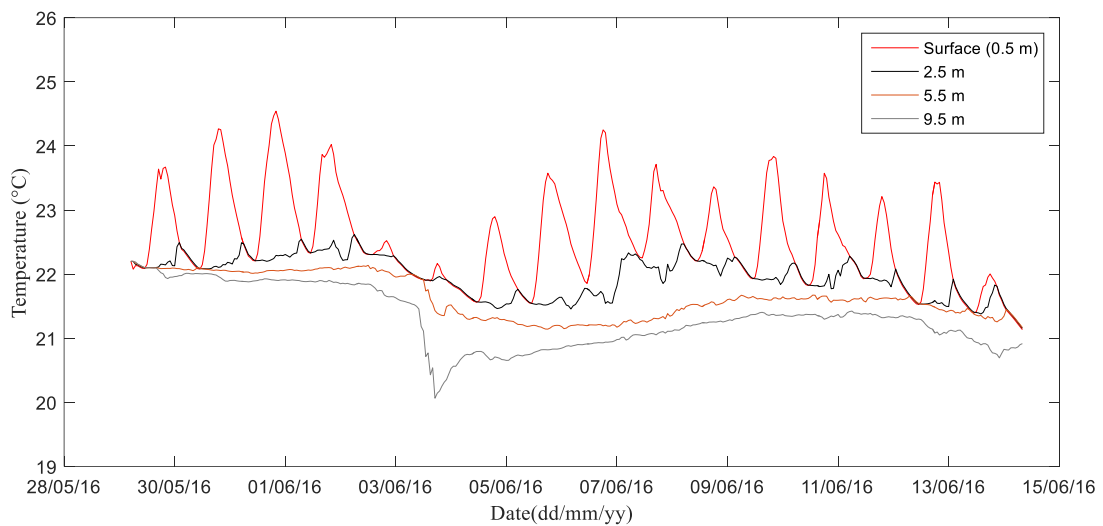


**Figure 17** – Simulated temperature for the validation period (May 29<sup>th</sup> to June 14<sup>th</sup> 2016) at surface (0.5 m), 2.5 m, 5.5 m and 9.5 m depths.

### Validation Period in 2015

A longer period of 88 days (from May 15<sup>th</sup> to August 10<sup>th</sup> 2015) was run with the calibrated parameters. For this period, only surface temperature data are available. The simulation results and data measurements during the period are presented in Figure 18. Even with a slightly warmer simulated water temperature, the MAE between the

measured and simulated values was very good (0.45°C), the RMSE (0.65°C), the RE (2.08%) and the R<sup>2</sup> (0.55) also presented good values.

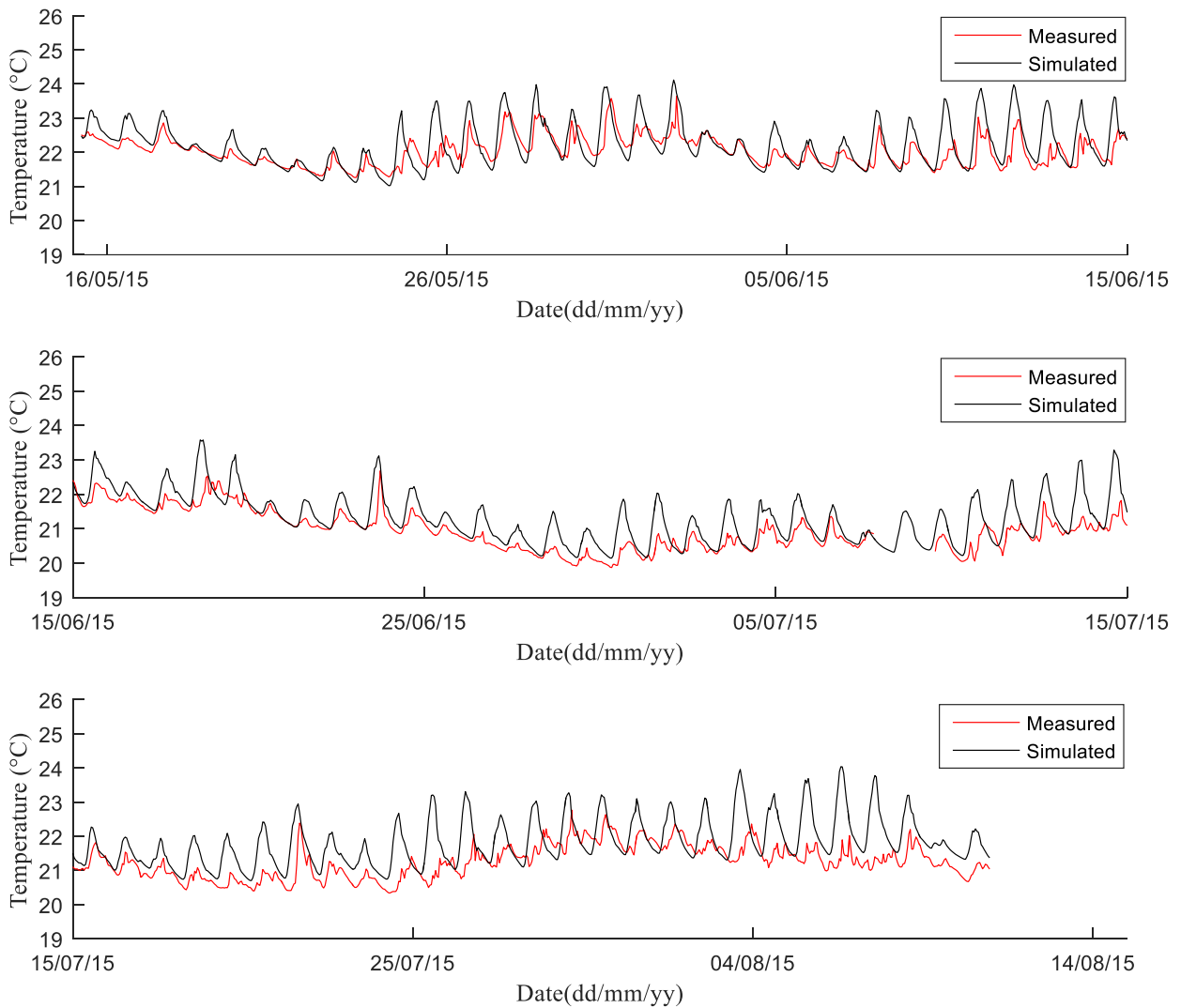


Figure 18 – Measured and simulated temperature at P<sub>1</sub> station at surface (0.5 m) depth from May 15<sup>th</sup> to August 10<sup>th</sup> 2015.

### Impact of the river inflow

On June 3<sup>rd</sup> 2016, during the validation period, the water temperature strongly decreased by 1.8 °C over 4 hours at 9.5 m and by 0.8 °C over 12 hours at 5.5 m (Figure 15 and Figure 17) at station P1. This strong temperature variation observed only in the deepest layers was not expected. The model was used as a tool to investigate what could be the reason for this cooling observed only below 5.5 m depth and more intense at 9.5 m depth. According to the computed water inflow temperature (Figure 19), the tributary water, just before the water cooling, presented a lower temperature (16.1 °C) and, therefore, a higher density, compared to the lake temperature (uniform at 22 °C). This colder inflow entered the reservoir during 15 hours (Figure 46), with a high discharge of 50 m<sup>3</sup>/s of the streams Ressaca and Sarandi. On 1<sup>st</sup> June at 17 h and 2<sup>nd</sup> June at 10 h other inflow high discharge events were observed, however with lower discharge (25.0 m<sup>3</sup>/s of Ressaca and Sarandi streams) and smaller duration (one to two hours). The inflow water temperature, respectively for June 1<sup>st</sup> and 2<sup>nd</sup> was 22.0 °C and 16.2 °C. Even though these events were secondary, compared to the event of June 3<sup>rd</sup>, they occurred in different condition of the water column stratification. On June 1<sup>st</sup>, the

lake was stratified, with water surface at 23.9 °C and bottom at 21.9 °C. On June 2<sup>nd</sup> the difference of water surface and bottom was less than 0.50 °C, with water surface at 22.3 °C and bottom at 21.85 °C, therefore, the lake was warmer than the water inflow.

During the peaks of water inflow on June 1<sup>st</sup> and 2<sup>nd</sup>, no decrease of temperature was measured and simulated at station P1, probably due to a lower inflow discharge and duration that was dissipated before reaching point P1. At the upstream very shallow region, on June 1<sup>st</sup>, no water temperature decrease was observed. However, the water inflow on 2<sup>nd</sup> June resulted in a water temperature decrease of 1.7 °C at 2.0 m depth (reaching 17.6 °C), 1.6 °C at 1.1 m depth (reaching 19.0 °C) and 0.6 °C at 0.5 m depth (reaching 20.7 °C). **Erro! Fonte de referência não encontrada.** shows the water temperature profiles at a point in the shallow region indicated in Figure 20 as UP point. Even being smaller, the event on June 2<sup>nd</sup> impacted the bottom temperature that remained colder until a higher inflow arrived on June 3<sup>rd</sup>, in which water temperature reached 16 °C at this point. This water temperature dynamics, during June 1<sup>st</sup> and 2<sup>nd</sup>, shows that the first water high inflow was dissipated fast and the second one impacted a wider region of the shallow part of the lake. The colder water remained

in the shallow region until a higher discharge arrived on June 3<sup>rd</sup>. In the supplementary material videos show the lake temperature at surface (Video 01) and bottom (Video 02) layers of the lake during the validation period. Videos also show the impact of the Tijuco and Mergulhão tributaries (Figure 43) that were not so intense due to a lower inflow rate (Figure 46).

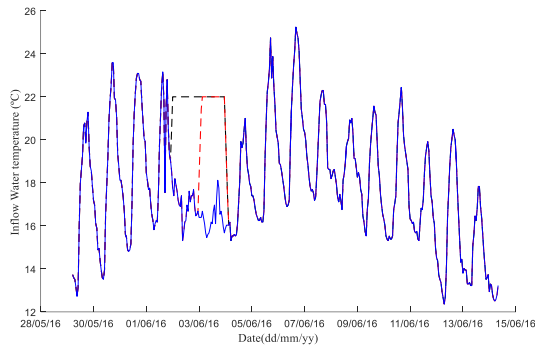


**Figure 19** – Computed inflow water temperature used as an input during the validation period (May 29<sup>th</sup> to June 14<sup>th</sup> 2016). Red dash line represents the sensitivity analysis with an inflow water temperature with a constant temperature during June 03<sup>rd</sup> (scenario D1) and the black dash line during June 02<sup>nd</sup> to 03<sup>rd</sup> (scenario D2).

Even with higher inflow, the simulated water level variations at station P1 were less than 12 cm during the passage of the higher inflow values (Figure 21). This small water variation is in agreement with the downstream condition, in which a water elevation of 0.5 m would spill 121 m<sup>3</sup>/s, much higher than 50 m<sup>3</sup>/s, the maximum inflow discharge during the simulated period.

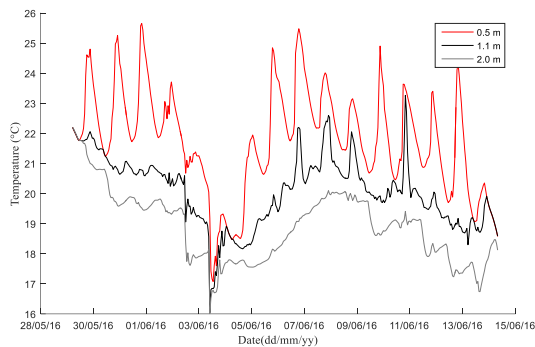


**Figure 20** – Simulated temperature for the validation period (May 29<sup>th</sup> to June 14<sup>th</sup> 2016) at surface (0.5 m), 2.5 m, 5.5 m and 9.5 m depths at the upstream region of the lake (UP point, see Figure 21).

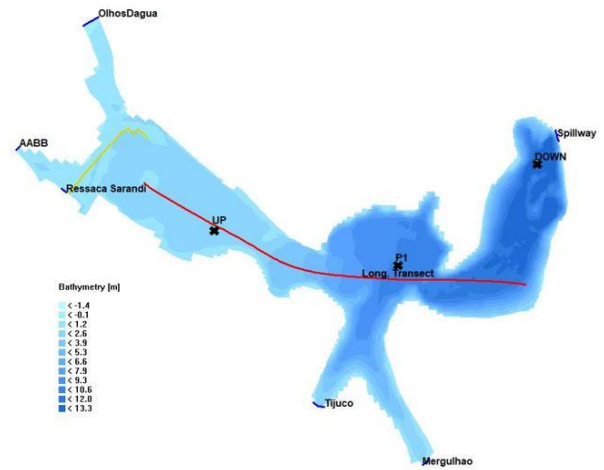


**Figure 21** – Longitudinal transect of the lake model in red and observation points in black cross.

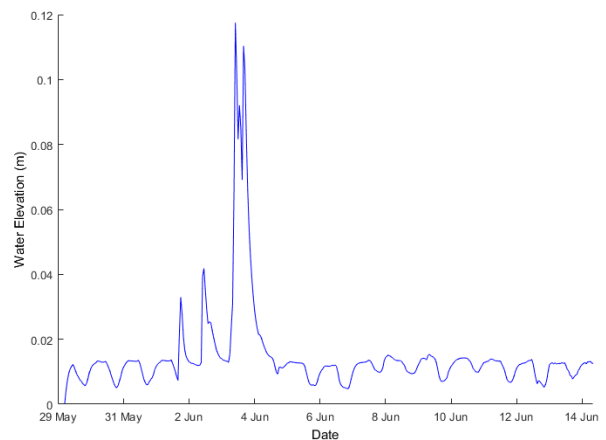


**Figure 22** – Water level variation during the validation period (May 29<sup>th</sup> to June 14<sup>th</sup> 2016)

On June 3<sup>rd</sup> 2016 at 13:00 hours, when the water velocity module in the bottom layer at P1 station is maximum, a longitudinal transect (Figure 20) of the simulated water temperature shows colder temperature in the lake deeper layers (Figure 22). The model suggests that the propagation of the inflow water on 3<sup>rd</sup> June occurred through the bottom of the lake (Figure 22 and Figure 23). The inflow water sank to the deepest layers of the lake. The plunging point is located 1500 m far from the inflow channel, where the lake shallow region ends. In the supplementary material a video shows the lake temperature evolution along the longitudinal transect (Video 03). Unfortunately, the stream inflow water temperature was not measured in this period to confirm this hypothesis. Therefore, to evaluate the influence of the inflow water temperature and to assess the impact of different intensity of inflow water conditions, two simulations considering the water inflow at a constant temperature of 22 °C were performed for two different scenarios (Figure 19). In the first scenario (D1), the water inflow temperature was considered constant (22°) on June 3<sup>rd</sup>. In the second scenario (D2), the water inflow temperature was considered constant (22°) on June 2<sup>nd</sup> to 3<sup>rd</sup>. In these simulations the main difference in the temperature profile was on the bottom of the lake (Figure 23) and more evident in the scenario considering the water inflow at a constant



temperature during two days (D2). In the simulations with the computed water inflow temperature (validation period) the lake bottom temperature presented a decrease of 1.8 °C at station P1. In scenario D1, with the inflow water temperature of 22.0 °C, the decrease was 0.8 °C. Changing the inflow water temperature to 20.0 °C, during 3<sup>rd</sup> June, the decrease was 1.4 °C, and, changing it to 18.0 °C the decrease was the same of the validated simulation (1.8 °C). Therefore, the variation of the inflow water temperature directly impacts the water stratification. For the scenario D2, with the inflow water temperature of 22.0 °C, the decrease of the lake bottom temperature was only 0.2 °C. The difference of water temperature decreases between scenario D1 and D2, with the inflow water temperature of 22.0 °C, shows that the event of 2<sup>nd</sup> June also influences the water temperature at station P1, even if indirectly. This probably happened because the shallow region of the lake remained at a lower temperature until the inflow peak arrives on 3<sup>rd</sup> June. Concerning the time evolution of the water velocity module, as expected, the higher values occurred on 3<sup>rd</sup> June, and due to the water sank to the deeper layers of the lake the higher values were at the bottom. At the moment of higher decrease of the water temperature, the bottom velocity module was 7 cm/s and the surface velocity was 1.5 cm/s. In the scenario D1, the bottom velocity module was 5.8 cm/s and the surface velocity 1 cm/s. Changing the inflow water temperature to 20 °C and 18 °C the water velocity module presented a very slight increase in almost all depths with a higher increase at 9.5 m depth (Table 39). In the scenario D2, the bottom velocity was 4.5 cm/s and the surface velocity 0.5 cm/s. Table 39 presents the water velocity module in different depths for the presented scenarios.

**Table 39** – Water velocity module (cm/s) at station P1 during the passage of 3<sup>rd</sup> June peak flow.

D epth (m)	Scenario		
	Validation period (cm/s)	D1 (cm/s)	D2 (cm/s)
0. 50	1.5	1.0*/1.1**/1.3***	0.50
2. 50	1.4	0.9*/1.1**/1.2***	0.50
5. 50	1.4	1.4*/1.3**/1.3***	0.50
9. 50	7.0	5.8*/6.1**/6.2***	4.5

Inflow water temperature: \*22 °C \* 20 °C, \*\*18 °C

Close to the spillway, according to the model results, the lake presented a water temperature decrease with a higher intensity at the bottom (Figure 24). This water cooling happened 6 hours later that the cooling observed at station P1 and with a lower intensity (decrease of 1.1 °C). Analysing the profile of the water velocity module, the highest value was at bottom (6.1 cm/s). The simulated surface velocity module was 2.5 cm/s. This point (DOWN in Figure 20) is located about 3.0 km far from the Ressaca

and Sarandi inflow channel. Figure 25 and Figure 26 present the profiles of the water velocity module for the UP and DOWN points (Figure 21). According to the simulation values, the dynamics of the upstream region of the lake is different of the downstream region. At the upstream region the lake presents higher velocity module values at surface. At the downstream region the bottom layers present higher velocity values. In the supplementary material videos show the lake velocity module at surface (Video 04) and bottom (Video 05).

Schmidt Stability represents the resistance to mechanical mixing (Idso, 1973). It corresponds to the energy required to completely mix a stratified lake. For the validation period, Schmidt stability shows a pattern of day-night oscillations (Figure 27), induced by the heating and cooling alternation period. It corresponds to the same pattern of the water temperature difference between surface and bottom depths (Figure 16). However, just before of the cooling of the bottom depth on June 3<sup>rd</sup> (Figure 45 and Figure 17) a mixing of the water column occurs that strongly reduces the value of Schmidt Stability index. This mixing event reduced the daily variation on June 3<sup>rd</sup>, which shows a smaller amplitude. Before the mixing event, the daily variation was around 14 J/m<sup>2</sup>, on 3<sup>rd</sup> June it reduced to 4 J/m<sup>2</sup>. Figure 27 also shows that the model could represent this Schmidt stability evolution. However, after June 5<sup>th</sup>, the agreement between measurements and simulated results is weaker (Figure 15), with larger differences between surface and bottom depth (Figure 16), and directly impacting the Schmidt stability index computed from simulated results.

The Lake Number, defined by Imberger and Patterson (1990), is the ratio of the strength of stratification (Schmidt Stability) to the effect of the wind stress. Lake number below 1 means that the lake stratification is weak with respect to wind stress and the lake will probably mix. According to Figure 27 and Figure 28, the Lake Number peaks were coincident with the Schmidt Stability peaks for measured and simulated values. The high inflow discharge on 3<sup>rd</sup> and 4<sup>th</sup> June resulted in the cooling of the bottom of the lake. On 5<sup>th</sup> June, after the cooling of the bottom depth the water difference between surface and bottom depth increases (Figure 16), which increases the Lake Number to values higher than 600 J/m<sup>2</sup>. Thus, the stream inflow impacted the lake stratification strength and the three-dimensional model could represent this pattern.

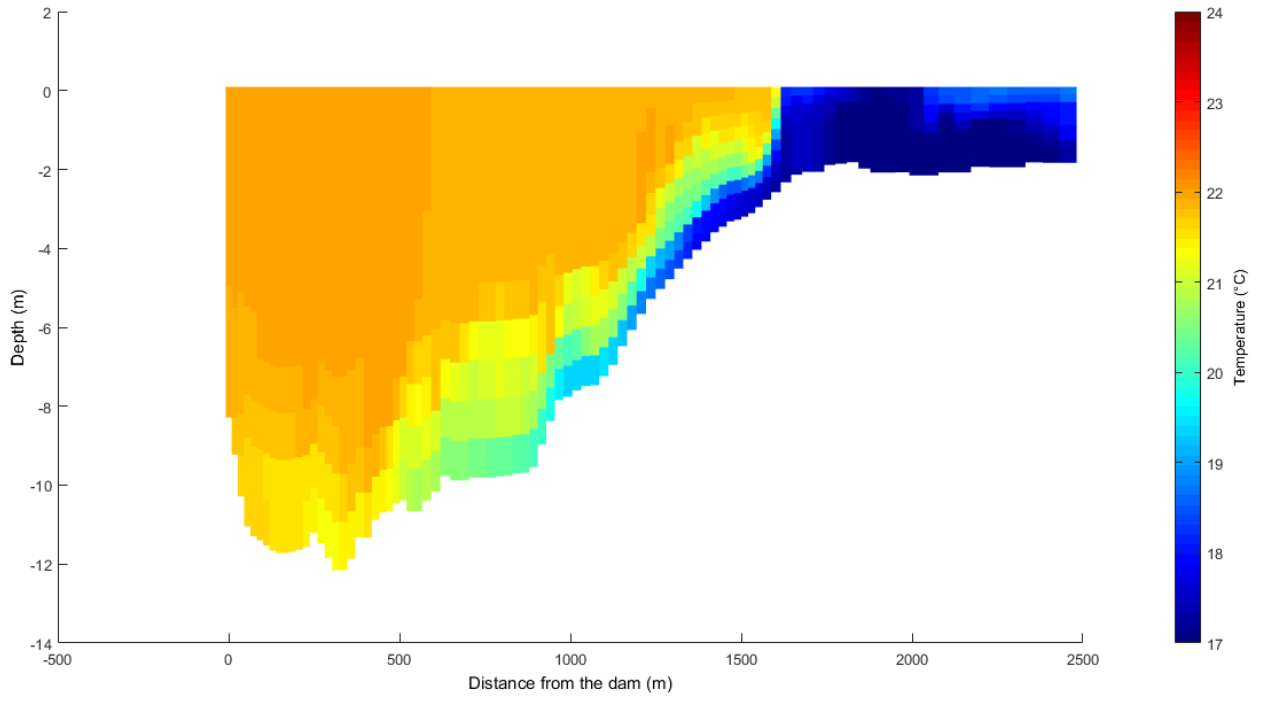
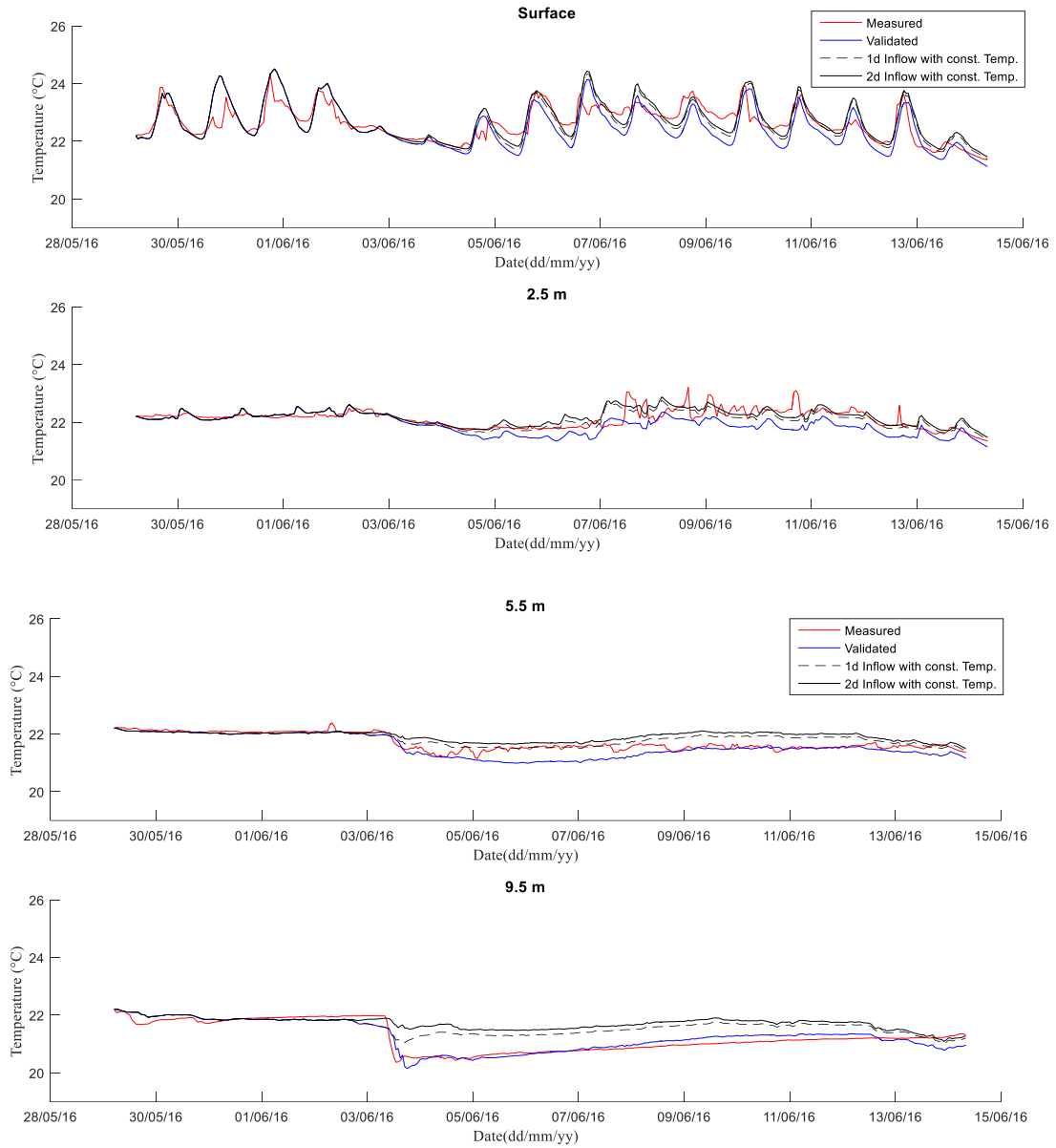
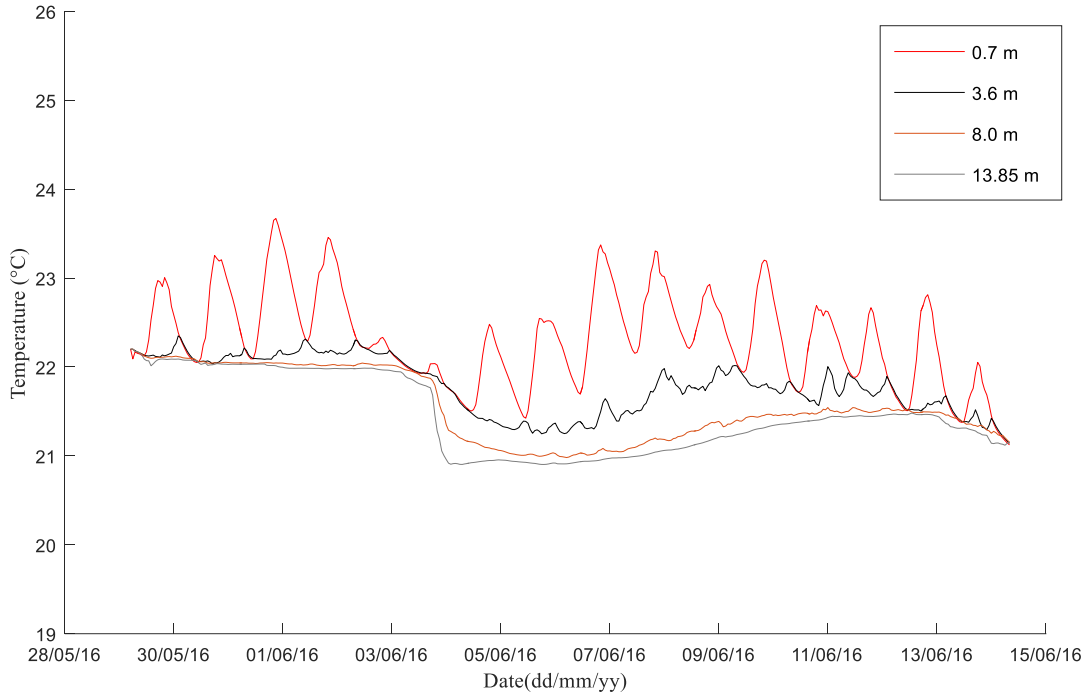


Figure 22 – Simulated lake water temperature during high inflow on June 03<sup>rd</sup> 2016 at 13:00 h along the reservoir longitudinal transect



**Figure 23** – Measured and simulated temperatures at point P1 at the surface (0.5 m), 2.5 m, 5.5 m, 9.5 m depths for the validation period simulated (May 29<sup>th</sup> to June 14<sup>th</sup> 2016) and for different inflow water temperatures scenarios.



**Figure 24** – Simulated temperature for the validation period (May 29<sup>th</sup> to June 14<sup>th</sup> 2016) at surface (0.5 m), 2.5 m, 5.5 m and 9.5 m depths at the downstream region of the lake (DOWN point in Figure 21).

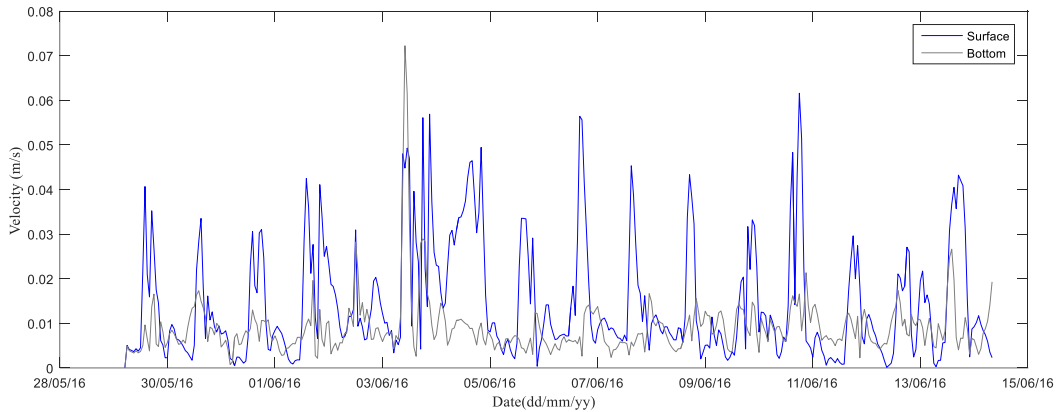


**Figure 25** – Simulated velocity module at UP point (see Figure 21) for the validation period (May 29<sup>th</sup> to June 14<sup>th</sup> 2016) at surface (0.5 m) and bottom (2.0 m).

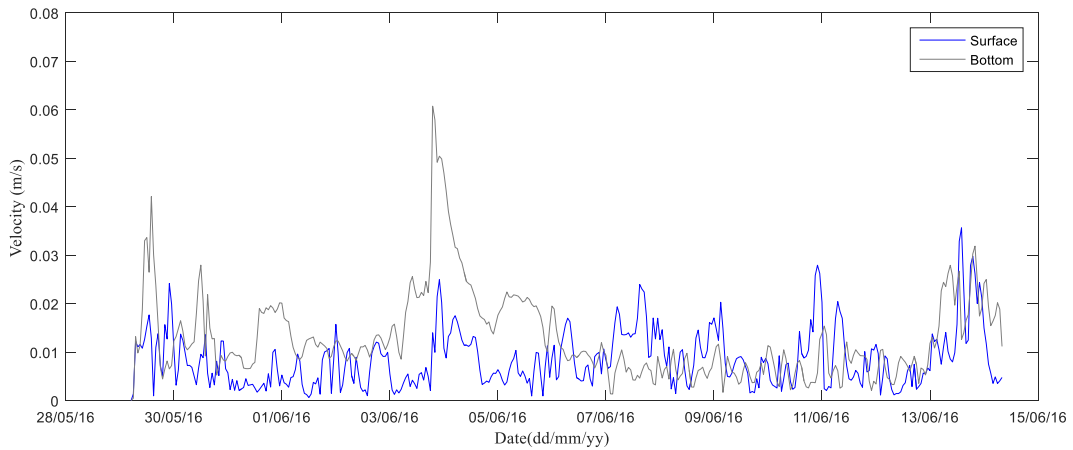


**Figure 26** – Simulated velocity module at DOWN point (see Figure 21) for the validation period (May 29<sup>th</sup> to June 14<sup>th</sup> 2016) at surface (0.5 m) and bottom (13.85 m)

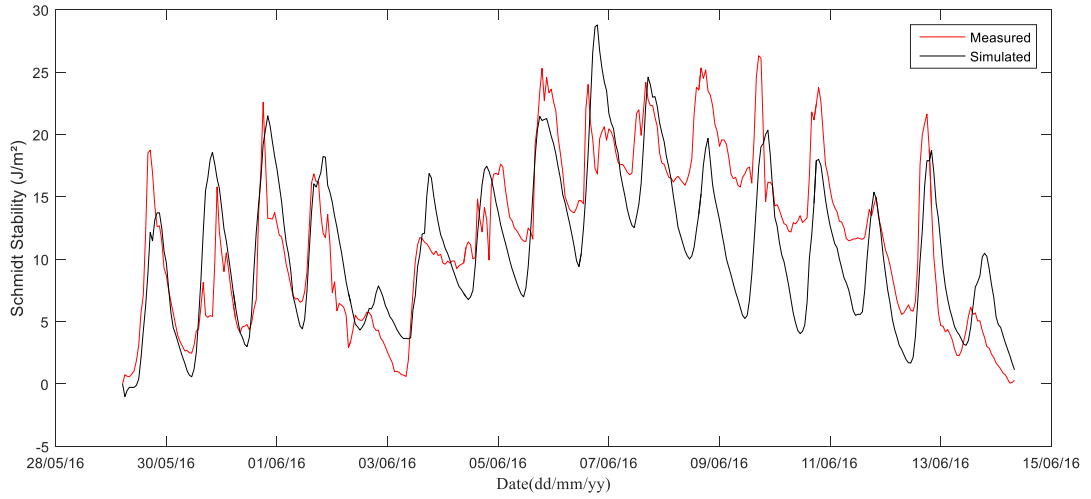


Figure 27 – Schmidt stability variation during the validation period (May 29<sup>th</sup> to June 14<sup>th</sup> 2016) at point P1

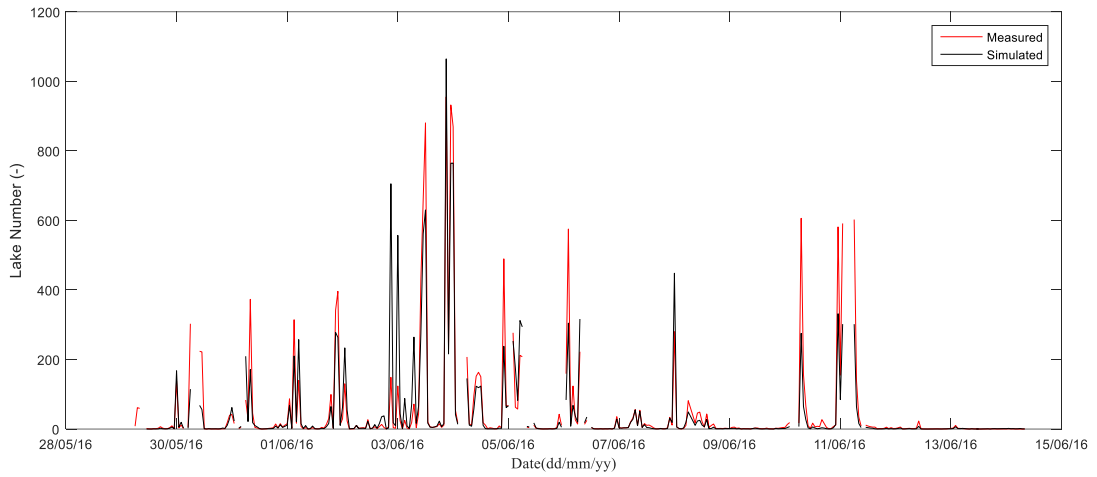


Figure 28 – Lake number variation during the validation period (May 29<sup>th</sup> to June 14<sup>th</sup> 2016) at point P1

## DISCUSSION

A literature review of papers published from 2000 to 2015, carried out by Meinson et al. (2016), showed that more than two-thirds of the studies that used high-frequency monitoring in lakes were carried out in northern temperate zone, either in North America or in Europe. The authors also showed that water temperature was the most common measured parameter, because of the sensor reasonable price and low maintenance and the most important, because water temperature is a controlling factor of biological, ecological and chemical processes (Meinson et al., 2016).

In our paper, a three-dimensional hydrodynamic model, Delft3D-FLOW, was implemented in Lake Pampulha, a shallow urban tropical reservoir. The calibration period lasted 18 days, from May 16<sup>th</sup> to May 29<sup>th</sup> 2016, corresponding to 440 hourly data at 0.5 m, 2.5 m, 5.5 m and 9.5 m depth. The model could accurately reproduce the alternation of stratification and mixing conditions along the period. The validation period lasted 16 days, from May 29<sup>th</sup> to June 14<sup>th</sup> 2016, corresponding to 388 hourly data at the same depths of calibration period. Performance indicators showed that the model performed well. The model was also validated for a longer period from May 15<sup>th</sup> to August 10<sup>th</sup> 2015, corresponding to 2107 hourly data at 0.5 m depth.

Mean absolute error (MAE) during all simulation periods for water temperature varied between 0.15 and 0.45 °C and was similar to other three-dimensional model studies. Soullignac et al. (2017) obtained values in a range between 0.25 and 2.34 °C for Lake Créteil (surface area of 0.4 km<sup>2</sup> and mean depth of 4.5 m,) using hourly temperature values at five depths (0.5, 1.5, 2.5, 3.5 and 4.5 m) over 8 months (around 5500 values). In Lake Yilong (surface area of 28.4 km<sup>2</sup> and mean depth of 3.9 m), Zhao et al. (2013) obtained a R<sup>2</sup> between 0.65 and 0.74 calculated from measured data of 15 campaigns throughout one year, in the same range of our values (0.55 to 0.93). In Lake Minnetonka (maximum depth of 25.0 m and surface area of 8.01 km<sup>2</sup>), Missaghi and Hondzo (2010) obtained a R<sup>2</sup> between 0.91 and 0.98 using 6 months of bi-weekly measured profiles of temperature for calibration and validation period.

Belico (2017) investigated the thermal regime of Lake Pampulha during rain events from 2011 to 2015 with a one-dimensional model using hourly measurements of water temperature at surface and monthly vertical profiles. The unidimensional modelling provided a Root Mean Square Error (RMSE) of 1.08 °C at surface. The author highlighted that the model could not rightly simulated the lake bottom layers. Other studies were also applied to Lake Pampulha (Silva, 2014; Silva et al., 2016, 2019) however, none of them used three-dimensional modelling with high-frequency measurement in different depths.

In the present paper, high-frequency measurement could detect sudden changes of water temperature with different amplitudes depending on the depth.

The water temperature measurements in the centre of the lake were performed at surface (0.5 m), 2.5 m, 5.5 m and bottom (9.5 m) and were compared to three-dimensional hydrodynamic model results, allowing a

thorough analysis of the lake hydrodynamics. In our paper, the RMSE varied between 0.15 and 0.65 °C and high-frequency measurement coupled with three-dimensional model could appropriately represent high vertical temperature gradient.

The good simulation results indicate that the meteorological data, collected at a weather station located 3 km from the lake (and from 9.5 km for the cloud cover data) reproduce well the meteorological conditions over the lake most of the time. However, the performance of the model may have been affected due to high sensibility of the lake hydrodynamics to external forcing such as nebulosity and wind intensity and direction. Another source of uncertainties was the inflow water temperature that was estimated using air temperature.

Using high-frequency time series, a good model performance was obtained using short simulation period, which is suitable in terms of computation time demand. However, the simulations were not performed for all seasons. We focused on the dry season because it is the period with higher episodes of cyanobacteria blooms in Lake Pampulha. The model must be validated over longer periods representing other hydro-meteorological conditions.

Despite using data from only one monitoring station to calibrate the model and despite the limitation in water inflow temperatures measurements, the model was useful to understand and evaluate the impact of forcing scenarios. During high discharge events, when the river temperature is colder than the lake water, it flows through the deepest layers of the lake. In the simulated episode, the inflow water sank to the bottom of the lake, 1500 m far from the inflow channel. The model showed that the colder water underflow in the deepest part of the lake is still visible almost 3.5 km far from the river entrance. The 3D hydrodynamic model could be further used for investigating in other hydro-meteorological conditions the complex spatio-temporal dynamics of Lake Pampulha or similar reservoirs.

Lake Pampulha water quality is severely impaired, with recurring hypoxia in the bottom layers (Friese et al., 2010; von Sperling and Campos, 2011). The water current caused by the inflow, through the deepest layers of the lake, may help to renew and oxygenate the water. It also may impact the lake ecological status by affecting the sediment resuspension and nutrient release. Thus, providing a modelling tool which can help to investigate the physical conditions of hypolimnion aeration is an important outcome of this study.

Due to the importance of water stratification and hydrodynamics on phytoplankton growth, our results may also help to understanding algal blooms. The good results of the hydrodynamic model allow, for the next steps, to study phytoplankton and nutrient dynamics by coupling the water quality module.

## CONCLUSION

In this paper, a three-dimensional hydrodynamic model, Delft3D-FLOW, was implemented in Lake Pampulha, a shallow urban tropical reservoir. For the three simulated periods, the agreement between the

modelled and hourly measured temperatures were considered very satisfactory.

This paper highlights the complex hydrodynamics of a shallow reservoir and the importance in monitoring the inflow water temperature and discharge. The model outcomes made it possible to investigate the cause of sudden changes in the water temperature. Future studies may focus on extending the simulation period to include rainy season and obtaining data in other monitoring stations in the lake to provide a further assessment of the 3D hydrodynamic model performance.

Investigating the inflow impact on the lake hydrodynamics may contribute to assess the efficiency of restoration techniques, supporting the decision-making for water management of urban lakes.

## ACKNOWLEDGEMENTS

This research was embedded with a collaboration between LEESU-ENPC (France) within OSS-Cyano research project supported by ANR (French National Research Agency) and EHR-UFGM (Brazil) within MoMa-SE research project, supported by CAPES and ANA (Brazilian National Water Agency) and MAPLU-2 funded by Brazilian research funding agency FINEP with funds from the Brazilian Water Resources Sectorial Fund. The authors are grateful to CAPES and ARF for providing financial resource and for all staff involved. The first author received a doctoral fellowship by Ecole des Ponts ParisTech (France) and by CAPES (Brazil). The 4<sup>th</sup> author benefits of a CNPq-PQ fellowship.

## REFERENCES

- Aparicio Medrano, E., Uittenbogaard, R.E., Dionisio Pires, L.M., van de Wiel, B.J.H., and Clercx, H.J.H. (2013). Coupling hydrodynamics and buoyancy regulation in *Microcystis aeruginosa* for its vertical distribution in lakes. *Ecol. Model.* 248, 41–56.
- Barçante, B., Nascimento, N.O., Silva, T.F.G., Reis, L.A., and Giani, A. (2020). Cyanobacteria dynamics and phytoplankton species richness as a measure of waterbody recovery: Response to phosphorus removal treatment in a tropical eutrophic reservoir. *Ecol. Indic.* 117, 106702.
- Belico, J.C.B. (2017). Impactos de eventos chuvosos na dinâmica físico-química e biológica em reservatórios urbanos estudo de caso: Lagoa da Pampulha.
- Bennett, N.D., Croke, B.F.W., Guariso, G., Guillaume, J.H.A., Hamilton, S.H., Jakeman, A.J., Marsili-Libelli, S., Newham, L.T.H., Norton, J.P., Perrin, C., et al. (2013). Characterising performance of environmental models. *Environ. Model. Softw.* 40, 1–20.
- Birch, S., and McCaskie, J. (1999). Shallow urban lakes: a challenge for lake management. *Hydrobiologia* 395–396, 365–378.
- Boegman, L., Imberger, J., Ivey, G.N., and Antenucci, J.P. (2003). High-frequency internal waves in large stratified lakes. *Limnol. Oceanogr.* 48, 895–919.
- Campos, R.G.D. (2004). Estudos Hidrológicos das Bacias do ribeirão Pampulha e do Córrego Cachoeirinha.
- Chanudet, V., Fabre, V., and van der Kaaij, T. (2012). Application of a three-dimensional hydrodynamic model to the Nam Theun 2 Reservoir (Lao PDR). *J. Gt. Lakes Res.* 38, 260–269.
- Chen, G., and Fang, X. (2015). Accuracy of Hourly Water Temperatures in Rivers Calculated from Air Temperatures. *Water* 7, 1068–1087.
- Chen, G., and Fang, X. (2016). Estimating Hourly Water Temperatures in Rivers from Air Temperatures. *World Environ. Water Resour. Congr.* 2016.
- CPRM (2001). Projeto Pampulha – Estudo Hidrogeológico da Bacia da Lagoa da Pampulha, (PBH).
- Davidson, K., Anderson, D.M., Mateus, M., Reguera, B., Silke, J., Sourisseau, M., and Maguire, J. (2016). Forecasting the risk of harmful algal blooms. *Harmful Algae* 53, 1–7.
- Deltares (2014). Delft3D-FLOW User Manual. Version: 3.15.36498.
- Diário Oficial do Município (2016). Prefeitura dá início à recuperação da qualidade da água da lagoa da pampulha.
- Elliott, J.A. (2012). Is the future blue-green? A review of the current model predictions of how climate change could affect pelagic freshwater cyanobacteria. *Water Res.* 46, 1364–1371.
- Felisberto, H., Rocha, F., and Palmier, L.R. (2015). Mapeamento da área inundada resultante da propagação de onda de cheia oriunda de ruptura hipotética de barragem - estudo de caso: Barragem da Pampulha. SBRH 8.
- Friese, K., Schmidt, G., de Lena, J.C., Arias Nalini, H., and Zachmann, D.W. (2010). Anthropogenic influence on the degradation of an urban lake – The

- Pampulha reservoir in Belo Horizonte, Minas Gerais, Brazil. *Limnol. - Ecol. Manag. Inland Waters* 40, 114–125.
- Gonçalves, A.L., Pires, J.C.M., and Simões, M. (2016). The effects of light and temperature on microalgal growth and nutrient removal: an experimental and mathematical approach. *RSC Adv.* 6, 22896–22907.
- Gong, R., Xu, L., Wang, D., Li, H., and Xu, J. (2016). Water Quality Modeling for a Typical Urban Lake Based on the EFDC Model. *Environ. Model. Assess.* 21, 643–655.
- Grimaud, G.M., Mairet, F., Sciandra, A., and Bernard, O. (2017). Modeling the temperature effect on the specific growth rate of phytoplankton: a review. *Rev. Environ. Sci. Biotechnol.* 16, 625–645.
- Hébert, C., Caissie, D., Satish, M.G., and El-Jabi, N. (2015). Predicting Hourly Stream Temperatures Using the Equilibrium Temperature Model. *J. Water Resour. Prot.* 07, 322.
- Ho, J.C., and Michalak, A.M. (2015). Challenges in tracking harmful algal blooms: A synthesis of evidence from Lake Erie. *J. Gt. Lakes Res.* 41, 317–325.
- IBGE (2014). Anuário Estatístico do Brasil.
- Idso, S.B. (1973). On the concept of lake stability. *Limnol. Oceanogr.* 18, 681–683.
- Imberger, J., and Patterson, J.C. (1990). Physical Limnology. In *Advances in Applied Mechanics*, J.W. Hutchinson, and T.Y. Wu, eds. (Elsevier), pp. 303–475.
- Jin, K.-R., Hamrick, J.H., and Tisdale, T. (2000). Application of Three-Dimensional Hydrodynamic Model for Lake Okeechobee. *J. Hydraul. Eng.* 126, 758–771.
- Jöhnk, K.D., Huisman, J., Sharples, J., Sommeijer, B., Visser, P.M., and Stroom, J.M. (2008). Summer heatwaves promote blooms of harmful cyanobacteria. *Glob. Change Biol.* 14, 495–512.
- Li-Kun, Y., Sen, P., Xin-hua, Z., and Xia, L. (2017). Development of a two-dimensional eutrophication model in an urban lake (China) and the application of uncertainty analysis. *Ecol. Model.* 345, 63–74.
- Matos, A.C. de S., Lemos, R.S., Silva, T.F. das G., Eleutério, J.C., and Nascimento, N. (2017). Evolução do uso e ocupação do solo em mananciais de abastecimento metropolitano na região metropolitana de Belo Horizonte, Estado de Minas Gerais. 8.
- Meinson, P., Idrizaj, A., Noges, P., Noges, T., and Laas, A. (2016). Continuous and high-frequency measurements in limnology: history, applications, and future challenges. *Environ. Rev.* 24, 52–63.
- Missaghi, S., and Hondzo, M. (2010). Evaluation and application of a three-dimensional water quality model in a shallow lake with complex morphometry. *Ecol. Model.* 221, 1512–1525.
- Nogueira, M.M. (2015). Elaboração da curva chave dos córregos Ressaca e Sarandi utilizando métodos computacionais (UFMG).
- Phlips, E.J., Badylak, S., and Grosskopf, T. (2002). Factors Affecting the Abundance of Phytoplankton in a Restricted Subtropical Lagoon, the Indian River Lagoon, Florida, USA. *Estuar. Coast. Shelf Sci.* 55, 385–402.
- PMS (2017). POLÍTICA MUNICIPAL DE SANEAMENTO DE BELO HORIZONTE.
- Polli, B.A., Bleninger, T., Polli, B.A., and Bleninger, T. (2019). Comparison of 1D and 3D reservoir heat transport models and temperature effects on mass transport. *RBRH* 24.
- Qin, B., Li, W., Zhu, G., Zhang, Y., Wu, T., and Gao, G. (2015). Cyanobacterial bloom management through integrated monitoring and forecasting in large shallow eutrophic Lake Taihu (China). *J. Hazard. Mater.* 287, 356–363.
- Read, J.S., Hamilton, D.P., Jones, I.D., Muraoka, K., Winslow, L.A., Kroiss, R., Wu, C.H., and Gaiser, E. (2011). Derivation of lake mixing and stratification indices from high-resolution lake buoy data. *Environ. Model. Softw.* 26, 1325–1336.
- Reynolds, C.S. (1998). What factors influence the species composition of phytoplankton in lakes of different trophic status? *Hydrobiologia* 369, 11–26.
- Scriban, A., Lemaire, B., and Vinçon-Leite, B. (2015). Configuration d'un modèle de prévision de l'évolution à court terme des dynamiques hydrodynamiques et biogéochimiques dans le plan d'eau urbain de Champs-sur-Marne.
- Silva, T.F. das G. (2014). Suivi et modélisation de la dynamique des cyanobactéries dans les lacs urbains au sein de leur bassin versant. Université



- Paris-Est and Universidade Federal de Minas Gerais.
- Silva, T.F. das G., Vinçon-Leite, B., Giani, A., Figueredo, C.C., Petrucci, G., Lemaire, B., Sperling, E.V., Tassin, B., Seidl, M., Khac, V.T., et al. (2016). Modelagem da Lagoa da Pampulha: uma ferramenta para avaliar o impacto da bacia hidrográfica na dinâmica do fitoplâncton. *Eng. Sanit. E Ambient.* *21*, 95–108.
- Silva, T.F.G., Vinçon-Leite, B., Lemaire, B.J., Petrucci, G., Giani, A., Figueredo, C.C., and Nascimento, N. de O. (2019). Impact of Urban Stormwater Runoff on Cyanobacteria Dynamics in A Tropical Urban Lake. *Water* *11*, 946.
- Simpson, J.H., Lucas, N.S., Powell, B., and Maberly, S.C. (2015). Dissipation and mixing during the onset of stratification in a temperate lake, Windermere. *Limnol. Oceanogr.* *60*, 29–41.
- Siqueira, R.C., Moura, P.M., and Silva, T.F. das G. (2019). Methodology for the construction of an urban flood hazard chart. *RBRH* *24*.
- Soullignac, F., Vinçon-Leite, B., Lemaire B. J., Scarati R, Bonhomme, C., Dubois, P., Mezemate, Y., Tchiguirinskaia I, Schertzer, D., and Tassin B (2017). Performance assessment of a 3D hydrodynamic model using high temporal resolution measurements in a shallow urban lake. *Environ. Model. Assess. in press*.
- Soullignac, F., Danis, P.-A., Bouffard, D., Chanudet, V., Dambrine, E., Guénand, Y., Harmel, T., Ibelings, B.W., Trevisan, D., Uittenbogaard, R., et al. (2018). Using 3D modeling and remote sensing capabilities for a better understanding of spatio-temporal heterogeneities of phytoplankton abundance in large lakes. *J. Gt. Lakes Res.*
- von Sperling, E., and Campos, M.O. (2011). Restoration of Lake Pampulha, Brazil by using sanitation and in-lake techniques.
- Stefan, H.G., and Preud'homme, E.B. (1993). Stream Temperature Estimation from Air Temperature1. *JAWRA J. Am. Water Resour. Assoc.* *29*, 27–45.
- UNESCO (1981). Background papers and supporting data on the practical salinity scale 1978. Unesco/ICES/SCOR/IAPSO Joint Panel on Oceanographic Tables and Standards. UNESCO Tech. Pap. Mar. Sci. Doc. Tech. Unesco Sur Sci. Mer.
- Van Donk, E. (1984). Factors influencing phytoplankton growth and succession in Lake Maarsseveen I. *Hydrobiol. Bull.* *18*, 69–71.
- Vinçon-Leite, B., and Casenave, C. (2019). Modelling eutrophication in lake ecosystems: A review. *Sci. Total Environ.* *651*, 2985–3001.
- Vinnå, L.R., Wüest, A., and Bouffard, D. (2017). Physical effects of thermal pollution in lakes. *Water Resour. Res.* *53*, 3968–3987.
- Whyte, C., Swan, S., and Davidson, K. (2014). Changing wind patterns linked to unusually high Dinophysis blooms around the Shetland Islands, Scotland. *Harmful Algae* *39*, 365–373.
- Wu, T., Qin, B., Zhu, G., Luo, L., Ding, Y., and Bian, G. (2013). Dynamics of cyanobacterial bloom formation during short-term hydrodynamic fluctuation in a large shallow, eutrophic, and wind-exposed Lake Taihu, China. *Environ. Sci. Pollut. Res. Int.* *20*, 8546–8556.
- Wu, T., Qin, B., Brookes, J.D., Shi, K., Zhu, G., Zhu, M., Yan, W., and Wang, Z. (2015). The influence of changes in wind patterns on the areal extension of surface cyanobacterial blooms in a large shallow lake in China. *Sci. Total Environ.* *518–519*, 24–30.
- Yi, X., Zou, R., and Guo, H. (2016). Global sensitivity analysis of a three-dimensional nutrients-algae dynamic model for a large shallow lake. *Ecol. Model.* *327*, 74–84.
- Zbiciński, I., and Ziemińska-Stolarska, A. (2017). Analysis of factors affecting the ecological status of the large water bodies on the basis of monitoring and integrated 3D models. *E3S Web Conf.* *19*, 02009.
- Zhao, L., Li, Y., Zou, R., He, B., Zhu, X., Liu, Y., Wang, J., and Zhu, Y. (2013). A three-dimensional water quality modeling approach for exploring the eutrophication responses to load reduction scenarios in Lake Yilong (China). *Environ. Pollut.* *177*, 13–21.